



ENGINEERING INFORMATION RECORD

Document Identifier 51 - 1258768-01

Title Ginna Spent Fuel Pool Re-racking Licensing Report

PREPARED BY:

REVIEWED BY:

Name See below

Name See below

Signature Date

Signature Date

Technical Manager Statement: Initials WPH

Reviewer is Independent.

Remarks:

Prepared by:

Reviewed by:

Criticality

L. A. Hassler 3/19/97
L. A. Hassler

B. M. Palmer 3/19/97
B. M. Palmer

Structural

J. R. Biddle 3/19/97
J. R. Biddle

M. K. Punatar 3/19/97
M. K. Punatar

Thermal-Hydraulic

P. J. Henningson 3/19/97
P. J. Henningson

D. A. Farnsworth 3/19/97
D. A. Farnsworth

VENDOR'S DOCUMENT REVIEW

1. ☒ APPROVED-MANUFACTURING MAY PROCEED
2. ☒ APPROVED-SUBMIT FINAL DOCUMENTS-MANUFACTURING MAY PROCEED
3. ☐ APPROVED AS NOTED-MAKE CHANGES AND SUBMIT FINAL DOCUMENTS. MANUFACTURING MAY PROCEED AS APPROVED.
4. ☐ NOT APPROVED-CORRECT AND RESUBMIT
5. ☐ REVIEW NOT REQUIRED-MANUFACTURING MAY PROCEED

APPROVAL OF THIS DOCUMENT DOES NOT RELIEVE SUPPLIER FROM FULL COMPLIANCE WITH CONTRACT OR PURCHASE ORDER REQUIREMENTS.

BY: DAVID L. DEWITT DATE: 3/31/97
ROCHESTER GAS & ELECTRIC CORP.
ROCHESTER, NEW YORK

M. A. Rutherford 3/19/97
M. A. Rutherford

S. Q. King 3/19/97
S. Q. King

TABLE OF CONTENTS

	<u>Page</u>
1.0 INTRODUCTION	
1.1 GENERAL	19
1.2 NEW SPENT FUEL POOL CONFIGURATION	20
1.3 BORATED STAINLESS STEEL RACK DESCRIPTION	21
1.3.1 Description of Region 1, Type 3 Racks	21
1.3.2 Description of Region 2, Type 2 Racks	22
1.3.3 Description of Region 2, Type 4 Racks	23
1.3.4 Neutron Absorber Material	24
1.3.5 Structural Materials	25
1.4 SUPPLIER QUALIFICATION AND EXPERIENCE	26
1.4.1 Team Qualifications	26
1.4.2 Team Experience	26
2.0 PRINCIPAL DESIGN CRITERIA	
2.1 General Design Criteria	52
2.2 Structural Criteria	52
2.3 Criticality Criteria	52
2.4 Thermal-Hydraulic Criteria	53
2.5 Radiological Criteria	53
3.0 STRUCTURAL EVALUATION	
3.1 SCOPE	54
3.2 DESIGN CRITERIA	55
3.2.1 Applicable Codes and Standards	55
3.2.2 Acceptance Criteria, Load Combinations and Stress Limits	57
3.3 STRUCTURAL DESIGN FEATURES	63
3.4 MATERIALS OF CONSTRUCTION	65
3.4.1 Structural Materials	65
3.4.2 Non-structural Materials	65
3.5 STRUCTURAL ANALYSIS	72
3.5.1 Loading Conditions	73
3.5.1.1 Overview	73
3.5.1.2 Seismic Input Compliance	77
3.5.2 Structural Analysis Methods	100
3.5.2.1 Assumptions - Seismic/Structural	100
3.5.2.2 Analytical Procedure	101
3.5.2.2.1 Seismic Analysis	101
3.5.2.2.2 Structural Analysis	103
3.5.2.2.2.1 Rack Stresses	103
3.5.2.2.2.2 Support Legs and Concrete Bearing Stresses	104
3.5.2.2.2.3 Weld Stresses	104

TABLE OF CONTENTS

	<u>Page</u>
3.5.2.2.2.4 Fuel-to-Rack Impact Loads Evaluation	105
3.5.2.2.2.5 Sliding and Tipping	105
3.5.2.2.2.6 Expected Loads on Floor From Racks	106
3.5.2.2.2.7 Pool Liner Plate Integrity Evaluation	106
3.5.2.3 Detailed Descriptions of Mathematical Models	106
3.5.2.4 Detailed Documentation of Computer Codes	117
3.5.2.4.1 General	117
3.5.2.4.2 Structural/Seismic Computer Codes	117
3.5.2.4.2.1 ANSYS	117
3.5.2.4.2.1.1 Summary of Element Types Used in the ANSYS Models	118
3.5.2.4.2.1.2 Summary of ANSYS Error Reports for Element Types Used	119
3.5.2.4.2.2 SIMQKE	119
3.5.2.5 Hydrodynamic Fluid Coupling	120
3.5.2.5.1 Fuel-To-Rack Hydrodynamic Coupling	120
3.5.2.5.2 Rack-To-Rack and Rack-To-Pool Hydrodynamic Coupling	123
3.5.2.6 Seismic Time History Factor Determinations	130
3.5.2.7 Rack Stiffness Sensitivity Study	132
3.5.3 Structural Evaluation	136
3.5.3.1 Normal, Upset and Faulted Conditions	136
3.5.3.1.1 Various Inputs to the 3-D Single Rack and Whole Pool Finite Element Models	136
3.5.3.1.1.1 Rack Structural Properties	136
3.5.3.1.1.2 Fuel Structural Properties	142
3.5.3.1.1.2.1 Consolidated Fuel Canister Structural Properties	142
3.5.3.1.1.2.2 Fuel Assembly Structural Properties	143
3.5.3.1.1.3 Interface Stiffness Between Fuel and Rack	143
3.5.3.1.1.4 Damping	144
3.5.3.1.1.5 Perforated Plates	146
3.5.3.1.1.6 Local Gaps Surrounding Each Rack	149
3.5.3.1.2 Rack Tube Connecting Tabs and Tube Retainer Plate Welds	150
3.5.3.1.2.1 Tab/Weld Stresses Due to Seismic Loads	150
3.5.3.1.2.2 Tab/Weld Stresses Due to Fuel-to-Tube Impact	152
3.5.3.1.2.3 Thermal Stresses in Tabs/Welds	158
3.5.3.1.2.4 Total Tab/Weld Stresses	159
3.5.3.1.2.5 Borated Stainless Steel Retainer Plates Weld Stresses	159
3.5.3.1.2.6 Rack Tube Buckling Strength and Tab Weld Spacing	161
3.5.3.1.2.7 Rack Tube Maximum Stress Evaluation	164
3.5.3.1.3 Bottom of Rack Tube to Base Plate Welds	167
3.5.3.1.4 Welding of Support Legs	171

TABLE OF CONTENTS

	<u>Page</u>
3.5.3.1.5 Summary of Support Pad Loads	173
3.5.3.1.6 Fuel-to-Rack Impact Loads	185
3.5.3.1.7 Summary of Single Rack 3-D Model Results	191
3.5.3.1.7.1 Brief Description of 3-D Single Rack Model	191
3.5.3.1.7.2 Study of Effects of Rack Height Increase	192
3.5.3.1.7.2.1 Purpose of Rack Height Increase Study	192
3.5.3.1.7.2.2 Modifications Required in the Rack Model	192
3.5.3.1.7.2.3 Results of Rack Height Increase Study	192
3.5.3.1.7.3 Peripheral Rack Attachment Study	196
3.5.3.1.7.3.1 Purpose of Peripheral Rack Attachment Study	196
3.5.3.1.7.3.2 Peripheral Rack Model Input Adjustments	196
3.5.3.1.7.3.3 Summary of Results	196
3.5.3.1.7.4 Off-Centered Loading Study	200
3.5.3.1.7.4.1 Purpose of Off-Centered Loading Study	200
3.5.3.1.7.4.2 Modifications Required to Analyze Off-Centered Loading Cases	200
3.5.3.1.7.4.3 Summary of Off-Centered Loading Results	201
3.5.3.1.7.5 Comparison of Connected and Disconnected Fuel Beam Models	201
3.5.3.1.8 Summary of Whole Pool Model Results	203
3.5.3.1.8.1 Rack Forces and Moments for Each Load Case	206
3.5.3.1.8.2 Final Rack Displacements for Each Load Case	218
3.5.3.1.8.3 Final Rack Rotations For Each Load Case	230
3.5.3.1.8.4 Representative Plots	236
3.5.3.1.9 Support Leg and Bearing Pad Analysis	254
3.5.3.1.9.1 Support Leg Analysis	256
3.5.3.1.9.1.1 Existing Rack Support Analysis	256
3.5.3.1.9.1.2 Concrete and Spent Fuel Pool Liner Qualification	257
3.5.3.1.9.1.2.1 Average Concrete Bearing Stress	257
3.5.3.1.9.1.2.2 Boussinesq's Solution	257
3.5.3.1.10 Rack Thermal Stress Analysis	260
3.5.3.1.11 Fatigue Analysis	266
3.5.3.1.12 Rack Base Plate Evaluation	269
3.5.3.1.13 Sloshing	272
3.5.3.1.14 Summary of Gap Closure from Five (5) OBE's Plus One (1) SSE	279
3.5.3.1.15 Borated Stainless Steel Functionality	283
3.5.3.1.16 U.S. Tool & Die Rack Structural Evaluation	284
3.5.3.1.17 Spent Fuel Pool and Liner Structural Evaluation	287
3.5.3.1.18 Stuck Fuel Assembly - Uplift Force	289
3.5.3.1.19 Storage Racks Lifting Analysis	292

TABLE OF CONTENTS

	<u>Page</u>
3.5.3.2 Accident Conditions	294
3.5.3.2.1 Methodology and Assumptions	294
3.5.3.2.2 Acceptance Criteria	295
3.5.3.2.3 Fuel Assembly Drop Analysis	295
3.5.3.2.3.1 Fuel Assembly-Straight Deep Drop	296
3.5.3.2.3.1.1 Fuel Assembly Falls Through Cell to Base Plate	296
3.5.3.2.3.1.2 Fuel Assembly Drops into Cell and Strikes Support Leg	301
3.5.3.2.3.2 Fuel Assembly - Shallow Drops	304
3.5.3.2.3.2.1 Flat Impact on Top Interface of the Racks	305
3.5.3.2.3.2.2 End-On Impact	306
3.5.3.2.4 Tornado Missile Impact	308
3.5.3.2.5 Gate Drop	310
3.5.3.2.6 Rack Drops	310
3.5.3.2.7 Cask Drop	314
3.5.3.2.8 Summary of Accident Drop Results	314
3.5.3.2.9 Loss of Spent Fuel Pool Cooling	316
3.5.3.3 Tabulation of Results	317
3.5.3.4 Discussion of Results and Significance	323
3.5.3.5 Conclusion	323
3.5.3.6 Anticipated Impact on Operations of R.E. Ginna Nuclear Plant	324
3.6 REFERENCES	325
 4.0 CRITICALITY EVALUATION	
4.1 INTRODUCTION	328
4.1.1 Region 1 Normal Condition	328
4.1.2 Region 2 Normal Condition	329
4.1.3 Abnormal Conditions	329
4.2 ANALYTICAL METHODS	330
4.2.1 Criticality Analysis Methodology	331
4.2.2 Tolerance Evaluation/Burnup Isotopic Generation with CASMO-3	331
4.2.3 Burnup Credit Methodology	332
4.2.4 Boraflex Degradation/Shrinkage Methodology	333
4.3 CRITICALITY ANALYSES	334
4.3.1 Input Parameters	335
4.3.1.1 Fuel Assembly Description	335
4.3.1.2 Spent Fuel Storage Rack Dimensions	335
4.3.1.3 Material Specifications	335
4.3.2 Tolerance/Uncertainty Evaluation	335
4.3.2.1 Fuel Rack Tolerance Analysis Methodology	336
4.3.2.2 Off-Center Fuel Assembly Analysis	336

TABLE OF CONTENTS

	<u>Page</u>
4.3.2.3 Storage Pool Coolant Temperature Effects	336
4.3.2.4 Fuel Assembly Mechanical Tolerances	337
4.3.2.5 Most Reactive Fuel Type	337
4.3.2.5.1 Intact Fuel Assemblies	337
4.3.2.5.2 Consolidated Fuel Containers	338
4.3.2.6 Summary of Biases, Penalties, and Uncertainties in Analysis	338
4.3.3 Region 1 Analysis	338
4.3.3.1 Region 1 Geometry Models	338
4.3.3.2 Burnup Credit	339
4.3.4 Region 2 Analysis	339
4.3.4.1 Region 2 Geometry Models	340
4.3.4.1.1 Rack Type 1 - Boraflex Rack	340
4.3.4.1.2 Rack Type 2 - Borated Stainless Steel Rack	340
4.3.4.1.3 Region 2 Combined Model for Rack Type 4 Evaluation	340
4.3.4.2 Region 2 Loading Curve Generation	341
4.3.4.2.1 Base Burnup vs Enrichment Curve Generation	341
4.3.4.3 Generation of the Loading Curve for Abnormal Assemblies	341
4.3.5 Interface Effects	342
4.3.6 Accident Analysis	343
4.3.6.1 Region 1 Assembly Drop Analyses	343
4.3.6.2 Region 2 Assembly Drop Analyses	344
4.3.6.3 Seismic Analysis	345
4.3.6.3.1 Region 1 Seismic Analysis	346
4.3.6.3.2 Region 2 Seismic Analysis	346
4.3.6.3.3 Interface Region Seismic Analysis	346
4.3.7 Summary of Results	346
4.3.7.1 Analytical Results for Region 1	347
4.3.7.1.1 Normal Condition Results	347
4.3.7.1.2 Burnup Versus Enrichment Curve	348
4.3.7.1.3 IFBA Rod Requirements	348
4.3.7.1.4 Accident Conditions	348
4.3.7.2 Analytical Results for Region 2	349
4.3.7.2.1 Analytical Results for Normal Conditions	349
4.3.7.2.2 Base Burnup Versus Enrichment Curve	350
4.3.7.2.3 Loading Curve for Abnormally Burned Assemblies	351
4.3.7.2.4 Results for Accident Conditions	351
4.3.8 Fuel Rod Consolidation	352
4.3.9 Acceptance Criteria for Criticality	353
4.4 SUPPLEMENTARY INFORMATION	354
4.4.1 KENO V.a Bias	354
4.4.1.1 Critical Experiments	354
4.4.1.2 CASMO-3/KENO V.a Benchmarks	357

TABLE OF CONTENTS

	<u>Page</u>
4.4.1.3 KENO V.a Infinite to Finite Model Comparison	357
4.4.2 Burnup Credit Methodology	358
4.4.2.1 Axial Profile Generation	358
4.4.2.2 Axial Profile Isotopic Concentration Generation	359
4.4.2.3 Axial Reactivity Effects	360
4.4.2.4 Boraflex Degradation Model Margin	361
4.4.3 Westinghouse IFBA Documentation	361
4.5 REFERENCES	367
 5.0 THERMAL-HYDRAULIC EVALUATION	
5.1 INTRODUCTION	429
5.2 CRITERIA	430
5.3 ASSUMPTIONS	430
5.4 DISCUSSION OF SPENT FUEL COOLING	430
5.5 SPENT FUEL POOL CAPACITY AND DISCHARGE SCENARIOS	431
5.5.1 Spent Fuel Pool Capacity	431
5.5.2 Core Offload Scenarios	431
5.5.2.1 Normal Discharge Scenario	431
5.5.2.2 Full Core Discharge Scenario	432
5.6 DECAY HEAT LOAD	434
5.6.1 Full Core Decay Heat Load	434
5.6.2 Single Fuel Assembly Decay Heat Load	435
5.7 REQUIRED CORE DECAY TIMES	435
5.7.1 Single Batch Offload	435
5.7.2 Full Core Offload	436
5.8 LOCAL FUEL BUNDLE THERMAL-HYDRAULICS	436
5.8.1 Natural Circulation in the Spent Fuel Pool Storage Canisters	437
5.8.2 Effects of Gamma Heating in the Flux Trap Regions and Inter-Canister Gaps	439
5.8.2.1 Region I Type 3 Flux Traps	439
5.8.2.2 Region II Type 2 Inter-Canister Gaps	440
5.8.3 Flow Blockages	441
5.8.4 Natural Circulation in the Consolidated Fuel Canisters	441
5.9 SPENT FUEL POOL THERMAL-HYDRAULICS ANALYSIS RESULTS ..	442
5.9.1 Region I with Type 3 ATEA Racks	442
5.9.2 Region II with Type 2 ATEA Racks	443
5.9.3 Region II with Type 4 ATEA Side Racks	444
5.9.4 Natural Circulation in the Region I Flux Trap Region	445
5.9.5 Natural Circulation in the Region II Inter-Canister Gaps	446
5.9.6 The Effect of Flow Blockage	446
5.9.7 Natural Circulation in the Consolidated Fuel Canister	447



TABLE OF CONTENTS

	<u>Page</u>
5.10 LOSS OF THE SPENT FUEL COOLING SYSTEM	447
5.11 COMPARISON BETWEEN ORIGEN2 RESULTS AND ASB 9-2 METHODOLOGY	449
5.12 REFERENCES	449
 6.0 RADIOLOGICAL EVALUATION	
6.1 ACCEPTANCE CRITERIA	451
6.1.1 Offsite Dose Exposure	451
6.1.2 Occupational Dose Exposure	452
6.2 OFFSITE DOSE CONSEQUENCES	452
6.2.1 Rack Drop Accident	452
6.2.2 Cask Drop/Tip Accident	452
6.2.3 Gate Drop Accident	452
6.2.4 Consolidated Canister Drop Accident	452
6.2.5 Fuel Handling Accident	453
6.2.6 Tornado Missile Accident	453
6.3 OCCUPATIONAL EXPOSURE	455
6.4 SOLID RADWASTE	458
6.5 GASEOUS RELEASES	460
6.6 RACK DISPOSAL	461
6.7 CONCLUSIONS	461
6.8 REFERENCES	461
 7.0 QUALITY ASSURANCE	
7.1 DESCRIPTION OF SUPPLIER'S QUALITY ASSURANCE PROGRAM	468
7.2 DESCRIPTION OF QUALITY ASSURANCE PLAN AND IMPLEMENTATION	468
7.2.1 Organization	469
7.2.2 Quality Assurance	469
7.2.3 Design Control	469
7.2.4 Procurement Document Control	469
7.2.5 Instructions, Procedures, and Drawings	469
7.2.6 Document Control	469
7.2.7 Control of Purchased Material, Equipment, and Services	469
7.2.8 Identification and Control of Materials, Parts, and Components	470
7.2.9 Control of Special Processes	470
7.2.10 Inspection	470
7.2.11 Test Control	470
7.2.12 Control of Measuring and Test Equipment	471
7.2.13 Handling, Storage, and Shipping	471
7.2.14 Inspections, Tests, and Operating Status	471
7.2.15 Non-Conforming Materials, Parts, or Components	471

TABLE OF CONTENTS

	<u>Page</u>
7.2.16 Corrective Action	472
7.2.17 Audits	472
 8.0 ENVIRONMENTAL COST/BENEFIT ASSESSMENT	
8.1 NEED FOR INCREASED STORAGE CAPACITY	473
8.2 ESTIMATED CONSTRUCTION COSTS	473
8.3 ALTERNATIVES TO INCREASED STORAGE CAPACITY	473
8.4 COMMITMENT OF MATERIAL RESOURCES	474
8.5 HEAT RELEASED TO THE ENVIRONMENT	475

List of Tables

Table 1.3-1	Number of Cells by Rack Type	29
Table 1.3-2	Rack Dimensions, Weight, Supports	30
Table 1.3-3	Design Data for Region 1, Type 3 Racks (Fresh Fuel and Spent Fuel)	31
Table 1.3-4	Design Data for Region 2, Type 2 Racks (Spent Fuel)	32
Table 1.3-5	Design Data for Region 2, Type 4 Racks (Spent Fuel)	33
Table 1.4-1	Framatome/ATEA Spent Fuel Racks	34
Table 1.4-2	Borated Stainless Steel Experience (Wet Storage)	35
Table 3.2-1	Stress Acceptance Criteria - Storage Racks	61
Table 3.2-2	304L Stainless Steel - Stress Acceptance Criteria	62
Table 3.4-1	Materials of Construction	67
Table 3.4-2	Material: 304 L Stainless Steel Plate, Bar and Pipe	68
Table 3.4-3	Material: 304 Stainless Steel Plate and Bar	69
Table 3.4-4	Material: 630 Precipitation Hardened Steel	70
Table 3.4-5	Concrete	71
Table 3.4-6	Zircaloy-4 Tubing Material	71
Table 3.4-7	Borated Stainless Steel	71
Table 3.4-8	Boraflex	71
Table 3.5-1	Regulatory Guide 1.60 Horizontal Spectra	78
Table 3.5-2	SSE Horizontal Spectra	78
Table 3.5-3	OBE Horizontal Spectra	79
Table 3.5-4	Regulatory Guide 1.60 Vertical Spectra	79
Table 3.5-5	SSE Vertical Spectra	79
Table 3.5-6	OBE Vertical Spectra	80
Table 3.5-7	Cross-Correlation Factors for SSE Time Histories	80
Table 3.5-8	Cross-Correlation Factors for OBE Time Histories	81
Table 3.5-9	Geometric Parameters for Hydrodynamic Mass Coupling - Summary Table	127

TABLE OF CONTENTS

	<u>Page</u>
Table 3.5-10 Rack Hydrodynamic Coupling Masses Standard Configuration (No Type 4 Racks Installed)	128
Table 3.5-11 Rack Hydrodynamic Coupling Masses Extended Configuration (Type 4 Racks Installed)	129
Table 3.5-12 Summary of Determination of SSE Time History Factor (Using Rack 8 (2B) Loaded with Consolidated Fuel, $\mu=0.8$)	131
Table 3.5-13 Summary of Determination of OBE Time History Factor (Using Rack 8 (2B) Loaded with Unconsolidated Fuel, $\mu=0.8$)	132
Table 3.5-14 Mechanical Tab/Weld Stresses	158
Table 3.5-15 Tabs/Welds Thermal Stresses	158
Table 3.5-16 Rack Cross-Section Properties for Tubes	162
Table 3.5-17 Compressive Rack Corner Tube Stresses [psi]	163
Table 3.5-18 Summary of Tube Stresses	166
Table 3.5-19 Base Plate Welds Cross-Section Properties for New ATEA Racks	168
Table 3.5-20 Base Plate & Weld Stress Summary for New ATEA Racks	170
Table 3.5-21 Summation of Support Leg Weld Stresses	172
Table 3.5-22 Max. Horiz. Model Leg Forces SRSS - LC#1	173
Table 3.5-23 Max. Vertical Pool Floor Forces -LC#1	173
Table 3.5-24 Max. Horiz. Leg Forces SRSS - LC#2	174
Table 3.5-25 Max. Vertical Pool Floor Forces - LC#2	174
Table 3.5-26 Max. Horiz. Model Leg Forces SRSS - LC#3	175
Table 3.5-27 Max. Vertical Pool Floor Forces - LC#3	175
Table 3.5-28 Max. Horiz. Leg Forces SRSS - LC#4	176
Table 3.5-29 Max. Vertical Pool Floor Forces - LC#4	176
Table 3.5-30 Max. Horiz. Model Leg Forces SRSS - LC#5	177
Table 3.5-31 Max. Vertical Pool Floor Forces - LC#5	177
Table 3.5-32 Max. Horiz. Model Leg Forces SRSS - LC#6	178
Table 3.5-33 Max. Vertical Pool Floor Forces - LC#6	178
Table 3.5-34 Max. Horiz. Leg Forces SRSS - LC#7	179
Table 3.5-35 Max. Vertical Pool Floor Forces - LC#7	179
Table 3.5-36 Max. Horiz. Leg Forces SRSS - LC#8	180
Table 3.5-37 Max. Vertical Pool Floor Forces - LC#8	180
Table 3.5-38 Max. Horiz. Leg Forces SRSS - LC#9	181
Table 3.5-39 Max. Vertical Pool Floor Forces - LC#9	181
Table 3.5-40 Max. Horiz. Leg Forces SRSS - LC#10	182
Table 3.5-41 Max. Vertical Pool Floor Forces - LC#10	182
Table 3.5-42 Max. Horiz. Leg Forces SRSS - LC#11	183
Table 3.5-43 Max. Vertical Pool Floor Forces - LC#11	183
Table 3.5-44 Max. Horiz. Leg Forces SRSS - LC#12	184
Table 3.5-45 Max. Vertical Pool Floor Forces - LC#12	184
Table 3.5-46 Local Fuel/Rack Impact Forces - LC#1	185



TABLE OF CONTENTS

	<u>Page</u>
Table 3.5-47 Local Fuel/Rack Impact Forces - LC#2	185
Table 3.5-48 Local Fuel/Rack Impact Forces - LC#3	186
Table 3.5-49 Local Fuel/Rack Impact Forces - LC#4	186
Table 3.5-50 Local Fuel/Rack Impact Forces - LC#5	187
Table 3.5-51 Local Fuel/Rack Impact Forces - LC#6	187
Table 3.5-52 Local Fuel/Rack Impact Forces - LC#7	188
Table 3.5-53 Local Fuel/Rack Impact Forces - LC#8	188
Table 3.5-54 Local Fuel/Rack Impact Forces - LC#9	189
Table 3.5-55 Local Fuel/Rack Impact Forces - LC#10	189
Table 3.5-56 Local Fuel/Rack Impact Forces - LC#11	190
Table 3.5-57 Local Fuel/Rack Impact Forces - LC#12	190
Table 3.5-58 Summary of Maximum Fuel/Rack Cell Wall Impact Loads	191
Table 3.5-59 Comparison of Results for Rack Model With and Without a Height Increase	195
Table 3.5-60 Summary of OBE Results in Peripheral Rack Analysis	197
Table 3.5-61 Summary of SSE Results in Peripheral Rack Analysis	198
Table 3.5-62 Comparison of Results for Half-Loaded Consolidated Rack 8, SSE 1, Mu=0.8	201
Table 3.5-63 Summary of Connected and Disconnected Fuel Beam Model Comparison Results	203
Table 3.5-64 Summary of Whole Pool Model Load Cases	203
Table 3.5-65 Summary of Rack Loadings for Load Case #11	204
Table 3.5-66 Summary of Rack Loadings for Load Case #12	205
Table 3.5-67 Rack Forces Fx, Fy & Fz - LC#1	206
Table 3.5-68 Rack Moments Mx, My & Mz - LC#1	206
Table 3.5-69 Rack Forces Fx, Fy & Fz - LC#2	207
Table 3.5-70 Rack Moments Mx, My & Mz - LC#2	207
Table 3.5-71 Rack Forces Fx, Fy & Fz - LC#3	208
Table 3.5-72 Rack Moments Mx, My & Mz - LC#3	208
Table 3.5-73 Rack Forces Fx, Fy & Fz - LC#4	209
Table 3.5-74 Rack Moments Mx, My & Mz - LC#4	209
Table 3.5-75 Rack Forces Fx, Fy & Fz - LC#5	210
Table 3.5-76 Rack Moments Mx, My & Mz - LC#5	210
Table 3.5-77 Rack Forces Fx, Fy & Fz - LC#6	211
Table 3.5-78 Rack Moments Mx, My & Mz - LC#6	211
Table 3.5-79 Rack Forces Fx, Fy & Fz - LC#7	212
Table 3.5-80 Rack Moments Mx, My & Mz - LC#7	212
Table 3.5-81 Rack Forces Fx, Fy & Fz - LC#8	213
Table 3.5-82 Rack Moments Mx, My & Mz - LC#8	213
Table 3.5-83 Rack Forces Fx, Fy & Fz - LC#9	214
Table 3.5-84 Rack Moments Mx, My & Mz - LC#9	214

TABLE OF CONTENTS

	<u>Page</u>
Table 3.5-85 Rack Forces Fx, Fy & Fz - LC#10	215
Table 3.5-86 Rack Moments Mx, My & Mz - LC#10	215
Table 3.5-87 Rack Forces Fx, Fy & Fz - LC#11	216
Table 3.5-88 Rack Moments Mx, My & Mz - LC#11	216
Table 3.5-89 Rack Forces Fx, Fy & Fz - LC#12	217
Table 3.5-90 Rack Moments Mx, My & Mz - LC#12	217
Table 3.5-91 Final Rack Relative East-West Disp. - LC#1	218
Table 3.5-92 Final Rack Relative North-South Disp. - LC#1	218
Table 3.5-93 Final Rack Relative East-West Disp. - LC#2	219
Table 3.5-94 Final Rack Relative North-South Disp. - LC#2	219
Table 3.5-95 Final Rack Relative East-West Disp. - LC#3	220
Table 3.5-96 Final Rack Relative North-South Disp. - LC#3	220
Table 3.5-97 Final Rack Relative East-West Disp. - LC#4	221
Table 3.5-98 Final Rack Relative North-South Disp. - LC#4	221
Table 3.5-99 Final Rack Relative East-West Disp. - LC#5	222
Table 3.5-100 Final Rack Relative North-South Disp. - LC#5	222
Table 3.5-101 Final Rack Relative East-West Disp. - LC#6	223
Table 3.5-102 Final Rack Relative North-South Disp. - LC#6	223
Table 3.5-103 Final Rack Relative East-West Disp. - LC#7	224
Table 3.5-104 Final Rack Relative North-South Disp. - LC#7	224
Table 3.5-105 Final Rack Relative East-West Disp. - LC#8	225
Table 3.5-106 Final Rack Relative North-South Disp. - LC#8	225
Table 3.5-107 Final Rack Relative East-West Disp. - LC#9	226
Table 3.5-108 Final Rack Relative North-South Disp. - LC#9	226
Table 3.5-109 Final Rack Relative East-West Disp. - LC#10	227
Table 3.5-110 Final Rack Relative North-South Disp. - LC#10	227
Table 3.5-111 Final Rack Relative East-West Disp. - LC#11	228
Table 3.5-112 Final Rack Relative North-South Disp. - LC#11	228
Table 3.5-113 Final Rack Relative East-West Disp. - LC#12	229
Table 3.5-114 Final Rack Relative North-South Disp. - LC#12	229
Table 3.5-115 Final Rack Rotations - LC #1	230
Table 3.5-116 Final Rack Rotations - LC #2	230
Table 3.5-117 Final Rack Rotations - LC #3	231
Table 3.5-118 Final Rack Rotations - LC #4	231
Table 3.5-119 Final Rack Rotations - LC #5	232
Table 3.5-120 Final Rack Rotations - LC #6	232
Table 3.5-121 Final Rack Rotations - LC #7	233
Table 3.5-122 Final Rack Rotations - LC #8	233
Table 3.5-123 Final Rack Rotations - LC #9	234
Table 3.5-124 Final Rack Rotations - LC #10	234
Table 3.5-125 Final Rack Rotations - LC #11	235



TABLE OF CONTENTS

	<u>Page</u>
Table 3.5-126 Final Rack Rotations - LC #12	235
Table 3.5-127 Material Properties for the Pool Liner and Support Legs	254
Table 3.5-128 Forces Used in Qualification of the Pool Liner and Support Legs	254
Table 3.5-129 Support Legs Force Comparison for Existing Racks	256
Table 3.5-130 Summation of Concrete Stresses	258
Table 3.5-131 Summation of Spent Fuel Pool Liner Stresses	258
Table 3.5-132 Summation of Support Leg Stresses	259
Table 3.5-133 Relative Disp. Due to East-West Translation	280
Table 3.5-134 Relative East-West Disp. Due to Rotation	280
Table 3.5-135 Relative Disp. Due to North-South Translation	281
Table 3.5-136 Relative North-South Disp. Due to Rotation	281
Table 3.5-137 Summary of East-West Relative Disp.	282
Table 3.5-138 Summary of North-South Relative Disp.	282
Table 3.5-139 Seismic Loads on Racks 1 through 6 - at the Base of Rack	286
Table 3.5-140 Seismic Support Pad Load on Racks 1 through 6 Load on Each Pad	287
Table 3.5-141 Results of Support Leg Stresses	317
Table 3.5-142 Results of Concrete Stresses	318
Table 3.5-143 Results of Spent Fuel Pool Liner Stresses	318
Table 3.5-144 Results of Tab Stresses	319
Table 3.5-145 Results of Tube Stresses	321
Table 3.5-146 Results of Base Plate Stresses	322
Table 4.1-1 Polynomial Generated for Spent Fuel Burnup vs Enrichment Requirements for the Region 1 Racks	370
Table 4.1-2 Polynomial Generated Burnup vs Enrichment Requirements for the Region 2 Racks	371
Table 4.1-3 KENO V.a Region 1 (Rack Type 3) Results of Burnup vs Enrichment Calculations	372
Table 4.1-4 KENO V.a Region 2 (Rack Types 1, 2, & 4) Results of Burnup vs Enrichment Calculations	373
Table 4.3-1 Fuel Assembly Parameters	374
Table 4.3-2 Consolidation Canister Specifications	375
Table 4.3-3a Region 1, Rack Type 3 Cell Dimensions	376
Table 4.3-3b Region 1, Rack Type 3 Damaged Fuel Cell Dimensions	376
Table 4.3-4 Region 2, Rack Type 1 Cell Dimensions	377
Table 4.3-5 Region 2, Rack Type 2 Cell Dimensions	377
Table 4.3-6 Region 2, Rack Type 4 Cell Dimensions	378
Table 4.3-7 Material Compositions for Non-Fuel Regions	379
Table 4.3-8 Fuel Material Number Densities	380
Table 4.3-9 Assembly Tolerance Penalties (Δk)	381
Table 4.3-10 Reactivity Uncertainty Associated With Fuel Assembly Type	381

TABLE OF CONTENTS

	<u>Page</u>
Table 4.3-11 Consolidation Container Results	381
Table 4.3-12 Summary of Rack Type Uncertainties, Penalties, And Credits	382
Table 4.3-13 Region 1, Rack Type 3, Dropped Assembly Accident Results	383
Table 4.3-14 Region 2, Rack Types 1, 2, & 4, Dropped Assembly Accident Results	383
Table 4.3-15 Seismic Event Accident Results	383
Table 4.4-1 KENO V.a BIAS vs Separation Distance	384
Table 4.4-2 Additional UO ₂ Critical Experiment Comparisons	385
Table 4.4-3 Mixed Oxide Critical Experiment Comparisons	386
Table 4.4-4 International Handbook Critical Experiments	387
Table 4.4-5 CASMO-3/KENO V.a Benchmark Configurations	387
Table 4.4-6 CASMO-3/KENO V.a Infinite Array Benchmark Comparison	388
Table 4.4-7 CASMO-3/KENO V.a Infinite Array Benchmark Comparison	388
Table 4.4-8 KENO V.a Infinite to Finite Model Comparison	388
Table 4.4-9 Ginna Fuel Assemblies Used for Axial Shape Evaluation	389
Table 4.4-10 Relative Axial Shapes for Typical Non-Axial Blanket Standard Fuel Assemblies	390
Table 4.4-11 Relative Axial Shapes for the Seven Zone Axial Model	391
Table 4.4-12 Axial Burnup Shapes for the Region 2 Loading Curve	391
Table 4.4-13 Irradiation Input Data and Isotopic Concentrations for 3 Wt% Initial Enrichment Fuel at 21 GWD/mtU Burnup In Region 2	392
Table 4.4-14 Irradiation Input Data and Isotopic Concentrations for 4 Wt% Initial Enrichment Fuel at 34 GWD/mtU Burnup in Region 2	393
Table 4.4-15 Irradiation Input Data and Isotopic Concentrations for 5 Wt% Initial Enrichment Fuel at 45 GWD/mtU Burnup in Region 2	394
Table 4.4-16 Isotopic Concentrations for Fuel for Region 2 Auxiliary Curves	395
Table 4.4-17 Average Isotopic Concentrations for Region 1 Loading Curve	395
Table 4.4-18 Evaluation of Axial Shape Effects for All Rack Types	396
Table 4.4-19 Evaluation of Margin Provided by the Boraflex Degradation Model for Rack Type 1	397
Table 5.5-1 Ginna Spent Fuel Pool Inventory (Actual & Projected)	433
Table 5.9-1 Region I Type 3 Rack Local Pool Cooling Results	443
Table 5.9-2 Region II Type 2 Rack Local Pool Cooling Results	444
Table 5.9-3 Region II Type 4 & Boraflex Rack Local Pool Cooling Results	445
Table 5.10-1 Loss of Pool Cooling and Heat-Up Time	448
Table 5.11-1 Comparison between ORIGEN2 and ASB 9-2 Results for a full core with 15 GWD/MTU burnup	449
Table 6.2-1 Offsite Radiological Consequences of a Hypothetical Tornado Missile Accident	455
Table 6.3-1 Dose Rates at Locations of Interest Around Spent Fuel Pool	457
Table 6.3-2 Gamma Isotopic Analysis of Spent Fuel Pool Water for 1996	457

TABLE OF CONTENTS

	<u>Page</u>
Table 6.4-1 Radionuclide Analysis Report - Resin Activity, from the Spent Resin Tanks	458
Table 6.5-1 Gaseous Releases from the Auxiliary Building	460
Table 6A-1 Assumptions and Inputs Used in Determining Offsite Doses Due to Tornado Missile Accident Inside Auxiliary Building	464
Table 6A-2 Tornado Missile Accident Source Terms for Region 1 (100 Hours of Decay)	465
Table 6A-3 Tornado Missile Accident Source Terms for Region 2 (60 Days of Decay)	466
Table 6A-4 Dose Conversion Factors	467

List of Figures

Figure 1.1-1 Spent Fuel Pool - General Arrangement	37
Figure 1.3-1 Type 3 Rack - Perspective	38
Figure 1.3-2 Type 3 Rack - General Arrangement	39
Figure 1.3-3 Type 3 Rack - Detail of Base	40
Figure 1.3-4 Type 3 Rack - Vertical Section	41
Figure 1.3-5 Type 3 Rack - Top View	42
Figure 1.3-6 Type 3 Rack - Details of Connecting Tabs	43
Figure 1.3-7 Type 2 Rack - Details of Top	44
Figure 1.3-8 Type 2 Rack - Perspective	45
Figure 1.3-9 Type 2 Rack - Detail of Base	46
Figure 1.3-10 Type 2 Rack - Vertical Section	47
Figure 1.3-11 Type 2 Rack - Top View	48
Figure 1.3-12 Type 2 Rack - Detail of Connecting Tabs	49
Figure 1.3-13 Type 4 Rack	50
Figure 1.3-14 Type 4 Rack - Top View	51
Figure 3.5-1 Avg. Calculated vs. Design Response Spectra for SSE (EW) X-Dir.	82
Figure 3.5-2 Avg. Calculated vs. Design Response Spectra for SSE (NS) Y-Dir.	83
Figure 3.5-3 Avg. Calculated vs. Design Response Spectra for SSE Z-Dir.	84
Figure 3.5-4 Avg. Calculated vs. Design Response Spectra for OBE (EW) X-Dir.	85
Figure 3.5-5 Avg. Calculated vs. Design Response Spectra for OBE (NS) Y-Dir.	86
Figure 3.5-6 Avg. Calculated vs. Design Response Spectra for OBE Z-Dir.	87
Figure 3.5-7 SSE Acceleration Time History #1 for (EW) X-Dir.	88
Figure 3.5-8 SSE Acceleration Time History #2 for (EW) X-Dir.	88
Figure 3.5-9 SSE Acceleration Time History #3 for (EW) X-Dir.	89
Figure 3.5-10 SSE Acceleration Time History #4 for (EW) X-Dir.	89
Figure 3.5-11 SSE Acceleration Time History #1 for (NS) Y-Dir.	90
Figure 3.5-12 SSE Acceleration Time History #2 for (NS) Y-Dir.	90
Figure 3.5-13 SSE Acceleration Time History #3 for (NS) Y-Dir.	91

TABLE OF CONTENTS

	<u>Page</u>
Figure 3.5-14 SSE Acceleration Time History #4 for (NS) Y-Dir.	91
Figure 3.5-15 SSE Acceleration Time History #1 for Vertical Z-Dir.	92
Figure 3.5-16 SSE Acceleration Time History #2 for Vertical Z-Dir.	92
Figure 3.5-17 SSE Acceleration Time History #3 for Vertical Z-Dir.	93
Figure 3.5-18 SSE Acceleration Time History #4 for Vertical Z-Dir.	93
Figure 3.5-19 OBE Acceleration Time History #1 for (EW) X-Dir.	94
Figure 3.5-20 OBE Acceleration Time History #2 for (EW) X-Dir.	94
Figure 3.5-21 OBE Acceleration Time History #3 for (EW) X-Dir.	95
Figure 3.5-22 OBE Acceleration Time History #4 for (EW) X-Dir.	95
Figure 3.5-23 OBE Acceleration Time History #1 for (NS) Y-Dir.	96
Figure 3.5-24 OBE Acceleration Time History #2 for (NS) Y-Dir.	96
Figure 3.5-25 OBE Acceleration Time History #3 for (NS) Y-Dir.	97
Figure 3.5-26 OBE Acceleration Time History #4 for (NS) Y-Dir.	97
Figure 3.5-27 OBE Acceleration Time History #1 for Vertical Z-Dir.	98
Figure 3.5-28 OBE Acceleration Time History #2 for Vertical Z-Dir.	98
Figure 3.5-29 OBE Acceleration Time History #3 for Vertical Z-Dir.	99
Figure 3.5-30 OBE Acceleration Time History #4 for Vertical Z-Dir.	99
Figure 3.5-31 3D-Single Rack Model	111
Figure 3.5-32 Ginna 3D Whole Pool Rack Model	112
Figure 3.5-33 Single Rack Finite Element Model	113
Figure 3.5-34 Ginna Type 2 Rack Cell Finite Element Model	114
Figure 3.5-35 Ginna Type 3 Rack Cell Finite Element Model	115
Figure 3.5-36 Plan View of Spent Fuel Pool	116
Figure 3.5-37 Percent of Value at Stiffness of Continuous Structure vs. Stiffness Factor	135
Figure 3.5-38 Longitudinal Tab Impact Model	153
Figure 3.5-39 Lateral Tab Impact Model	156
Figure 3.5-40 Dimensions, Support Leg, and Gusset Plates Used for Weld Qualification	172
Figure 3.5-41 Representation of Model for Single Rack Analysis	193
Figure 3.5-42 Representation of Model for Analysis of Rack 1 With Attached Rack 4A	194
Figure 3.5-43 Vertical Leg Force Fz, Rack 1, Leg 1 - LC#1	236
Figure 3.5-44 Sum of Vert. Leg Forces Fz, Rack 1 - LC#1	237
Figure 3.5-45 Rack 1 Horizontal Force Fy - LC#1	238
Figure 3.5-46 Rack 1 Moment Mx - LC#1	239
Figure 3.5-47 Rack 7 Moment My - LC#1	240
Figure 3.5-48 Fuel/Rack Impact Lds. +X, Rack 1 Top - LC#1	241
Figure 3.5-49 Relative Displ. DX Rack5/Rack7, Top - LC#1	242
Figure 3.5-50 Rel. Displ. DX Rack5/Rack7, Base - LC#1	243
Figure 3.5-51 Rel. Displ. DY Rack1/Rack2, Base - LC#1	244



TABLE OF CONTENTS

	<u>Page</u>
Figure 3.5-52 Vertical Leg Force Fz, Rack 1, Leg 1 - LC#2	245
Figure 3.5-53 Sum of Vertical Leg Forces Fz, Rack 1 - LC#2	246
Figure 3.5-54 Rack 1 Horizontal Force Fy - LC#2	247
Figure 3.5-55 Rack 1 Moment Mx - LC#2	248
Figure 3.5-56 Rack 7 Moment My - LC#2	249
Figure 3.5-57 Fuel/Rack Impact Loads +X, Rack 1 Top - LC#2	250
Figure 3.5-58 Relative Displ. DX Rack5/Rack7, Top - LC#2	251
Figure 3.5-59 Relative Displ. DX Rack5/Rack7, Base - LC#2	252
Figure 3.5-60 Relative Displ. DY Rack1/Rack2, Base - LC#2	253
Figure 3.5-61 Support Leg Details	255
Figure 3.5-62 Support Leg Gusset Plate Details	256
Figure 3.5-63 Stress Locations For Boussinesq's Bearing Solution	257
Figure 3.5-64 Rack Tubes Stress Contours - To (Top Plane)	261
Figure 3.5-65 Rack Tubes Stress Contours - To (Mid Plane)	261
Figure 3.5-66 Base Plate Stress Contours - To (Top Plane)	262
Figure 3.5-67 Base Plate Stress Contours - To (Mid Plane)	262
Figure 3.5-68 Deformed Base Plate with Legs - Ta	263
Figure 3.5-69 Bottom Corner Tubes Stress Contours - Ta (Top Plane)	264
Figure 3.5-70 Bottom Corner Tubes Stress Contours - Ta (Mid Plane)	264
Figure 3.5-71 Base Plate Stress Contours - Ta (Top Plane)	265
Figure 3.5-72 Base Plate Stress Contours - Ta (Mid Plane)	265
Figure 3.5-73 Base Plate Membrane Stress Contours	271
Figure 3.5-74 Base Plate Memb. + Bend. Stress Contours	272
Figure 4.1-1 Region 1 Spent Fuel Burnup vs Enrichment Curve	398
Figure 4.1-2 Region 2 Burnup vs Enrichment Curve	399
Figure 4.1-3 Sketch of Allowable Loading Configurations for Region 1	400
Figure 4.1-4 Sketch of Allowable Loading Configurations for Region 2	401
Figure 4.3-1 Ginna Spent Fuel Pool Configuration	402
Figure 4.3-2 Region 1 Type 3 Base Cell Structure for Infinite Model	403
Figure 4.3-3 Axial Profile Of Finite And Infinite Base Models	404
Figure 4.3-4 Region 1 - Rack Type 3 Finite Model	405
Figure 4.3-5 Region 2 Boraflex Rack (Type 1) - KENO V.a Model	406
Figure 4.3-6 Region 2 Borated Stainless Steel (Type 2) Racks - KENO V.a Model	407
Figure 4.3-7 Areas Modeled to Examine Interface Effects between Rack Types and Regions	408
Figure 4.3-8 KENO V.a Model Used to Examine Interface Effect between (1) Rack Types 3C & 2B, and (2) Rack Types 2B & 3E	409
Figure 4.3-9 KENO V.a Model Used to Examine Interface Effects between Rack Types 1, 4F, and 3A	410

TABLE OF CONTENTS

	<u>Page</u>
Figure 4.3-10 KENO V.a Model Used to Examine Interface Effects between Rack Types 1, 4C, and 2A	411
Figure 4.3-11 KENO V.a Shallow Drop Accident Models	412
Figure 4.3-12 KENO V.a Side Drop Accident Model	413
Figure 4.3-13 KENO V.a Deep Drop Accident Model for Rack Types 2, 3, and 4	414
Figure 4.3-14 KENO V.a Region 1 Misplaced Assembly Model	415
Figure 4.3-15 KENO V.a Region 2 Misplaced Assembly Model	416
Figure 4.3-16 KENO V.a Rack Type 1 Deep Drop Accident Model	417
Figure 4.3-17 Sketch of Consolidation Canister	418
Figure 4.4-1 KENO V.a Results for B&W Criticals for Spacing Variations	419
Figure 4.4-2 Results for Water Spacing Experiments from KENO V.a 27 and 44 Group and MCNP Continuous Group Cross Sections	420
Figure 4.4-3 Least Squares Fit Through Results B&W Interspersed Absorber Experiments	421
Figure 4.4-4 Typical Ginna Axial Burnup Shapes for Burnups between 10 and 20 GWd/mtU	422
Figure 4.4-5 Typical Ginna Axial Burnup Shapes for Burnups between 20 and 30 GWd/mtU	423
Figure 4.4-6 Typical Ginna Axial Burnup Shapes for Burnups between 30 and 40 GWd/mtU	424
Figure 4.4-7 Typical Ginna Axial Burnup Shapes for Burnups between 40 and 50 GWd/mtU	425
Figure 4.4-8 Non-Axial Blanket Shapes Used for Analysis	426
Figure 4.4-9 Relative Non-Blanket Axial Shapes Used in Analysis	427
Figure 4.4-10 Illustration of Seven Zone Representation	428
 Figure 5.8-1 Spent Fuel Pool	 437
Figure 5.8-2 Natural Circulation Flow Path	439
Figure 5.8-3 Flux Trap Region	440
Figure 5.8-4 Region II Type 2 Inter-Canister Gap	441
Figure 5.9-1 Natural Circulation Flow Path - Type 3 Rack	443
 Figure 6-1 Overview of Proposed Re-racking of the Ginna Spent Fuel Pool	 463
Figure 6-2 Overview of Spent Fuel Pool Concrete Wall Thicknesses	463

List of Appendices

Appendix 6A Assumptions and Input	464
---	-----

1.0 INTRODUCTION

1.1 GENERAL

The licensing analysis presented in the following sections is applicable to Rochester Gas and Electric's R. E. Ginna Nuclear Power Plant. The Ginna Nuclear Plant is located approximately 16 miles east of Rochester in Wayne County, New York. The reactor is a Westinghouse 2-Loop Pressurized Water Reactor (PWR) design configuration, and utilizes a 14 x 14 fuel assembly.

The plant's spent fuel pool was originally racked in 1968. Subsequently, the pool was re-racked in 1977 and 1985. The present pool is configured with two types of racks. Region 1 consists of three flux trap type racks providing storage for 176 fuel assemblies, and Region 2 consists of six high density fixed poison (Boraflex) type racks accommodating 840 fuel assemblies for a total capacity of 1016 fuel assemblies.

The new spent fuel pool rack analysis contained in this report provides the necessary licensing analyses to reconfigure the pool to accommodate a net increase of 353 locations. This is accomplished by retaining the six existing high density racks (840 minus 12 for attachment of new racks = 828 locations), and installing new Borated Stainless Steel (BSS) racks with up to 541 additional storage locations for a new total of 1,369 locations. The analyses presented herein demonstrate that a total of 1,879 fuel assemblies can be accommodated in these 1,369 locations by storing consolidated rod canisters in some spent fuel locations. The number of fuel rods contained in the intact fuel assemblies and/or consolidated rod storage canisters stored in these locations is limited to no more than the number of rods contained in 1,879 fuel assemblies (179 fuel rods per assembly x 1,879 assemblies = 336,341 fuel rods.)

The re-configured pool will have four types of racks in two regions. Region 1 will contain only fresh fuel/spent fuel racks designated Type 3. Region 2 will contain spent fuel racks including the existing Boraflex racks, designated Type 1, and new high density racks designated Types 2 and 4. The Type 2 racks will occupy the main portion of the available space while the Type 4 racks will be placed between the existing Type 1 Boraflex racks and the pool wall. The Regions and Types are summarized below; Figure 1.1-1 shows the new pool arrangement.

Region	Type	Description
1	3	BSS racks for fresh fuel/spent fuel
2	1	Existing Boraflex racks for spent fuel
2	2	Interior BSS racks for spent fuel
2	4*	Peripheral BSS racks for spent fuel

* Only Type 2 and 3 racks will be installed at this time. The Type 4 racks are being presented as a means of achieving the maximum storage capacity of the pool and to license the configuration, but will not be installed, unless needed in the future.

The new racks will consist of a grid arrangement of vertical square-section parallel cells each designed to take one fuel assembly. The distance between cells is minimized by inserting neutron absorber plates between the cells to ensure adequate margin against criticality.

To facilitate manufacturing and assembly, these racks are not of monolithic construction but are made of modules placed side by side. Each module is comprised of multiple cells and is sized to match the geometry of the storage pool zone available and to allow for handling constraints.

The racks are designed for a forty-year service life. The materials used in their construction provide corrosion resistance in pure or borated water and dimensional and structural stability under irradiation. In addition, their structure ensures the integrity of the nuclear fuel stored in them under all circumstances, notably in the event of an earthquake.

The racks use borated stainless steel neutron absorbers in the form of rigid plates which have not been subjected to operations like bending, welding, or mechanical fastening which can reduce their strength and subsequent integrity under operating conditions. The fabrication method allows the neutron absorber plates to be held in place without bending, welding, or mechanical fastening.

The design of the proposed racks incorporates two fundamental features:

- Stainless steel containing boron is used as a neutron absorber material only and not as a structural member.
- This equipment is fabricated and installed without bending, welding or mechanical fastening of the borated stainless steel.

1.2 NEW SPENT FUEL POOL CONFIGURATION

Figure 1.1-1 shows the general layout of the re-configured spent fuel pool. The racks are located in two regions as detailed below.

REGION 1 - Fresh fuel and spent fuel stored in a checkerboard arrangement.

Type 3: Five borated stainless steel racks accommodating:
145 spent fuel assemblies
144 fresh fuel assemblies
5 damaged fuel assemblies

REGION 2 - Spent fuel.

Type 1: Six existing Boraflex racks accommodating:
840 spent fuel assemblies. When the six peripheral Type 4 racks are installed, 12 of the 840 locations are used to support the Type 4 racks.

Type 2: Two new borated stainless steel racks accommodating:
187 spent fuel assemblies

Type 4: Six peripheral Borated Stainless Steel racks accommodating: 60 spent fuel assemblies. The type 4 racks are located between the existing Type 1 Boraflex racks and the pool wall and are attached to the Type 1 racks.

1.3 BORATED STAINLESS STEEL RACK DESCRIPTION

The racks consist of vertically oriented, square cross-section cells each designed to hold one fuel assembly (see Figure 1.3-1). The number and type of racks, the number of cells per rack, and the total number of cells are shown in Table 1.3-1.

The Region 1, Type 3 and Region 2, Type 2 racks are free standing and self supporting. The Region 2, Type 4 racks have two legs each for support and are attached to the Region 2, Type 1 racks to provide lateral support. The dimensions, weight and number of supports for each rack are listed in Table 1.3-2.

1.3.1 Description of Region 1, Type 3 Racks

These racks accommodate fresh fuel and spent fuel in a checkerboard pattern. The geometry and dimensions of the square cells are given in Figure 1.3-5 and Table 1.3-3. The rack constituent parts are shown in Figures 1.3-1 to 1.3-6 and described below.

a) Cells for Fresh Fuel Assemblies (Figure 1.3-2, callout 2) - These cells are composed of:

- Four Borated Stainless Steel (BSS) sheets forming a square cell. The sheets are linked together at the corners and rest on the base plate.
- Eight horizontal Stainless Steel (SS) belts maintaining the BSS geometry and ensuring a very precise pitch dimension. Seven of these belts are located in the same vertical position as the seven intermediate spacer grids on the fuel assemblies.
- Stainless Steel square cross-section funnels are welded to the adjacent SS cells. These funnels guide the fresh fuel assembly into the cells and prevent the inadvertent extraction of the BSS sheets when a fuel assembly is removed.

In the cells facing a pool wall or the cask area, the corresponding BSS sheet facing the wall or the cask area is replaced by a SS sheet.

b) Cells for Spent Fuel Assemblies (Figure 1.3-2, callout 1). These cells are composed of:

- External SS square tubes. The tubes are formed either by welding two channel sections or by expanding a round tube into a square tube.
- Four internal BSS sheets. The sheets are linked together at the corners and rest on lower tabs which are welded to the surrounding stainless steel cell walls as in the Type 2 racks (Figure 1.3-10, callout 8). At the top, stainless steel tabs are also welded to the surrounding SS cell walls to restrain the BSS plates from upward motion.



In the cells facing a pool wall or the cask area, the BSS sheet facing the wall or the cask area is replaced by a SS sheet.

c) Base Plate - This plate provides a continuous horizontal surface for supporting the fuel assemblies (Figure 1.3-3, callout 1). Holes in the base plate, concentric to each cell, provide the necessary path for the cooling water flow. Grooves are machined on the upper surface of the base plate for positioning each square cell. This groove ensures a very precise center- to-center spacing of the cells (pitch). The SS square tubes are fillet welded to the base plate.

d) Connecting Tabs - The SS cells are joined together along their length by SS connecting tabs welded to the SS square tube faces (Figure 1.3-6). This forms the cells in each rack into a continuous structure. Rack assembly is performed in a machined assembly fixture resulting in a very precise center-to-center spacing of the cell (pitch).

e) Support Legs - The rack support legs are of the adjustable type (Figure 1.3-3, callout 2). The number of support legs on each rack is shown in Table 1.3-2. Each leg is composed of four pieces:

- An upper SS part that is welded to the base plate and containing four flow holes for cooling.
- A threaded pin with a convex spherical shape at its bottom. The pin is made of ASTM 630 steel in order to avoid galling.
- A SS support plate with a concave spherical bearing surface in contact with the threaded pin.
- A SS washer welded to the support plate.

f) Flat Plate and Corner Plate - The BSS cells located either on a rack edge or on a rack corner incorporate a SS flat plate or corner plate to restrain the corresponding BSS plate (Figure 1.3-2, callout 7.)

1.3.2 Description of Region 2, Type 2 Racks

This rack design accommodates spent fuel in two types of square cells: SS cells and BSS cells arranged in a checkerboard array. The geometry and dimensions of the square cells are given in Figure 1.3-10 and Table 1.3-4. The rack constituent parts are shown in Figures 1.3-7 to 1.3-12 and described below.

a) Stainless Steel Cells - These cells are made either by welding two channel sections or by expanding a round tube to a square tube (see Figure 1.3-7, callout 1).

b) Borated Stainless Steel Cells - These cells are composed of four BSS sheets linked together at the corners forming a square (see Figure 1.3-7, callout 2). The Borated Stainless Steel sheets are supported by a lower tab which is welded to the surrounding stainless steel cells (Figure 1.3-10, callout 8). At the top a stainless steel tab is welded to the SS cell to retain the BSS plates from upward motion (Figure 1.3-10, callout 7).

c) Neutron Absorber Material - The joining tabs on both long edges of each full-length sheet of BSS are laser cut to ensure precise alignment of the sheets (see Figure 1.3-7, callout 2). The BSS sheets are located in front of the active fuel length of the fuel assembly.

d) Base Plate - The base plate provides a continuous horizontal surface for supporting the fuel assemblies (Figure 1.3-9, callout 6). Holes in the base plate, concentric to the cells, correspond to the necessary section for the cooling water flow. Grooves are machined on the upper surface of the base plate for positioning each square cell prior to welding. These grooves ensure a very precise center-to-center spacing of the cell (pitch).

e) Connecting Tabs - The SS cells are joined together along their length by SS connecting tabs welded to the SS square tube faces (Figure 1.3-12). This forms the cells in each rack into a continuous structure. Rack assembly is performed in a machined assembly fixture resulting in a very precise center- to-center spacing of the cell (pitch).

f) Support Legs - The rack support legs are of the adjustable type (Figure 1.3-9, callout 5). The number of support legs on each rack is shown in Table 1.3-2. Each leg is composed of four pieces:

- An upper SS part that is welded to the base plate and containing four flow holes for cooling.
- A threaded pin with a convex spherical shape at its bottom. The pin is made of ASTM 630 steel in order to avoid galling.
- A SS support plate with a concave spherical bearing surface in contact with the threaded pin.
- A SS washer welded to the support plate.

g) Flat Plate and Corner Plate - The BSS cells located either on a rack edge or on a rack corner incorporate a SS flat plate or corner plate to restrain the corresponding BSS plate.

1.3.3 Description of Region 2, Type 4 Racks

The rack design employs square cell locations. The racks and their constituent parts are shown in Figure 1.3-13).

a) Cells - These SS cells are made either by welding two channel sections or by expanding a round tube to a square tube. BSS sheets are inserted between adjacent cells. Each BSS sheet is continuous over the active length of a fuel assembly. The lower part of the BSS sheets rest on the base plate. On the sides facing the existing Boraflex racks and the pool wall, there are no BSS sheets. The geometry and dimensions of the square cells are given in Figure 1.3-14 and Table 1.3-5.

b) Base Plate - The base plate provides a continuous horizontal surface for supporting the fuel assemblies. Holes in the base plate, concentric to the cells, correspond to the necessary section for the cooling water flow. Grooves are machined on the upper surface of the base plate for positioning each square cell prior to welding. These grooves ensure a very precise center-to-center spacing of the cell (pitch).

c) Connecting Tabs - On the cell sides facing the existing Boraflex racks and the pool wall, connecting tabs are welded between the SS square tube faces. This forms each rack into a continuous structure.

d) Rack Attachment - In the upper part and the lower part of the rack, two connecting devices attach each Type 4 rack to an existing Boraflex rack (Figure 1.3-13.) Each upper connecting device consists of a square tube inserted into a cell of the existing Boraflex rack, which is taken out of service. Each lower connecting device consists of a locking arm inserted into the cooling flow hole in the existing Boraflex rack.

e) Support Legs - There are two support legs on each Type 4 rack. The rack support legs are of the adjustable type. Each leg is composed of four pieces:

- An upper SS part that is welded to the base plate and containing four flow holes for cooling.
- A threaded pin with a convex spherical shape at its bottom. The pin is made of ASTM 630 steel in order to avoid galling.
- A SS support plate with a concave spherical bearing surface in contact with the threaded pin.
- A SS washer welded to the support plate.

1.3.4 Neutron Absorber Material

The neutron absorber material is borated stainless steel (BSS) sheet. It is a type 304 austenitic chromium stainless steel modified by the addition of boron. The BSS is inserted in the racks for neutron absorption but, due to the design of the racks, no stresses are induced in the BSS. Moreover, the BSS sheets are fabricated using processes designed to prevent the formation of residual stresses.

The neutron absorber material is borated stainless steel (BSS) type 304 B6/B7 in accordance with ASTM Specification A 887-89. The minimum percentage of boron in the BSS is 1.70 in weight %.

The chemical composition of borated stainless steel to be used at Ginna is in accordance with ASTM A 887-89 type 304 B6/B7, as listed below:

<u>Element</u>	<u>Maximum Weight %</u>
Carbon	0.08
Manganese	2.00
Phosphorous	0.045
Sulfur	0.030
Silicon	0.75
Chromium	18.00-20.00
Nickel	12.00 - 15.00
Boron	1.70 (min.)

Boron is added to the austenitic stainless steel for its neutron absorption properties. It is present as an alloying element and not as particles in a mixture. The microstructure consists of an austenitic stainless steel matrix with a fine, uniform dispersion of complex chromium borides.

The uniformity of the boron distribution is ensured by the manufacturing practice and may be confirmed by a number of methods, including elemental and isotopic boron analysis or direct attenuation measurement of samples taken from the finished sheet. When compared to plain 304 type stainless steel, borated stainless steels have higher strength but lower ductility and lower impact resistance. However, these properties have no impact on the Ginna rack design since the borated stainless steel plates are not part of the rack structure.

Borated stainless steels are used for neutron attenuation in spent nuclear fuel storage pool racks and in cask baskets for storage and transportation of spent fuel. These applications dictate that the borated stainless steel be exposed to aqueous environments with and without boric acid. The BSS to be used in the Ginna racks has exceptional resistance to corrosion by electrolytic hydration, oxidation, or other chemical reactions in borated or pure water for the following reasons:

- Austenitic stainless steels are not susceptible to any type of corrosion leading to hydride products.
- In BSS, boron is present as an alloying element which eliminates microcell effects and not as a dispersion of an heterogeneous boron component.
- The proposed design, wherein the neutron absorber material is neither bent nor welded, thus preventing any cracking or thermal alteration of the metal, is an essential factor that also contributes to ensuring corrosion-resistance of this material.

Early studies of the corrosion behavior BSS with boron contents up to 2.3 wt% confirmed that BSS exhibits corrosion resistance similar to that of Type 304 stainless steel in environments present in nuclear reactors^{1-1,1-2}. Corrosion rates for BSS containing 1.35 wt% boron in boiling 10% nitric acid have also been measured¹⁻³. The results were consistent with other stainless steel behavior with a rapid change in weight (passivation) within 48 hours and no further weight change. The maximum penetration was 0.09 mils. Corrosion tests of BSS with boron contents of 1.0 wt% and 1.75 wt% exposed to 2000 PPM boric acid solutions at 154°F for six month durations have also been recently reported¹⁻⁴. The 154°F test temperature represents the maximum normal operating temperature in spent fuel pools. Various coupon configurations representing simple immersion, creviced, and galvanically-coupled conditions were included in these tests. The test showed essentially no detectable corrosion for all test conditions.

There are no significant changes to the mechanical properties of borated stainless steel due to exposure to the levels of irradiation experienced over the design life of the Ginna fuel storage racks¹⁻⁵.

1.3.5 Structural Materials

The principal structural materials are stainless steel meeting the following standards:

- ASTM A 240 for structure
- ASTM A 312 for welded pipes expanded to square tubes

- ASTM A 564 for bar of adjustable support
- ASTM A 479 for support legs.
- ASTM A 630 for threaded pins in support legs

These materials, described further in Section 3, are of proven durability in spent fuel pools.

1.4 SUPPLIER QUALIFICATION AND EXPERIENCE

1.4.1 Team Qualifications

The Team of Framatome Technologies, Inc. (FTI), Societe Atlantique de Techniques Avancees (ATEA), Framatome Cogema Fuels (FCF), and Peyla Consulting & Management Services, Inc. (PCM) bring an impressive array of experience and resources to the Ginna re-racking project which ensures high quality rack design, fabrication, and installation. The technology and skills required for an overall successful project demands a Team with complimentary strengths.

FTI has demonstrated experience in the management of complex nuclear projects as a supplier of Nuclear Steam Supply Systems (NSSS) and service maintenance projects to the nuclear industry for over 30 years. The employees within the Integrated Nuclear Services Division have excelled in providing a wide range of management and maintenance services to the nuclear utility industry. Now FTI's capabilities have been expanded through the new Framatome ownership by providing access to additional European resources and technologies.

ATEA, with Framatome, has been involved for more than 15 years in the design, manufacturing, licensing, and field erection of more than 38,000 fuel storage cells. ATEA is equipped with specialized equipment and nuclear production areas to fabricate spent fuel racks. In the last MAANSHAN project, ATEA has shown its capability to manufacture more than 4300 cells with borated stainless steel as neutron poison absorber.

For the Ginna project, all fabrication and assembly will be performed by ATEA. The ATEA rack fabrication facility in Nantes, France consists of 2500 square meters with a 25 ton crane capability. FCF has been providing nuclear fuel and fuel services to the domestic commercial nuclear industry for over 30 years. Included in this experience is the evaluation of high density fuel storage racks. These evaluations included criticality, structural, thermal-hydraulic, and radiological analyses using NRC approved methods to demonstrate compliance with NRC requirements.

PCM will provide on-site management and coordination for the on-site project work. PCM's manager, David Peyla, has over twenty years of field experience in completing rack replacement services.

1.4.2 Team Experience

The Framatome Group, with a 1995 revenue of 3.6 billion dollars and 19,000 employees, is involved in four main industrial sectors:

- *Nuclear Engineering:* nuclear power plant design, manufacturing, erection and maintenance and nuclear fuel services,

- *Mechanical Engineering:* PWR heavy components, turbines and compressors, and precision components,
- *Connectors for electrical industry and electronics,*
- *Computer services:* computer aided design (CAD), structural analysis, and artificial intelligence.

In the nuclear field, Framatome is currently the primary nuclear power plant designer, manufacturer and exporter in the world, with 60 PWR units delivered and five under construction. Framatome's scope involves the design of all the main systems and components of the Nuclear Steam Supply System (NSSS), including fuel handling equipment and fuel storage racks. Therefore, Framatome has very strong teams specializing in nuclear physics, thermal-hydraulics, structural and seismic analysis, shielding and radiological analysis and has at its disposal the relevant computer codes for such calculations.

Framatome has been involved in the design, manufacturing, licensing, onsite mounting and testing of more than 38,000 fuel storage cells, of which more than 10,000 were high density cells with neutron absorber at sixteen units worldwide (see Table 1.4-1). In the Framatome Group organization, ATEA is responsible for rack design, fabrication and installation.

Since 1976, PCM worked in the Nuclear Industry performing maintenance, repair, retrofit and re-rack projects. Many of these projects were one of a kind or the first ever attempted. Responsibilities and positions have been varied and extensive. Dave Peyla served as a Diver, Foreman, Project Superintendent and Project Manager and Consultant performing this work and twenty three re-racking projects for utilities in the United States and Overseas.

Ginna Nuclear Power Plant
Vermont Yankee
Nine Mile Point Nuclear Station
Surry Power Station
Pilgrim Nuclear Station
Kewaunee Nuclear Power Plant
Oconee
Duane Arnold
Salem
Davis Besse
Brunswick Steam & Electric

Arkansas Nuclear One
H.B. Robinson
Indian Point -2
Arkansas Nuclear One
Indian Point - 3
Indian Point - 2
Fitzpatrick Nuclear Power
Taiwan Power Co
Zion Nuclear Generating Station
Fort Calhoun
Salem

Borated stainless steel has been used in spent fuel pool applications worldwide for over 20 years (see Table 1.4-2). A brief synopsis of this experience is shown below.

Foreign Experience - Borated stainless steel has been used in various applications in Europe for over 20 years. Some of these applications are proprietary; the user is generally not willing to provide specific information. However, information obtained from two European suppliers of borated

stainless steel, BOHLER Bleche GmbH and KRUPP Thyssen Nirosta GmbH, indicates they have not had any claims concerning the materials that they have supplied. All indications are that the users have been satisfied for up to 20 years with the material supplied.

Domestic Experience - Consolidated Edison Company installed spent fuel storage racks utilizing borated stainless steel as the neutron absorber in the Indian Point Unit 2 spent fuel pool in 1982. In 1990 these racks were removed from the pool in order to expand fuel storage by utilizing more densely packed racks. The racks were viewed during removal from the spent fuel pool and showed negligible, if any, corrosion; the overall appearance of the racks was good.

REFERENCES

- 1-1 N.R. Grant, "Corrosion of Boron Stainless Steel," Reactor Eng. Div. Quarterly Report, pp 57-60, April-June 1965, ANL 5601
- 1-2 W. Kermit Anderson and J. S. Theilacker, "Neutron Absorber Materials for Reactor Control," US Atomic Energy Commission, 1962
- 1-3 T.L. Hoffman and T.L. Adams, "Corrosion of Alloys in Various ICPP Decontaminating Solutions," Phillips Petroleum Co., Atomic Energy Division, April 14, 1961
- 1-4 R.J. Smith, G.W. Loomis, C. Paul Deltete, "Borated Stainless Steel Applications in Spent fuel Pool Environments," EPRI Report TR_100784, Project 2813-21, June 1992
- 1-5 S.E. Soliman and Baratta, D.L. Youchison, T.A. Balliet, "Neutron Effects on Borated Stainless Steel," Nuclear Technology, Vol. 96, Dec. 1991



Table 1.3-1 Number of Cells by Rack Type

Region 1				
Type 3 Rack Number	Number of Cells	No. of Spent FA Locations	No. of Fresh FA Locations	No. of Damaged FA Locations
3A	70	35	35	0
3B	62	31	31	0
3C	50	25	25	0
3D	50	25	25	0
3E	62	29	28	5
TOTAL TYPE 3	294	145	144	5

Region 2				
Type 2 Rack Number	Number of Cells	No. of Spent FA Locations	No. of Fresh FA Locations	No. of Damaged FA Locations
2A	88	88	0	0
2B	99	99	0	0
TOTAL TYPE 2	187	187	0	0
TOTAL TYPE 2 & 3	481	332	144	5

Region 2				
Type 4 Rack Number	Number of Cells	No. of Spent FA Locations	No. of Fresh FA Locations	No. of Damaged FA Locations
4A	10	10	0	0
4B	10	10	0	0
4C	10	10	0	0
4D	10	10	0	0
4E	10	10	0	0
4F	10	10	0	0
TOTAL	60	60	0	0

Table 1.3-2 Rack Dimensions, Weight, Supports

Region 1				
Type 3 Rack No.	N-S Length	E-W Length	Dead Weight (long tons)	Number of support legs
3A	1642 mm (64.6 in)	2345 mm (92.3 in)	8.8	12
3B	1642 mm (64.6 in)	2345 mm (92.3 in)	8.0	11
3C	1173 mm (46.2 in)	2345 mm (92.3 in)	6.3	8
3D	1173 mm (46.2 in)	2345 mm (92.3 in)	6.3	8
3E	1642 mm (64.6 in)	2345 mm (92.3 in)	8.0	12

Region 2				
Type 2 Rack No.	N-S Length	E-W Length	Dead Weight (long tons)	Number of support legs
2A	1729 mm (68.1 in)	2370 mm (93.3 in)	7.8	12
2B	1942 mm (76.5 in)	2370 mm (93.3 in)	8.8	16

Region 2				
Type 4 Rack No.	N-S Length	E-W Length	Dead Weight (long tons)	Number of support legs
4A	241 mm (9.5 in)	2138 mm (84.2 in)	1.1	2
4B	241 mm (9.5 in)	2138 mm (84.2 in)	1.1	2
4C	241 mm (9.5 in)	2138 mm (84.2 in)	1.1	2
4D	241 mm (9.5 in)	2138 mm (84.2 in)	1.1	2
4E	241 mm (9.5 in)	2138 mm (84.2 in)	1.1	2
4F	241 mm (9.5 in)	2138 mm (84.2 in)	1.1	2

Table 1.3-3 Design Data for Region 1, Type 3 Racks (Fresh Fuel and Spent Fuel)

- Cells
 - Cells for Fresh Fuel (BSS cells)
 - Inner dimension 206.8 x 206.8 mm (8.14 x 8.14 in)
 - Height 4115 mm (162 in)
 - Material Borated Stainless Steel 304 B6
 - BSS sheet
 - Height 3770 mm (148.4 in)
 - Width 211 mm (8.3 in)
 - Thickness 2.5 mm (0.1 in)
- Cells for Spent Fuel (BSS/SS cells)
 - Inner dimension 206.8 x 206.8 mm (8.14 x 8.14 in)
 - Height 4115 mm (162 in)
 - Material Borated Stainless Steel 304 B6
304 L
- BSS sheet
 - Height 3700 mm (145.7 in)
 - Width 211 mm (8.3 in)
 - Thickness 2.5 mm (0.1 in)
- Pitch 234.5 mm (9.23 in)
- Base Plate
 - Thickness 30 mm (1.2 in)
 - Material 304 L



Table 1.3-4 Design Data for Region 2, Type 2 Racks (Spent Fuel)

- Cells
 - SS cell
 - Inner dimension 206.8 x 206.8 mm (8.14 x 8.14 in)
 - Height 4026 mm (158.5 in)
 - Thickness 2 mm (0.08 in)
 - Material 304 L
 - BSS cell
 - Inner dimension 206.8 x 206.8 mm (8.14 x 8.14 in)
 - Height 4026 mm (158.5 in)
 - Material Borated Stainless Steel 304 B6
- BSS sheet
 - Height 3700 mm (145.7 in)
 - Width 213 mm (8.4 in)
 - Thickness 3 mm (0.12 in)
- Pitch 214 mm (8.43 in)
- Base plate
 - Thickness 30 mm (1.2 in)
 - Material 304 L



Table 1.3-5 Design Data for Region 2, Type 4 Racks (Spent Fuel)

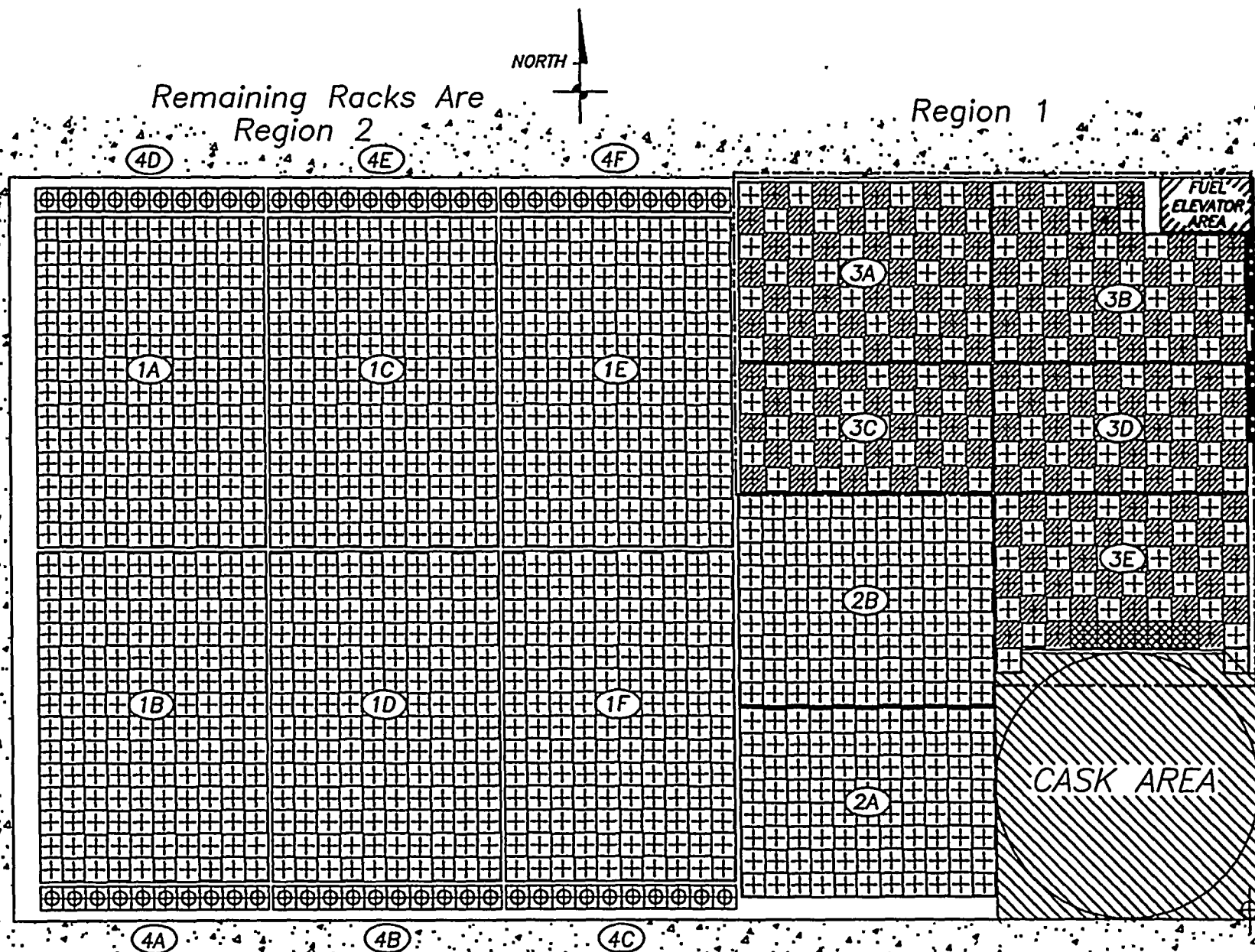
- Cells
 - Inner dimension 206.8 x 206.8 mm (8.14 x 8.14 in)
 - Height 4026 mm (158.5 in)
 - Thickness 2 mm (0.08 in) (SS material)
 - Materials 304L
- BSS sheet
 - Width 208 mm (8.18 in)
 - Height 3770 mm (148.42 in)
 - Thickness 2.5 mm (0.1 in)
 - Material Borated Stainless Steel 304 B6
- Pitch 214 mm (8.43 in)

Table 1.4-1 Framatome/ATEA Spent Fuel Racks

Plant	Number of Storage Cells	Poison Material and Pitch	Year of Design	Year of Fabrication	Year Licensed	Customer				
<u>FRANCE / 1300 MWE PLANTS</u>										
CATTENOM -1 CATTENOM - 2 CATTENOM - 3 CATTENOM - 4] 2520]]]	BORAL (11.3 inches)	1983	1984-1985 1985 1986-1987 1989	August 86	E.D.F.				
BELLEVILLE - 1 BELLEVILLE - 2] 1260]			1985 1985-1986						
NOGENT - 1 NOGENT - 2] 1260]			1985 1986						
PENLY - 1 PENLY - 2] 1260]			1987 1989-1990						
GOLFECH - 1 GOLFECH - 2] 1260]			1988 1990-1991						
<u>FRANCE : 1450 MWE PLANTS</u>										
CHOOZ - 1 CHOOZ - 2] 1224]	CADMIUM (11 inches)	1988	1989 1990-1991	Sept. 90					
CIVAUX - 1 CIVAUX - 2] 1224]			1993-1994						
<u>CHINA : 1000 MWE PLANTS</u>										
GUANGDONG - 1 GUANGDONG - 2] 1380]	BORATED SS Region 1: 11.1" Region 2 : 9.0"	1991	1989 1990	Jan. 88	GNPJVC				
<u>TAIWAN : 1000 MWE PLANTS</u>										
MAANSHAN 1 MAANSHAN 2	2160 2160							1993 1994 1995	1993	TPC
<u>USA: 500 MWE PLANTS</u>										
GINNA	480	BORATED SS Region 2: 9.2" Region 3: 8.4"	1996	later in 1997	in progress	RG&E				

Table 1.4-2 Borated Stainless Steel Experience (Wet Storage)				
No.	Country	Nuclear Facility	Type	Year
1	Austria	Tullnerfeld	BWR	1978
2	Belgium	Doel 3	PWR	
3	Belgium	Tihange 2	PWR	
4	Brazil	Angra 2	PWR	Under Constr.
5	Czech Republic	Temelin 1-2	VVER	Under Constr.
6	Czech Republic	Dukovany 1-2-3-4	VVER	1985 - 1987
7	Czech Republic	Mochovce 1-2-3-4	VVER	Under Constr.
8	Finland	Olkiluoto 1	BWR	1981
9	Finland	Olkiluoto 2	BWR	1981
10	France	La Hague	PWR	1976 - 1991
11	Germany	Karlsruhe	FBR	
12	Germany	Stade	PWR	
13	Germany	Wuerpassen	PWR	
14	Germany	Brunsbuettel	PWR	
15	Germany	Philippsburg 2	PWR	1980
16	Germany	Neckarwestheim 1	PWR	1976
17	Germany	Neckarwestheim 2	PWR	1989
18	Germany	Grohnde (re-racking)	BWR	1986
19	Germany	Unterweser	BWR	1977
20	Germany	Grafenrheinfeld	PWR	1982
21	Germany	Grohnde	PWR	1985
22	Germany	Grundremmingen 2-B	BWR	1984
23	Germany	Grundremmingen 2-C	PWR	1985
24	Germany	Brokdorf	PWR	1986
25	Germany	Brokdorf (re-racking)	PWR	1984
26	Germany	Krummel	FBR	1984
27	Germany	Isar 1	PWR	1979
28	Germany	Isar 2	BWR	1988
29	Germany	Emsland	PWR	
30	Germany	Biblis A/B	PWR	

Table 1.4-2 Borated Stainless Steel Experience (Wet Storage)				
No.	Country	Nuclear Facility	Type	Year
31	Hungary	Paks 1	VVER	1985
32	Hungary	Paks 2	VVER	1985
33	Hungary	Paks 3	VVER	1985
34	Hungary	Paks 4	VVER	1985
35	Spain	Almaraz 1	PWR	1991
36	Spain	Almaraz 2	PWR	1991
37	Spain	Asco 1	PWR	1992
38	Spain	Asco 2	PWR	1992
39	Spain	Trillo 1	PWR	1985
40	Korea	Kori 3	PWR	1992
41	Sweden	CLAB interim spent fuel storage pool	PWR & BWR	1990
42	Taiwan	Maanshan 1	PWR	1995
43	Taiwan	Maanshan 2	PWR	1995
44	USA	Indian Pt 2	PWR	1982
45	USA	Indian Pt 3	PWR	1978



⊕ SPENT FUEL
 ▨ FRESH FUEL

Figure 1.1-1 Spent Fuel Pool - General Arrangement

Figure 1.3-1 Type 3 Rack - Perspective

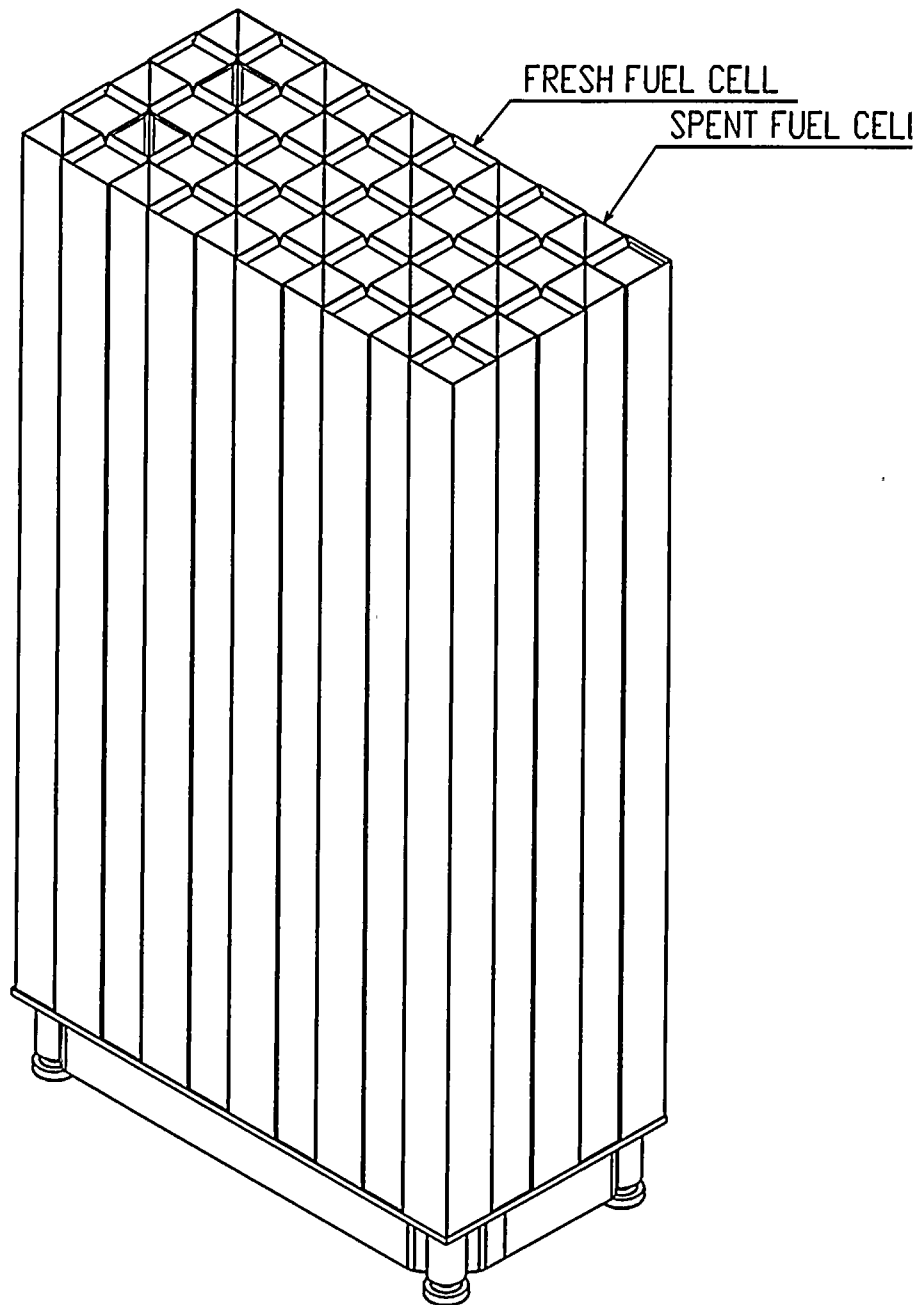


Figure 1.3-2 Type 3 Rack - General Arrangement

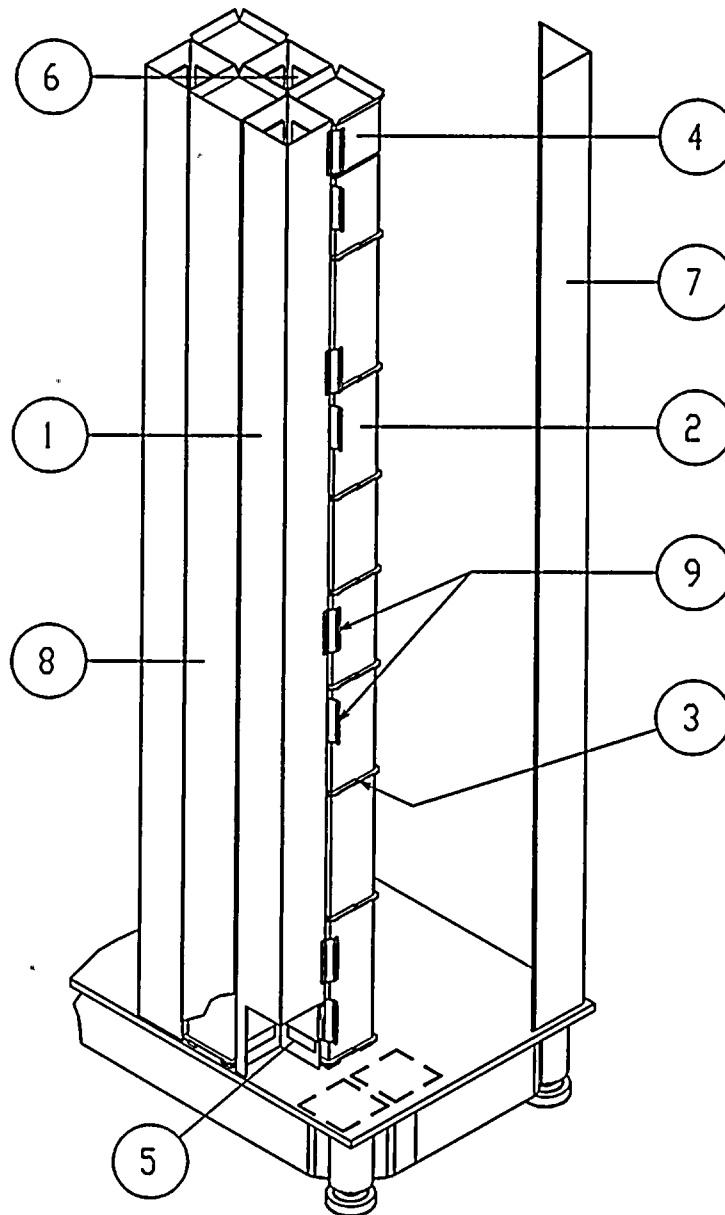


Figure 1.3-3 Type 3 Rack - Detail of Base

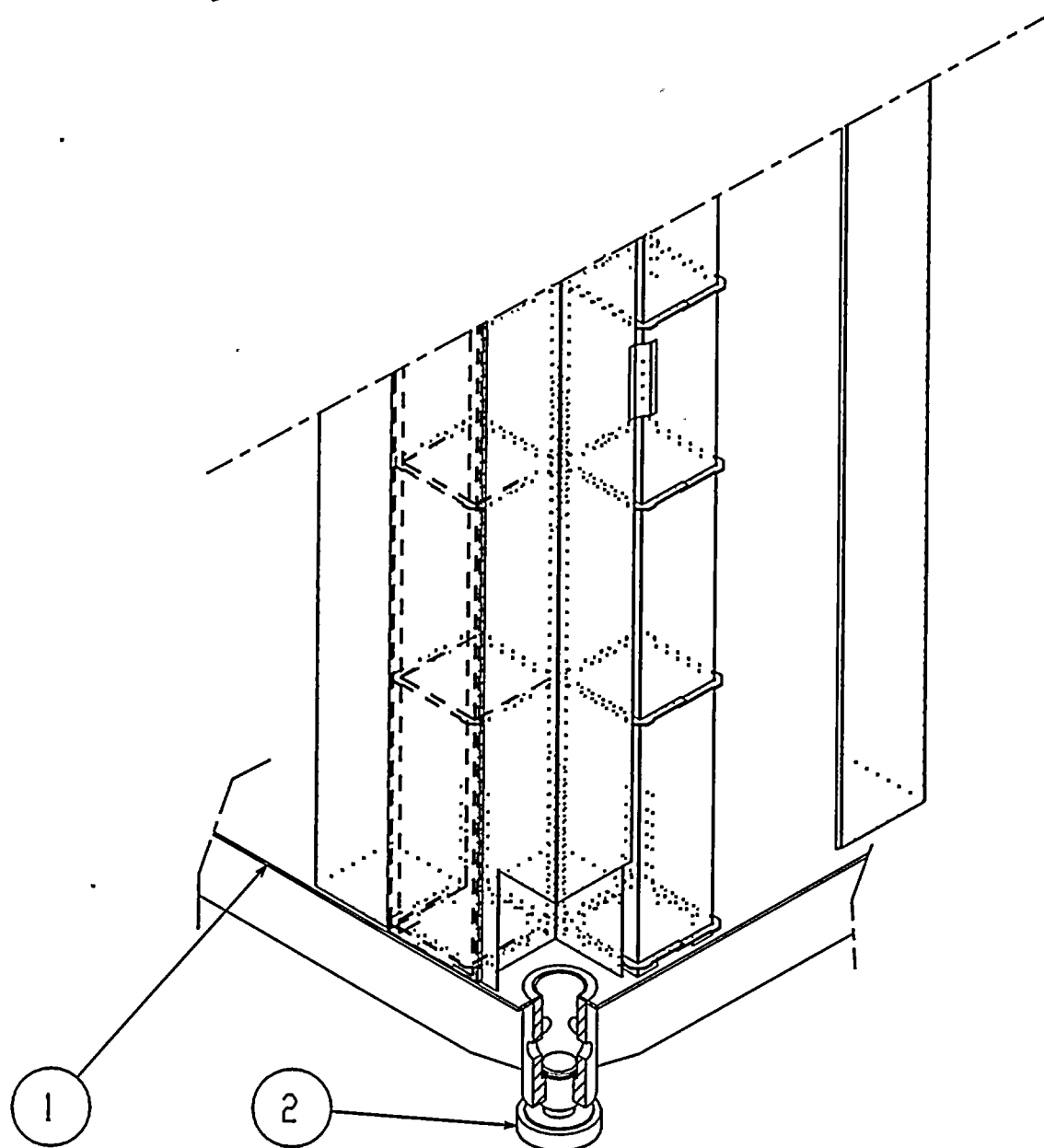


Figure 1.3-4 Type 3 Rack - Vertical Section

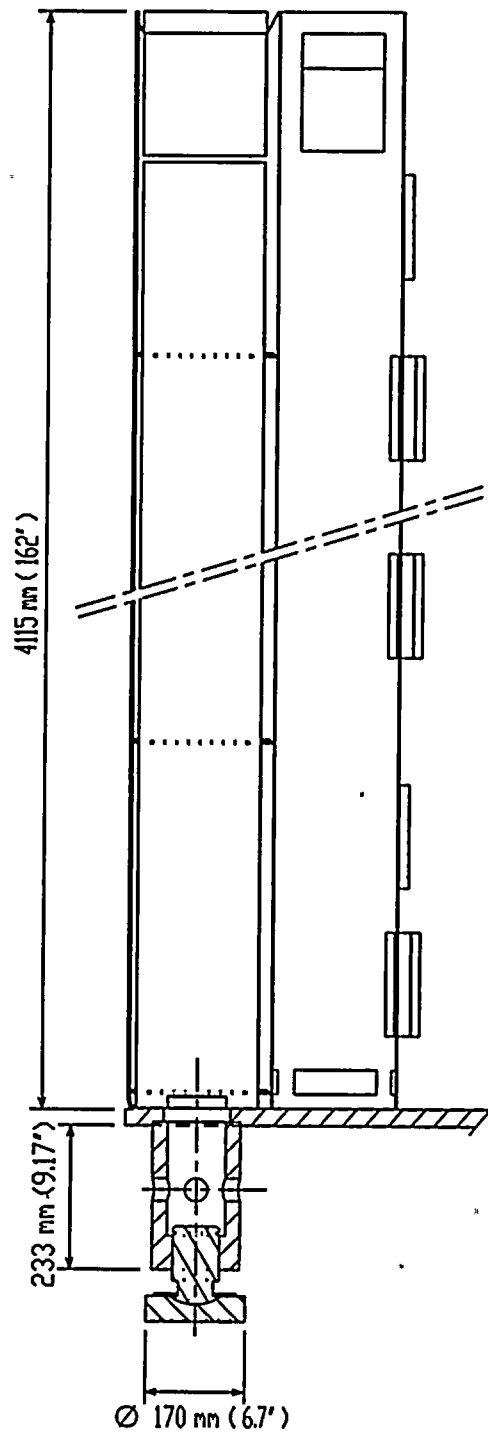


Figure 1.3-5 Type 3 Rack - Top View

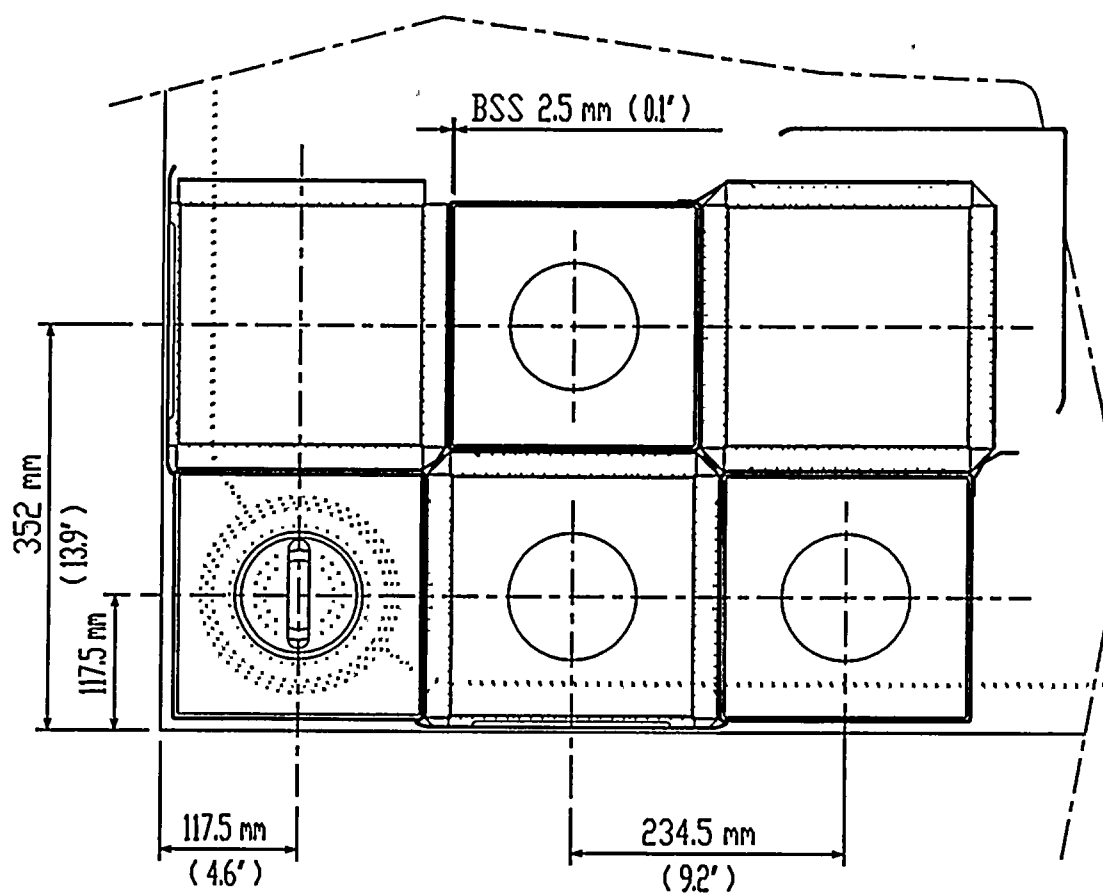


Figure 1.3-6 Type 3 Rack - Details of Connecting Tabs

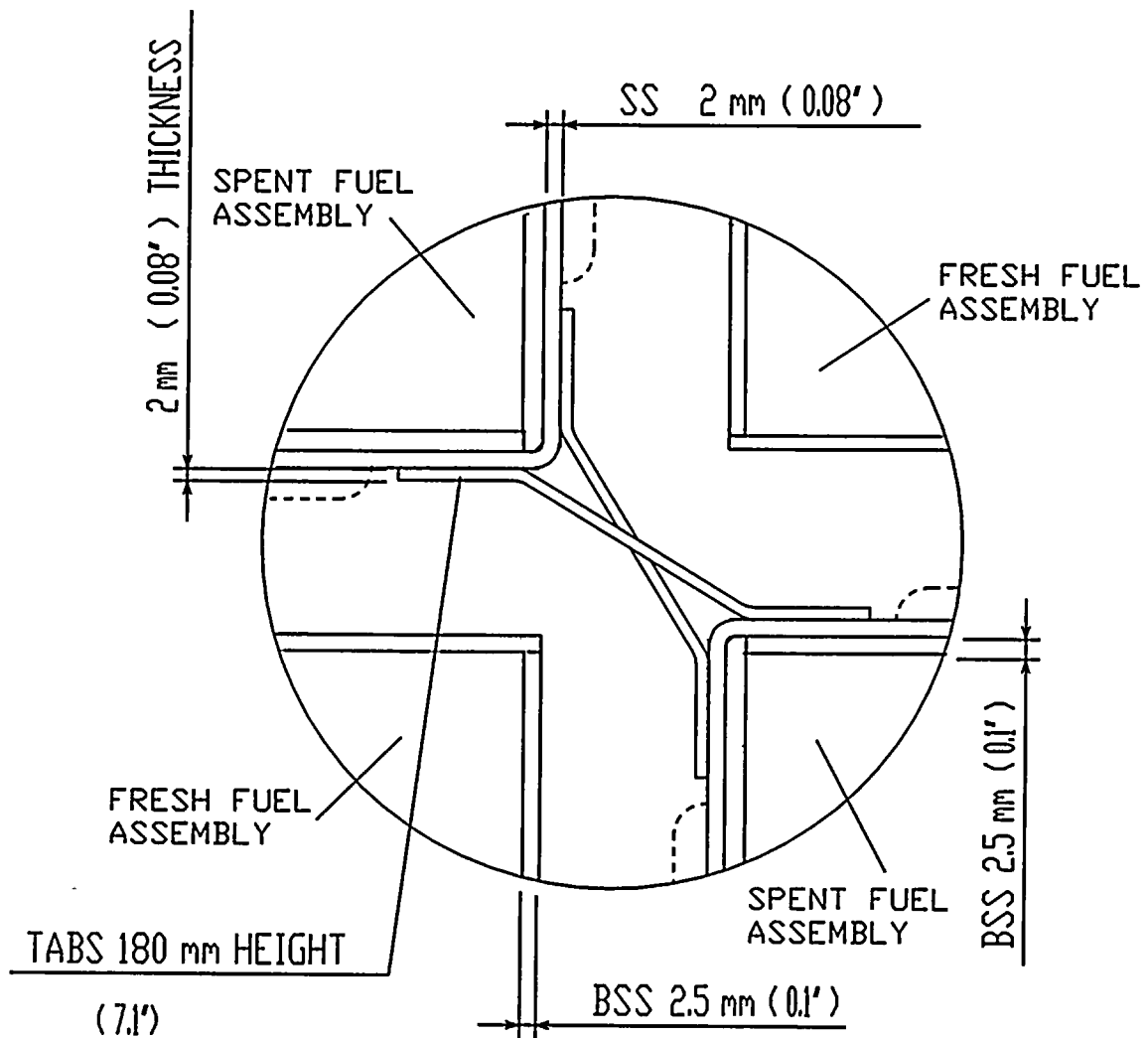


Figure 1.3-7 Type 2 Rack - Details of Top

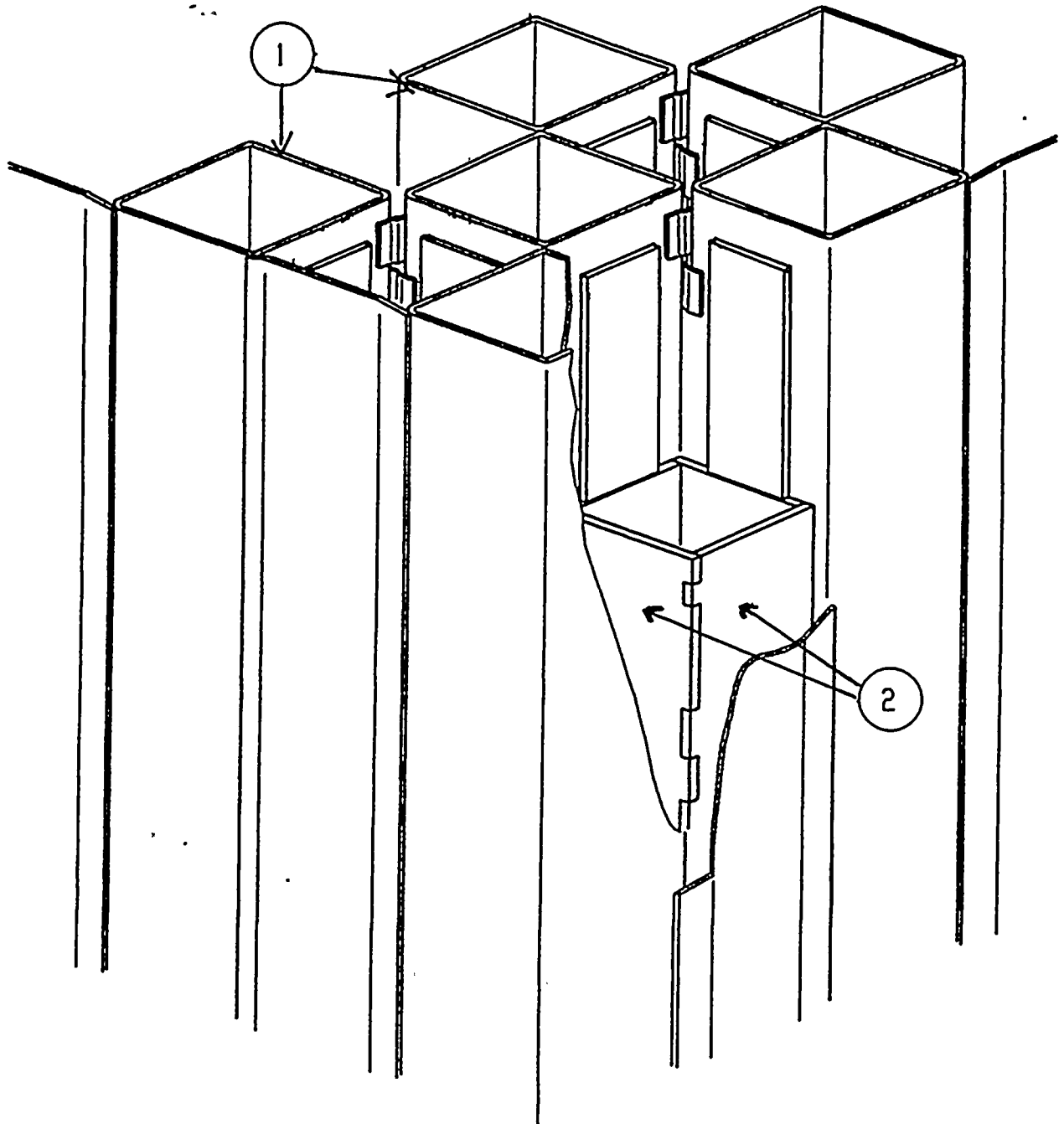


Figure 1.3-8 Type 2 Rack - Perspective

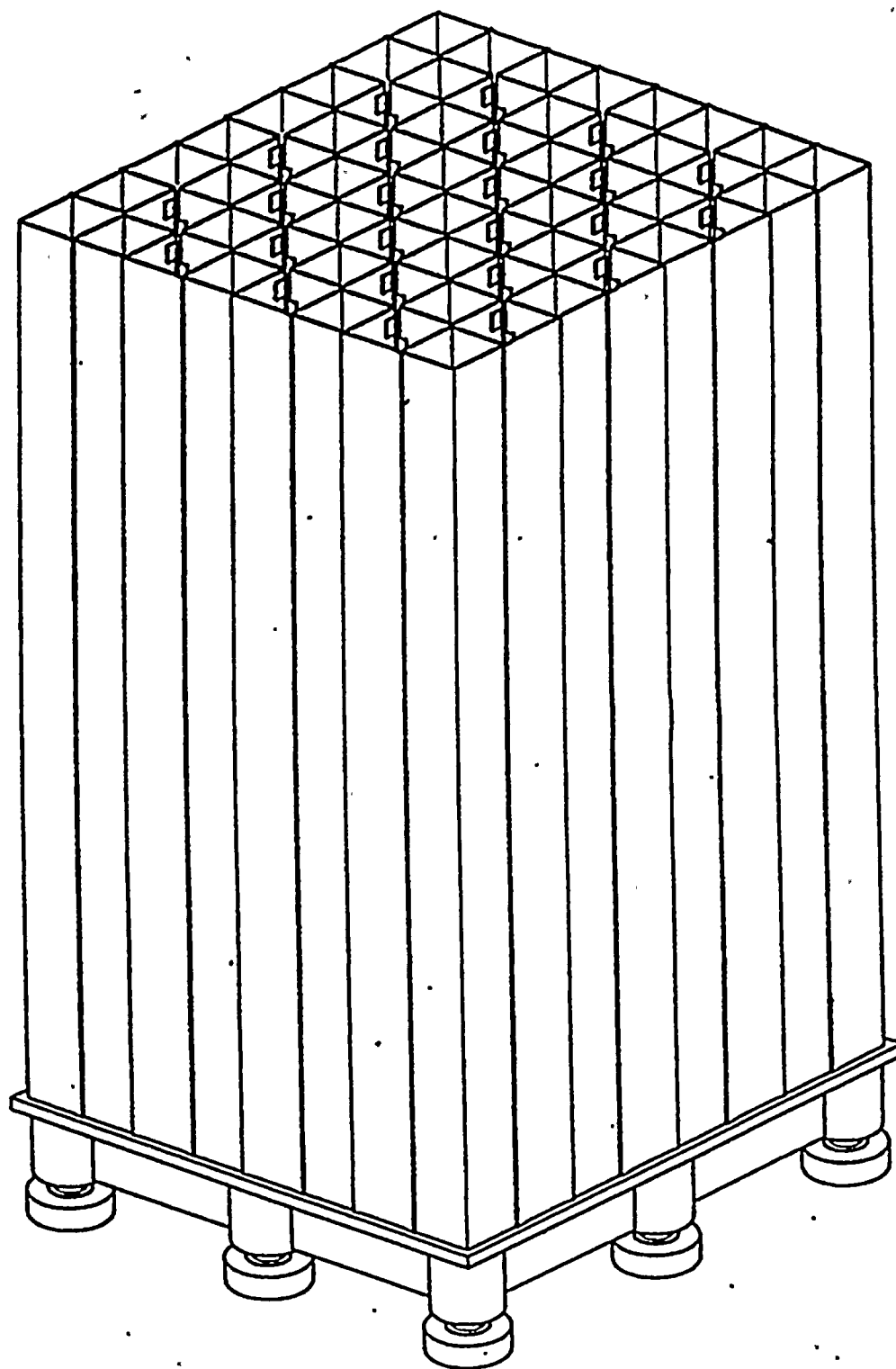


Figure 1.3-9 Type 2 Rack - Detail of Base

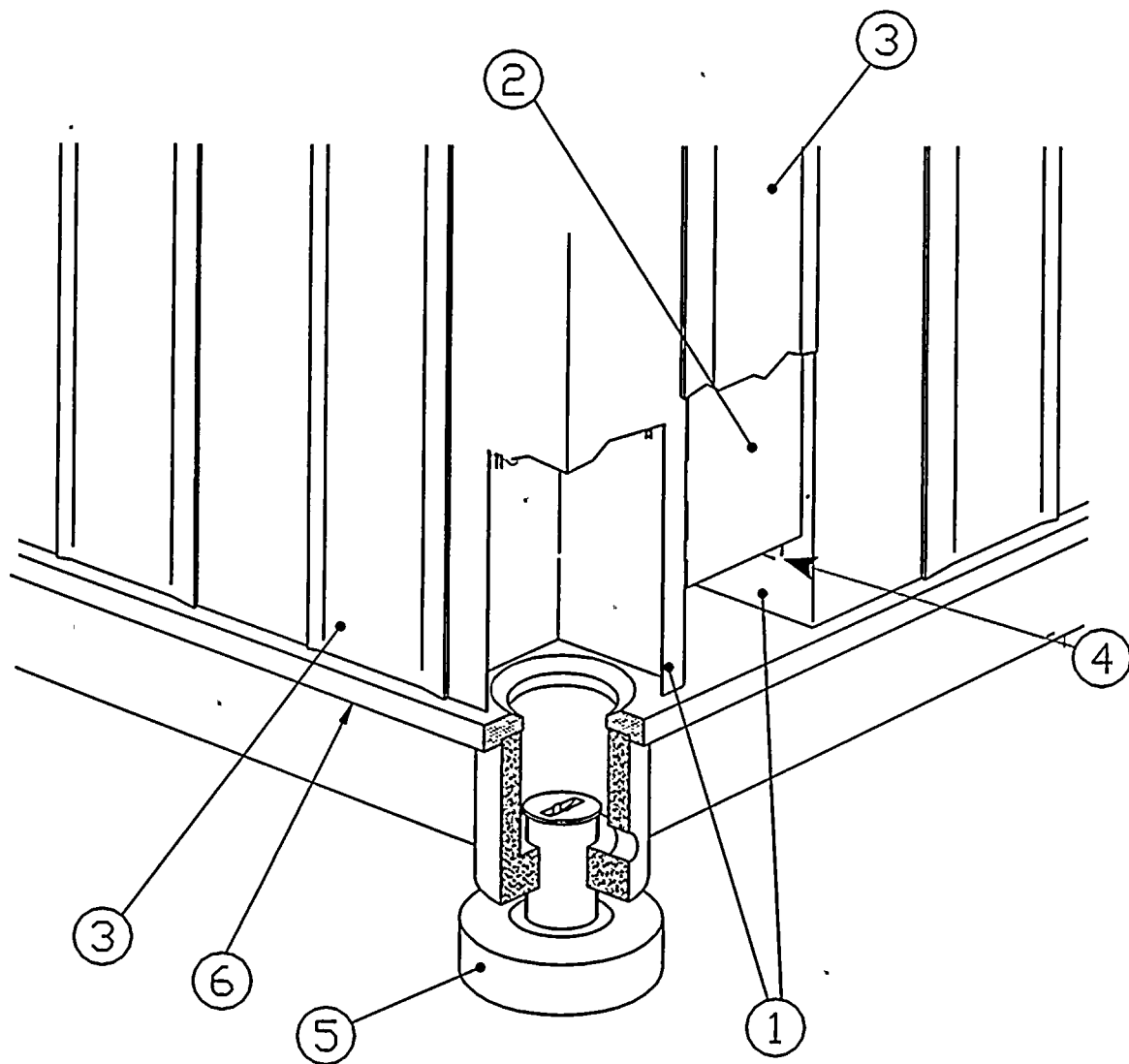


Figure 1.3-10 Type 2 Rack - Vertical Section

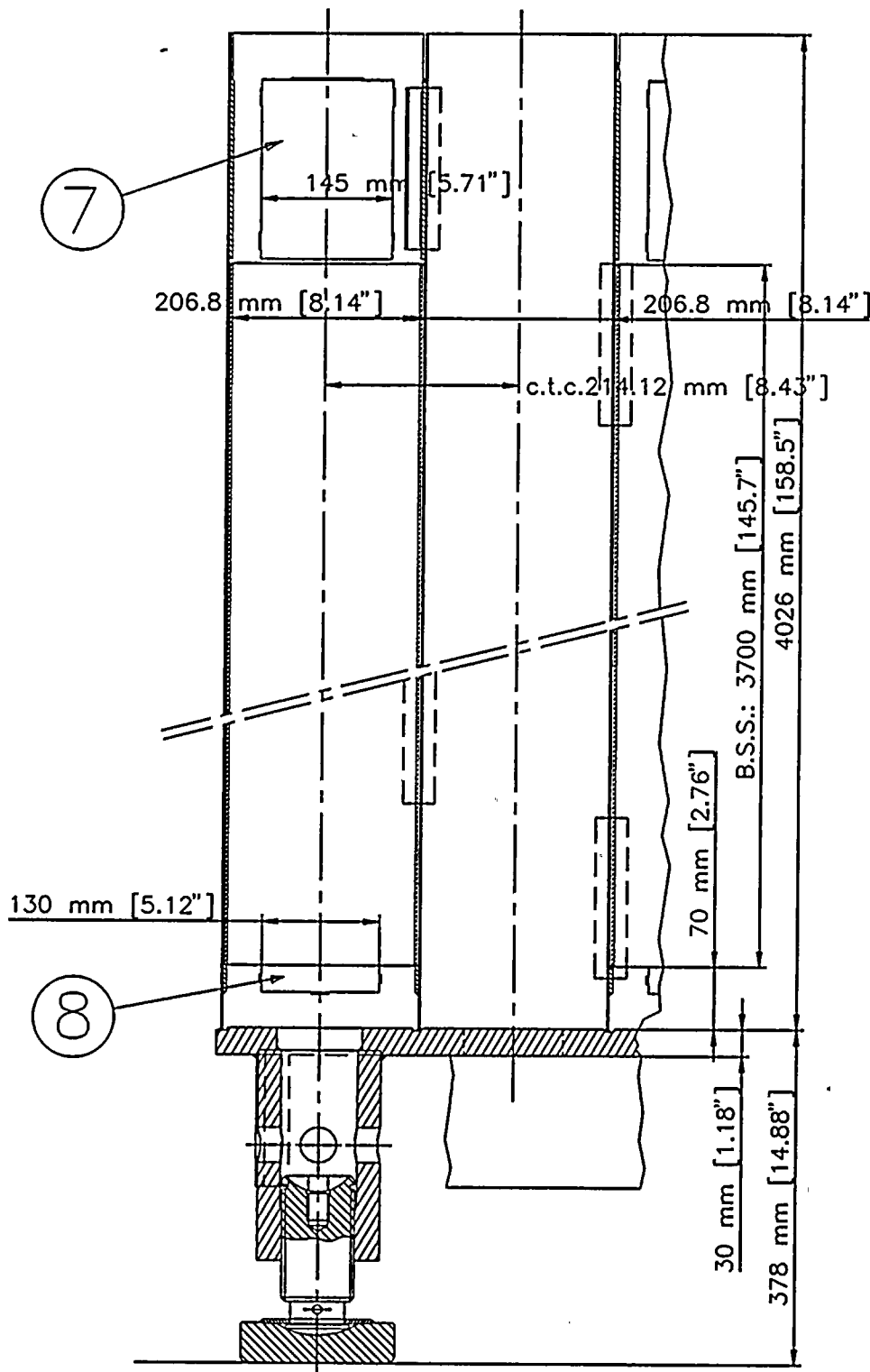


Figure 1.3-11 Type 2 Rack - Top View

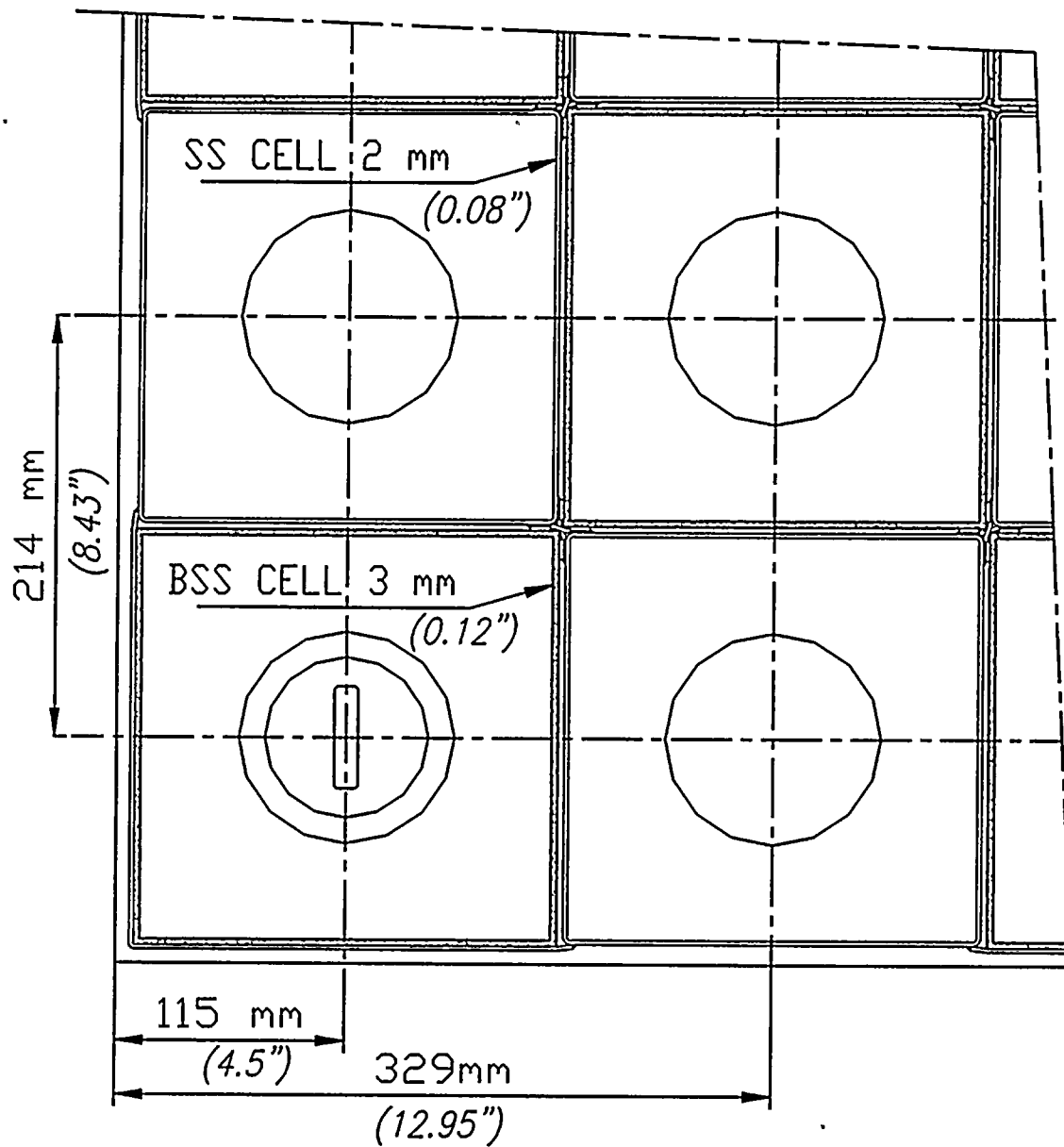


Figure 1.3-12 Type 2 Rack - Detail of Connecting Tabs

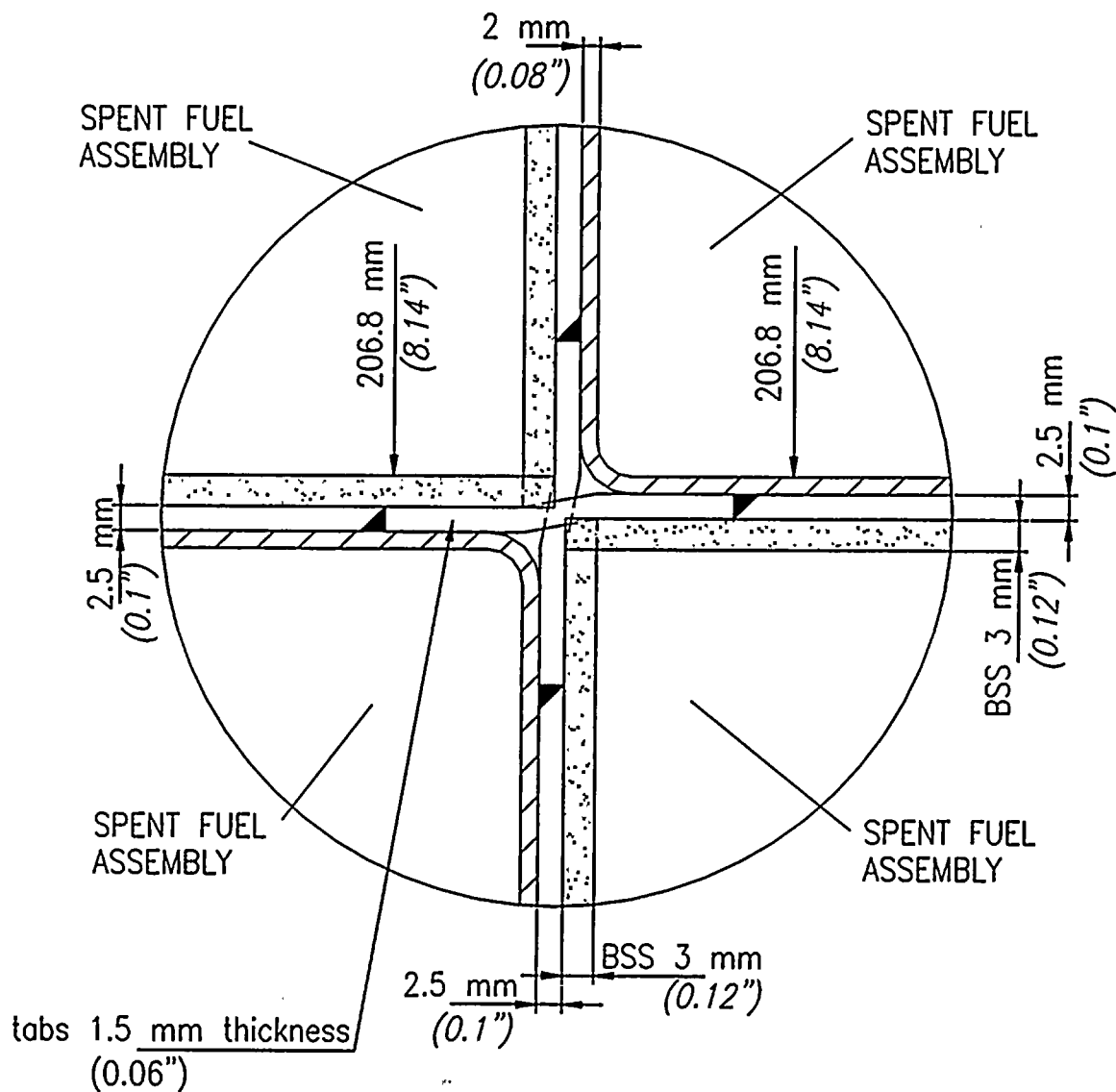


Figure 1.3-13 Type 4 Rack

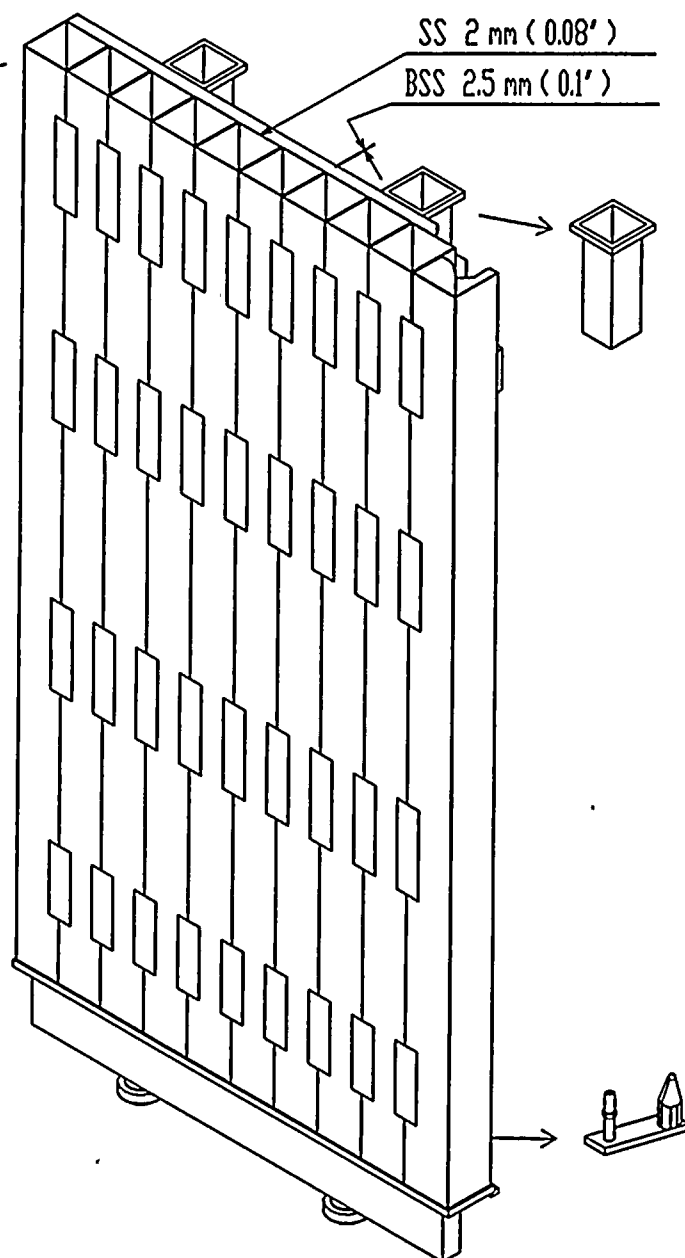
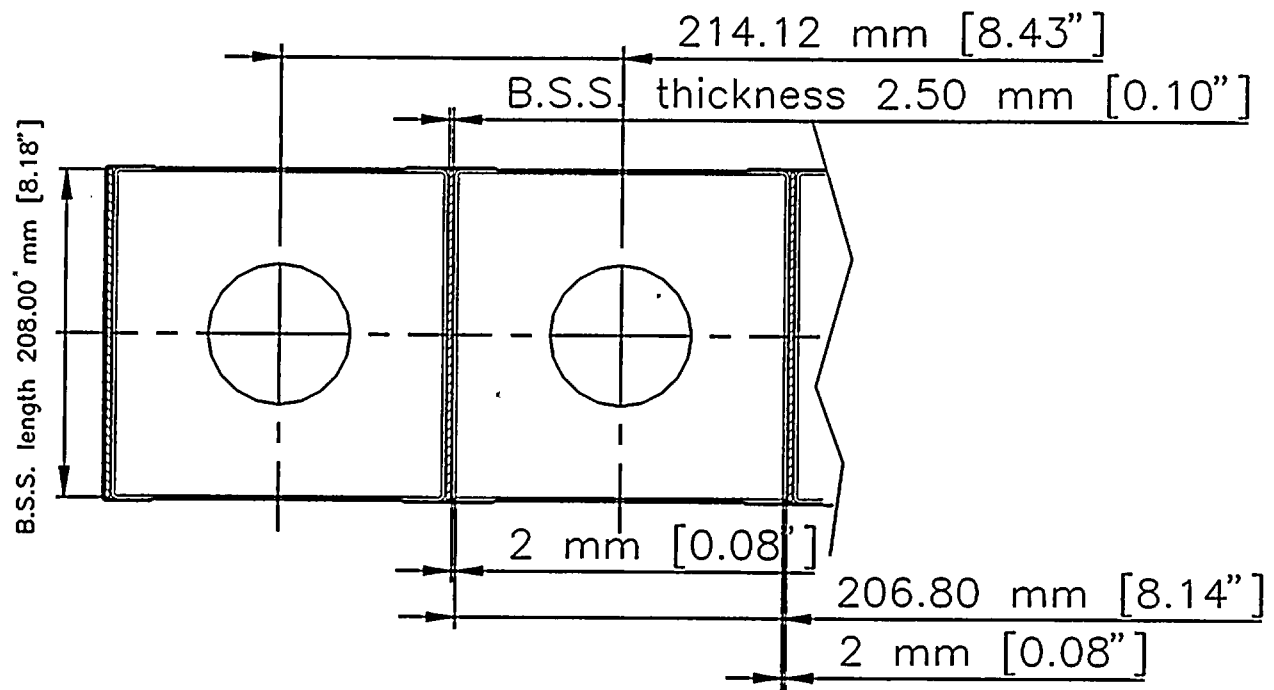


Figure 1.3-14 Type 4 Rack - Top View



2.0 PRINCIPAL DESIGN CRITERIA

2.1 General Design Criteria

The nuclear fuel storage racks are required to have a minimum service life of 40 years in an environment that includes high radiation fields, continuous exposure to pure and borated water; must be designed to withstand severe accidents due to natural phenomena (i.e., seismic, tornado missiles), and drop accidents associated with plant operations. The primary function of the racks is to insure subcriticality of the fresh and spent nuclear fuel for a variety of accident scenarios.

The racks are categorized as safety related products and are designed to comply with stringent licensing requirements of the U.S. Nuclear Regulatory Commission's (NRC), Regulatory Guides; the American Society of Mechanical Engineers (ASME) Boiler and Pressure Vessel Code (Code), Section III, Subsection NF; American Institute of Steel Construction (AISC) Manual of Steel Construction; various American National Standards Institute (ANSI) and industry standards; and meet other RG&E design specifications.

Four main areas (structural, criticality, thermal-hydraulics, and radiological) are examined and analyzed to meet the design criteria. Sections 3.0, 4.0, 5.0, and 6.0 describe in detail the particular design scenarios and the results of these analyses.

2.2 Structural Criteria

The storage racks are considered as seismic Class I components and are designed to meet the allowable stresses of the ASME Code, Section III, Subsections NF for Class 3 Component Supports, applicable Regulatory Guides, and Standard Review Plan (SRP) NUREG-0800.

A detailed stress analysis was performed to determine the resulting stresses for deadweight, thermal, seismic and other accident impact loads (i.e., dropped fuel, canisters, and other missiles). The seismic analysis includes effects due to both Operating Basis Earthquake (OBE) and Safe Shutdown Earthquake (SSE) loading conditions. Factors of Safety against gross sliding and overturning of the racks are in accordance with NUREG-0800, SRP, Section 3.8.5, II-5.

The spent fuel pool liner shall not permit leakage of the pool water, and the resulting concrete bearing loads shall meet the allowable concrete stresses of ACI 349-85. Impacts that are determined that could penetrate the liner shall be mitigated or prevented by RG&E by invoking the requirements of NUREG-0612, Control of Heavy Loads at Nuclear Power Plants. This may be accomplished by using load paths that would avoid the spent fuel pool area, or designing handling and lifting equipment to meet the requirements of 'Single-Failure Proof' Handling Systems.

The structural analytical methodology and results are presented in Section 3.0.

2.3 Criticality Criteria

The criticality analysis of the storage racks demonstrates that both the fresh and spent fuel assemblies remain subcritical ($k_{\max} \leq 0.95$) in either the normal or accident condition. Criticality control is maintained by geometrical spacing of the fuel assemblies, and the use of neutron absorption with fixed neutron poisons.



The criticality analytical methodology and results are presented in Section 4.0. The analyses are performed using NRC-approved computer codes CASMO-3, and SCALE 4.2 (KENO-V.a).

2.4 Thermal-Hydraulic Criteria

Thermal-hydraulic analyses were performed to ensure that the spent fuel pool cooling system has adequate capacity to cool and maintain water and fuel assembly temperatures within the current licensing criteria given the added heat load of the larger number of spent fuel assemblies. The analyses were performed to the requirements in the following NRC documents:

- SRP 9.1.3, Spent Fuel Cooling and Cleanup System
- OT Position for Review and Acceptance of Spent Fuel Storage and Handling Applications, dated April 14, 1978 and revised January 18, 1979.

The thermal-hydraulic analytical methodology and results are presented in Section 5.0.

2.5 Radiological Criteria

Reference offsite dose values for evaluating hypothetical accidents involving fission product releases are specified in 10 CFR Part 100 and are 25 rem to the whole body and 300 rem to the thyroid from iodine exposure. Both values are applicable to the exclusion area boundary (EAB) and the low population zone boundary (LPZ). Section 15.7.4. of the Standard Review Plan (SRP) specifies acceptance criteria of 25% of 10 CFR Part 100 guidelines for postulated fuel handling accidents. However, the Ginna Station was designed and built prior to the SRP and is not required to meet the SRP limits. A previous fuel handling accident analysis showed an offsite dose of 96 rem thyroid which has been previously accepted by the NRC as being "well within" 10 CFR Part 100 limits (see Section 6.1.1).

Occupational exposure dose limits are specified in 10 CFR Part 20 and are further controlled by plant procedures. The recommended dose rate that shall not be exceeded in accessible spaces adjacent the spent fuel pool is given in ANSI/ANS 57.2 and is 2.5 mrem/hr to any persons occupying those spaces. The rate is specified for when the pool is at its design fuel inventory and at the minimum design water depth.

The radiological analytical methodology and results are presented in Section 6.0

3.0 STRUCTURAL EVALUATION

This section presents the structural evaluation to ensure that the Rochester Gas and Electric's Ginna Unit 1 Spent Fuel Storage System meets all applicable structural criteria to maintain a subcritical array for the spent fuel and to keep radiation exposure within federal limits. The analysis of the Spent Fuel Storage System demonstrates that the structure satisfies the requirements of Title 10 of the Code of Federal Regulations Part 50. Results of the analysis show the design satisfies the statutory requirements for licensing. The results also demonstrate the ruggedness of the spent fuel rack design.

Current state-of-the-art methods are used in the structural analyses. The storage rack structural evaluation is based on a conservative interpretation of the American Society of Mechanical Engineers (ASME) Boiler and Pressure Vessel (B&PV) Code. The spent fuel pool evaluation is based on a conservative interpretation of the American Concrete Institute's Code Requirements for Nuclear Safety Related Concrete Structures and American Institute of Steel Construction's Building Code. It is shown that the spent fuel system structures are robust and provide safe storage of spent fuel under any of the normal, upset or hypothetical accident conditions.

Section 3.2 summarizes the structural design criteria. Section 3.3 provides the structural design features of the Spent Fuel Storage Racks. Section 3.4 summarizes the materials of construction and the corresponding material properties. Section 3.5 summarizes the structural analysis. Specifically, section 3.5.3.3 summarizes the analytically determined minimum design factors for the major components.

3.1 SCOPE

The scope of this structural evaluation includes the RG&E's Ginna Unit 1 Spent Fuel Storage System. The structural evaluation includes the spent fuel storage racks and the floor and liner of the spent fuel pool. Structural evaluation of the storage racks include both the resident U.S. Tool and Die racks and the new ATEA racks. The U.S. Tool and Die racks hereafter are referred to as Racks 1 through 6. The new ATEA racks are referred to as Racks 7 through 13 or as 2A, 2B, 3A, 3B, 3C, 3D, 3E. The perimeter racks are referred to as Type 4 Racks.

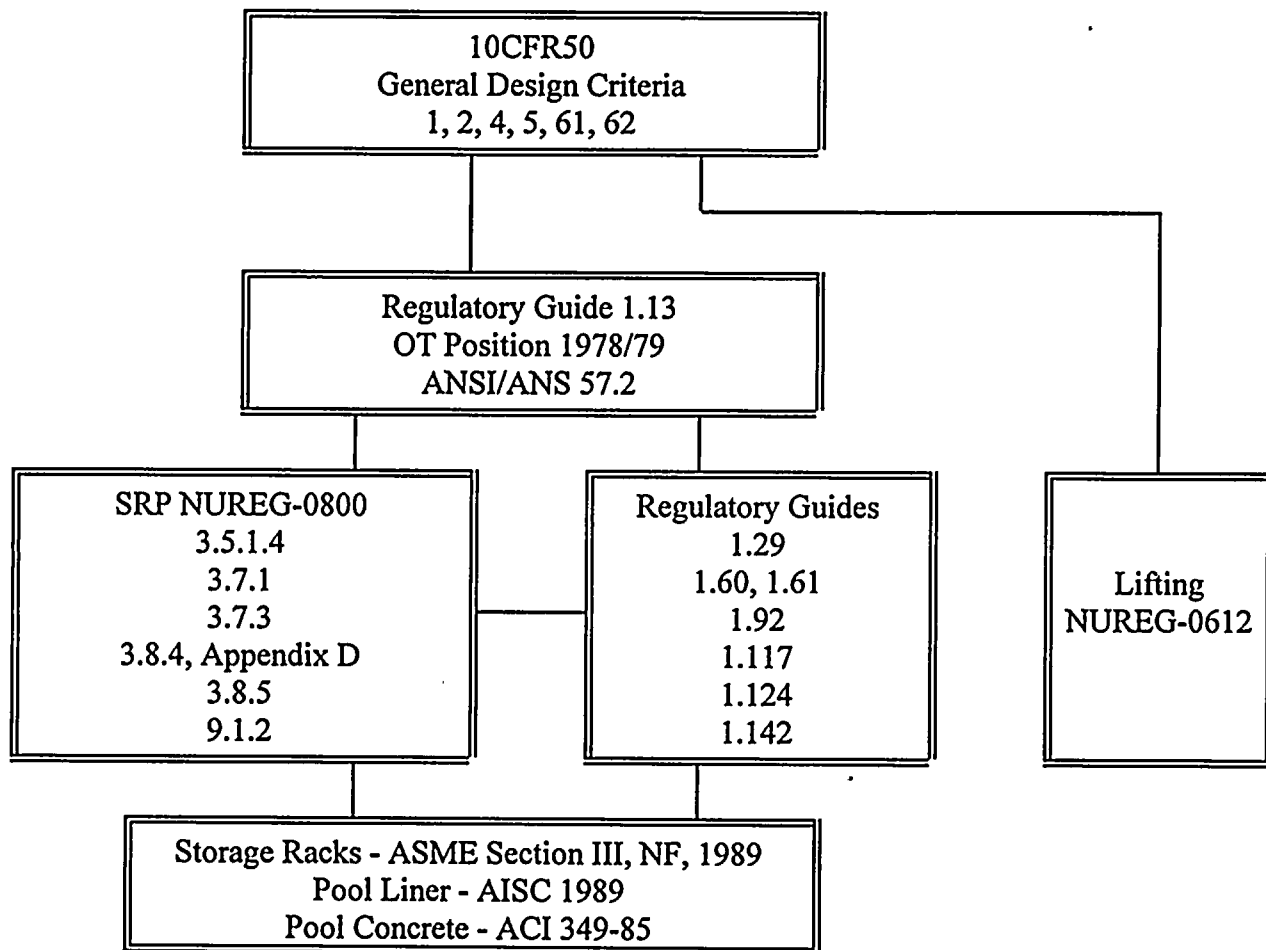
The design of the new high density storage racks is such that it preserves the original licensing basis (NRC SER dated November 14, 1984), hereafter referred to as the 1985 licensing basis, for Racks 1 through 6, and for the spent fuel pool liner and pool concrete. The new ATEA storage racks are free standing racks and are supported on the pool floor only. The gaps between the racks, and those between the rack and the pool wall, are designed such that the new racks do not impose any additional loadings on the resident racks or on the pool wall. These conditions are verified throughout the analysis. The new racks are high density storage racks and are capable of storing additional fuel. The number of support legs are designed such that the new racks do not impose any higher loading on the pool liner or the pool concrete. This is also verified in the analysis. The seismic analysis is performed for both the resident and new racks. The 1985 licensing basis is preserved for all hypothetical accidental drop cases on the resident U.S. Tool and Die racks. Therefore, the hypothetical accident evaluation is performed only on the new ATEA racks.

3.2 DESIGN CRITERIA

3.2.1 Applicable Codes and Standards

This section outlines the applicable design codes, standards, specifications, regulations, general design criteria, regulatory guides, and other industry standards used in the Spent Fuel Storage System structural evaluation. The following flowchart provides an overview of the codes and standards applicable to the structural evaluation.

Structural Evaluation - Spent Fuel Storage Racks



10CFR50, General Design Criteria

Relevant requirements for the Spent Fuel Storage System include:

- General Design Criterion 1: Safety related structure should be designed, fabricated,... to quality standards commensurate with the importance of safety function to be performed.
- General Design Criterion 2: Design of the safety related structures being capable to withstand the most severe natural phenomena such as tornado, earthquake,... and the appropriate combination of all loads.
- General Design Criterion 4: Safety related structure being capable of withstanding the dynamic effects of equipment failure.
- General Design Criterion 5: Relates to sharing of structure important to safety unless it can be shown that such sharing will not significantly impair their validity to perform their safety function.
- General Design Criterion 61: Fuel storage capacity requirements for full core down load.
- General Design Criterion 62: Prevention of criticality by a physical and geometric safe configuration.

USNRC "OT Position for Review and Acceptance of Spent Fuel Storage and Handling Applications," dated April 14, 1978 and the modifications to this document dated January 18, 1979.

Regulatory Guides:

The following recommendations and guidance by the NRC Staff are used in the structural evaluation:

- 1.13 Spent Fuel Storage Facilities Design Basis, Revision 1, December 1975
- 1.29 Seismic Design Classification, Revision 3, September 1978
- 1.60 Design Response Spectra for Seismic Design of Nuclear Power Plants, Revision 1, December 1973
- 1.61 Damping Values for Seismic Design of Nuclear Power Plants, Revision 0, October 1973
- 1.92 Combining Modal Responses and Spatial Components in Seismic Response Analysis, Revision 1, February 1976
- 1.117 Tornado Design Classification, Revision 1, April 1978

1.124 Service Limits and Loading Combinations for Class I Linear-Type Components Supports, Revision 1, January 1978

1.142 Safety-Related Concrete Structures for Nuclear Power Plants (Other than Reactor Vessels and Containments), Revision 1, October 1981

Standard Review Plan - NUREG-0800

3.5.1.4 Missile Generated by Natural Phenomena, Revision 2, July 1981

3.7 Seismic Design

3.7.1 Seismic Design Parameters, Revision 2, August 1989

3.7.3 Seismic Subsystem Analysis, Revision 2, August 1989

3.8.4 Other Seismic Category I Structures, Appendix D: Technical Position on Spent Fuel Pool Racks, Revision 1, July 1981

3.8.5 Foundations, Revision 1, July 1981

9.1.2 Spent Fuel Storage, Revision 3, July 1981

NUREG-0612 Control of Heavy Loads at Nuclear Power Plant, July 1980

ANSI-57.2-1983 Design Requirements for Light Water Reactor Spent Fuel Storage Facilities at Nuclear Power Plants, approved Oct. 1983

Industry Standard

ASME Section III, Division 1, Subsection NF, 1989 Edition

1989 American Society of Mechanical Engineers, Section III, Pressure Vessel and Piping Code, Subsection NF - Rules for Construction of Nuclear Power Plant Component Supports.

ACI 349-85 Code Requirements for Nuclear Safety Related Concrete Structures, American Concrete Institute 1985.

AISC Manual of Steel Construction, 9th Edition

1989, American Institute of Steel Construction, Specification for Structural Steel Buildings, June 1989.

3.2.2 Acceptance Criteria, Load Combinations and Stress Limits

The structural design meets the basic requirements specified in 10 CFR 50 (General Design Criteria) and NRC Regulatory Guide 1.13, and can be summarized as:

The design protects the health and safety of the general public and personnel involved in spent fuel handling under normal, abnormal and accident conditions. In addition, the design of spent fuel storage racks and pool:



- Maintains the capability to remove and insert fuel assemblies
- Prevents physical damage to the stored fuel assemblies
- Maintains the stored fuel in a coolable geometry
- Maintains the stored fuel in a subcritical configuration

Per requirements of Regulatory Guide 1.29, the spent fuel system structures are classified as "Seismic Category I" and are designed to remain functional under the effects of the SSE. The system is designated as a safety-related system. The spent fuel storage racks are designed and will be constructed to conform to ASME Section III, Subsection NF for Class 3 component supports. All structural materials selected for the spent fuel storage racks are compatible with the fuel pool environment to minimize corrosion and galvanic effects.

All safety related structures conform to:

Spent Fuel Storage Racks:

- ASME Code - Section III, Subsection NF, Class 3 Component Supports, 1989 Edition.
- Regulatory Guide 1.124

Spent Fuel Pool Liner:

- AISC - 1989 Specification for Structural Steel Buildings, 9th Edition, June 1989.

Spent Fuel Pool - Concrete

- ACI 349 - 85 Code Requirements for Nuclear Safety-Related Structures, American Concrete Institute
- Regulatory Guide 1.142

Load Combinations

The following section provides the load combinations considered in the structural analysis. These load combinations meet the requirements of Standard Review Plan 3.8.4, Appendix D for Seismic Category I Structures. Where possible, load combinations were enveloped and compared with lower Acceptance Limits to reduce the number of load combinations to be analyzed. The analysis provides details on the enveloped cases considered, where applicable.

Design Factor

A term of "Design Factor" is used to relate actual values with allowable values, given as a percentage. The form of the calculation is as follows:

$$\text{Design Factor (\%)} = [(\text{Allowable} - \text{Actual}) / \text{Actual}] \times 100$$

Load Combinations - Storage Racks

<u>Load Combination</u>	<u>Acceptance Limit</u>
$D + L$	Level A service limits
$D + L + T_o$	Level A service limits
$D + L + T_o + E$	Level A service limits
$D + L + T_a + E$	Level B service limits
$D + L + T_o + P_f$	Level B service limits
$D + L + T_a + E'$	Level D service limits
$D + L + F_d$	The functional capability of the fuel racks should be demonstrated

The abbreviations used here are:

D	Dead loads and their related internal forces and moments
L	Live load, zero for storage racks since no moving objects in the rack
E	Load generated by the Operating Basis Earthquake
E'	Load generated by the Safe Shutdown Earthquake
T_o	Thermal effects and load during normal operating or shutdown conditions, based on the most critical transient or steady state condition
T_a	Thermal effects at the highest temperature associated with the postulated abnormal conditions
P_f	Upward force on the racks caused by postulated stuck fuel assembly
F_d	Force caused by the accidental drop of the heaviest load from the maximum possible height

Note: Provision of ASME Section III, Subsection NF-3251.2 is amended by the requirements of paragraphs c.2.3 and 4 of Regulatory Guide 1.124 entitled "Design Limits and Load Combinations for Class 1 Linear-Type Component Supports."



ACCEPTANCE CRITERIA

This section provides the acceptance criteria used to qualify Spent Fuel System structures. To stay within the 1985 licensing basis, several self-imposed acceptance criteria are established and are also defined here. The acceptance criteria summarized here meet all the regulatory requirements and meets all the self-imposed requirements.

Acceptance Criteria - Storage Racks

The storage racks are designed per the requirements of Subsection NF of the ASME Section III Code. Table 3.2-1 shows the Class 3 Component Support stress allowables for the structure. The structural evaluation is based on a conservative interpretation of the ASME B&PV Code. The design factors provided here are margins above the ASME Code. The Code has large built-in safety factors. Table 3.2-2 provides the stress allowables for 304L (ASTM A240 and ASTM A479) stainless steel material. This table is developed using criteria outlined in Table 3.2-1, and is provided as an example. For all other materials, the stress allowables are calculated where applicable.

Table 3.2-1 Stress Acceptance Criteria - Storage Racks

	Service Level A	Service Level B	Service Level D
Primary Membrane Stress σ_1	1.0 S	1.33 S	Lower of 1.2 Sy or 0.7 Su
Primary Membrane + Bending $\sigma_1 + \sigma_2$	1.5 S	1.995 S	Lower of 1.8 Sy or 1.05Su
Range of Primary + Secondary Stress	Lower of 2Sy or Su	Lower of 2Sy or Su	Lower of 2Sy or Su
Bearing Average Large distance from Edge	Sy 1.5 Sy	Sy 1.5 Sy	No Evaluation Required
Pure Shear Average Primary Shear Maximum Primary Shear	0.6 S 0.8 S	0.6 S 0.8 S	0.42 Su 0.42 Su
Weld Stress - Fillet Weld Weld metal Base metal	0.3 Su 0.4 Sy	0.4 Su 0.532 Sy	0.42 Su 0.42 Su

Per ASME Section III, Subsection NF, SRP 3.8.4, & Reg Guide 1.124

where: S = Allowable stress value at temperature, from the applicable table of Appendix I
 Sy = Yield strength at temperature
 Su = Tensile strength at temperature

Notes: Per sections of ASME Section III, Subsection NF and Appendix F:
 Line 1: Per NF-3251, NF-3261 and F-1332 of ASME Section III
 Line 2: Per NF-3251, NF-3261 and F-1332 of ASME Section III
 Line 3: Per footnote 6 of Table NF-3523(b)-1 and conservative interpretation of ASME
 Section III
 Line 4: Per NF-3252.1, and F-1332.3 of ASME Section III
 Line 5: Per NF-3252.2, and F-1332.4 of ASME Section III
 Line 6: Per NF-3266, Table NF-3324.5(a)-1 of ASME Section III

Deformations should preclude damage to the fuel assemblies. In addition to the stress acceptance, the structure is evaluated against stability (buckling).

**Table 3.2-2 304L Stainless Steel - Stress Acceptance Criteria ASME III,
Class 3 Component Support**

	Service Level A ksi	Service Level B ksi	Service Level D ksi
Primary Membrane Stress σ_1	15.7	20.881	26.448 @ 180° F
Primary Membrane + Bending $\sigma_1 + \sigma_2$	23.55	31.322	39.672 @ 180° F
Range of Primary + Secondary Stress	46.3	44.08 @ 180° F	44.08 @ 180° F
Bearing Average Large distance from Edge	23.15 34.725	22.04 33.06 @ 180° F	No Evaluation Required
Pure Shear Average Primary Shear Maximum Primary Shear	9.42 12.56	9.42 12.56	28.123 @ 180° F 28.123 @ 180° F
Weld Stress - Fillet Weld Weld metal Base metal	21 9.26	27.93 11.725 @ 180° F	29.40 28.123 @ 180° F

Per ASME Section III, Subsection NF, SRP 3.8.4, & Reg Guide 1.124

Notes: Per sections of ASME Section III, Subsection NF and Appendix F:

- Line 1: Per NF-3251, NF-3261 and F-1332 of ASME Section III
- Line 2: Per NF-3251, NF-3261 and F-1332 of ASME Section III
- Line 3: Per footnote 6 of Table NF-3523(b)-1 of ASME Section III
- Line 4: Per NF-3252.1, and F-1332.3 of ASME Section III
- Line 5: Per NF-3252.2, and F-1332.4 of ASME Section III
- Line 6: Per NF-3266, Table NF-3324.5(a)-1 of ASME Section III

For other materials, the acceptable stress values are calculated where applicable.

Acceptance Criteria - Lifting

Some of the old fuel storage racks will be removed from the spent fuel pool, and new racks will be installed. These operations involve lifting of the racks. Due to weight of these racks, they are considered as heavy load. The Criteria of NUREG-0612 are applied for the lifting analysis.

NUREG-0612 (Control of Heavy Loads at Nuclear Power Plants), Section 5.1.6

	<u>Safety Factor</u>	<u>Design Criteria</u>
Redundant Lift (Single-Failure Proof)	5	Ultimate
Non-redundant Lift	10	Ultimate

Acceptance Criteria - Spent Fuel Pool Liner

The spent fuel pool liner is designed in accordance with the AISC-1989 Code. The storage rack support pads are designed such that they do not rest on any liner weld seams. The support pads primarily transmit the rack loads as bearing loads on the liner.

- The redesign only changes the floor bearing loads
- Bearing Allowable $0.9 F_y$
Per AISC
- Liner Fatigue Analysis per AISC, Appendix K

Acceptance Criteria - Spent Fuel Pool Concrete

The spent fuel pool concrete is designed per requirements ACI 349-85. The storage racks, being free standing structures, primarily induce bearing loads on the concrete at support pad locations. The redesign only changes the floor bearing loads.

Bearing Allowable $\phi (0.85 f_c)$
Per ACI 349, Section 10.15

- Demonstrate that there are no rack-to-wall impacts

3.3 STRUCTURAL DESIGN FEATURES

The ATEA spent fuel rack design objective was to maximize the number of available fuel assembly storage cells while ensuring that all criticality, thermal-hydraulic, and structural requirements were met. Specific to these structural design features, the ATEA racks consist of three fundamental rack types, grouped as Types 2A-2B, 3A-3E, and 4. The rack modules are freestanding structures that minimize the loadings on the pool liner and floor, in that only friction loads and bearing loads are transmitted. In addition, rack structural loads are minimized by the compliance offered by the free-standing boundary condition. Rack modules are sized to ensure sufficient lateral gaps between modules and the pool wall such that no impacts are made during the faulted events.

The rack pedestals are positioned such that they are sufficiently removed from the existing pool liner leak chases, thus minimizing the effects of additional loads in these areas. The pedestals are also

sized and numbered to ensure a stable rack structure, thus minimizing tilting, and also to equally distribute and minimize the resulting bearing loads onto the pool liner and floor. The pedestals also provide threaded connections to ensure the overall rack module levelness during installation, thus minimizing any load eccentricities and imbalances. The pedestal and rack baseplate designs provide sufficient cutouts for fluid cooling while ensuring adequate structural strength. The ATEA baseplate thickness is greater than that of the resident racks. In addition, the entire rack foundation is designed with a gusset plate network tying the baseplate and pedestals throughout the rack module. The gusset plate network further strengthens the rack, increasing structural margins for the baseplate and pedestals.

Type 2 racks have a primary structural design whose features include cell junction weld tabs, which are used to physically connect the stainless steel structural cells axially along the cell length. These weld tabs laterally position the structural cells and provide a load path between these cells. The weld tabs are sized and numbered to ensure sufficient structural margins. The structural cells are also fabricated with welded stainless steel retainer plates located at the top and bottom of the cell. These plates serve to axially constrain the adjacent borated stainless steel (BSS) cells while providing a gap to accommodate any axial differential thermal expansion. The retainer plates also serve as a bearing surface through which loads are transmitted from structural cell to structural cell through the top and bottom nozzles of the fuel assembly within the BSS cell. The retainer plate welds are sized and numbered to ensure a sufficient structural margin for all loading cases, including a stuck fuel assembly.

Type 3 racks have a primary structural design whose features include a series of stainless steel "bands" located at discrete axial locations along the length of the BSS cells. These axial locations correspond to those of the fuel assembly spacer grids. The spacer grids are the primary lateral load interface for the fuel assembly in addition to the top and bottom nozzles. The band is assembled as two pieces fitting into mortice joints on the BSS plates and then welded to each other to form an integral band around the BSS cell. These bands serve as the load path through the BSS cell to the structural cells. The bands coupled with the rack-to-rack cell gaps ensure that only compressive loads and no bending loads are transmitted to the BSS plates. The type 3 racks also utilize the cell junction weld tabs, which are used to physically connect the stainless steel structural cells axially along the cell length. These weld tabs laterally position the structural cells and provide a load path between these cells, similar to type 2 racks. The weld tabs are sized and numbered to ensure sufficient structural margins.

Type 4 racks are special racks located on the periphery of the resident rack modules (type 1) to further increase storage capacity. These racks consist of 10 rack cells per module which are secured by two custom mounting fixtures located in the top of the outer cells of the adjacent resident racks. Type 4 racks are also positioned on the pool floor using two pedestals, allowing it to be self-supporting and stable. For additional lateral constraint, tie bars fixtured to the bottom of two type 4 rack cells (adjacent to the pedestal cells) interface with the diagonally adjacent type 1 rack cells. The type 4 racks and corresponding mounting fixtures are designed and positioned to minimize rack displacement and maximize structural margins while ensuring that no impacts with the pool wall occur.

3.4 MATERIALS OF CONSTRUCTION

General Standards

This section addresses the general 'structural material' requirements of Standard Review Plan, NUREG-0800, Section 3.8.4, Appendix D in the design of the spent fuel storage racks. The internal and external environmental conditions of the storage pool were considered in the selection of the component materials. All of the structural materials selected conform to the ASTM Specifications and meet the intent of ASME Section III, Subsection NF requirements. Any benefits of the structural strength of Boraflex and borated stainless steel are not considered in the structural analysis.

Table 3.4-1 summarizes the materials of construction for the spent fuel storage racks, spent fuel pool liner, and the spent fuel pool.

3.4.1 Structural Materials

Type 304L and 630 stainless steel materials were selected for the storage rack construction because of:

- Corrosion resistance (low carbon content which minimizes the sensitization),
- Strength,
- Fracture toughness, and
- ASME acceptability.

The 630 bolting material is selected for its high strength and resistance to stress corrosion cracking, even at temperature to 300° F, and under severe chloride and H₂S environment. Galvanic reactions are not expected between the 304L and borated stainless steel, or between 304L and 630 austenitic stainless steel.

The resident U.S. Tool & Die storage racks and pool liner are fabricated from 304 stainless steel. The spent fuel pool walls and floor are constructed using 3,000 psi minimum strength concrete - 28 days cured.

Tables 3.4-2 through 3.4-6 report the material properties used in the structural analyses.

3.4.2 Non-Structural Materials

Borated stainless steel and Boraflex are used as neutron absorber materials. They are considered non-structural materials in the structural analyses.

Borated Stainless Steel

The borated stainless steel (BSS) is grade 304 B6/B7, Type B in accordance with ASTM-A887-89 and A-480.

Natural Boron (B10) is added to the austenitic stainless steel with a minimum content of 1.7 percent in weight and a carbon content less than or equal to 0.03%. The microstructure consists of an austenitic stainless steel matrix with fine, uniform dispersion of complex chromium borides.



Borated stainless steels are used for neutron attenuation in spent fuel storage and transportation applications. BSS has been used in spent fuel storage pools since 1978. Currently, more than 4,000 metric tons of BSS are in use in spent fuel pools. BSS has been licensed in 13 countries including the U.S.A. for use in spent fuel pools. BSS has been licensed for use in spent fuel pools at Indian Point 2, Indian Point 3 and Millstone 2 in the U.S.A. For these applications, BSS was exposed to aqueous environments including boric acid, and these applications have proven the corrosion resistance of BSS. Borated stainless steel has an exceptional resistance to corrosion by electrolytic hydridation, oxidation, or other chemical reactions in borated and pure water.

As compared to 304 type stainless steel, borated stainless steel has a higher strength but lower ductility and lower impact resistance. The coefficient of thermal expansion and density for borated stainless steel are very similar to 304L stainless steel (Table 3.4-7). BSS corrosion resistance is very similar to conventional austenitic stainless steel in a spent fuel pool environment. There are no significant changes to the mechanical properties of the borated stainless steel upon exposure to the levels of irradiation, over the design life of the fuel storage rack.

In the ATEA rack design, the borated stainless steel plate is a free standing member. The borated stainless steel is neither bent nor welded in the storage rack design. This will preclude any cracking or thermal alteration of the metal. The borated stainless steel is not considered as a structural member in the structural analysis, and its contribution to the strength of the racks is neglected.

In summary, the neutron absorber material selected for the rack construction provide:

- Homogeneous Boron in austenitic stainless steel matrix
- Corrosion resistance over the life of the racks
- High stability under irradiation (no blistering, no creep, ...)
- No degradation, swelling or ballooning.

Boraflex

Boraflex is used as a neutron absorber in the resident U.S. Tool & Die racks. The Boraflex is not considered as a structural member in the strength analysis. The analysis reflects only the weight of the Boraflex. Table 3.4-8 reports the material density used in the weight calculation.

Table 3.4-1 Materials of Construction

Component	Material Specification
ATEA New Storage Racks	
Cell Wall	ASTM - A240 Type 304L or ASTM - A312 Type 304L
Base Support Plate	ASTM - A240 Type 304L
Support Pads	ASTM - A479 Type 304L
Perimeter Rack Connection (Lower)	ASTM - A240 Type 304
Bolts (Part of Support Pad)	ASTM - A564 Type 630, Condition H1100
Weld Material	Grade 308L in accordance with AWS AS-9
Neutron Absorber	ASTM - A887-89, Type 304 B6/B7, Grade B Borated Stainless Steel
Resident Storage Racks (US Tool & Die Racks on Wachter's Base Support)	
Rack Cell Wall Cell Insert Wall Filler	ASTM - A240 Type 304 ASTM - A240 Type 304 ASTM - A240 Type 304
Base Support Assembly	ASTM - A240 Type 304
Base Corner Support Shims	ASTM - A240 Type 304
Boraflex	0.020 gm/cm ² Minimum B ₁₀
Hold Down Bolts	Type 304 Stainless steel
Spent Fuel Pool	
Liner	ASTM-A240 Type 304
Concrete	3,000 psi minimum strength, 28 days cured
Consolidated Fuel	
Fuel Can Wall Cell Divider Can Bottom	ASTM A240 Type 304 ASTM A240 Type 304 ASTM A240 Type 304

**Material Properties - RG&E Ginna High Density Spent Fuel
Storage Racks**

The mechanical properties of the structural material used in the RG&E Ginna high density storage racks, fuel pool liner and the fuel pool concrete are reported here. These are linear elastic properties for use in the structural analyses. The material property for weld metal is per table NF-3324.5 (a)-1 of the ASME Code Section III. The weld metal minimum tensile strength is 70 KSI.

Table 3.4-2
Material : 304L Stainless Steel Plate
Material : 304L Stainless Steel Bar
Material : 304L Stainless Steel Welded and Seamless Pipe

Spec: ASTM-A240, Type 304L
Spec: ASTM-A479, Type 304L
Spec: ASTM-A312, Type 304L
Composition 18Cr-8Ni

Temperature °F	70	100	150	200	300
Allowable Stress S - ksi		15.7	15.7	15.7	15.3
Minimum Yield Strength - ksi	25	25	23.15	21.3	19.1
Minimum Ultimate Strength - ksi	70	70	68.1	66.2	60.9
Elastic Modulus - $\times 10^6$ psi	28.3	-	27.869	27.6	27.0
Linear Thermal Expansion α - $\times 10^{-6}$ in/in/°F Mean coefficient going from 70° F		8.55	8.67	8.79	9.00
Density - lb/in ³	0.29				

Source References:

Allowable Stress S from Table I-7.2 of ASME Section III, Appendix I
Minimum Sy from Table I-2.2 of ASME Section III, Appendix I
Minimum Su from Table I-3.2 of ASME Section III, Appendix I
Linear Thermal Expansion α from Table I-5.0 of ASME Section III, Appendix I
Elastic Modulus E from Table I-6.0 of ASME Section III, Appendix I

Table 3.4-3
Material : 304 Stainless Steel Plate
Material : 304 Stainless Steel Bar

Spec: ASTM-A240, Type 304
Spec: ASTM-A479, Type 304
Composition 18Cr-8Ni

Temperature °F	70	100	200	300
Allowable Stress S - ksi		18.8	17.8	16.6
Minimum Yield Strength Sy - ksi	30	30	25	22.5
Minimum Ultimate Strength Su - ksi	75	75	71	66
Elastic Modulus E - x10 ⁶ psi	28.3	-	27.6	27.0
Linear Thermal Expansion α - x 10 ⁻⁶ in/in/°F Mean coefficient going from 70° F		8.55	8.79	9.00
Density - lb/in ³	0.29			

Source References:

Allowable Stress S from Table I-7.2 of ASME Section III, Appendix I

Minimum Sy from Table I-2.2 of ASME Section III, Appendix I

Minimum Su from Table I-3.2 of ASME Section III, Appendix I

Linear Thermal Expansion α from Table I-5.0 of ASME Section III, Appendix I

Elastic Modulus E from Table I-6.0 of ASME Section III, Appendix I

Table 3.4-4
Material : 630 Precipitation Hardened Steel

Spec: ASTM-A564, Type 630 Bolting Material
Nominal Composition: 17Cr-4Ni-4Cu, Precipitation hardened steel
Minimum temper temperature 1100° F

Temperature °F	70	100	200	300
Allowable Stress S - ksi		28	28	28
Minimum Yield Strength - ksi	115	115	106.3	101.9
Minimum Ultimate Strength - ksi	140	140	140	140
Elastic Modulus - x10 ⁶ psi	28.3		27.6	27.0
Linear Thermal Expansion α - x 10 ⁻⁶ in/in/°F Mean coefficient going from 70° F		5.89	5.90	5.90
Density - lb/in ³	0.29			

Source References:

Allowable Stress S from Table I-7.3 of ASME Section III, Appendix I
Minimum Sy from Table I-2.1 of ASME Section III, Appendix I
Minimum Su from Table I-3.1 of ASME Section III, Appendix I
Linear Thermal Expansion α from Table I-5.0 of ASME Section III, Appendix I
Elastic Modulus E from Table I-6.0 of ASME Section III, Appendix I

Table 3.4-5 Concrete**3,000 PSI Minimum Strength 28 days Cured Concrete**

		Concrete
Young's Modulus (psi)	Note 1	3.122×10^6
Poisson's Ratio		0.25
Density (lb/ft ³)		150
Coefficient of Thermal Expansion (in/in/°F)		5.5×10^{-6}
Compressive Strength - f_c (psi)		3,000 minimum

Source: Ginna UFSAR, Table 3.8-20 (Reference 3.22)

Note 1: Per Section 8.5 of ACI 349-85 (Reference 3.20)

Table 3.4-6 Zircaloy-4 Tubing Material

Material Properties for Cold worked, stress relieved Zircaloy-4 Tubing	
Modulus of Elasticity	12×10^6 lb/in ² @ 150° F

Source: Framatome Cogema Fuel Test Results

Table 3.4-7 Borated Stainless Steel
ASTM - A887-89, Grade 304 B6/B7, Type B

Weight density and coefficient of thermal expansion taken same as 304L stainless steel.

Note: This material is not used as a structural material in the structural analysis.

Source: EPRI Report #EPRI TR-100784, "Borated Stainless Steel Application in Spent Fuel Storage Racks," June 1992 (Reference 3.31) and ASME Code Case N-510-1 (Reference 3.43).

Table 3.4-8 Boraflex
Spec: 0.020 gm/cm² Minimum B₁₀

Specific Gravity	1.7 g/cc
------------------	----------

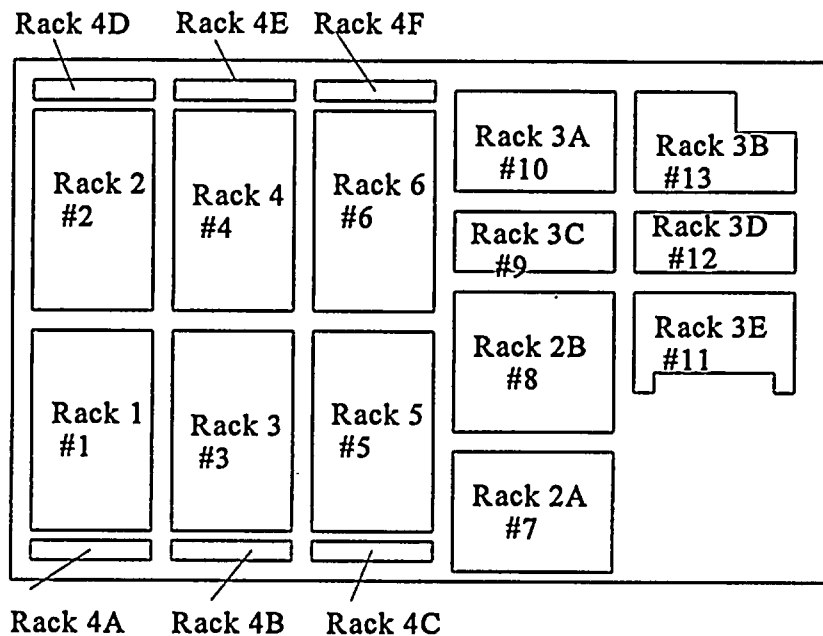
The Boraflex material is not to be used as a structural material in the structural analysis.

Source Reference: Table A-2 of EPRI NP-6159, "An Assessment of Boraflex Performance in Spent-Nuclear-Fuel Storage Racks," December 1988 (Reference 3.30).

3.5 STRUCTURAL ANALYSIS

The RG&E Ginna Unit 1 Spent Fuel Storage System structure is analyzed to meet the codes and standards specified in Section 3.2.1. This section covers the structural analysis of the storage racks, spent fuel pool and the pool liner.

The re-racking at Ginna utilizes high density, free-standing spent fuel storage racks to replace selected resident, low density racks. The racks are of four basic design variations; namely Type 1 Type 2, Type 3 and Type 4 racks. All racks are designed to store consolidated spent fuel canisters with a 2:1 consolidation ratio. The following sketch provides a general layout of the array of racks in the pool.



Storage Racks - Rack Locations
And General Arrangement

Section 3.5.1 presents the method used in generating the seismic input, the fuel assembly loading and various loads considered in the analysis. Section 3.5.2 presents the structural and seismic analysis methodology and assumptions. Section 3.5.3 presents analyses and results for normal (Level A), upset (Level B), faulted (Level D) and hypothetical accident loading conditions.

Finite element methods were used extensively to analyze loads, deformations and stresses in the structural components. Computer codes used for structural analysis are certified and benchmarked to known solutions. Section 3.5.2.4 provides a listing of computer programs used. The computer program, ANSYS, was used for a majority of these calculations.

Several mathematical models were used with features to represent the sliding and tipping of the racks and hydrodynamic coupling which can occur between fuel assemblies and rack cells, between racks, and between racks and reinforced concrete walls. These mathematical models account for differences in rack modules in the pool. Fuel loadings analyzed included all possible combinations,

loading conditions of empty, half-loaded, unconsolidated and consolidated fuel. Due to the fact that the racks are free to slide and tip, a nonlinear dynamic analysis was performed to evaluate seismic loadings. The analysis was a time history analysis, which permitted both sliding and tipping. Section 3.5.2.3 provides detailed descriptions of the mathematical models. An overview of the main mathematical models is provided here.

3-D Single Rack Dynamic Analysis Models

These mathematical models are used for various sensitivity studies. Figure 3.5-31 provides a schematic of the 3-D single rack model. These evaluations reduce the number of discrete whole pool evaluations, thus making the analysis of the spent fuel pool racks more efficient. Section 3.5.2.7 presents the results of the rack stiffness sensitivity study. The results presented conclude that the seismic loadings and hence stresses are not sensitive to the rack stiffness. For this reason, it is concluded that structural testing is not required to verify stiffness calculations.

3-D Whole Pool Multi-Rack Dynamic Analysis Model

A three-dimensional whole pool multi-rack (WPMR) model (Figure 3.5-32) was used for the re-racking seismic and structural analysis. The racks in the model reflect the use of six racks currently in use at Ginna and the additional seven (7) new ATEA racks for a total of thirteen (13) racks in the spent fuel pool. The use of six additional perimeter racks (Type 4), which may be installed at a future time, is also addressed in analyzing several pool configurations. The seismic input is site-specific to the Ginna plant. Rack loads and displacements were determined from this analysis for all load cases.

3-D Single Rack Plate Models

These mathematical models were used for static stress, thermal, base plate and lifting analyses. Figure 3.5-33 provides an isometric view of the 3-D Single Rack Plate Model.

Isolated Component Models

Extensive use has been made of various isolated mathematical models for calculation of global or isolated stiffness, support tab stiffness and tab stresses, etc. Figures 3.5-34 and 3.5-35 provide an isometric view of type 2 and type 3 fuel cell finite element models with tabs respectively. Section 3.5.3.1.1.3 describes the isolated model for fuel-to-rack interface stiffness calculation. Section 3.5.3.1.2 describes the isolated mathematical model for the tab stresses.

3.5.1 Loading Conditions

3.5.1.1 Overview

FUEL ASSEMBLY LOADING

The empty, half full and fully loaded racks were considered in the seismic analysis. The weight of 1450 pounds was used for a single fuel assembly. This weight envelopes all three fuel designs, namely W-standard, W-OFA, and Exxon. The 1450 pound fuel assembly weight includes the weight of control components. Two full rack loading conditions were analyzed. The first, referred to as unconsolidated, represents a rack filled with fuel assemblies. The second, referred to as consolidated, represents a rack filled with full consolidation canisters, each weighing 2323 pounds. The half-full condition considered is a rack which is filled with fuel assemblies in one half and

empty in the other half, so that the worst case eccentricity would exist. The empty rack condition considered is a rack with no fuel assemblies or consolidation canisters.

DEAD WEIGHT

The dead weight loading includes: 1) empty storage racks, 2) racks fully loaded with fuel assemblies, 3) racks fully loaded with the consolidated canisters, and 4) racks partially loaded with a mixture of fuel assemblies and consolidated canisters. The results presented for seismic loadings include the effect of dead weight loadings. Section 3.5.3.1.5 provides a summary of the support pad loads which includes the dead weight loads.

LIVE LOADS

There are no live loads on the storage racks. For this reason, all live loads are zero in the load combination considered.

SEISMIC LOAD

For the RG&E Ginna Unit 1, the ground seismic response is 0.08 g for OBE and 0.2 g SSE (Ginna UFSAR, Section 3.7.1.2). The spent fuel pool is built on top of hard rock. Therefore, the ground response spectra are also applicable to the pool foundation. The shape of response spectra is per U.S. NRC Regulatory Guide 1.60.

Synthetic Time History

Four sets of statistically independent synthetic acceleration time histories were generated for 2% damping for OBE and 4% damping for SSE conditions with each set containing horizontal and vertical acceleration time histories. The most current version of the computer program SIMQKE was used to generate synthetic seismic time histories.

It was demonstrated that each of the generated time histories was statistically independent from all of the others. In order to prove statistical independence, the normalized cross-correlation coefficient between any two sets is less than 0.1 (Section N-1213.1 of ASME Section III, Reference 3.19). The largest coefficient was less than 0.1. The time history was based on a time step of 0.01 seconds.

The synthetic time histories used had a duration of 20 seconds, and the three orthogonal components of each set were simultaneously applied in the rack time history seismic analyses.

The floor response spectra were regenerated from 1.1 times the average of all four developed time histories. The regenerated floor response spectra are found to match very well throughout the frequency range of the Criteria Floor Response Spectra to meet the requirements specified in SRP 3.7.1 of NUREG-0800, Reference 3.2. The specified OBE and SSE response spectra are per Ginna UFSAR, Section 3.7.1.2. The comparison of the calculated and the Ginna specific SSE response spectra are shown in Figures 3.5-1 through 3.5-6.

Four SSE and OBE time histories were used in an analysis of the Rack 8 (Rack 2B). The parametric study was based upon a friction coefficient of 0.8, which produced the maximum loads. For this study, several parameters were examined, such as maximum rack forces and moments, support leg loads, and fuel to rack impact loads. From the comparison, it was found that using a factor on a single time history would envelop the other three. Section 3.5.2.6 presents the determination of the

"single" OBE and "single" SSE time histories and associated factors. To simplify calculations, the remaining analyses were based on single OBE and single SSE time histories.

From the results of the four different time histories upon the single rack model, factors were applied to selected single OBE and SSE forces and moments for the stress analysis calculations in order to cover all possibilities. The four OBE's indicated that a factor of 1.12 applied to the OBE-4 loads would completely envelop all four of the generated OBE loads. The four SSE's indicated that a factor of 1.20 applied to the SSE-1 loads would completely envelop all four of the generated SSE loads. These factors used were 1.12 and 1.20 for OBE and SSE, respectively.

THERMAL LOADS

The conditions T_a and T_o cause local thermal stresses to be produced.

Two cases of thermal effects were considered. First, an isolated storage location containing a fuel assembly was considered, in which it was assumed that the fuel assembly is generating heat at the maximum postulated rate. The surrounding storage locations were assumed empty. The heated water was assumed to make contact with the inside of the storage walls, thereby producing the maximum possible temperature difference, T_o , between the adjacent cells. In the second case, it was assumed that there is a loss of cooling such that the entire rack expands, setting up shear forces in the support legs which are assumed to be held from sliding by the horizontal friction force between the support legs bearing pad and pool floor liner, see Section 3.5.3.1.9.

Single Hot Cell (T_o)

The worst situation was assumed to exist when an isolated storage location has a fuel assembly which is generating heat at the maximum postulated rate. The surrounding storage location is assumed to contain no fuel. The heated water makes unobstructed contact with the inside of the storage walls, thereby producing the maximum possible temperature difference between the adjacent cells. The sum of primary plus secondary stresses is limited to the lesser of two times the material yield strength, $2 S_y$, and ultimate strength, S_u at the design temperature.

Loss of Spent Fuel Pool Cooling (T_a)

This thermal condition is produced when the pool water bulk temperature increases to 180° F due to loss of artificial cooling. The pool liner temperature is kept the same as the normal operating temperature to generate conservative stresses in the rack.

FATIGUE ANALYSIS

The peak stress range in the rack structure and the pool liner due to the cyclic loading was evaluated against fatigue criteria. For purposes of evaluating fatigue compliance, one SSE and five OBE events were used. It was demonstrated, by analysis, that the Cumulative Usage Factor in accordance with the procedures of NB 3222.4 (Reference 3.19) did not exceed 1.0 for storage racks. The pool liner fatigue strength was evaluated per Part 5, Appendix K of the AISC Code - 9th edition. The analysis is contained in Section 3.5.3.1.11.

STUCK FUEL ASSEMBLY - UPLIFT FORCE

The ability of the racks to withstand a vertical or inclined (at 45°) force of 2000 pounds applied at any point without damaging the racks as to violate the sub-criticality criteria (K_{eff} less than 0.95) for the stored fuel was demonstrated by analysis. The analysis is contained in Section 3.5.3.1.18.

SLOSHING EFFECTS

The effect of sloshing of the pool water during the seismic event on the rack motion is negligible, as demonstrated by classical methods in Section 3.5.3.1.13. The hydrodynamic pressures from sloshing of the pool surface water have no effect upon the racks. The sloshing water rises and lowers at the ends of the pool by about 1 ft under OBE conditions and 3 ft under SSE. The effect of this and the resulting changes in pressure are minimal.

HYPOTHETICAL ACCIDENT DROPS

The major hypothetical accident conditions addressed in Section 3.5.3.2 are:

- a) Fuel assembly drop during fuel handling in the spent fuel pool
- b) Spent fuel pool canal gate drop
- c) Spent fuel pool storage rack drop
- d) Tornado missile impact
- e) Spent fuel cask drop.

The straight deep drop cases required an exactitude, (i.e., falls through cell with no contact), which has a very low probability of occurring. Nevertheless, the consequences of such an accident were examined. While damage to the fuel rack bottom plate or support leg could be expected, no damage would occur to the spent fuel pool floor.

The shallow drop was examined and it was found that with a ductility factor less than 20 and deformation less than one inch, the distortion of the cells would be confined to the portion of cells above the borated stainless steel, and hence, would not affect the K factor used in the criticality analysis.

The conservatism used in the mechanical accident analyses for various drops indicated that minor distortion of the rack is limited to the vicinity of the impact area. There is no gross deformation of the rack away from the impact area.

Consolidated fuel, the pool canal gate, storage racks and spent fuel shipping casks were considered heavy loads per NUREG-0612. There will be administrative control for movement of these hardware in the spent fuel pool area. Also they will be lifted using a single-failure proof crane and a single-failure proof lifting system. Handling of these hardware in the spent fuel pool area will be performed in accordance with the guidelines of NUREG-0612 with regard to limiting the chance of unacceptable heavy load drop. Reference 3.23, NRC Staff safety evaluation report, provides exclusion of heavy load drops meeting these criteria.

3.5.1.2 Seismic Input Compliance

This section demonstrates compliance of RG&E's Ginna spent fuel storage seismic analysis time histories input with:

- a) U.S. NRC Regulatory Guides 1.60 and 1.61.
- b) Standard Review Plan - NUREG-0800, Section 3.7.1., "Seismic Design Parameters" requirement, and
- c) ASME Code, Appendix N, Sections N-1212.2 and N-1213.1, 1989 edition.

Design Response Spectra

References 3.2 and 3.10 provide criteria for design floor response spectra in the three orthogonal directions as a function of the fundamental frequency for Operational Basis Earthquake (OBE). Per reference 3.10, the Safe Shutdown Earthquake (SSE) ground response spectra is 0.20 G's (horizontal) and 0.133 G's (vertical), while the OBE ground spectra is 0.08 G's for horizontal and 0.053 G's for vertical motion components. Per reference 3.3, structural damping values for welded steel structures are taken as 2% and 4% (percent of critical damping) for OBE and SSE respectively. These spectrum curves were used for the seismic analysis of all racks in the pool. The numerical values of accelerations for the RG&E Ginna Unit 1 spent fuel pool specified ground response spectra are given in Tables 3.5-1 through 3.5-6. These acceleration values are consistent with the U.S. NRC Regulatory Guide 1.60 requirements.

Synthetic Time Histories

Per Reference 3.2, Paragraph 1 "Design ground Motion", Option 2 "Multiple Time Histories" is chosen as an analysis basis. Per same reference, acceptance criteria for the Option 2 requires a minimum of four independently generated time histories. Therefore, four sets of statistically independent synthetic acceleration time histories were generated assuming 2% damping for OBE and 4% damping for SSE conditions, each set containing horizontal and vertical acceleration time histories. Averages of the calculated response spectra with an assigned factor of 1.1 envelop each design spectra ground motion component, as shown in Figures 3.5-1 through 3.5-6. Total seismic activity time duration was taken to be 20 seconds. Reference 3.19, Section N-1212.2 "Duration of Time History" suggests duration time larger than 6 seconds for strong seismic motion. Reference 3.4, Section II "Acceptance Criteria", paragraph 1-b "Design Time History" requires a total time duration between 10 and 25 seconds. Thus, both requirements are met with a 20 seconds time history duration. All time histories were based on a 0.01 second time step. Plots of the developed acceleration time histories are given in Figures 3.5-7 through 3.5-30.

Time Histories Independence

Per Reference 3.19, Section N-1213.1 "Time Phase Relationship", all artificially generated time histories met cross-correlation limit requirement (maximum correlation coefficient per time history pair of 0.16 or 16%). It was demonstrated that each of the generated time histories was statistically independent from all of the others, since a normalized cross-correlation coefficient between any two sets was less than 0.10 (Reference 3.43). The results of this analysis for the four sets of synthetic SSE and OBE time histories are given in Tables 3.5-7 and 3.5-8, respectively.

Multiple Time History Inputs

Three orthogonal components of each synthetic time history set were simultaneously applied in all three directions.

Seismic runs were made for both SSE and OBE conditions, with a single time history set chosen for each condition (one out of four) for all of the 3D whole pool multi-rack analyses. The chosen time history set was used in conjunction with load factors to envelop the loads and displacements of all four time history sets. These factors are 1.20, for SSE, using time history set number 1, and 1.12 for OBE, using time history set number 4. Section 3.5.2.6. covers Time History Factor Determination.

Synthetic Time Histories Generation

The artificial time history generation program SIMQKE was used to obtain all sets of acceleration time histories.

Table 3.5-1

Regulatory Guide 1.60 Horizontal Spectra (Scaled to 1G ground acceleration)					
Damping %	Acceleration [G's]				Displace. [in]
	33 [Hz]	9 [Hz]	2.5 [Hz]	0.25 [Hz]	0.25 [Hz]
0.5	1.00	4.96	5.95	0.736	3.2
2	1.00	3.54	4.25	0.575	2.5
4 (*)	1.000	2.84	3.40	0.496	2.159
5	1.00	2.61	3.13	0.471	2.05
7	1.00	2.27	2.72	0.432	1.88
10	1.00	1.9	2.28	0.391	1.7

(*) logarithmic interpolation using values for 2 and 5 % critical damping

Table 3.5-2

SSE Horizontal Spectra (0.20 G ground acceleration)					
Damping %	Acceleration [G's]				Displace. [in]
	33 [Hz]	9 [Hz]	2.5 [Hz]	0.25 [Hz]	0.25 [Hz]
0.5	0.2	0.992	1.19	0.1471	0.64
2	0.2	0.708	0.85	0.1149	0.5
4 (*)	0.2	0.5673	0.6806	0.0993	0.4319
5	0.2	0.522	0.626	0.0943	0.41
7	0.2	0.454	0.544	0.0864	0.376
10	0.2	0.38	0.456	0.0782	0.34

Table 3.5-3

OBE Horizontal Spectra (0.08 G ground acceleration)					
Damping %	Acceleration [G's]				Displac. [in]
	33 [Hz]	9 [Hz]	2.5 [Hz]	0.25 [Hz]	0.25 [Hz]
0.5	0.08	0.3968	0.4760	0.0588	0.256
2	0.08	0.2832	0.3400	0.0460	0.2
4 (*)	0.080	0.2269	0.2720	0.0397	0.1728
5	0.08	0.2088	0.2504	0.0377	0.164
7	0.08	0.1816	0.2176	0.0346	0.1504
10	0.08	0.1520	0.1824	0.0313	0.136

Table 3.5-4

Regulatory Guide 1.60 Vertical Spectra (Scaled to 1G ground acceleration)					
Damping %	Acceleration [G's]				Displac. [in]
	33 [Hz]	9 [Hz]	2.5 [Hz]	0.25 [Hz]	0.25 [Hz]
0.5	1	4.96	5.67	0.4896	2.13
2	1	3.54	4.05	0.3839	1.67
4 (*)	1	2.84	3.24	0.3317	1.443
5	1	2.61	2.98	0.3149	1.37
7	1	2.27	2.59	0.2874	1.25
10	1	1.9	2.17	0.2598	1.13

(*) logarithmic interpolation using values for 2 and 5 % critical damping

Table 3.5-5

SSE Vertical Spectra (0.13 G ground acceleration)					
Damping %	Acceleration [G's]				Displac. [in]
	33 [Hz]	9 [Hz]	2.5 [Hz]	0.25 [Hz]	0.25 [Hz]
0.5	0.1333	0.6613	0.7560	0.0653	0.2840
2	0.1333	0.4720	0.5400	0.0512	0.2227
4 (*)	0.1333	0.3782	0.4321	0.0442	0.1924
5	0.1333	0.3480	0.3973	0.0420	0.1827
7	0.1333	0.3027	0.3453	0.0383	0.1667
10	0.1333	0.2533	0.2893	0.0346	0.1507

Table 3.5-6

OBE Vertical Spectra (0.053 G ground acceleration)					
Damping %	Acceleration [G's]				Displac. [in]
	33 [Hz]	9 [Hz]	2.5 [Hz]	0.25 [Hz]	0.25 [Hz]
0.5	0.0533	0.2645	0.3024	0.0261	0.1136
2	0.0533	0.1888	0.2160	0.0205	0.0891
4 (*)	0.0533	0.1513	0.1728	0.0177	0.0770
5	0.0533	0.1392	0.1589	0.0168	0.0731
7	0.0533	0.1211	0.1381	0.0153	0.0667
10	0.0533	0.1013	0.1157	0.0139	0.0000

Table 3.5-7 Cross-Correlation Factors for SSE Time Histories

X-axes:	R	Y-axes:	R	Z-axes:	R
x1 to x2	-0.0062	y1 to y2	-0.0471	z1 to z2	+0.0509
x1 to x3	-0.0288	y1 to y3	+0.0899	z1 to z3	-0.0481
x1 to x4	-0.0664	y1 to y4	-0.0608	z1 to z4	+0.0087
x2 to x3	-0.0548	y2 to y3	+0.0164	z2 to z3	+0.0166
x2 to x4	+0.0459	y2 to y4	+0.0189	z2 to z4	+0.0122
x3 to x4	+0.0097	y3 to y4	-0.0004	z3 to z4	+0.0357
X-Y axes:	R	X-Z axes:	R	Y-Z axes:	R
x1 to y1	+0.0205	y1 to z1	+0.0573	x1 to z1	+0.0480
x1 to y2	-0.0194	y1 to z2	+0.0213	x1 to z2	-0.0398
x1 to y3	+0.0505	y1 to z3	+0.0055	x1 to z3	-0.0523
x1 to y4	-0.0214	y1 to z4	+0.0236	x1 to z4	-0.0597
x2 to y1	-0.0344	y2 to z1	+0.0350	x2 to z1	+0.0247
x2 to y2	-0.0049	y2 to z2	-0.0974	x2 to z2	-0.0591
x2 to y3	-0.0266	y2 to z3	-0.0090	x2 to z3	+0.0096
x2 to y4	+0.0218	y2 to z4	-0.0573	x2 to z4	-0.0013
x3 to y1	+0.0032	y3 to z1	-0.0203	x3 to z1	-0.0149
x3 to y2	+0.0522	y3 to z2	-0.0414	x3 to z2	-0.0277
x3 to y3	+0.0033	y3 to z3	-0.0542	x3 to z3	-0.0422
x3 to y4	-0.0639	y3 to z4	+0.0220	x3 to z4	+0.0835
x4 to y1	-0.0054	y4 to z1	+0.0133	x4 to z1	+0.0705
x4 to y2	-0.0414	y4 to z2	-0.0282	x4 to z2	-0.0016
x4 to y3	-0.0206	y4 to z3	-0.0146	x4 to z3	+0.0171
x4 to y4	-0.0152	y4 to z4	+0.0185	x4 to z4	+0.0327

Table 3.5-8 Cross-Correlation Factors for OBE Time Histories

X-axes:	R	Y-axes:	R	Z-axes:	R
x1 to x2	-0.0294	y1 to y2	-0.0066	z1 to z2	+0.0128
x1 to x3	+0.0605	y1 to y3	+0.0791	z1 to z3	-0.0163
x1 to x4	-0.0985	y1 to y4	+0.0236	z1 to z4	-0.0679
x2 to x3	+0.0345	y2 to y3	+0.0173	z2 to z3	+0.0040
x2 to x4	-0.0160	y2 to y4	+0.0114	z2 to z4	-0.0112
x3 to x4	-0.0268	y3 to y4	+0.0473	z3 to z4	+0.0429
X-Y axes:	R	X-Z axes:	R	Y-Z axes:	R
x1 to y1	+0.0120	y1 to z1	-0.0856	x1 to z1	+0.0240
x1 to y2	-0.0241	y1 to z2	+0.0222	x1 to z2	+0.0570
x1 to y3	+0.0435	y1 to z3	-0.0159	x1 to z3	+0.0605
x1 to y4	-0.0360	y1 to z4	-0.0187	x1 to z4	+0.0121
x2 to y1	-0.0140	y2 to z1	+0.0219	x2 to z1	+0.0012
x2 to y2	+0.0380	y2 to z2	+0.0028	x2 to z2	+0.0270
x2 to y3	-0.0019	y2 to z3	+0.0530	x2 to z3	-0.0206
x2 to y4	+0.0144	y2 to z4	+0.0536	x2 to z4	-0.0418
x3 to y1	+0.0029	y3 to z1	+0.0478	x3 to z1	+0.0121
x3 to y2	+0.0449	y3 to z2	+0.0186	x3 to z2	+0.0727
x3 to y3	-0.0202	y3 to z3	+0.0271	x3 to z3	-0.0543
x3 to y4	+0.0234	y3 to z4	+0.0046	x3 to z4	+0.0278
x4 to y1	+0.0063	y4 to z1	+0.0331	x4 to z1	-0.0246
x4 to y2	+0.0234	y4 to z2	+0.0296	x4 to z2	+0.0186
x4 to y3	+0.0565	y4 to z3	-0.0310	x4 to z3	+0.0237
x4 to y4	-0.0065	y4 to z4	+0.0134	x4 to z4	-0.0223

Figure 3.5-1 Avg. Calculated vs. Design Response Spectra for SSE (EW) X-dir

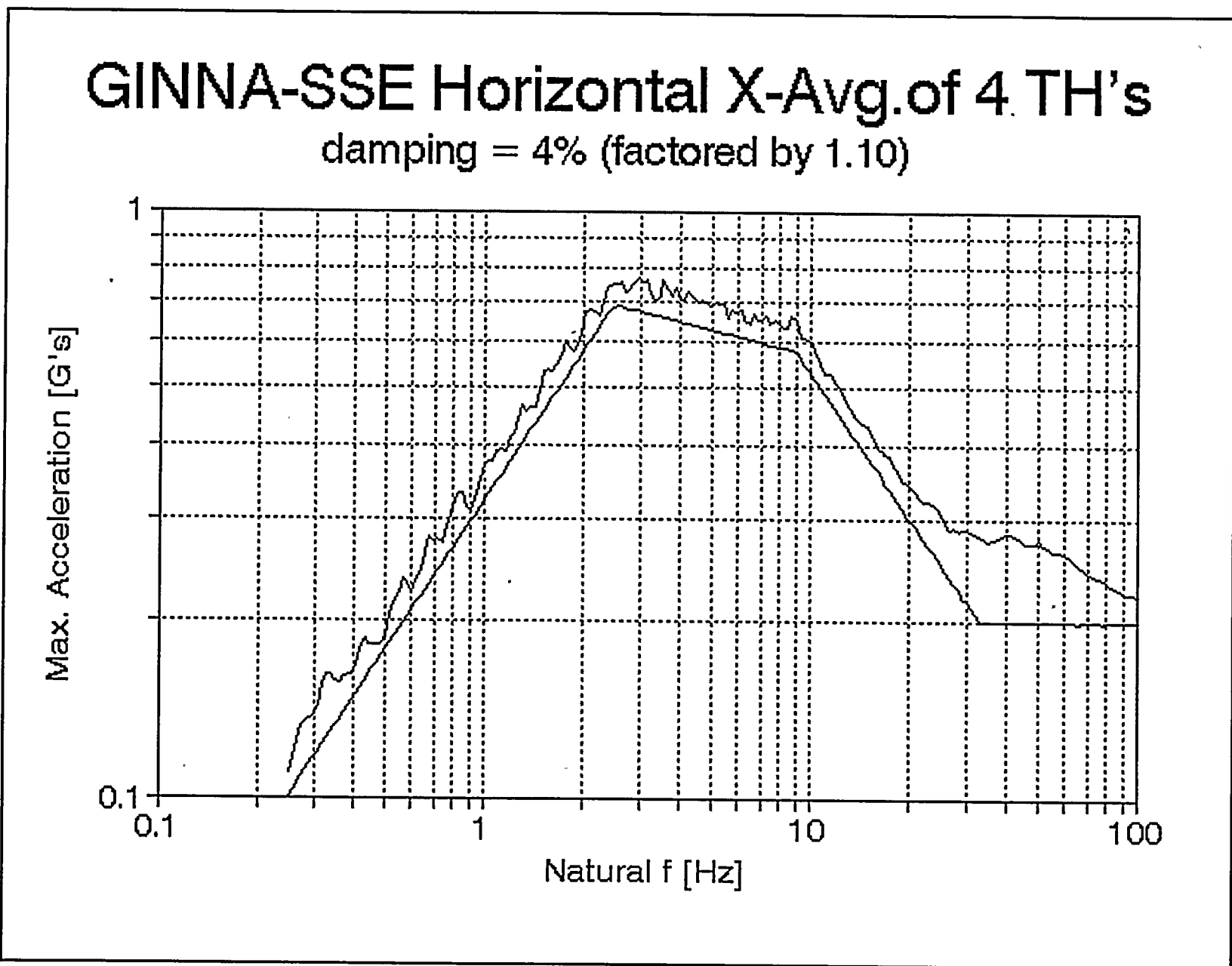




Figure 3.5-2 Avg. Calculated vs. Design Response Spectra for SSE (NS) Y-dir

GINNA-SSE Horizontal Y-Avg.of 4 TH's damping = 4% (factored by 1.10)

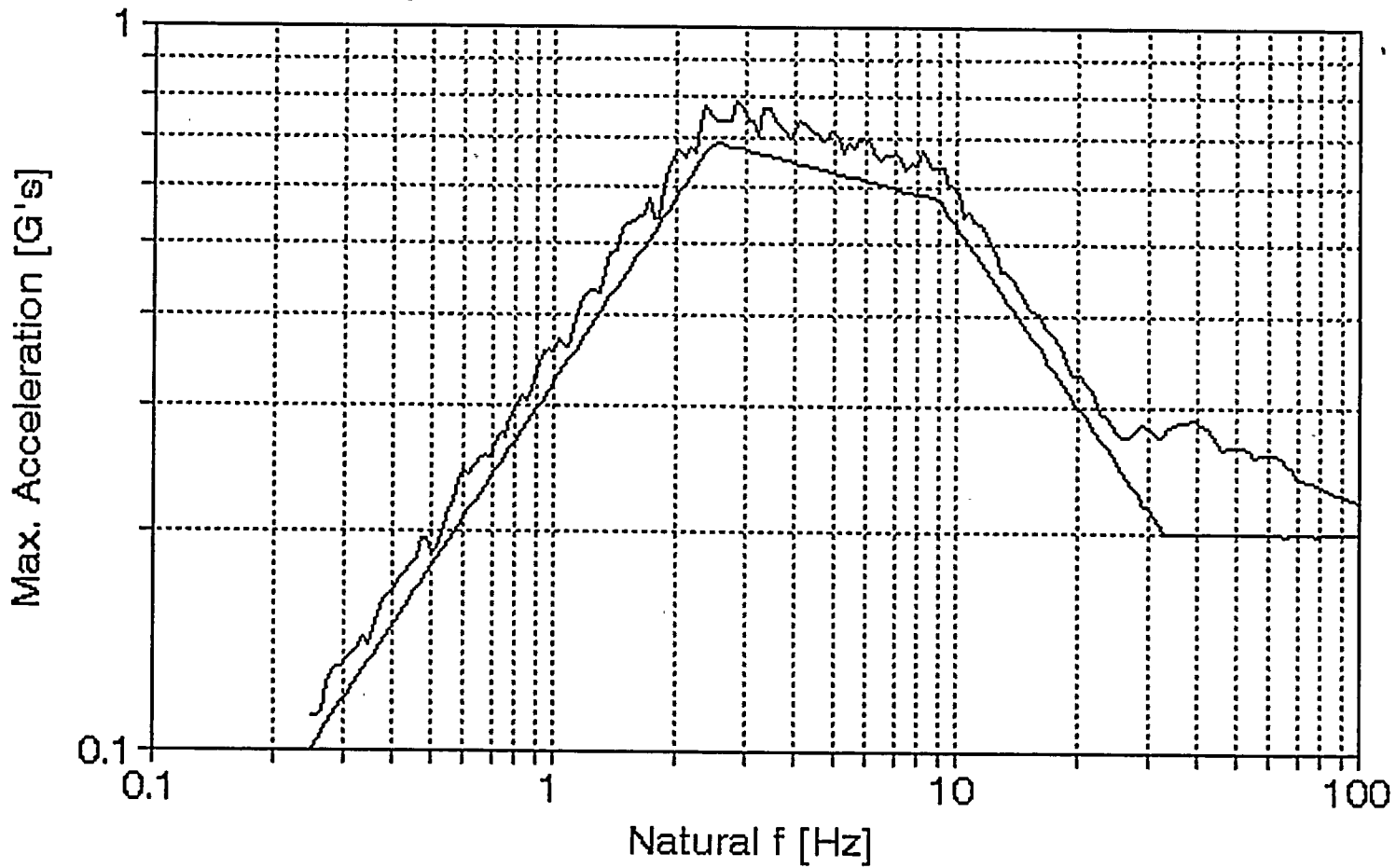
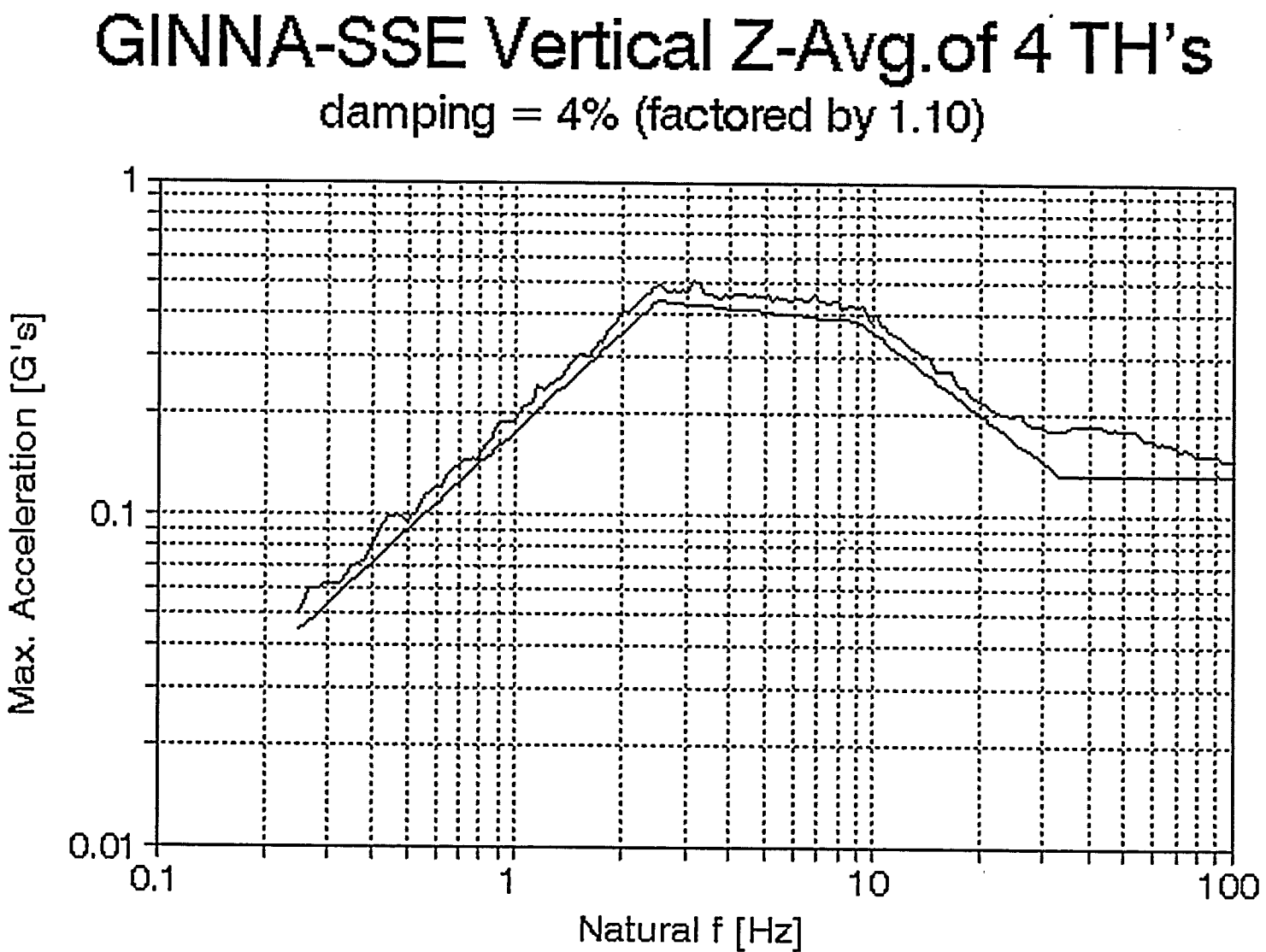


Figure 3.5-3 Avg. Calculated vs. Design Response Spectra for SSE Z-dir



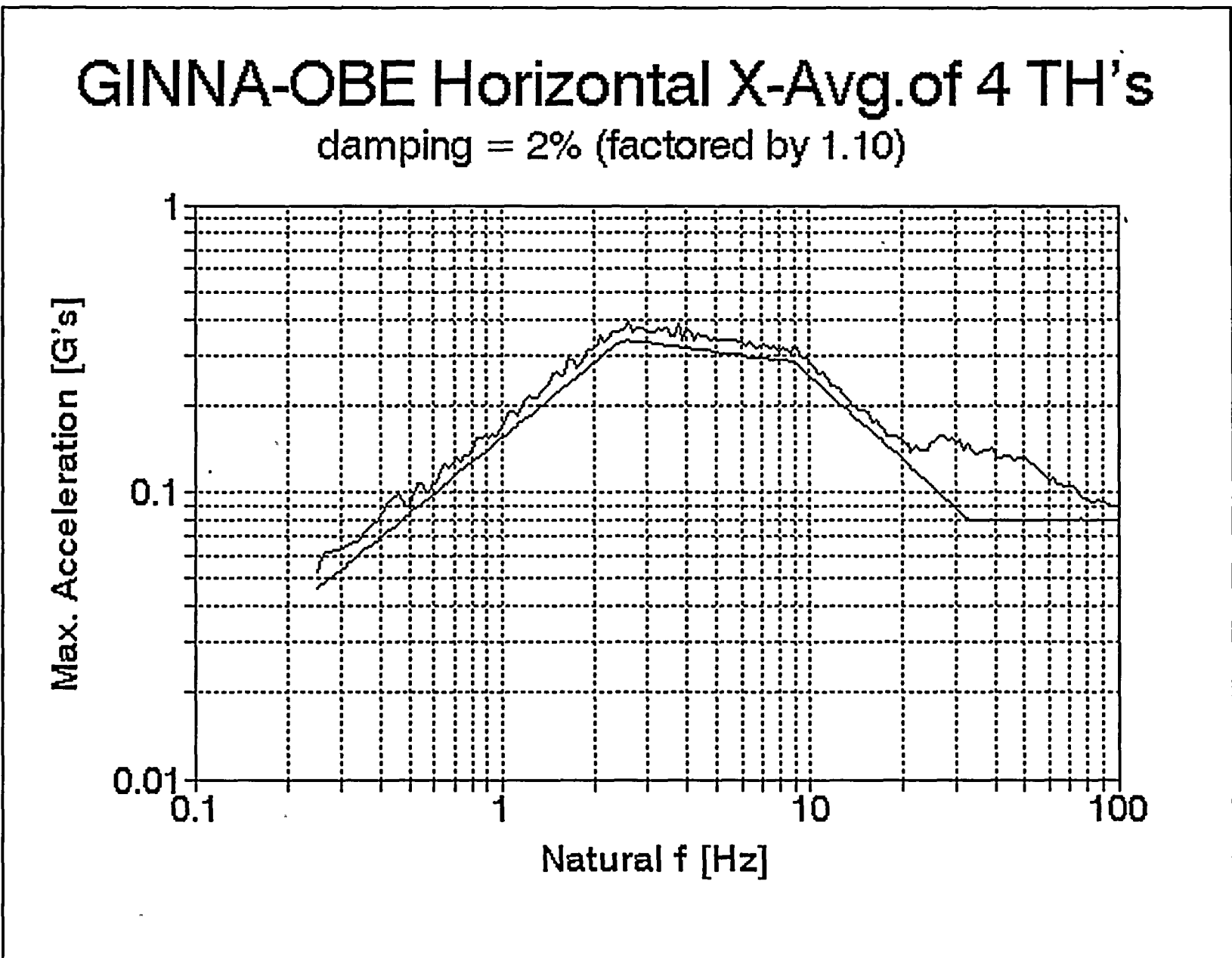


Figure 3.5-4 Avg. Calculated vs. Design Response Spectra for OBE (EW) X-dir

Figure 3.5-5 Avg. Calculated vs. Design Response Spectra for OBE (NS) Y-dir

GINNA-OBE Horizontal Y-Avg.of 4 TH's

damping = 2% (factored by 1.10)

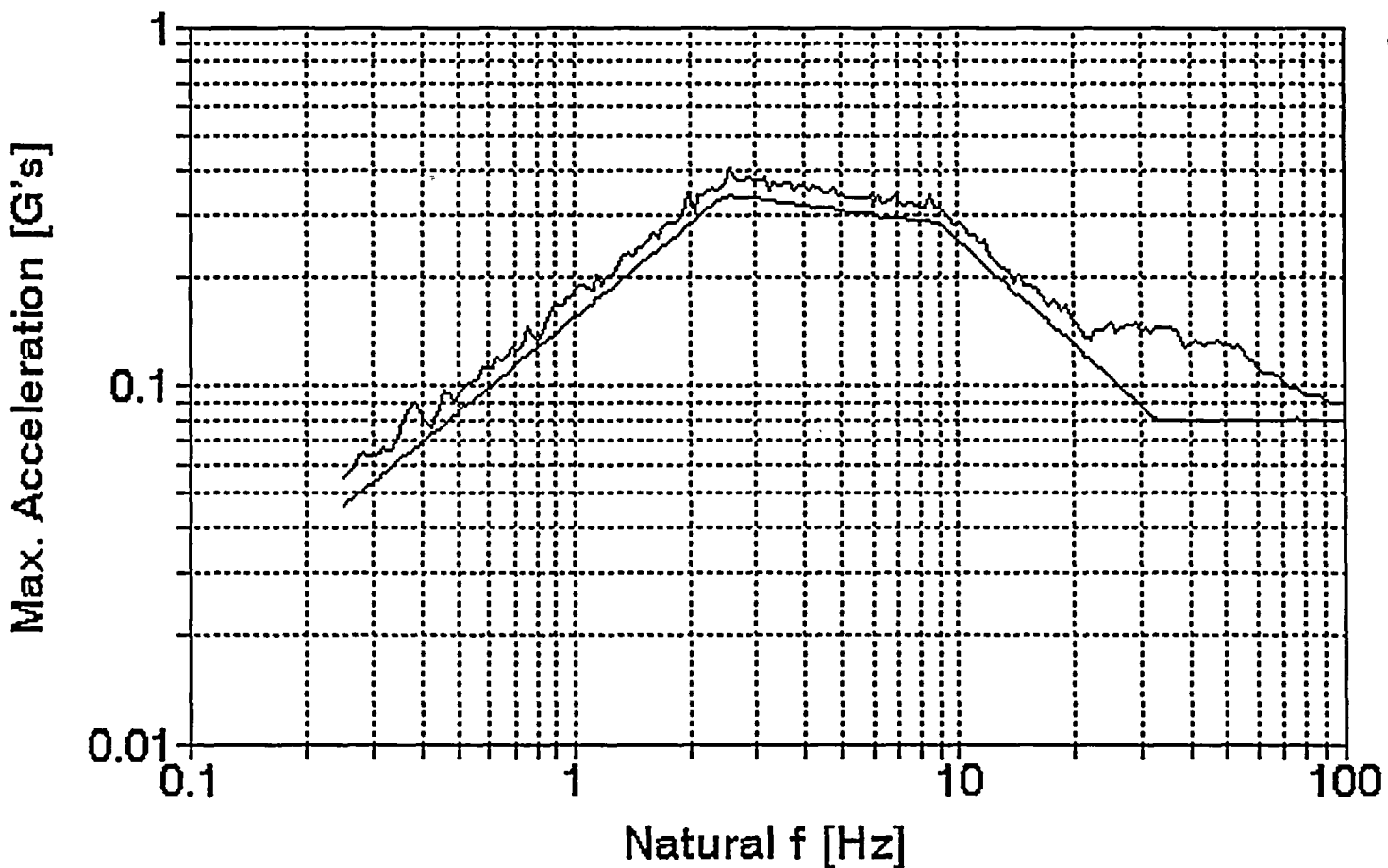


Figure 3.5-6 Avg. Calculated vs. Design Response Spectra for OBE Z-dir

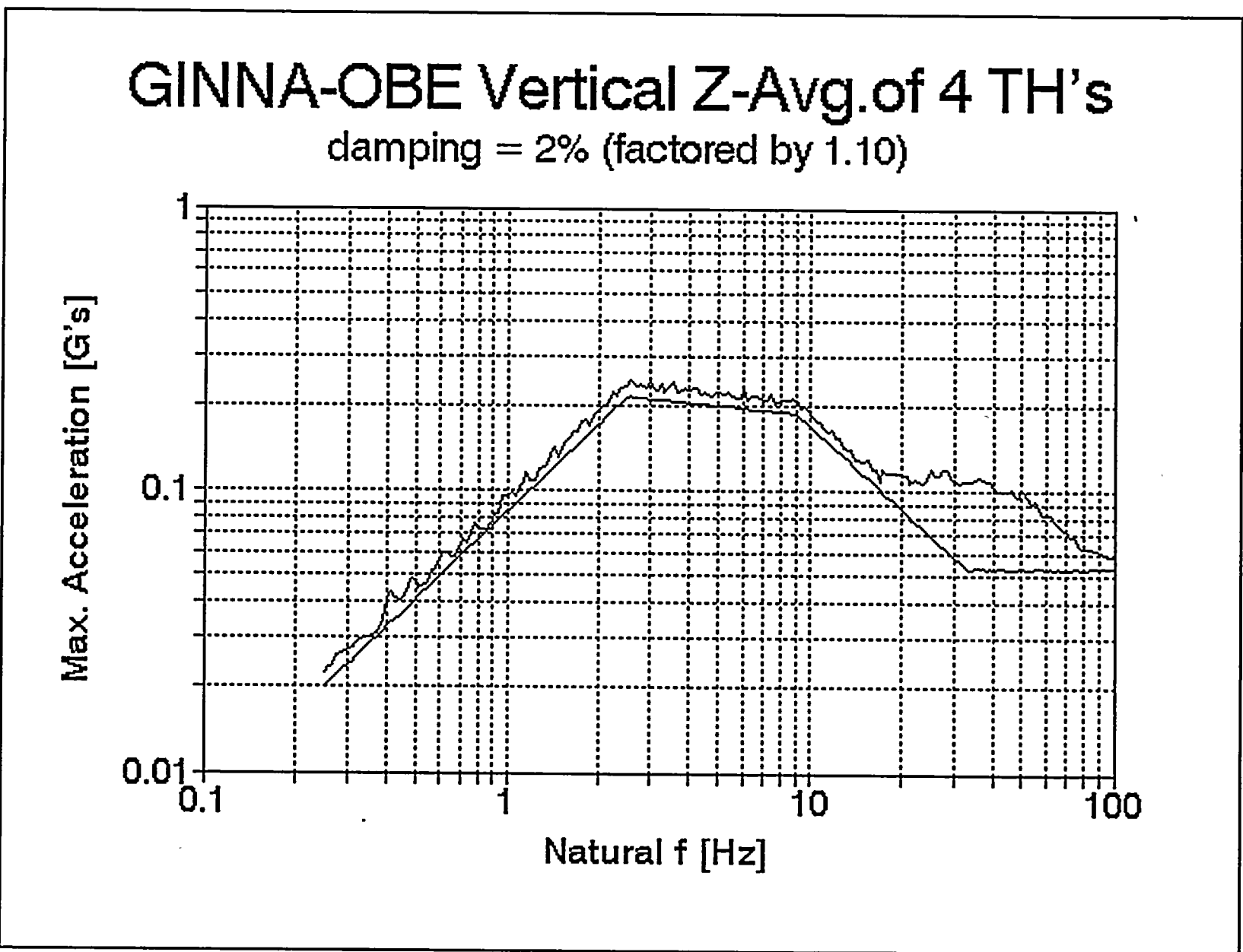


Figure 3.5-7 SSE Acceleration Time History #1 for (EW) X Direction

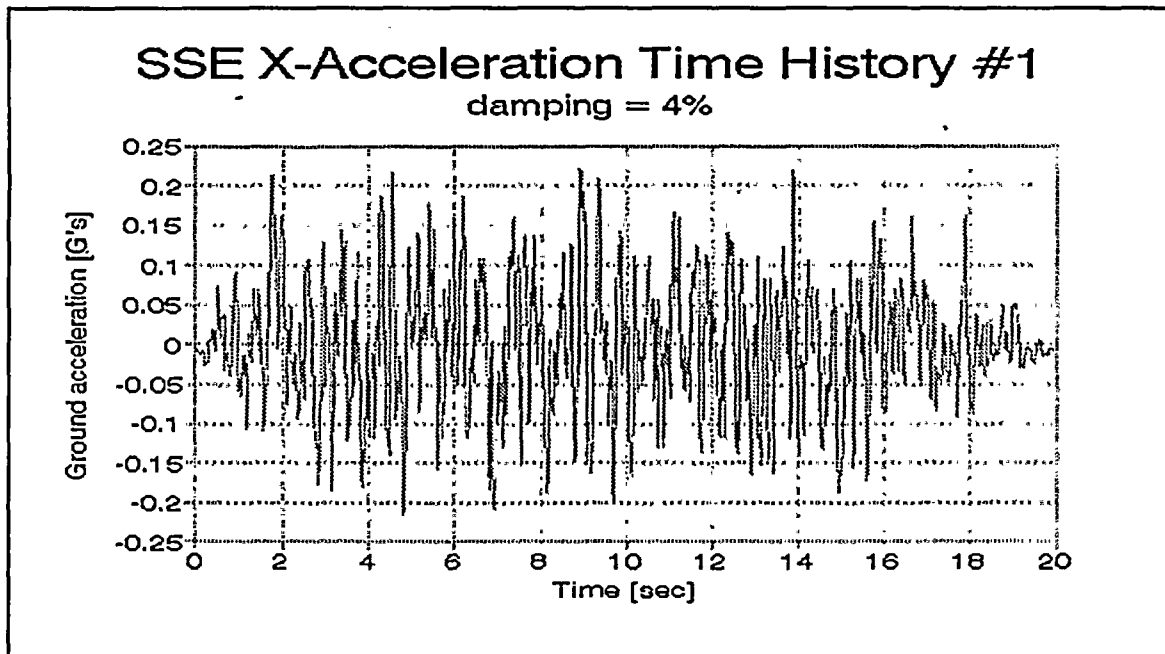


Figure 3.5-8 SSE Acceleration Time History #2 for (EW) X direction

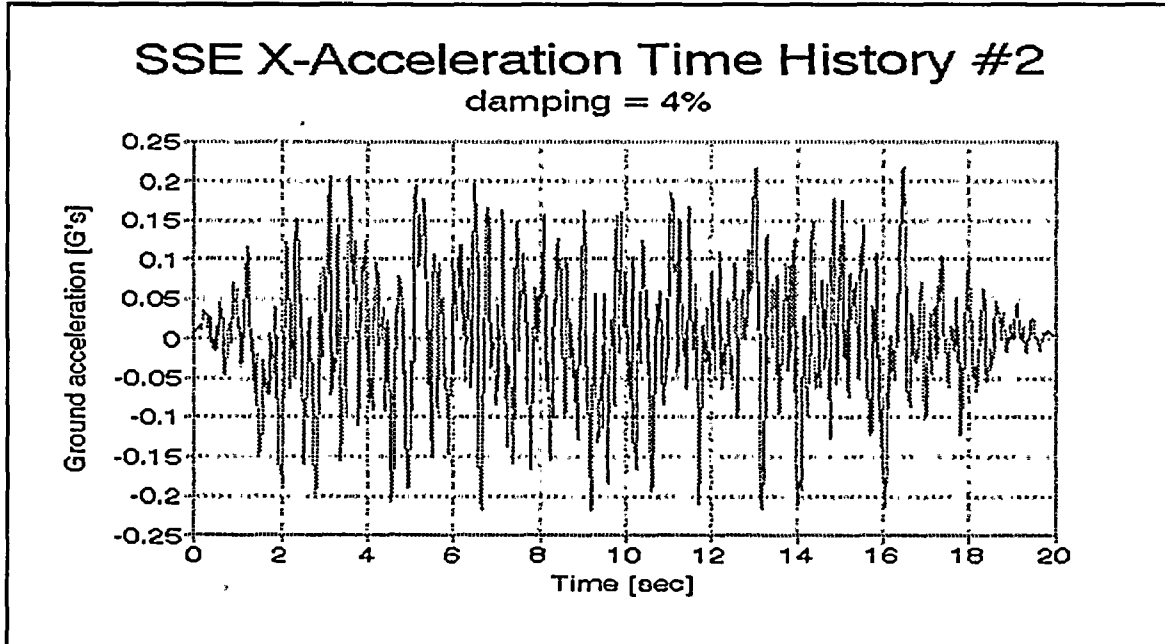


Figure 3.5-9 SSE Acceleration Time History #3 for (EW) X direction

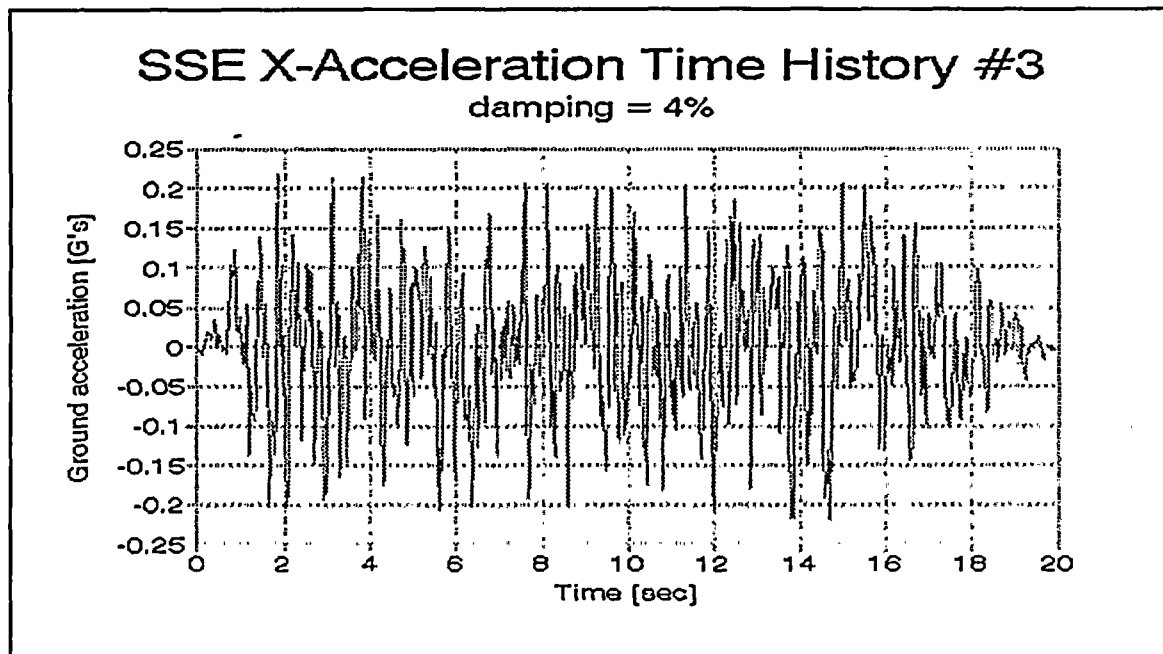


Figure 3.5-10 SSE Acceleration Time History #4 for (EW) X direction

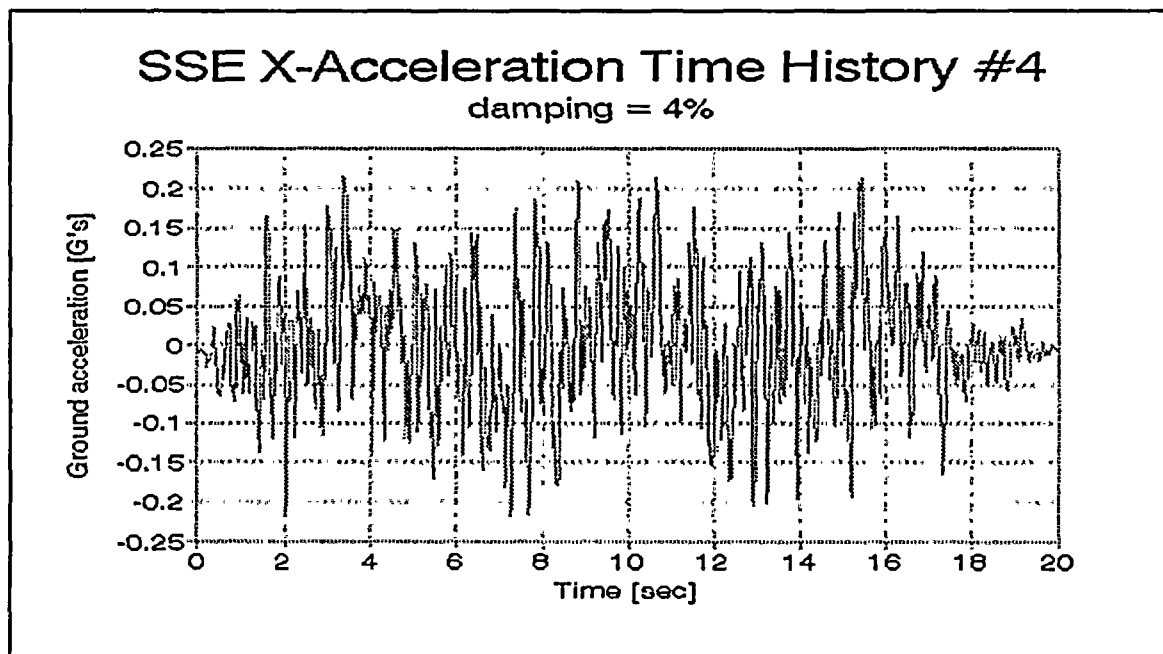




Figure 3.5-11 SSE Acceleration Time History #1 for (NS) Y direction

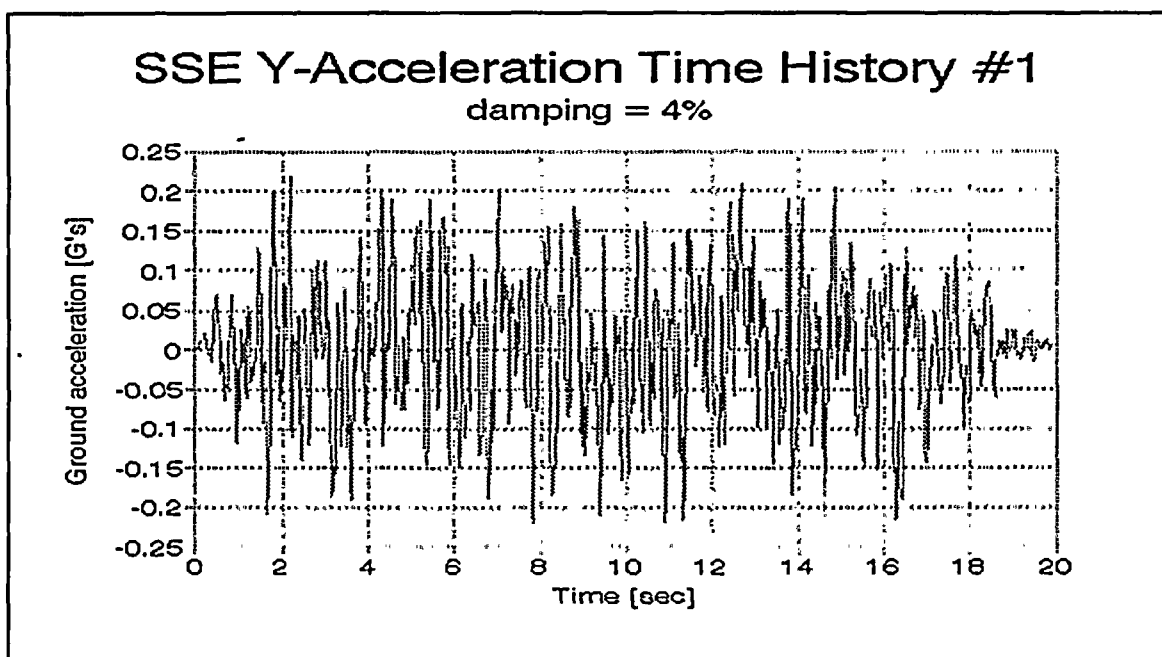


Figure 3.5-12 SSE Acceleration Time History #2 for (NS) Y direction

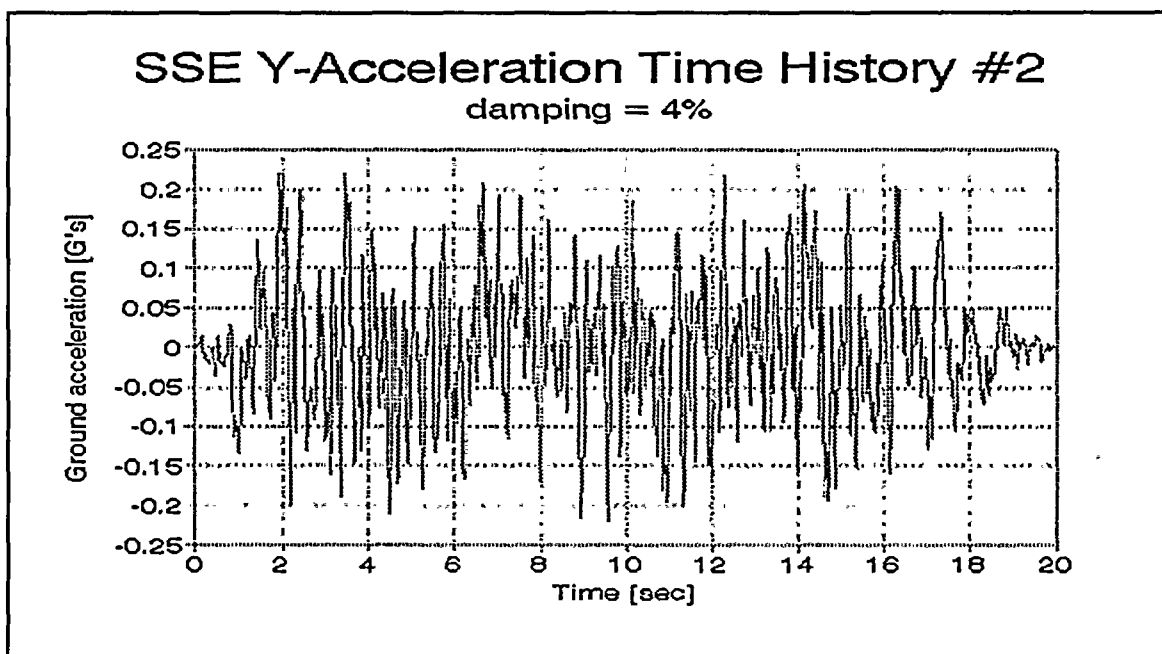


Figure 3.5-13 SSE Acceleration Time History #3 for (NS) Y direction

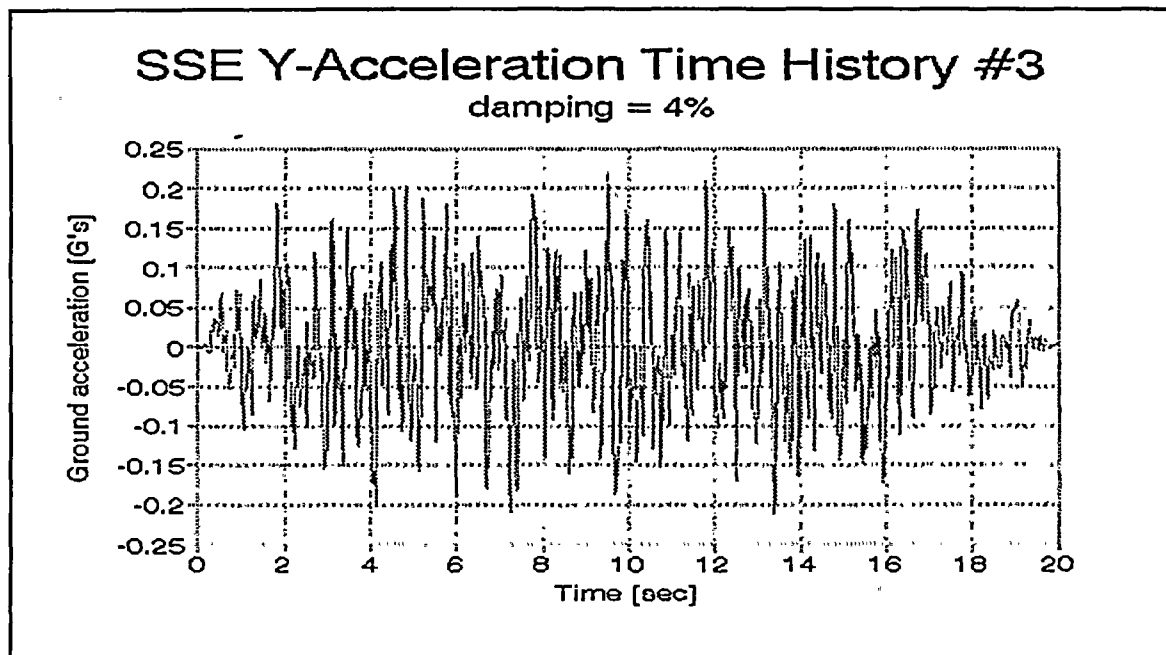


Figure 3.5-14 SSE Acceleration Time History #4 for (NS) Y direction

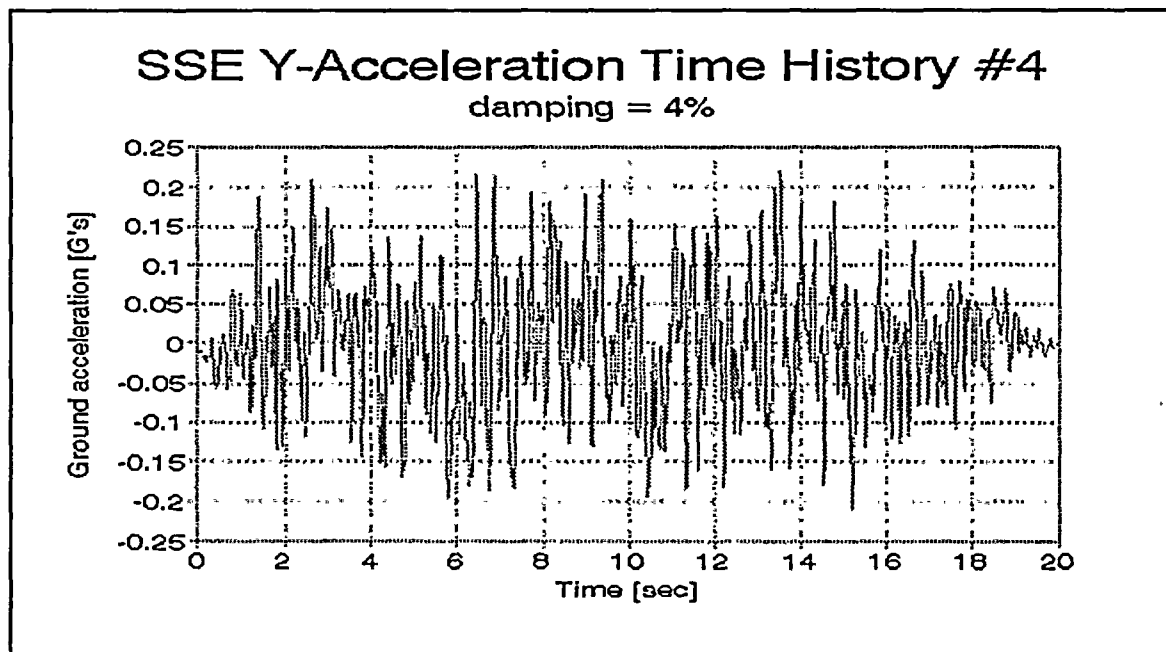


Figure 3.5-15 SSE Acceleration Time History #1 for vertical Z direction

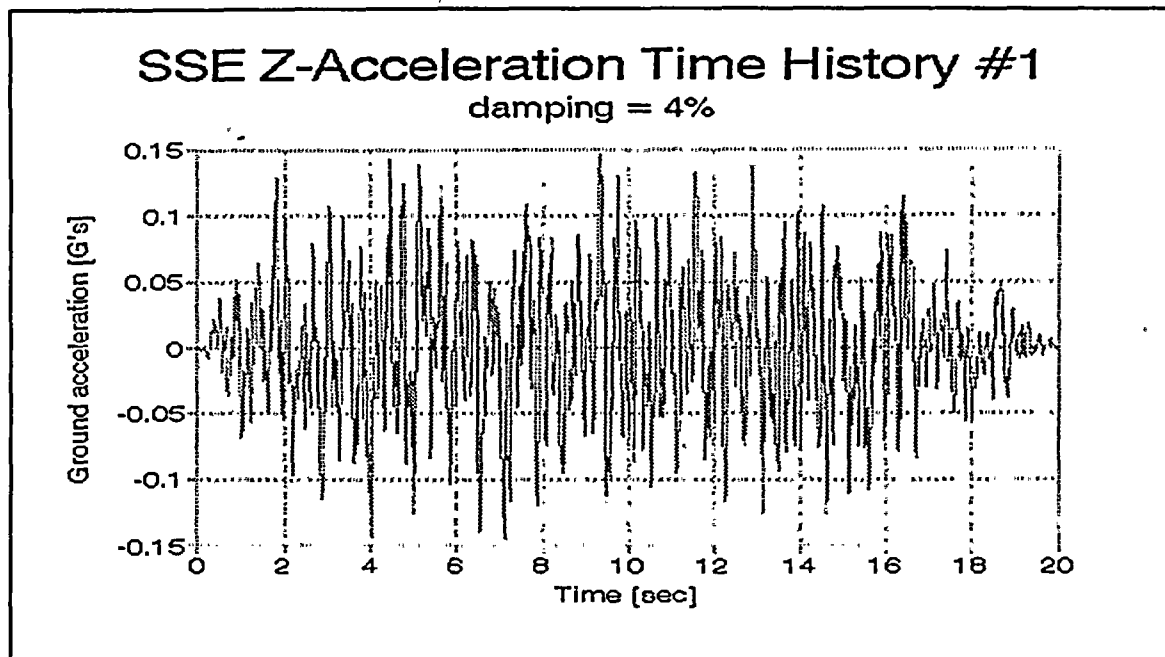


Figure 3.5-16 SSE Acceleration Time History #2 for vertical Z direction

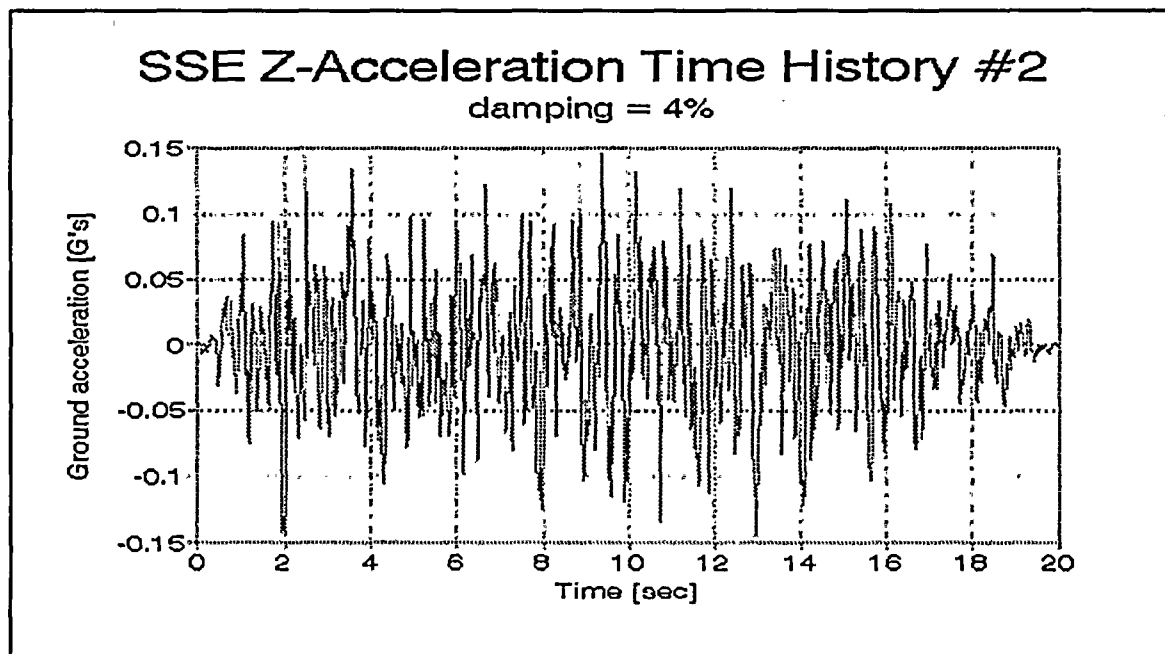


Figure 3.5-17 SSE Acceleration Time History #3 for vertical Z direction

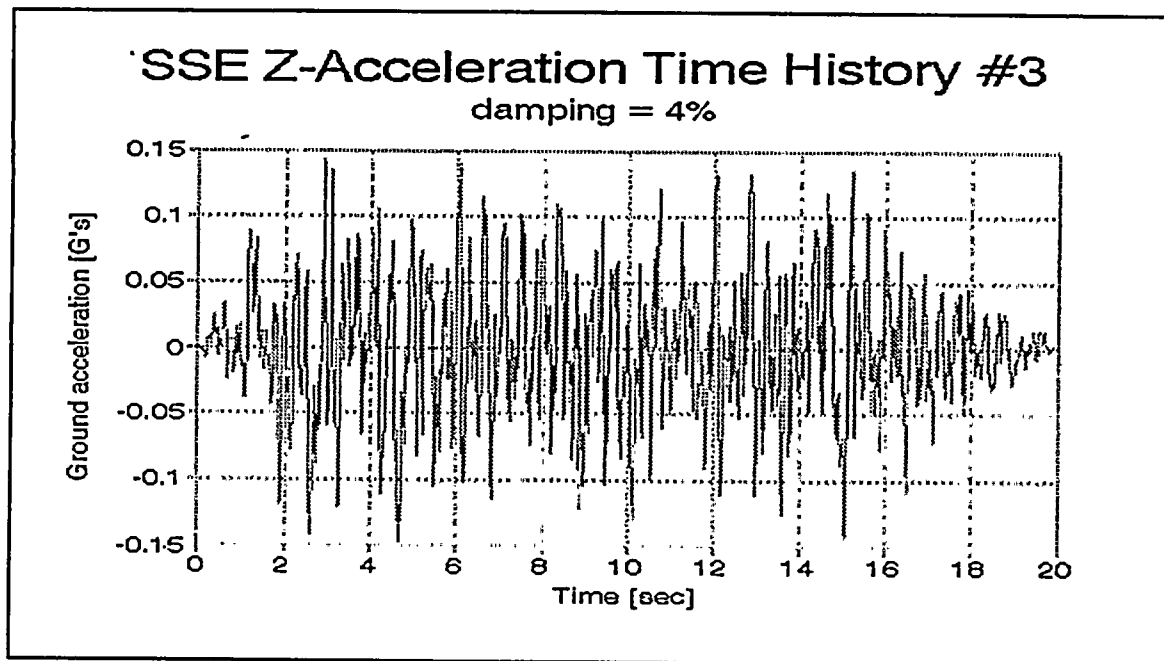


Figure 3.5-18 SSE Acceleration Time History #4 for vertical Z direction

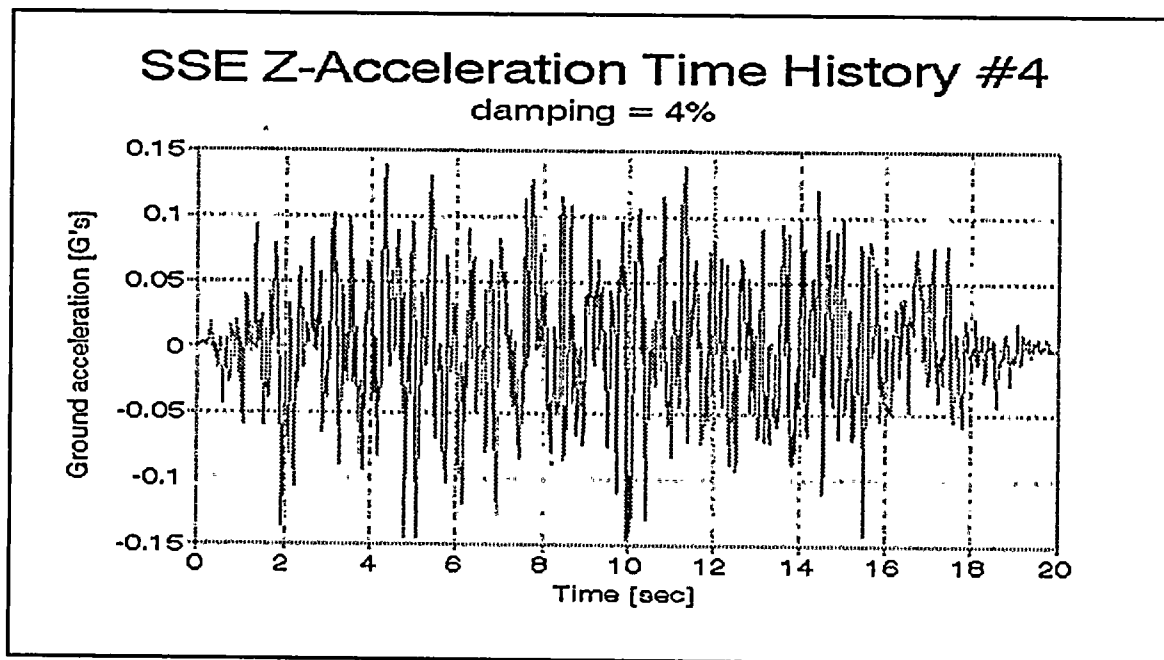


Figure 3.5-19 OBE Acceleration Time History #1 for (EW) X direction

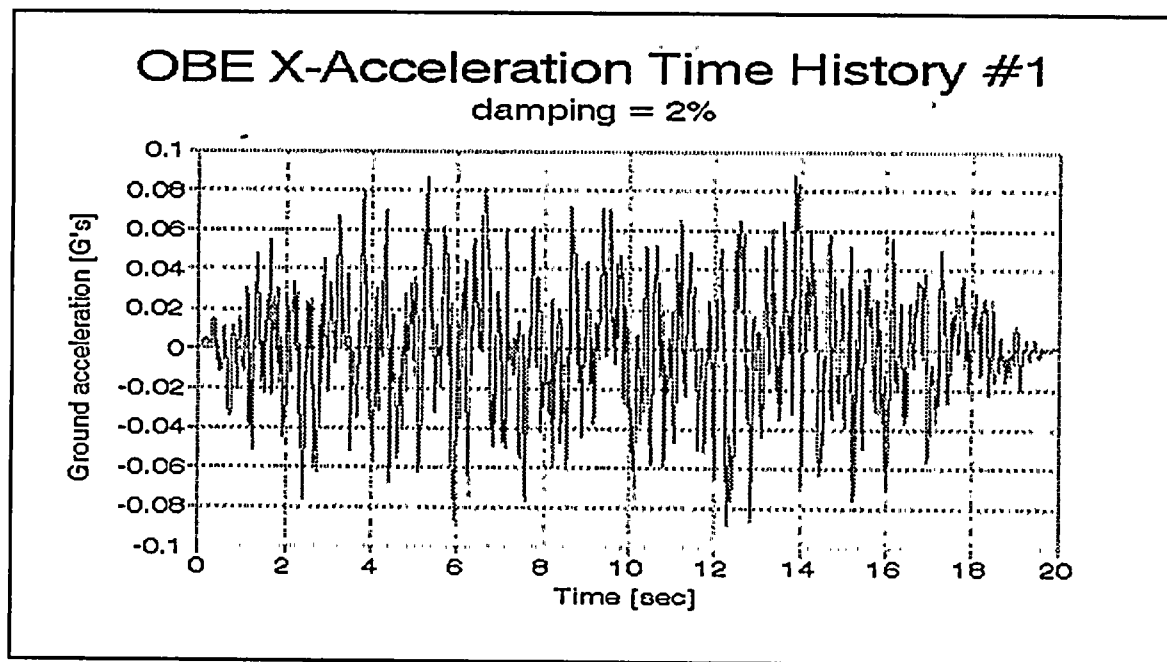


Figure 3.5-20 OBE Acceleration Time History #2 for (EW) X direction

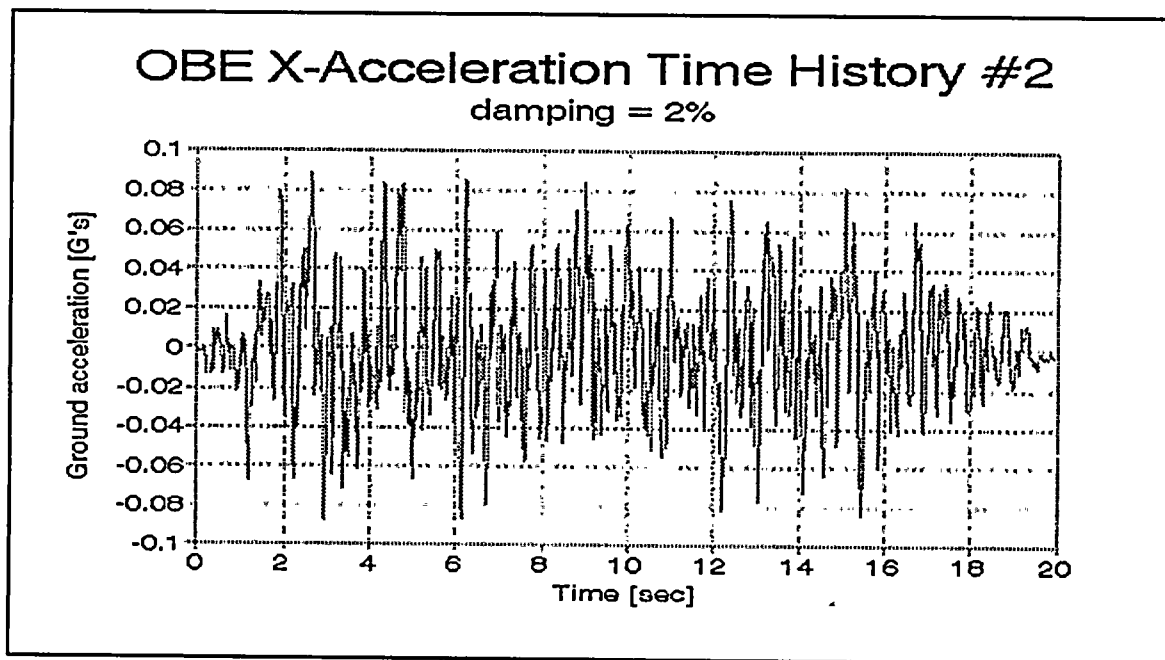




Figure 3.5-21 OBE Acceleration Time History #3 for (EW) X direction

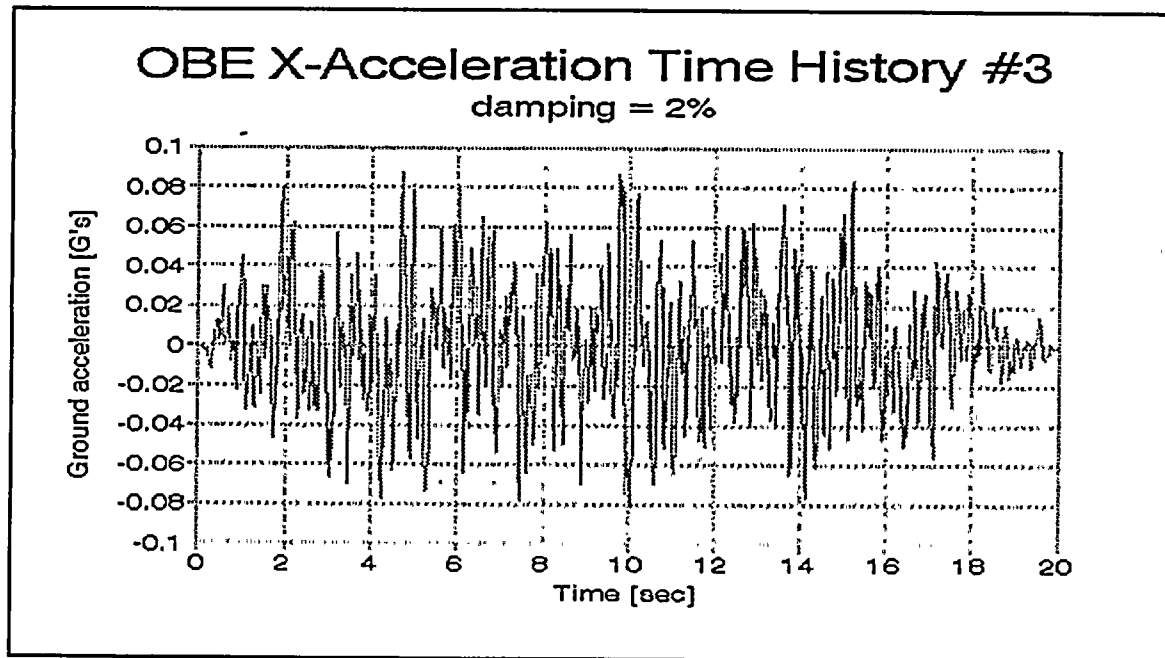


Figure 3.5-22 OBE Acceleration Time History #4 for (EW) X direction

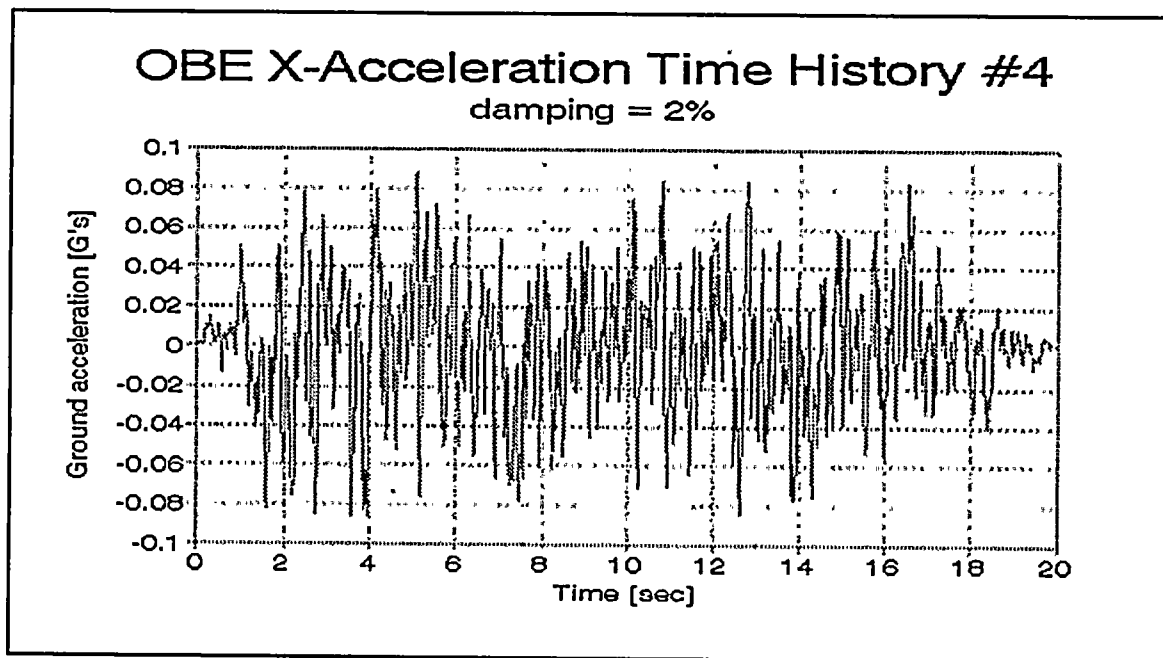


Figure 3.5-23 OBE Acceleration Time History #1 for (NS) Y direction

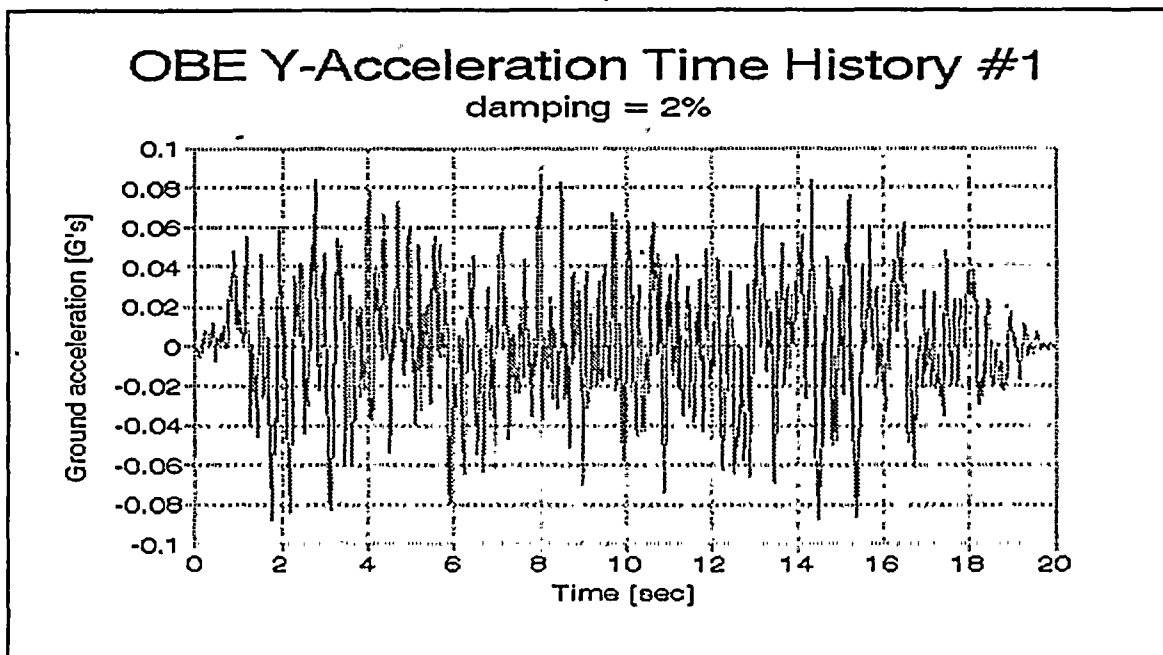


Figure 3.5-24 OBE Acceleration Time History #2 for (NS) Y direction

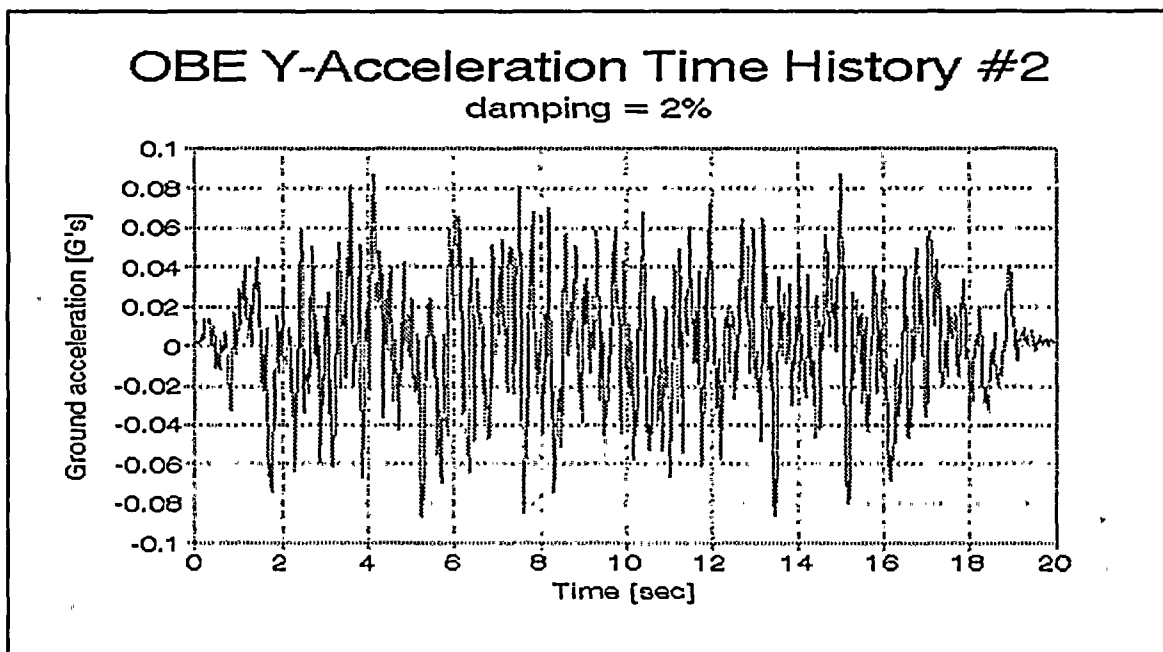


Figure 3.5-25 OBE Acceleration Time History #3 for (NS) Y direction

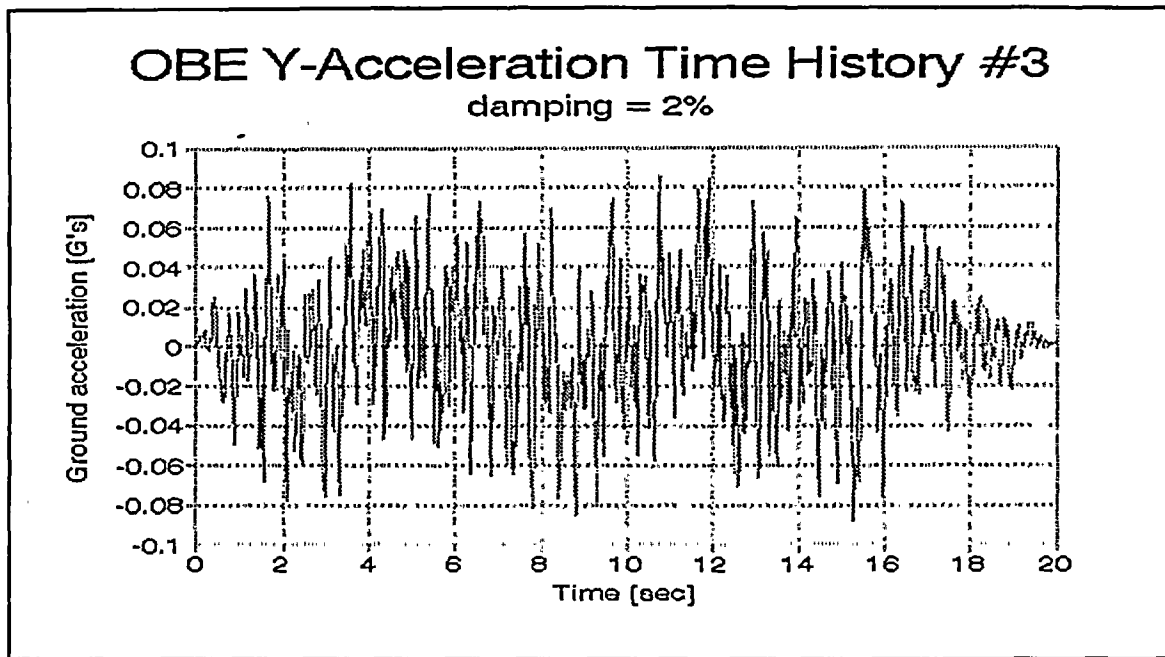


Figure 3.5-26 OBE Acceleration Time History #4 for (NS) Y direction

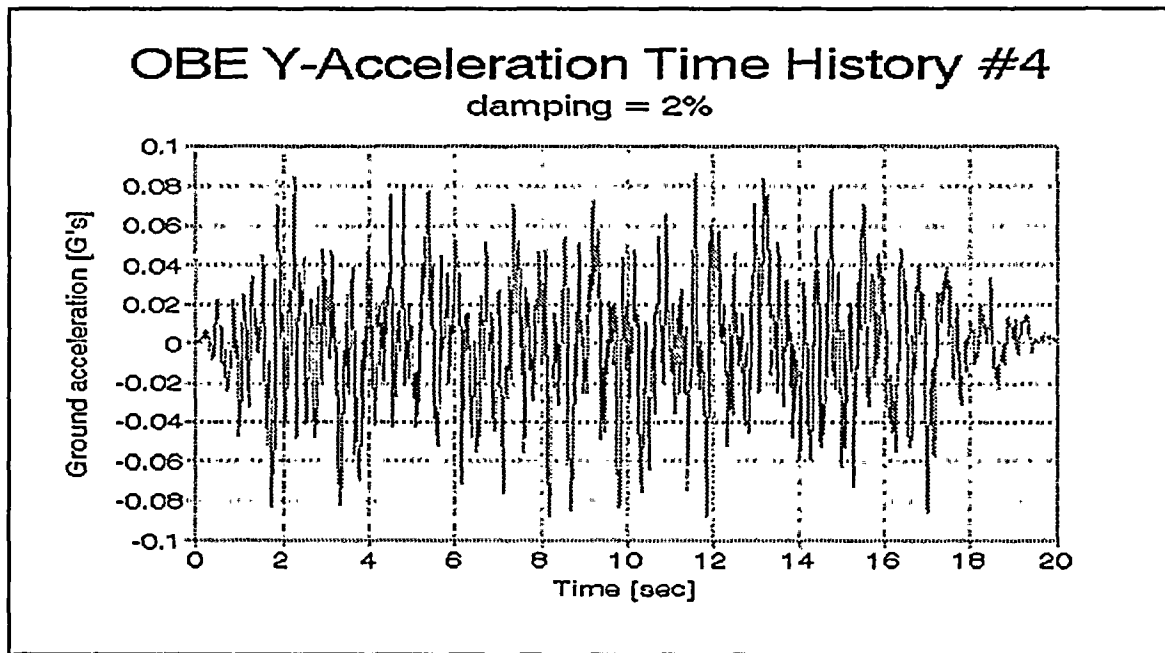


Figure 3.5-27 OBE Acceleration Time History #1 for vertical Z direction

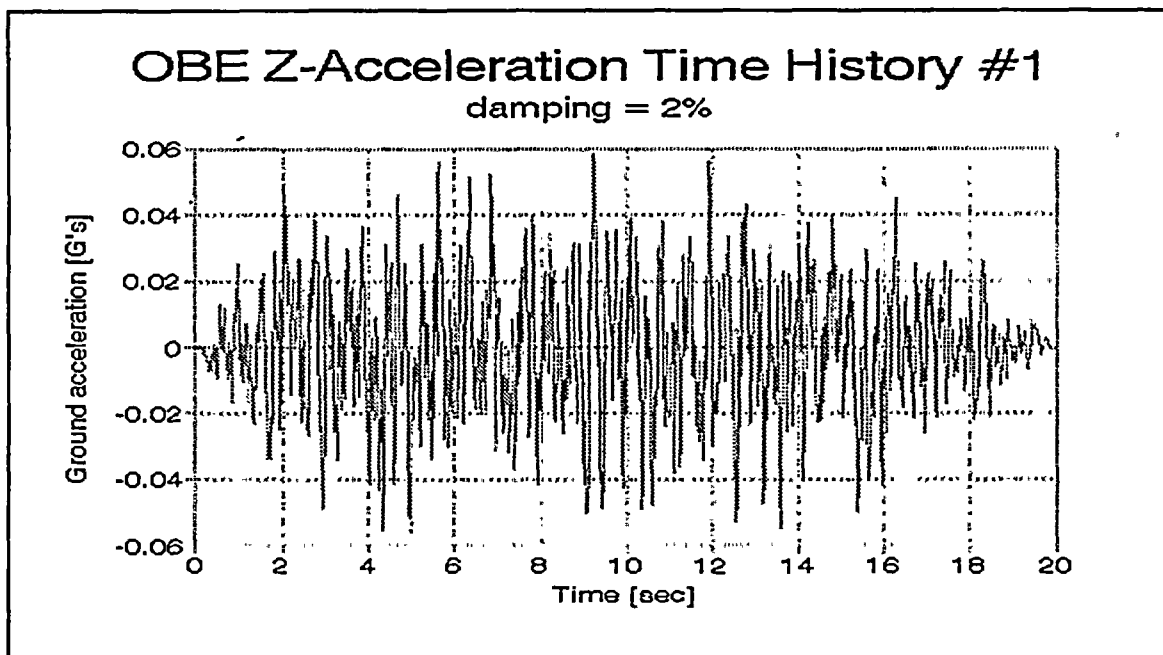


Figure 3.5-28 OBE Acceleration Time History #2 for vertical Z direction

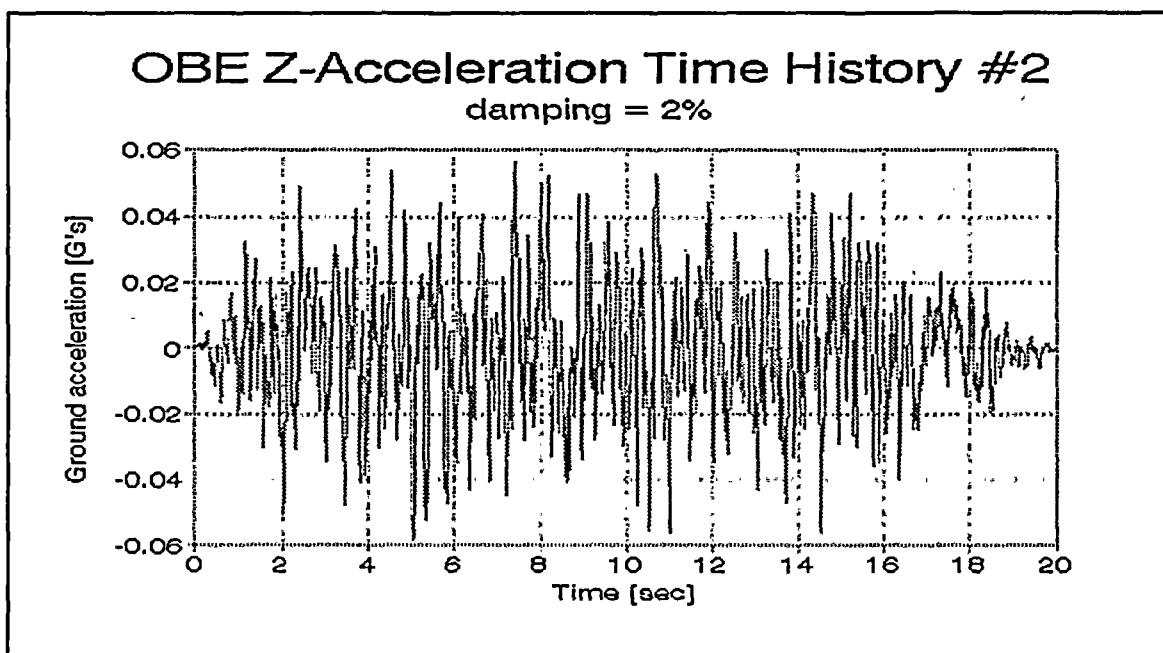


Figure 3.5-29 OBE Acceleration Time History #3 for vertical Z direction

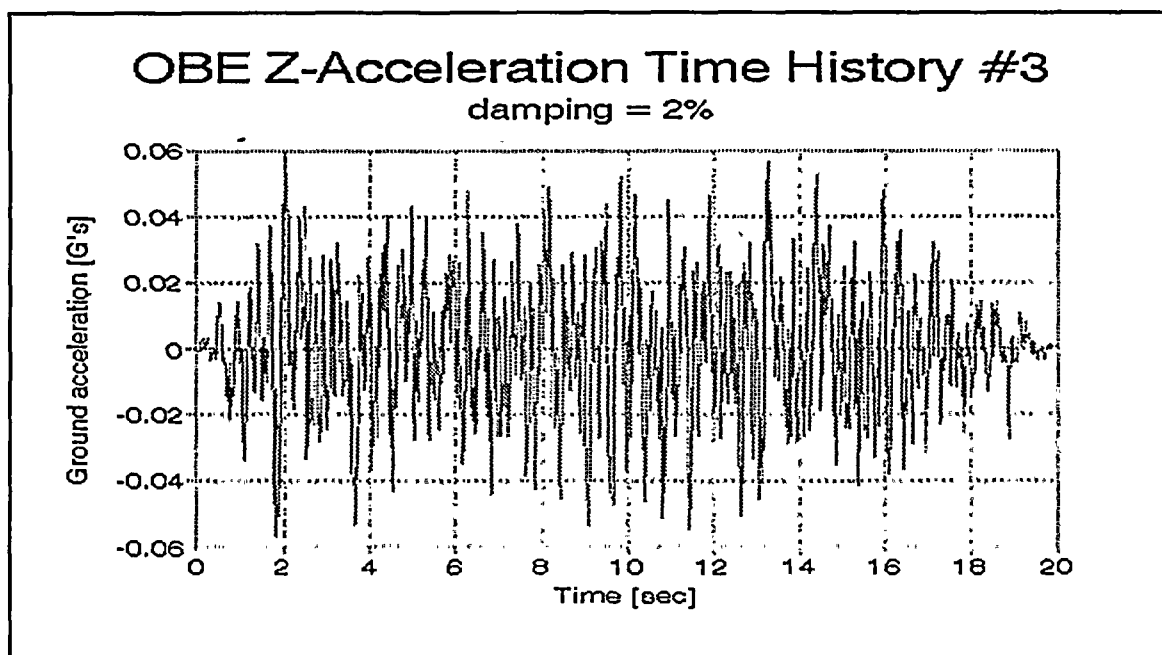
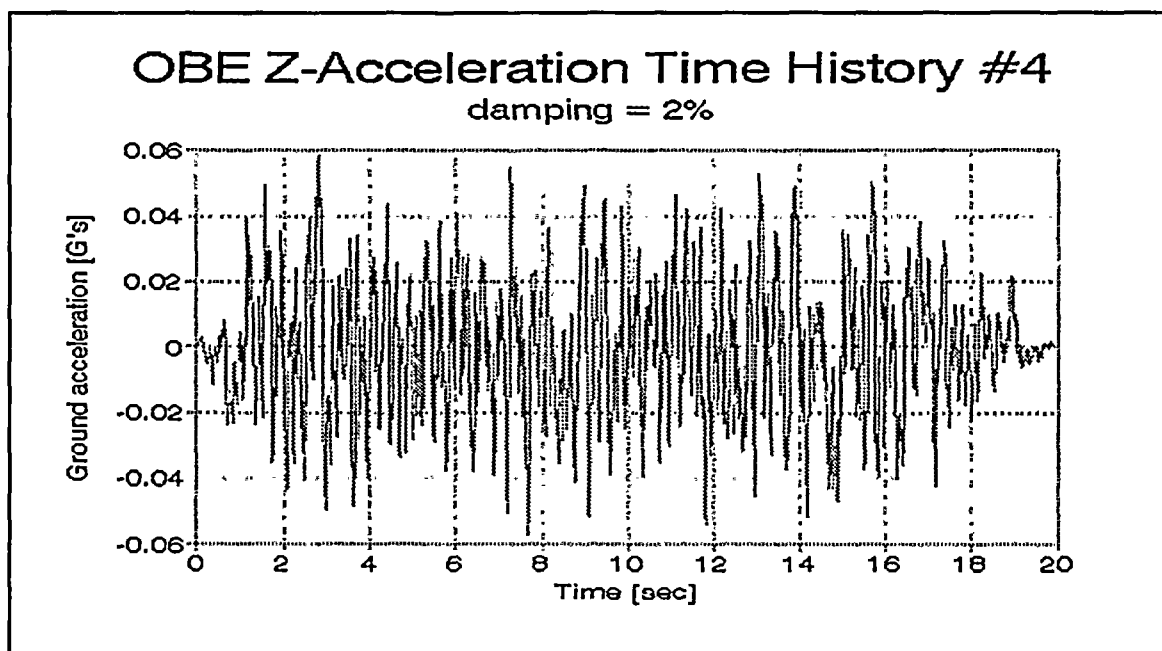


Figure 3.5-30 OBE Acceleration Time History #4 for vertical Z direction





3.5.2 Structural Analysis Methods

RG&E Ginna Nuclear Plant spent fuel storage system structure is evaluated using state-of-the-art analytical methods. To expedite Staff review, the methods used in current license applications are used here. The methods of analysis used are well documented in text books and open literature. The method and source references are identified throughout the report. The following subsections provide more details on these methods.

3.5.2.1 Assumptions - Seismic/Structural

1. Rack stainless steel responds elastically under all loading, including seismic OBE and SSE.
2. Hydrodynamic coupling terms were calculated based upon potential flow theory with consideration of horizontal flow.
3. For the 3-D single rack model and the 3-D whole pool model, a number of actual support legs were modeled by four legs placed at the corners of the rack base plate.
4. Seismic input consists of three statistically independent orthogonal time histories of motion, simultaneously applied at each pool point under rack legs, and at pool wall points hydrodynamically coupled to the rack beams.
5. Four sets of earthquake inputs were generated. All effects of the earthquake were examined; i.e., leg and pool wall reaction forces, displacements, tipping, etc. A single earthquake time history was selected for OBE and SSE conditions. In each case, a seismic response spectra enveloping factor was determined, such that the average of four developed time histories would envelop the specified floor response spectra throughout the frequency range, to meet the requirements specified in SRP 3.7.1 of NUREG 0800. A time history factor was then applied to the final results to ensure that the results would remain the most conservative and envelope all time history cases.
6. It was assumed that the hydrodynamic coupling forces were dependent upon the initial gap. The results of the 3-D whole pool analysis showed the suitability of this assumption. This was due to the fact that increases in gaps on one side of the rack tended to be offset by decreases in gaps on the other side. Further gap closures would produce higher hydrodynamic coupling forces, which would decrease further closure.
7. Coefficients of friction between 0.2 and 0.8 are adequate to cover the range between the lower and the upper friction values between the rack legs and the pool floor. A selective run was made with the coefficient of friction of 0.5 to show that loads were bounded for the coefficient of friction of 0.8, and the displacements were bounded for the coefficient of friction of 0.2.
8. Buoyancy was considered for the calculations of rack and fuel weights.

9. The use of 20.0 seconds for the duration of the seismic time histories is sufficient. It was shown that the developed time histories match the requirements specified in SRP 3.7.1 of NUREG-0800, Reference 3.2.
10. Nominal dimensions were used in the analysis.
11. Allowable material properties as specified in the ASME Code, Section III were used.
12. Hydrodynamic coupling between fuel and rack cells, between racks and between racks and pool wall was taken into account.
13. All the fuel assemblies act simultaneously to produce the maximum loading effect.
14. All rack stresses, excluding the legs and the leg weld attachments, are evaluated based upon maximum forces rather than upon time dependent forces.
15. The pool was considered as a rigid structure with regard to the seismic excitation.
16. A damping coefficient of 2% was used for OBE and 4% for SSE.
17. Borated stainless steel density and coefficient of thermal expansion were taken as the same as 304L stainless steel.

3.5.2.2 Analytical Procedure

3.5.2.2.1 Seismic Analysis

The methodology used to perform the seismic analysis of the racks is described in this section. The racks are free standing modules which are independent of each other as well as the walls. The racks are simply supported by the pool floor with no structural connection. Therefore, the racks may slide and tip.

A wide range of seismic analyses were performed accounting for:

- A. variation in coefficient of friction,
- B. variation in fuel loading,
- C. various levels of seismic activity,
- D. hydrodynamic coupling,
- E. sliding and tipping of racks, and
- F. impact of fuel assemblies within the racks.

The new racks (racks 7 through 13) to be added at the Ginna Station utilize high density, free standing spent fuel storage racks. Due to the fact that the new high density spent fuel racks are free-standing structures which are free to slide and tip, a nonlinear dynamic analysis is required to evaluate the cases of Operational Basis Earthquake (OBE) and Safe Shutdown Earthquake (SSE). The racks are of two basic design variations: namely those in Region 1 and Region 2. Region 1 is designed to accommodate fresh fuel assemblies, while Region 2 is designed to accommodate spent

fuel assemblies. In addition, Region 1 and 2 are designed to store consolidated spent fuel canisters with a 2:1 consolidation ratio. A general layout of the array of racks, Region 1 and 2, are shown in Figure 3.5-36.

The analyses were performed using several mathematical models. The models included features to allow sliding and tipping of the racks and to represent the hydrodynamic coupling which occurs between fuel assemblies and rack cells, between racks, and between racks and reinforced concrete pool walls.

A 3-D single rack beam model was used to select the appropriate parameters for the multi-rack whole pool nonlinear analysis. The 3-D single rack model simulated the three-dimensional characteristics of the rack modules in a comprehensive manner. The physical degrees of freedom such as lifting, twisting, bending, sliding, overturning, etc., were incorporated into the dynamic model as required. The 3-D single rack model could not evaluate multi-rack effects, such as relative rack-to-rack displacements, so a 3-D whole pool model was used. The 3-D single rack model was used to determine the sensitivity of various parameters on the structural response and to simplify the input for the 3-D whole pool analysis. To detect any impact between racks and/or any impact between the racks and the pool wall, additional gap elements were introduced into the 3D whole pool model. The 3-D whole pool model was used to determine all forces and moments for each rack module, and then used for the stress analysis of the racks. This model was also used to determine the relative rack-to-rack and the rack-to-wall motions.

The 3-D single rack model determined the following:

- 1) A single enveloping seismic time history factor (see Section 3.5.2.6).
- 2) Effects of rack stiffness on forces, moments and displacements (see Section 3.5.2.7).
- 3) Forces transmitted to the inter-rack connections from the peripheral racks to the existing Region 2 racks. Including parameters for these connections in the 3-D whole pool model would have made the model too complex to run for the nonlinear analysis. The 3-D single rack model was run for the rack that produced the highest load for the peripheral rack (see Section 3.5.3.1.7.3).
- 4) Effects of off-centered fuel loadings (see Section 3.5.3.1.7.4).
- 5) Comparison of single 3-D rack models with connected and disconnected fuel beams (see Section 3.5.3.1.7.5).
- 6) Effect of rack height increase (see Section 3.5.3.1.7.2).

In both the 3-D single rack model and the 3-D whole pool multi-rack model, the racks and the fuel assemblies in each rack were represented as a single member. Hydrodynamic coupling and impact forces were obtained for fuel to rack impact. Impact forces from rack support legs to pool floors were also obtained, as well as maximum loadings (both vertical and lateral) on the support legs.

Detailed descriptions of the 3-D single rack model and the 3-D whole pool model used in the analysis are given in Section 3.5.2.3.

The other models used in the stress analysis included (1) a 3-D single rack plate model and (2) single cell models with tabs. The 3-D single rack plate model was used for the static stress, thermal, and the base plate stress analysis. The single cell models with tabs were used to determine the distribution of the local fuel to rack impact loadings.

The 3-D whole pool model was run for twelve (12) different pool loading configurations as described in Section 3.5.2.3 and provided in Table 3.5-64. To account for all possible combinations, fuel loading conditions of empty, half-loaded, and fully-loaded racks were analyzed. Both normal fuel assemblies and consolidated fuel canisters were considered. Interface coefficients of friction considered for the racks were as follows:

- a) all at 0.2,
- b) one run of all at 0.5
- c) all at 0.8, and
- d) mixed, which were statistically determined as provided in Tables 3.5-65 and 3.5-66.

Maximum sliding occurs when the interface coefficient of friction is 0.2 and maximum tipping and stress occurs when the interface coefficient of friction is 0.8. Therefore, only selective runs were made with the mixed coefficients of friction.

The maximum loads for each rack and relative gap closures between racks were determined. The maximum loads generated onto the resident racks were then compared with the loads used for the original licensing of the racks (racks 1 through 6).

3.5.2.2.2 Structural Analysis

3.5.2.2.2.1 Rack Stresses

The results of all the dynamic analysis runs included both seismic and dead loads. For both OBE and SSE conditions, all acceleration time histories were amplified by a seismic response spectra enveloping factor of 1.1. As described in Section 3.5.2.6, a time history factor of 1.2 applied to the SSE loads would completely envelop loads generated from all four of the SSE time histories. Similarly, a factor of 1.12 was developed for the OBE loads.

The accompanying Tables 3.5-141 through 3.5-146 list the stress allowable and the results of the analyses. Stresses in the tubes were calculated from the 3-D whole pool model based upon the overall moments and shears applied to the rack. In addition, the fuel to rack impacts causes bending stresses in the walls of the structural tubes. Since the tubes act together in resisting seismic loads, shear forces must be transferred through the connecting tabs. Due to these shear forces, the tab plates are subjected to shear and bending moments. The welds are, therefore, subject to stresses due to tab plate bending and shear.

The connecting tabs are used to connect structural tubes together so that the rack acts as a structural element. The tab and weld arrangements and results are described in Section 3.5.3.1.2.



The tabs are designed to be capable of carrying the shear flow from one tube to the next. Due to the grid arrangement, the shear stress in each direction will tend to be uniform in plan. Maximum base shear force, calculated from the 3-D whole pool analysis, was found in two orthogonal directions; i.e., N-S, E-W. All tabs and welds for ATEA racks are designed for the worst load cases. Results from the 3-D whole pool model analysis provide information on overall maximum stresses in cells. The output forces and stresses of all bounding runs using the 3-D whole pool model are provided in Section 3.5.3.1.8.

3.5.2.2.2.2 Support Legs and Concrete Bearing Stresses

The bearing stresses in the concrete slab and the stresses in the support legs were determined for deadweight, thermal and seismic (OBE & SSE) loadings. Boussinesq's solution (Reference 3.35) for half-space was also used to estimate bearing stresses in the concrete (see Section 3.5.3.1.5 for loads).

The maximum horizontal and vertical load inputs to the model were taken from the results from the 3-D whole pool analyses (see Section 3.5.3.1.5 for loads). The maximum support reactions, overall bending moments and forces calculated from the time history analyses were used to determine stresses in the support legs and reinforced concrete.

According to Reference 3.22, the average concrete strength of the spent fuel pool concrete is 3,000 psi. The average pressure (bearing) under the bearing pad shall not exceed the design basis pressure for a dead load or seismic load.

The maximum bearing stress in the concrete was calculated by taking the maximum vertical support leg loads determined from the 3-D whole pool analyses and dividing by the area of the bearing pad.

As another check for bearing stresses, Boussinesq's solution for half-space was used. In this method, it was assumed that a normal force is acting on the plane boundary of a semi-infinite solid. All results are summarized in Section 3.5.3.1.9.

The stress allowable pertaining to the support leg, analysis details and tabulated results are given in Section 3.5.3.1.9.

3.5.2.2.2.3 Weld Stresses

The weld patterns of connecting tabs were calculated for each rack in Region 1 and Region 2. The controlling load combinations were the consolidated fuel case for both OBE and SSE conditions with the coefficient of friction of 0.8.

The structural tubes are welded to the base plate by means of fillet welds. The welds transfer the base shear forces and the base bending moments from the tubes to the base plate. The base shear in either the E-W or N-S direction is assumed to cause longitudinal shear stresses in the welds oriented in the E-W and N-S directions, respectively. The bending moments cause vertical shear stresses in the welds.

The weld material is 308L, for which the minimum tensile strength is
 $S_u = 70,000$ psi

Weld stress limit to $0.3S_u$ for Service Level A

= 21,000 psi.

Weld stress limit to $0.42S_u$ for Service Level D

= 29,400 psi @ $T_0 = 180^\circ\text{F}$

The results of the maximum tab and tube weld stresses are listed in Tables 3.5-144 and 3.5-145.

3.5.2.2.2.4 Fuel-to-Rack Impact Loads Evaluation

The loading due to fuel assemblies was considered for unconsolidated, consolidated, half-full and empty conditions. The impact forces between the fuel assemblies and rack cell are presented in Section 3.5.3.1.6. In all cases for the OBE and SSE, the case of unconsolidated fuel caused the greatest seismic fuel-to-rack impact loading to occur. The hydrodynamic coupling between the unconsolidated fuel and the rack cells was much lower than the hydrodynamic coupling between the consolidated fuel canisters and the rack cells, thus permitting greater impact to occur.

The analysis was performed to demonstrate the fuel rack-cell wall structural integrity due to impact loading of fuel assemblies. The local stress in the rack cell was calculated from the peak impact load obtained from all the dynamic analysis runs that included both seismic and dead loads. The stress limits specified for Level B loadings (OBE) and Level D loadings (SSE) given in the ASME Section III Code (Reference 3.19) were used to obtain the limiting impact load.

The stresses in the rack cell were determined using a finite element model of a single cell. For this analysis, the base of the plate was assumed fixed, the other edges along the height of the cell were assumed simply-supported, and the top edge of the cell was assumed free. The model was constructed of shell elements with ANSYS 5.2 (Reference 3.40)

Table 3.5-58 provides the allowable load and the maximum load obtained for all of the load cases analyzed. As described in Section 3.5.2.6, a time history factor, of 1.2 and 1.12 was applied to the maximum SSE and OBE loads respectively. The calculated maximum fuel assembly-rack cell wall impact loads for the SSE and OBE cases, accounting for the time history factor, are well below the allowable load limit. This confirms the local cell wall integrity for the maximum fuel to rack cell wall impact loads.

3.5.2.2.2.5 Sliding and Tipping

In addition to the results of the 3-D whole pool analysis used to determine stresses, data is also provided on the maximum relative sliding and tipping.

The results indicate that the vibratory nature of the seismic effects precludes a significant degree of sliding and tipping. The sliding and tipping have three major effects: 1) the sliding is an energy dissipator, 2) the sliding precludes the effect of resonance since energy is not stored, and 3) both tipping and sliding limit the forces that can be introduced into the rack.



The horizontal seismic displacements of the pool floor are transferred to the racks through the support legs. The base shear force is limited by the coefficient of friction in sliding. The effective bending moment at the base of the rack is limited to that bending moment which causes some support legs to lift off. However, even after tipping has occurred, resistance to tipping is provided by the moments attributed to the extreme support legs still bearing upon the floor.

Supporting calculations for the 3-D single rack model and the 3-D whole pool model are provided in Section 3.5.3.1.1.

3.5.2.2.2.6 Expected Loads on Floor From Racks

Each rack responds to the seismic input causing peak maximum support pad loads in addition to maximum average support pad loads. The concrete bearing stresses were checked for maximum peak and average support pad loads and found to be within the allowables, as presented in Table 3.5-142. Due to the supporting surface (concrete) being wider on all sides than the loaded area (support pads), the design bearing strength was increased by a factor of two per ACI 349-85, Section 10.15, Reference 3.20. Information on the floor loads is provided in Section 3.5.3.1.5.

3.5.2.2.2.7 Pool Liner Plate Integrity Evaluation

The pool liner is subject to a top surface shearing load due to the frictional reaction load. By definition, the maximum shear force imposed by the support leg is 0.8 times the vertical force. The vertical reaction is transferred directly downward to the concrete through the liner plate. The maximum bearing stresses and tensile stresses induced on the liner are provided in Section 3.5.3.1.17.

3.5.2.3 Detailed Descriptions of Mathematical Models

The ANSYS (Reference 3.40) Finite-Element Analysis Code was used for the structural/seismic analysis of the racks. Both elastic shell element and beam element models were created. These models included features to allow for sliding and tipping of the racks and to represent the hydrodynamic coupling which can occur between fuel assemblies and rack cells, between racks, and between the racks and the reinforced concrete walls. The models used in the analysis are described in the following paragraphs.

Model 1 - 3-D Single Rack Plate Model

A 3-D Single Rack Plate Model (See Figure 3.5-33) was prepared for use in the static stress, thermal, and the base plate stress analysis. This model consisted of shell elements representing the cells of the rack. A 9x11 rack module was chosen since it holds the largest number of consolidated fuel assemblies, which will result in the greatest support pad loadings.

In the static analysis, all support pads are restrained against sliding and tipping. The maximum horizontal and vertical loads and bending moments input to the model were taken from the results of the 3-D whole pool model seismic analyses. Upper bound values are used in the selection of the seismic g loads. Therefore, though results of this analysis are considered conservative, they provide important information on pad bearing forces and stresses in the rack.

Model 2 - 3-D Single Rack Beam Model

A 3-D Single Rack Beam Model (see Figure 3.5-31) was used for parametric studies relating to the seismic dynamic analyses of the racks. The rack modules in the pool were modeled as non-linear dynamic structures taking the geometric and physical nonlinearities into consideration, and analyzed by the nonlinear time history analysis method.

The nonlinearities arise primarily from the following:

1. The support legs are free to slide in any horizontal direction and can lift off, vertically upward.
2. The fuel assembly, whether consolidated in a canister or not, is not structurally tied to the fuel rack cell. This results in either a fluid gap or an impact at any time during the seismic event.

All structural members are modeled by the ANSYS BEAM4 element. The BEAM4 element is a 3-D elastic beam with six degrees of freedom at each node. Beam elements are used to model the rack legs, the base plate, the rack tubes, and the fuel.

The fuel beam and the rack beam are vertical beams located at the centroid of the rack in the horizontal plane. The fuel beam and the rack beam are connected at the bottom end. The baseplate beams extend horizontally from the bottom of the rack beam to the centers of the corner rack cells. At the corner rack cells, rack leg beams extend vertically downward from the ends of the baseplate beams. Each leg beam represents one fourth of the total number of rack legs.

All mass is represented by MASS21 elements. The MASS21 element is a lumped mass element which can be applied in all three directions. The MASS21 element can also apply rotary inertia to represent the lumped mass more as a distributed mass.

All contact elements between the rack legs and pool liner and between the rack tubes and fuel are modeled with CONTACT52 elements. The CONTACT52 element is a 3-D point to point contact element which allows for gaps, interface stiffness, and sliding friction.

All hydrodynamic coupling between the fuel and rack, and between the rack and adjacent racks are modeled with the FLUID38 elements. The FLUID38 element is a hydrodynamic coupling element with two degrees of freedom at each node, i.e. horizontal translation in two orthogonal axes perpendicular to the vertical axes of the coupled cylinders.

The rack analysis incorporates inertial fluid coupling terms which model the effects of fluid in the gaps between the fuel assemblies and racks, between adjacent racks, and between the racks and the pool walls. The corresponding hydrodynamic masses were calculated using established methods, based on potential theory described in References 3.38.

The inter-rack hydrodynamic masses were calculated using formulations developed for rectangular shapes (Reference 3.38) assuming nominal gaps between racks. The hydrodynamic mass for concentric long cylinders given in Reference 3.38 was used for fuel-to-rack coupling terms.



Gap elements were provided in the mathematical model as follows:

- a. The fuel assembly to cell gap included an elastic spring which became effective when the gap is closed. This spring stiffness was based upon the bending stiffness of the cell walls restrained at corners.
- b. The support leg to pool floor gap was represented separately in the vertical and horizontal directions. The horizontal reaction was based upon the coefficient of friction times the vertical reaction up until the summation of horizontal reaction exceeded the horizontal inertial force, at which time the rack is assumed to slide. As a conservatism, the Rayleigh damping effect in the reinforced concrete slab was not considered, for the vertical impact support leg load.

There are two basic single rack models. The first is a representation of rack 8(2B), a 9x11 Region 2 rack designed by ATEA. The second is a representation of rack 1, an existing Region 2 rack in the R.E. Ginna spent fuel pool, with a peripheral rack, rack 4A, attached.

Model 3 - 3-D Whole Pool Model

A 3-D Whole Pool Model was used to determine the relative rack-to-rack and the rack-to-wall motions. This model was also used to determine all maximum forces and moments for each rack module. The arrangements of the Ginna spent fuel pool with seven new ATEA spent fuel racks and six resident racks are shown in Figure 3.5-36. Note in this figure that racks 1, through 6 are the resident racks and 7 through 13 are the new racks.

The individual rack models were combined as shown in Figure 3.5-32. The rack properties were taken from the rack properties for each rack. The major difference between this rack model and the 3-D single rack model was in the representation of the fuel. The individual rack model used in the 3-D whole pool model used a common node between the rack beam and the fuel beam at the base plate of the rack as shown in Figure 3.5-40. It was shown that this common node does not affect the rack forces and moments obtained from the analysis (see Table 3.5-63). The base location nodes of the rack beam and the fuel beam are connected by a spring element in the 3-D single rack model.

The fuel mass in the 3-D whole pool model is distributed with 1/4 of the total fuel mass located at the top node of the fuel beam element. One half of the total fuel mass and one half of the rack mass are located at the middle nodes of the fuel and rack beams. The remaining 1/4 of the fuel mass, 1/4 of the rack mass and the bottom rack plate mass, as well as the leg masses are combined at the bottom node.

Hydrodynamic coupling terms were calculated for each rack and then averaged for the connection between any two racks. The coupling for any perimeter rack to the pool wall was taken simply as the hydrodynamic coupling for that specific rack.

The fuel to rack hydrodynamic coupling was accounted for with one half of the coupling placed between the top nodes of the rack and fuel beams. The other half of the fuel to rack coupling was placed between the middle two nodes of the rack and fuel beams.

The other parameters used in the 3-D whole pool model are similar to the 3-D single rack analysis.

Buoyancy was considered for the calculations of rack and fuel weights.

The coefficient of friction between the rack support legs and pool liner used in the 3-D whole pool analysis corresponded to the following cases:

- i) All coefficient of friction = 0.2
- ii) All coefficient of friction = 0.8
- iii) All coefficient of friction = 0.5
- iv) Combination of friction coefficients between 0.2 and 0.8. The coefficients of friction between the rack support legs and pool liner were generated using a Gaussian distribution random number generator with 0.52 as the mean and 0.148 standard deviations. Separate calculations were carried out for both OBE and SSE conditions.

Conditions of full, empty and half-loaded with fuel assemblies were analyzed. The storage locations occupied by fuel in the half-loaded conditions were selected in such a manner that the center of gravity of the loaded racks is farthest from its geometric plane of symmetry (i.e., torsional response of rack was considered).

A total of twelve separate cases were analyzed with the 3-D whole pool model. There is a total of thirteen (13) racks in the 3-D whole pool model. The load cases analyzed are summarized in Table 3.5-64. The first ten cases assumed each rack filled with unconsolidated fuel or consolidated fuel with the coefficient of friction being varied with values of 0.8, 0.5 and 0.2. The seismic loads consist of both the SSE and OBE conditions. The last two cases (11 and 12) were run with the racks assigned various fuel loadings as given in Tables 3.5-65 and 3.5-66. Also, the racks were assigned random coefficients of friction with values of 0.8, 0.5 and 0.2 as given in Tables 3.5-65 and 3.5-66.

The kinematic criterion seeks to ensure that the rack is a physically stable structure. The physical stability of the rack must be considered with the criterion that inter-rack impact or rack-to-wall impacts do not occur. However, the impact of the fuel assembly on the cell does occur and was evaluated and accounted for.

Forces generated from the impact events between the fuel assemblies and the rack cells were considered for local as well as overall effects on the cell walls and rack module. It was demonstrated that such an impact does not lead to damage of the rack modules.

Single Cell Models with Tabs

Two 3-D finite element models of type 2 and type 3 individual spent fuel storage rack cells were made with ANSYS 5.2 using a SHELL63 element. The models were used to determine the distribution of connecting tab translational reaction loads. The finite element models for the type 2 rack cell and the type 3 rack cell are shown in Figures 3.5-34 and 3.5-35 respectively. The type 2 cell is subjected to a pressure load on the inside surface of one cell face, and a pressure load on the



outside surface of an opposite cell face. The type 3 cell is subjected to a pressure load on the inside surface of one cell face, and concentrated loads at eight belt elevations on the outside surface of an opposite cell face. The entire length of the connecting tabs is modeled such that the stiffness of the tab is represented properly.

The type 2 and type 3 cell models were loaded as described above with an arbitrary load to represent a fuel assembly loading inside and outside of a cell. The connecting tab reaction loads were then ratioed up or down based on the actual loading. These reaction loads were used to determine the stresses in the tab, and in the tab weld at each tab location. The maximum stress intensity of the cell was also obtained for the type 2 and type 3 cells from these finite element models.

Stress analysis details on the connection tabs, welds, and tube (rack cell) are given in Section 3.5.3.1.2.

Figure 3.5-31 3D - Single Rack Model

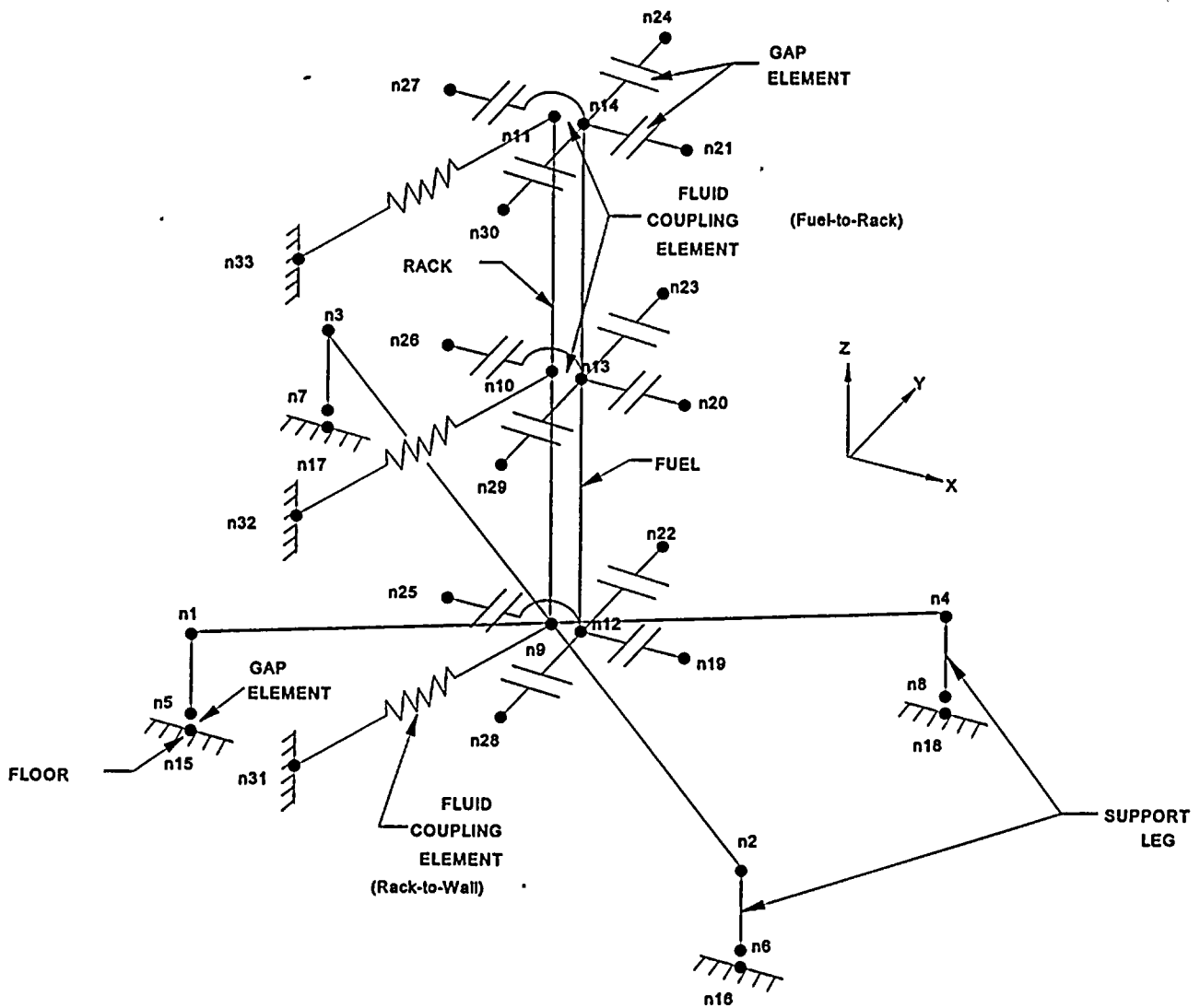


Figure 3.5-32 GINNA 3D Whole Pool Rack Model

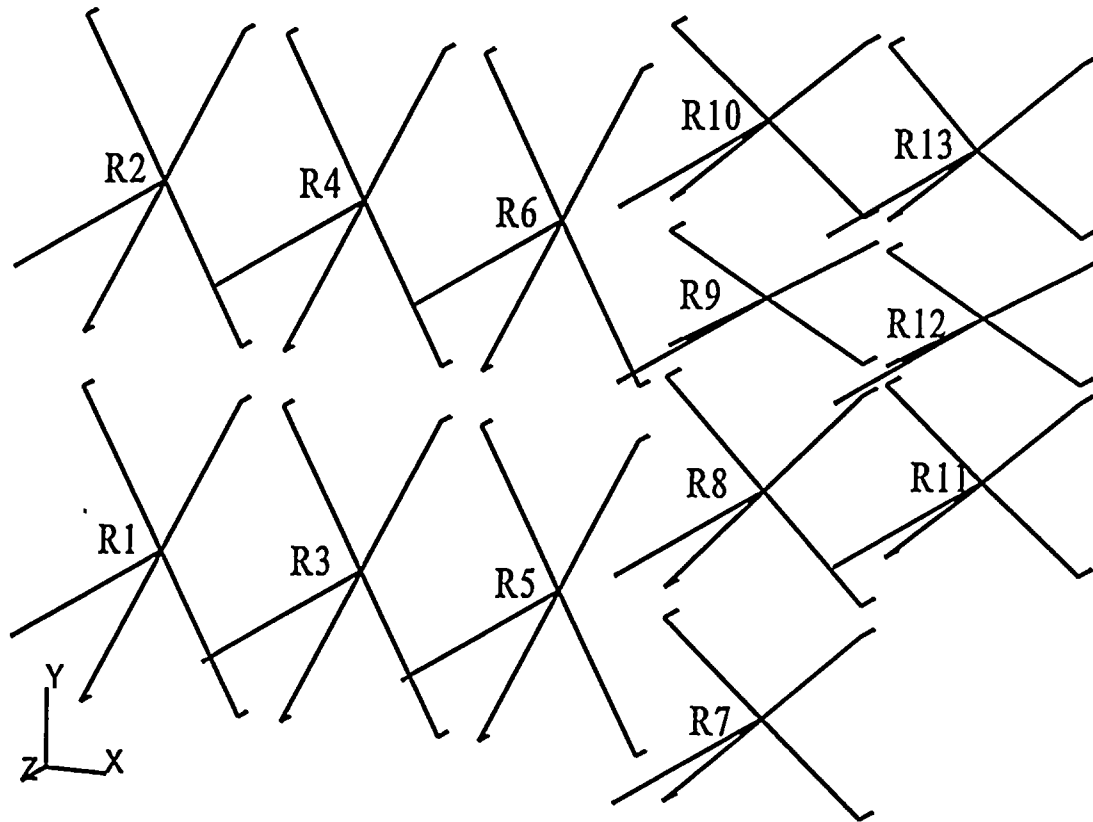




Figure 3.5-33 Single Rack Finite Element Model

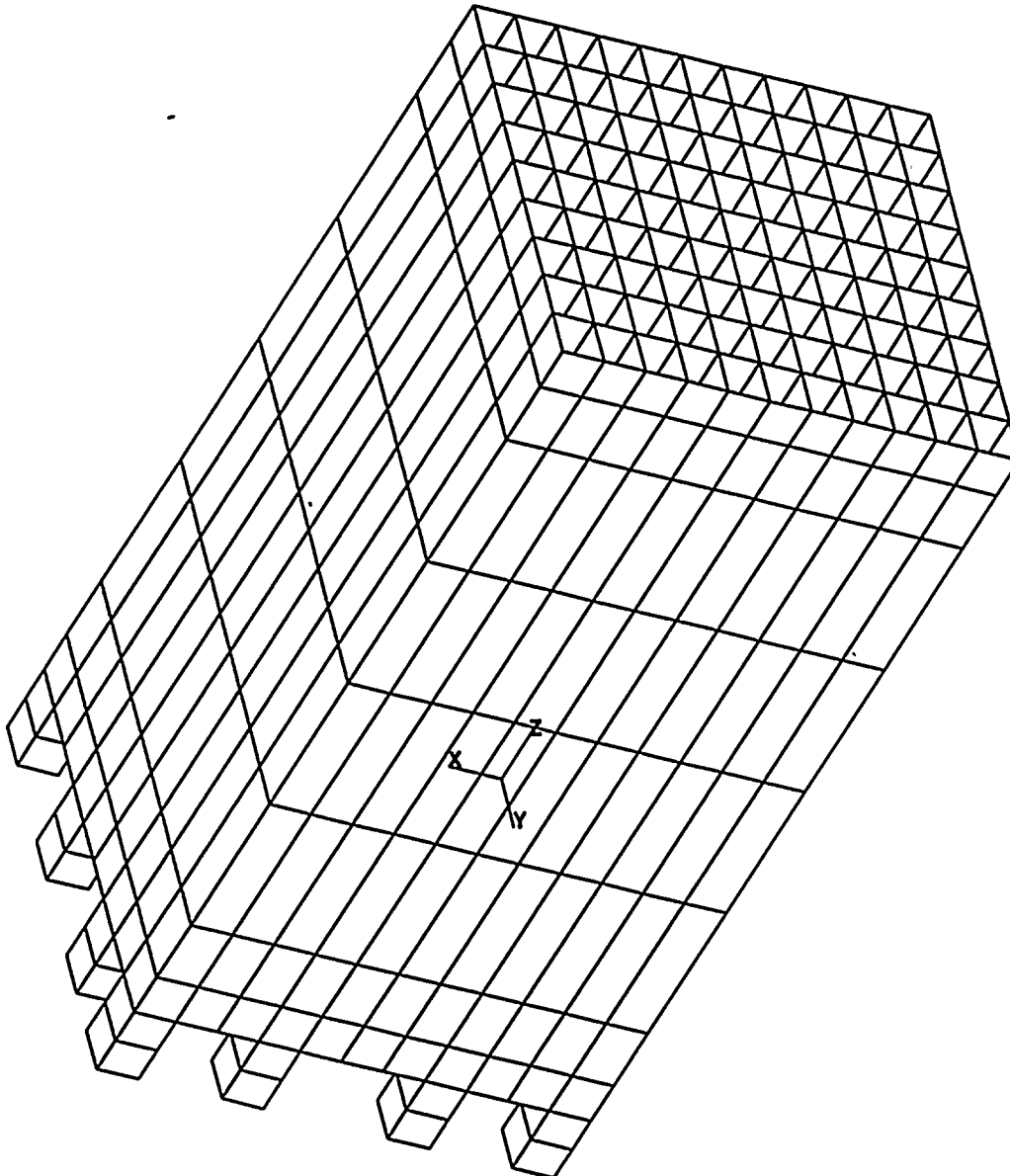


Figure 3.5-34 Ginna Type 2 Rack Cell Finite Element Model

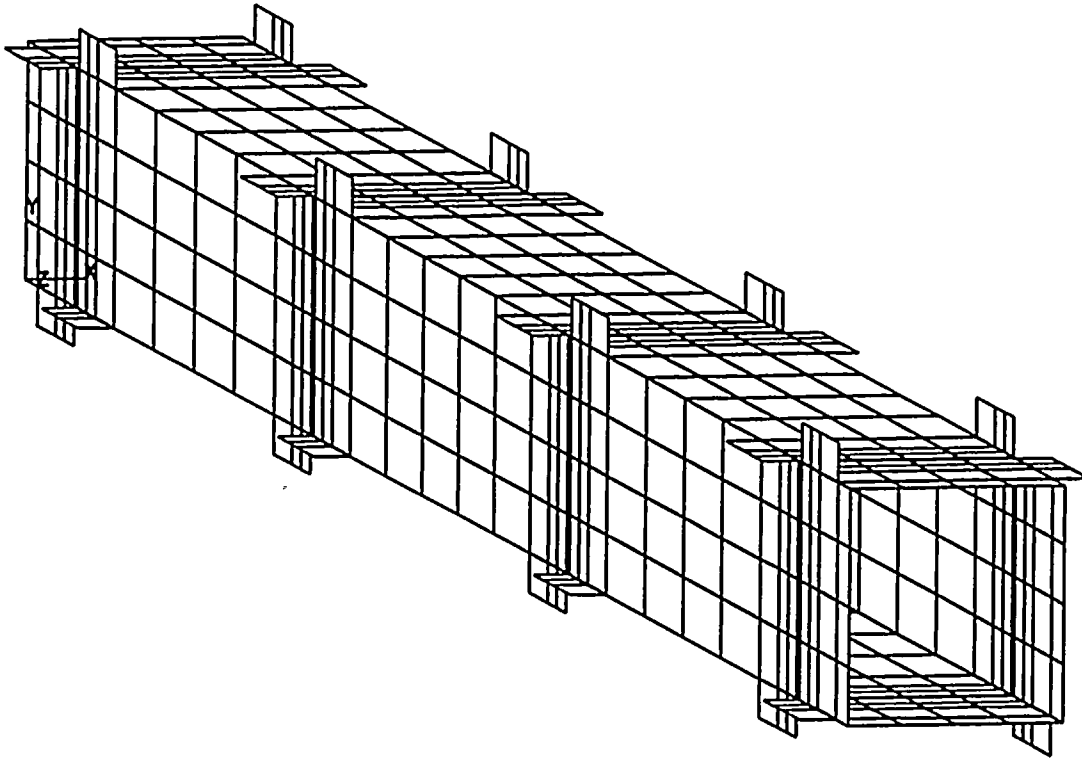
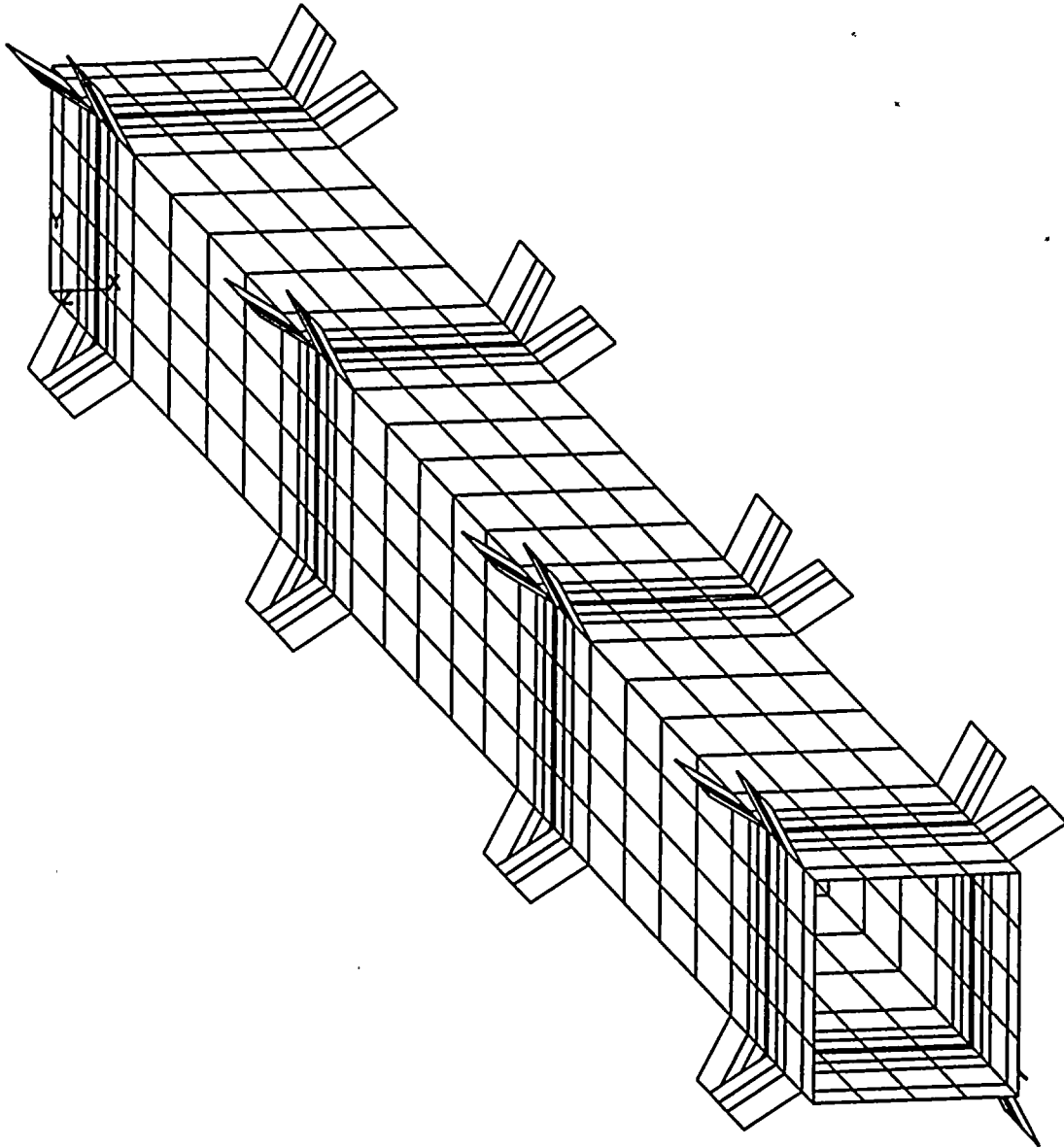




Figure 3.5-35 Ginna Type 3 Rack Cell Finite Element Model



North

REGION 2 — REGION 1
(INCLUDES 2A & 2B)

Note: Racks 1 thru 6 are existing racks
+X=East, +Y=North, +Z=Up

51-1258768-01
Ginna SFP Re-racking Licensing Report



姓名: _____ 性别: _____ 年龄: _____ 职业: _____ 住址: _____ 电话: _____ 邮编: _____

11

1

48

3.5.2.4 Detailed Documentation of Computer Codes

3.5.2.4.1 General

The following is a description of the computer codes and verification/validation methods (as applicable) used in the structural/seismic analyses performed by FCF for the Ginna Station Spent Fuel Storage Racks. A copy of the user's manual and documentation for SIMQKE is available in the Public Domain.

3.5.2.4.2 Structural/Seismic Computer Codes

Two computer codes were utilized for the structural/seismic calculations, ANSYS (Reference 3.40) and SIMQKE (Reference 3.41).

3.5.2.4.2.1 ANSYS

The primary code which was used for the structural analyses is ANSYS Version 5.2. ANSYS is a general purpose, finite element program for solving a wide variety of engineering analysis problems. ANSYS employs the latest finite element technology for the solution of several classes of engineering problems. ANSYS has a large library of elements and an extensive selection of material properties, both linear and nonlinear. The software services a wide spectrum of uses, from the linear elastic analysis of two dimensional and three-dimensional solids to applications in which nonlinear material and geometric effects dominate. These applications must be included in conjunction with sophisticated geometric modeling. The regime of applications varies from static to dynamic structural problems. Mesh generators and extensive pre-processing and post-processing graphics help in establishing the correct analysis.

Since 1970, this program has been used extensively by analysts in the nuclear, chemical, construction, and electronic industries. Extensive use has led to a high degree of reliability in obtained computer results. The ANSYS analysis types include the following:

- Static analysis
- Dynamic analysis
- Nonlinear transient, linear transient, harmonic response, mode-frequency, modal seismic, random vibration.
- Buckling and stability analysis
- Linear buckling, nonlinear buckling
- Heat transfer analysis
- Nonlinearities
- Material, geometric, element
- Substructures

All ANSYS analysis types are based on classical engineering concepts. Through proven numerical techniques, these concepts can be formulated into matrix equations that are suitable for analysis using the finite element method. The system to be analyzed is represented by a mathematical model consisting of elements and nodes. Structural element types include spars, pipes and elbows, beams, plates, shells, solids, masses, springs, dampers, sliding interfaces, and gap interfaces. Also, arbitrary stiffness, mass and damping matrix elements are available.

Loading input for structural analyses may be nodal forces, body forces, displacements, velocities, accelerations, pressures, or temperatures. These inputs may be sinusoidal, random or an arbitrary function of time for the linear and nonlinear dynamic analyses. Mode frequency analyses may include force spectrum or response spectrum loadings. Structural analysis outputs are usually forces, displacements, stresses, and strains.

ANSYS has been used at FCF for the last 21 years, and analyses are performed per procedures that include the guidelines for the certification of computer codes. FCF has verified that ANSYS 5.2 is acceptable for this analysis and that all applicable error reports have been reviewed and have been shown to have no effect on these analyses.

3.5.2.4.2.1.1 Summary of Element Types Used in the ANSYS Models

The following is a list of the element types which were used in the ANSYS models:

- | | |
|------------------|--|
| BEAM4 | The BEAM4 element is a 3-D elastic beam with six degrees of freedom at each node. Beam elements were used to model the rack legs, the baseplate, the rack tubes, and the fuel. |
| MASS21 | The MASS21 element is a lumped mass element which can be applied in all three orthogonal directions. The MASS21 element can also apply rotary inertia to represent the lumped mass more as a distributed mass. |
| CONTACT52 | The CONTACT52 element is a 3-D point-to-point contact element which allows for gaps, interface stiffness, and sliding friction. |
| FLUID38 | The FLUID38 element is a hydrodynamic coupling element with two degrees of freedom at each node, translation perpendicular to the axes of the coupled cylinders. |
| SHELL63 | The SHELL63 element is an elastic shell element that has both bending and membrane capabilities. Both in-plane and normal loads are permitted. The element has six degrees of freedom at each node. The SHELL63 element was used in the single 3D plate models of the racks, and in the local rack cell models with connecting tabs. |

3.5.2.4.2.1.2 Summary of ANSYS Error Reports for Element Types Used

Error No: 96-14 Use of SHELL63 elements with: (1) NON-UNIFORM thermal loads, and (2) any nonlinearity in the model, and (3) extra displacement shapes. This error is not applicable for our analyses since we didn't use any non-uniform thermal loads.

Error No: 96-26 Use of SHELL63 elements with the Allman in-plane rotational stiffness (KEYOPT(3)=2) in any one of the following: (1) a buckling analysis, or (2) a prestressed analysis, or (3) in a nonlinear analysis with stress stiffening. This error is not applicable for our analysis since we didn't use the Allman in-plane rotational stiffness (KEYOPT(3)=2).

Conclusion: None of the ANSYS Error Reports had any effect on the results of the analyses.

3.5.2.4.2.2 SIMQKE

The program SIMQKE has these capabilities: it computes a power spectral density function from a specified smooth response spectrum; it generates statistically independent artificial acceleration times histories and tries, by iteration, to match the specified response spectrum; it performs a baseline correction on the generated motion to ensure zero final ground velocity; and it calculates response spectra with the time histories as input.

The artificial motion generated by the program is a series of sinusoidal waves multiplied by an intensity envelope function:

$$Z(t) = I(t) \sum_n A_n \sin(\omega_n t + \phi_n)$$

A_n is the amplitude and ϕ_n is the phase angle of the n^{th} contributing sinusoid. By fixing an array of amplitudes and generating different arrays of phase angles, one obtains different motions with the same general appearance but different details.

The computer uses a random number generator to produce strings of phase angles with uniform likelihood in the range between 0 and 2π .

The amplitudes A_n are related to the (one-sided) spectral density function $G(\omega)$ in the following way:

$$G(\omega_n) \delta\omega = A_n^2/2$$

The total power may be expressed as:

$$\sum A_n^2/2 = \sum G(\omega_n) \delta\omega$$

Three different intensity envelope functions $I(t)$ are available "Trapezoidal," "Exponential" and "Compound." The program artificially raises or lowers the generated peak acceleration to match the target peak acceleration exactly. The response spectra corresponding to the motion are then

computed. The response spectrum for one chosen damping value is called the "target" response spectrum which the program will attempt to "match."

To smooth the calculated spectrum and to improve the matching, an iterative procedure is implemented. In each cycle of the iteration, the calculated response is compared with the target at a set of control frequencies specified by the user.

3.5.2.5 Hydrodynamic Fluid Coupling

The present rack analysis incorporates inertial fluid coupling terms which model the effects of fluid in the gaps between fuel assemblies and racks, between adjacent racks, and between the racks and the pool wall. The corresponding hydrodynamic masses are calculated using established methods, based on potential theory, and documented in References 3.38. The following sections describe hydrodynamic masses and their methods of application.

The relative contribution of fluid coupling is dependent upon fluid gaps and the relative motion between the bodies considered. The values calculated for the present analysis are based on nominal gaps. The coupling terms for "in-phase" rack motion are determined for gaps equivalent to nominal, and for "out-of-phase" rack motion are determined for gaps equal to 1/2 nominal. A general description of the methods used is given herein.

The equations indicate that the hydrodynamic coupling forces would become infinite as the gaps approach zero, so to be conservative, the calculation of the hydrodynamic mass is based on the original gaps. Impact forces would be calculated if gaps are too close to zero.

ANSYS Element STIF38 is used. The option of calculating hydrodynamic masses both on diagonal and off diagonal terms of the mass matrix is selected. The hydrodynamic element masses inserted in the mass matrix are:

$$\begin{bmatrix} m_{11} & 0 & m_{13} & 0 \\ 0 & m_{22} & 0 & m_{24} \\ m_{31} & 0 & m_{33} & 0 \\ 0 & m_{42} & 0 & m_{44} \end{bmatrix} \quad \text{where:} \quad \begin{aligned} m_{11} &= M_{nx}, m_{22} = M_{ny} \\ m_{13} &= m_{31} = -(M_1 + M_{nx}) \\ m_{33} &= M_1 + M_2 + M_{nx} \\ m_{24} &= m_{42} = -(M_1 + M_{nz}) \\ m_{44} &= M_1 + M_2 + M_{nz} \end{aligned}$$

The general equation for fluid kinetic energy is used to estimate the hydrodynamic mass. The values of these masses is based upon the equations developed by Singh-90 (Reference 3.38).

3.5.2.5.1 Fuel-to-Rack Hydrodynamic Coupling

Fuel Assemblies

The fuel assembly contains 179 individual fuel rods, 16 guide tubes and one instrument tube. These rods and tubes are held in position by spacer grids. There is no outside sheathing, so the hydrodynamic coupling is based upon each fuel rod, assumed to be at the center of the cell.

For concentric long cylinders, the hydrodynamic mass is given by Singh-90 (Reference 3.38):

$$M_H = \left| \frac{R_2^2 + R_1^2}{R_2^2 - R_1^2} \right| n \pi \rho R_1^2 h$$

where R_1 = fuel rod radius
 R_2 = rack cell "equivalent" radius
 h = height of fuel within rack
 ρ = density of fluid
 n = number of fuel rods and tubes

Therefore: Since $R_1 \ll R_2$ $\frac{R_2^2 + R_1^2}{R_2^2 - R_1^2} \rightarrow 1$

$$M_H = \sum_{i=1}^n \rho \pi R_1^2 h$$

Fuel Assembly Parameters:

	W-Standard	W- OFA	Exxon
Fuel Assembly	14x14	14x14	14x14
Rods per Assembly	179	179	179
Clad O.D. - inch	0.422	0.4	0.424
No. Of guide Tubes	16	16	16
Guide Tube O.D. - in	0.539	0.528	0.524
No. Of Instrument Tube	1	1	1
Instrument Tube O.D. - in	0.422	0.399	0.424

Also using: $\rho = 9.345 \times 10^{-5} \text{ lb-sec}^2 / \text{in}^4$
 $h = 158.5 \text{ in}$ (rod and tubes length taken as full length of rack)
 $R_1 = \text{rod or tube (O.D. / 2)}$

we obtain, the M_H - hydrodynamic masses for the fuel coupling, and result are summarized at the end of section.

M_1 = mass of fluid displaced by the inner body
 = this is same as M_H for long concentric cylinders with $R_1 \ll R_2$

M_2 = mass of fluid inside the outer body in the absence of the inner body
 = area \times height \times fluid density

For ATEA racks (Type 2, 3 or 4) inside fuel cell dimension 8.1417 in

For U.S. Tool & Die Racks, inside fuel cell dimension is 8.113 in

Height is 158.5 in

Density of fluid is 9.345×10^{-5} lb-sec² / in⁴

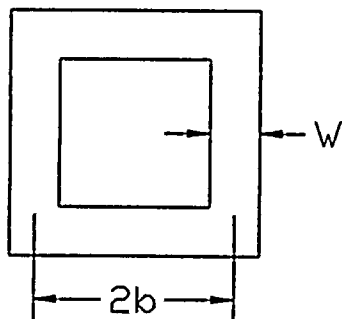
The results of M_H , M_1 and M_2 are summarized below for both ATEA and U.S. Tool & Die Racks:

Summary - Fuel to Rack Hydrodynamic Masses - lb-sec² / in

	W-Standard Fuel	W-OFA Fuel	Exxon Fuel
M_H	0.427	0.387	0.428
M_1	0.427	0.387	0.428
M_2	0.982	0.982	0.982

Consolidated Fuel Canisters

Consolidated fuel storage consists of fuel rods stored within a closed canister. The hydrodynamic coupling to the cell is based upon the canister rather than the individual fuel rods.



For concentric long rectangular bodies, the hydrodynamic mass along x and y-directions is given by Singh-90 (Reference 3.38).

$$M_H = \frac{16}{3} \rho \frac{b^3 h}{W}$$

where h = height of rectangular body
 = 158.5 in

ρ = density of fluid
 = 9.345×10^{-5} lb-sec² / in⁴

$$M_1 = (2b - w)^2 \times h \times \rho$$

$$M_2 = (2b + w)^2 \times h \times \rho$$

The results for the consolidated fuel hydrodynamic masses are summarized with input parameters.

Outside dimension of consolidated fuel 8.0 x 8.0 in

Inside dimension of ATEA rack fuel cell 8.1417 in

Inside dimension of U.S. Tool & Die rack fuel cell 8.113 in

Summary - Hydrodynamic coupling Masses for Consolidated Fuel - Each

	ATEA Rack	U.S. Tool & Die Rack	
b	4.035	4.036	inch
w	0.071	0.0715	inch
M_H	73.27	91.39	lb-sec ² / in
M_1	0.948	0.948	lb-sec ² / in
M_2	0.982	0.975	lb-sec ² / in

3.5.2.5.2 Rack-to-Rack and Rack-to-Pool Hydrodynamic Coupling

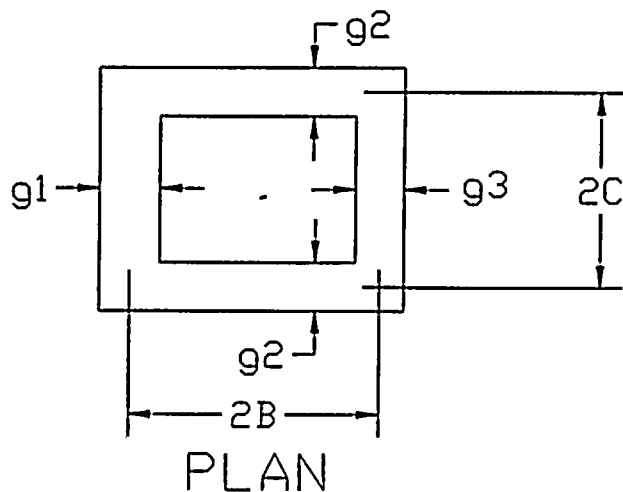
For eccentric long rectangular bodies, the hydrodynamic mass along x and y-directions is given by Singh-90 (Reference 3.38).

$$M_H (HORIZ) = 2\rho h C^2 \left[\frac{C}{3g_1} + \frac{C}{3g_3} + \frac{2B}{g_2} \right]$$

$$M_1 = \rho h (2C - g_2) \left[2b - \left(\frac{g_1 + g_3}{2} \right) \right]$$

$$M_2 = \rho h (2C + g_2) \left[2b + \left(\frac{g_1 + g_3}{2} \right) \right]$$



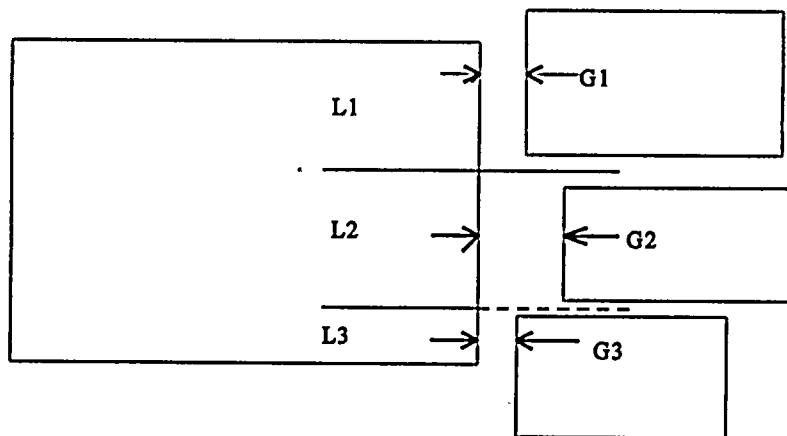


where h = height of rack
 ρ = density of fluid
 g_1, g_2, g_3 = gaps

If g_2 gaps are different among North or South side of rack, the average gaps are used in the hydrodynamic mass calculations. For cases when there is overlap of two or more racks on the side of a rack, the weighted average gaps are used in the calculations.

Weighted Gaps

For the idealization of gaps, if more than one rack with different gaps is in the vicinity of the rack under consideration, a weighted gap is used. The weighted gap is based on length of overlap between the racks.



Weighted average gap

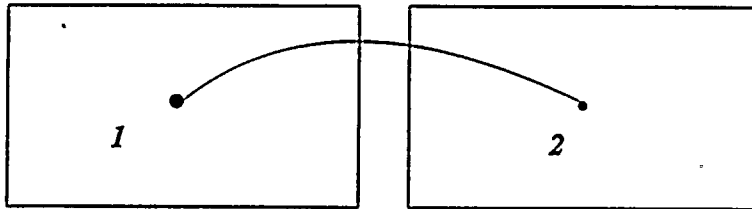
$$G = \frac{\sum Li Gi}{\sum Li}$$

Table 3.5-9 summarizes geometric parameters and also the weighted gaps.

Weighted Average Rack Coupling

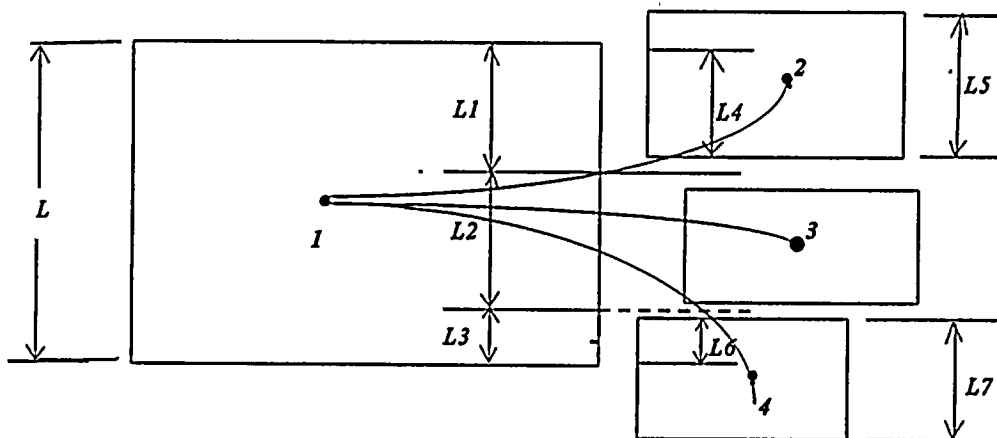
The hydrodynamic mass coupling between rack to rack motion under seismic events is based on weighted mass coupling. The weighted mass is based on length of overlap between the racks.

Case 1



$$M_{H_{1,2}} = \frac{M_{H_1} + M_{H_2}}{2}$$

Case 2



Using Effective Coupled Lengths for Hydrodynamic Mass:

$$M_{H_{1,2}} = \frac{M_{H_1} \frac{L_1}{L} + M_{H_2} \frac{L_4}{L_5}}{2}$$

$$M_{H_{1,3}} = \frac{M_{H_1} \frac{L_2}{L} + M_{H_3}}{2}$$

$$M_{H_{1,4}} = \frac{M_{H_1} \frac{L_3}{L} + M_{H_4} \frac{L_6}{L_7}}{2}$$

Tables 3.5-10 and -11 summarize hydrodynamic masses.



**Table 3.5-9 Geometric Parameters for Hydrodynamic
Mass Coupling - Summary Table
Gaps at the Top of the Rack**

Rack	h in	Rack W E-W Length in	Rack L N-S Length in	Gaps at the Top of the Rack			
				g1 West Gap in	g2 North Gap in	g3 East Gap in	g2' South Gap in
1	159	84.30	118.02	10.50	0.50	1.75	14.75
1 and Type 4	159	84.30	127.21	10.50	0.50	1.75	5.53
2	159	84.30	118.02	9.75	15.25	1.25	0.50
2 and Type 4	159	84.30	127.21	9.75	6.03	1.25	0.50
3	159	84.30	118.02	1.75	0.75	0.75	15.50
3 and Type 4	159	84.30	127.21	1.75	0.75	0.75	6.28
4	159	84.30	118.02	1.25	14.25	0.63	0.75
4 and Type 4	159	84.30	127.21	1.25	5.03	0.63	0.75
5	159	84.30	118.02	0.75	0.75	0.84	17.00
5 and Type 4	159	84.30	127.21	0.75	0.75	0.84	7.78
6	159	84.30	118.02	0.63	12.75	3.18	0.75
6 and Type 4	159	84.30	127.21	0.63	3.53	3.21	0.75
7 or 2A	159.68	92.73	67.5	0.84	1.36	96.77	7.34
8 or 2B	159.68	92.73	75.88	0.84	1.29	1.29	1.36
10 or 3A	159.68	91.93	64.23	3.59	1.93	1.20	1.21
13 or 3B	159.68	91.93	64.23	1.20	1.93	3.45	1.21
9 or 3C	159.68	91.93	45.76	3.55	1.21	1.20	1.21
12 or 3D	159.68	91.93	45.76	1.20	1.21	3.51	1.21
11 or 3E	159.68	91.92	55.77	1.29	1.21	3.48	96.39

Using these geometric parameters, the hydrodynamic masses are calculated for the rack to pool and rack to rack coupling. The results are summarized in the following table. The X-direction corresponds to East direction. The Y-direction corresponds to North direction.



**Table 3.5-10 Rack Hydrodynamic Coupling Masses
Standard Configuration (No Type 4 Racks Installed)**

	M _{hx} lb.sec ² /in	M _{hy} lb.sec ² /in	M ₁ lb.sec ² /in	M ₂ lb.sec ² /in
Individual Rack Coupling				
1	3028.21	3139.21	147.83	191.19
2	3572.70	3223.44	148.83	189.42
3	5978.95	6570.86	147.83	173.17
4	7176.08	8284.38	147.83	170.33
5	7532.38	9648.98	147.83	173.27
6	6050.91	4735.82	147.83	172.18
7 (Rack 2A)	1807.09	3292.76	93.40	216.43
8 (Rack 2B)	4273.00	6308.24	105.00	111.16
9 (Rack 3C)	1426.57	3036.12	62.77	69.51
10 (Rack 3A)	2334.69	3226.97	88.11	97.23
11 (Rack 3E)	1668.51	3782.04	76.50	221.28
12 (Rack 3D)	1426.71	3045.61	62.77	69.48
13 (Rack 3B)	2337.26	3275.97	88.11	97.09
Weighted Average Rack Coupling				
Racks 1 and 2	3300.45	3181.32	147.83	190.30
Racks 1 and 3	4503.58	4855.03	147.83	182.18
Racks 2 and 4	5374.39	5753.91	147.83	179.88
Racks 3 and 5	6755.66	8109.92	147.83	173.22
Racks 3 and 4	6577.51	7427.62	147.83	171.75
Racks 4 and 6	6613.5	6510.10	147.83	171.26
Racks 5 and 6	6791.65	7192.40	147.83	172.73
Racks 5 and 7	2638.77	3797.74	76.52	135.35
Racks 5 and 8	3570.42	4900.17	78.34	87.16
Racks 6 and 10	2352.86	2421.95	70.37	79.72
Racks 6 and 9	1917.37	2460.45	60.80	69.02
Racks 6 and 8	901.66	1028.22	22.09	24.52
Racks 7 and 8	3040.04	4800.50	99.20	163.79
Racks 8 and 11	2970.75	5045.14	90.75	166.22
Racks 8 and 9	2849.78	4672.18	83.89	90.33
Racks 10 and 13	2335.97	3251.47	88.11	97.16
Racks 9 and 10	1880.63	3131.55	75.44	83.37
Racks 12 and 13	1881.98	3160.79	75.44	83.29
Racks 9 and 12	1426.64	3040.86	62.77	69.49
Racks 11 and 12	1547.61	3413.82	69.63	145.38

**Table 3.5-11 Rack Hydrodynamic Coupling Masses
Extended Configuration (Type 4 Racks Installed)**

	M _{hx} lb.sec ² /in	M _{hy} lb.sec ² /in	M _I lb.sec ² /in	M ₂ lb.sec ² /in
Individual Rack Coupling				
1	5601.65	3288.11	159.34	191.15
2	5960.82	3363.23	159.34	189.38
3	8358.80	6843.52	159.34	173.13
4	10218.21	8646.03	159.34	170.30
5	9664.24	10012.09	159.34	173.23
6	10096.49	5003.73	159.34	172.20
7 (Rack 2A)	1807.09	3292.76	93.40	216.43
8 (Rack 2B)	4273.00	6308.24	105.00	111.16
9 (Rack 3C)	1426.57	3036.12	62.77	69.51
10 (Rack 3A)	2334.69	3226.97	88.11	97.23
11 (Rack 3E)	1668.51	3782.04	76.50	221.28
12 (Rack 3D)	1426.71	3045.61	62.77	69.48
13 (Rack 3B)	2337.26	3275.97	88.11	97.09
Weighted Average Rack Coupling				
Racks 1 and 2	5781.24	3325.67	159.34	190.26
Racks 1 and 3	6980.22	5065.82	159.34	182.14
Racks 2 and 4	8089.52	6004.63	159.34	179.84
Racks 3 and 5	9011.52	8427.81	159.34	173.18
Racks 3 and 4	9288.51	7744.78	159.34	171.71
Racks 4 and 6	10157.35	6824.88	159.34	171.25
Racks 5 and 6	9880.37	7507.91	159.34	172.72
Racks 5 and 7	3480.84	4316.44	89.19	154.41
Racks 5 and 8	3926.36	4803.67	78.25	83.90
Racks 6 and 10	3681.77	2859.61	83.74	91.50
Racks 6 and 9	2572.73	2439.58	60.73	66.47
Racks 6 and 8	928.71	690.69	20.23	22.07
Racks 7 and 8	3040.04	4800.50	99.20	163.79
Racks 8 and 11	2970.75	5045.14	90.75	166.22
Racks 8 and 9	2849.78	4672.18	83.89	90.33
Racks 10 and 13	2335.97	3251.47	88.11	97.16
Racks 9 and 10	1880.63	3131.55	75.44	83.37
Racks 12 and 13	1881.98	3160.79	75.44	83.29
Racks 9 and 12	1426.64	3040.86	62.77	69.49
Racks 11 and 12	1547.61	3413.82	69.63	145.38



3.5.2.6 Seismic Time History Factor Determinations

Approach

Four Safe Shutdown Earthquake (SSE) and four Operating Basis Earthquake (OBE) time histories are developed to evaluate the racks for the RG&E Ginna Spent Fuel Pool. The development of the time histories is documented in Section 3.5.1. Each time history is applied to a 3-D single rack model for Rack 8(2B), a 9x11 rack manufactured by ATEA. After applying each time history to the model, a multiplication factor is found that, when applied to the critical results of one of the time histories, would envelope the results produced when running the other three time histories. After the time history factors are determined for the SSE and OBE time histories, only the time histories for which factors have been calculated are used on the whole pool model. The calculated factors for SSE and OBE are then applied to the results of the evaluations.

SSE Time History Factor

Table 3.5-12 lists key results of the single rack model evaluations for the four SSE time histories. The last column of the table gives the results of multiplying the results of SSE1 by the calculated factor. These results provide verification that the results from all of the other SSE time histories are enveloped. The result from SSE1 which requires the highest enveloping factor is the horizontal rack load. The factor required to envelope the horizontal rack load from SSE2 is:

$$\text{Factor} = 73,320/62,980 = 1.164$$

Thus, the enveloping factor determined for the SSE time histories is $1.20 \times \text{SSE1}$. Therefore, all SSE evaluations will be performed using SSE1. The factor of 1.20 is applied to all results taken from the evaluation.

The factor of 1.20 also envelopes a factor from the effects of an increase in rack height, see Section 3.5.3.1.7.

OBE Time History Factor

Table 3.5-13 lists key results of the single rack model evaluations for the four OBE time histories. The last column of the table gives the results of multiplying the results of OBE4 by the calculated factor. These results provide verification that the results from all of the other OBE time histories are enveloped. The result from OBE4 which requires the highest enveloping factor is the horizontal rack load. The factor required to envelope the horizontal rack load from OBE1 is:

$$\text{Factor} = 32,420/29,810 = 1.088$$



Thus, the enveloping factor determined for the OBE time histories is $1.12 \times \text{OBE4}$. Therefore, all OBE evaluations will be performed using OBE4. The factor of 1.12 is applied to all results taken from the evaluation.

The factor of 1.12 also envelopes a factor from the effects of an increase in rack height, see Section 3.5.3.1.7.

**Table 3.5-12 Summary of Determination of SSE Time History Factor
(Using Rack 8(2B) Loaded with Consolidated Fuel, $\mu=0.8$)**

	Item	SSE1	SSE2	SSE3	SSE4	1.20*SSE1
Max. Leg Load (lbs.)	Single Model Leg Horizontal	34,910	24,660	37,390	31,580	41,892
	Single Model Leg Vertical	138,000	122,700	129,000	127,300	165,600
	Leg Total Vertical	322,800	307,100	320,200	307,100	387,360
Max. Rack Load (lbs.)	Horizontal	62,980	73,320	71,190	59,000	75,576
	Vertical	13,480	12,820	13,370	12,820	16,176
Max. Rack Moments (in.-lbs.)	Bending	6.645×10^6	6.267×10^6	7.001×10^6	5.875×10^6	7.974×10^6
Max. Impact Load (lbs.)	Fuel to Rack	12,950	12,710	11,050	11,740	15,540
Displacement of Leg (in.)	Horizontal	0.03354	0.02938	0.02765	0.02548	0.04025



1. The first part of the document is a list of names and addresses of the members of the committee.

2. The second part of the document is a list of names and addresses of the members of the committee.

**Table 3.5-13 Summary of Determination of OBE Time History Factor
(Using Rack 8(2B) Loaded with Unconsolidated Fuel, $\mu=0.8$)**

	Item	OBE1	OBE2	OBE3	OBE4	1.12*OBE4
Max. Leg Load (lbs.)	Single Model Leg Horizontal	8,630	7,696	7,347	8,723	9,770
	Single Model Leg Vertical	64,440	62,410	59,740	63,090	70,661
	Leg Total Vertical	159,400	157,700	156,400	156,500	175,280
Max. Rack Load (lbs.)	Horizontal	32,420	25,590	26,500	29,810	33,387
	Vertical	11,230	11,110	11,020	11,030	12,354
Max. Rack Moments (in.-lbs.)	Bending	3.382×10^6	3.206×10^6	3.070×10^6	3.114×10^6	3.488×10^6
Max. Impact Load (lbs.)	Fuel to Rack	42,980	38,980	42,330	51,440	57,613
Displacement of Leg (in.)	Horizontal	0.008675	0.007697	0.007348	0.008731	0.009779

3.5.2.7 Rack Stiffness Sensitivity Study

Statement of Concern

In the July 1996 meeting between the Nuclear Regulatory Commission, (NRC), RG&E, and Framatome Cogema Fuels, the NRC expressed concerns about the stiffness of the rack structures. The issue raised was that the rack stiffness used in the analytical models may not necessarily represent the actual stiffness of the rack. The difference in stiffness may exist because the rack stiffness in the model is based on a continuous structure, while the rack is made up of tubes connected by welded tabs. The NRC expected this method of fabrication to result in a structure with a potentially lower stiffness than that used in the structural analysis of the rack. The NRC recommended testing to verify that the rack stiffness is close to the stiffness used in the analyses.

The objectives of this study are to determine the difference in stiffness between a continuous structure and a segmented structure, if any, and to show that the rack seismic loads and hence stresses are not sensitive to the rack stiffness.

Resolution of Concern

The approach taken to resolve this concern is to approximate the difference in stiffness between a continuous structure and a structure connected by tabs and then to determine the impact that the difference in stiffness would have on critical results of the rack analysis, such as the reaction forces on the pool floor, the moments generated in the rack, and the movement of the rack.

To determine the difference in stiffness, a continuous structure was modeled using ANSYS and loaded to calculate its stiffness. The finite element computer program ANSYS was verified against experimental test data. The model was then modified to separate the structure into segments which were then connected with tabs. The stiffness of the segmented structure connected by four tabs as in the actual rack design was found to be about 13.5% lower than the stiffness of the continuous structure.

Because the stiffness of the structure was lower for the segmented structure connected by tabs, the impact of this stiffness was examined. A model for dynamic analysis of a single rack was modified to have rack stiffnesses ranging from 50% to 200% of the stiffness of the continuous structure. The model was of a free standing spent fuel rack which included rack to rack hydrodynamic coupling, rack to fuel gaps, and rack to fuel hydrodynamic coupling. Because the racks were free standing, the gaps and hydrodynamic coupling had a larger effect than rack stiffness on the loads, moments, and rack movements since there was rigid body motion.

These models were evaluated using a single specified safe shutdown earthquake (SSE) time history. The results of these analyses were then plotted as percentages of the values calculated using the stiffness of the continuous structure vs. the factor applied to the stiffness. The results plotted were the maximum total reaction load at the floor, the maximum horizontal displacement at two corners of the rack, and the maximum moments at the base of the rack. As can be seen in the following table and plot, the maximum reaction forces at the floor are essentially independent of the rack stiffness. The moments at the base of the rack showed slight dependence on the stiffness with the moments increasing with increasing stiffness. The rack displacements showed the greatest variation with changing stiffness, following the general trend of increasing displacement with increasing stiffness. Note that the displacements referred to are rack translations caused by fuel to rack impacts. A stiffer rack beam causes more energy from the impact to generate translation of the entire rack rather than bending of the rack beam.

Conclusions

The comparison of a continuous structure and a segmented structure connected with tabs indicates that using tabs as the method of fabricating the rack will result in a stiffness about 13.5% lower than that of a continuous structure. SSE analyses performed on a single rack model with stiffnesses ranging from 50% to 200% of the stiffness of a continuous structure indicates that the reaction loads at the floor remain constant, bending moments in the rack increase slightly with increasing stiffness, and rack displacements increase with increasing stiffness. These results are listed in the following table and are plotted in Figure 3.5-37.



Rack Stiffness Sensitivity Study Results

Percentage of Stiffness of Continuous Structure	Percentage of Maximum Total Reaction Forces at Floor vs. Results for 100% Stiffness	Percentage of Maximum Total Bending Moment at Tube Connection to Baseplate vs. Results for 100% Stiffness	Percentage of Maximum Total Horizontal Displacement of Corner of Rack vs. Results for 100% Stiffness
50%	100%	85%	55% (0.018 in.)
80%	100%	97%	73% (0.023 in.)
100%	100%	100%	100% (0.032 in.)
120%	100%	105%	124% (0.040 in.)
150%	100%	108%	155% (0.049 in.)
200%	100%	111%	176% (0.056 in.)

Results are based on fully consolidated rack loading and coefficient of friction of 0.8. Displacements listed are given for comparison purposes only. For rack displacements and gap closures, see Section 3.5.3.1.14.

Rack stiffness is not a critical parameter in the determination of pool floor reaction loads, rack moments, or rack displacements. Therefore, experimental verification of the rack stiffness is unnecessary. The stiffness used in the model of the Ginna racks is slightly higher than the actual stiffness of the rack (based on the stiffness of a continuous structure rather than a segmented structure connected by tabs). The result of using a higher rack stiffness is higher bending moments and rack displacements, thus making the use of a higher than actual rack stiffness conservative for the seismic analyses.

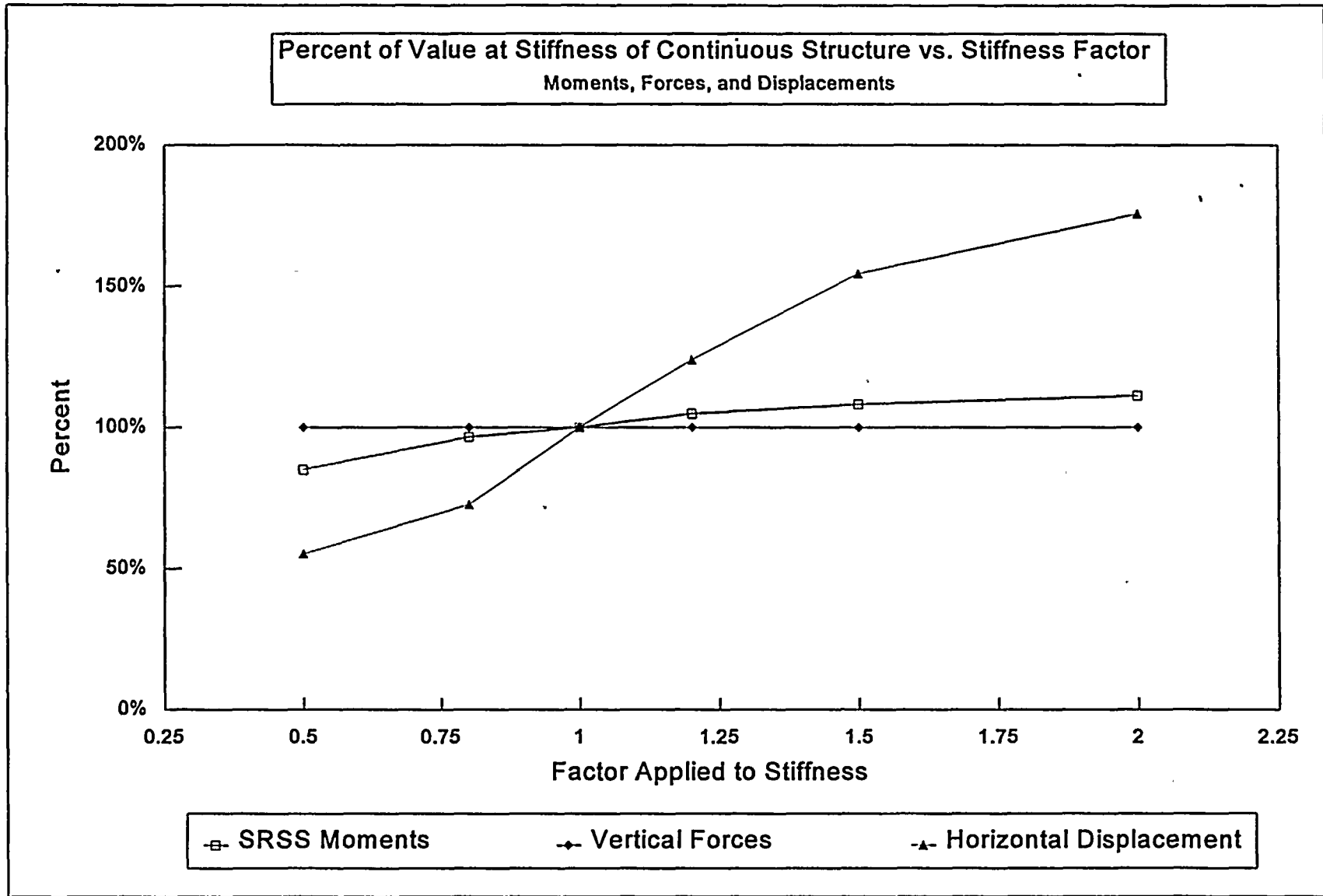


Figure 3.5-37 Percent of Value at Stiffness of Continuous Structure vs. Stiffness Factor



1. The first part of the document is a list of names and addresses of the members of the committee.

3.5.3 Structural Evaluation

The RG&E Ginna Unit 1 Spent Fuel Storage system structure, i.e., new ATEA storage racks, the resident U.S. Tool and Die racks, spent fuel pool and liner, was evaluated for license application. For all these structures, the normal, upset, faulted, and the hypothetical accident conditions were evaluated. The structural evaluation methods used proven design practices and current technology with innovative engineering principles. Details of these evaluations are provided in the next subsections.

3.5.3.1 Normal, Upset and Faulted Conditions

The Spent Fuel Storage System was designed to meet all applicable structural criteria for normal (Level A), upset (Level B) and faulted (Level D) conditions as defined in NUREG-0800, SRP 3.8.4, Appendix D. The dead weight, thermal, seismic and stuck fuel assembly loadings were considered. The load combinations were performed per SRP 3.8.4, Appendix D. The combined loads were used to assess storage rack structural integrity based on allowable stress limits provided for Class 3 component support of ASME Section III, Subsection NF of the ASME Boiler and Pressure Vessel Code. All rack components were shown to meet the ASME Section III structural requirements. In addition, the storage rack lifting stresses were shown to meet the NUREG-0612 lifting requirements of the heavy load lift in the nuclear power plant. The spent fuel pool evaluation was based on allowable stress limits provided in ACI 349-85. The spent fuel pool was shown to meet these stress requirements. The pool liner evaluation was based on stress limits provided in AISC-9th edition. The pool liner was shown to meet these stress requirements. The structural integrity was evaluated using conservative analytical methods.

3.5.3.1.1 Various Inputs to the 3-D Single Rack and Whole Pool Finite Element Models

3.5.3.1.1.1 Rack Structural Properties

Type 2 Rack General Information

SS Wall Thickness = 0.08 in.
Cell Size = 8.30 in.
Cell Height = 158.5 in.
Density of SS 304 L = 0.290 lb/in³

Borated SS thickness = 0.12 in.
Borated SS OD = 8.38 in.
Borated SS Height = 145.7 in.
Density of Borated SS = 0.290 lb/in³

Rack Baseplate thickness = 1.18 in.
Cell bottom hole diameter = 3.74 in.

Length of Rack Support Leg = 13.70 in.
Center-center dimension (pitch) = 8.43 in

Type 2 Rack Structural Properties

Rack No.	Rack Type	Size	Area (in ²)	Width W-E (in)	Length N-S (in)	I N-S (in ⁴)	I W-E (in ⁴)
7	2A	8x11	113.9	93.31	68.07	43,971	82,250
8	2B	9x11	129.5	93.31	76.46	64,009	95,291

Type 2 Rack Total Dry Weights

Rack No.	Rack Type	Total No. of Legs	Total No. of Cells	Total Rack Dry Weight (lbs.)	Total Leg and Baseplate Dry Weight (lbs.)	Total Dry Unconsolidated Fuel Wt. (lbs.)	Total Dry Consolidated Fuel Wt. (lbs.)
7	2A	12	88	14,072	3,038	127,600	232,170
8	2B	16	99	15,701	3,640	143,550	261,192

Type 2 Rack Total Wet Weights

Rack No.	Rack Type	Total No. of Legs	Total No. of Cells	Total Rack Wet Weight (lbs.)	Total Leg and Baseplate Wet Weight (lbs.)	Total Wet Unconsolidated Fuel Wt. (lbs.)	Total Wet Consolidated Fuel Wt. (lbs.)
7	2A	12	88	12,319	2,659	114,980	204,385
8	2B	16	99	13,747	3,187	129,353	229,933

Type 2 Rack Total Combined (Rack+Baseplate+Legs+Fuel) Wet and Dry Weights (in lbs.)

Rack No.	Rack Type	Total Dry Unconsolidated Combined Wts.	Total Dry Consolidated Combined Wts.	Total Wet Unconsolidated Combined Wts.	Total Wet Consolidated Combined Wts.
7	2A	144,710	249,280	129,958	219,363
8	2B	162,891	280,533	146,287	246,867

Type 2 Rack Maximum Wet and Dry Weights Per Support Leg (in lbs.)

Rack No.	Rack Type	Total Dry Unconsolidated Wt. on One Leg	Total Dry Consolidated Wt. on One Leg	Total Wet Unconsolidated Wt. on One Leg	Total Wet Consolidated Wt. on One Leg
7	2A	12,059	20,773	10,830	18,280
8	2B	10,181	17,533	9,143	15,429

Type 3 Rack General Information

SS Wall Thickness = 0.08 in.	Borated SS thickness = 0.10 in.
Cell Size = 8.50 in.	Borated SS OD = 8.34 in.
Cell Height = 162.0 in.	Borated SS Height = 145.7 in.
Density of SS 304 L = 0.290 lb/in ³	Density of Borated SS = 0.290 lb/in ³
Rack Baseplate thickness = 1.18 in	Length of Rack Support Leg = 13.70 in
Cell bottom hole diameter = 3.74 in.	Center-center dimension (pitch) = 9.23 in

Type 3 Rack Structural Properties

No.	Rack Type	Size	Area (in ²)	Width W-E (in)	Length N-S (in)	I N-S (in ⁴)	I W-E (in ⁴)
9	3C	5x10	66.2	92.34	46.18	12,079	47,402
10	3A	7x10	92.7	92.34	64.65	32,726	66,359
11	3E	6x10+2	84.8	92.34	56.19, 64.63	26,008	66,040
12	3D	5x10	66.2	92.34	46.18	12,079	47,402
13	3B	5x10+12	82.1	92.34, 55.41	64.65, 46.18	25,998	55,479



Type 3 Rack Total Dry Weights

Rack No.	Rack Type	Total No. of Legs	Total No. of Cells	Total Rack Dry Weight (lbs.)	Total Leg and Baseplate Dry Weight (lbs.)	Total Dry Unconsolidated Fuel Wt. (lbs.)	Total Dry Consolidated Fuel Wt. (lbs.)
9	3C	8	50	11,548	2,142	72,500	131,915
10	3A	12	70	16,232	2,958	101,500	184,681
11	3E	12	62	14,547	2,771	89,900	163,575
12	3D	8	50	11,548	2,142	72,500	131,915
13	3B	11	62	14,651	2,672	89,900	163,575

Type 3 Rack Total Wet Weights

Rack No.	Rack Type	Total No. of Legs	Total No. of Cells	Total Rack Wet Weight (lbs.)	Total Leg and Baseplate Wet Weight (lbs.)	Total Wet Unconsolidated Fuel Wt. (lbs.)	Total Wet Consolidated Fuel Wt. (lbs.)
9	3C	8	50	10,111	1,875	65,330	116,128
10	3A	12	70	14,211	2,589	91,461	162,461
11	3E	12	62	12,735	2,425	81,009	143,999
12	3D	8	50	10,111	1,875	65,330	116,128
13	3B	11	62	12,827	2,340	81,009	143,999

Type 3 Rack Total Combined (Rack+Baseplate+Legs+Fuel) Wet and Dry Weights (in lbs.)

Rack No.	Rack Type	Total Dry Unconsolidated Combined Wts.	Total Dry Consolidated Combined Wts.	Total Wet Unconsolidated Combined Wts.	Total Wet Consolidated Combined Wts.
9	3C	86,190	145,605	77,316	128,114
10	3A	120,690	203,871	108,261	179,261
11	3E	107,218	180,893	96,169	159,159
12	3D	86,190	145,605	77,316	128,114
13	3B	107,223	180,898	96,176	159,166

Type 3 Rack Maximum Wet and Dry Weights Per Support Leg (in lbs.)

Rack No.	Rack Type	Total Dry Unconsolidated Wt. on One Leg	Total Dry Consolidated Wt. on One Leg	Total Wet Unconsolidated Wt. on One Leg	Total Wet Consolidated Wt. on One Leg
9	3C	10,774	18,201	9,665	16,014
10	3A	10,058	16,989	9,022	14,938
11	3E	8,935	15,074	8,014	13,263
12	3D	10,774	18,201	9,665	16,014
13	3B	9,748	16,445	8,743	14,470

Type 4 Rack General Information

Center-center dimension (pitch) = 8.43 in

SS Wall Thickness = 0.08 in.

Borated SS thickness = 0.10 in.

Cell Size = 8.30 in.

Borated SS OD = 8.18 in. (length)

Cell Height = 158.5 in.

Borated SS Height = 148.4 in.

Density of SS 304 L = 0.290 lb/in³

Density of SS 304 L = 0.290 lb/in³

Rack Baseplate thickness = 1.18 in.

Cell bottom hole diameter = 3.74 in.

Length of Rack Support Leg = 13.69 in.

Type 4 Rack Structural Properties

Rack Type	Size	Area (in ²)	Width W-E (in)	Length N-S (in)	I N-S (in ⁴)	I W-E (in ⁴)
4A-F	1x10	25.9	8.30	84.56	292	15,471

Type 4 Rack Total Dry Weights

Rack Type	Total No. of Legs	Total No. of Cells	Total Rack Dry Weight (lbs.)	Total Leg and Baseplate Dry Weight (lbs.)	Total Dry Unconsolidated Fuel Wt. (lbs.)	Total Dry Consolidated Fuel Wt. (lbs.)
4A-F	2	10	1,919	418	14,500	26,383

Type 4 Rack Total Wet Weights

Rack Type	Total of Legs	Total No. of Cells	Total Rack Wet Weight (lbs.)	Total Leg and Baseplate Wet Weight (lbs.)	Total Wet Unconsolidated Fuel Wt. (lbs.)	Total Wet Consolidated Fuel Wt. (lbs.)
4A-F	2	10	1,680	365	13,066	23,266

Type 4 Rack Total Combined (Rack+Baseplate+Legs+Fuel) Wet and Dry Weights (in lbs.)

Rack Type	Total Dry Unconsolidated Combined Wts.	Total Dry Consolidated Combined Wts.	Total Wet Unconsolidated Combined Wts.	Total Wet Consolidated Combined Wts.
4A-F	16,837	28,720	15,111	25,311

Type 4 Rack Maximum Wet and Dry Weights Per Support Leg (in lbs.)

Rack Type	Total Dry Unconsolidated Wt. on One Leg	Total Dry Consolidated Wt. on One Leg	Total Wet Unconsolidated Wt. on One Leg	Total Wet Consolidated Wt. on One Leg
4A-F	8,419	14,360	7,556	12,656



3.5.3.1.1.2 Fuel Structural Properties

3.5.3.1.1.2.1 Consolidated Fuel Canister Structural Properties

The consolidated fuel canister is represented by a beam element in the seismic analysis. Both the structural canister and the 358 fuel rods are represented by a single beam (single A, I and E). Since the canister (304 SS) and the fuel cladding (Zircaloy) are fabricated of different materials, the equivalent A_{eff} and I_{eff} are calculated for a beam with E of the canister.

Outside Length of Fuel Canister = 8.00 in.

Canister Thickness = 0.093 in.

Inside Length of Fuel Canister/Divider Plate Length = 7.814 in.

Divider Plate Width = 0.093 in.

Area of Canister = 3.6681 in²

Average Moment of Inertia of Canister = 32.5031 in⁴

The elastic modulus of the canister material (304SS) = 27.87×10^6 psi.

Fuel Rod Structural Properties

Fuel Cladding Outer Diameter = 0.424 in. (Exxon)

Fuel Cladding Thickness = 0.03 in. (Exxon)

Number of Rods = 358

Area of Fuel Cladding = 13.2938 in²

Momentum of Inertia of Cladding = 0.2595 in⁴

The elastic modulus of the fuel rod cladding (Zircaloy) is only 12×10^6 psi.

Effective Cross-Section Properties of Consolidated Canister

The individual properties of the fuel cladding and the consolidated canister are used to calculate the combined cross-section properties as follow. The elastic modulus of the canister is used for the beam representation in the seismic analysis.

Effective Area

$$A_{eff} = (E_f / E_c) A_f + A_c = 9.3920 \text{ in}^2$$

Effective Moment of Inertia

$$I_{eff} = (E_f / E_c) I_f + I_c = 32.6148 \text{ in}^4$$

Where: E_f = Fuel Cladding Elastic Modulus, 12×10^6 psi

A_f = Fuel Cladding Cross Sectional Area = 13.2938 in²

I_f = Fuel Cladding Moment of Inertia = 0.2595 in⁴

E_c = Canister Elastic Modulus, 27.87×10^6 psi

A_c = Canister Cross Sectional Area = 3.6681 in²

I_c = Canister Moment of Inertia = 32.5031 in⁴

3.5.3.1.1.2.2 Fuel Assembly Structural Properties

The following structural properties were used in the rack analysis to represent the fuel assembly. The properties envelope Exxon's and Westinghouse's (standard and optimized) fuel assemblies. Each fuel assembly represents 179 fuel rods, 16 guide tubes, and 1 instrument tube. The properties closely resemble the previous analysis (Reference 3.25, section 5.10).

Fuel Assembly's Cross Sectional Area = 7.1419 in²

Fuel Assembly's Beam Shear Factor Used in ANSYS = 1.89

Fuel Assembly's Area Moment of Inertia = 2.17 in⁴

The Elastic Modulus of the Fuel Assembly (Zircaloy) = 12.0×10^6 psi.

Fuel Assembly's Width = 7.763 in

Fuel Assembly Wet Weight = 1306.6 lbs (per assembly)

3.5.3.1.1.3 Interface Stiffness Between Fuel and Rack

The calculations were performed to generate the interface stiffness between the fuel and rack cells. The interface of interest was the impact of the upper end fitting with the stainless steel tube of the rack. This stiffness was calculated using a plate finite element model of a single cell and computer program ANSYS 5.2. A pressure load was applied in the area of contact between the upper end fitting and the cell wall while constraints prevent beam bending of the cell. The stiffness desired was only the local effect because the beams in the model already account for beam deflection. The stiffness was then determined by dividing the total load applied by the average deflection at the top edge of the cell wall.

Contact area between upper end fitting and cell wall:

Type 1 (Existing Racks)

Cell Height = 159 in.

Outside Tube Width = 8.43 in.

Tube Wall Thickness = 0.090 in.

Types 2 and 3 (New ATEA Racks):

Cell Height: Type 2 = 158.5 in.
 Type 3 = 162 in.

Inside Tube Width: Type 2 = 8.1417 in.
 Type 3 = 8.3386 in.

Tube Wall Thickness = 0.07874 in.

Fuel Assembly Heights Exxon - 160.13 in. Westinghouse OFA - 159.710 in.
Upper End Fitting Heights Exxon - 6.865 in. Westinghouse OFA - 3.480 in.



Elevation of beginning of contact between upper end fitting and cell wall:

Exxon: $h = 153.265$ in.

Westinghouse_OFA: $h = 156.230$ in.

The model used was constructed of shell elements which were placed at the midplane of the tube walls. In the type 1 racks, there was a tube for each fuel assembly. Therefore, the load was applied to only one side of the cell. For the type 2 and 3 racks, there was one tube for every two fuel assemblies. Therefore, the load was applied in the same direction on opposite sides of the tube.

The deflections were generated from the finite element model. The stiffness was then determined by dividing the total load applied by the average deflection at the top edge of the cell wall, which is summarized below:

Fuel Cell Impact Stiffness summary:

Type 1 (Existing U.S. Tool & Die Racks): 4449 lb/in.

Type 2 and Type 4 (New ATEA Racks): 7036 lb/in.

Type 3 (New ATEA Racks): 6595 lb/in.

3.5.3.1.1.4 Damping

Structural damping was specified in the seismic analysis. The computer program ANSYS provided five choices (or five forms) to input damping values. Among them Rayleigh Damping (also called as alpha and beta damping) method was used in the Ginna seismic analysis, where

The Damping Matrix. $[C] = \alpha[M] + \beta[K]$

The values of α and β are not generally known directly, but can be calculated from modal damping ratios, ξ_i . Where ξ_i is the ratio of actual damping to critical damping for a particular mode of vibration, i . If ω_i is the natural circular frequency of mode i , α and β satisfy the relation:

$$\xi_i = \frac{\alpha}{2 \omega_i} + \frac{\beta \omega_i}{2}$$

$$\text{since } \omega_i = 2 \pi f_i$$

$$\xi_i = \frac{\alpha}{4 \pi f_i} + \pi f_i \beta$$

Only one set of α and β are input in an analysis, so one needs to select the dominant frequency active in that load step, to calculate α and β . In the storage rack seismic analysis, the fuel assembly impact was dominant. For that reason, the fuel assembly frequencies were used in the calculations of α and β values. Also, it was considered that the first three modes of the fuel assembly were important in the seismic analysis. The values for α and β were developed for first three modes of fuel assembly frequencies.

The damping (ξ) values were taken from U.S. NRC Regulatory Guide 1.61 (Reference 3.11), for welded steel structure. The α and β values were developed for both OBE and SSE loadings using fuel frequencies and Regulatory guide damping.

Fuel Assembly:

First mode frequency is $f_1 = 3$ Hz (Page 19, U.S. Tool & Die Seismic Report, Reference 3.25)

$$f_n = C_n \sqrt{\frac{g E I}{W L^4}}$$

For hinged-free beam:

(Mark's Handbook 7th Edition Page 5-101, Reference 3.33)

Where $C_n = 2.45$ for first mode hinged-free beam, and

$C_n = 16.6$ for third mode hinged free beam.

Using this the third mode frequency is

$$\begin{aligned} f_3 &= \frac{16.6}{2.45} \times 3 \\ &= 20.3 \text{ Hz} \end{aligned}$$

Using damping values from U.S. NRC Regulatory Guide 1.61 for welded steel structure:

$$\xi_{OBE} = 2 \% \text{ or } 0.02$$

$$\xi_{SSE} = 4 \% \text{ or } 0.04$$

Mode Number	Frequency Hz	ξ damping OBE	SSE
1	3	0.02	0.04
3	20.3	0.02	0.04



For OBE:

$$\text{@ Mode 1} \quad 0.02 = \frac{1}{4 \pi \times 3} \alpha + \pi \times 3 \times \beta$$

$$\text{@ Mode 3} \quad 0.02 = \frac{1}{4 \pi \times 20.3} \alpha + \pi \times 20.3 \times \beta$$

$$\text{Solving:} \quad \alpha = 0.6568 \text{ and} \\ \beta = 2.7323 \times 10^{-4}$$

For SSE:

$$\text{Similiarly solving for SSE:} \\ \alpha = 1.3136 \text{ and} \\ \beta = 5.4647 \times 10^{-4}$$

Summary:

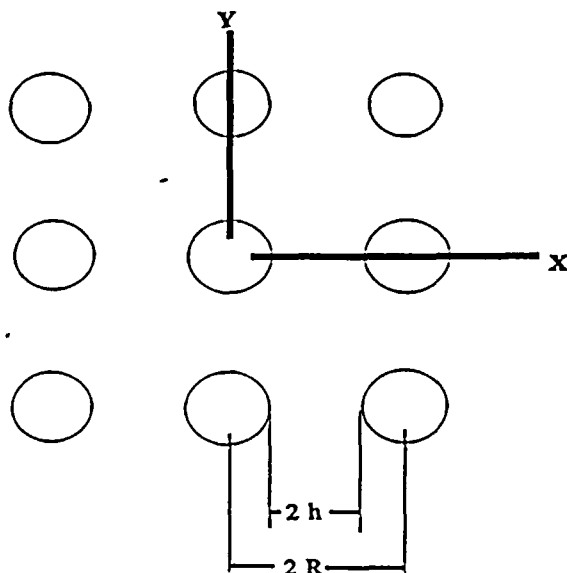
α and β values for damping:

OBE	$\alpha = 0.6568$	$\beta = 2.7323 \times 10^{-4}$
SSE	$\alpha = 1.3136$	$\beta = 5.4647 \times 10^{-4}$

3.5.3.1.1.5 Perforated Plates

The bottom plates for the spent fuel storage racks are plates with flow holes. The equivalent homogeneous plate was idealized for plates with circular holes arranged in square pattern. The plate thickness was kept the same in the analysis. The Young's Modulus (E^*) and Poisson's Ratio (ν^*) was modified to reflect square pattern perforation in the plate. ASME Section III, Appendix A, Article A-8000 addresses the perforated plate. However, the Article A-8000 only addresses the holes in array of equilateral triangle.

The Welding Research Council Bulletin #151, June 1970 (Reference 3.28) titled, "Further Theoretical Treatment of Perforated Plates with Square Penetration Pattern" was used. This bulletin addressed the loading in pitch and diagonal direction. For the seismic analyses, the pitch direction loading was more appropriate and was used.



Nomenclature:

h / R Ligament efficiency
 E Young's Modulus of material
 E^* effective Young's Modulus of perforated plate with the same thickness
 v^* effective Poisson's ratio of perforated plate with the same thickness

Type 2 and Type 4 (ATEA) Racks - Perforated Plate

Thickness of plate $t = 1.18$ in
 Flow hole size 3.74 in
 Rectangular Pitch $2R = 8.43$ in

Width of ligament $2h = \text{Pitch} - \text{Hole diameter}$
 $= 8.43 - 3.74$
 $= 4.69$ in

Ligament efficiency $h / R = 4.69 / 8.43$
 $= 0.56$

From Figure 3 of WRCB #151 for loading in pitch direction:

$$\frac{E^*}{E} = 0.68 \quad \text{and} \quad v^* = 0.28$$

Type 3 (ATEA) Rack - Perforated Plate

Thickness of plate $t = 1.18$ in
Flow hole size 3.74 in
Rectangular Pitch $2R = 9.23$ in

Width of ligament $2h = \text{Pitch} - \text{Hole diameter}$
 $= 9.23 - 3.74$
 $= 5.49$ in

Ligament efficiency $h / R = 5.49 / 9.23$
 $= 0.59$

From Figure 3 of WRCB #151 for loading in pitch direction:

$$\frac{E^*}{E} = 0.72 \quad \text{and} \quad \nu^* = 0.285$$

Summary of Perforated Plates

For perforated plates, using same thickness as drawing, the equivalent E^* Young's Modulus and equivalent ν^* Poisson's Ratio for homogeneous idealization is as follows. These values were used in the stress analysis of the perforated plates.

	Plate Thickness <u>in</u>	<u>E^*/E</u>	<u>ν^*</u>
ATEA Type 2 Rack	1.18	0.68	0.28
ATEA Type 3 Rack	1.18	0.72	0.285
ATEA Type 4 Rack	1.18	0.68	0.28

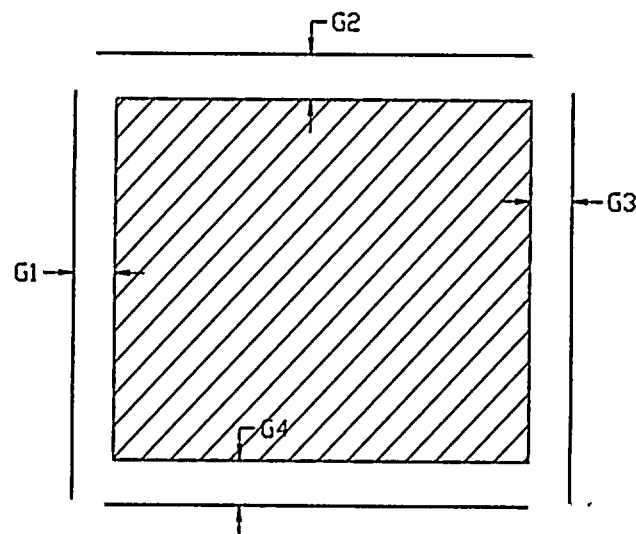


3.5.3.1.1.6 Local Gaps Surrounding Each Rack

Gaps Surrounding Rack - Without Perimeter Racks - At Base (Inches)				
Rack	Gap 1	Gap 2	Gap 3	Gap 4
1	10.500	0.500	1.750	14.750
2	9.750	15.250	1.250	0.500
3	1.750	0.750	0.750	15.500
4	1.250	14.250	0.630	0.750
5	0.750	0.750	0.550	17.000
6	0.630	12.750	3.380	0.750
7	0.550	0.790	96.480	7.050
8	0.550	0.790	0.790	0.790
9	3.380	0.790	0.790	0.790
10	3.380	1.720	0.790	0.790
11	0.790	0.790	3.270	96.180
12	0.790	0.790	3.270	0.790
13	0.790	1.720	3.270	0.790

Gaps Surrounding Rack - With Perimeter Racks - At Base (Inches)				
Rack	Gap 1	Gap 2	Gap 3	Gap 4
1	10.500	0.500	1.750	5.250
2	9.750	5.750	1.250	0.500
3	1.750	0.750	0.750	6.000
4	1.250	4.750	0.630	0.750
5	0.750	0.750	0.550	7.500
6	0.630	3.250	3.380	0.750
7	0.550	0.790	96.480	7.050
8	0.550	0.790	0.790	0.790
9	3.380	0.790	0.790	0.790
10	3.380	1.720	0.790	0.790
11	0.790	0.790	3.270	96.180
12	0.790	0.790	3.270	0.790
13	0.790	1.720	3.270	0.790

Note: Gap1=G1(West), Gap2=G2(North), Gap3=G3(East), Gap4=G4(South)
For gap dimensions, see the following sketch.



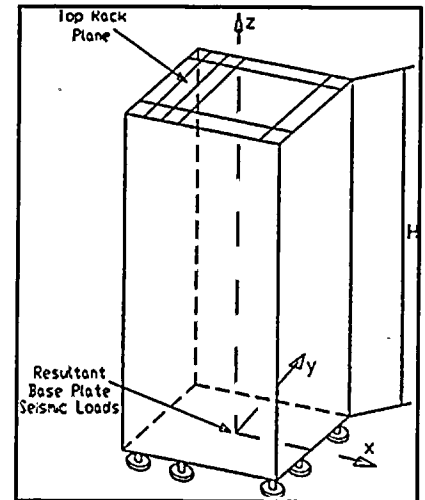


3.5.3.1.2 Rack Tube Connecting Tabs and Tube Retainer Plate Welds

The tab plates are welded to rack cells (tubes) in order to maintain the structural integrity of the rack. The primary function of tabs is to provide a transfer of the shear flow between the tubes. In ATEA racks, mutually perpendicular pairs of tabs are welded to adjacent interior stainless tubes. For both type 2 and type 3 racks, there are 4 pairs of uniformly spaced tabs per each interior tube edge.

Tab stresses are derived from the following three stress components:

- a) Interior rack beam loads resulting from seismic full pool rack analyses. Base plate shear force components are assumed to act as uniformly distributed loads along rack height, and develop shear stresses acting upon tabs. Resultant interior rack bending moments induce normal stresses in rack tubes, but not in tabs which are exposed to shear only. The rack forces and moments are provided from the full pool runs.
- b) Rack-to-fuel beam (regular fuel assembly or consolidated fuel canister) impact loads. Depending on an impact direction relative to tab orientation, two impact models are considered. Section 3.5.3.1.2.2 describes the rack to fuel beam impact models in more detail. Obtained tab loads are superimposed to the condition "a)" shear stresses. Note that the internal rack force and moment resultants obtained from the full pool analyses are reflected in the "a" tab shear stress components calculation. Impact loads also produce normal (axial) stresses in tabs, as well as bending moment in both tabs and tab welds.
- c) Thermally induced stresses due to "Normal - To" and "Abnormal - Ta" thermal conditions. Section 3.5.3.1.10 covers thermal stress calculation. Depending on the load combinations, thermal stresses for the two conditions are superimposed to the combined "a" and "b" stresses.



3.5.3.1.2.1 Tab/Weld Stresses due to Seismic Loads

This section evaluates the maximum shear stresses developed in rack tubes interconnecting tabs, developed as a result of seismic rack shear forces F_x and F_y . Assuming clamped simple beam as an equivalent of rack tubes, seismic shear force resultants F_x and F_y are considered uniformly distributed across the rack tube height. At any rack tube cross-section parallel to the base plate, parabolic shear stress distribution is developed. Maximum shear stresses occur nearby the base plate, i.e. in the lowest tab group, and also along the rack tube cross section neutral axes:

$$\tau_{\max} = \frac{V}{I(\Sigma t)} Q$$



where: V Rack shear load resultant, Fx or Fy.
I Moment of inertia for a rack tubes cross section about its principal axes perpendicular to the shear force (V) direction.
Q First moment of inertia at the neutral axis location of the rack tubes cross section.
Σt Cumulative tab thickness, for all tubes along the neutral axis to the shear force direction.

Extreme OBE load case is number 8, with maximum shear loads developed in rack 3E (#11):

Fx = 51,930 lbs and Fy = 20,820 lbs; (section 3.5.3.1.8)

Extreme SSE load case is number 3, with maximum shear loads developed in rack 2B (#8):

Fx = 98,880 lbs and Fy = 60,740 lbs; (section 3.5.3.1.8)

Cross section properties for racks 3E(#11) and 2B(#8) are listed in the table below:

ATEA Rack	3E (#11)	2B (#8)
t [in]	0.0787	0.0591
Ix [in ⁴]	31,335	75,257
Iy [in ⁴]	77,073	110,201
Qx [in ³]	1,073	1,506.5
Qy [in ³]	607.8	1,222.7
(Σt) _x	5t	8t
(Σt) _y	9t	10t

Maximum Tab (Base Metal) Shear Stresses for OBE Case

Seismic stress enveloping factor for OBE cases is f=1.12. The shear stresses are:

$$\tau_x = f \frac{F_x Q_x}{I_y (\Sigma t)_x} = 1.12 \frac{51,930 \times 1,073}{77,073 \times (5 \times 0.0787)} \approx 2,058 \text{ p.s.i.}$$

$$\tau_y = f \frac{F_y Q_y}{I_x (\Sigma t)_y} = 1.12 \frac{20,820 \times 607.8}{31,335 \times (9 \times 0.0787)} \approx 639 \text{ p.s.i.}$$

Combined tab shear stress acting in vertical-Z direction is

$$\tau_{\max} = \tau_x + \tau_y \approx 2,697 \text{ p.s.i.}$$

Maximum Tab (Base Metal) Shear Stresses for SSE Case

Seismic stress enveloping factor for SSE cases is $f=1.20$. The shear stresses are:

$$\tau_x = f \frac{F_x Q_x}{I_y (\Sigma t)_x} = 1.20 \frac{98,880 \times 1,506.5}{110,201 \times (8 \times 0.0591)} \approx 3,431 \text{ p.s.i.}$$

$$\tau_y = f \frac{F_y Q_y}{I_x (\Sigma t)_y} = 1.20 \frac{60,740 \times 1,222.7}{75,257 \times (10 \times 0.0591)} \approx 2,004 \text{ p.s.i.}$$

Combined tab shear stress acting in vertical-Z direction is

$$\tau_{\max} = \tau_x + \tau_y \approx 5,435 \text{ p.s.i.}$$

Maximum Weld Stresses

Tabs are welded to the tubes via fillet welds, with the following effective weld throats:

Type 2 tabs: $a = 0.8 \text{ mm} = 0.0315''$

Type 3 tabs: $a = 1.2 \text{ mm} = 0.0472''$

Weld stresses can be obtained by linearly scaling tab τ_{\max} shear stress, acting in vertical-Z direction, due to combined influence of F_x and F_y shear forces:

Rack #8 (type 2): $(\tau_{\max})_w = (\tau_{\max})_{\text{tab}} t/a = (\tau_{\max})_{\text{tab}} 1.5/0.8 = 1.875 (\tau_{\max})_{\text{tab}}$

Rack #11 (type 3): $(\tau_{\max})_w = (\tau_{\max})_{\text{tab}} t/a = (\tau_{\max})_{\text{tab}} 2.0/1.2 = 1.667 (\tau_{\max})_{\text{tab}}$

Results are summarized in the table below:

Shear Stresses	OBE (Rack #11)	SSE (Rack #8)
$(\tau_{\max})_{\text{tab}}$ [psi]	2,697	5,435
$(\tau_{\max})_{\text{weld}}$ [psi]	5,057	9,058

Note: Estimated stresses are conservative, since maximum of the two component shear forces F_x and F_y may not occur at the same time instant.

3.5.3.1.2.2 Tab/Weld Stresses due to Fuel-to-Tube Impact

This section discusses a tab strength when a fuel assembly or consolidated canister impacts a rack tube. The impact load is further transmitted through the set of tab pairs to the adjacent tubes. Maximum fuel to rack beams cumulative impact loads for new ATEA racks are listed in Section 3.5.3.1.8:



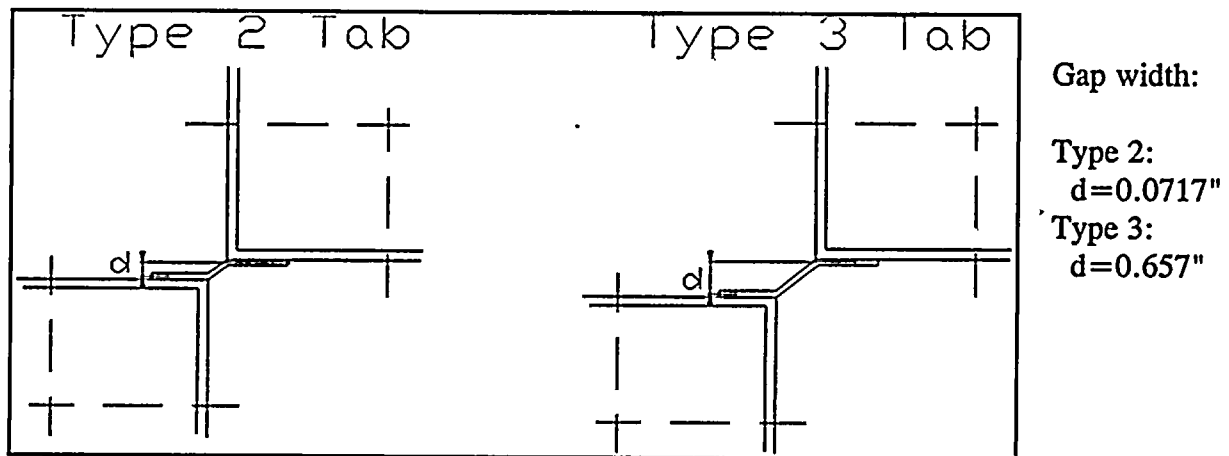
OBE: $811 \text{ lbs} \times 1.12 \text{ (stress enveloping factor)} = 908 \text{ lbs}$
SSE: $1,331 \text{ lbs} \times 1.20 \text{ (stress enveloping factor)} = 1,597 \text{ lbs}$

Considering tab and tab-to-tube welds strength, two possible impact scenarios are distinguished:

- a) Longitudinal tab impact
- b) Lateral tab impact

A) *Longitudinal tab impact* refer to a case where the impact force is transmitted along the tab, so that the force direction is parallel to the tab plane. Each stainless steel tube corner is connected to its neighboring SS tubes with a set of tab pairs, mutually perpendicular to each other. This design enables transmission of fuel to rack tubes impacts in either X or Y directions. This analysis also conservatively assumes that series of tabs perpendicular to the assumed impact direction do not contribute as stress bearing elements. Actual stresses in longitudinal tabs are therefore lower than predicted. Figure 3.5-38 depicts top view of a pair of SS tubes connected with a tab set parallel to the direction of the impacting force, assumed here to act horizontally.

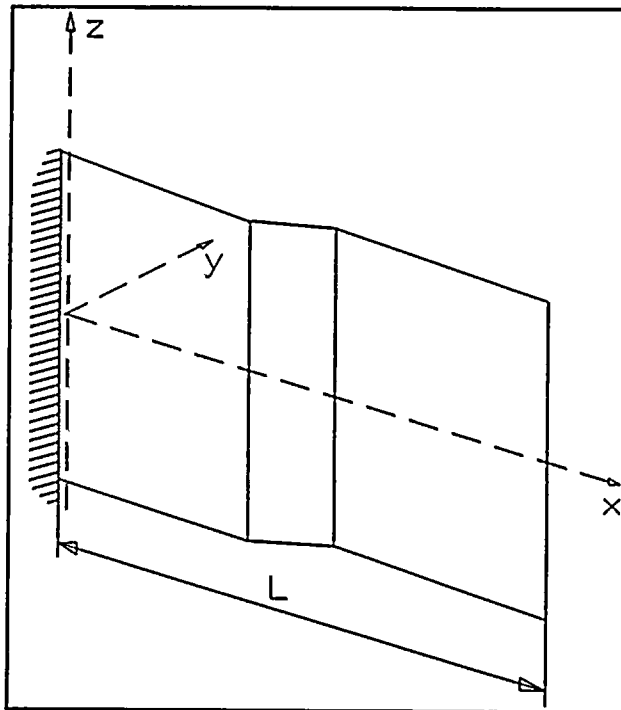
Figure 3.5-38 Longitudinal Tab Impact Model



A finite element model of the rack tube with integral tabs is constructed to obtain impact load distribution across all tube tabs. Impact resultants are obtained for all tube model tabs, and are based on 1,000 lbs total impact force. Maximum resultant impact reactions acting upon a single tab for type 2 and 3 rack tubes are then applied to a single tab finite element model with neighboring SS tubes, as shown in Fig.3.5-38. Tab model consists of 3 shell finite elements, while half of an each SS tube side is discretized into six shell elements. Tab to tube welds are modeled so that welded tab edges share common edges of the corresponding SS tube finite elements. Obtained stress reactions used for tab (base metal) and weld strength qualification are listed in the table below:

Load components	Type 2 tab	Type 3 tab
Fx [lbs]	304	215.3
Fy [lbs]	45.3	110.3
Fz [lbs]	9.5	58.4
Mx [in-lbs]	negligible	negligible
My [in-lbs]	21.6	136
Mz [in-lbs]	21.38	41.32

Local tab coordinate system where the force and moment components are defined is shown in the sketch below:



Overall tab length :

type 2: $L = 1.3487''$

type 3: $L = 2.329''$

Tab height: $h = 7.0866''$

Tab thickness :

type 2: $t = 0.0591''$

type 3: $t = 0.0787''$

Tab weld throat :

type 2: $t = 0.0315''$

type 3: $t = 0.0472''$

The following stress components are considered:

Tab (base metal):

- membrane stress σ_m - tab cross section perpendicular to x-axis.
- average shear $\tau = V/A$; where $V = ((F_y)^2 + (F_z)^2)^{1/2}$, and $A = h t$
- normal stress σ_{by} - due M_y : $\sigma_{by} = M_y h / 2I_y$, where $I_y = h^3 t / 12$
- normal stress σ_{bz} - from single tab finite element model



- Total normal stress : $\sigma = \sigma_m + \sigma_{by} + \sigma_{bz}$
- Maximum principal stress : $\sigma_1 = 1/2[\sigma + (\sigma^2 + 4\tau^2)^{1/2}]$

Weld:

- a) average shear $\tau = V/A$; where $V = ((F_x)^2 + (F_y)^2 + (F_z)^2)^{1/2}$, and $A = h a$
- b) normal stress σ_{by} - due M_y : $\sigma_{by} = M_y h/2I_y$, where $I_y = h^3 a/12$
- c) normal stress σ_{bz} - from single tab finite element model, scaled for the throat thickness

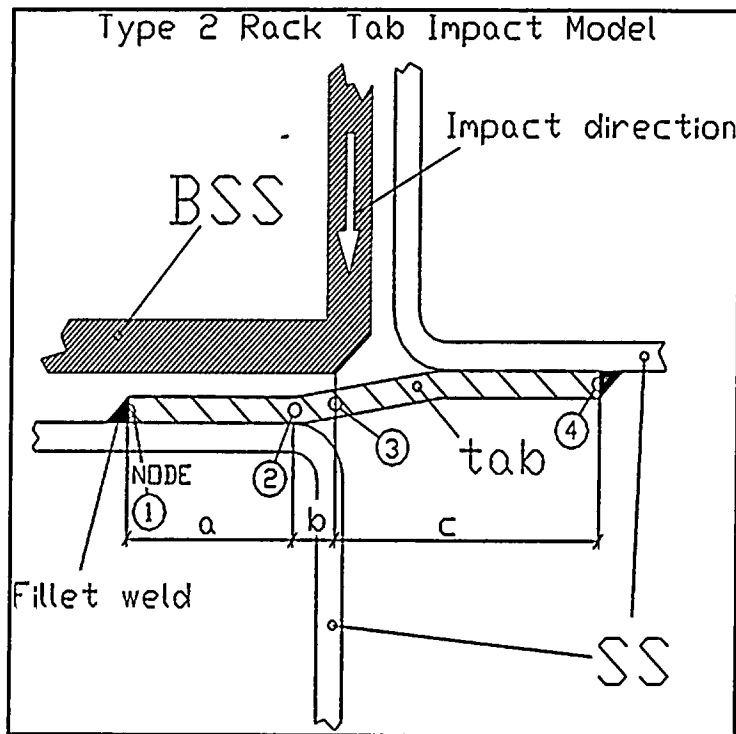
- Total normal stress : $\sigma = \sigma_{by} + \sigma_{bz}$
- Maximum principal stress : $\sigma_1 = 1/2[\sigma + (\sigma^2 + 4\tau^2)^{1/2}]$

Results for type 2 and 3 tabs and welds are tabulated below:

Stress Components	Base Metal (Tab) (stress, psi)		Weld (stress, psi)	
	Type 2	Type 3	Type 2	Type 3
Membrane - σ_m	726.3	444.7	N/A	N/A
Avg.shear - τ	110.5	224	1377.7	745
Normal - σ_{by}	25.9	206.5	82	344.2
Normal - σ_{bz}	2901	4961	4685.5	8268
Normal - σ	3653	5612	4768	8613
Principal - σ_1	3656	5621	5138	8677

B) Lateral tab impact relates to tab strength in a situation where fuel assembly or consolidated canister impacts a borated stainless steel (BSS) tube in which case the impact load can be further transmitted to a tab interconnecting adjacent stainless steel (SS) tubes. Typical layout is shown in Fig.3.5-39, in case of the type 2 rack tabs. This consideration is not fully applicable to the type 3 rack tabs, due to the existence of belt connectors that bridge BSS to adjacent SS cell tubes for load transmission.

Figure 3.5-39 Lateral Tab Impact Model



Characteristic dimensions:

$$a = 0.485 \text{ in}$$

$$b = 0.096 \text{ in}$$

$$c = 0.800 \text{ in}$$

$$\text{Tab thickness } t = 0.0591" \text{ (1.5 mm)}$$

$$\text{Tab length } l = 7.087" \text{ (180 mm)}$$

The tab is modeled as a beam clamped at both ends (weld locations, nodes 1 and 4) and simply supported at node 2, the point where surface contact between the tab and the SS tube wall ends. BSS tube is assumed to impact the tab at the point marked as node 3. For this twice statically indeterminate beam, a three beam segment finite element model was made (ANSYS) with a vertical unit load $P=1$ lbs, acting in the assumed impact direction. The following results were obtained:

Node #	1	2	3	4
Shear Force [lbs] (*)	$0.145*P$	$-1.077*P$	P	$-0.077*P$
Bending Moment [in-lbs]	$0.0248*P$	$0.0496*P$	$0.039*P$	$0.0226*P$

(*) positive shear force direction is assumed to be in direction of applied P , ie. downward.

The largest bending moment will be developed at node 2, if P reaches limit value P_L , causing yielding of the tab cross section. The corresponding bending moment limit is:

$$M_L = \sigma_y \frac{bt^2}{4} = 143.3 \text{ in-lbs}$$

where σ_y is the tab material yield strength (21.3 ksi for SS 304L, taken at 150°F). Hence, the limit load is then $P_L = M_L / 0.0496 = 2,888$ lbs. The average shear at that cross section can be estimated as $\tau = (0.145 + 1.077)P_L / (bt) = 8,343$ psi < 9,420 psi (Service Level A or B Stress Acceptance Criteria for pure shear). The maximum cumulative impact loads between fuel and rack beam, for the new ATEA racks are for both OBE and SSE conditions less than limit load estimated value P_L . Hence, it is concluded that the *type 2 rack tabs will not undergo permanent deformation if impacted* by an adjacent loaded BSS tube. This consideration excludes the fact that only part of the above expected impact loads would be transmitted to a single tab, as well as that the other BSS tube corner or edge would impact another tab group welded to the other SS tube corner.

The maximum combined stress developed in fillet weld at node 1 in Fig.3.5-39 is estimated as

$$S = \sqrt{\sigma^2 + \tau^2}$$

where σ is the bending moment induced stress in weld, and τ is the vertical shear at the same location. Hence,

$$\sigma = \left(\frac{M_1}{I} \right) \left(\frac{a}{2} \right) \quad \text{and} \quad \tau = \frac{V_1}{A_s}$$

where

$M_1 = 0.0248 * (0.5 * P_{imp})$, and P_{imp} = the total BSS tube to tab impact load (listed above)
 $I = (ba^3)/12$, the tab cross section moment of inertia ($a=0.0315$ " or 0.8mm the weld throat)

$V_1 = 0.145 * (0.5 * P_{imp})$

$A_s = ba$, the effective weld shear area (reduced to its throat)

Results are tabulated below:

OBE	$P_{imp} = 908$ lbs	$\sigma = 9.65$ ksi	$\tau = 0.295$ ksi	$S = 9.654$ ksi
SSE	$P_{imp} = 1597$ lbs	$\sigma = 16.9$ ksi	$\tau = 0.52$ ksi	$S = 16.91$ ksi

The allowable fillet weld metal stresses are 21 ksi for Service Level A (OBE), and 31.5 ksi for Service Level D (SSE). Therefore, tab welds can withstand estimated impact forces with margin of safety greater than 86% (for both SSE and OBE conditions).

Summary of the mechanically induced tab stresses



Superimposed loading conditions are:

- 1) Seismically induced tab/weld stresses (Section 3.5.3.1.2.1).
- 2a) Stresses due to the longitudinal impact (Section 3.5.3.1.2.2.A). Stresses are obtained for 1,000 lbs total impact force, and scaling factors have to be applied for OBE (0.908) and SSE (1.6) conditions.
- 2b) Stresses due to the lateral impact (Section 3.5.3.1.2.2.B).

Results are summarized in the table below:

Table 3.5-14 Mechanical Tab/Weld Stresses

Type	Stress Category	OBE Stress (psi) (1) + (max of 2a or 2b)	SSE Stress (psi) (1) + (max of 2a or 2b)
Base Metal (Tab)	Pm	$726.3(2a) \times 0.908 = 659.5$	$726.3(2a) \times 1.6 = 1162$
	Pm+Pb	$5621(2a) \times 0.908 = 5104$ or $5759(2b)$	$5621(2a) \times 1.6 = 8994$ or $10148(2b)$
	Avg. Shear	$2697(1) + 1324(2b)$ or $224(2a) \times 0.908$	$5435(1) + 2333(2b)$ or $224(2a) \times 1.6$
Weld	Avg. Shear	$5057(1) + 1377.7(2a) \times 0.908 = 1251$ or $295(2b)$	$9058(1) + 1377.7(2a) \times 1.6 = 2204$ or $520(2b)$
	Pm+Pb	$8677(2a) \times 0.908 = 7879$ or $9659(2b)$	$8677(2a) \times 1.6 = 13883$ or $9659(2b)$

3.5.3.1.2.3 Thermal Stresses in Tabs/Welds

Maximum thermally induced stresses in tabs and tab welds are taken from section 3.5.3.1.10. An assumption is made that maximum thermal stresses occurring in rack tubes conservatively envelop tab/welds thermal stresses. The rack thermal finite element model (section 3.5.3.1.10) assumes rigid connections between the rack tubes. In reality, the tubes are connected via tabs and tab-to-tube line welds. In return, the whole rack structure is more flexible than the assumed rack finite element model. Hence, the obtained stresses from the model envelop real thermal stresses in tabs and tab-to-tubes welds. Table 3.5-15 summarizes thermal stresses for Normal (To) and Abnormal (Ta) thermal conditions.

Table 3.5-15 Tabs/Welds Thermally Induced Stresses

Stress [psi]	To - condition	Ta - condition
membrane	3,837	9,654
membrane + bending	9,856	9,803



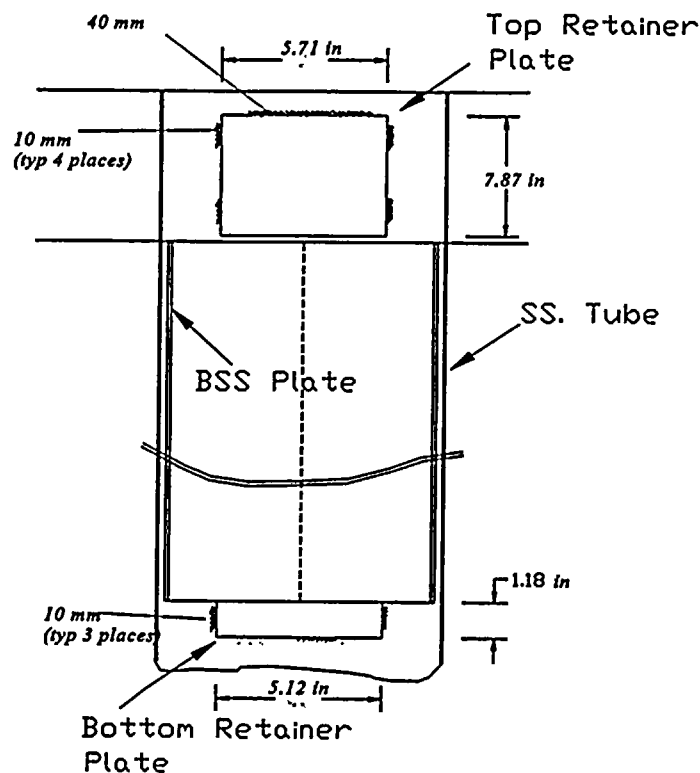
3.5.3.1.2.4 Total Tab/Weld Stresses

Stress components from summary table in Section 3.5.3.1.2.1, Tables 3.5-14 and 3.5-15 are superimposed in order to arrive to maximum estimated stresses in tabs and tab welds.

Summarized values are reported in Section 3.5.3.3, Table 3.5-144. It is therefore concluded that tabs and tab welds has adequate margin against ASME code allowables for levels A,B and D.

3.5.3.1.2.5 Borated Stainless Steel Retainer Plates Weld Stresses

Type 2 and 3 Racks Borated Stainless Steel cells are held in place by 4 mm thick plates. The following calculations qualify the retainer plates and welds for maximum impact loadings (shear) on the rack cell. The following figure shows the retainer plate locations and dimensions.



Type 2 and 3 Retainer Plate Dimensions:

<u>Plates</u>	<u>Top Retainer Plates</u>	<u>Bottom Retainer</u>
Height (vertical)	7.87 in (200 mm)	1.18 in (30 mm)
Length (horizontal)	5.71 in (145 mm)	5.12 in (130 mm)
Plate Thickness	0.16 in (4 mm)	0.16 in (4 mm)

The retaining plates are the same size for both rack types 2 and 3.

The minimum weld throat equals 0.0313 inches (0.8 mm) for both top and bottom plates.

The total weld length required for the top retainer plate equals 3.15 inches (80 mm),
 $A_w = 0.10 \text{ in}^2$

The total weld length for the bottom retainer plate equals 1.18 inches (30 mm), $A_w = 0.04 \text{ in}^2$.

The BSS's deadweight equals 164.9 lbs. Each lower retainer plate receives 165/4 or 41.25 lbs.

The maximum stresses result from a stuck fuel assembly accident condition where the total uplift force acting on all four sides of the BSS tube equals 2000 lbs. Each top retainer plate receives 1/4 of the uplift or 500 lbs. The stuck fuel assembly condition affects the upper retainer plate and occurs only in the Service Level B stresses.

For Service Level D stresses, a "g" value (acceleration) was determined for SSE. The maximum rack weight is rack number 8 (2B) equaling 246,867 lbs per section 3.5.3.1.1.1. The maximum SSE plus deadweight for rack 8 equals 322,400 (per section 3.5.3.1.5 for Load case 3). The ratio of the highest deadweight plus SSE over the rack deadweight gave an acceleration value of 1.31 g (includes deadweight). Using the time history factor of 1.2 gives a "g" value of 1.57. Therefore, the SSE loading of the BSS cell (per plate) equals $41.25 * 1.57 = 64.8 \text{ lbs}$.

Obtained stresses and corresponding allowables are summarized below:

<u>Load Service Level</u>	<u>Base Metal</u> <u>Maximum Weld Stress</u>	<u>Allowable Stress</u>
Service Level A	1,031 psi	$0.4 * S_y = 9,260 \text{ psi}$
Service Level B	5,000 psi	$0.532 * S_y = 11,725 \text{ psi}$
Service Level D	1,620 psi	$0.42 * S_u = 28,120 \text{ psi}$

Retainer Plates welds are shown qualified.



THE UNIVERSITY OF CHICAGO LIBRARY 1207 EAST 58TH STREET CHICAGO, ILL. 60637

3.5.3.1.2.6 Rack Tube Buckling Strength and Tab Weld Spacing

This section evaluates the strength of the Rochester Gas & Electric GINNA spent fuel ATEA rack tube against buckling requirements. This section demonstrates the compliance of Standard Review Plan, Section 3.8.4, Appendix D, and ASME Section III, Subsection NF. The results are applicable to ATEA type 2, 3, and 4 racks.

Compressive stresses in rack tubes are evaluated at the lower, base plate level, as a result of combined action of bending moments about principal axes M_x and M_y and vertical inertial load F_z ($\sigma_a = F_z/A$, A -material cross section for all tubes), all due to seismic activity. Total stress thus obtained is scaled with the time history enveloping factor f_{th} equal to 1.20 for SSE or 1.12 for OBE conditions (section 3.5.2.6), as

$$\sigma_z = f_{th} \sqrt{\left(M_x \frac{y_{ct}}{I_x} \right)^2 + \left(M_y \frac{x_{ct}}{I_y} \right)^2 + \sigma_a^2}$$

Square root of sum of squares of each peak compressive load component is taken since generally they do not occur at the same time instant.

As depicted in the sketch shown below, the total compressive tube stress is evaluated for the farthest edge of the corner tube for each rack (distances x_{ct} and y_{ct} , measured with respect to shown principal coordinate system). This ensures conservatism of calculated stresses. Cross section properties (tube racks) for all racks are summarized in the Table 3.5-16.

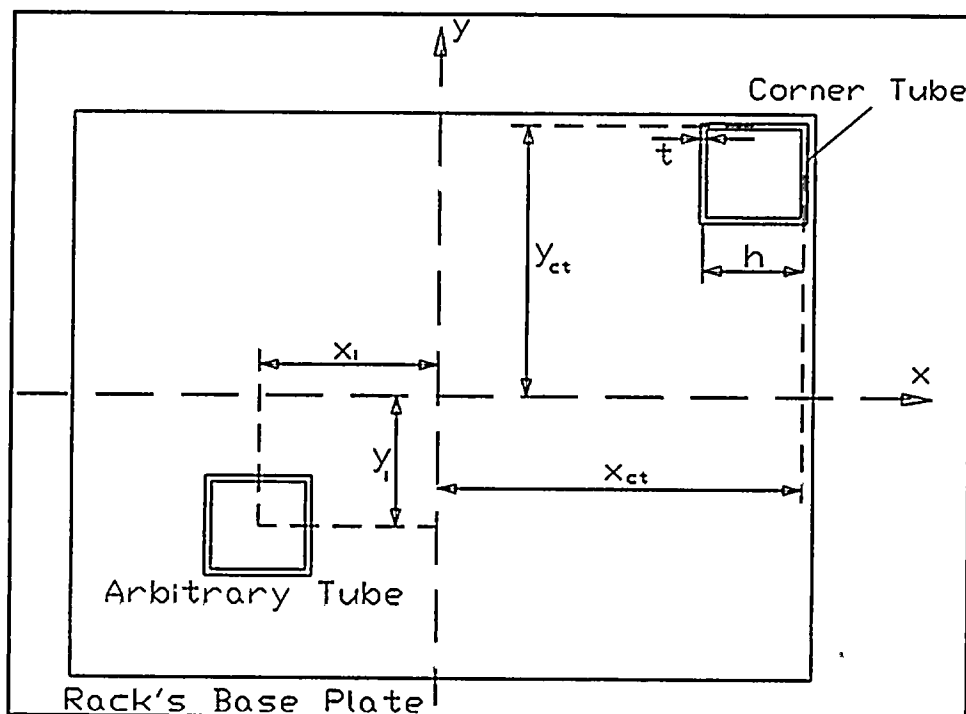


Table 3.5-16 Rack Cross-section Properties for Tubes

Rack #	Xpr [in]	Ypr [in]	Ix-pr [in^4]	Iy-pr [in^4]	At [in^2]	Xct [in]	Yct [in]
7	46.4	33.7	53,893	98,523	126.2	46.37	33.72
8	46.4	37.9	75,257	110,201	141.1	46.37	37.94
9	46.2	23.1	16,308	59,240	76.2	46.15	23.08
10	46.1	32.3	41,407	81,057	104.1	46.15	32.31
11	46.1	35.5	31,335	77,073	94.7	46.15	35.49
12	46.2	23.1	16,308	59,240	76.2	46.15	23.08
13	42.7	29.4	33,486	69,215	93.5	49.55	35.19

Note:

- Xpr - X-location of Y (NS) principal axis *
- Ypr - Y-location of X (EW) principal axis *
- Ix-pr - Principal moment of inertia (tubes) about X axis
- Iy-pr - Principal moment of inertia (tubes) about Y axis
- At - Total cross section area (all tubes)
- Xct - Max.corner tube edge to base plate center distance in X
- Yct - Max.corner tube edge to base plate center distance in Y

(*) principal axes are obtained for ensemble of all tubes in particular rack base plate

Moments of inertia for all tubes in given rack are calculated via

$$I_x = \sum_{i=1}^{i=n_t} (I_{pr}^x + A_t y_i^2) \quad ; \quad I_y = \sum_{i=1}^{i=n_t} (I_{pr}^y + A_t x_i^2)$$

where n_t is the total number of tubes for particular rack and I_{pr}^x and I_{pr}^y are principal tube moments of inertia, A_t - material tube cross section and x_i, y_i - tube centroid location with respect to the principal coordinate system (as shown in the sketch above).

Obtained stresses for types 2 and 3 ATEA racks are listed in Table 3.5-17 for all load cases.

Table 3.5-17 Compressive Rack Corner Tube Stresses [psi]

rack #	7	8	9	10	11	12	13
Load Case #							
1	4,286	4,537	4,137	4,198	4,997	3,965	4,941
2	3,671	4,050	4,160	3,724	4,436	3,914	4,663
3	5,675	5,683	6,979	5,793	6,393	6,461	6,964
4	4,140	4,477	4,076	4,071	4,864	3,947	5,217
5	4,297	4,600	4,130	4,318	5,030	4,060	5,323
6	5,481	5,674	5,619	5,209	6,143	6,238	6,502
7	3,439	3,689	3,851	3,482	4,310	3,739	4,609
8*	2,755	2,966	4,113	2,767	4,543	4,446	4,214
9*	2,188	2,294	3,058	2,431	2,929	2,838	2,805
10*	2,487	2,414	3,129	2,308	2,885	2,872	2,730
11	2,789	650	6,175	825	4,428	3,848	4,653
12*	488	2,108	2,986	642	4,029	2,925	3,653

(*) OBE load cases.

Highest compressive stresses developed for service levels A and B (OBE condition) are from load case #8 for rack #11, where $\sigma_{OBE} = 4,543$ psi. In case of service level D (SSE condition), the worst stresses are from load case #3 for rack #9, where $\sigma_{SSE} = 6,979$ psi.

Per Reference 3.19 (ASME Section III, subsection NF3322 (c)(2) (eq.6a, for austenitic stainless steel), the allowable stress in compression for stainless steel gross section column member (for $kL/r = 11.28$ (types 2&4), 11.02 (type 3)) < 120 is

$$F_a = S_y \left(0.47 - \frac{kL_{max}/r}{444} \right) = \begin{matrix} 10.29 \text{ ksi (type 2 and 4)} \\ 12.31 \text{ ksi (type 3)} \end{matrix}$$

where: $S_y =$ 23.15 ksi @ $T=150^\circ\text{F}$ for SS tube material (ASME Section III, Appendix I)
 $k =$ 1.0, compressive buckling coefficient (ASME Section III, subsection NF3322.2 (b)(1)), for braced frames
 $L_{max} =$ 37.9 [in], interconnecting tab welds spacing for tube's peripheral edges (type 3 rack)
 $r =$ 3.36 [in], tube cross section radius of gyration (type 2 rack), 3.44 [in], tube cross section radius of gyration (type 3 rack)



● 1981.11.24(日) 1981年11月24日 火曜 晴 15℃ 11℃ 湿度75% 風速1.0m/s 風向 北北東 雲量 100% 月相 上弦月 11月24日 火曜 晴 15℃ 11℃ 湿度75% 風速1.0m/s 風向 北北東 雲量 100% 月相 上弦月

The tube radius of gyration is obtained from:

$$r = \sqrt{\frac{I}{A}} = \begin{array}{l} 3.36 \text{ in, for rack tube types 2 and 4} \\ 3.44 \text{ in, for type 3 rack tube} \end{array}$$

where $I = (2/3)h^3t = 0.667 \times 8.22^3 \times 0.0787 = 29.16 \text{ in}^4$, is the type 2 tube cross section moment of inertia, and its area is $A = 4ht = 2.59 \text{ in}^2$. Similarly for the type 3 rack, $I = 31.29 \text{ in}^4$, and $A = 2.65 \text{ in}^2$.

Gross tube cross section buckling is not controlling, since both σ_{OBE} and σ_{SSE} are lower than the allowable F_a .

Local elastic buckling stress is evaluated from Reference 3.42, and in the case of type 2 and 3 rack tubes:

$$\sigma_{cr} = \frac{k_h \pi^2 E}{12 (1 - \nu_e^2)} \left(\frac{t_h}{h} \right)^2 = \begin{array}{l} 9.24 \text{ ksi (types 2\&4)} \\ 8.82 \text{ ksi (type 3)} \end{array}$$

where: $\nu_e = 0.3$, Poison's ratio for SS steel @ 150°F
 $t = 0.0787 \text{ [in]}$, tube wall thickness
 $h = 8.22 \text{ [in]}$, tube side width (median line) (types 2&4 rack)
 8.417 [in] , tube side width (median line) (type 3 rack)
 $k_n = 4$

Again, both σ_{OBE} and σ_{SSE} for rack types 2, 3 and 4 are lower than the corresponding critical stress limit σ_{cr} . Consequently, buckling is not a concern for Rochester Gas & Electric GINNA Unit 1 Spent Fuel racks, for given level of seismic conditions, and maximum tab welds peripheral tube spacing is adequate.

3.5.3.1.2.7 Rack Tube Maximum Stress Evaluation

In this section, maximum rack tube stresses are evaluated and compared with ASME code allowable stresses for Service Levels A, B and D.

In addition to axial (compressive) tube stresses, shear stresses are acting upon bottom tube ends. It will be shown that shear stresses contribution is only a fraction of total tube stress. Therefore it is sufficient to consider shear loads for SSE condition (load case #3) acting upon rack 3C (#9), where the highest corner tube axial stress occurs. The obtained shear stresses conservatively envelope OBE induced shear stresses.

a) Shear stresses due to rack base plate seismic loads F_x and F_y :

$$\tau_F = F_{TH} \sqrt{\tau^2(F_x) + \tau^2(F_y)} \approx 1,240 \text{ psi}$$

where

$f_{TH} = 1.20$, time history enveloping factor for SSE condition
 $\tau(F_x), \tau(F_y)$ - average shear stresses acting at the base plate level:

$$\tau(F_x) = \frac{F_x}{n_t 0.5 A_t} = 981.9 \text{ psi}$$

$$\tau(F_y) = \frac{F_y}{n_t 0.5 A_t} = 321.5 \text{ psi}$$

where $F_x = 65,050 \text{ lb}$ and $F_y = 21,300 \text{ lb}$ (load case #3, rack #9, section 3.5.3.1.8.1)

$A_t = 2.65 \text{ in}^2$, the tube (type 3) cross section area (section 3.5.3.1.2.6).

Note that a reduction factor of 0.5 is used since each pair of neighboring tubes shares a common SS wall.

$n_t = 5 \times 10 = 50$, total number of tubes for rack #9 (3C)

b) Shear stresses due to rack torsion M_z :

$$\tau_T = f_{TH} \frac{M_z r}{J} = 184.6 \text{ psi}$$

where $M_z = 221,000 \text{ in-lb}$ (load case #3, rack #9, section 3.5.3.1.8.1)

$r = 52.6 \text{ in}$, the rack corner to center distance for rack #9

$J = 75,548 \text{ in}^4$, torsional constant for rack #9 ($= I_x + I_y$, Table 3.5-16)

Generally torsion adds little to the overall maximum tube stress. It is therefore conservatively taken $\tau_T = 250 \text{ psi}$.

Combined shear stress is evaluated as a square root of sum of squares of the shear components:

$$\tau_{\max} = \sqrt{\tau_F^2 + \tau_T^2} = 1,265 \text{ psi}$$

Principal tube (type 3 rack) stresses are now obtained:

$$\sigma_{1/2} = \frac{1}{2} [\sigma_z \pm \sqrt{\sigma_z^2 + 4\tau_{\max}^2}] \approx 7,202 \text{ psi} / -223 \text{ psi}$$

where $\sigma_z = \sigma_{SSE} = 6,979 \text{ psi}$, maximum axial tube (type 3) stress (Table 3.5-17).

Similarly for type 2 and 4 rack tubes, using conservative estimate for maximum shear $\tau_{\max} = 1,265$ psi obtained previously, principal stresses are:

$$\sigma_{1/2} = \frac{1}{2} [\sigma_z \pm \sqrt{\sigma_z^2 + 4\tau_{\max}^2}] \approx 4,872 \text{ psi} / -329 \text{ psi}$$

where $\sigma_z = \sigma_{\text{OBE}} = 4,543$ psi, maximum axial tube (type 2&4) stress (Table 3.5-17).

Thermally induced stresses in tube walls (section 3.5.3.1.10) are obtained for rack #8 (2B). Since they are conservative, they are superimposed to the obtained seismic principal stresses for racks 9 and 11. The table below summarizes tube wall stresses for both thermal conditions:

Thermal Condition	Secondary Membrane [psi]	Secondary Membrane + Bending [psi]
Normal (To)	3,837	9,856
Abnormal (Ta)	9,654	9,803

Finally, the principal stresses compared to ASME Code Service Levels A,B and D allowables are listed in Table 3.5-18.

Table 3.5-18 Summary of Tube Stresses

Load Combinations	Maximum Stress [psi]	Allowable Stress [psi]	Design Factor [%]
<i>D + L + E + To (Level A)</i>			
Primary Membrane	4,543	15,700	246
Primary Membrane + Bending	4,872	23,550	383
Range of Primary + Secondary	14,728	46,300	214
Average Primary Shear	1,265	9,420	644

Table 3.5-18 (Cont'd)

Load Combinations	Maximum Stress [psi]	Allowable Stress [psi]	Design Factor [%]
<i>D + L + E + Ta (Level B)</i>			
Primary Membrane	4,543	20,881	360
Primary Membrane + Bending	4,872	31,322	542
Range of Primary + Secondary	14,675	44,080	200
Average Primary Shear	1,265	9,420	644
<i>D + L + E' + Ta (Level D)</i>			
Primary Membrane	6,979	26,448	279
Primary Membrane + Bending	7,202	39,672	450
Range of Primary + Secondary	17,005	44,080	159
Average Primary Shear	1,265	28,123	2123

3.5.3.1.3 Bottom of Rack Tube to Base Plate Welds

This section demonstrates compliance of Rochester Gas & Electric GINNA spent fuel storage racks with allowable base plate welds stress limits for service levels B and D, per ASME Section III, Subsection NF for Class 3 component supports.

Base Plate Welds Layout

Square rack tubes are welded to the base plate via a pair of 2 mm fillet welds per designated rack tube sides. Total weld length per tube side varies from minimum 3.150 in (2x40 mm) to maximum 6.299 in (2x80 mm). Weld lengths are optimized so that adequate design factors are obtained for all new ATEA racks and all 12 load cases (both OBE (level B) and SSE (level D) conditions). Additional requirements specified actual weld lengths in 10 mm increments. Weld throat is taken to be 0.047 in (1.2 mm). Adopted weld lengths are:

Weld Type	1	2	3	4	5
L [mm]	40	50	60	70	80



Depending on the allowable stress limits lower design factors can be developed either in welds or in the base metal (rack tube material). Critical cross section for welds is assumed to be the throat area (throat width times weld length). In case of base metal, critical cross section is equal to a total weld length per tube side times the tube wall thickness. Base plate welds/base metal cross section properties for each rack are listed in the Table 3.5-19. For both welds and base metal, *shear area* represents total weld area for all welded rack tube sides, for all tubes of a particular rack. Same welds or base metal lines are taken into account for calculating their cross section principal moments of inertia. Positions of corresponding principal axes are also listed in the Table 3.5-19. So obtained cross section properties are used for stress calculations.

Table 3.5-19 Base Plate Welds Cross-section Properties for New ATEA Racks

Rack #	Shear A [in ²]		Principal I _x [in ⁴]		Principal I _y [in ⁴]		Principal Axes	
	Weld	Base Metal	Weld	Base Metal	Weld	Base Metal	x [in]	y [in]
7	28.6	47.7	13,667	22,778	24,157	40,262	46.37	33.58
8	32.5	54.2	19,801	33,001	28,540	47,567	46.22	37.94
9	25.0	41.6	5,808	9,680	23,166	38,610	46.40	23.08
10	23.9	39.9	10,814	18,023	20,595	34,326	45.99	32.22
11	33.6	55.9	12,142	20,236	31,068	51,780	46.12	35.18
12	28.2	47.0	6,783	11,304	24,044	40,074	46.44	23.08
13	29.0	48.3	11,621	19,368	24,089	40,149	42.44	29.36

(Note: x - direction is in EW, y - direction is in NS)

Weld Loads

The following tube-to-base plate weld load components are considered:

- Seismic loads - acting upon bottom rack beam node, and also shared by the base plate cross beams. Load components are obtained from the full pool analyses (section 3.5.3.1.8) and consist of transverse F_x and F_y components, vertical F_z component normal to the base plate, bending moments M_x and M_y , and torsion M_z . Transverse F_x and F_y forces are assumed to be uniformly distributed across all welds. Loads are distributed similarly for torsion induced shear from M_z . All the loads are then assumed to act at the top rack plane. Load components (forces and moments) taken from section 3.5.3.1.8 are multiplied by the time history enveloping factor (1.20 for SSE and 1.12 for OBE condition).

Resulting weld / base metal stresses are calculated as:

$$\sigma_{tot} = \sqrt{\sigma_x^2 + \sigma_y^2 + \tau^2}$$



where σ_x and σ_y are the normal stresses due to base plate bending moments M_x and M_y . The stresses which act upon the tube bottom (base metal), are normal stresses, as well as combined shear stresses in tube-to-base plate welds:

$$\sigma_x = f_{TH} \frac{M_x}{I_x} (y_i - y_{pr}) \quad ; \quad \sigma_y = f_{TH} \frac{M_y}{I_y} (x_i - x_{pr})$$

where I_x and I_y are principal moments of inertia for the whole weld or corresponding base metal group, (x_i, y_i) is welded tube side center location with respect to the weld group principal coordinate system. The principal coordinate system origin is located at (x_{pr}, y_{pr}) with respect to SE (lower left) base plate corner.

Horizontal weld and base metal total (average) shear stress τ is due to transverse F_x and F_y , vertical F_z and torsion M_z , all reduced to the weld or base metal group total area A :

$$\tau = \sqrt{\tau_x^2 + \tau_y^2 + \tau_z^2 + \tau_T^2} \quad \text{where} \quad \tau_x = f_{TH} \frac{F_x}{A} \quad ; \quad \tau_y = f_{TH} \frac{F_y}{A} \quad ; \quad \tau_z = f_{TH} \frac{F_z}{A} \quad ; \quad \tau_T = f_{TH} \frac{M_z}{J} r$$

Note that stress components are evaluated at the rack corner which is farthest from the weld group principal coordinate system origin (at distance r). Polar moment of inertia for the weld/base plate group is $J = I_x + I_y$. Results are summarized in Table 3.5-20.

- b) Thermally induced loads - due to the difference in thermal expansion of the base plate and the tubes. Two conditions were considered (section 3.5.3.1.10):

Normal (To) operating condition "To" - An ANSYS model yields the maximum stress of 5,031 psi at the "hot" cell-to-base plate interface (minimum - type 1 weld length of 40 mm is assumed).

Abnormal (Ta) condition "Ta" - free thermal expansion of the base plate and tubes is partially constrained due to the existence of friction between legs and pool liner. Maximum induced stresses are in the corner tubes, and estimated (ANSYS model) stress is 6,676 psi for corner tube-to base plate welds (80 mm weld length, for type 2B rack).



**Table 3.5-20 Base Plate & Weld Stress Summary for
New ATEA Racks**

Load Case #		Rack #						
		7 (2A)	8 (2B)	9 (3C)	10 (3A)	11 (3E)	12 (3D)	13 (3B)
1	bm	10,506	10,611	5,900	8,837	7,170	5,151	7,286
	w	17,510	17,686	9,834	14,729	11,950	8,585	12,143
2	bm	8,986	9,442	5,960	7,918	6,229	5,105	6,848
	w	14,976	15,737	9,933	13,196	10,381	8,509	11,414
3	bm	13,976	13,388	9,565	12,046	8,724	8,234	10,296
	w	23,293	22,313	15,942	20,077	14,541	13,723	17,160
4	bm	10,159	10,475	5,812	8,600	6,914	5,123	7,669
	w	16,932	17,459	9,687	14,334	11,524	8,539	12,782
5	bm	10,537	10,770	5,999	9,196	7,181	5,314	7,828
	w	17,562	17,950	9,998	15,327	11,969	8,857	13,047
6	bm	13,504	13,311	7,941	10,986	8,356	8,029	9,617
	w	22,507	22,186	13,236	18,309	13,927	13,382	16,029
7	bm	8,397	8,615	5,478	7,485	6,027	4,826	6,766
	w	13,996	14,358	9,129	12,475	10,044	8,044	11,277
8	bm	6,768	6,926	5,593	5,930	6,205	5,611	6,197
	w	11,280	11,544	9,322	9,884	10,341	9,351	10,328
9	bm	5,386	5,382	4,232	5,095	3,946	3,597	4,134
	w	8,977	8,970	7,053	8,491	6,577	5,995	6,889
10	bm	6,091	5,653	4,387	4,863	3,898	3,656	4,021
	w	10,152	9,422	7,312	8,105	6,497	6,094	6,072
11	bm	6,869	1,622	8,454	1,845	6,243	4,984	6,864
	w	11,448	2,704	14,090	3,075	10,405	8,306	11,440
12	bm	1,211	4,959	4,042	1,425	5,311	3,719	5,381
	w	2,018	8,264	6,736	2,374	8,851	6,199	8,969

NOTE: *bm* - base metal, *w* - weld stresses



Weld/Base Metal Stresses

The following table summarizes the maximum stresses in the tube-to-base plate welds and in the base metal.

Service Level	Type	Max. Stresses [psi]	Allowable* Stresses [psi]
D+L+E +To (Level A)	Base Metal	6,926	$0.40*(S_y)=9,260$
	Weld	11,544	$0.3*(S_u)=21,000$
D+L+E+Ta (Level B)	Base Metal	6,926	$0.532*(S_y)=11,725$
	Weld	11,544	$0.40*(S_u)=27,930$
D+L+E'+Ta (Level D)	Base Metal	13,976	$0.42*(S_u)=28,123$
	Weld	23,293	$0.42*(S_u)=29,400$

(*) Allowable stresses are taken from Table 3.2-2.

Conclusion

ATEA type 2 and 3 racks tube to base plate welds meet the Service Levels A, B and D weld stress limits. The base plate weld stresses in the Type 4 racks are enveloped by the Type 2 and Type 3 racks, due to the additional top and bottom lateral supports on the Type 4 racks.

3.5.3.1.4 Welding of Support Legs

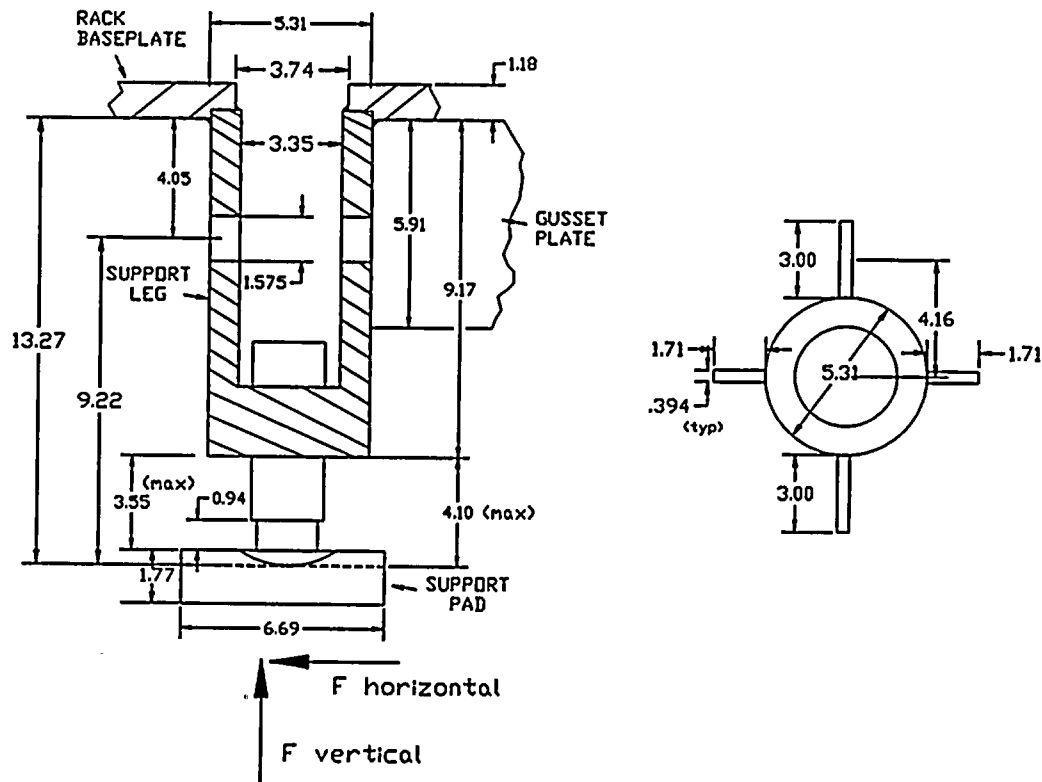
The weld stress calculation was based on a linear stress distribution using the Section Modulus for both the circular weld (leg cylinder), and linear welds (gusset plates). The support legs welds were qualified using a minimum weld throat size of 0.157 in (4.0 mm). The upper weld (above the baseplate) was qualified using a 0.118 in (3.0 mm) throat size.

The maximum weld stresses are given in Table 3.5-21 (below). Figure 3.5-40 shows support cylinder and gusset plates used in weld stress evaluations.

Table 3.5-21 Summation of Support Leg Weld Stresses

Load Combinations	Max Weld Stress (psi)	Allowable Stress (psi)
Welds: $D + E$ (Level A)	11,677	$0.3*(Su)=21,000$
$D + E + Ta$ (Level B)	11,733	$0.40*(Su)=27,930$
$D + E' + Ta$ (Level D)	18,302	$0.42*(Su)=29,400$
Base Metal: $D+E$ (Level A)	8,257	$0.40*(Sy)=9,260$
$D+E + Ta$ (Level B)	8,297	$0.532*(Sy)=11,725$
$D+E' + Ta$ (Level D)	12,942	$0.42*(Su)=28,123$

Figure 3.5-40 Dimensions, Support Leg, and Gusset Plates Used For Weld Qualification





3.5.3.1.5 Summary of Support Pad Loads

The following horizontal and vertical loads are given for the model legs. The actual leg loads for each rack must then be modified by the actual number of legs per rack. The tables also do not include the time history factors of 1.12 for OBE and 1.20 for SSE.

Table 3.5-22 Max. Horiz. Model Leg Forces SRSS - LC#1
GINNA 3D Whole Pool Model - Without Perimeter Racks
Load Case #1 - Unconsolidated Fuel - SSE - Mu = 0.8

Absolute Values - Horizontal SRSS (Fx & Fy) - Lbs					
Rack	Leg 1	Leg 2	Leg 3	Leg 4	Max.
1	54,570	66,620	66,480	54,970	66,620
2	46,600	73,030	57,700	55,550	73,030
3	45,260	43,400	45,920	37,630	45,920
4	39,250	49,040	41,130	38,380	49,040
5	37,320	43,870	48,310	39,890	48,310
6	42,710	45,530	52,510	42,380	52,510
7	30,340	33,280	35,090	42,120	42,120
8	38,050	41,800	33,650	40,040	41,800
9	26,470	27,520	22,920	23,770	27,520
10	39,200	36,240	32,370	25,480	39,200
11	32,430	35,750	32,480	29,750	35,750
12	31,090	26,220	25,250	22,610	31,090
13	34,870	33,920	25,230	24,590	34,870

Table 3.5-23 Max. Vertical Pool Floor Forces -LC#1
GINNA 3D Whole Pool Model - Without Perimeter Racks
Load Case #1 - Unconsolidated Fuel - SSE - Mu = 0.8

Vertical Leg and Rack Forces - Lbs						
Rack	Leg 1	Leg 2	Leg 3	Leg 4	Max. Leg	Rack Total
1	122,700	149,700	161,200	130,000	161,200	274,100
2	124,400	146,600	151,800	117,300	151,800	265,300
3	113,400	128,600	156,700	107,800	156,700	263,900
4	114,100	130,500	142,600	109,600	142,600	262,500
5	115,600	119,900	156,400	114,600	156,400	269,100
6	119,400	135,700	144,400	116,400	144,400	272,100
7	83,640	96,810	83,730	91,750	96,810	162,100
8	100,200	117,500	98,640	116,400	117,500	186,900
9	55,490	68,410	57,780	62,330	68,410	104,300
10	71,970	82,670	70,700	82,940	82,940	135,600
11	67,570	89,030	68,160	74,000	89,030	132,200
12	57,240	68,560	53,260	62,620	68,560	105,400
13	73,390	85,750	74,280	70,590	85,750	121,000

Table 3.5-24 Max. Horizontal Leg Forces SRSS - LC#2
GINNA 3D Whole Pool Model - Without Perimeter Racks
Load Case #2 - Unconsolidated Fuel - SSE - Mu = 0.2

Absolute Values - Horizontal SRSS (Fx & Fy) - Lbs

Rack	Leg 1	Leg 2	Leg 3	Leg 4	Max.
1	24,180	22,550	23,340	21,270	24,180
2	23,270	23,620	23,530	21,620	23,620
3	20,680	20,190	18,570	20,200	20,680
4	20,260	20,980	19,280	21,180	21,180
5	21,790	21,240	18,970	20,760	21,790
6	22,540	22,850	21,310	22,420	22,850
7	15,750	15,510	13,270	15,380	15,750
8	17,130	17,360	16,240	17,610	17,610
9	10,020	10,490	9,930	11,240	11,240
10	12,880	12,790	11,780	13,160	13,160
11	12,000	12,830	12,350	12,440	12,830
12	10,200	10,420	9,813	10,850	10,850
13	12,550	11,470	10,930	10,720	12,550

Table 3.5-25 Max. Vertical Pool Floor Forces -LC#2
GINNA 3D Whole Pool Model - Without Perimeter Racks
Load Case #2 - Unconsolidated Fuel - SSE - Mu = 0.2

Vertical Leg and Rack Forces - Lbs

Rack	Leg 1	Leg 2	Leg 3	Leg 4	Max. Leg	Rack Total
1	121,000	112,800	116,600	107,600	121,000	262,200
2	116,400	117,800	117,600	107,900	117,800	263,300
3	103,500	101,700	106,200	100,400	106,200	262,200
4	102,400	104,800	97,280	105,900	105,900	262,200
5	108,900	106,200	98,680	103,600	108,900	262,800
6	112,700	114,200	106,400	112,000	114,200	264,700
7	78,680	77,520	71,790	76,930	78,680	157,700
8	85,340	86,710	81,180	87,950	87,950	184,900
9	50,070	52,390	51,190	56,080	56,080	109,100
10	64,290	63,870	63,120	65,780	65,780	132,500
11	60,670	63,920	61,700	62,160	63,920	118,200
12	50,930	52,030	49,070	54,050	54,050	101,800
13	62,430	56,870	54,640	54,300	62,430	115,700

Table 3.5-26 Max. Horiz. Model Leg Forces SRSS - LC#3
GINNA 3D Whole Pool Model - Without Perimeter Racks
Load Case #3 - Consolidated Fuel - SSE - Mu = 0.8

Absolute Values - Horizontal SRSS (Fx & Fy) - Lbs

Rack	Leg 1	Leg 2	Leg 3	Leg 4	Max.
1	64,980	86,330	60,800	71,860	86,330
2	52,630	67,460	53,260	57,290	67,460
3	34,640	39,730	46,300	32,760	46,300
4	31,450	36,720	41,280	30,310	41,280
5	29,520	31,240	42,720	27,820	42,720
6	36,740	48,460	47,630	38,870	48,460
7	41,300	46,780	34,940	39,010	46,780
8	48,820	62,630	46,830	39,380	62,630
9	31,900	27,590	28,850	32,820	32,820
10	29,910	34,090	31,260	34,670	34,670
11	43,730	38,600	37,620	45,190	45,190
12	35,090	32,790	32,170	38,020	38,020
13	38,160	38,210	28,970	32,360	38,210

Table 3.5-27 Max. Vertical Pool Floor Forces -LC#3
GINNA 3D Whole Pool Model - Without Perimeter Racks
Load Case #3 - Consolidated Fuel - SSE - Mu = 0.8

Vertical Leg and Rack Forces - Lbs

Rack	Leg 1	Leg 2	Leg 3	Leg 4	Max. Leg	Rack Total
1	189,900	199,800	208,900	198,700	208,900	465,500
2	190,100	201,400	190,100	174,900	201,400	465,500
3	162,800	174,200	162,000	150,800	174,200	465,500
4	162,200	175,500	163,600	154,800	175,500	465,500
5	155,000	174,900	172,500	162,000	174,900	465,500
6	164,400	182,500	186,000	172,300	186,000	465,500
7	123,600	119,600	129,600	128,000	129,600	276,700
8	145,600	150,300	149,000	146,500	150,300	322,400
9	87,060	85,000	87,990	84,370	87,990	166,300
10	107,600	101,100	111,600	108,900	111,600	221,600
11	112,000	107,500	112,200	101,100	112,200	204,200
12	85,290	85,680	85,210	85,570	85,680	173,300
13	115,600	101,900	103,600	91,960	115,600	203,400

Table 3.5-28 Max. Horizontal Leg Forces SRSS - LC#4
GINNA 3D Whole Pool Model - Without Perimeter Racks
Load Case #4 - Unconsolidated Fuel - SSE - Mu = 0.5

Absolute Values - Horizontal SRSS (Fx & Fy) - Lbs					
Rack	Leg 1	Leg 2	Leg 3	Leg 4	Max.
1	49,660	58,720	63,070	53,360	63,070
2	46,000	62,790	56,070	50,660	62,790
3	37,750	48,600	42,300	35,920	48,600
4	37,200	54,050	34,590	38,450	54,050
5	35,860	41,160	46,070	40,880	46,070
6	43,140	49,180	50,860	44,050	50,860
7	34,910	32,500	31,310	34,740	34,910
8	41,410	41,160	33,140	35,980	41,410
9	26,620	26,340	20,690	21,840	26,620
10	33,430	34,010	29,910	26,790	34,010
11	31,800	31,980	26,960	23,870	31,980
12	26,040	24,000	20,780	22,470	26,040
13	31,710	33,870	22,840	23,450	33,870

Table 3.5-29 Max. Vertical Pool Floor Forces -LC#4
GINNA 3D Whole Pool Model - Without Perimeter Racks
Load Case #4 - Unconsolidated Fuel - SSE - Mu = 0.5

Vertical Leg and Rack Forces - Lbs

Rack	Leg 1	Leg 2	Leg 3	Leg 4	Max. Leg	Rack Total
1	121,900	146,000	156,600	120,400	156,600	267,000
2	123,600	146,100	152,600	122,500	152,600	266,800
3	110,700	124,800	148,500	108,300	148,500	264,200
4	110,300	126,100	138,100	109,500	138,100	263,400
5	117,900	124,700	145,100	118,500	145,100	270,100
6	122,600	135,800	138,800	121,200	138,800	272,600
7	83,560	93,060	83,070	94,390	94,390	166,400
8	94,660	112,100	96,740	115,400	115,400	187,000
9	55,680	64,070	58,490	62,260	64,070	108,800
10	74,910	83,920	68,540	84,410	84,410	139,300
11	69,850	82,020	69,320	67,990	82,020	127,500
12	58,750	66,020	56,200	61,220	66,020	106,900
13	76,110	82,910	72,920	67,630	82,910	123,800



Table 3.5-30 Max. Horiz. Model Leg Forces SRSS - LC#5
GINNA 3D Whole Pool Model - With Perimeter Racks
Load Case #5 - Unconsolidated Fuel - SSE - Mu = 0.8

Absolute Values - Horizontal SRSS (Fx & Fy) - Lbs

Rack	Leg 1	Leg 2	Leg 3	Leg 4	Max.
1	63,630	69,790	70,000	65,030	70,000
2	59,600	68,830	53,420	57,670	68,830
3	47,590	49,960	47,740	50,310	50,310
4	48,470	45,070	41,900	48,760	48,760
5	45,470	47,040	50,270	44,580	50,270
6	49,920	53,920	55,280	48,220	55,280
7	34,960	37,890	43,690	31,480	43,690
8	45,840	36,860	35,400	33,860	45,840
9	26,520	29,040	25,910	25,290	29,040
10	34,550	31,770	26,900	25,560	34,550
11	38,320	32,730	27,060	30,930	38,320
12	31,100	26,790	22,820	24,000	31,100
13	37,720	35,320	26,650	29,960	37,720

Table 3.5-31 Max. Vertical Pool Floor Forces -LC#5
GINNA 3D Whole Pool Model - With Perimeter Racks
Load Case #5 - Unconsolidated Fuel - SSE - Mu = 0.8

Vertical Leg and Rack Forces - Lbs

Rack	Leg 1	Leg 2	Leg 3	Leg 4	Max. Leg	Rack Total
1	136,400	150,600	148,200	136,900	150,600	297,200
2	132,200	154,400	139,600	139,400	154,400	290,400
3	123,300	121,600	125,100	128,500	128,500	283,200
4	114,800	127,300	122,400	130,200	130,200	283,200
5	121,300	117,800	128,800	116,600	128,800	288,500
6	123,400	121,900	127,600	123,700	127,600	288,300
7	86,270	84,320	77,570	94,180	94,180	162,500
8	103,100	108,100	91,970	110,700	110,700	192,900
9	57,440	64,340	55,680	60,480	64,340	97,710
10	69,560	80,340	65,370	82,460	82,460	134,800
11	69,750	78,530	67,680	72,820	78,530	122,800
12	55,990	64,930	52,810	59,040	64,930	99,740
13	78,470	83,720	65,960	67,610	83,720	119,600

Table 3.5-32 Max. Horiz. Model Leg Forces SRSS - LC#6
GINNA 3D Whole Pool Model - With Perimeter Racks
Load Case #6 - Consolidated Fuel - SSE - Mu = 0.8

Absolute Values - Horizontal SRSS (Fx & Fy) - Lbs

Rack	Leg 1	Leg 2	Leg 3	Leg 4	Max.
1	64,020	68,460	65,790	66,380	68,460
2	64,040	55,950	59,800	61,780	64,040
3	38,470	42,420	47,920	31,300	47,920
4	34,610	36,920	44,150	31,980	44,150
5	32,940	31,790	45,240	31,820	45,240
6	38,650	43,820	50,170	38,620	50,170
7	36,910	35,890	36,960	39,040	39,040
8	51,210	58,980	46,330	48,230	58,980
9	29,390	28,500	27,970	33,190	33,190
10	38,770	34,290	34,650	34,870	38,770
11	40,260	40,830	37,110	42,830	42,830
12	28,130	32,830	31,540	30,390	32,830
13	39,660	39,600	28,120	31,650	39,660

Table 3.5-33 Max. Vertical Pool Floor Forces -LC#6
GINNA 3D Whole Pool Model - With Perimeter Racks
Load Case #6 - Consolidated Fuel - SSE - Mu = 0.8

Vertical Leg and Rack Forces - Lbs

Rack	Leg 1	Leg 2	Leg 3	Leg 4	Max. Leg	Rack Total
1	213,400	220,000	204,000	194,800	220,000	496,500
2	206,600	215,100	195,800	186,000	215,100	494,100
3	168,000	188,200	167,900	163,700	188,200	494,100
4	170,100	185,000	172,600	160,700	185,000	494,100
5	159,300	185,900	173,900	165,400	185,900	494,100
6	170,200	187,800	189,800	181,200	189,800	494,100
7	121,100	130,400	117,500	106,600	130,400	276,600
8	140,000	156,000	136,500	138,900	156,000	322,500
9	81,330	86,280	82,300	82,540	86,280	169,800
10	107,700	109,600	97,400	95,920	109,600	221,600
11	102,100	102,800	108,100	94,940	108,100	204,800
12	82,060	87,480	83,810	86,770	87,480	170,900
13	105,900	109,500	98,730	88,910	109,500	202,600



THESE DOCUMENTS SONT LOANES DE LA BIBLIOTHEQUE DE LA COMMISSION EUROPEENNE A BRUXELLES

1974

1974

Table 3.5-34 Max. Horizontal Leg Forces SRSS - LC#7
GINNA 3D Whole Pool Model - With Perimeter Racks
Load Case #7 - Unconsolidated Fuel - SSE - Mu = 0.2

Absolute Values - Horizontal SRSS (Fx & Fy) - Lbs

Rack	Leg 1	Leg 2	Leg 3	Leg 4	Max.
1	23,400	23,290	22,140	21,960	23,400
2	24,300	24,350	22,490	22,930	24,350
3	20,640	20,700	19,940	21,570	21,570
4	21,100	21,490	19,810	22,680	22,680
5	21,760	21,630	20,390	22,750	22,750
6	22,680	22,680	22,010	24,140	24,140
7	15,810	14,540	13,560	14,550	15,810
8	17,420	16,590	16,280	17,100	17,420
9	10,210	10,330	9,787	10,210	10,330
10	12,750	11,910	11,630	12,520	12,750
11	12,830	12,870	12,230	11,690	12,870
12	9,865	9,967	9,546	10,240	10,240
13	12,100	11,320	11,160	10,490	12,100

Table 3.5-35 Max. Vertical Pool Floor Forces -LC#7
GINNA 3D Whole Pool Model - With Perimeter Racks
Load Case #7 - Unconsolidated Fuel - SSE - Mu = 0.2

Vertical Leg and Rack Forces - Lbs

Rack	Leg 1	Leg 2	Leg 3	Leg 4	Max. Leg	Rack Total
1	117,100	116,400	110,600	109,700	117,100	283,200
2	121,400	121,600	112,500	114,600	121,600	283,200
3	103,300	104,200	103,800	107,700	107,700	283,200
4	105,400	107,300	101,900	113,500	113,500	283,200
5	108,800	108,100	102,000	113,900	113,900	283,200
6	113,400	113,200	110,000	120,600	120,600	284,100
7	78,700	73,230	71,030	72,690	78,700	158,500
8	86,310	82,890	81,400	85,120	86,310	181,600
9	50,950	51,650	50,450	51,090	51,650	100,900
10	63,790	59,600	62,780	62,540	63,790	131,800
11	63,330	64,210	61,140	58,290	64,210	117,600
12	49,350	49,810	47,740	51,100	51,100	101,800
13	60,750	56,560	56,210	52,440	60,750	115,900



Table 3.5-36 Max. Horizontal Leg Forces SRSS - LC#8
GINNA 3D Whole Pool Model - With Perimeter Racks
Load Case #8 - Consolidated Fuel - OBE - $\mu = 0.8$

Absolute Values - Horizontal SRSS (Fx & Fy) - Lbs

Rack	Leg 1	Leg 2	Leg 3	Leg 4	Max.
1	22,850	22,690	22,690	22,860	22,860
2	19,440	19,380	19,380	19,440	19,440
3	12,600	12,450	12,450	12,600	12,600
4	13,020	12,860	12,860	13,020	13,020
5	14,650	14,630	14,620	14,650	14,650
6	16,660	16,580	16,580	16,660	16,660
7	10,200	10,200	10,200	10,200	10,200
8	11,580	11,420	11,420	11,580	11,580
9	16,790	17,510	17,030	14,050	17,510
10	7,674	7,665	7,665	7,674	7,674
11	30,050	25,330	29,100	27,190	30,050
12	22,040	23,820	22,740	25,990	25,990
13	15,890	14,940	16,190	15,470	16,190

Table 3.5-37 Max. Vertical Pool Floor Forces -LC#8
GINNA 3D Whole Pool Model - With Perimeter Racks
Load Case #8 - Consolidated Fuel - OBE - $\mu = 0.8$

Vertical Leg and Rack Forces - Lbs

Rack	Leg 1	Leg 2	Leg 3	Leg 4	Max. Leg	Rack Total
1	162,100	159,700	151,600	151,900	162,100	424,500
2	160,300	150,400	149,200	145,000	160,300	424,500
3	128,500	134,500	127,200	121,100	134,500	424,500
4	129,000	131,300	128,300	123,500	131,300	424,500
5	126,900	125,100	128,200	124,100	128,200	424,500
6	132,600	128,900	135,900	128,000	135,900	424,500
7	82,210	91,200	90,440	79,420	91,200	238,200
8	97,560	111,100	106,800	97,250	111,100	270,000
9	58,900	68,610	67,460	58,700	68,610	138,100
10	70,910	76,170	77,600	68,890	77,600	195,200
11	86,550	89,140	81,740	83,450	89,140	172,600
12	75,850	68,970	66,210	68,600	75,850	141,300
13	87,540	78,730	75,190	64,670	87,540	170,900



Table 3.5-38 Max. Horizontal Leg Forces SRSS - LC#9
GINNA 3D Whole Pool Model - With Perimeter Racks
Load Case #9 - Unconsolidated Fuel - OBE - Mu = 0.2

Absolute Values - Horizontal SRSS (Fx & Fy) - Lbs

Rack	Leg 1	Leg 2	Leg 3	Leg 4	Max.
1	21,850	20,120	19,370	19,750	21,850
2	20,480	19,740	18,530	20,410	20,480
3	18,240	15,340	15,830	16,810	18,240
4	17,210	15,890	15,290	16,370	17,210
5	17,190	14,820	15,540	16,660	17,190
6	18,010	16,950	16,540	17,120	18,010
7	11,940	12,000	12,410	11,810	12,410
8	13,910	14,320	14,290	12,550	14,320
9	8,885	8,383	8,952	7,969	8,952
10	9,791	9,606	10,960	9,834	10,960
11	10,990	10,380	10,120	9,703	10,990
12	9,115	8,351	8,172	7,959	9,115
13	10,790	9,172	9,128	8,687	10,790

Table 3.5-39 Max. Vertical Pool Floor Forces -LC#9
GINNA 3D Whole Pool Model - With Perimeter Racks
Load Case #9 - Unconsolidated Fuel - OBE - Mu = 0.2

Vertical Leg and Rack Forces - Lbs

Rack	Leg 1	Leg 2	Leg 3	Leg 4	Max. Leg	Rack Total
1	109,300	101,600	96,840	98,720	109,300	243,100
2	102,400	98,830	92,630	102,000	102,400	243,100
3	91,190	84,180	84,340	86,620	91,190	243,100
4	86,060	85,420	86,760	87,430	87,430	243,100
5	87,120	84,460	78,810	83,970	87,120	243,100
6	90,990	91,190	85,710	89,370	91,190	243,100
7	59,730	62,090	62,050	59,140	62,090	139,600
8	69,530	71,630	71,460	67,910	71,630	156,500
9	44,420	41,910	44,760	39,840	44,760	84,790
10	48,950	48,030	54,770	49,180	54,770	116,000
11	54,970	52,930	50,590	48,520	54,970	103,700
12	45,560	41,760	40,840	39,800	45,560	85,220
13	53,960	46,370	45,640	44,170	53,960	102,900



Table 3.5-40 Max. Horizontal Leg Forces SRSS - LC#10
GINNA 3D Whole Pool Model - Without Perimeter Racks
Load Case #10 - Unconsolidated Fuel - OBE - $\mu = 0.2$

Absolute Values - Horizontal SRSS (F_x & F_y) - Lbs

Rack	Leg 1	Leg 2	Leg 3	Leg 4	Max.
1	21,950	20,700	19,350	20,790	21,950
2	20,840	20,450	17,540	19,150	20,840
3	17,940	15,480	16,480	14,370	17,940
4	17,120	16,540	15,530	14,620	17,120
5	16,060	15,220	14,810	14,490	16,060
6	15,890	14,750	16,110	15,720	16,110
7	13,110	12,530	12,440	12,160	13,110
8	14,550	14,190	13,740	14,030	14,550
9	9,077	8,366	8,621	8,631	9,077
10	10,240	10,450	10,420	10,160	10,450
11	10,940	10,390	10,530	10,290	10,940
12	8,795	8,395	8,453	7,793	8,795
13	10,520	9,309	9,974	8,717	10,520

Table 3.5-41 Max. Vertical Pool Floor Forces -LC#10
GINNA 3D Whole Pool Model - Without Perimeter Racks
Load Case #10 - Unconsolidated Fuel - OBE - $\mu = 0.2$

Vertical Leg and Rack Forces - Lbs

Rack	Leg 1	Leg 2	Leg 3	Leg 4	Max. Leg	Rack Total
1	109,800	103,500	98,070	103,900	109,800	230,700
2	104,100	102,300	92,250	96,510	104,100	230,700
3	89,690	84,500	82,630	83,230	89,690	230,700
4	85,590	88,680	79,490	81,240	88,680	230,700
5	82,920	77,290	82,810	84,620	84,620	230,700
6	88,260	84,010	82,450	84,740	88,260	230,700
7	65,530	62,630	62,200	60,790	65,530	139,600
8	72,720	70,960	68,700	70,620	72,720	156,500
9	45,390	41,830	43,100	43,150	45,390	84,740
10	51,210	52,230	52,090	50,990	52,230	115,400
11	54,700	51,950	52,660	51,480	54,700	102,800
12	43,980	41,960	42,270	38,960	43,980	83,740
13	52,830	48,040	49,860	43,620	52,830	103,700

Table 3.5-42 Max. Horizontal Leg Forces SRSS - LC#11
GINNA 3D Whole Pool Model - With Perimeter Racks
Load Case #11 - Mixed Fuel - SSE - Mu = Mixed

Absolute Values - Horizontal SRSS (Fx & Fy) - Lbs

Rack	Leg 1	Leg 2	Leg 3	Leg 4	Max.
1	27,670	42,710	30,140	34,540	42,710
2	26,650	46,550	30,160	34,760	46,550
3	29,110	23,620	28,690	28,060	29,110
4	33,220	26,880	31,720	26,770	33,220
5	26,010	24,160	24,320	29,550	29,550
6	29,080	32,900	26,880	25,670	32,900
7	21,190	19,490	21,920	23,150	23,150
8	10,700	11,030	10,260	10,600	11,030
9	29,420	28,710	25,160	30,590	30,590
10	5,478	6,009	5,581	5,647	6,009
11	30,610	23,580	22,490	27,850	30,610
12	31,130	22,550	23,100	23,760	31,130
13	31,360	23,780	24,640	24,250	31,360

Table 3.5-43 Max. Vertical Pool Floor Forces -LC#11
GINNA 3D Whole Pool Model - With Perimeter Racks
Load Case #11 - Mixed Fuel - SSE - Mu = Mixed

Vertical Leg and Rack Forces - Lbs

Rack	Leg 1	Leg 2	Leg 3	Leg 4	Max. Leg	Rack Total
1	57,750	89,720	81,920	95,520	95,520	158,000
2	57,780	91,080	76,440	93,560	93,560	154,600
3	68,950	54,710	101,400	70,060	101,400	157,100
4	106,700	116,900	104,200	108,300	116,900	283,200
5	89,810	127,800	63,930	92,180	127,800	262,600
6	154,400	172,800	166,800	169,300	172,800	494,200
7	68,510	45,190	81,980	75,950	81,980	142,600
8	19,750	19,940	19,850	19,380	19,940	22,240
9	80,430	84,210	71,500	77,170	84,210	157,500
10	18,210	19,740	18,830	18,520	19,740	20,040
11	70,230	74,500	65,100	66,890	74,500	117,700
12	54,060	59,370	54,640	54,410	59,370	101,400
13	72,440	72,320	67,860	62,970	72,440	118,700

Table 3.5-44 Max. Horizontal Leg Forces SRSS - LC#12
GINNA 3D Whole Pool Model - With Perimeter Racks
Load Case #12 - Mixed Fuel - OBE - Mu = Mixed

Absolute Values - Horizontal SRSS (Fx & Fy) - Lbs

Rack	Leg 1	Leg 2	Leg 3	Leg 4	Max.
1	16,070	15,450	14,380	15,660	16,070
2	4,260	4,240	4,377	3,874	4,377
3	11,900	11,810	11,810	11,900	11,900
4	7,782	8,076	7,644	7,512	8,076
5	12,770	11,620	15,520	14,740	15,520
6	16,770	10,030	14,500	13,650	16,770
7	5,781	6,153	5,363	6,728	6,728
8	10,850	14,050	14,090	11,660	14,090
9	16,800	13,800	15,350	15,190	16,800
10	6,366	6,685	6,241	6,287	6,685
11	20,720	20,240	21,010	19,950	21,010
12	14,260	16,760	13,330	13,940	16,760
13	12,360	11,430	12,130	11,600	12,360

Table 3.5-45 Max. Vertical Pool Floor Forces -LC#12
GINNA 3D Whole Pool Model - With Perimeter Racks
Load Case #12 - Mixed Fuel - OBE - Mu = Mixed

Vertical Leg and Rack Forces - Lbs

Rack	Leg 1	Leg 2	Leg 3	Leg 4	Max. Leg	Rack Total
1	113,400	75,210	77,770	42,910	113,400	222,300
2	17,820	17,730	18,310	16,210	18,310	33,710
3	73,340	74,460	72,650	74,090	74,460	243,300
4	18,360	17,970	18,680	18,440	18,680	32,970
5	53,630	33,660	66,410	46,090	66,410	136,500
6	55,720	32,650	70,440	47,450	70,440	136,200
7	14,900	15,120	14,170	15,820	15,820	16,890
8	63,280	70,740	69,880	62,510	70,740	156,500
9	42,880	44,330	42,730	39,760	44,330	85,330
10	15,640	16,840	15,140	15,360	16,840	19,270
11	75,890	79,160	75,270	74,700	79,160	170,900
12	54,600	49,010	33,950	25,660	54,600	78,400
13	72,830	69,600	69,740	59,920	72,830	170,800

3.5.3.1.6 Fuel-to-Rack Impact Loads

Table 3.5-46 Local Fuel/Rack Impact Forces - LC#1
GINNA 3D Whole Pool Model - Without Perimeter Racks
Load Case #1 - Unconsolidated Fuel - SSE - $\mu = 0.8$

Local Fuel/Rack Impact Forces Fx & Fy (lbs) per Fuel Assy.

Rack	East Fx	North Fy	West Fx	South Fy
1	1,388	1,224	1,350	1,348
2	1,163	1,053	1,299	1,322
3	1,518	1,291	1,231	1,289
4	1,136	1,261	1,304	1,240
5	1,299	1,341	1,247	1,289
6	1,380	1,305	1,122	1,432
7	803	1,011	690	1,206
8	1,237	873	1,114	1,174
9	988	915	771	1,171
10	1,082	978	832	1,128
11	1,323	870	1,204	1,173
12	1,107	944	891	1,181
13	1,307	991	1,046	1,175

Table 3.5-47 Local Fuel/Rack Impact Forces - LC#2
GINNA 3D Whole Pool Model - Without Perimeter Racks
Load Case #2 - Unconsolidated Fuel - SSE - $\mu = 0.2$

Local Fuel/Rack Impact Forces Fx & Fy (lbs) per Fuel Assy.

Rack	East Fx	North Fy	West Fx	South Fy
1	1,288	1,199	1,317	1,253
2	1,367	1,160	1,432	1,159
3	1,542	1,290	1,307	1,223
4	1,204	1,142	1,304	1,231
5	1,306	1,300	1,270	1,291
6	1,524	1,219	1,299	1,394
7	1,119	1,149	860	1,288
8	795	777	746	1,136
9	1,131	917	1,001	1,223
10	1,060	978	841	1,097
11	1,199	971	1,044	1,251
12	1,254	940	1,079	1,227
13	1,054	988	907	1,233



1. The first part of the document is a list of names and addresses of the members of the committee.

2. The second part of the document is a list of names and addresses of the members of the committee.

Table 3.5-48 Local Fuel/Rack Impact Forces - LC#3
GINNA 3D Whole Pool Model - Without Perimeter Racks
Load Case #3 - Consolidated Fuel - SSE - $\mu = 0.8$

Local Fuel/Rack Impact Forces Fx & Fy (lbs) per Fuel Assy.

Rack	East Fx	North Fy	West Fx	South Fy
1	299	317	331	262
2	281	305	333	290
3	293	290	367	314
4	292	269	359	302
5	293	339	395	325
6	307	344	396	328
7	260	176	354	221
8	291	178	380	227
9	306	166	366	198
10	278	155	330	199
11	330	156	392	203
12	310	163	366	191
13	289	142	338	188

Table 3.5-49 Local Fuel/Rack Impact Forces - LC#4
GINNA 3D Whole Pool Model - Without Perimeter Racks
Load Case #4 - Unconsolidated Fuel - SSE - $\mu = 0.5$

Local Fuel/Rack Impact Forces Fx & Fy (lbs) per Fuel Assy.

Rack	East Fx	North Fy	West Fx	South Fy
1	1,267	1,194	1,335	1,421
2	1,374	1,274	1,121	1,261
3	1,075	1,082	1,229	1,301
4	1,414	1,134	1,304	1,364
5	1,523	1,131	1,508	1,328
6	1,423	1,208	1,174	1,376
7	815	1,218	788	1,239
8	1,328	1,123	1,117	1,227
9	1,083	874	974	1,172
10	1,213	1,264	966	1,121
11	1,103	888	1,045	1,198
12	1,210	1,149	982	1,220
13	1,280	990	1,018	1,202



Table 3.5-50 Local Fuel/Rack Impact Forces - LC#5
GINNA 3D Whole Pool Model - With Perimeter Racks
Load Case #5 - Unconsolidated Fuel - SSE - $\mu = 0.8$

Local Fuel/Rack Impact Forces Fx & Fy (lbs) per Fuel Assy.

Rack	East	North	West	South
	Fx	Fy	Fx	Fy
1	1,451	1,205	1,258	1,457
2	1,316	1,043	1,304	1,448
3	1,501	1,274	1,532	1,244
4	1,525	1,295	1,324	1,330
5	1,516	1,139	1,501	1,380
6	1,308	1,213	1,327	1,439
7	1,087	1,215	994	1,248
8	994	939	1,036	1,301
9	1,112	807	1,031	898
10	1,043	990	967	1,331
11	950	1,013	821	1,185
12	925	944	819	1,228
13	1,127	1,136	969	1,229

Table 3.5-51 Local Fuel/Rack Impact Forces - LC#6
GINNA 3D Whole Pool Model - With Perimeter Racks
Load Case #6 - Consolidated Fuel - SSE - $\mu = 0.8$

Local Fuel/Rack Impact Forces Fx & Fy (lbs) per Fuel Assy.

Rack	East	North	West	South
	Fx	Fy	Fx	Fy
1	318	314	342	265
2	317	298	340	301
3	313	289	353	311
4	311	269	348	300
5	309	349	385	320
6	318	355	385	324
7	250	177	331	223
8	267	176	363	223
9	302	164	363	197
10	272	155	318	201
11	301	153	389	198
12	286	164	368	191
13	282	144	343	189



Table 3.5-52 Local Fuel/Rack Impact Forces - LC#7
GINNA 3D Whole Pool Model - With Perimeter Racks
Load Case #7 - Unconsolidated Fuel - SSE - $\mu = 0.2$

Local Fuel/Rack Impact Forces Fx & Fy (lbs) per Fuel Assy.

Rack	East Fx	North Fy	West Fx	South Fy
1	1,329	842	1,143	1,102
2	1,389	843	1,431	1,184
3	1,570	843	1,470	1,116
4	1,423	1,017	1,186	1,308
5	1,464	1,227	1,493	1,397
6	1,466	1,236	1,370	1,450
7	1,289	1,006	1,026	1,216
8	781	858	913	1,210
9	939	1,272	757	1,203
10	998	981	911	1,232
11	964	946	804	1,273
12	1,258	1,267	1,099	1,106
13	1,000	991	883	1,230

Table 3.5-53 Local Fuel/Rack Impact Forces - LC#8
GINNA 3D Whole Pool Model - With Perimeter Racks
Load Case #8 - Consolidated Fuel - OBE - $\mu = 0.8$

Local Fuel/Rack Impact Forces Fx & Fy (lbs) per Fuel Assy.

Rack	East Fx	North Fy	West Fx	South Fy
1	115	141	132	110
2	109	137	140	106
3	109	133	142	100
4	103	132	144	100
5	108	132	144	94
6	104	132	144	94
7	80	97	122	84
8	75	95	121	81
9	76	100	119	88
10	67	81	110	77
11	79	79	120	78
12	69	103	112	92
13	65	75	111	73

Table 3.5-54 Local Fuel/Rack Impact Forces - LC#9
GINNA 3D Whole Pool Model - With Perimeter Racks
Load Case #9 - Unconsolidated Fuel - OBE - $\mu = 0.2$

Local Fuel/Rack Impact Forces Fx & Fy (lbs) per Fuel Assy.

Rack	East	North	West	South
	Fx	Fy	Fx	Fy
1	382	682	459	571
2	661	421	691	573
3	696	469	748	596
4	640	738	699	519
5	362	563	419	743
6	561	703	573	690
7	378	620	448	785
8	446	356	574	426
9	441	603	695	565
10	765	467	735	587
11	411	589	518	522
12	376	609	489	698
13	497	621	514	811

Table 3.5-55 Local Fuel/Rack Impact Forces - LC#10
GINNA 3D Whole Pool Model - Without Perimeter Racks
Load Case #10 - Unconsolidated Fuel - OBE - $\mu = 0.2$

Local Fuel/Rack Impact Forces Fx & Fy (lbs) per Fuel Assy.

Rack	East	North	West	South
	Fx	Fy	Fx	Fy
1	618	707	605	504
2	357	503	392	608
3	440	590	604	577
4	803	417	959	515
5	465	751	523	720
6	629	670	794	946
7	333	461	389	608
8	413	681	524	472
9	343	575	582	797
10	485	574	574	724
11	358	489	436	649
12	583	598	521	491
13	461	624	546	658

Table 3.5-56 Local Fuel/Rack Impact Forces - LC#11
GINNA 3D Whole Pool Model - With Perimeter Racks
Load Case #11 - Mixed Fuel - SSE - Mu = Mixed

Local Fuel/Rack Impact Forces Fx & Fy (lbs) per Fuel Assy.

Rack	East Fx	North Fy	West Fx	South Fy
1	1,577	1,056	1,407	1,311
2	1,488	1,167	1,520	1,409
3	1,451	1,165	1,495	1,411
4	1,449	952	1,497	1,232
5	322	293	365	304
6	330	248	372	286
7	258	173	304	219
8	0	0	0	0
9	266	167	284	194
10	0	0	0	0
11	1,029	898	1,043	1,239
12	1,193	1,034	990	1,261
13	1,070	977	1,026	1,272

Table 3.5-57 Local Fuel/Rack Impact Forces - LC#12
GINNA 3D Whole Pool Model - With Perimeter Racks
Load Case #12 - Mixed Fuel - OBE - Mu = Mixed

Local Fuel/Rack Impact Forces Fx & Fy (lbs) per Fuel Assy.

Rack	East Fx	North Fy	West Fx	South Fy
1	107	126	143	106
2	0	0	0	0
3	618	666	895	758
4	0	0	0	0
5	590	674	640	788
6	521	667	730	749
7	0	0	0	0
8	568	646	582	683
9	506	629	738	536
10	0	0	0	0
11	80	68	117	64
12	83	98	122	80
13	69	77	109	73

Table 3.5-58 Summary of Maximum Fuel/Rack Cell Wall Impact Loads

Seismic Conditions	Calculated Load (lbs)	TH Factor Load	Maximum Load (lbs)	Maximum ¹ Allowable Load (lbs)
SSE	1331	1.20	1600	2902
OBE	811	1.12	908	2291

Note: 1) Max. allowable load determined as load to produce max. allowable stresses in rack cell walls per ASME Section III criteria, as provided in Table 3.2-1.

3.5.3.1.7 Summary of Single Rack 3-D Model Results

These special studies on single rack models are performed to evaluate the effects of certain parameters on the results of seismic analyses. These evaluations reduce the number of whole pool evaluations which are required, thus making the analysis of the R.E. Ginna spent fuel pool racks more efficient. Two studies have already been reported. Section 3.5.2.6 covers the determination of time history factors for SSE and OBE, and Section 3.5.2.7 covers a study of the effects of rack stiffness on stresses and deflections. Four additional studies are reported in this section. The first study is an evaluation of the effects that increasing the rack tube height will have on the forces, moments, and displacements of the rack. The second study reported is an evaluation of the effects of attaching a peripheral rack onto the existing region 2 racks. This study includes the evaluation of the connection between the peripheral rack and the existing region 2 rack. The third study reported is an evaluation of three off-centered loading cases for half-loaded racks to find the most critical loading to be used in the whole pool model. The fourth study is a comparison of models with connected and disconnected fuel beams.

3.5.3.1.7.1 Brief Description of 3-D Single Rack Model

The analyses of the 3-D single rack model are performed using ANSYS 5.2, a finite element code accepted by the United States Nuclear Regulatory Commission (USNRC) for seismic and stress analysis. The model is made up of beam elements, mass elements, contact elements and hydrodynamic coupling elements.

All structural members are modeled by the BEAM4 element. The BEAM4 element is a 3-D elastic beam with six degrees of freedom at each node. Beam elements are used to model the rack legs, the baseplate, the rack tubes, and the fuel.

The fuel beam and the rack beam are vertical beams located at the centroid of the rack in the horizontal plane. The fuel beam and rack beam are connected at the bottom end. The baseplate beams extend horizontally from the bottom of the rack beam to the centers of the corner rack cells. At the corner rack cells, rack leg beams extend vertically downward from the ends of the baseplate beams. Each leg beam represents one fourth of the total number of rack legs.

All mass is represented by MASS21 elements. The MASS21 element is a lumped mass element which can be applied in all three orthogonal directions. The MASS21 element can also apply rotary inertia to represent the lumped mass more as a distributed mass.

All contacts between the rack legs and pool liner and between the rack tubes and fuel are modeled with CONTAC52 elements. The CONTAC52 element is a 3-D point to point contact element which allows for gaps, interface stiffness, and sliding friction.

All hydrodynamic coupling between the fuel and rack, and between the rack and adjacent racks are modeled with FLUID38 elements. The FLUID38 element is a hydrodynamic coupling element with two degrees of freedom at each node, translation perpendicular to the axes of the coupled cylinders.

There are two basic single rack models. The first is a representation of rack 8 (2B), a 9x11 region 2 rack designed by ATEA, see Figure 3.5-41. The second is a representation of rack 1, an existing region 2 rack in the R.E. Ginna spent fuel pool, with a peripheral rack, rack 4A attached, see Figure 3.5-42.

3.5.3.1.7.2 Study of Effects of Rack Height Increase

3.5.3.1.7.2.1 Purpose of Rack Height Increase Study

During evaluation of the racks, it became apparent that the height of the racks would have to be increased. The original design height of the tubes on the racks was 158.5 in. This height, for this study, was increased 3 in. to 161.5 in. All of the previous analyses had been performed using the shorter rack height, so this study was performed to determine the effects that this change will have on the structural seismic performance of the racks.

3.5.3.1.7.2.2 Modifications Required in the Rack Model

The following modifications were made to the standard model for rack 8 (rack 2B, 11x9) in order to represent a rack in which the tube height had been increased 3 in.

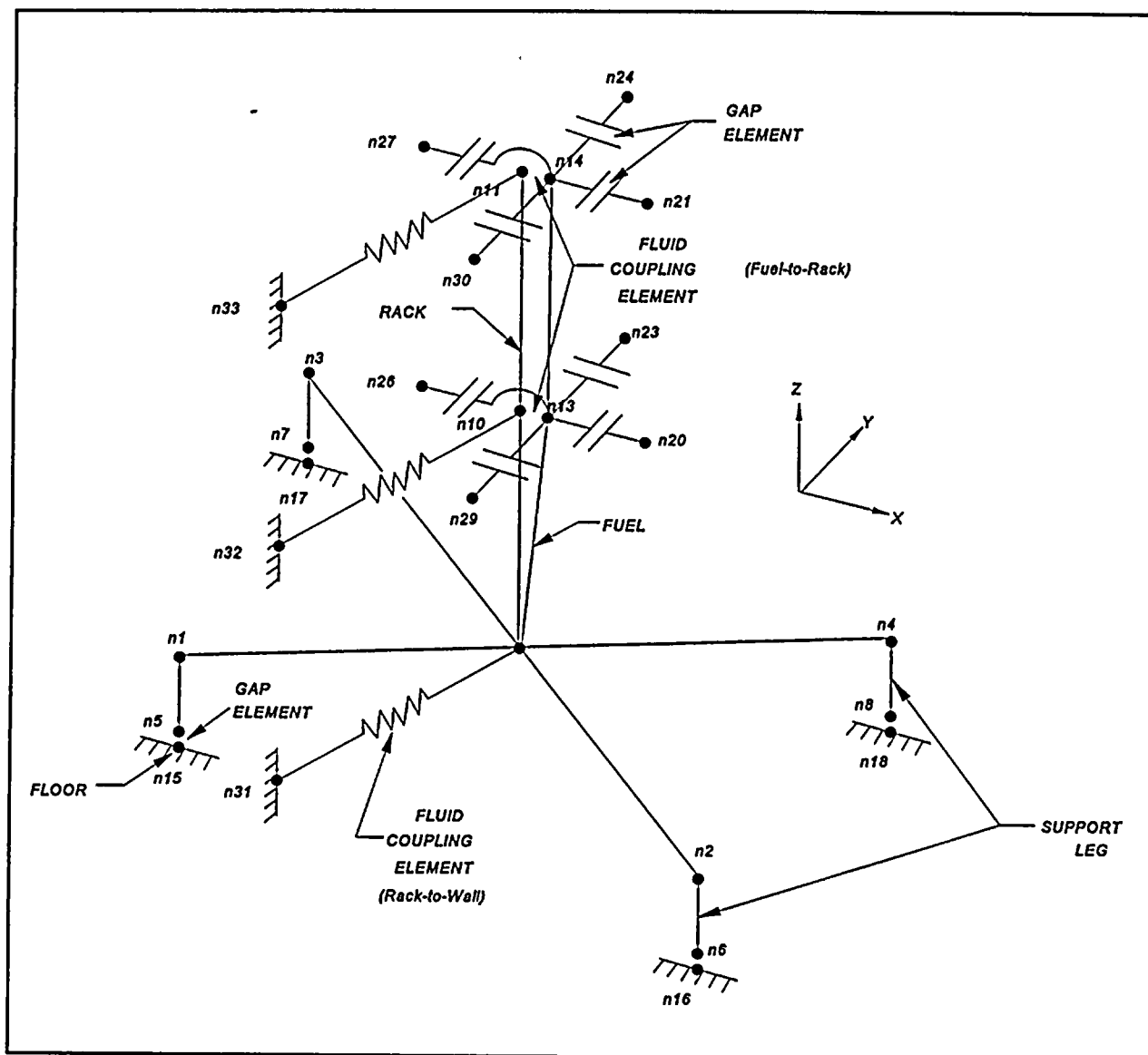
1. Increase rack beam height by 3 in.
2. Add mass of additional rack tube height, 98.6 lbs
3. Recalculated Mass Moments of Inertia for height of 161.5 in.
4. Scale fuel to rack hydrodynamic coupling masses by $(161.5/158.5)$.
5. Scale rack to rack hydrodynamic coupling masses by $(162.68/159.68)$.

3.5.3.1.7.2.3 Results of Rack Height Increase Study

A 3 in. increase in the height of the rack tubes was found to have only minor effects on the resulting rack loads, moments, and displacements. Table 3.5-59 provides a comparison of the results of a rack analyzed without and with the height increase.

The actual height increase of the racks was 3.5 in. (to 162.0 in) rather than the 3.0 in. used in this study. However, comparing this difference with the highest analyzed ratio produced in Table 3.5-59 equals $(3.5/3.0)(0.028) = 0.033$, which when rounded to two significant figures still shows a maximum of 3 percent increase due to the actual height increase of the racks by 3.5 inches.

Figure 3.5-41 Representation of Model for Single Rack Analysis



Note: Comparison with the above simplified model and the model shown in Figure 3.5-31 is provided in Section 3.5.3.1.7.5.



Figure 3.5-42 Representation of Model for Analysis of Rack 1 with Attached Rack 4A

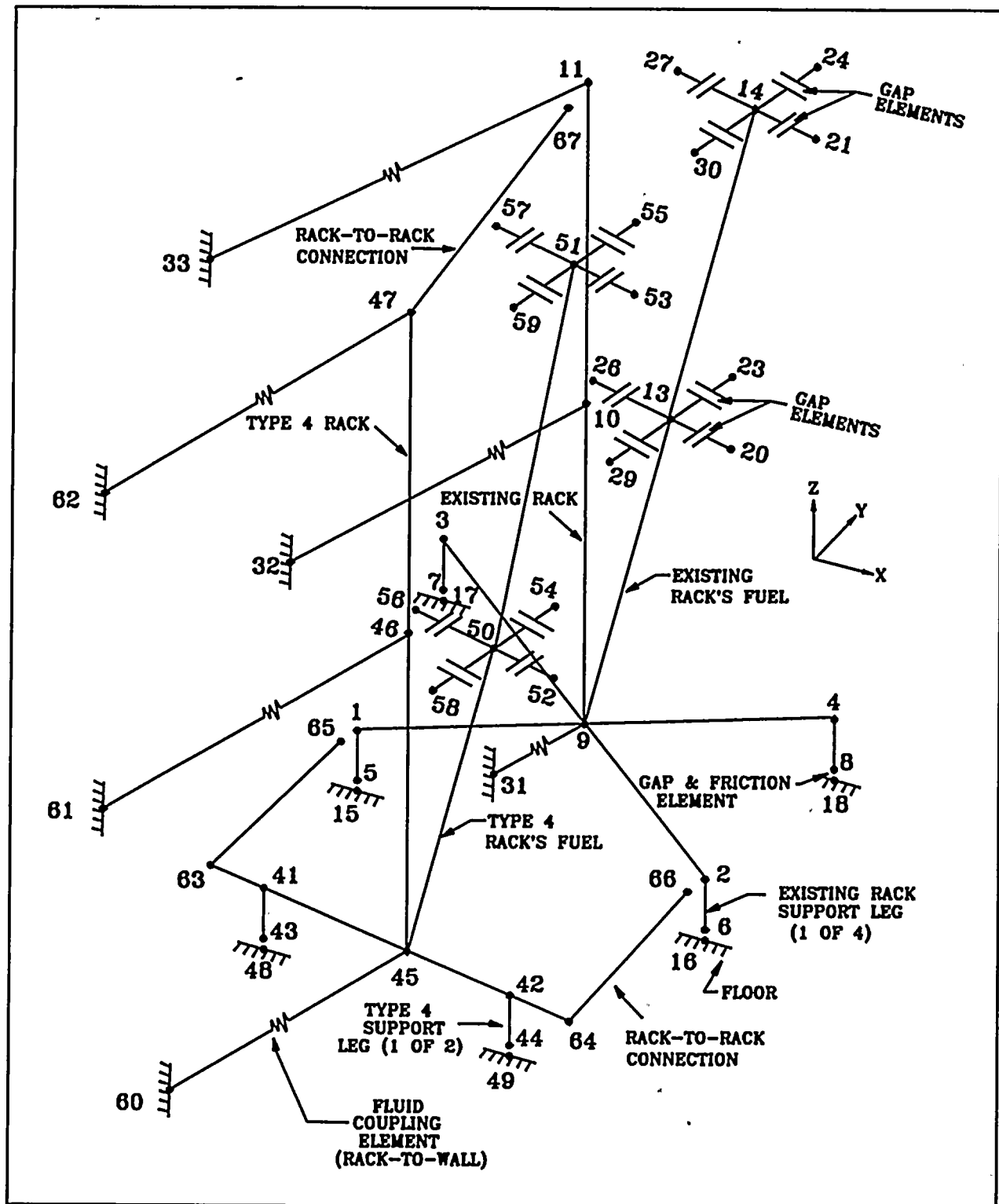




Table 3.5-59 Comparison of Results for Rack Model With and Without a Height Increase

	Item	Without Height Increase	With Height Increase	Increased Height Original Height
Max. Leg Load (lbs)	Single Model Leg Horizontal	34,910	33,570	0.962
	Single Model Leg Vertical	138,000	133,500	0.967
	Leg Total Vertical	322,800	322,800	1.000
Max. Rack Load (lbs)	Horizontal	62,980	64,740	1.028
	Vertical	13,480	13,570	1.007
Max. Rack Moments (in-lbs)	Rack Bending Moment	6.645×10^6	6.701×10^6	1.008
Max. Impact Loads (lbs)	Fuel-to-Rack	12,950	11,870	0.917
Displacement of Leg (in)	Horizontal	0.03354	0.03178	0.948

Included in the table is the factor which would have to be applied to the results of the analysis without the height increase to envelope the results of the analysis with the height increase. This factor is 1.028 and is governed by horizontal rack load. This factor needs to be increased by $(3.5/3.0)(.028) = 0.033$ for a total of 1.033 to account for the actual height increase of 3.5 in. rather than 3.0 in. as used in this study. This factor applies to all racks which have been increased 3.5 in. in height. However, this factor was accounted for when selecting the enveloping time history factors in Section 3.5.2.6. The actual time history factor calculated for SSE is 1.164. The combined time history factor is:

$$\text{SSE Time History Factor} = 1.164 * 1.033 = 1.2024 \approx 1.20$$

Thus, the time history factor selected for SSE is 1.20. Likewise, the actual time history factor calculated for OBE is 1.088. The combined time history factor is:

$$\text{OBE Time History Factor} = 1.088 * 1.033 = 1.1239 \approx 1.12$$

Thus, the time history factor selected for OBE is 1.12. Because the factor for increased rack height has already been accounted for in the time history factor, no additional factors need to be applied.

3.5.3.1.7.3 Peripheral Rack Attachment Study

3.5.3.1.7.3.1 Purpose of Peripheral Rack Attachment Study

In the whole pool models, the global effects of the peripheral racks was studied by adding the corresponding size and weight to the resident racks. However, the size and complexity of the whole pool model did not allow detailed modeling of the peripheral racks. Therefore, a model of a single peripheral rack attached to a resident rack was developed. This model includes separate beam models for the two racks, with beams connecting the two racks. The finer detail of this model provides loadings for the connections, the legs of the peripheral rack, and the loads on the peripheral rack itself. A representation of the model used in this analysis is included as Figure 3.5-42.

3.5.3.1.7.3.2 Peripheral Rack Model Input Adjustments

The model to analyze the connections between the Type 4 peripheral racks consists of beam element models of the Type 1 resident rack and the Type 4 peripheral rack connected by additional beams. The beams for the lower connection link the legs of the Type 1 rack to the baseplate of the Type 4 rack. The type 4 racks are modeled with 2 legs. The upper connection is modeled as a single beam which connects the centers of the two racks.

Connection Dimensions

Bottom Connection (2 per model)

Material is SS Type 304

width = 90 mm (3.543 in.)

height = 20 mm (0.787 in.)

length = 285 mm (11.22 in.)

Section Properties: Area = 2.788 in², $I_{yy} = 0.144$ in⁴, $I_{zz} = 2.917$ in⁴

Top Connection (1 per model)

Material is SS Type 304L

width = 140 mm (5.512 in.)

height = 40 mm (1.575 in.)

length = 57.4 mm (2.26 in.)

Section Properties: Area = 8.681 in², $I_{yy} = 1.795$ in⁴, $I_{zz} = 3,778.695$ in⁴

3.5.3.1.7.3.3 Summary of Results

The results of this model are analyzed to find the loads in each of the individual racks and in the connections between the two racks. Tables 3.5-60 and 3.5-61 provide summaries of the displacements and the forces and moments on the racks and the connections for OBE and SSE respectively.

In calculating the stresses in the connection, the loads encountered during thermal accident conditions, a temperature rise from 150°F to 180°F, must be included. The maximum loads caused by the thermal accident are horizontal leg forces equal to the dead load of the rack multiplied by the coefficient of friction between the leg and the pool liner. The top end of the friction range is 0.8.

Table 3.5-60 Summary of OBE Results in Peripheral Rack Analysis ¹

	Item	Resident Rack 1	Peripheral Rack 4A
Max. Leg Load (lbs)	Single Model Leg Horizontal	16,190	8,708
	Single Model Leg Vertical	137,100	27,110
	Leg Total Vertical	424,800	
Max. Rack Load (lbs)	Horizontal Rack Load	19,560	13,700
	Vertical Rack Load	16,990	1,340
Rack Moments (in-lbs)	Rack Moment Mx	978,000	502,600
	Rack Moment My	747,800	583,800
Max. Rack Moments (in-lbs)	Rack Bending Moment	1.042×10^6	6.661×10^5
Max. Impact Load (lbs)	Fuel-to-Rack Impact Loads	5,614	5,699
Displacement of Leg (in)	Horizontal	0.01620	0.01770
Axial Load (lbs)	Bottom Connection	Tension: 11,034 Compres.: -2,063	
	Upper Connection	Tension: 7,618 Compres.: -7,753	
Bending Load (lbs)	Bottom Connection Vertical	-703	
	Upper Connection Horizontal	1,218	

¹ - OBE results need to be multiplied by a seismic load factor of 1.12.

Top Connection Stresses for OBE

$$\sigma_{\text{memb.}} = 1,000 \text{ psi} \leq 1.0 * S = 15,700 \text{ psi (304L S.S.)}$$

$$\sigma_{\text{shear}} = 157 \text{ psi} \leq 0.6 * S = 9,420 \text{ psi}$$

Bottom Connection Stresses for OBE

$$\sigma_{\text{memb.}} = 4,433 \text{ psi} \leq 1.0 * S = 18,300 \text{ psi (304 S.S.)}$$

$$\sigma_{\text{memb.+bend.}} = 25,740 \text{ psi} \leq 1.5 * S = 27,450 \text{ psi}$$



Table 3.5-61 Summary of SSE Results in Peripheral Rack Analysis ¹

	Item	Resident Rack 1	Peripheral Rack 4A
Max. Leg Load (lbs)	Single Model Leg Horizontal	41,410	18,080
	Single Model Leg Vertical	184,900	31,170
	Leg Total Vertical	484,500	
Max. Rack Load (lbs)	Horizontal Rack Load	42,870	25,710
	Vertical Rack Load	23,200	1,518
Rack Moments (in-lbs)	Rack Moment Mx	2.081*10 ⁶	8.634*10 ⁵
	Rack Moment My	1.323*10 ⁶	6.569*10 ⁵
Max. Rack Moments (in-lbs)	Rack Bending Moment	2.196*10 ⁶	9.676*10 ⁵
Max. Impact Load (lbs)	Fuel-to-Rack Impact Loads	24,050	11,910
Displacement of Leg (in)	Horizontal	0.03793	0.03682
Axial Load (lbs)	Bottom Connection	Tension: 25,724 Compres.: -5,164	
	Upper Connection	Tension: 17,153 Compres.: -17,319	
Bending Load (lbs)	Bottom Connection Vertical	-901	
	Upper Connection Horizontal	2,297	

¹ - SSE results need to be multiplied by a seismic load factor of 1.20.

Top Connection Stresses for SSE

$$\sigma_{\text{memb.}} = 2,394 \text{ psi} \leq 1.2 * S_y = 26,450 \text{ psi (304L S.S.)}$$

$$\sigma_{\text{shear}} = 318 \text{ psi} \leq 0.42 * S_u = 28,123 \text{ psi}$$

Bottom Connection Stresses for SSE

$$\sigma_{\text{memb.}} = 11,072 \text{ psi} \leq 1.2 * S_y = 31,200 \text{ psi (304 S.S.)}$$

$$\sigma_{\text{memb.+bend.}} = 31,914 \text{ psi} \leq 1.8 * S_y = 46,800 \text{ psi}$$

Type 4 Rack Stresses for OBE Loads

$$I_{xx} = 292 \text{ in}^4$$

$$I_{yy} = 15,471 \text{ in}^4$$

$$A = 25.9 \text{ in}^2$$

$$c_{xx} = 8.3/2 = 4.15 \text{ in}$$

$$c_{yy} = 84.56/2 = 42.28 \text{ in}$$

$$\sigma_{\text{memb}} (\text{X-Dir}) = 8,000 \text{ psi} \leq 1.0 * S = 15,700 \text{ psi (304L S.S.)}$$

$$\sigma_{\text{memb}} (\text{Y-Dir}) = 1,787 \text{ psi} \leq 1.0 * S = 15,700 \text{ psi (304L S.S.)}$$

Note: Rack Overturning moments result in local cell wall membrane stresses

Type 4 Rack Stresses for SSE Loads

$$\sigma_{\text{memb}} (\text{X-Dir}) = 14,725 \text{ psi} \leq 1.2 * S_y = 26,450 \text{ psi (304L S.S.)}$$

$$\sigma_{\text{memb}} (\text{Y-Dir}) = 2,145 \text{ psi} \leq 1.2 * S_y = 26,450 \text{ psi (304L S.S.)}$$

Note: Rack Overturning moments result in local cell wall membrane stresses

Loading Effects on the Resident Racks Due to Rack 4 Attachment

Upper Connection

$$\sigma_{\text{memb}} = 687 \text{ psi} \leq 1,194 \text{ psi local critical buckling stress}$$

Lower Connection

This connection runs the entire 84.56 in. interface between the Type 4 Rack and the Resident Racks

$$\text{Area in compression} = 42.28 \text{ in}^2$$

$$\sigma_{\text{memb}} = 1,453 \text{ psi} \leq 31,200 \text{ psi (Level D loading with Level A allowables)}$$

3.5.3.1.7.4 Off-Centered Loading Study

3.5.3.1.7.4.1 Purpose of Off-Centered Loading Study

One of the scenarios which is analyzed using the whole pool model is a mixed load case. The mixed load case represents any of the following rack loading configurations:

1. Full, Unconsolidated
2. Full, Consolidated
3. Half Loaded, Unconsolidated
4. Half Loaded, Consolidated
5. Empty

The cases which involve half loaded racks can be loaded off-centered, causing the higher loadings and displacements than if they are partially loaded with an even distribution. There are three different ways to load the fuel to provide off-centered loading:

1. Load half of rack on one side of short axis.
2. Load half of rack on one side of long axis.
3. Load half of rack on one side of diagonal.

Each of these three conditions are analyzed to determine which provides the highest loads, moments, and displacements for the half loaded racks. It should be noted that the absolute maximum racks loads occur with fully loaded racks with consolidated fuel. Further, the maximum rack displacements occur with fully loaded racks with unconsolidated fuel.

3.5.3.1.7.4.2 Modifications Required to Analyze Off-Centered Loading Cases

The rack modeled is rack 8 (2B), a region 2 11x9 rack. The half loaded case is modeled with 50 consolidation canisters. The fuel beam area, fuel beam moment of inertia, fuel weight, fuel to rack interface stiffness, and fuel to rack hydrodynamic coupling are all adjusted by multiplying by 50 canisters rather than 99. The centroids of the racks are adjusted for each case to represent the off-centered loading, and the appropriate mass moments of inertia are applied.

Centroid of centered loading case:

x: 46.655 in. y: 38.23 in.

Case 1: Load on one side of short axis.

x: 66.5193 in. y: 38.23 in.

Case 2: Load on one side of long axis.

x: 46.655 in. y: 22.0442 in.

Case 3: Load on one side of diagonal.

x: 60.6336 in. y: 27.9300 in.

3.5.3.1.7.4.3 Summary of Off-Centered Loading Results

A summary of the results of the loadings is provided in Table 3.5-62. The results indicate that in general, the diagonal loading pattern provides the highest loads, moments and displacements. Maximum values are shown in bold text. Five of the seven items are highest for the diagonal loading pattern. For the two items which are higher for the short axis loading case, the values for the diagonal loading are within 5 percent.

**Table 3.5-62 Comparison of Results for Half-Loaded
Consolidated Rack 8, SSE1, Mu=0.8**

Loading on one side of:	Short Axis	Long Axis	Diagonal
Single Model Leg Horizontal Load	17,480 lbs	13,720 lbs	19,210 lbs
Single Model Leg Vertical Load	85,820 lbs	84,060 lbs	91,880 lbs
Total Vertical Load on Legs	165,700 lbs	164,000 lbs	166,100 lbs
Rack Load - Horizontal	30,830 lbs	27,970 lbs	29,640 lbs
Rack Load - Vertical	12,830 lbs	12,700 lbs	12,870 lbs
Rack Bending Moment	3.361*10⁶ in-lbs	2.873*10 ⁶ in-lbs	3.222*10 ⁶ in-lbs
Leg Displacement - Horiz.	0.02273 in.	0.01478 in.	0.02325 in.

3.5.3.1.7.5 Comparison of Connected and Disconnected Fuel Beam Models

All of the models used thus far have connected the fuel beam to the rack at the lower end. This model simplification was performed to aid convergence in the whole pool model. In order to maintain consistency between the single rack models and the whole pool models, the same simplification was made on the single rack models. However, the single rack model, having less complexity than the whole pool models, converged with the fuel beam essentially disconnected from the rack (weak springs were used to connect the fuel to the rack at the base, in order to aid convergence). The purpose of this study was to compare the results of two analyses, one with the fuel connected and one with fuel disconnected, to determine the effects of connecting the fuel on the forces, moments, and displacements seen in the rack. The objective was to justify use of the connected fuel beam model for the whole pool models.



1. The first part of the document is a list of names and addresses of the members of the committee.

2. The second part of the document is a list of names and addresses of the members of the committee.

Differences Between Connected and Disconnected Fuel Beam Models

The first analysis was performed using a connected fuel beam (Figure 3.5-41), and the second analysis was performed using the disconnected fuel beam (Figure 3.5-31). Both analyses modeled Rack 8 (2B) with consolidated fuel, and used a coefficient of friction of 0.8 and SSE time history set number 1. The following is a list of the differences between the two models:

1. Separate node for bottom of fuel beam.
2. The fuel mass was separated from rack mass and applied at new node.
3. New node was attached to rack beam by weak linear and torsional springs.
4. A hydrodynamic coupling element was added at the bottom of the fuel beam. The fuel to rack hydrodynamic coupling was redistributed, 25% at top of rack, 50% at middle of rack, and 25% at bottom of rack.
5. Fuel to rack gap elements were added at the bottom of the fuel beam for the +X, +Y, -X, and -Y directions.

Results of Connected and Disconnected Fuel Beam Model Comparison

Table 3.5-63 contains the results of the comparison between the connected and disconnected beam models. The table reports the results of the individual evaluations and the ratio of the results of the connected beam model with the disconnected beam model. The comparison shows that the differences between the results of the two models is small, and the connected beam model results are slightly higher and are therefore more conservative. Therefore, use of the simpler connected fuel beam model is justified.

Table 3.5-63 Summary of Connected and Disconnected Fuel Beam Model Comparison Results

Component	Connected Fuel Beam Model	Disconnected Fuel Beam Model	Ratio: Connected Fuel Disconnected Fuel
Single Model Leg Horizontal Force	34,910 lbs	29,070 lbs	1.201
Single Model Leg Vertical Force	138,000 lbs	134,500 lbs	1.026
Sum of Legs Vertical Force	322,800 lbs	322,600 lbs	1.001
Horizontal Rack Force	62,980 lbs	57,090 lbs	1.103
Vertical Rack Force	13,480 lbs	13,470 lbs	1.001
Horizontal Rack Moment	6.645×10^6 in-lbs	6.342×10^6 in-lbs	1.048
Horizontal Leg Displacement	0.03354 in.	0.03120 in.	1.075

3.5.3.1.8 Summary of Whole Pool Model Results

The results of the whole pool multi-rack analysis are presented in this section, except for selected topics (ie, Fuel-to-Rack Impact Loads) which are covered in other sections.

The subsections are as follows:

- 3.5.3.1.8.1 Rack Forces and Moments for Each Load Case
- 3.5.3.1.8.2 Final Rack Displacements for Each Load Case
- 3.5.3.1.8.3 Final Rack Rotations for Each Load Case
- 3.5.3.1.8.4 Representative Plots

Table 3.5-64 Summary of Whole Pool Model Load Cases

Load Case	Seismic Loading	Fuel Loading	Perimeter Racks	Coefficient of Friction, μ
1	SSE	Unconsolidated	No	0.8
2	SSE	Unconsolidated	No	0.2
3	SSE	Consolidated	No	0.8
4	SSE	Unconsolidated	No	0.5
5	SSE	Unconsolidated	Yes	0.8
6	SSE	Consolidated	Yes	0.8
7	SSE	Unconsolidated	Yes	0.2
8	OBE	Consolidated	Yes	0.8
9	OBE	Unconsolidated	Yes	0.2
10	OBE	Unconsolidated	No	0.2
11	SSE	Mixed ¹	Yes	Mixed ²
12	OBE	Mixed ¹	Yes	Mixed ²

Notes: 1) Fuel loadings of Empty, Half-Consolidated, Half-Unconsolidated, Full-Consolidated and Full-Unconsolidated were randomly assigned to the racks in the pool.

2) Coefficients of Friction ranging from 0.2 to 0.8 (with a mean of 0.5, and a standard deviation of 0.15) were randomly assigned to the racks in the pool.

Table 3.5-65 Summary of Rack Loadings for Load Case #11

Rack	Fuel Loading	Coefficient of Friction, μ
1	Half-Unconsolidated, NE ¹	0.48
2	Half-Unconsolidated, NE	0.53
3	Half-Unconsolidated, NW	0.58
4	Full Unconsolidated	0.75
5	Half-Consolidated, SE	0.66
6	Full Consolidated	0.25
7	Half-Consolidated, NW	0.43
8	Empty	0.59
9	Full Consolidated	0.42
10	Empty	0.31
11	Full Unconsolidated	0.59
12	Full Unconsolidated	0.71
13	Full Unconsolidated	0.47

- Notes:
- 1) Fuel loadings of half full used a diagonal fuel loading for worst eccentricity. The locations of the centroid for the half loaded conditions were randomly assigned to one of the four corners of the rack. Thus, NE = North-East, NW = North-West, SW = South-West and SE = South-East.
 - 2) Coefficients of friction in the range between 0.2 and 0.8 were randomly assigned to the racks. The mean of the values for Load Case #11 is 0.52 and the standard deviation is 0.148.

Distribution of Fuel Loads for Load Case #11

Loading	Qty
Full Consolidated	2
Full Unconsolidated	4
Half Consolidated	2
Half Unconsolidated	3
Empty	2



Table 3.5-66 Summary of Rack Loadings for Load Case #12

Rack	Fuel Loading	Coefficient of Friction, μ
1	Half-Consolidated, SW ¹	0.42
2	Empty	0.24
3	Full Unconsolidated	0.50
4	Empty	0.45
5	Half-Unconsolidated, NW	0.55
6	Half-Unconsolidated, NW	0.40
7	Empty	0.43
8	Full Unconsolidated	0.77
9	Full Unconsolidated	0.65
10	Empty	0.41
11	Full Consolidated	0.43
12	Half-Consolidated, SW	0.75
13	Full Consolidated	0.36

- Notes:
- 1) Fuel loadings of half full used a diagonal fuel loading for worst eccentricity. The locations of the centroid for the half loaded conditions were randomly assigned to one of the four corners of the rack. Thus, NE = North-East, NW = North-West, SW = South-West and SE = South-East.
 - 2) Coefficients of friction in the range between 0.2 and 0.8 were randomly assigned to the racks. The mean of the values for Load Case #12 is 0.49 and the standard deviation is 0.153.

Distribution of Fuel Loads for Load Case #12

<u>Loading</u>	<u>Qty</u>
Full Consolidated	2
Full Unconsolidated	3
Half Consolidated	2
Half Unconsolidated	2
Empty	4



3.5.3.1.8.1 Rack Forces and Moments for Each Load Case

Table 3.5-67 Rack Forces Fx, Fy & Fz - LC#1
GINNA 3D Whole Pool Model - Without Perimeter Racks
Load Case #1 - Unconsolidated Fuel - SSE - Mu = 0.8

Rack Forces Fx, Fy & Fz (lbs)

Rack	Min Fx	Max Fx	Min Fy	Max Fy	Min Fz	Max Fz
1	-52,790	48,960	-95,430	90,500	-23,460	-13,890
2	-47,730	56,870	-92,630	84,690	-22,930	-13,650
3	-52,960	40,220	-105,000	77,030	-22,810	-14,190
4	-54,020	45,660	-95,510	76,140	-22,690	-14,190
5	-73,610	54,300	-81,040	82,450	-23,260	-13,720
6	-67,270	46,410	-84,280	88,820	-23,510	-14,200
7	-56,650	51,990	-24,720	33,780	-11,460	-6,824
8	-64,390	59,140	-37,730	42,310	-13,140	-7,841
9	-35,110	32,440	-14,060	13,790	-10,260	-5,674
10	-42,430	42,910	-24,340	22,980	-13,330	-8,283
11	-44,190	50,490	-19,790	25,570	-13,090	-6,938
12	-37,490	35,780	-10,180	16,220	-10,310	-5,847
13	-42,010	44,180	-23,340	25,000	-12,090	-7,388

Table 3.5-68 Rack Moments Mx, My & Mz - LC#1
GINNA 3D Whole Pool Model - Without Perimeter Racks
Load Case #1 - Unconsolidated Fuel - SSE - Mu = 0.8

Rack Moments Mx, My & Mz (in-lbs) x 1E6

Rack	Min Mx	Max Mx	Min My	Max My	Min Mz	Max Mz
1	-10.640	10.950	-6.556	5.899	-0.522	0.595
2	-10.130	11.070	-5.283	6.042	-0.606	0.677
3	-8.325	9.978	-4.775	4.350	-0.577	0.535
4	-8.653	9.440	-4.703	4.680	-0.377	0.272
5	-8.884	8.926	-7.813	5.227	-0.366	0.425
6	-9.460	9.826	-7.416	5.542	-0.508	0.582
7	-3.154	3.051	-5.735	6.323	-0.208	0.239
8	-4.669	4.223	-7.030	6.729	-0.281	0.331
9	-1.325	1.182	-3.710	3.533	-0.237	0.215
10	-2.556	2.253	-5.044	4.902	-0.146	0.166
11	-2.783	2.404	-4.405	4.538	-0.166	0.185
12	-1.138	1.110	-3.575	3.699	-0.135	0.125
13	-2.424	2.284	-3.972	4.515	-0.189	0.185

Table 3.5-69 Rack Forces Fx, Fy & Fz - LC#2
GINNA 3D Whole Pool Model - Without Perimeter Racks
Load Case #2 - Unconsolidated Fuel - SSE - Mu = 0.2

Rack Forces Fx, Fy & Fz (lbs)

Rack	Min Fx	Max Fx	Min Fy	Max Fy	Min Fz	Max Fz
1	-50,330	47,920	-63,490	72,310	-22,660	-13,900
2	-52,770	51,310	-61,840	68,070	-22,710	-13,570
3	-46,020	46,440	-61,140	58,390	-22,660	-13,460
4	-53,420	44,680	-61,420	68,470	-22,660	-13,460
5	-43,320	46,070	-60,860	68,440	-22,720	-13,460
6	-43,000	44,000	-73,570	90,930	-22,880	-13,470
7	-47,250	41,460	-28,000	25,570	-11,200	-7,134
8	-44,110	46,200	-33,770	42,680	-12,980	-7,788
9	-28,350	30,650	-12,860	13,250	-10,630	-5,653
10	-36,730	37,950	-26,080	22,730	-13,010	-8,373
11	-35,370	37,460	-23,670	20,420	-11,750	-7,460
12	-27,700	28,630	-12,070	12,540	-9,960	-6,047
13	-33,300	33,330	-25,230	19,060	-11,570	-7,651

Table 3.5-70 Rack Moments Mx, My & Mz - LC#2
GINNA 3D Whole Pool Model - Without Perimeter Racks
Load Case #2 - Unconsolidated Fuel - SSE - Mu = 0.2

Rack Moments Mx, My & Mz (in-lbs) x 1E6

Rack	Min Mx	Max Mx	Min My	Max My	Min Mz	Max Mz
1	-9.342	7.955	-5.506	5.003	-0.370	0.292
2	-9.097	7.384	-5.325	4.779	-0.291	0.250
3	-7.066	6.519	-4.635	3.415	-0.194	0.196
4	-7.515	6.430	-4.343	3.630	-0.225	0.235
5	-8.004	6.563	-3.653	3.186	-0.235	0.270
6	-8.725	7.941	-4.092	3.375	-0.323	0.368
7	-2.767	2.418	-5.137	5.355	-0.144	0.167
8	-4.418	3.836	-5.276	6.024	-0.159	0.196
9	-1.398	1.042	-3.387	3.650	-0.120	0.129
10	-2.449	2.226	-4.289	4.280	-0.112	0.136
11	-2.274	2.197	-4.102	4.423	-0.095	0.103
12	-1.277	0.985	-3.468	3.481	-0.072	0.075
13	-2.405	2.260	-3.788	4.120	-0.129	0.100

Table 3.5-71 Rack Forces Fx, Fy & Fz - LC#3
GINNA 3D Whole Pool Model - Without Perimeter Racks
Load Case #3 - Consolidated Fuel - SSE - Mu = 0.8

Rack Forces Fx, Fy & Fz (lbs)

Rack	Min Fx	Max Fx	Min Fy	Max Fy	Min Fz	Max Fz
1	-66,330	71,480	-147,200	137,700	-24,060	-12,630
2	-57,400	54,080	-131,900	119,500	-24,060	-12,730
3	-60,520	57,640	-101,700	108,600	-24,060	-12,750
4	-60,290	51,580	-106,500	107,600	-24,060	-12,750
5	-65,780	54,300	-98,050	108,000	-24,060	-12,750
6	-69,900	56,790	-104,700	117,800	-24,060	-12,750
7	-79,380	86,280	-40,040	45,420	-11,650	-6,779
8	-82,650	98,880	-51,140	60,740	-13,460	-7,888
9	-52,350	65,050	-18,540	21,300	-9,837	-5,310
10	-65,250	72,760	-35,700	36,290	-13,170	-7,864
11	-63,300	74,980	-31,200	32,490	-12,250	-6,996
12	-49,740	59,820	-19,800	23,530	-10,250	-5,530
13	-61,500	67,090	-35,060	33,130	-12,290	-7,212

Table 3.5-72 Rack Moments Mx, My & Mz - LC#3
GINNA 3D Whole Pool Model - Without Perimeter Racks
Load Case #3 - Consolidated Fuel - SSE - Mu = 0.8

Rack Moments Mx, My & Mz (in-lbs) x 1E6

Rack	Min Mx	Max Mx	Min My	Max My	Min Mz	Max Mz
1	-15.840	14.950	-6.339	7.307	-0.888	0.898
2	-14.260	13.600	-5.366	5.321	-0.419	0.491
3	-11.160	10.730	-3.900	3.441	-0.340	0.272
4	-10.480	9.842	-3.957	3.580	-0.220	0.173
5	-9.832	10.420	-4.897	4.318	-0.199	0.171
6	-11.480	12.050	-5.369	4.969	-0.275	0.293
7	-3.848	3.310	-7.457	8.648	-0.180	0.231
8	-5.114	4.909	-8.893	9.440	-0.324	0.353
9	-1.579	1.678	-5.341	6.813	-0.221	0.217
10	-2.821	2.857	-6.487	7.517	-0.182	0.213
11	-2.451	2.661	-6.969	7.333	-0.260	0.266
12	-1.403	1.435	-5.424	6.399	-0.211	0.230
13	-2.468	2.972	-6.146	6.830	-0.284	0.322

Table 3.5-73 Rack Forces Fx, Fy & Fz - LC#4
GINNA 3D Whole Pool Model - Without Perimeter Racks
Load Case #4 - Unconsolidated Fuel - SSE - Mu = 0.5

Rack Forces Fx, Fy & Fz (lbs)

Rack	Min Fx	Max Fx	Min Fy	Max Fy	Min Fz	Max Fz
1	-51,490	59,470	-92,040	86,220	-23,050	-13,740
2	-46,580	53,850	-87,100	89,180	-23,060	-13,460
3	-61,530	44,990	-91,480	73,310	-22,840	-13,940
4	-53,010	43,260	-89,380	79,110	-22,770	-13,810
5	-64,430	49,920	-77,530	86,680	-23,340	-13,920
6	-65,330	60,210	-82,560	88,100	-23,550	-13,900
7	-57,600	50,180	-29,510	33,700	-11,810	-6,715
8	-63,580	56,170	-39,670	43,280	-13,170	-7,906
9	-34,780	33,070	-13,050	12,650	-10,720	-5,496
10	-44,950	44,390	-26,660	29,750	-13,680	-8,234
11	-41,200	43,380	-20,200	23,600	-12,640	-7,326
12	-35,730	35,100	-10,890	11,350	-10,530	-5,671
13	-35,060	42,560	-24,380	24,200	-12,310	-7,174

Table 3.5-74 Rack Moments Mx, My & Mz - LC#4
GINNA 3D Whole Pool Model - Without Perimeter Racks
Load Case #4 - Unconsolidated Fuel - SSE - Mu = 0.5

Rack Moments Mx, My & Mz (in-lbs) x 1E6

Rack	Min Mx	Max Mx	Min My	Max My	Min Mz	Max Mz
1	-10.430	11.490	-5.788	5.872	-0.504	0.654
2	-10.430	10.890	-4.886	5.981	-0.543	0.376
3	-8.321	9.106	-5.468	4.240	-0.289	0.336
4	-8.416	9.020	-5.542	4.720	-0.417	0.366
5	-8.156	8.685	-7.789	5.785	-0.325	0.336
6	-9.294	9.577	-7.997	5.935	-0.366	0.360
7	-3.055	2.896	-6.100	5.839	-0.159	0.192
8	-4.580	3.926	-6.961	6.673	-0.341	0.391
9	-1.289	1.309	-3.650	3.535	-0.151	0.138
10	-2.474	2.271	-4.894	4.835	-0.169	0.140
11	-2.634	2.109	-4.448	4.576	-0.172	0.158
12	-1.000	1.158	-3.657	3.606	-0.141	0.163
13	-2.680	2.662	-3.946	4.622	-0.155	0.138

Table 3.5-75 Rack Forces Fx, Fy & Fz - LC#5
GINNA 3D Whole Pool Model - With Perimeter Racks
Load Case #5 - Unconsolidated Fuel - SSE - Mu = 0.8

Rack Forces Fx, Fy & Fz (lbs)

Rack	Min Fx	Max Fx	Min Fy	Max Fy	Min Fz	Max Fz
1	-46,410	51,270	-103,900	109,100	-25,870	-14,070
2	-48,550	54,790	-104,600	105,200	-25,430	-14,320
3	-51,080	42,070	-96,110	95,890	-24,700	-14,680
4	-49,500	42,440	-97,660	97,740	-24,700	-14,740
5	-71,970	47,940	-97,320	89,390	-25,160	-14,430
6	-81,550	53,640	-102,900	97,700	-25,140	-14,280
7	-57,340	54,570	-29,000	34,340	-11,510	-7,102
8	-70,580	59,840	-45,040	40,210	-13,580	-7,830
9	-33,960	35,270	-14,720	12,700	-9,535	-5,702
10	-42,600	46,360	-28,250	26,680	-13,250	-8,087
11	-38,990	55,460	-24,760	21,800	-12,170	-7,055
12	-35,120	35,700	-12,600	13,370	-9,740	-5,515
13	-39,010	42,250	-28,440	26,050	-11,970	-7,140

Table 3.5-76 Rack Moments Mx, My & Mz - LC#5
GINNA 3D Whole Pool Model - With Perimeter Racks
Load Case #5 - Unconsolidated Fuel - SSE - Mu = 0.8

Rack Moments Mx, My & Mz (in-lbs) x 1E6

Rack	Min Mx	Max Mx	Min My	Max My	Min Mz	Max Mz
1	-12.430	13.460	-4.887	4.697	-0.709	0.548
2	-12.060	11.920	-4.816	4.164	-0.739	0.750
3	-11.410	11.080	-4.913	3.486	-0.491	0.406
4	-11.310	11.560	-4.252	4.234	-0.421	0.511
5	-10.040	10.960	-7.132	4.671	-0.598	0.506
6	-10.650	11.830	-6.449	4.974	-0.332	0.424
7	-3.145	3.003	-6.261	6.354	-0.212	0.252
8	-4.538	4.946	-6.909	6.916	-0.295	0.273
9	-1.453	1.309	-3.539	3.488	-0.180	0.132
10	-2.573	2.868	-4.944	4.813	-0.155	0.203
11	-2.199	2.715	-4.412	4.752	-0.230	0.241
12	-1.121	1.307	-3.527	3.633	-0.138	0.135
13	-2.800	2.742	-4.133	4.633	-0.180	0.145

Table 3.5-77 Rack Forces Fx, Fy & Fz - LC#6
GINNA 3D Whole Pool Model - With Perimeter Racks
Load Case #6 - Consolidated Fuel - SSE - Mu = 0.8

Rack Forces Fx, Fy & Fz (lbs)

Rack	Min Fx	Max Fx	Min Fy	Max Fy	Min Fz	Max Fz
1	-70,290	59,940	-144,000	145,800	-25,950	-13,170
2	-65,800	50,590	-129,300	123,700	-25,800	-13,170
3	-62,710	49,580	-107,200	119,700	-25,800	-13,170
4	-67,340	47,810	-107,000	118,800	-25,800	-13,170
5	-71,790	56,630	-101,600	114,300	-25,800	-13,170
6	-72,390	63,110	-108,400	125,100	-25,800	-13,170
7	-65,260	90,640	-39,500	45,210	-11,650	-6,815
8	-84,380	84,640	-54,980	63,020	-13,470	-7,838
9	-53,660	56,940	-18,140	19,660	-10,040	-5,575
10	-56,100	72,920	-36,530	36,960	-13,170	-8,024
11	-63,610	63,840	-31,290	31,350	-12,290	-6,851
12	-53,130	66,960	-20,620	18,890	-10,110	-5,598
13	-61,190	62,430	-35,200	33,010	-12,240	-6,846

Table 3.5-78 Rack Moments Mx, My & Mz - LC#6
GINNA 3D Whole Pool Model - With Perimeter Racks
Load Case #6 - Consolidated Fuel - SSE - Mu = 0.8

Rack Moments Mx, My & Mz (in-lbs) x 1E6

Rack	Min Mx	Max Mx	Min My	Max My	Min Mz	Max Mz
1	-15.390	15.930	-5.518	5.541	-0.516	0.701
2	-15.050	12.780	-6.292	5.465	-0.533	0.845
3	-12.430	11.700	-3.967	3.993	-0.250	0.208
4	-11.420	10.850	-4.713	3.987	-0.248	0.217
5	-10.490	10.770	-5.261	4.634	-0.144	0.123
6	-12.310	12.160	-5.664	4.884	-0.179	0.149
7	-4.070	3.288	-6.997	8.054	-0.215	0.246
8	-5.555	4.608	-9.052	7.925	-0.323	0.395
9	-1.646	1.553	-5.132	5.212	-0.285	0.212
10	-2.882	2.712	-6.343	6.517	-0.214	0.241
11	-2.305	2.565	-6.481	7.035	-0.232	0.227
12	-1.408	1.504	-5.596	6.085	-0.197	0.209
13	-2.387	2.648	-5.881	6.491	-0.233	0.197



Table 3.5-79 Rack Forces Fx, Fy & Fz - LC#7
GINNA 3D Whole Pool Model - With Perimeter Racks
Load Case #7 - Unconsolidated Fuel - SSE - Mu = 0.2

Rack Forces Fx, Fy & Fz (lbs)

Rack	Min Fx	Max Fx	Min Fy	Max Fy	Min Fz	Max Fz
1	-59,090	55,910	-70,350	75,780	-24,700	-14,790
2	-48,380	46,530	-67,240	72,950	-24,700	-14,880
3	-43,220	39,650	-61,890	74,530	-24,700	-14,430
4	-41,430	53,070	-69,170	68,820	-24,700	-14,430
5	-38,700	44,670	-73,460	71,530	-24,700	-14,430
6	-46,190	43,210	-82,560	96,500	-24,780	-14,430
7	-40,620	38,760	-25,540	24,890	-11,260	-7,219
8	-39,420	46,990	-42,170	40,080	-12,770	-7,940
9	-28,900	29,180	-19,840	12,640	-9,851	-5,949
10	-34,250	37,820	-29,830	24,800	-12,960	-8,340
11	-34,050	35,070	-25,470	19,900	-11,700	-7,545
12	-27,760	29,200	-16,670	11,610	-9,956	-5,840
13	-31,360	31,690	-25,500	25,950	-11,590	-7,417

Table 3.5-80 Rack Moments Mx, My & Mz - LC#7
GINNA 3D Whole Pool Model - With Perimeter Racks
Load Case #7 - Unconsolidated Fuel - SSE - Mu = 0.2

Rack Moments Mx, My & Mz (in-lbs) x 1E6

Rack	Min Mx	Max Mx	Min My	Max My	Min Mz	Max Mz
1	-9.349	8.796	-4.441	4.246	-0.221	0.278
2	-9.193	8.662	-4.681	4.140	-0.262	0.273
3	-7.675	7.100	-4.205	3.691	-0.185	0.181
4	-7.884	6.818	-3.670	3.461	-0.276	0.308
5	-8.760	7.679	-3.272	3.114	-0.231	0.304
6	-9.640	9.303	-3.292	3.066	-0.319	0.407
7	-2.710	2.441	-4.906	4.767	-0.125	0.171
8	-4.177	4.001	-4.897	5.319	-0.132	0.187
9	-1.220	1.164	-3.468	3.364	-0.105	0.122
10	-2.426	2.240	-3.856	3.779	-0.108	0.108
11	-2.026	2.161	-4.191	4.385	-0.103	0.134
12	-1.055	1.006	-3.488	3.507	-0.074	0.083
13	-2.354	2.132	-3.620	4.100	-0.094	0.090

[illegible]

100

Table 3.5-81 Rack Forces Fx, Fy & Fz - LC#8
GINNA 3D Whole Pool Model - With Perimeter Racks
Load Case #8 - Consolidated Fuel - OBE - Mu = 0.8

Rack Forces Fx, Fy & Fz (lbs)

Rack	Min Fx	Max Fx	Min Fy	Max Fy	Min Fz	Max Fz
1	-46,380	42,380	-85,620	99,540	-20,850	-15,980
2	-38,460	37,830	-74,010	88,260	-20,850	-15,980
3	-30,360	34,950	-56,530	56,640	-20,850	-15,980
4	-31,580	33,650	-52,960	53,880	-20,850	-15,980
5	-33,460	29,110	-73,110	56,470	-20,850	-15,980
6	-32,590	27,990	-79,430	61,010	-20,850	-15,980
7	-39,830	30,610	-28,490	23,870	-10,030	-8,295
8	-39,420	34,930	-37,940	32,400	-11,270	-9,219
9	-39,680	31,630	-12,420	10,900	-8,178	-6,987
10	-30,590	25,110	-21,120	21,760	-11,600	-9,608
11	-51,930	42,770	-20,820	17,420	-10,360	-8,628
12	-41,410	40,770	-13,350	10,070	-8,363	-6,845
13	-36,700	30,680	-20,950	20,830	-10,330	-8,692

Table 3.5-82 Rack Moments Mx, My & Mz - LC#8
GINNA 3D Whole Pool Model - With Perimeter Racks
Load Case #8 - Consolidated Fuel - OBE - Mu = 0.8

Rack Moments Mx, My & Mz (in-lbs) x 1E6

Rack	Min Mx	Max Mx	Min My	Max My	Min Mz	Max Mz
1	-10.640	10.160	-3.968	3.628	-0.000	0.000
2	-9.256	8.347	-3.412	2.817	-0.000	0.000
3	-5.797	5.391	-2.581	2.199	-0.000	0.000
4	-5.071	5.030	-2.299	2.043	-0.000	0.000
5	-5.902	6.957	-2.596	1.876	-0.000	0.000
6	-6.334	7.592	-2.647	1.992	-0.000	0.000
7	-2.145	2.129	-4.378	3.184	-0.000	0.000
8	-2.828	3.605	-4.575	3.933	-0.003	0.004
9	-1.000	0.994	-4.348	3.959	-0.061	0.063
10	-1.602	2.066	-3.283	2.888	-0.000	0.000
11	-1.314	2.093	-5.220	5.494	-0.093	0.083
12	-0.888	0.922	-4.740	4.811	-0.100	0.102
13	-1.584	2.150	-4.199	4.197	-0.081	0.054

Table 3.5-83 Rack Forces Fx, Fy & Fz - LC#9
GINNA 3D Whole Pool Model - With Perimeter Racks
Load Case #9 - Unconsolidated Fuel - OBE - Mu = 0.2

Rack Forces Fx, Fy & Fz (lbs)

Rack	Min Fx	Max Fx	Min Fy	Max Fy	Min Fz	Max Fz
1	-38,300	33,270	-67,440	63,890	-21,210	-17,510
2	-31,830	28,850	-62,750	58,130	-21,210	-17,510
3	-28,990	30,150	-51,200	51,070	-21,210	-17,510
4	-31,420	30,130	-52,740	53,580	-21,210	-17,510
5	-33,230	25,920	-60,110	61,870	-21,210	-17,510
6	-27,350	26,080	-51,230	52,200	-21,210	-17,510
7	-37,940	30,520	-19,910	19,400	-9,922	-8,542
8	-38,580	32,790	-24,210	22,590	-11,030	-9,418
9	-25,390	27,430	-10,250	9,799	-8,312	-6,978
10	-30,010	27,280	-12,680	15,040	-11,420	-9,830
11	-29,570	30,460	-14,600	11,950	-10,300	-8,733
12	-21,520	21,650	-9,840	8,599	-8,321	-6,895
13	-24,810	25,070	-15,740	14,310	-10,290	-8,832

Table 3.5-84 Rack Moments Mx, My & Mz - LC#9
GINNA 3D Whole Pool Model - With Perimeter Racks
Load Case #9 - Unconsolidated Fuel - OBE - Mu = 0.2

Rack Moments Mx, My & Mz (in-lbs) x 1E6

Rack	Min Mx	Max Mx	Min My	Max My	Min Mz	Max Mz
1	-8.108	8.336	-2.595	2.956	-0.185	0.185
2	-7.581	7.526	-2.804	2.557	-0.128	0.198
3	-4.687	5.683	-2.539	2.455	-0.167	0.190
4	-4.809	5.491	-2.068	2.085	-0.087	0.085
5	-4.988	5.074	-2.342	2.201	-0.066	0.050
6	-5.782	5.553	-2.086	2.102	-0.078	0.088
7	-1.783	1.765	-3.404	3.391	-0.072	0.059
8	-2.363	2.289	-3.956	3.940	-0.078	0.094
9	-0.875	0.783	-2.935	3.121	-0.054	0.042
10	-1.327	1.469	-3.231	2.359	-0.062	0.058
11	-1.242	1.176	-3.527	3.677	-0.054	0.050
12	-0.674	0.703	-2.988	2.966	-0.032	0.032
13	-1.198	1.390	-2.838	2.692	-0.051	0.063



Table 3.5-85 Rack Forces Fx, Fy & Fz - LC#10
GINNA 3D Whole Pool Model - Without Perimeter Racks
Load Case #10 - Unconsolidated Fuel - OBE - Mu = 0.2

Rack Forces Fx, Fy & Fz (lbs)

Rack	Min Fx	Max Fx	Min Fy	Max Fy	Min Fz	Max Fz
1	-34,740	37,840	-56,520	54,270	-19,950	-16,470
2	-30,270	34,120	-59,450	63,300	-19,950	-16,470
3	-34,310	29,990	-48,080	54,760	-19,950	-16,470
4	-29,010	34,490	-51,390	47,610	-19,950	-16,470
5	-27,410	31,400	-58,770	58,870	-19,950	-16,470
6	-39,260	29,050	-50,920	52,150	-19,950	-16,470
7	-32,790	32,780	-17,130	17,400	-9,922	-8,542
8	-32,820	36,590	-27,360	24,230	-11,030	-9,418
9	-25,420	27,080	-9,398	9,521	-8,316	-7,041
10	-25,500	26,770	-16,720	15,820	-11,360	-9,830
11	-29,520	24,890	-13,850	14,260	-10,200	-8,896
12	-24,000	24,940	-10,900	8,519	-8,211	-7,018
13	-23,010	21,090	-14,930	17,800	-10,370	-8,844

Table 3.5-86 Rack Moments Mx, My & Mz - LC#10
GINNA 3D Whole Pool Model - Without Perimeter Racks
Load Case #10 - Unconsolidated Fuel - OBE - Mu = 0.2

Rack Moments Mx, My & Mz (in-lbs) x 1E6

Rack	Min Mx	Max Mx	Min My	Max My	Min Mz	Max Mz
1	-6.622	7.304	-3.373	3.973	-0.155	0.188
2	-6.944	7.149	-2.751	3.710	-0.117	0.093
3	-5.023	5.296	-2.292	2.587	-0.121	0.106
4	-4.659	5.205	-2.365	2.543	-0.112	0.132
5	-5.158	4.490	-2.328	2.257	-0.092	0.098
6	-4.850	5.218	-2.557	2.510	-0.063	0.055
7	-1.831	1.764	-4.039	3.705	-0.080	0.093
8	-2.428	2.586	-4.076	3.572	-0.080	0.083
9	-0.890	0.989	-3.006	3.101	-0.062	0.043
10	-1.387	1.481	-2.990	2.947	-0.050	0.049
11	-1.254	1.105	-3.584	3.252	-0.047	0.054
12	-0.709	0.722	-3.016	2.970	-0.044	0.038
13	-1.364	1.468	-2.631	2.486	-0.061	0.061

Table 3.5-87 Rack Forces Fx, Fy & Fz - LC#11
GINNA 3D Whole Pool Model - With Perimeter Racks
Load Case #11 - Mixed Fuel - SSE - Mu = Mixed

Rack Forces Fx, Fy & Fz (lbs)

Rack	Min Fx	Max Fx	Min Fy	Max Fy	Min Fz	Max Fz
1	-31,020	26,090	-70,390	46,510	-24,290	-15,070
2	-32,360	26,290	-61,450	47,210	-23,730	-15,370
3	-27,940	25,100	-55,930	55,930	-24,100	-15,410
4	-31,290	42,990	-68,710	61,970	-24,700	-14,440
5	-34,340	33,510	-59,820	74,510	-25,370	-14,390
6	-58,400	62,020	-81,720	98,510	-25,800	-13,160
7	-39,090	40,390	-27,180	23,810	-11,240	-7,180
8	-15,480	15,380	-17,430	22,320	-13,490	-7,898
9	-53,780	55,230	-14,180	16,250	-9,322	-6,032
10	-10,960	12,070	-12,090	13,520	-12,710	-8,540
11	-41,190	39,650	-18,910	20,720	-11,640	-7,394
12	-33,950	33,810	-12,700	15,990	-9,940	-5,738
13	-42,590	35,970	-22,810	22,310	-11,870	-7,756

Table 3.5-88 Rack Moments Mx, My & Mz - LC#11
GINNA 3D Whole Pool Model - With Perimeter Racks
Load Case #11 - Mixed Fuel - SSE - Mu = Mixed

Rack Moments Mx, My & Mz (in-lbs) x 1E6

Rack	Min Mx	Max Mx	Min My	Max My	Min Mz	Max Mz
1	-5.815	8.222	-2.948	2.718	-0.261	0.225
2	-5.501	7.580	-3.246	2.965	-0.248	0.198
3	-5.239	6.477	-2.098	1.894	-0.234	0.207
4	-6.993	7.257	-3.501	3.912	-0.094	0.074
5	-7.137	5.715	-2.399	2.777	-0.172	0.149
6	-9.980	8.469	-3.812	5.311	-0.235	0.285
7	-1.943	1.797	-3.506	4.205	-0.108	0.120
8	-0.734	0.704	-0.912	0.896	-0.102	0.118
9	-1.500	1.075	-5.366	6.015	-0.106	0.133
10	-0.585	0.514	-0.805	0.878	-0.039	0.048
11	-2.133	2.302	-4.109	4.356	-0.127	0.117
12	-0.997	1.094	-3.601	3.380	-0.088	0.092
13	-2.123	2.220	-3.954	4.322	-0.142	0.168



Table 3.5-89 Rack Forces Fx, Fy & Fz - LC#12
GINNA 3D Whole Pool Model - With Perimeter Racks
Load Case #12 - Mixed Fuel - OBE - Mu = Mixed

Rack Forces Fx, Fy & Fz (lbs)

Rack	Min Fx	Max Fx	Min Fy	Max Fy	Min Fz	Max Fz
1	-18,950	16,980	-40,320	45,930	-21,470	-17,750
2	-11,140	8,009	-15,440	14,010	-21,580	-17,860
3	-23,560	27,670	-38,210	41,050	-21,230	-17,520
4	-11,610	11,260	-17,270	18,840	-21,110	-18,360
5	-17,680	15,950	-32,500	34,200	-20,970	-18,100
6	-15,970	16,230	-37,820	34,780	-20,920	-18,110
7	-9,893	9,514	-6,669	6,994	-10,390	-8,539
8	-37,740	31,640	-22,830	20,060	-11,030	-9,418
9	-27,570	27,010	-8,257	9,215	-8,351	-6,886
10	-10,460	9,993	-8,776	8,304	-12,190	-9,684
11	-39,560	45,870	-13,820	13,750	-10,250	-8,628
12	-21,370	28,870	-7,209	7,718	-8,485	-6,851
13	-32,750	32,160	-20,110	15,010	-10,330	-8,691

Table 3.5-90 Rack Moments Mx, My & Mz - LC#12
GINNA 3D Whole Pool Model - With Perimeter Racks
Load Case #12 - Mixed Fuel - OBE - Mu = Mixed

Rack Moments Mx, My & Mz (in-lbs) x 1E6

Rack	Min Mx	Max Mx	Min My	Max My	Min Mz	Max Mz
1	-5.514	4.377	-1.124	1.190	-0.075	0.083
2	-1.665	1.678	-0.722	0.571	-0.034	0.029
3	-3.134	3.443	-1.472	1.220	-0.000	0.000
4	-1.722	1.654	-0.638	0.727	-0.031	0.037
5	-3.105	3.358	-1.257	1.356	-0.055	0.058
6	-3.231	4.070	-1.436	1.386	-0.052	0.059
7	-0.474	0.475	-0.647	0.653	-0.025	0.029
8	-1.809	1.985	-3.784	3.626	-0.040	0.034
9	-0.699	0.634	-3.083	3.175	-0.057	0.060
10	-0.467	0.477	-0.728	0.738	-0.040	0.033
11	-0.945	1.398	-4.905	5.392	-0.039	0.033
12	-0.496	0.686	-2.126	3.109	-0.049	0.062
13	-1.334	1.729	-3.454	3.780	-0.027	0.031

3.5.3.1.8.2 Final Rack Displacements for Each Load Case

Table 3.5-91 Final Rack Relative East-West Disp. - LC#1
GINNA 3D Whole Pool Model - Without Perimeter Racks
Load Case #1 - Unconsolidated Fuel - SSE - Mu = 0.8

Final Relative Horizontal X Disp. (E-W) for all racks:

Rack/Rack	Gap Status	Absolute Magnitude (in)
WW/1	Opening	0.02417
WW/2	Closing	0.02180
1/3	Closing	0.03667
2/4	Opening	0.00913
3/5	Closing	0.00336
4/6	Closing	0.00552
5/7	Opening	0.00267
5/8	Closing	0.00811
6/8	Closing	0.00578
6/9	Opening	0.03545
6/10	Opening	0.01840
8/11	Closing	0.00052
9/12	Closing	0.02312
10/13	Opening	0.01870
11/EW	Opening	0.02449
12/EW	Opening	0.00585
13/EW	Closing	0.01891

Table 3.5-92 Final Rack Relative North-South Disp. - LC#1
GINNA 3D Whole Pool Model - Without Perimeter Racks
Load Case #1 - Unconsolidated Fuel - SSE - Mu = 0.8

Final Relative Horizontal Y Disp. (N-S) for all racks:

Rack/Rack	Gap Status	Absolute Magnitude (in)
SW/1	Opening	0.01273
1/2	Opening	0.01073
2/NW	Closing	0.02345
SW/3	Closing	0.02392
3/4	Opening	0.00086
4/NW	Opening	0.02306
SW/5	Opening	0.00173
5/6	Closing	0.01910
6/NW	Opening	0.01737
SW/7	Closing	0.09708
7/8	Closing	0.02245
8/9	Opening	0.00235
9/10	Opening	0.04914
10/NW	Opening	0.06804
SW/11	Closing	0.14916
11/12	Opening	0.01488
12/13	Opening	0.02572
13/NW	Opening	0.10856

Table 3.5-93 Final Rack Relative East-West Disp. - LC#2
GINNA 3D Whole Pool Model - Without Perimeter Racks
Load Case #2 - Unconsolidated Fuel - SSE - Mu = 0.2

Final Relative Horizontal X Disp. (E-W) for all racks:

Rack/Rack	Gap Status	Absolute Magnitude (in)
WW/1	Closing	0.00763
WW/2	Opening	0.03430
1/3	Closing	0.00725
2/4	Closing	0.00208
3/5	Closing	0.01017
4/6	Closing	0.01164
5/7	Closing	0.19546
5/8	Closing	0.14137
6/8	Closing	0.18699
6/9	Closing	0.20772
6/10	Opening	0.05527
8/11	Closing	0.13015
9/12	Closing	0.03844
10/13	Closing	0.06719
11/EW	Opening	0.29656
12/EW	Opening	0.22558
13/EW	Closing	0.00865

Table 3.5-94 Final Rack Relative North-South Disp. - LC#2
GINNA 3D Whole Pool Model - Without Perimeter Racks
Load Case #2 - Unconsolidated Fuel - SSE - Mu = 0.2

Final Relative Horizontal Y Disp. (N-S) for all racks:

Rack/Rack	Gap Status	Absolute Magnitude (in)
SW/1	Closing	0.14172
1/2	Opening	0.05469
2/NW	Opening	0.08703
SW/3	Closing	0.15461
3/4	Closing	0.00441
4/NW	Opening	0.15902
SW/5	Closing	0.16020
5/6	Opening	0.01021
6/NW	Opening	0.14999
SW/7	Closing	0.21596
7/8	Closing	0.00728
8/9	Opening	0.04089
9/10	Opening	0.01931
10/NW	Opening	0.16304
SW/11	Closing	0.14911
11/12	Opening	0.07554
12/13	Closing	0.11141
13/NW	Opening	0.18498

Table 3.5-95 Final Rack Relative East-West Disp. - LC#3
GINNA 3D Whole Pool Model - Without Perimeter Racks
Load Case #3 - Consolidated Fuel - SSE - Mu = 0.8

Final Relative Horizontal X Disp. (E-W) for all racks:

Rack/Rack	Gap Status	Absolute Magnitude (in)
WW/1	Opening	0.05460
WW/2	Opening	0.00068
1/3	Closing	0.04984
2/4	Opening	0.00263
3/5	Closing	0.00095
4/6	Opening	0.00092
5/7	Closing	0.01745
5/8	Closing	0.00725
6/8	Closing	0.00766
6/9	Closing	0.03309
6/10	Closing	0.01143
8/11	Closing	0.03167
9/12	Opening	0.02419
10/13	Opening	0.02216
11/EW	Opening	0.03511
12/EW	Opening	0.00469
13/EW	Closing	0.01494

Table 3.5-96 Final Rack Relative North-South Disp. - LC#3
GINNA 3D Whole Pool Model - Without Perimeter Racks
Load Case #3 - Consolidated Fuel - SSE - Mu = 0.8

Final Relative Horizontal Y Disp. (N-S) for all racks:

Rack/Rack	Gap Status	Absolute Magnitude
SW/1	Closing	0.00154
1/2	Opening	0.01310
2/NW	Closing	0.01156
SW/3	Closing	0.00911
3/4	Opening	0.00329
4/NW	Opening	0.00582
SW/5	Closing	0.00878
5/6	Opening	0.01283
6/NW	Closing	0.00405
SW/7	Closing	0.00593
7/8	Closing	0.02483
8/9	Closing	0.02980
9/10	Opening	0.05161
10/NW	Opening	0.00894
SW/11	Closing	0.06063
11/12	Opening	0.04096
12/13	Closing	0.03245
13/NW	Opening	0.05212



Table 3.5-97 Final Rack Relative East-West Disp. - LC#4
GINNA 3D Whole Pool Model - Without Perimeter Racks
Load Case #4 - Unconsolidated Fuel - SSE - Mu = 0.5

Final Relative Horizontal X Disp. (E-W) for all racks:

Rack/Rack	Gap Status	Absolute Magnitude (in)
WW/1	Closing	0.00009
WW/2	Closing	0.00831
1/3	Opening	0.00309
2/4	Opening	0.01036
3/5	Closing	0.01917
4/6	Closing	0.00719
5/7	Opening	0.00068
5/8	Opening	0.03986
6/8	Opening	0.02883
6/9	Opening	0.04392
6/10	Opening	0.00794
8/11	Closing	0.03125
9/12	Closing	0.04378
10/13	Opening	0.09056
11/EW	Opening	0.00755
12/EW	Opening	0.00499
13/EW	Closing	0.09336

Table 3.5-98 Final Rack Relative North-South Disp. - LC#4
GINNA 3D Whole Pool Model - Without Perimeter Racks
Load Case #4 - Unconsolidated Fuel - SSE - Mu = 0.5

Final Relative Horizontal Y Disp. (N-S) for all racks:

Rack/Rack	Gap Status	Absolute Magnitude (in)
SW/1	Closing	0.00123
1/2	Opening	0.02532
2/NW	Closing	0.02409
SW/3	Closing	0.02282
3/4	Opening	0.00394
4/NW	Opening	0.01888
SW/5	Closing	0.00477
5/6	Closing	0.01137
6/NW	Opening	0.01614
SW/7	Closing	0.05839
7/8	Closing	0.02307
8/9	Opening	0.02080
9/10	Closing	0.03080
10/NW	Opening	0.09145
SW/11	Closing	0.08363
11/12	Closing	0.01634
12/13	Opening	0.05166
13/NW	Opening	0.04832

Table 3.5-99 Final Rack Relative East-West Disp. - LC#5
GINNA 3D Whole Pool Model - With Perimeter Racks
Load Case #5 - Unconsolidated Fuel - SSE - Mu = 0.8

Final Relative Horizontal X Disp. (E-W) for all racks:

Rack/Rack	Gap Status	Absolute Magnitude(in)
WW/1	Opening	0.03092
WW/2	Opening	0.00170
1/3	Closing	0.03663
2/4	Closing	0.00422
3/5	Opening	0.01847
4/6	Opening	0.03023
5/7	Opening	0.01569
5/8	Opening	0.01356
6/8	Closing	0.00138
6/9	Closing	0.02269
6/10	Closing	0.02717
8/11	Opening	0.02142
9/12	Opening	0.04883
10/13	Opening	0.05146
11/EW	Closing	0.04775
12/EW	Closing	0.05385
13/EW	Closing	0.05200

Table 3.5-100 Final Rack Relative North-South Disp. - LC#5
GINNA 3D Whole Pool Model - With Perimeter Racks
Load Case #5 - Unconsolidated Fuel - SSE - Mu = 0.8

Final Relative Horizontal Y Disp. (N-S) for all racks:

Rack/Rack	Gap Status	Absolute Magnitude(in)
SW/1	Opening	0.05042
1/2	Closing	0.01951
2/NW	Closing	0.03091
SW/3	Opening	0.00662
3/4	Closing	0.00933
4/NW	Opening	0.00271
SW/5	Closing	0.00474
5/6	Closing	0.00104
6/NW	Opening	0.00577
SW/7	Closing	0.05207
7/8	Closing	0.00228
8/9	Closing	0.04859
9/10	Opening	0.03773
10/NW	Opening	0.06522
SW/11	Closing	0.05260
11/12	Closing	0.01983
12/13	Opening	0.01740
13/NW	Opening	0.05503

Table 3.5-101 Final Rack Relative East-West Disp. - LC#6
GINNA 3D Whole Pool Model - With Perimeter Racks
Load Case #6 - Consolidated Fuel - SSE - Mu = 0.8

Final Relative Horizontal X Disp. (E-W) for all racks:

Rack/Rack	Gap Status	Absolute Magnitude (in)
WW/1	Opening	0.00454
WW/2	Opening	0.00660
1/3	Opening	0.00229
2/4	Closing	0.00002
3/5	Closing	0.00276
4/6	Closing	0.00357
5/7	Closing	0.00037
5/8	Opening	0.01589
6/8	Opening	0.01696
6/9	Closing	0.00648
6/10	Opening	0.00103
8/11	Closing	0.05180
9/12	Opening	0.00467
10/13	Opening	0.02688
11/EW	Opening	0.03183
12/EW	Closing	0.00120
13/EW	Closing	0.03092

Table 3.5-102 Final Rack Relative North-South Disp. - LC#6
GINNA 3D Whole Pool Model - With Perimeter Racks
Load Case #6 - Consolidated Fuel - SSE - Mu = 0.8

Final Relative Horizontal Y Disp. (N-S) for all racks:

Rack/Rack	Gap Status	Absolute Magnitude (in)
SW/1	Opening	0.05979
1/2	Closing	0.02341
2/NW	Closing	0.03639
SW/3	Closing	0.00631
3/4	Closing	0.00124
4/NW	Opening	0.00755
SW/5	Closing	0.01072
5/6	Opening	0.00798
6/NW	Opening	0.00274
SW/7	Closing	0.01255
7/8	Closing	0.02777
8/9	Closing	0.00780
9/10	Opening	0.02677
10/NW	Opening	0.02135
SW/11	Closing	0.04537
11/12	Opening	0.01638
12/13	Closing	0.02028
13/NW	Opening	0.04927

Table 3.5-103 Final Rack Relative East-West Disp. - LC#7
GINNA 3D Whole Pool Model - With Perimeter Racks
Load Case #7 - Unconsolidated Fuel - SSE - Mu = 0.2

Final Relative Horizontal X Disp. (E-W) for all racks:

Rack/Rack	Gap Status	Absolute Magnitude(in)
WW/1	Opening	0.00423
WW/2	Opening	0.04590
1/3	Opening	0.00530
2/4	Closing	0.04230
3/5	Opening	0.01537
4/6	Closing	0.00441
5/7	Opening	0.03429
5/8	Opening	0.03364
6/8	Opening	0.05936
6/9	Opening	0.00890
6/10	Opening	0.05444
8/11	Closing	0.21570
9/12	Closing	0.27550
10/13	Closing	0.03807
11/EW	Opening	0.15716
12/EW	Opening	0.26742
13/EW	Closing	0.01555

Table 3.5-104 Final Rack Relative North-South Disp. - LC#7
GINNA 3D Whole Pool Model - With Perimeter Racks
Load Case #7 - Unconsolidated Fuel - SSE - Mu = 0.2

Final Relative Horizontal Y Disp. (N-S) for all racks:

Rack/Rack	Gap Status	Absolute Magnitude(in)
SW/1	Closing	0.05938
1/2	Opening	0.02715
2/NW	Opening	0.03223
SW/3	Closing	0.04946
3/4	Closing	0.03572
4/NW	Opening	0.08518
SW/5	Closing	0.10125
5/6	Closing	0.06297
6/NW	Opening	0.16422
SW/7	Closing	0.20051
7/8	Closing	0.01969
8/9	Opening	0.02984
9/10	Opening	0.04274
10/NW	Opening	0.14762
SW/11	Closing	0.18976
11/12	Opening	0.04303
12/13	Closing	0.03887
13/NW	Opening	0.18560



Table 3.5-105 Final Rack Relative East-West Disp. - LC#8
GINNA 3D Whole Pool Model - With Perimeter Racks
Load Case #8 - Consolidated Fuel - OBE - Mu = 0.8

Final Relative Horizontal X Disp. (E-W) for all racks:

Rack/Rack	Gap Status	Absolute Magnitude (in)
WW/1	Closing	0.00249
WW/2	Closing	0.00309
1/3	Closing	0.00010
2/4	Opening	0.00014
3/5	Opening	0.00041
4/6	Opening	0.00022
5/7	Opening	0.00038
5/8	Opening	0.00062
6/8	Opening	0.00116
6/9	Closing	0.00595
6/10	Opening	0.00029
8/11	Opening	0.00085
9/12	Opening	0.00921
10/13	Closing	0.00965
11/EW	Opening	0.00071
12/EW	Closing	0.00054
13/EW	Opening	0.01209

Table 3.5-106 Final Rack Relative North-South Disp. - LC#8
GINNA 3D Whole Pool Model - With Perimeter Racks
Load Case #8 - Consolidated Fuel - OBE - Mu = 0.8

Final Relative Horizontal Y Disp. (N-S) for all racks:

Rack/Rack	Gap Status	Absolute Magnitude (in)
SW/1	Opening	0.00378
1/2	Closing	0.00074
2/NW	Closing	0.00304
SW/3	Closing	0.00012
3/4	Opening	0.00016
4/NW	Closing	0.00004
SW/5	Closing	0.00459
5/6	Closing	0.00071
6/NW	Opening	0.00530
SW/7	Closing	0.00452
7/8	Closing	0.00176
8/9	Opening	0.00041
9/10	Opening	0.00196
10/NW	Opening	0.00391
SW/11	Closing	0.00873
11/12	Closing	0.01088
12/13	Opening	0.01158
13/NW	Opening	0.00803



Table 3.5-107 Final Rack Relative East-West Disp. - LC#9
GINNA 3D Whole Pool Model - With Perimeter Racks
Load Case #9 - Unconsolidated Fuel - OBE - Mu = 0.2

Final Relative Horizontal X Disp. (E-W) for all racks:

Rack/Rack	Gap Status	Absolute Magnitude (in)
WW/1	Closing	0.01606
WW/2	Opening	0.00568
1/3	Opening	0.00633
2/4	Closing	0.00792
3/5	Opening	0.01220
4/6	Opening	0.01036
5/7	Opening	0.02389
5/8	Closing	0.01108
6/8	Closing	0.01672
6/9	Closing	0.02163
6/10	Closing	0.01534
8/11	Opening	0.04194
9/12	Opening	0.00088
10/13	Closing	0.09881
11/EW	Closing	0.03334
12/EW	Opening	0.01264
13/EW	Opening	0.10603

Table 3.5-108 Final Rack Relative North-South Disp. - LC#9
GINNA 3D Whole Pool Model - With Perimeter Racks
Load Case #9 - Unconsolidated Fuel - OBE - Mu = 0.2

Final Relative Horizontal Y Disp. (N-S) for all racks:

Rack/Rack	Gap Status	Absolute Magnitude (in)
SW/1	Closing	0.01179
1/2	Opening	0.05142
2/NW	Closing	0.03963
SW/3	Closing	0.01680
3/4	Opening	0.00275
4/NW	Opening	0.01405
SW/5	Opening	0.00012
5/6	Closing	0.02273
6/NW	Opening	0.02260
SW/7	Opening	0.00018
7/8	Closing	0.01966
8/9	Opening	0.03419
9/10	Closing	0.00781
10/NW	Closing	0.00691
SW/11	Closing	0.03325
11/12	Opening	0.03952
12/13	Closing	0.01329
13/NW	Opening	0.00702

Table 3.5-109 Final Rack Relative East-West Disp. - LC#10
GINNA 3D Whole Pool Model - Without Perimeter Racks
Load Case #10 - Unconsolidated Fuel - OBE - Mu = 0.2

Final Relative Horizontal X Disp. (E-W) for all racks:

Rack/Rack	Gap Status	Absolute Magnitude (in)
WW/1	Closing	0.01643
WW/2	Opening	0.02205
1/3	Opening	0.01620
2/4	Closing	0.01630
3/5	Opening	0.00108
4/6	Closing	0.00608
5/7	Opening	0.00685
5/8	Opening	0.01479
6/8	Opening	0.01596
6/9	Closing	0.01317
6/10	Closing	0.04331
8/11	Opening	0.06224
9/12	Closing	0.03278
10/13	Closing	0.08206
11/EW	Closing	0.07787
12/EW	Opening	0.04628
13/EW	Opening	0.12570

Table 3.5-110 Final Rack Relative North-South Disp. - LC#10
GINNA 3D Whole Pool Model - Without Perimeter Racks
Load Case #10 - Unconsolidated Fuel - OBE - Mu = 0.2

Final Relative Horizontal Y Disp. (N-S) for all racks:

Rack/Rack	Gap Status	Absolute Magnitude (in)
SW/1	Closing	0.06940
1/2	Opening	0.01541
2/NW	Opening	0.05399
SW/3	Closing	0.01715
3/4	Opening	0.00815
4/NW	Opening	0.00900
SW/5	Closing	0.02408
5/6	Opening	0.03233
6/NW	Closing	0.00825
SW/7	Closing	0.01177
7/8	Closing	0.00704
8/9	Opening	0.02116
9/10	Closing	0.00155
10/NW	Closing	0.00081
SW/11	Closing	0.02675
11/12	Opening	0.02555
12/13	Closing	0.01133
13/NW	Opening	0.01253

Table 3.5-111 Final Rack Relative East-West Disp. - LC#11
GINNA 3D Whole Pool Model - With Perimeter Racks
Load Case #11 - Mixed Fuel - SSE - Mu = Mixed

Final Relative Horizontal X Disp. (E-W) for all racks:

Rack/Rack	Gap Status	Absolute Magnitude (in)
WW/1	Opening	0.04614
WW/2	Opening	0.02864
1/3	Closing	0.07518
2/4	Closing	0.02314
3/5	Opening	0.03575
4/6	Opening	0.00171
5/7	Opening	0.02846
5/8	Closing	0.07895
6/8	Closing	0.07944
6/9	Opening	0.00281
6/10	Opening	0.02302
8/11	Opening	0.03253
9/12	Closing	0.06976
10/13	Closing	0.02095
11/EW	Opening	0.03970
12/EW	Opening	0.05973
13/EW	Closing	0.00929

Table 3.5-112 Final Rack Relative North-South Disp. - LC#11
GINNA 3D Whole Pool Model - With Perimeter Racks
Load Case #11 - Mixed Fuel - SSE - Mu = Mixed

Final Relative Horizontal Y Disp. (N-S) for all racks:

Rack/Rack	Gap Status	Absolute Magnitude (in)
SW/1	Closing	0.13654
1/2	Opening	0.06351
2/NW	Opening	0.07303
SW/3	Closing	0.01286
3/4	Opening	0.00753
4/NW	Opening	0.00533
SW/5	Closing	0.00882
5/6	Closing	0.00848
6/NW	Opening	0.01730
SW/7	Opening	0.01509
7/8	Closing	0.07944
8/9	Closing	0.01851
9/10	Opening	0.03341
10/NW	Opening	0.04945
SW/11	Closing	0.05967
11/12	Opening	0.02935
12/13	Closing	0.03841
13/NW	Opening	0.06872

Table 3.5-113 Final Rack Relative East-West Disp. - LC#12
GINNA 3D Whole Pool Model - With Perimeter Racks
Load Case #12 - Mixed Fuel - OBE - Mu = Mixed

Final Relative Horizontal X Disp. (E-W) for all racks:

Rack/Rack	Gap Status	Absolute Magnitude (in)
WW/1	Closing	0.00699
WW/2	Closing	0.00033
1/3	Opening	0.00579
2/4	Opening	0.00591
3/5	Closing	0.00297
4/6	Closing	0.01073
5/7	Opening	0.06792
5/8	Opening	0.00485
6/8	Opening	0.00583
6/9	Closing	0.00394
6/10	Opening	0.01772
8/11	Closing	0.00802
9/12	Opening	0.02732
10/13	Closing	0.02090
11/EW	Opening	0.00734
12/EW	Closing	0.01823
13/EW	Opening	0.00833

Table 3.5-114 Final Rack Relative North-South Disp. - LC#12
GINNA 3D Whole Pool Model - With Perimeter Racks
Load Case #12 - Mixed Fuel - OBE - Mu = Mixed

Final Relative Horizontal Y Disp. (N-S) for all racks:

Rack/Rack	Gap Status	Absolute Magnitude (in)
SW/1	Opening	0.00002
1/2	Closing	0.04807
2/NW	Opening	0.04804
SW/3	Opening	0.00094
3/4	Closing	0.00468
4/NW	Opening	0.00375
SW/5	Opening	0.00257
5/6	Closing	0.00058
6/NW	Closing	0.00199
SW/7	Opening	0.01027
7/8	Closing	0.01390
8/9	Closing	0.01017
9/10	Closing	0.02591
10/NW	Opening	0.03971
SW/11	Closing	0.00624
11/12	Closing	0.05434
12/13	Opening	0.05529
13/NW	Opening	0.00530



3.5.3.1.8.3 Final Rack Rotations for Each Load Case

Table 3.5-115 Final Rack Rotations - LC#1

GINNA 3D Whole Pool Model - Without Perimeter Racks

Load Case #1 - Unconsolidated Fuel - SSE - $\mu = 0.8$

Final Rack Rotations ROTZ (About Vertical)

Rack	Radians	Degrees
1	-0.00187	-0.10722
2	-0.00084	-0.04802
3	0.00004	0.00232
4	-0.00012	-0.00668
5	0.00032	0.01806
6	0.00009	0.00521
7	0.00035	0.02006
8	0.00078	0.04464
9	0.00128	0.07348
10	0.00027	0.01554
11	-0.00059	-0.03353
12	0.00102	0.05866
13	0.00044	0.02527

Table 3.5-116 Final Rack Rotations - LC#2

GINNA 3D Whole Pool Model - Without Perimeter Racks

Load Case #2 - Unconsolidated Fuel - SSE - $\mu = 0.2$

Final Rack Rotations ROTZ (About Vertical)

Rack	Radians	Degrees
1	-0.00180	-0.10340
2	-0.00054	-0.03108
3	-0.00014	-0.00784
4	-0.00029	-0.01672
5	0.00070	0.04014
6	0.00014	0.00827
7	0.00020	0.01139
8	0.00257	0.14719
9	0.00104	0.05966
10	0.00171	0.09772
11	0.00241	0.13786
12	0.00218	0.12486
13	0.00337	0.19320



Table 3.5-117 Final Rack Rotations - LC#3
GINNA 3D Whole Pool Model - Without Perimeter Racks
Load Case #3 - Consolidated Fuel - SSE - $\mu = 0.8$

Final Rack Rotations ROTZ (About Vertical)

Rack	Radians	Degrees
1	-0.00035	-0.02001
2	0.00003	0.00150
3	-0.00007	-0.00393
4	-0.00003	-0.00168
5	-0.00001	-0.00055
6	0.00001	0.00068
7	0.00084	0.04831
8	0.00095	0.05425
9	0.00110	0.06330
10	0.00068	0.03875
11	0.00071	0.04072
12	0.00222	0.12708
13	0.00080	0.04609

Table 3.5-118 Final Rack Rotations - LC#4
GINNA 3D Whole Pool Model - Without Perimeter Racks
Load Case #4 - Unconsolidated Fuel - SSE - $\mu = 0.5$

Final Rack Rotations ROTZ (About Vertical)

Rack	Radians	Degrees
1	0.00009	0.00506
2	0.00010	0.00551
3	0.00012	0.00713
4	-0.00003	-0.00197
5	0.00008	0.00436
6	-0.00009	-0.00542
7	-0.00054	-0.03118
8	-0.00063	-0.03630
9	0.00022	0.01281
10	-0.00017	-0.00999
11	0.00186	0.10635
12	0.00208	0.11894
13	0.00192	0.10978



Table 3.5-119 Final Rack Rotations - LC#5
GINNA 3D Whole Pool Model - With Perimeter Racks
Load Case #5 - Unconsolidated Fuel - SSE - Mu = 0.8

Final Rack Rotations ROTZ (About Vertical)

Rack	Radians	Degrees
1	-0.00029	-0.01645
2	-0.00067	-0.03828
3	-0.00022	-0.01269
4	-0.00010	-0.00583
5	-0.00014	-0.00830
6	0.00004	0.00208
7	-0.00079	-0.04528
8	-0.00056	-0.03183
9	0.00033	0.01918
10	-0.00017	-0.00950
11	0.00029	0.01665
12	-0.00011	-0.00611
13	-0.00169	-0.09679

Table 3.5-120 Final Rack Rotations - LC#6
GINNA 3D Whole Pool Model - With Perimeter Racks
Load Case #6 - Consolidated Fuel - SSE - Mu = 0.8

Final Rack Rotations ROTZ (About Vertical)

Rack	Radians	Degrees
1	-0.00019	-0.01111
2	-0.00018	-0.01018
3	-0.00005	-0.00305
4	-0.00006	-0.00352
5	-0.00000	-0.00022
6	0.00000	0.00027
7	0.00024	0.01367
8	0.00083	0.04735
9	0.00031	0.01753
10	0.00031	0.01797
11	0.00103	0.05896
12	0.00077	0.04432
13	0.00077	0.04391

Table 3.5-121 Final Rack Rotations - LC#7
GINNA 3D Whole Pool Model - With Perimeter Racks
Load Case #7 - Unconsolidated Fuel - SSE - $\mu = 0.2$

Final Rack Rotations ROTZ (About Vertical)

Rack	Radians	Degrees
1	-0.00041	-0.02349
2	-0.00046	-0.02647
3	-0.00029	-0.01673
4	-0.00007	-0.00418
5	0.00043	0.02491
6	0.00034	0.01946
7	-0.00039	-0.02234
8	0.00058	0.03297
9	0.00095	0.05457
10	0.00078	0.04482
11	0.00238	0.13637
12	0.00250	0.14296
13	0.00183	0.10472

Table 3.5-122 Final Rack Rotations - LC#8
GINNA 3D Whole Pool Model - With Perimeter Racks
Load Case #8 - Consolidated Fuel - OBE - $\mu = 0.8$

Final Rack Rotations ROTZ (About Vertical)

Rack	Radians	Degrees
1	-0.00000	-0.00000
2	-0.00000	-0.00000
3	0.00000	0.00000
4	-0.00000	-0.00000
5	-0.00000	-0.00000
6	-0.00000	-0.00000
7	-0.00000	-0.00000
8	0.00000	0.00005
9	-0.00001	-0.00067
10	0.00000	0.00000
11	0.00022	0.01275
12	0.00035	0.01986
13	0.00004	0.00212



Table 3.5-123 Final Rack Rotations - LC#9
GINNA 3D Whole Pool Model - With Perimeter Racks
Load Case #9 - Unconsolidated Fuel - OBE - $\mu = 0.2$

Final Rack Rotations ROTZ (About Vertical)

Rack	Radians	Degrees
1	-0.00013	-0.00762
2	-0.00022	-0.01233
3	0.00005	0.00297
4	-0.00001	-0.00038
5	-0.00003	-0.00171
6	-0.00002	-0.00132
7	-0.00002	-0.00133
8	-0.00004	-0.00225
9	0.00047	0.02666
10	0.00005	0.00302
11	0.00038	0.02201
12	0.00074	0.04259
13	0.00010	0.00590

Table 3.5-124 Final Rack Rotations - LC#10
GINNA 3D Whole Pool Model - Without Perimeter Racks
Load Case #10 - Unconsolidated Fuel - OBE - $\mu = 0.2$

Final Rack Rotations ROTZ (About Vertical)

Rack	Radians	Degrees
1	0.00026	0.01470
2	-0.00017	-0.00991
3	-0.00008	-0.00477
4	-0.00004	-0.00228
5	-0.00002	-0.00122
6	-0.00001	-0.00051
7	0.00038	0.02198
8	-0.00006	-0.00364
9	0.00072	0.04113
10	0.00035	0.02029
11	0.00001	0.00041
12	0.00045	0.02575
13	-0.00019	-0.01066



Table 3.5-125 Final Rack Rotations - LC#11
GINNA 3D Whole Pool Model - With Perimeter Racks
Load Case #11 - Mixed Fuel - SSE - Mu = Mixed

Final Rack Rotations ROTZ (About Vertical)

Rack	Radians	Degrees
1	0.00090	0.05143
2	0.00057	0.03237
3	-0.00049	-0.02835
4	-0.00001	-0.00050
5	-0.00007	-0.00393
6	0.00006	0.00321
7	0.00091	0.05229
8	0.00048	0.02730
9	0.00079	0.04531
10	0.00090	0.05152
11	0.00003	0.00152
12	0.00024	0.01352
13	0.00040	0.02318

Table 3.5-126 Final Rack Rotations - LC#12
GINNA 3D Whole Pool Model - With Perimeter Racks
Load Case #12 - Mixed Fuel - OBE - Mu = Mixed

Final Rack Rotations ROTZ (About Vertical)

Rack	Radians	Degrees
1	-0.00001	-0.00040
2	0.00023	0.01331
3	0.00000	0.00000
4	-0.00020	-0.01164
5	-0.00000	-0.00009
6	-0.00002	-0.00136
7	-0.00057	-0.03250
8	-0.00002	-0.00097
9	0.00024	0.01360
10	-0.00067	-0.03824
11	-0.00003	-0.00168
12	-0.00147	-0.08435
13	0.00001	0.00044

3.5.3.1.8.4 Representative Plots

The following plots are representative of all the plots that were obtained for each load case.

Figure 3.5-43 Vertical Leg Force Fz, Rack 1, Leg 1 - LC#1

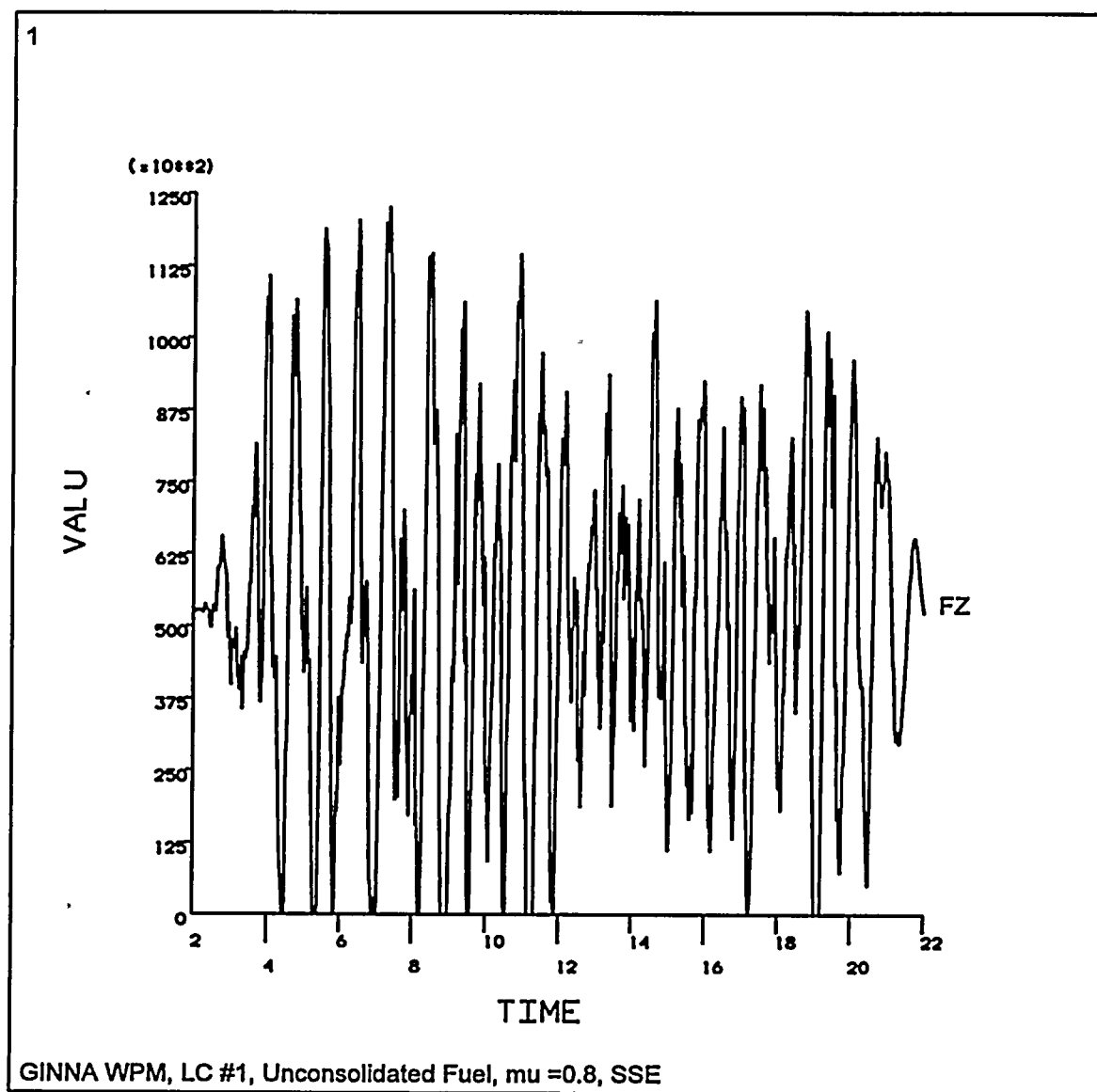


Figure 3.5-44 Sum of Vert. Leg Forces Fz, Rack 1 - LC#1

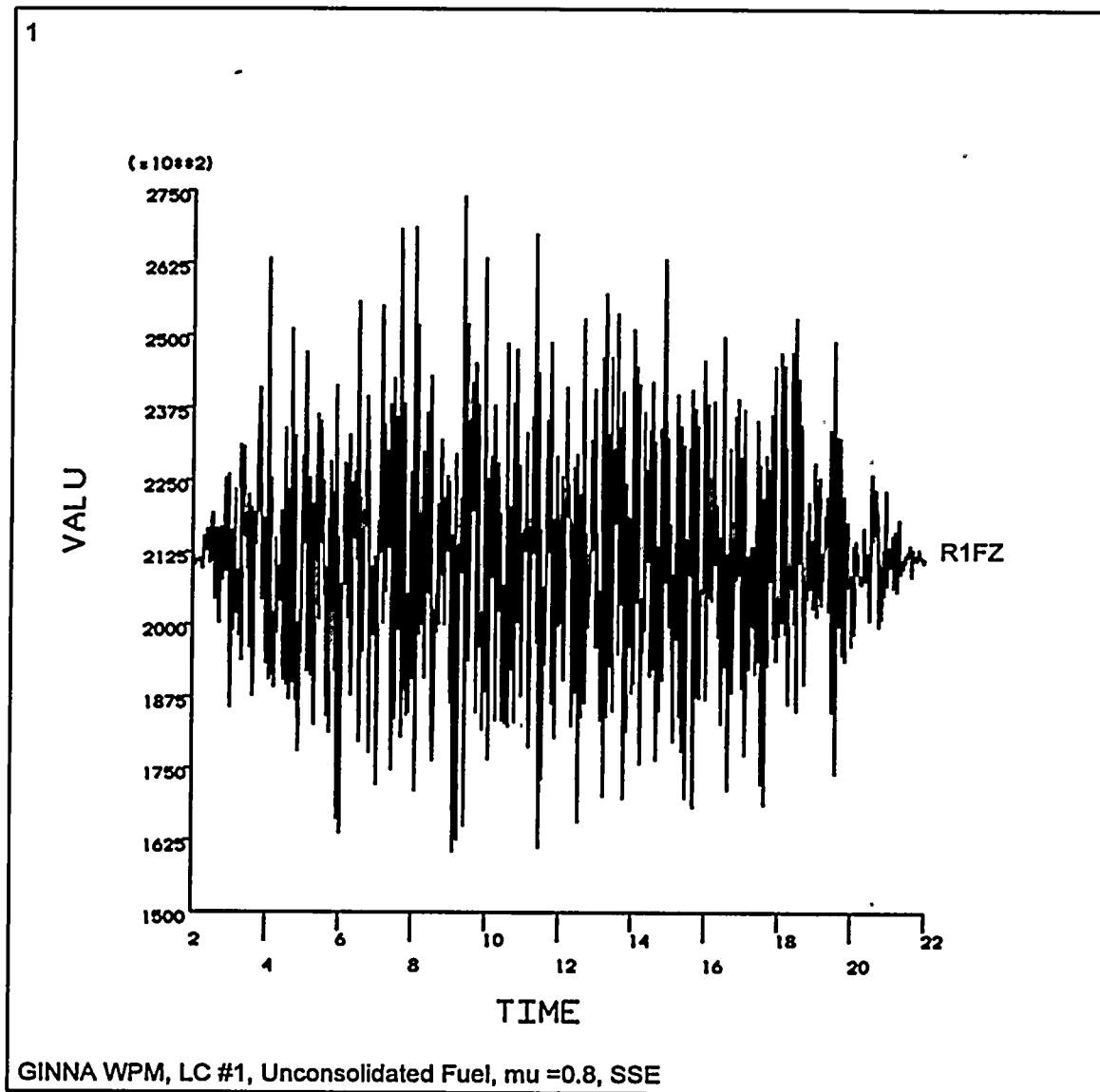


Figure 3.5-45 Rack 1 Horizontal Force Fy - LC#1

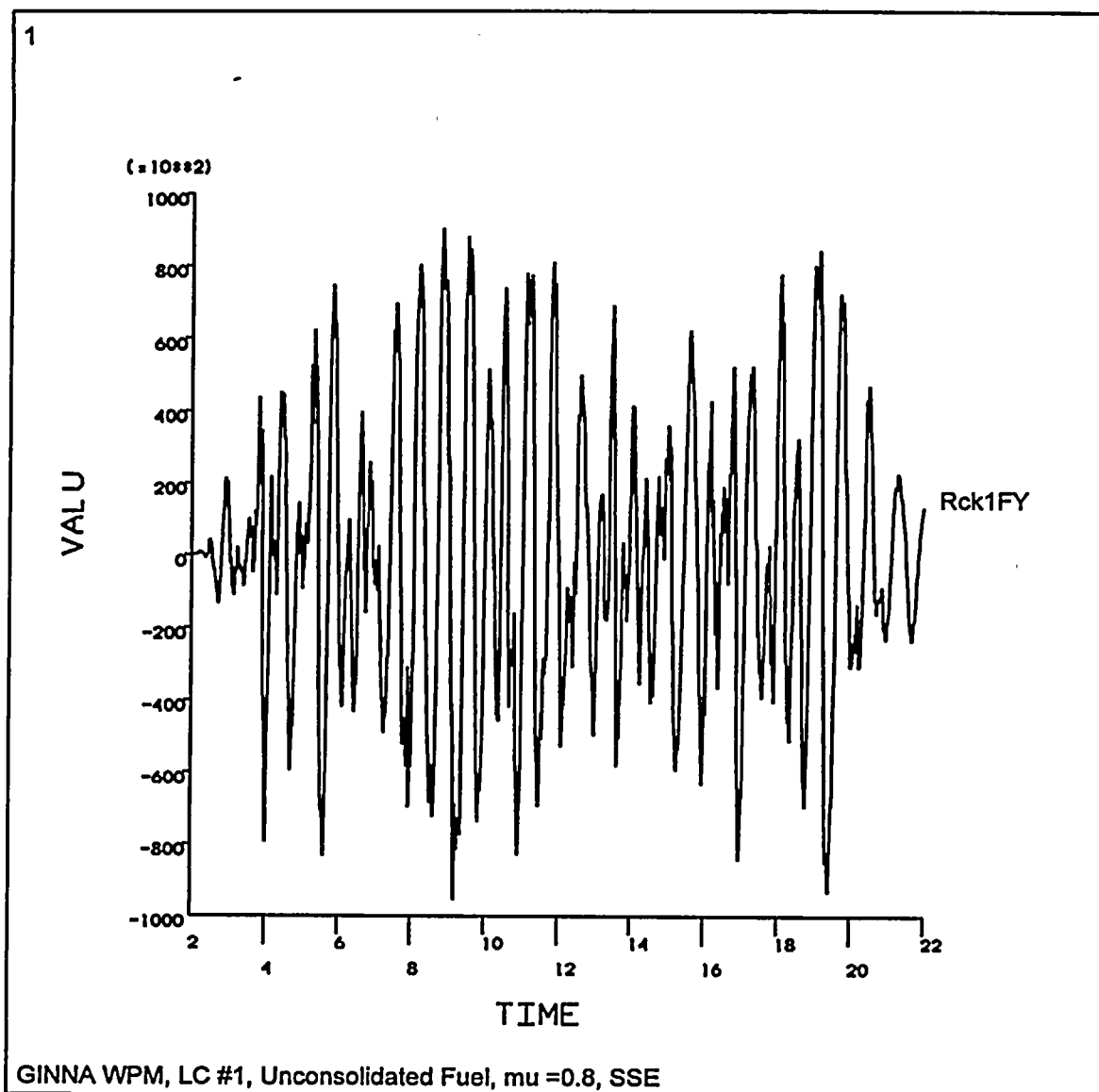


Figure 3.5-46 Rack 1 Moment Mx - LC#1

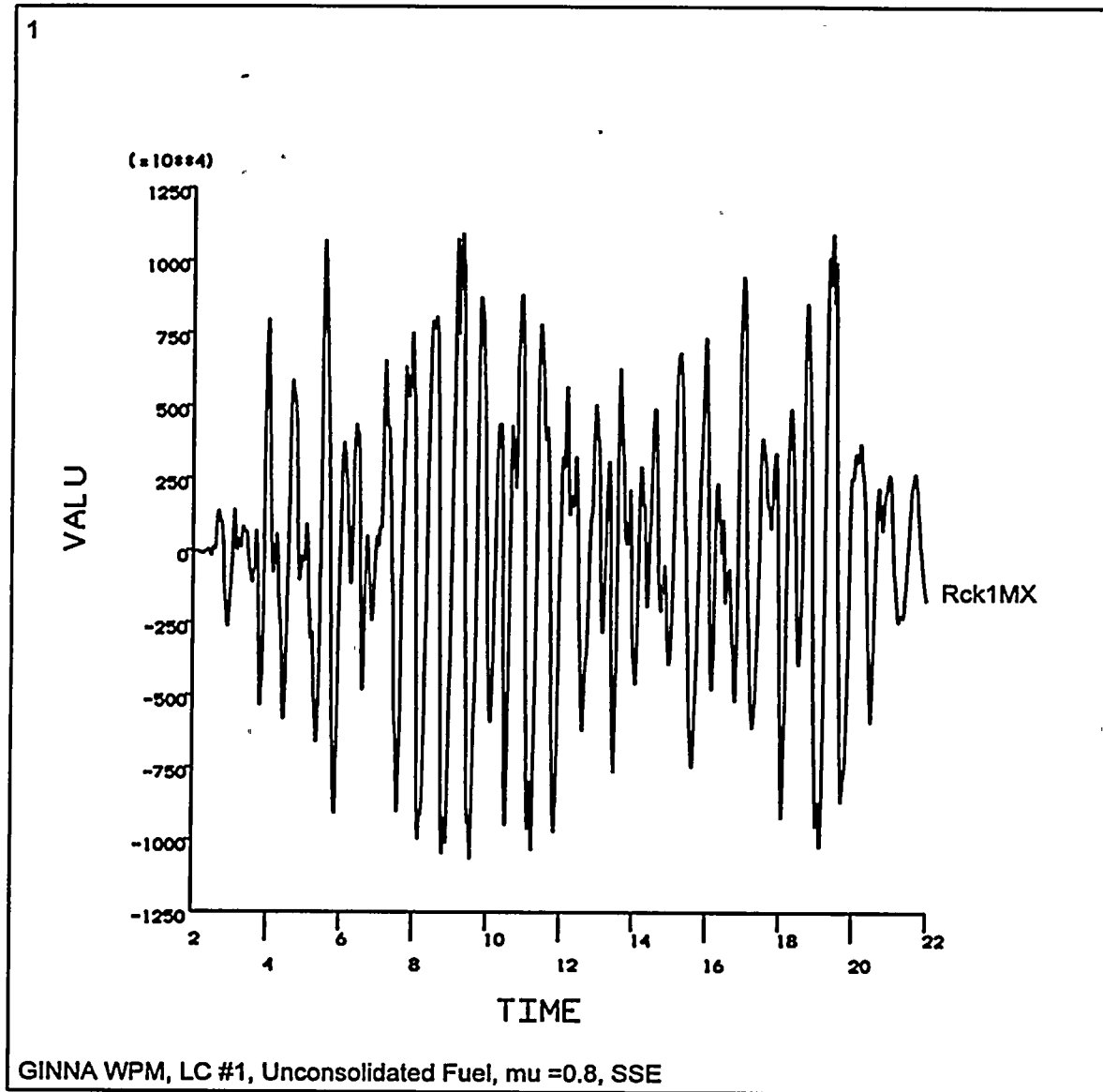


Figure 3.5-47 Rack 7 Moment My - LC#1

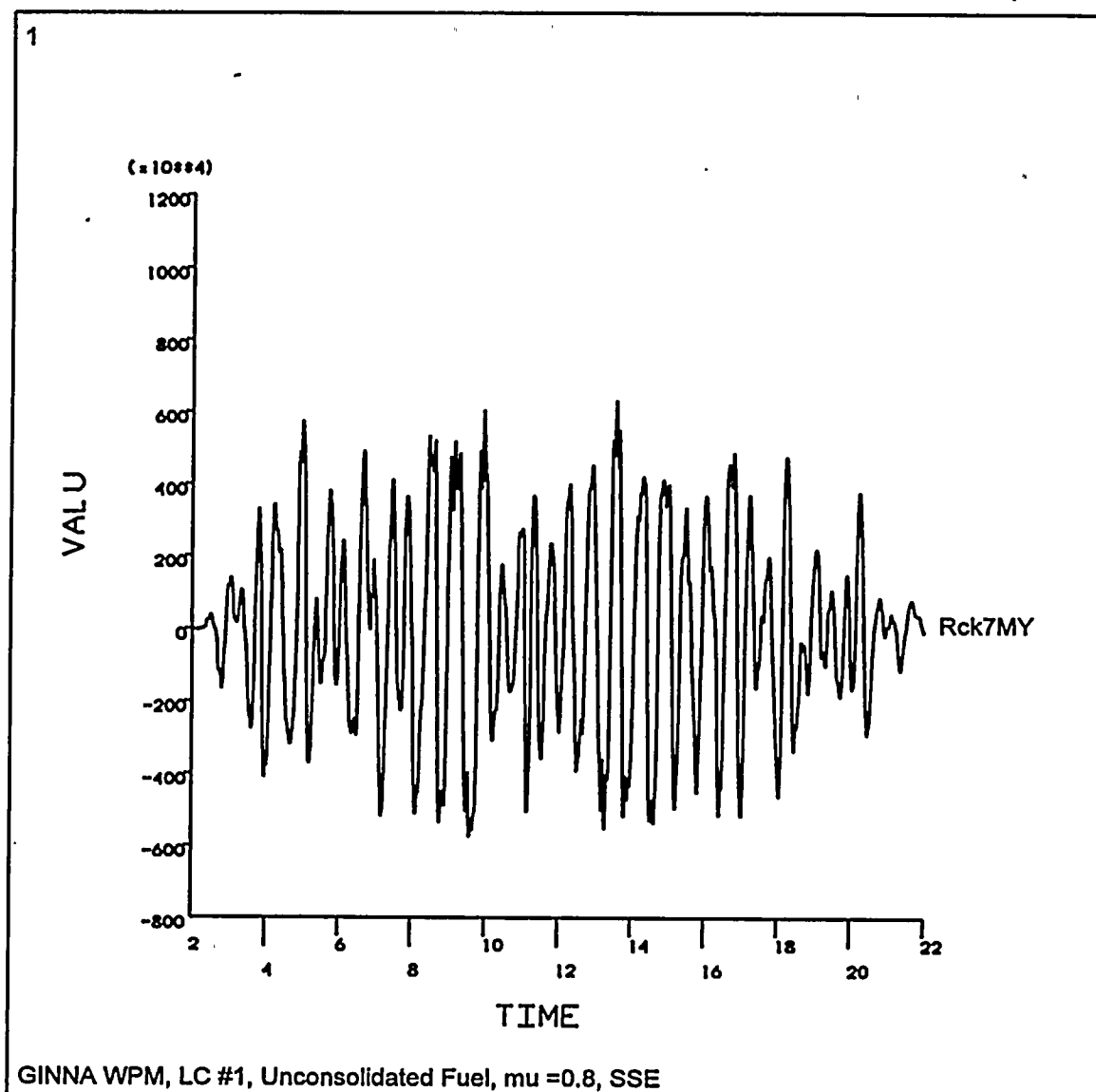


Figure 3.5-48 Fuel/Rack Impact Lds. +X, Rack 1 Top - LC#1

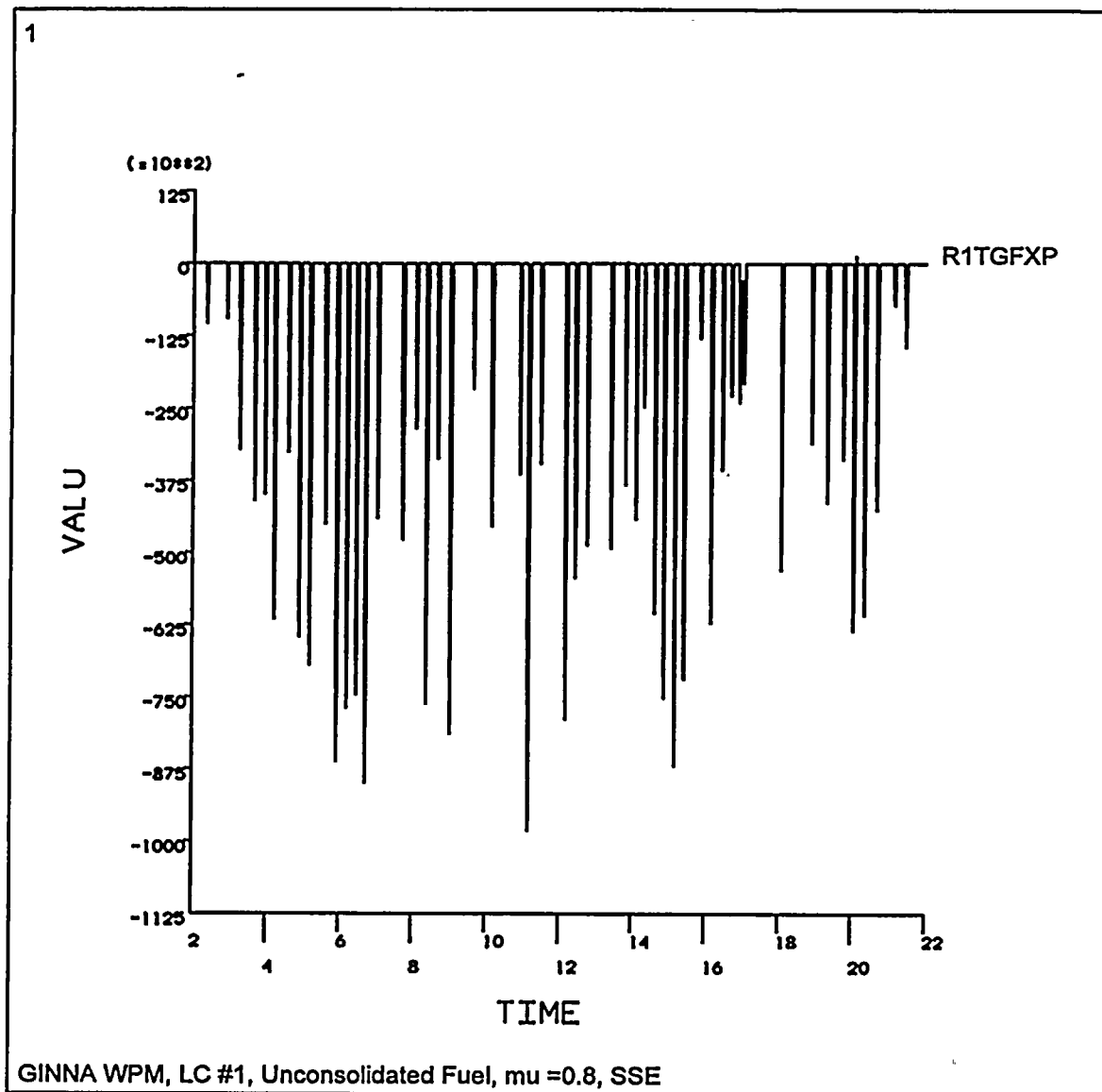


Figure 3.5-49 Relative Displ. DX Rack5/Rack7, Top - LC#1

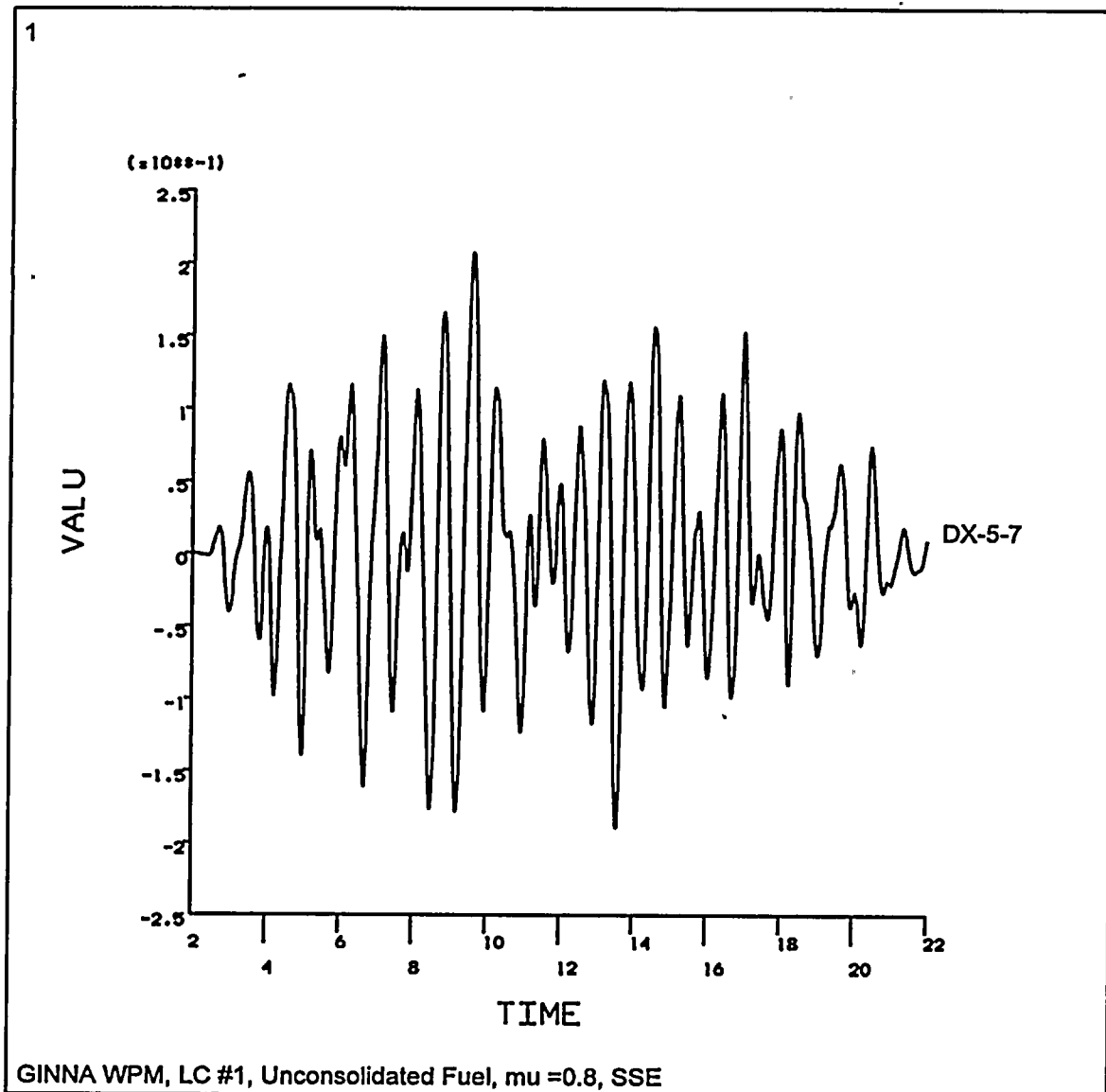
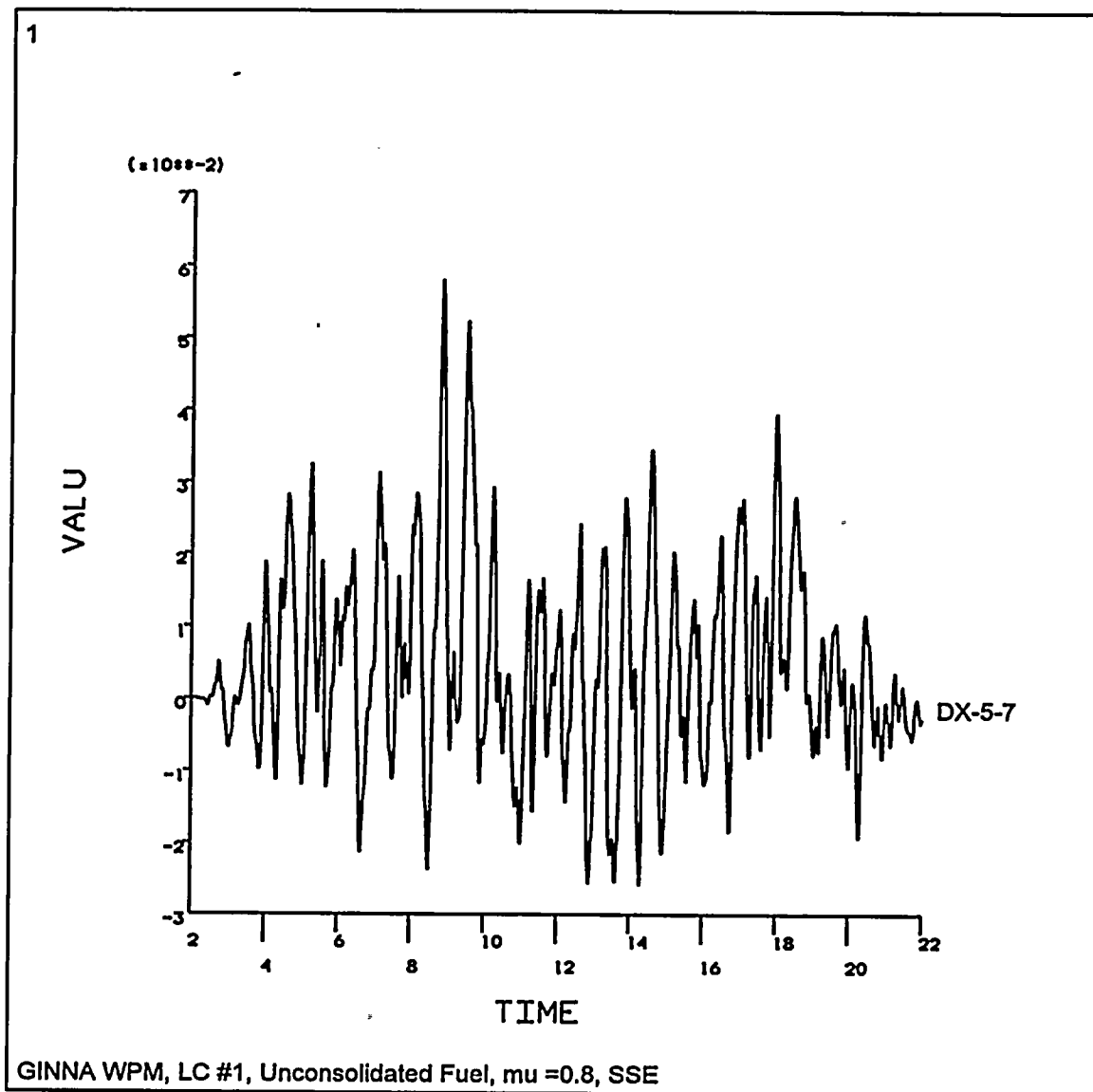


Figure 3.5-50 Rel. Displ. DX Rack5/Rack7, Base - LC#1





THE UNIVERSITY OF CHICAGO PRESS

CHICAGO, ILLINOIS 60607

Figure 3.5-51 Rel. Displ. DY Rack1/Rack2, Base - LC#1

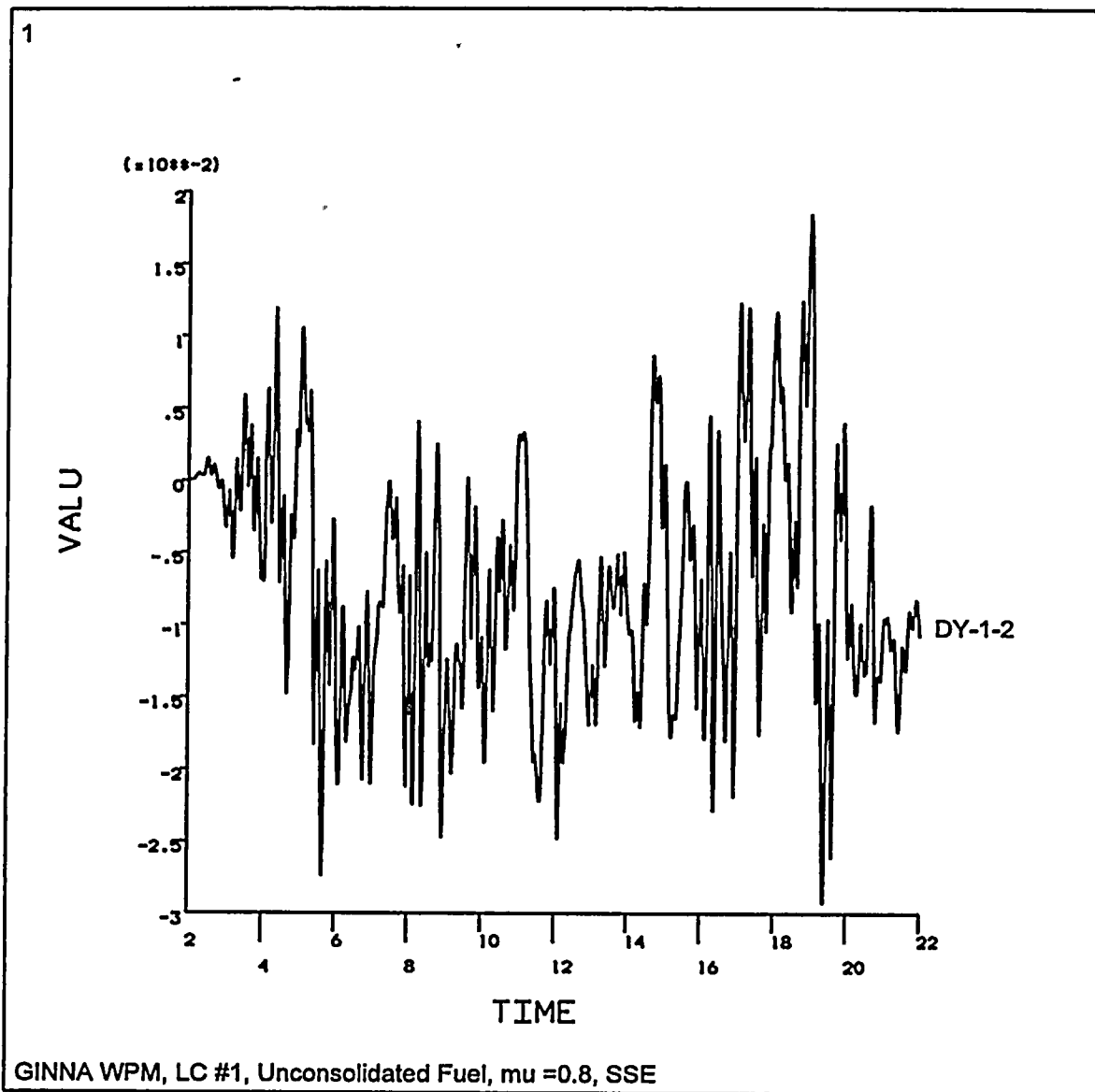




Figure 3.5-52 Vertical Leg Force Fz, Rack 1, Leg 1 - LC#2

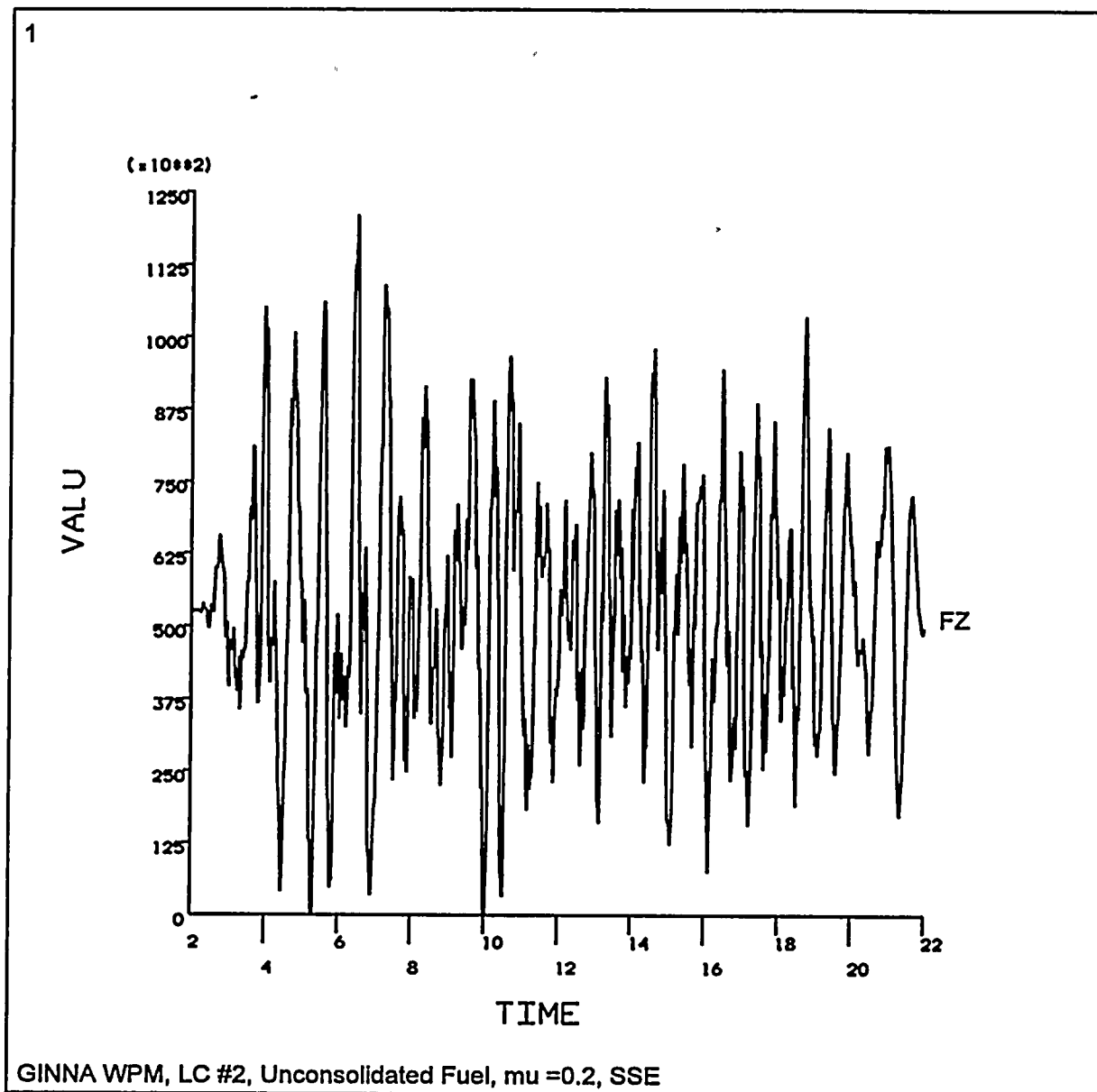


Figure 3.5-53 Sum of Vertical Leg Forces Fz, Rack 1 - LC#2

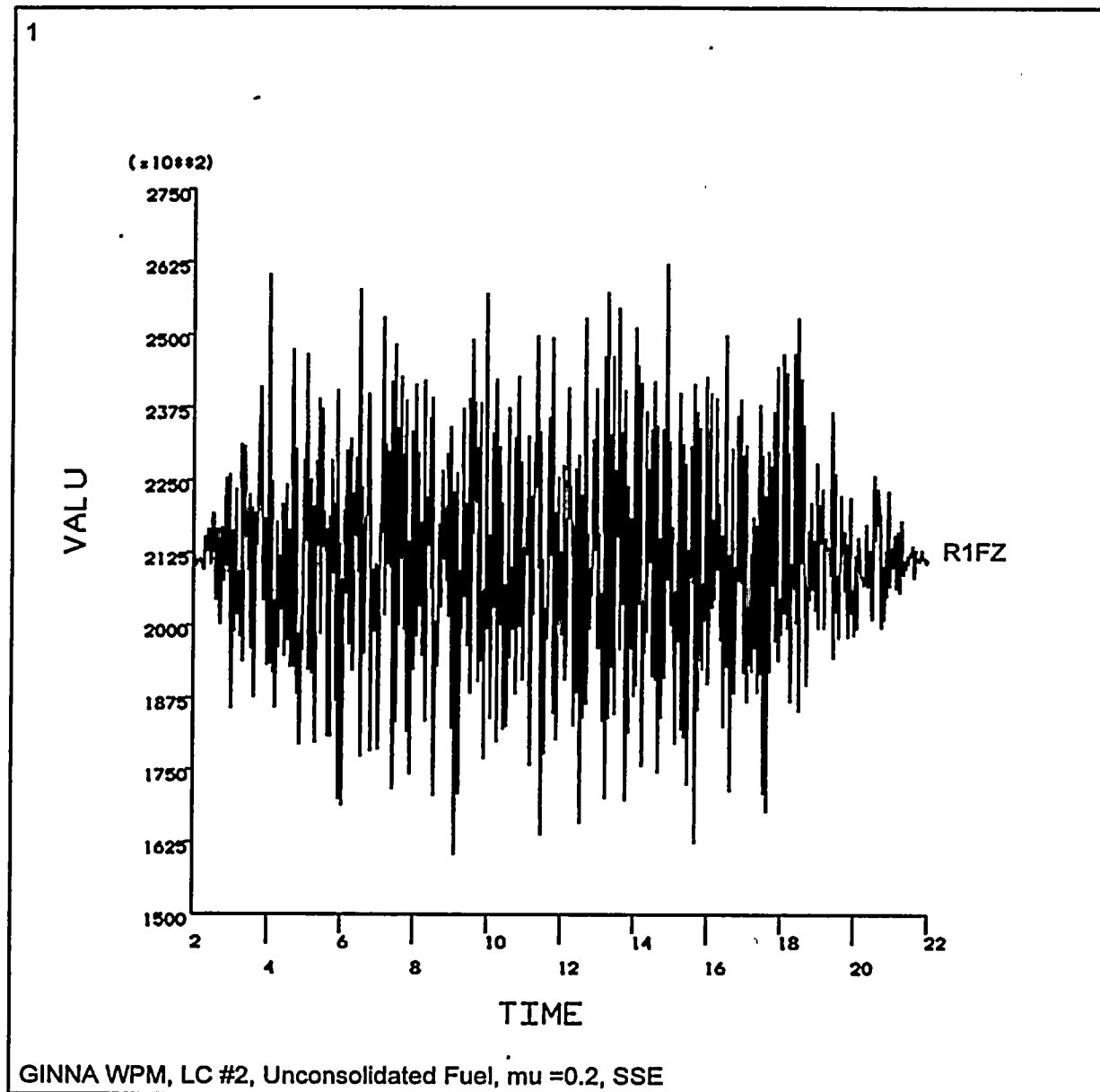
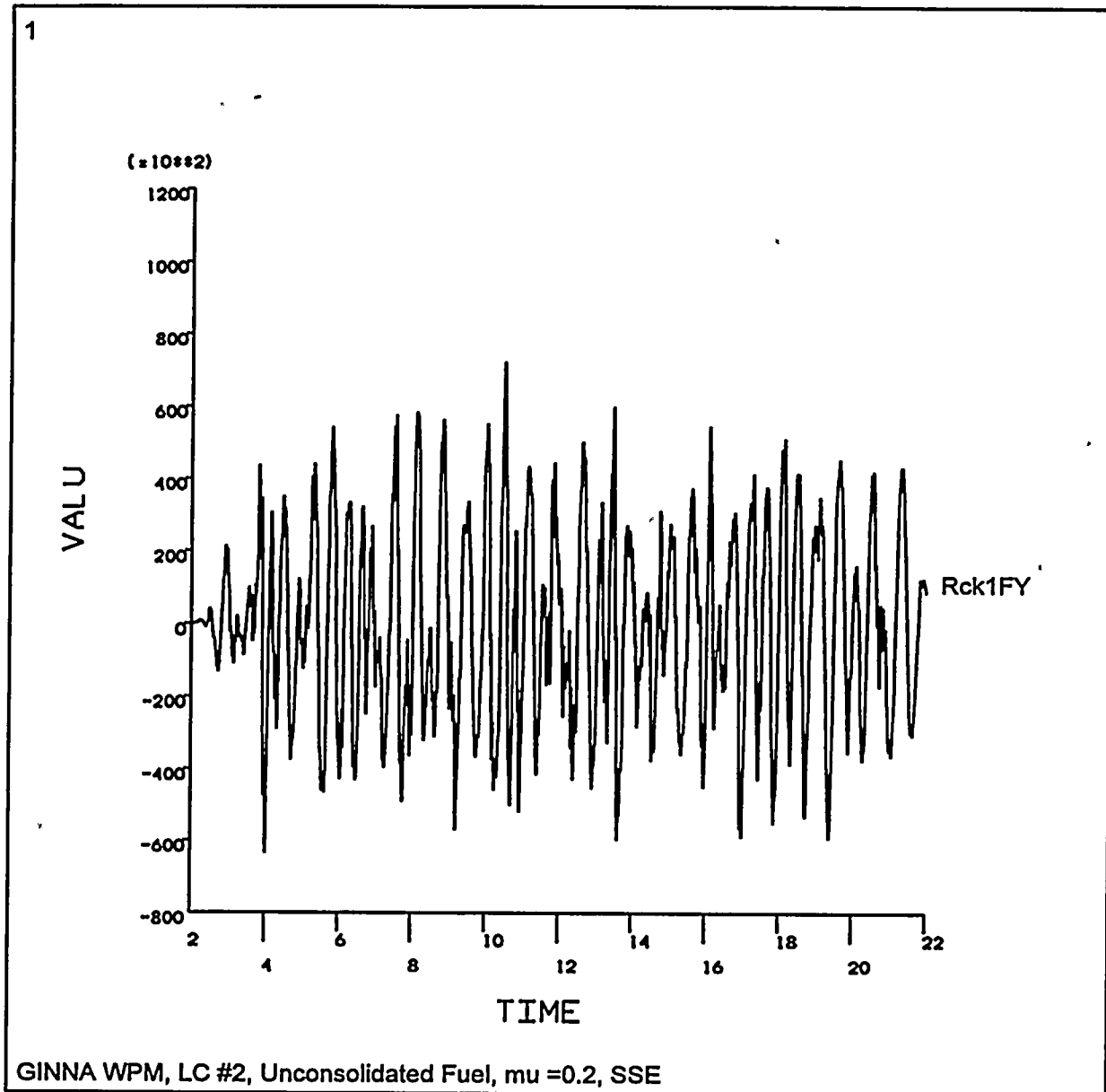


Figure 3.5-54 Rack 1 Horizontal Force Fy - LC#2



THE UNIVERSITY OF CHICAGO

DEPARTMENT OF THE HISTORY OF ARTS

1954-1955

1954-1955

1954-1955

1954-1955

1954-1955

1954-1955

1954-1955

1954-1955

1954-1955

1954-1955

1954-1955

1954-1955

1954-1955

1954-1955

1954-1955

1954-1955

1954-1955

1954-1955

1954-1955

1954-1955

1954-1955

1954-1955

1954-1955

1954-1955

1954-1955

1954-1955

1954-1955

1954-1955

1954-1955

Figure 3.5-55 Rack 1 Moment Mx - LC#2

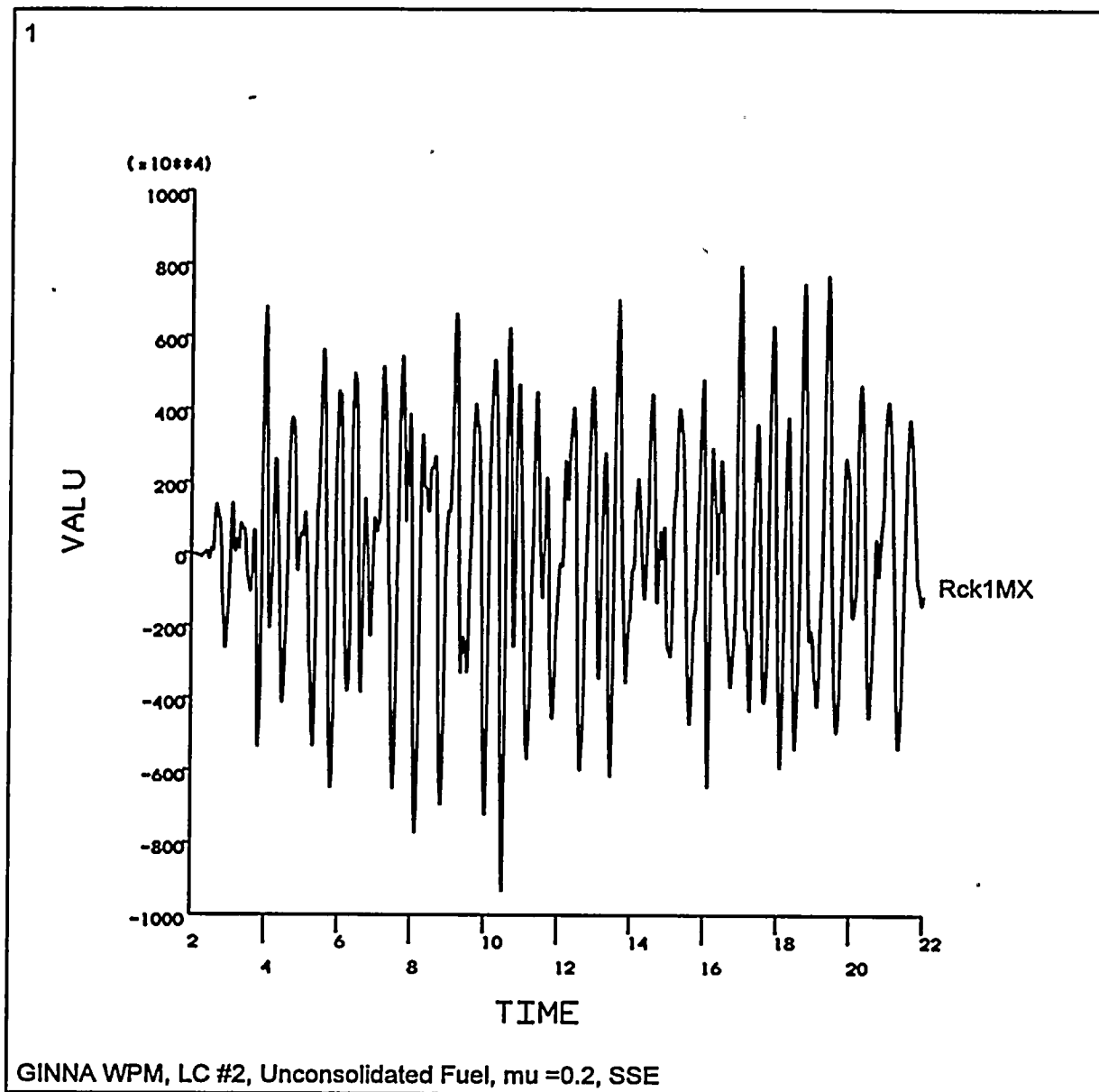




Figure 3.5-56 Rack 7 Moment My - LC#2

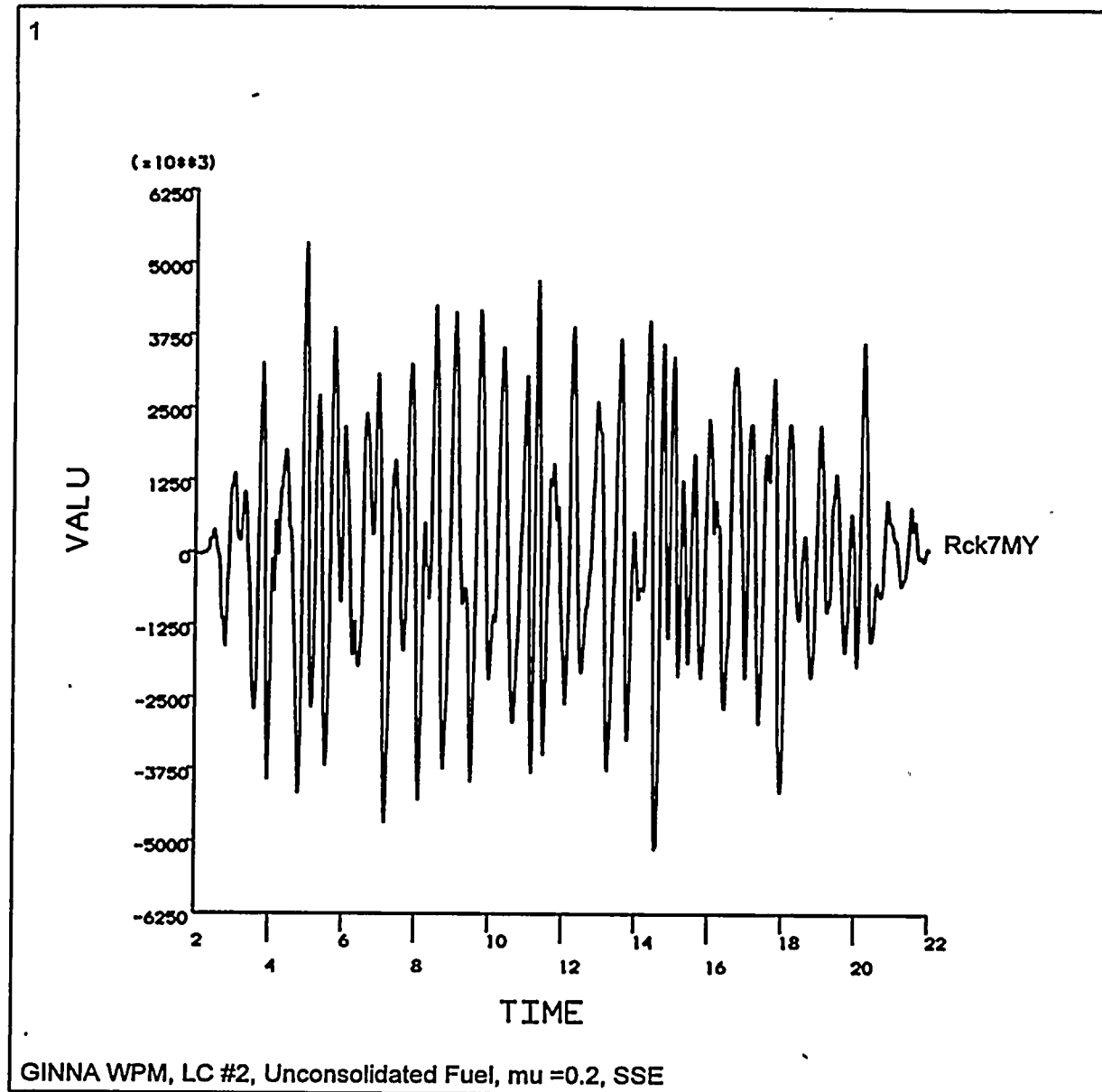


Figure 3.5-57 Fuel/Rack Impact Loads +X, Rack 1 Top - LC#2

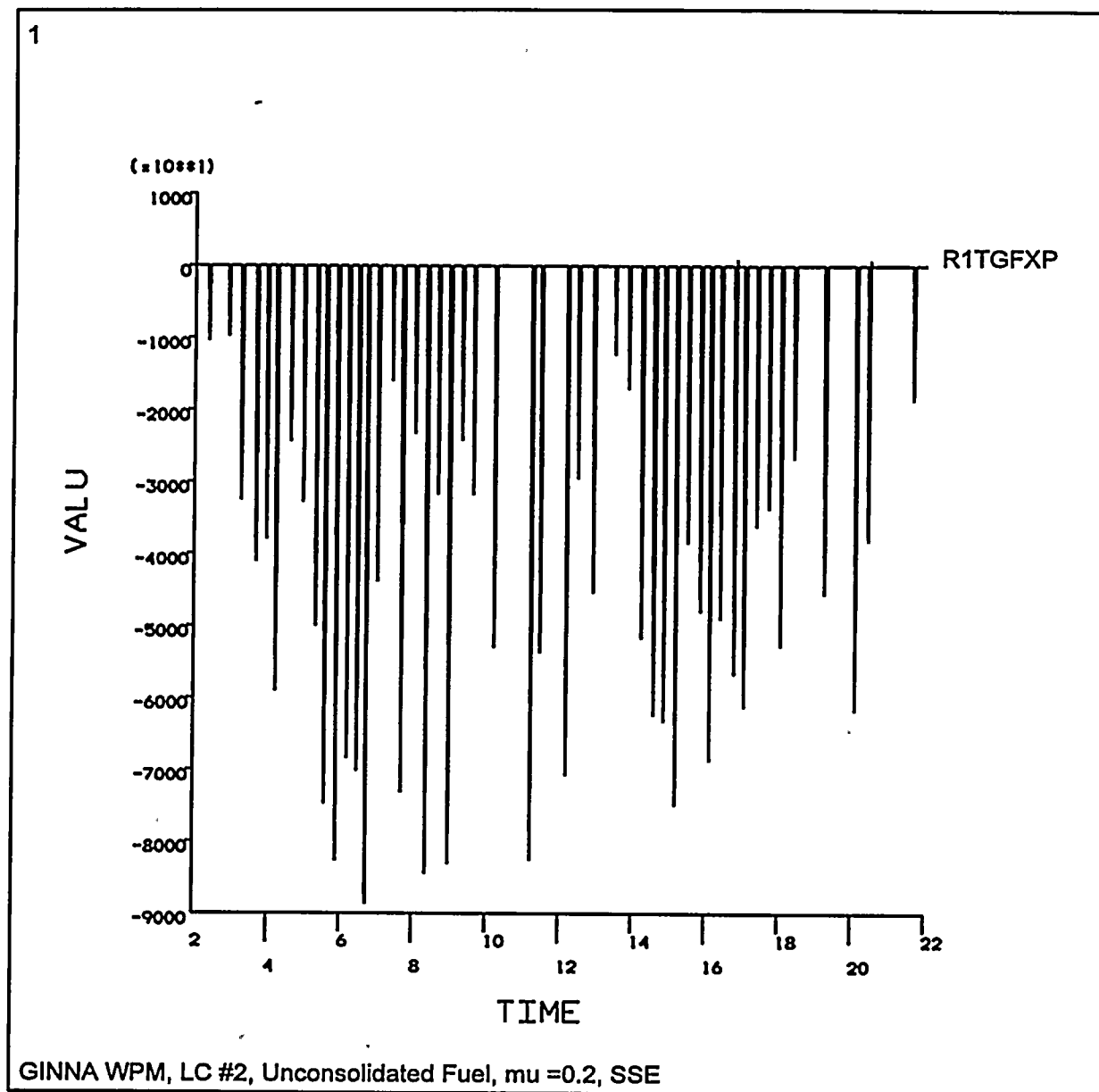




Figure 3.5-58 Relative Displ. DX Rack5/Rack7, Top - LC#2

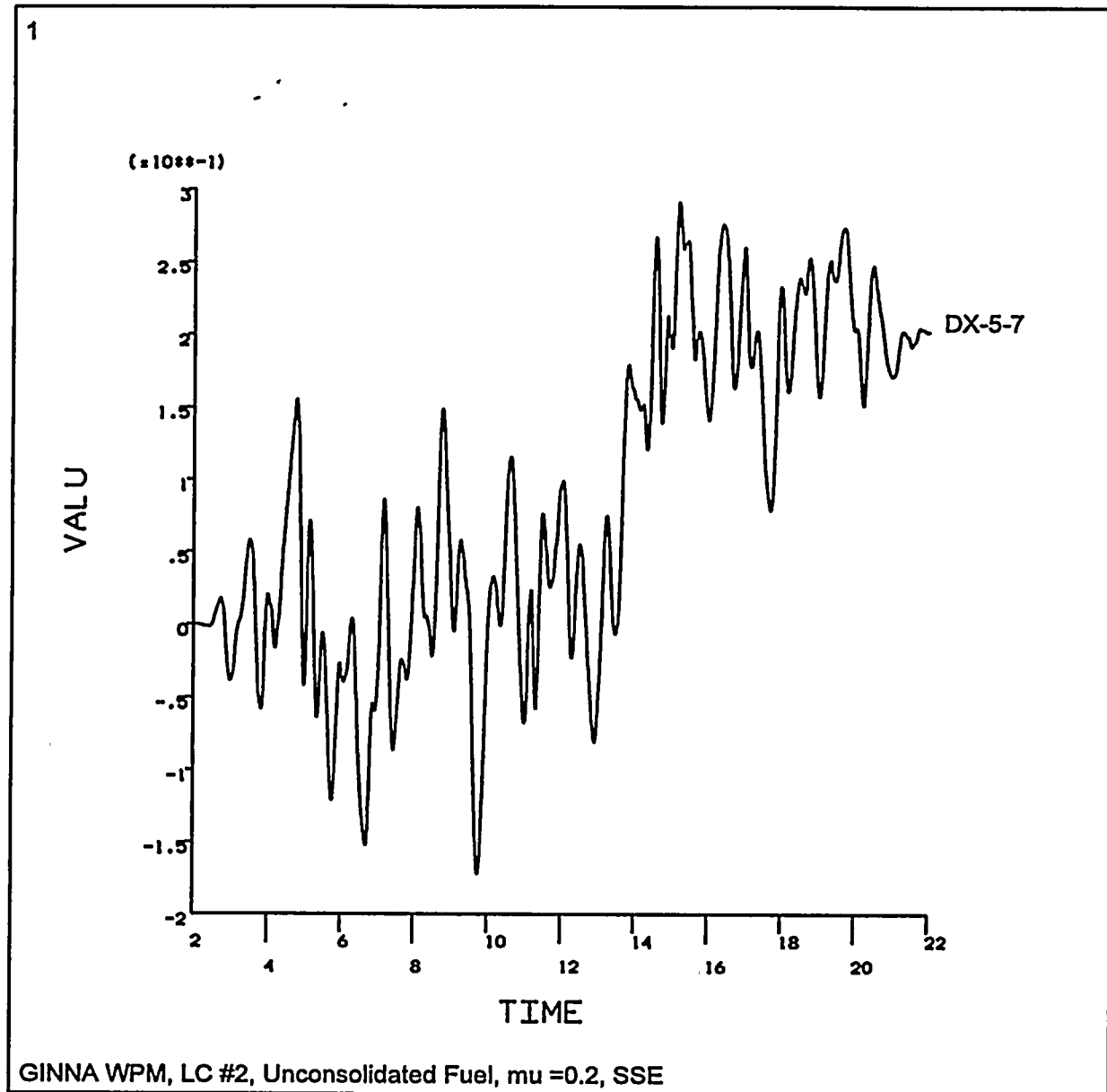




Figure 3.5-59 Relative Displ. DX Rack5/Rack7, Base - LC#2

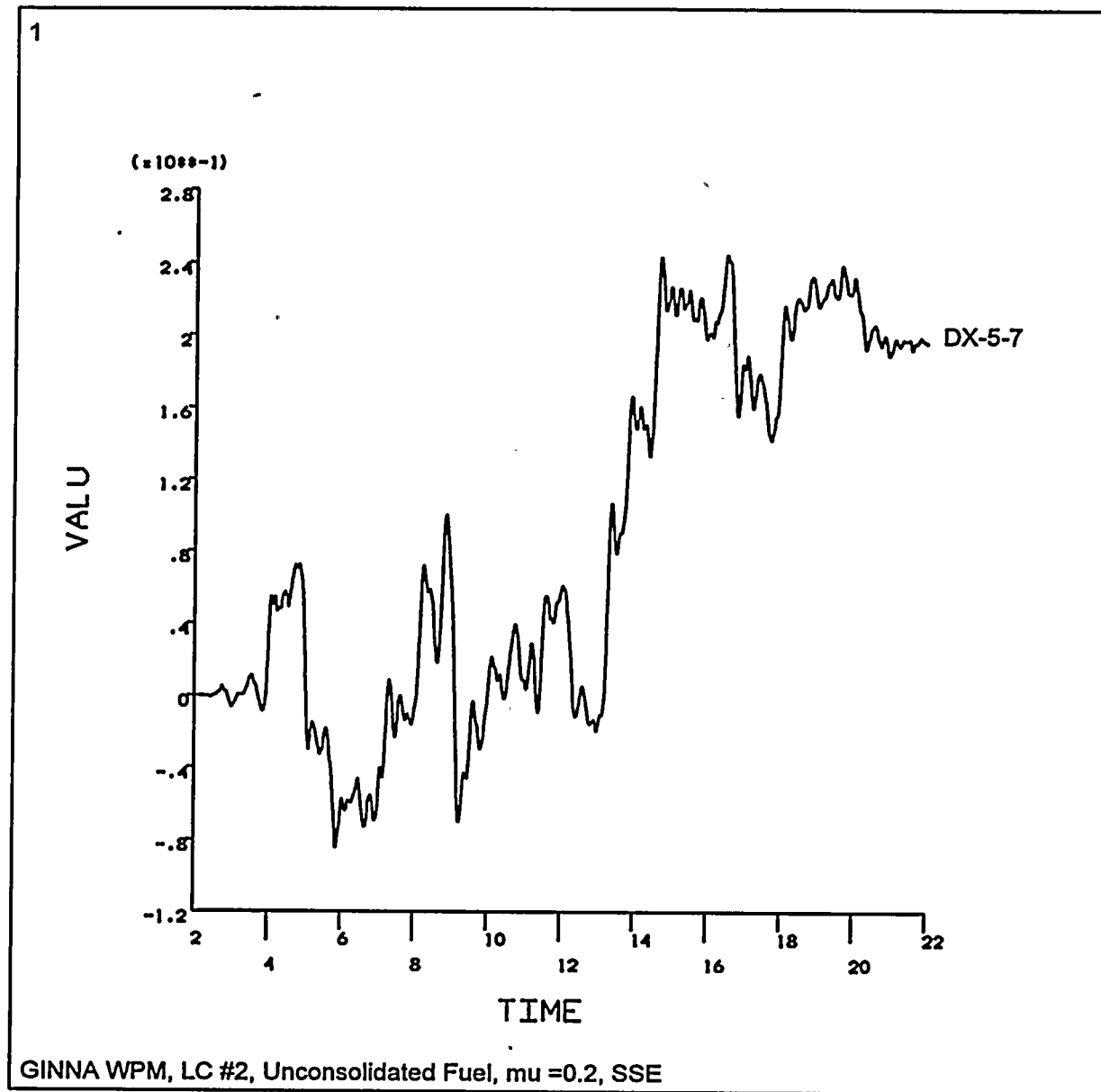
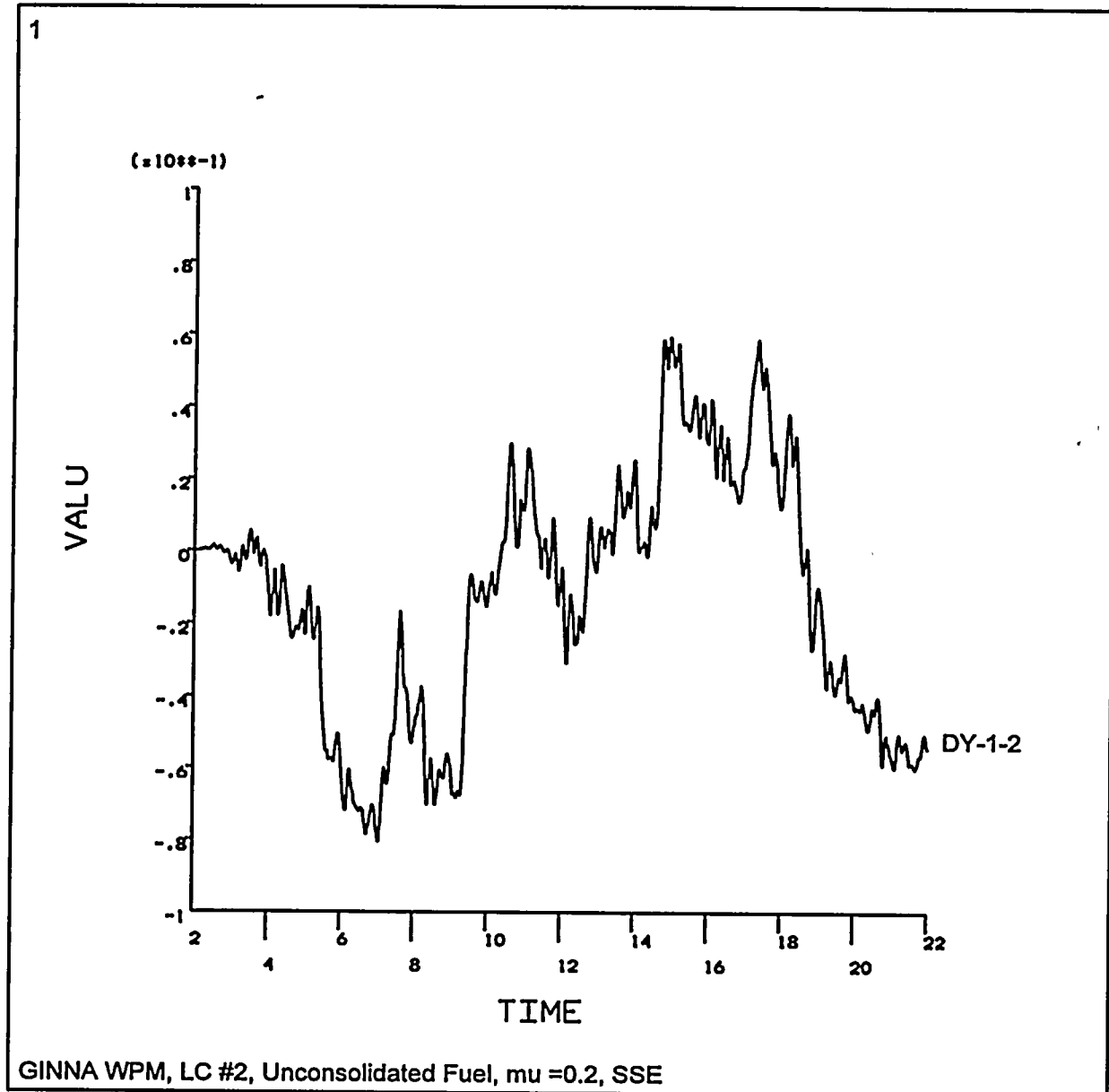




Figure 3.5-60 Relative Displ. DY Rack1/Rack2, Base - LC#2





3.5.3.1.9 Support Leg and Bearing Pad Analysis

The model shown in Figure 3.5-61 was used to determine the stresses in the support leg, and bearing stresses in the concrete for dead-weight, thermal and seismic (OBE & SSE) loadings. Boussinesq's solution for elastic half-space (Reference 3.35) was also used to estimate bearing stresses in the concrete.

The pool liner is a 1/4 inch ASTM A240 Type 304 SS plate. The support pads are 6.6929 inch diameter ASTM A479 Type 304L SS bar stock. The following material properties (and allowables) were used in this evaluation:

$$E (304L) = 27.9 \times 10^6 \text{ psi @ } 150^\circ \text{ F } (27.71 \times 10^6 \text{ psi @ } 180^\circ \text{ F})$$
$$\alpha (304L) = 8.74\text{E-}6 \text{ in/in}^\circ \text{ F @ } 180^\circ \text{ F } (8.67\text{E-}6 \text{ in/in}^\circ \text{ F @ } 150^\circ \text{ F})$$

Table 3.5-127 Material Properties for the Pool Liner and Support Legs
(Reference 3.19)

Material Type	To = Operating Temp. (150°F)			Ta = Abnormal Temperature (180°F)		
	S	Sy	Su	S	Sy	Su
A240 Type 304	18.3	27.5	73.0	18.0	26.0	71.8
A479 Type 304L	15.7	23.15	68.1	15.7	22.0	67.0

Note: All allowables are in ksi

The following per leg dead-weight, thermal, and OBE and SSE horizontal and vertical loads (i.e. support pad reactions) were taken from the results of the 3-D Full Rack and 2-D Multi-Rack analyses and used in the present analysis. The loads pertain to the new racks only.

Table 3.5-128 Forces Used in Qualification of the Pool Liner and Support Legs

Load Condition	Horizontal Force, SRSS (lbs)	Vertical Force (lbs)
Dead Weight (D)	--	18,280
Thermal (Ta)	14,624 ²	--
OBE (E)	14,554	42,476 ¹
SSE (E')	22,812	52,794 ¹

¹ includes deadweight in vertical force.

² maximum friction load allowed before slippage of the support leg occurs (less than calculated thermal load)



In the rack analysis models, each rack was represented by only the 4 corner legs. For example, a majority of the new racks in the pool have been designed to have twelve support legs. The 3-D single rack model has four legs to represent the twelve total legs. Therefore, the load per support leg is found by dividing by 12/4 or 3. The maximum support vertical leg loads for SSE were found at a single rack with eight support legs (rack number 9 for the vertical load and rack number 12 for the maximum horizontal load). Therefore, the load was divided by 8/4 or 2 to determine the maximum load per support leg. The vertical load was applied in the Z direction (compression) and the horizontal load was the Square Root Sum of the Squares of the X and Y directions (refer to Figure 3.5-61). For the seismic load cases, there existed significant lateral (horizontal) loads on the support leg.

Support leg stresses at two locations were evaluated. The first location (case 1) evaluated was at the location of the cylinder's holes (4.05 inches below the bottom of the baseplate). The cross-sectional area (A_2) = 6.90 in², and the section modulus (S_x) = 12.38 in³. This section was shown to produce the highest stresses.

The second location (case 2) was at the baseplate bottom (where moments are the largest). The cylinder's cross-sectional area (A_1) = 13.33 in², and the section modulus (S_x) = 17.58 in³.

Figure 3.5-61 - Support Leg Details

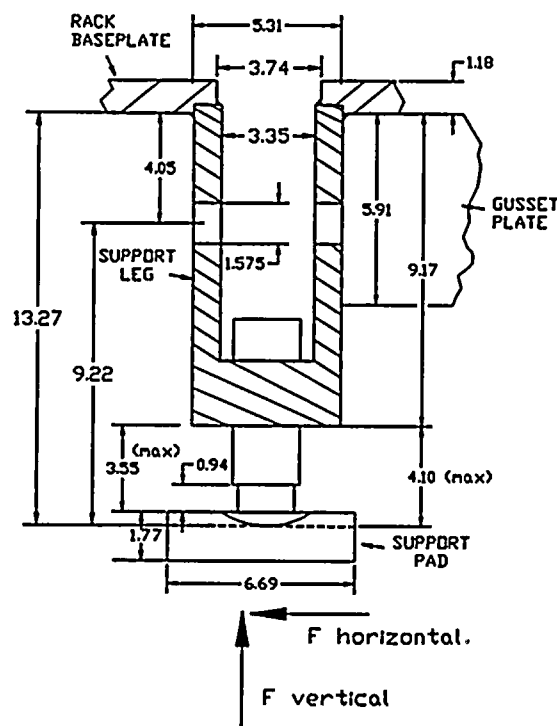
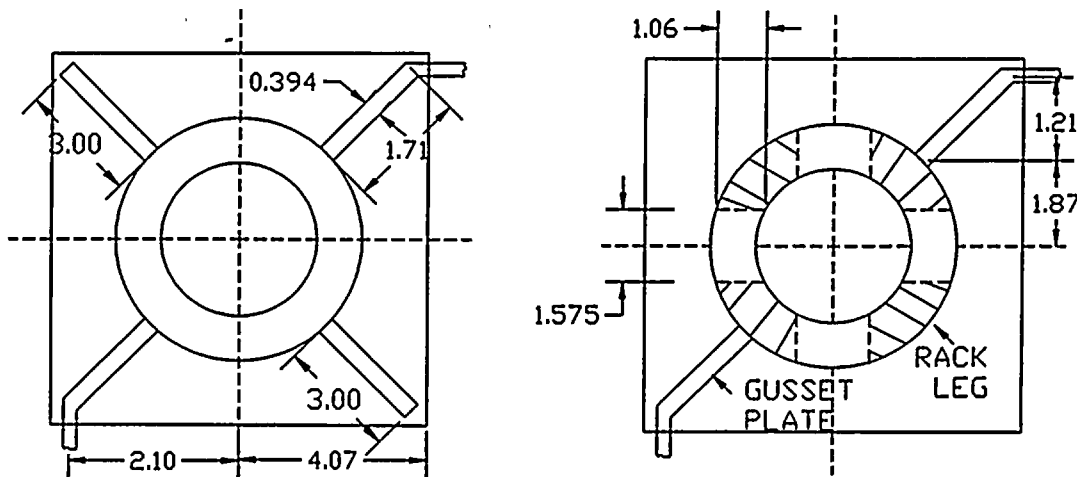




Figure 3.5-62 - Support Leg Gusset Plate Details



3.5.3.1.9.1 Support Leg Analysis

3.5.3.1.9.1.1 Existing Rack Support Analysis

Evaluation of the existing rack support was performed by comparison of new loads with the previous rack leg analysis (Reference 3.26). The following table gives the maximum loads of the new analysis compared with the previous analysis. Since the new rack analysis results in lower existing support loads than the previous analysis (Reference 3.26), existing racks and support loads are qualified per comparison to the previous rack analysis.

Table 3.5-129 Support Legs Force Comparison for Existing Racks
(New vs. Old Analyses)

Horizontal Load	U.S. Tool & Die Analysis Loads at Support Pad (lbs)		New Analysis Loads at Support Pad (lbs) ¹	
	Horizontal	Vertical	Horizontal	Vertical
Standard Fuel				
SSE (E')	141,939	237,862	87,636	193,440
Consolidated Fuel				
SSE (E')	151,144	282,782	103,596	250,680

¹ includes deadweight in vertical force. SSE loads are factored by 1.20

3.5.3.1.9.1.2 Concrete and Spent Fuel Pool Liner Qualification

The 28 days cured compressive strength of the spent fuel pool concrete is 3,000 psi. The average pressure (bearing) under the bearing pad shall not exceed the design basis pressure for dead load or seismic. The bearing stresses and comparison to allowables are presented in Table 3.5-130.

3.5.3.1.9.1.2.1 Average Concrete Bearing Stress

The maximum bearing stresses in the concrete are calculated below, whereas the average bearing stresses are calculated by taking the maximum vertical support leg loads determined from the single and multi-rack analyses and dividing by the area of the bearing pad as follows:

$$\sigma_{\text{BEARING}} = P/A, \text{ where } A = \pi d^2/4 = 35.18 \text{ in}^2 \\ d = 6.693 \text{ in. (support pad diameter)}$$

$\sigma_{\text{BEARING, DEAD LOAD}}$	$=$	$18,280 / 35.18$	$=$	520 psi.
$\sigma_{\text{BEARING, OBE + DL}}$	$=$	$42,476 / 35.18$	$=$	1,207 psi.
$\sigma_{\text{BEARING, SSE + DL}}$	$=$	$52,794 / 35.18$	$=$	1,501 psi.

3.5.3.1.9.1.2.2 Boussinesq's Solution

As another check for bearing stresses, Boussinesq's solution for elastic half-space is used (Reference 3.35, pages 398 through 402). In this method, it is assumed that a normal force, P , is acting on the plane boundary of a semi-infinite solid as shown in the following figure. All results are summarized in Table 3.5-130.

Figure 3.5-63 Stress Locations For Boussinesq's Bearing Solution

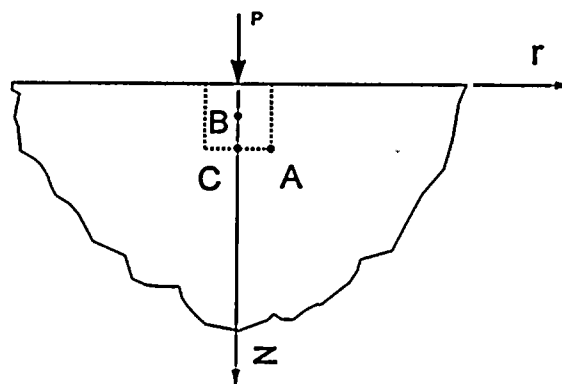


Table 3.5-130 Summation of Concrete Stresses

Load Combinations	Maximum Stress (psi)	Allowable Stress (psi)
<i>D</i>		
Maximum Slab Bearing	520	3,570
Boussinesq's Solution	779	3,570
<i>D + E</i>		
Maximum Slab Bearing	1,207	3,570
Boussinesq's Solution	1,811	3,570
<i>D + E'</i>		
Maximum Slab Bearing	1,501	3,570
Boussinesq's Solution	2,251	3,570

Concrete's bearing allowable = $\phi (0.85)fc' = 0.70(0.85)3000 \text{ psi} * 2^1 = 3,570 \text{ psi}$

¹ Since Area of concrete \gg area of pad = $\pi d^2/4 = 35.18 \text{ in}^2$, bearing allowable is increased by factor of 2 (Reference 3.20, section 10.15)

For the evaluation of compressive stresses in the concrete, the specified Boussinesq solution is considered valid.

Table 3.5-131 Summation of Spent Fuel Pool Liner Stresses

Load Combinations	Maximum Stress (psi)	Allowable Stress (psi)
<i>D + E</i>		
Liner Bearing Stress	1,207	$0.9*(F_y)=23,400$
<i>D + E'</i>		
Liner Bearing Stress	1,501	$0.9*(F_y)=23,400$

Pool Liner's Allowable Stress is from Reference 3.21

Table 3.5-132 Summation of Support Leg Stresses

Load Combinations	Maximum Stress (psi)	Allowable Stress (psi)
<i>D</i> (Level A)		
Primary Membrane (Pm)	6,156	1*(S) = 15,700
Primary Membrane+ Bending (Pm + Pb)	16,995	1.5*(S) = 23,550
<i>D + E</i> (Level B)		
Primary Membrane (Pm)	6,156	1.33*(S) = 20,880
Primary Membrane+ Bending (Pm + Pb)	16,995	1.995*(S) = 31,320
Average Shear Stress	2,109	0.6*(Sy) = 9,420
<i>D + E'</i> (Level D)		
Primary Membrane (Pm)	7,651	1.2*(Sy) = 26,448
Primary Membrane+ Bending (Pm + Pb)	24,640	1.8*(Sy) = 39,672
Average Shear Stress	3,306	0.42*(Su) = 28,123

3.5.3.1.10 Rack Thermal Stress Analysis

Two thermal accident conditions were considered. Analysis is performed on ANSYS 3D single rack plate model of the rack #8 (2B) with the largest plan projection (footprint), as well as largest number of cells. As a consequence, this will produce largest increase in overall linear dimensions of the rack structure.

1) Normal or Upset Condition (To) - This thermal condition is produced when an isolated storage location has a fuel assembly generating heat at the maximum postulated rate. Surrounding storage tubes are assumed to contain no fuel assemblies. In lieu of running a full thermal analysis to determine the actual temperature distribution along the inner and outer hot cell walls, it was conservatively assumed that the outside tube wall temperature remains at 150°F, while the inner wall temperature is kept at 212°F. This results in a conservative 62°F temperature differential across the 2 mm (0.0787 in) thick tube wall. This maximum ΔT assumption envelopes the actual thermal distribution in the cell walls due to a maximum outlet water bulk temperature which exits the cell at 224°F, and linearly drops to the tube inlet temperature of 150°F. The hot cell outside water bulk temperature is assumed to be 150°F, and temperature drop through the wall's adjacent boundary layers is not considered. Due to this temperature differential, thermal growth of the hot cell induces membrane and bending stresses in the rack base plate and tube walls.

Stress contours in rack cells around middle hot cell are shown in Figures 3.5-64 (top plane) and 3.5-65 (mid plane). Half of the rack is shown, since the stress distribution is symmetric about NS direction. Base plate stress contours are shown in Figures 3.5-66 (top plane) and 3.5-67 (mid plane).

Summarized, the local hot cell maximum thermal stresses are:

- a) Tube walls: membrane = 3,837 psi; membrane+bending = 9,856 psi
- b) Base plate : membrane = 1,198 psi; membrane+bending = 5,941 psi



Figure 3.5-64 Rack Tubes Stress Contours - To (Top Plane)

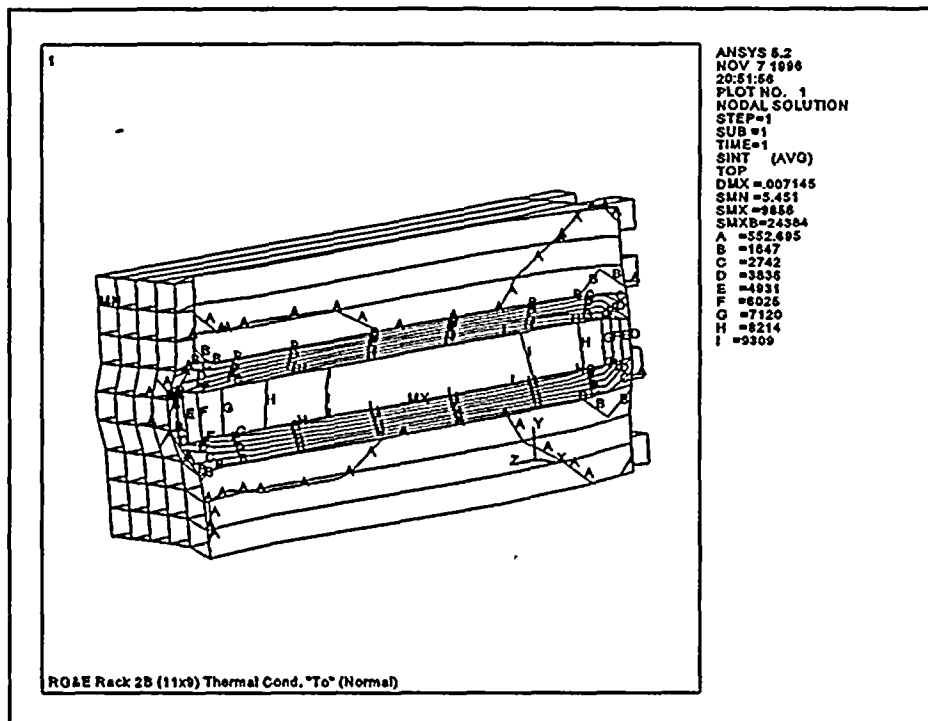


Figure 3.5-65 Rack Tubes Stress Contours - To (Mid Plane)

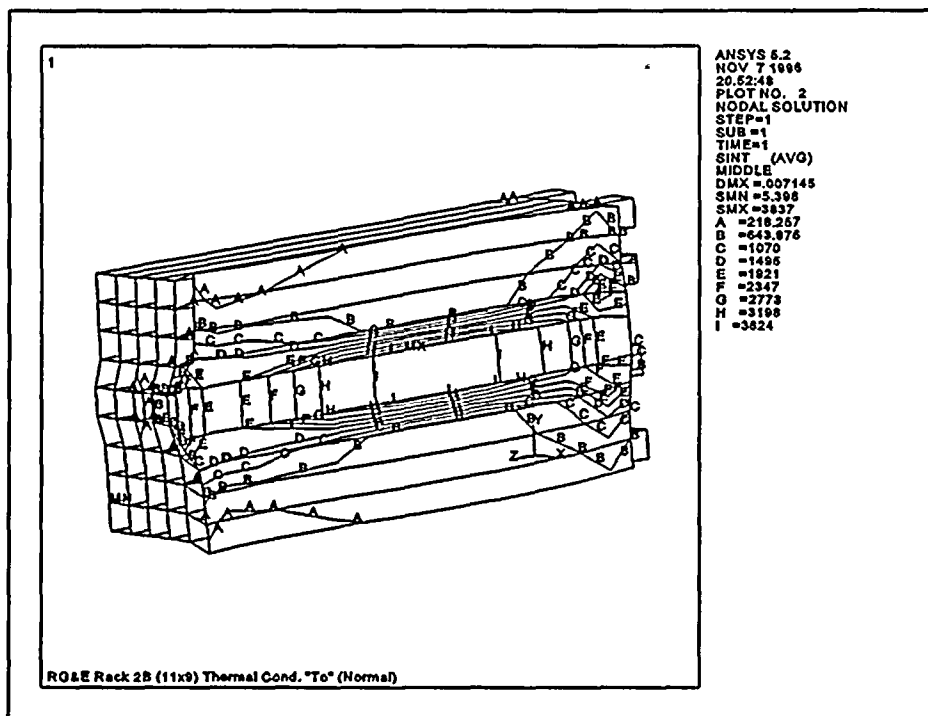




Figure 3.5-66 Base Plate Stress Contours - To (Top Plane)

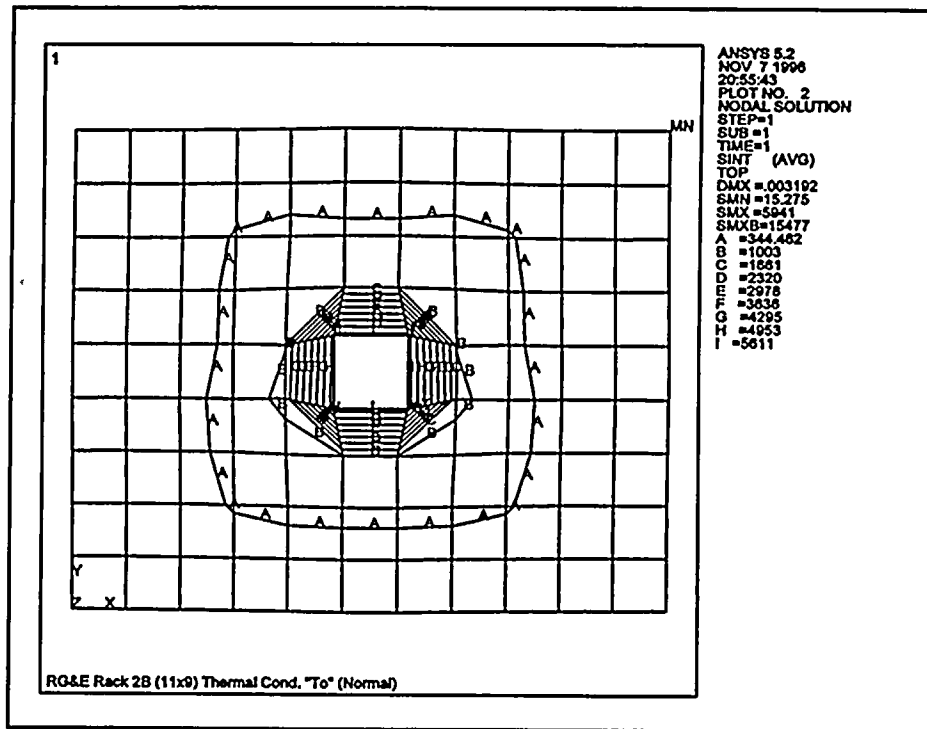
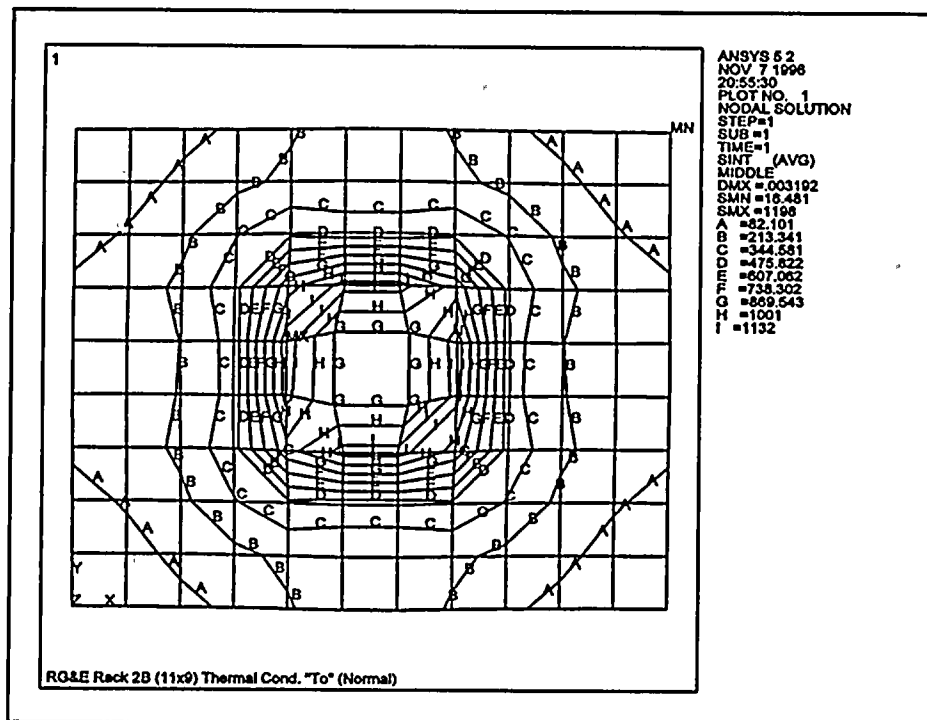


Figure 3.5-67 Base Plate Stress Contours - To (Mid Plane)



2) Abnormal Condition (Ta) - This thermal condition is produced when the pool water bulk temperature reaches a maximum allowable value of 180°F, when auxiliary pumps are activated. Reference temperature with no thermally induced stresses is assumed to be normal pool operating temperature of 150°F. Legs are fixed to the pool liner (Figure 3.5-68).

Stress contours at the bottom of the corner rack tubes are shown in Figures 3.5-69 (top plane) and 3.5-70 (mid plane). Base plate stress contours are shown in Figures 3.5-71 (top plane) and 3.5-72 (mid plane).

Summarized, thermally induced stresses are:

- a) Tube walls: membrane = 9,654 psi; membrane+bending = 9,803 psi
- b) Base plate : membrane = 596 psi; membrane+bending = 1,556 psi

Figure 3.5-68 Deformed Base Plate with Legs - Ta

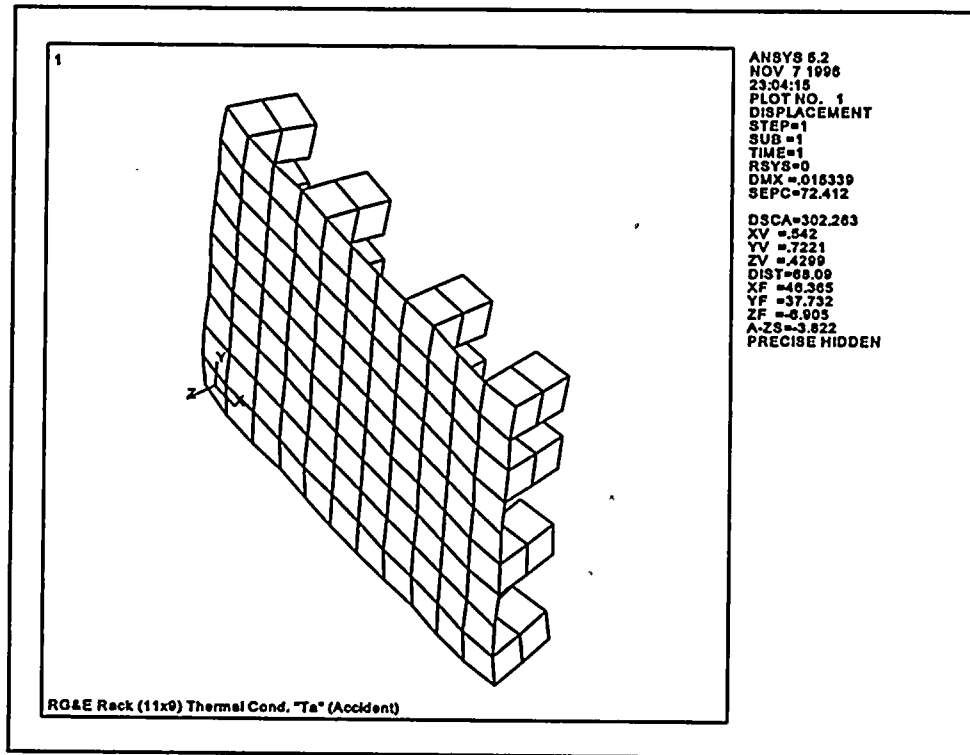


Figure 3.5-69 Bottom Corner Tubes Stress Contours - Ta (Top Plane)

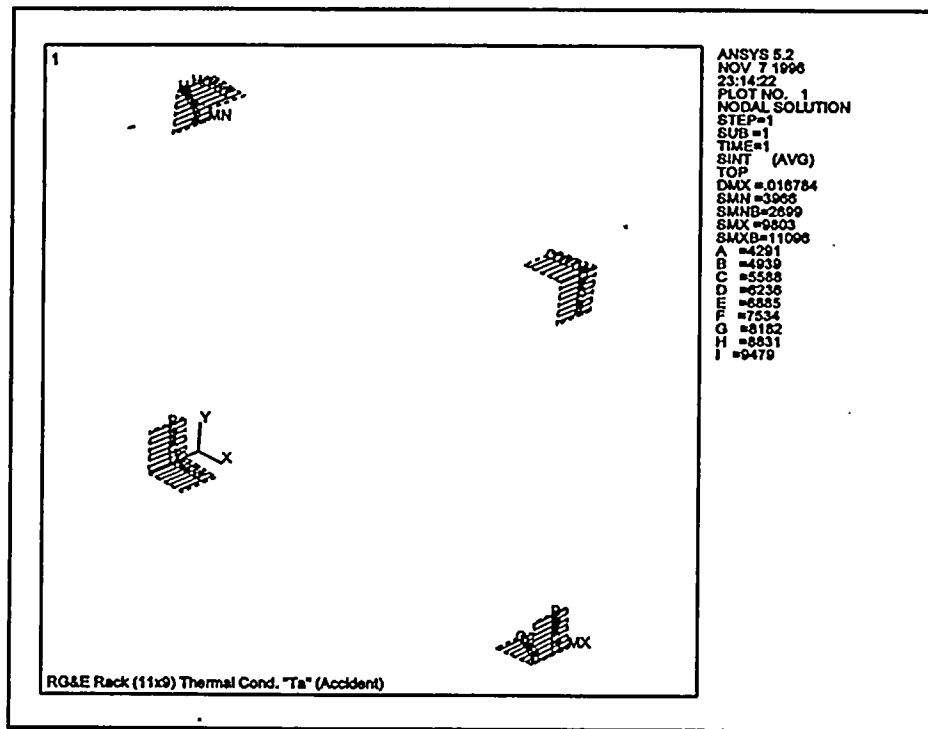
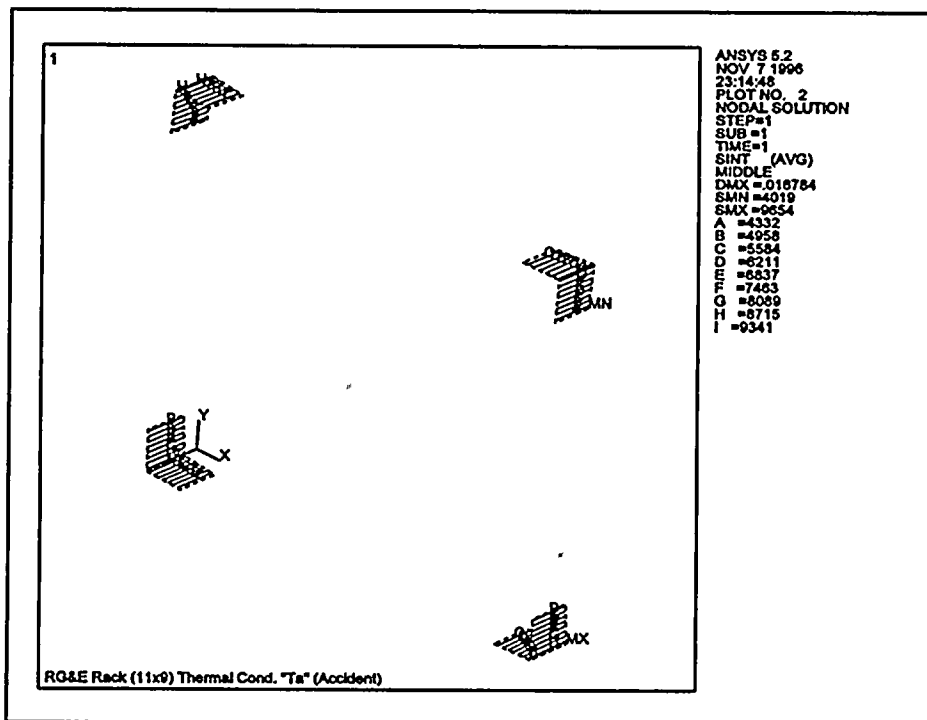


Figure 3.5-70 Bottom Corner Tubes Stress Contours - Ta (Mid Plane)





1. 2. 3. 4. 5. 6. 7. 8. 9. 10.



Figure 3.5-71 Base Plate Stress Contours - Ta (Top Plane)

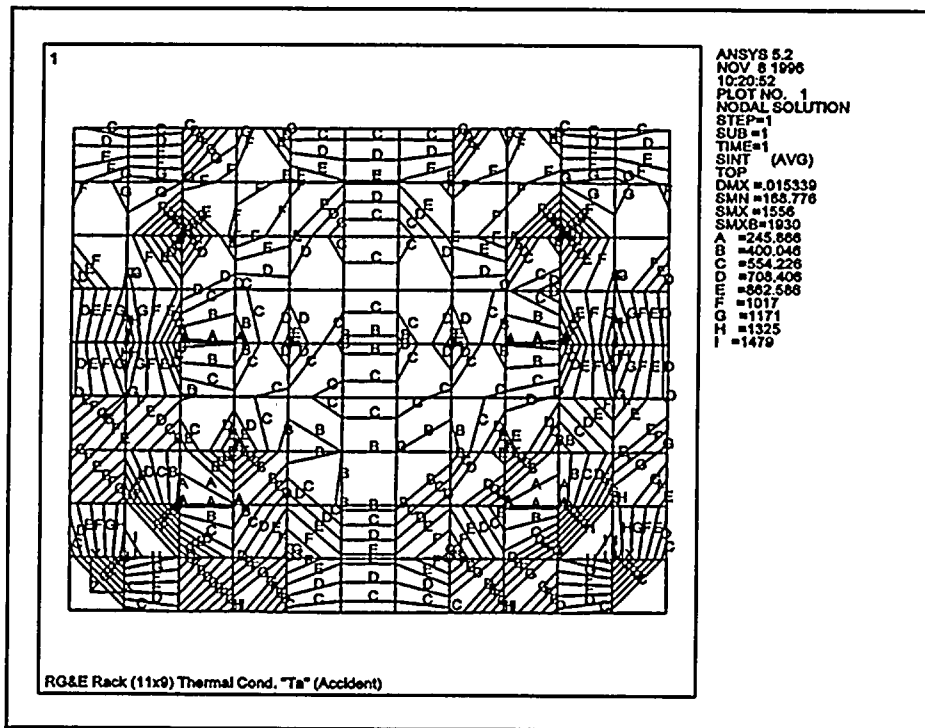
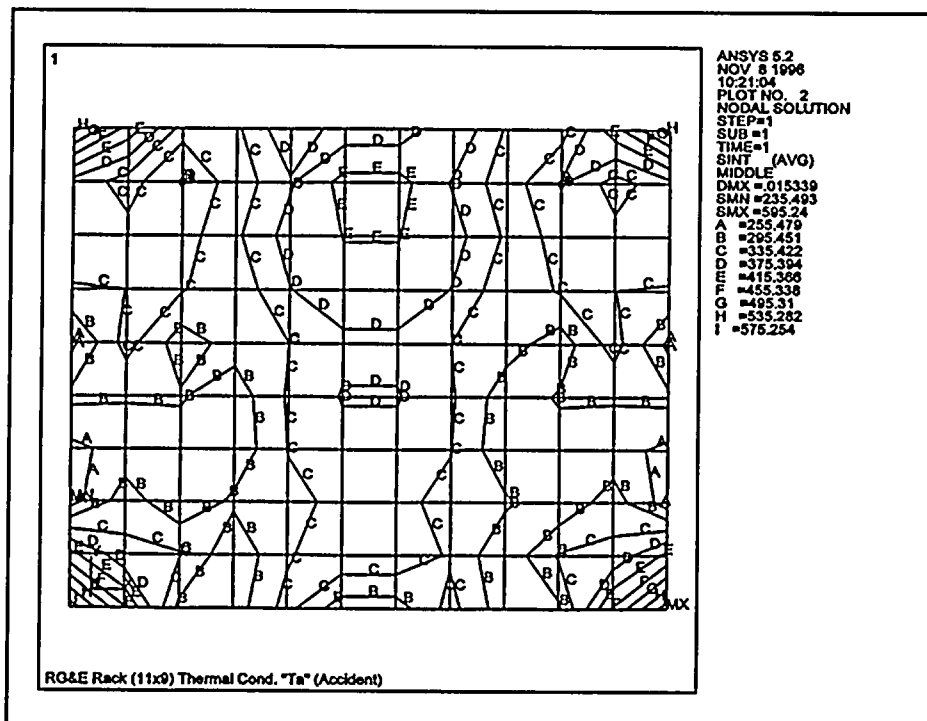


Figure 3.5-72 Base Plate Stress Contours - Ta (Mid Plane)



3.5.3.1.11 Fatigue Analysis

Applicable Codes and Standards - Structural fatigue analysis of the Rochester Gas and Electric's R. E. Ginna Unit 1 high density spent fuel storage racks and spent fuel pool liner is performed here. The design by analysis procedure is employed for qualification. The number of earthquake cycles is per Standard Review Plan, Section 3.7.3, Subsection II.2 (NUREG-0800). The acceptable maximum stress range in various storage rack structures is based on the design criteria given in the American Society of Mechanical Engineers Boiler and Pressure Vessel Code - Section III, Rules of Construction of Nuclear Power Plant Components, Division I, 1989 edition. Hereafter it is referred to as the ASME Code (Reference 3.19). The acceptable maximum stress range in pool liner structures is based on the design criteria given in the American Institution of Steel Construction, Manual of Steel Construction, Part 5- Specification and Codes, Ninth Edition. Hereafter it is referred to as the AISC Code (Reference 3.21).

The fuel storage racks are considered Class 3 component supports and are plate and shell type supports. Design rules given in Subsection NF of the Code are utilized in the evaluation. General requirements concerning stress determination, definitions, derivation of stress intensities, derivation of stress range, and classification of stresses are per Subsections NB and NF of the ASME Code.

Per Subsection NF of the Code, the secondary stresses evaluation is not required for the Class 3 supports. However, as a conservative approach, the range of primary plus secondary stresses is evaluated against the lower of two times yield strength or ultimate tensile strength at the design temperature.

For the pool liner, the definition of 'Loading Condition,' type and location of 'stress category,' and 'allowable stress range' are per Part 5, Appendix K of the AISC Code.

Fatigue Analysis and Methodology - Acronyms

E	Young's Modulus
Fy	Material yield strength
Hz	Hertz, Natural frequency in cycles per second
OBE	Operating Basis Earthquake
SSE	Safe Shutdown Earthquake
Sa	Alternating stress intensity
Sy	Material yield strength
Su	Material tensile strength
U	Cumulative usage factor

Other acronyms are explained where they first appear.

The earthquake stresses are included in the stress analysis. The structure is designed for five Operating Basis Earthquakes and one Safe Shutdown Earthquake (SRP Section 3.7.3, II.2, NUREG-0800).

Review of the natural frequencies of the structure indicates that the majority of the stresses in the structure will be induced during low frequency excitation. The frequency of the racks loaded with fuel assemblies ranges from 7 to 26 Hz (following table). The majority of rack first mode frequencies are less than 20 Hz. The frequency of the empty rack ranges from 24 to 72 Hz. Being of a high frequency structures, the empty racks will behave like a rigid structure. Loaded spent fuel storage racks will induce the majority of stresses. Therefore, most of the stresses in the structure will be induced by a frequency of less than 20 Hz. For a conservative fatigue analysis, the stress cycles are taken at 20 cycles per second.

Spent Fuel Storage Racks - First Mode Frequency

Rack Number	Empty Racks		Racks With Standard Fuel Assemblies		Racks With Consolidated Fuel Canisters	
	East-West Frequency Hz	N-S Frequency Hz	East-West Frequency Hz	N-S Frequency Hz	East-West Frequency Hz	N-S Frequency Hz
1 to 6	60.2	71.7	21.8	26.1	16.7	19.8
2A	38.3	46.4	12.8	15.6	9.8	11.8
2B	40.9	46.2	13.7	15.5	10.4	11.8
3A	30.9	38.6	12.1	15.1	9.3	11.6
3B	29.9	37.5	11.8	14.7	9.1	11.3
3C	23.7	38.5	9.2	15.0	7.1	11.6
3D	23.7	38.5	9.2	15.0	7.1	11.6
3E	30.3	39.8	11.9	15.7	9.1	12.0

Although earthquake motions can be expected to last for a duration of minutes, the strong motion portion of a shock, which is of concern for seismically designed structures, is generally not longer than a few seconds. Of motions based on 60 earthquakes ranging in magnitude from 5.0 to 8.0, the duration of the strong motion portion of these earthquakes ranges from about 1.5 seconds for magnitude 5.0 to about 15 seconds for magnitude 8.0. The average duration of the strong motion portion, however, is only about 2.2 seconds. To be somewhat conservative, it will be assumed that the duration of the strong motion portion will be 5 seconds for the OBE and 20 seconds for the SSE. When compared to the duration of the strong motion records of such earthquakes as the N-S component of the 1940 El Centro and the N 69 W component of the 1952 Taft, this assumed duration of strong motion earthquake is conservative. The high density fuel storage racks are designed for five OBE's and one SSE.

Number of stress cycles = Number of earthquakes x time in second for the strong motion earthquake x Fundamental mode in Hz.

Number of stress cycles during OBE = $5 \times 5 \times 20 = 500$ cycles

Number of stress cycles during SSE = $1 \times 20 \times 20 = 400$ cycles.

Storage Rack Fatigue Analysis - Per Subsection NF of the ASME Code, no peak stress or fatigue evaluation is required for Class 3 supports. However, as a conservative approach, the peak stress range, fatigue evaluation, and cumulative damage are calculated per Subsection NB-3222.4 of the Code.

The range of primary plus secondary stresses is limited to the lower of $2S_y$ or S_u , per ASME Code Section III, Table NF-3522(b)-1, Note 5. The material properties of the rack material are tabulated below at design temperature. The design temperature of the storage rack is 150°F. The material properties given in the ASME Code Section III, Appendix I, are interpolated to get properties at 150°F.

	S_y ksi	S_u ksi	E lb/in ²
ASTM A-240 Type 304L	23.15	63.1	27.9×10^6
ASTM A-479 Type 304L	23.15	68.1	27.9×10^6

The allowable range of primary plus secondary stress (lower of $2S_y$ or S_u at design temperature) is 46.3 ksi.

$$\begin{aligned} \text{Alternating stress } S_a &= \frac{1}{2} (\text{Stress Range}) \\ \therefore S_a &= \frac{1}{2} \times 46.3 = 23.15 \text{ ksi} \end{aligned}$$

The storage rack fatigue analysis is performed per ASME Code Section III, Subsection NB-3222.4. First, the effect of elastic modulus (E) is considered since the E for the fuel storage racks is different from the ASME Code Section III, Figures I-9.2.1, and I-9.2.2. The effect of elastic modulus is considered by multiplying S_a by the ratio of the modulus of elasticity given on the design fatigue curve to the value of the modulus of elasticity of the fuel storage racks.

$$\begin{aligned} S_a &= 23.15 \times (28.3 / 27.9) \\ S_a &= 23.48 \text{ ksi} \end{aligned}$$

In order to ensure that the fatigue analysis is conservative, a stress concentration factor of 4 is applied to S_a .

Therefore:

$$S_a = 4(23.48 \text{ ksi}) = 93.92 \text{ ksi}$$

Figure I-9.2.1 of the ASME Code Section III (Reference 3.19) is used to calculate the allowable number of cycles at the given alternating stress. The number of allowable cycle at 93.92 ksi alternating stress is 2000.

$$\begin{aligned} \text{Cumulative usage factor } U &= n_1/N_1 + n_2/N_2 \\ U &= (500/2000) + (400/2000) \\ U &= 0.25 + 0.20 \\ U &= 0.45 \end{aligned}$$

where U = Cumulative usage factor

n_1 = Number of OBE stress cycles

N_1 = Allowable cycles at OBE S_a

n_2 = Number of SSE stress cycles

N_2 = Allowable cycles at SSE S_a

The cumulative usage factor for the spent fuel storage racks is 0.45 which is less than the limit of 1.0, so the racks meet the requirements of the ASME Code Section III, Subsection NB-3222.4.

Pool Liner Fatigue Analysis - The pool liner fatigue analysis is performed per Part 5, Appendix K of the AISC Code - Ninth Edition. The allowable tensile stress for the liner is $0.6F_y$ (Part 5, Chapter D-1 of the AISC Code). The tensile property for the liner at 150°F is:

ASTM A-240 Type 304 Stainless steel $F_y = 27.5\text{ ksi}$ (Appendix I, ASME Section III)

\therefore Allowable tensile stress is $= 0.6F_y = 0.6 \times 27.5 = 16.5\text{ ksi}$

Stress range $= 2 \times 16.5 = 33\text{ ksi}$

The total number of OBE + SSE stress cycle is 900. These stress cycles are lower than 20,000. Therefore, Load Condition # 1 of the Table A-K4.1 (AISC Code) will be applicable to the pool liner. For the pool liner welded connections, the Stress Category B of the Table A-K4.2 (AISC Code) will be applicable. For Loading Condition #1 and Stress Category B, the allowable stress range is 49 ksi for fatigue strength, per Table A-K4.3 of the AISC Code. Since the pool liner stress range is 33 ksi, the pool liner meets the fatigue requirements of the AISC Code.

Conclusion - Rochester Gas & Electric's R.E. Ginna Unit 1 high density spent fuel storage racks meet the fatigue requirements of the ASME Code Section III, Subsection NB-3222.4, and the pool liner meets the fatigue requirements of the AISC Code, Section 5, Appendix K. All of these hardware have more than adequate fatigue life.

3.5.3.1.12 Rack Base Plate Evaluation

Rack #8 (2B), which is a 9×11 rack, was chosen for the thermal stress calculations since it has the largest plan projection (footprint). As a consequence, this will produce the largest thermal stresses due to the differential thermal growth during the faulted thermal accident, T_a .

The maximum rack loads generated during a seismic event (SSE) were applied to the ANSYS 3D single rack plate model. The fuel load consisted of consolidated fuel canisters (all cells loaded), with the coefficient of friction equal to 0.8. This set of conditions produced the maximum loads in the rack structure, and was used to envelope the maximum base plate stresses for all the new racks. Additional conservatism was introduced into the analysis by constraining all the rack legs. The loads obtained from the rack full pool seismic analysis were taken as the maximum values for each force and moment component (which generally do not achieve their maximums at the same time instant). The use of the individual maximum values assures a conservative combination of rack loads.

The highest stresses in the base plate occur in the vicinity of the supports. The highest loaded legs are the corner legs, which are subjected to compression due to the vertical load (weight) and also due to the maximum bending about the two horizontal axes.

The thermally induced stresses (section 3.5.3.1.10) further increase base plate corner stresses. The base plate membrane stress is shown in Figure 3.5-73, and Figure 3.5-74 shows the corresponding membrane plus bending stress.

The analysis results for the base plate are summarized in the table below:

Load Combination	Max. Stress [psi]	Allowable Stress [psi]
D+L+E+To (Level A)	membrane: 767* memb+bend: 4,286* range of m+b: 10,227	membrane: 15,700 memb+bend: 23,550 range of m+b: 46,300
D+L+E+Ta (Level B)	membrane: 767* memb+bend: 4,286* range of m+b: 5,842	membrane: 20,881 memb+bend: 31,322 range of m+b: 44,080
D+L+E'+Ta (Level D)	membrane: 767 memb+bend: 4,286 range of m+b: 5,842	membrane: 26,448 memb+bend: 39,672 range of m+b: 44,080

(*) Seismic stresses for Level D are reported since they envelop seismic OBE stresses

Figure 3.5-73 Base Plate Membrane Stress Contours

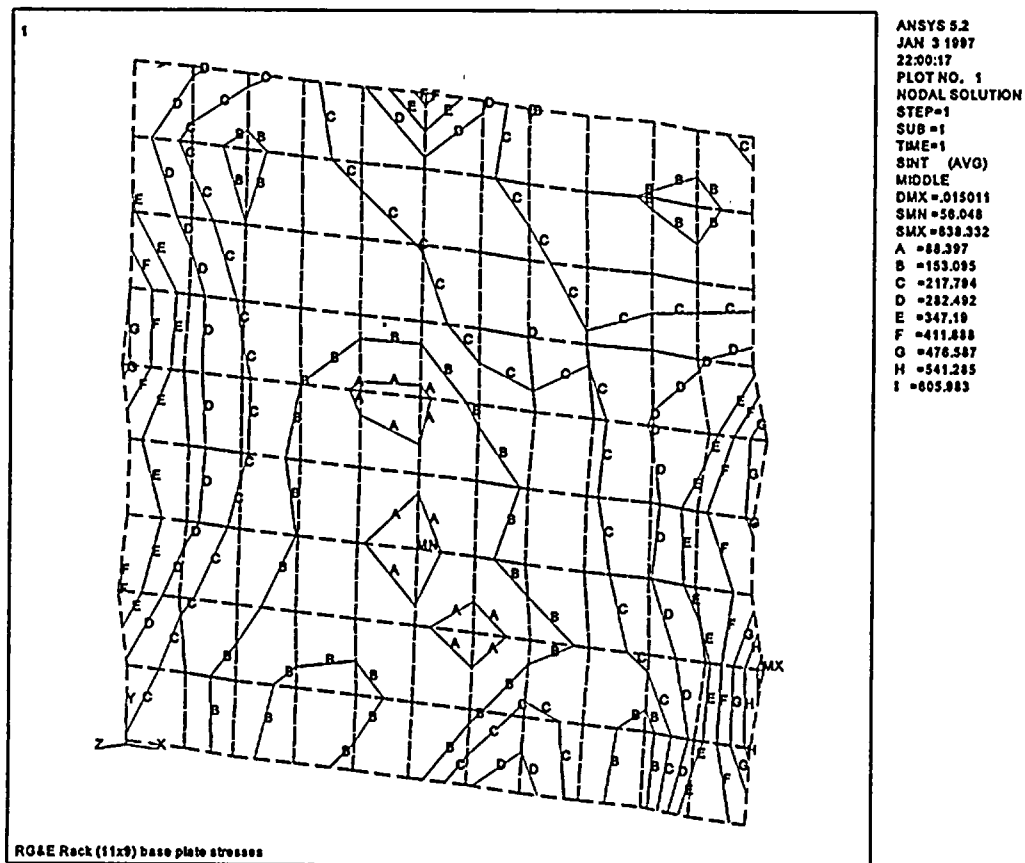
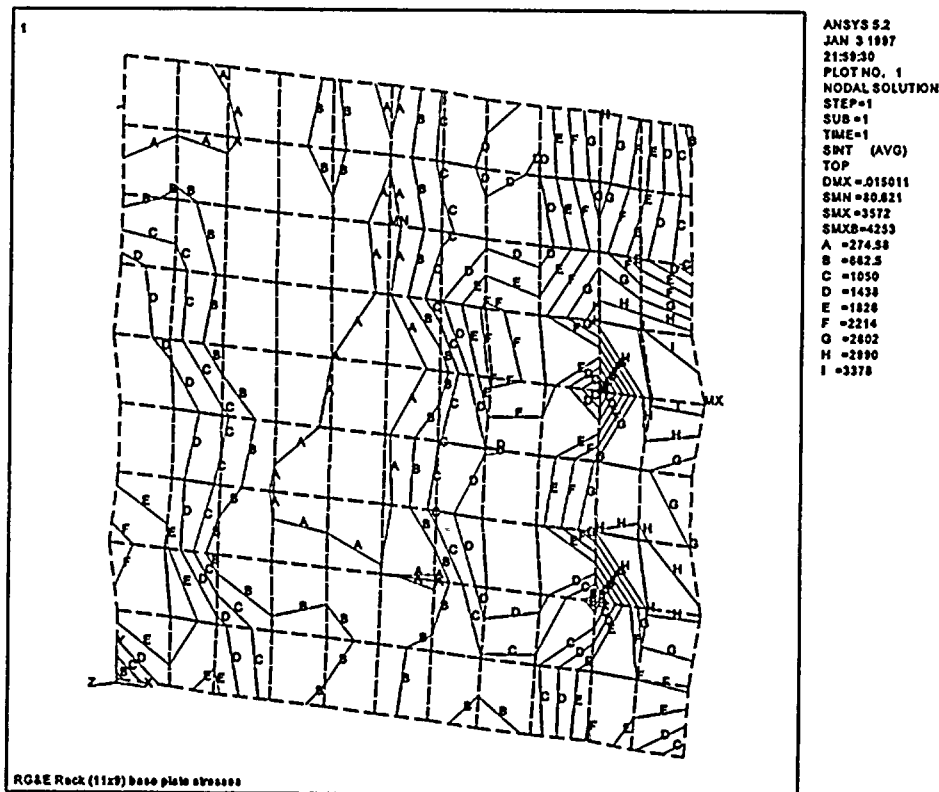


Figure 3.5-74 Base Plate Memb. + Bend. Stress Contours



3.5.3.1.13 Sloshing

This section demonstrates compliance of Rochester Gas & Electric's Ginna spent fuel storage racks with Standard Review Plan - NUREG-0800, Section 3.8.4, Appendix D, Subsection (5), 'sloshing water' requirements. The standard stipulates that the spent fuel assemblies should be in a safe configuration through earthquake including its sloshing effects. Both seismic OBE and SSE conditions are evaluated for the sloshing effects.

Acceptance Criteria:

The safe configuration of the spent fuel assemblies is validated by verifying:

- Change in hydrostatic pressure due to sloshing - impulsive force is negligible.
- Height of sloshing waves is small such that the spent fuel racks will remain submerged in spent fuel water at all times.

Sloshing Analysis

Nomenclature

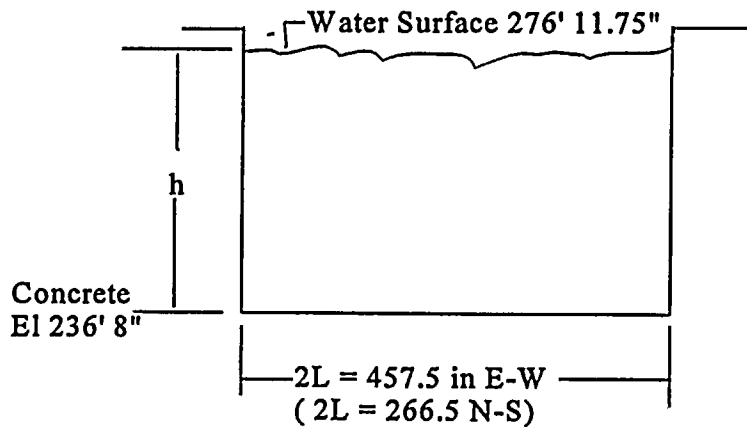
A_1	Maximum displacement of W_1
d_{max}	Maximum water-surface displacement
EBP	Excluding Bottom Pressure
IBP	Including Bottom Pressure
g	Acceleration of gravity
h	Height of water surface above the bottom of pool
h_o, h_1	Vertical distance from the pool bottom to W_o and W_1 respectively
ℓ	One half length of rectangular pool wall
M	Bending moment or overturning moment on horizontal section of pool at the bottom
P_o, P_1	Impulsive and convective forces, respectively
T	Period of vibration
\ddot{u}	Maximum horizontal acceleration of the ground during an earthquake
W	Weight of fluid in a pool
W_o	Equivalent weight of fluid to produce the impulsive force P_o on the pool wall
W_1	Equivalent oscillating weight to produce the convective force P_1 on pool wall
θ_h	Angular amplitude of free oscillations at the water surface
ρ	Mass density of fluid
ω_n	Circular frequency of free vibration for the n^{th} mode

Sloshing:

The method of calculating seismically induced fluid pressure and maximum wave motion has been developed by Housner (TID-7024, Reference 3.27). The method applies to a flat bottomed, vertically oriented tank of uniform rectangular section.

When a tank containing fluid of weight W is accelerated in horizontal direction, a certain portion of the fluid acts as if it were a solid mass of weight W_o in rigid contact with walls and remainder weight W_1 will oscillate. Assuming the tank moves as a rigid body, bottom and walls will undergo the same acceleration. The acceleration induces oscillations of the fluid, contributing additional dynamic pressure on the walls and bottom. The maximum amplitude, A_1 , of the horizontal excursion of the mass determines the vertical displacement, d_{max} , of the water surface, slosh height. Both impulsive pressure and the slosh height are calculated.

Impulsive Pressure:



using equation F.47 (Reference 3.27)

$$P_w = \rho \ddot{u} h \left[\frac{y}{h} - \frac{1}{2} \left(\frac{y}{h} \right)^2 \right] \sqrt{3} \tanh \left(\sqrt{3} \frac{\ell}{h} \right)$$

Where: $\rho = 62.4 \text{ lb/ft}^3$ density of water
 \ddot{u} = horizontal acceleration (zero period acceleration)
 = $0.2g$ for horizontal SSE
 $h = 276' 11 \frac{3}{4}" - (236' 8" + \text{linear thickness})$
 Neglecting liner thickness of $1/4"$

$$h \approx 40.33 \text{ ft}$$

$$2L = \text{East West length of pool} = 457.50" \text{ or } 38.125 \text{ ft.}$$

$$\therefore L \approx 19.1 \text{ ft}$$

$$\frac{\ell}{h} = \frac{19.1}{40.33} = 0.47$$

Impulsive Pressure at $y = h$

$$P_w = \frac{62.4}{g} \times 0.2g \times 40.33 \left[1 - \frac{1}{2} \right] \sqrt{3} \tanh \left(\sqrt{3} \frac{19.1}{40.33} \right)$$

$$\begin{aligned}
&= 435.9 \times \tanh(0.8203) \\
&= 435.9 \times (0.6752) \\
&= 294.3 \text{ lb/ft}^2 \quad \text{or} \quad 2 \text{ psi}
\end{aligned}$$

The maximum pressure on the wall is 2 psi. This reduces to zero at water surface. This is acceptable considering hydrostatic pressure due to height of water 40.33 ft under normal condition.

MAXIMUM WATER-SURFACE DISPLACEMENT - d_{\max} UNDER OBE:

For $\ell/h = 0.474$

$$\begin{aligned}
\frac{W_1}{W} &= 0.527 \frac{\ell}{h} \tanh\left(1.58 \frac{h}{\ell}\right) \quad \text{Equation 6.5 of Reference (3.27)} \\
&= 0.527 \times 0.474 \times \tanh\left(\frac{1.58}{0.474}\right) \\
&= 0.249
\end{aligned}$$

EBP - Excluding bottom Pressure on bottom

$$\begin{aligned}
\frac{h_1}{h} &= 1 - \left[\frac{\cosh\left(1.58 \frac{h}{\ell}\right) - 1}{1.58 \frac{h}{\ell} \sinh\left(1.58 \frac{h}{\ell}\right)} \right] \\
&= 1 - \left[\frac{\cosh\left(\frac{1.58}{0.474}\right) - 1}{\frac{1.58}{0.474} \times \sinh\left(\frac{1.58}{0.474}\right)} \right] \\
&= 0.72
\end{aligned}$$



1. The first part of the document is a list of names and addresses of the members of the committee.

2. The second part of the document is a list of names and addresses of the members of the committee.

Using Equation 6.8 (Reference 3.27)

$$\begin{aligned}\omega^2 &= \frac{1.58 g}{\ell} \tanh \left(1.58 \frac{h}{\ell} \right) \\ &= \frac{1.58 \times 32.2}{19.1} \tanh \left(1.58 \times \frac{40.33}{19.1} \right) \\ &= 2.6569\end{aligned}$$

$$\therefore \omega = \sqrt{2.6569} = 1.63 \text{ rad/sec}$$

$$T = \frac{2\pi}{\omega} = \frac{2\pi}{1.63} = 3.85 \text{ seconds}$$

$$\text{or } f = \frac{\omega}{2\pi} = \frac{1.63}{2 \times \pi} = 0.26 \text{ Hz}$$

From OBE horizontal response spectra at 0.25 Hz at 1/2% damping, the spectra acceleration is 0.0588 g's (derived from 0.08 g's Regulatory Guide 1.60, horizontal spectra, References 3.10, and 3.22).

$$\therefore A_1 = \frac{\text{spectra accln}}{\omega^2} = \frac{0.0588 \times 32.2}{2.6569} = 0.71 \text{ ft}$$

Using Equation 6.9 of Reference 3.27

$$\begin{aligned}\theta_h &= 1.58 \frac{A_1}{\ell} \tanh \left(1.58 \frac{h}{\ell} \right) \\ &= 1.58 \times \frac{0.71}{19.1} \tanh \left(1.58 \times \frac{40.33}{19.1} \right) \\ &= 0.05858 \text{ radian}\end{aligned}$$

Using Equation 6.11 of Reference 3.27:

$$d_{\max} = \left[\frac{0.527 \ell \coth(1.58 \frac{h}{\ell})}{\frac{g}{\omega^2 \theta_h \ell} - 1} \right]$$

$$= \left[\frac{0.527 \times 19.1 \times \coth(1.58 \times \frac{40.33}{19.1})}{\frac{32.2}{2.6569 \times 0.05858 \times 19.1} - 1} \right]$$

$$= 1.026 \text{ ft}$$

Due to sloshing during OBE the water surface will rise and lower by 1.026 feet. The distance from pool water level to top of fuel storage racks is approximately 25 feet. This depth is significantly higher than the sloshing wave (d_{\max}) height. Therefore, spent fuel will remain submerged in the spent fuel pool water throughout the OBE event.

MAXIMUM WATER SURFACE DISPLACEMENT - d_{\max} UNDER SSE:

The frequency of sloshing is the same as that of OBE, i.e., 0.26 Hz. From SSE horizontal response spectra at 0.25 Hz at 1/2% damping, the spectra acceleration is 0.1471 g's (derived from 0.2 g's Regulatory Guide 1.60, horizontal spectra, References 3.11, and 3.22).

$$\therefore A_1 = \frac{\text{spectra accln}}{\omega^2} = \frac{0.1471 \times 32.2}{2.6569} = 1.7828 \text{ ft}$$

Using Equation 6.9 of Reference 3.27

$$\theta_h = 1.58 \frac{A_1}{\ell} \tanh(1.58 \frac{h}{\ell})$$

$$= 1.58 \times \frac{1.7828}{19.1} \tanh(1.58 \times \frac{40.33}{19.1})$$

$$= 0.1471 \text{ radian}$$

Using Equation 6.11 of Reference 3.27:

$$d_{\max} = \left[\frac{0.527 \ell \coth \left(1.58 \frac{h}{\ell} \right)}{\frac{g}{\omega^2 \theta_h \ell} - 1} \right]$$

$$= \left[\frac{0.527 \times 19.1 \times \coth \left(1.58 \times \frac{40.33}{19.1} \right)}{\frac{32.2}{2.6569 \times 0.1471 \times 19.1} - 1} \right]$$

$$= 3.054 \text{ ft}$$

During SSE event the water surface will rise and lower by 3.054 ft. The distance from pool water level to top of fuel storage racks is approximately 25 feet. This depth is significantly higher than the sloshing wave (d_{\max}) height. Therefore, spent fuel will remain submerged in the spent fuel pool water throughout the SSE event.

Sloshing Summary:

During earthquake the pool water will oscillate with frequency of 0.26 Hz (or with a period of 3.85 seconds). During OBE the water surface will rise 1.026 ft. above it's undisturbed level. During postulated OBE event the water will not spill above pool wall. During SSE the water surface will rise and fall 3.054 ft from it's undisturbed level. During both OBE and SSE events, spent fuel will remain submerged in the spent fuel pool water.



3.5.3.1.14 Summary of Gap Closure from Five (5) OBE's Plus One (1) SSE

The cumulative movement of the racks within the pool due to a combination of seismic events is addressed in this section. A total of five (5) OBE events and one (1) SSE event is accounted for. The relative closure between the racks is tabulated for both East-West and North-South directions. The maximum rack displacements occur with the lowest coefficient of friction equal to 0.2, and the racks completely loaded with unconsolidated fuel. The low hydrodynamic coupling values for unconsolidated fuel (versus higher hydrodynamic coupling for the consolidated fuel) combined with the maximum fuel load per rack (full racks) cause the maximum displacements to occur. Therefore, the total closure calculated from this section is taken from loading cases with racks completely loaded with unconsolidated fuel and coefficients of friction equal to 0.2.

The final position of the racks (both translations and rotations) for the OBE events is combined using the SRSS method. The time-history factor for the OBE events (1.12) is then multiplied by the SRSS value for the 5 OBEs. This process is applied to both displacements and rotations.

The maximum motions during the entire SSE event (displacements at the top of the racks) were then used for SSE. The time-history factor of 1.20 was used for the SSE events.

For conservatism, all OBE final relative displacements were taken as "closure", even though many were actually showing an "opening" between the two bodies. Further, to add to the overall conservatism, the relative lateral displacements due to rack rotations were additive for each rack rotation, regardless as to the actual rotations between the two bodies. For example, for small angles of rotation, with two racks rotating the same direction for similar angles, the relative gap between two corners would remain the same. Also the effects of higher hydrodynamic coupling between two bodies that have a smaller gap between them during successive seismic events are not accounted for.

The nomenclature for the following tables are as follows: WW = West Wall, NW = North Wall, EW = East Wall and SW = South Wall.

In conclusion, using a conservative approach, none of the racks impact with any other rack or with the walls during the cumulative effects of 5 OBE's and 1 SSE.

Maximum Gap Closure for 5 OBE's + 1 SSE (With Perimeter Racks)
Horizontal East-West Relative Displacements (in)

Table 3.5-133 Relative Disp. Due to East-West Translation

1st Rack	2nd Rack	1 OBE	5 OBE's	1.12 X 5 OBE's	1 SSE	1.2 X 1 SSE	Total Disp.
WW	1	0.0161	0.0359	0.0402	0.1680	0.2016	0.2418
WW	2	0.0057	0.0127	0.0142	0.1903	0.2284	0.2426
1	3	0.0063	0.0141	0.0158	0.0731	0.0877	0.1035
2	4	0.0079	0.0177	0.0198	0.0924	0.1109	0.1308
3	5	0.0122	0.0273	0.0306	0.0592	0.0711	0.1017
4	6	0.0104	0.0233	0.0261	0.0619	0.0743	0.1004
5	7	0.0239	0.0534	0.0598	0.1595	0.1914	0.2512
5	8	0.0111	0.0248	0.0278	0.2060	0.2472	0.2750
6	8	0.0167	0.0374	0.0419	0.1844	0.2213	0.2632
6	9	0.0216	0.0484	0.0542	0.2151	0.2581	0.3123
6	10	0.0153	0.0343	0.0384	0.1230	0.1476	0.1860
8	11	0.0419	0.0937	0.1049	0.2750	0.3300	0.4349
9	12	0.0009	0.0020	0.0022	0.3473	0.4168	0.4190
10	13	0.0988	0.2209	0.2474	0.1738	0.2086	0.4560
11	EW	0.0333	0.0746	0.0836	0.2076	0.2491	0.3327
12	EW	0.0126	0.0282	0.0316	0.1312	0.1574	0.1890
13	EW	0.1060	0.2370	0.2654	0.1991	0.2389	0.5044

Table 3.5-134 Relative East-West Disp. Due to Rotation

1st Rack	2nd Rack	1 OBE	5 OBE's	1.12 X 5 OBE's	1 SSE	1.2 X 1 SSE	Total Disp.
WW	1	0.0089	0.0199	0.0223	0.0274	0.0329	0.0552
WW	2	0.0144	0.0322	0.0361	0.0308	0.0370	0.0730
1	3	0.0123	0.0275	0.0308	0.0469	0.0563	0.0871
2	4	0.0148	0.0331	0.0371	0.0357	0.0428	0.0799
3	5	0.0055	0.0123	0.0138	0.0485	0.0582	0.0720
4	6	0.0020	0.0045	0.0050	0.0275	0.0330	0.0380
5	7	0.0028	0.0063	0.0070	0.0423	0.0508	0.0578
5	8	0.0035	0.0078	0.0088	0.0510	0.0612	0.0700
6	8	0.0030	0.0067	0.0075	0.0447	0.0536	0.0612
6	9	0.0123	0.0275	0.0308	0.0447	0.0536	0.0844
6	10	0.0032	0.0072	0.0080	0.0480	0.0576	0.0656
8	11	0.0139	0.0311	0.0348	0.0989	0.1187	0.1535
9	12	0.0279	0.0624	0.0699	0.0796	0.0955	0.1654
10	13	0.0050	0.0112	0.0125	0.0844	0.1013	0.1138
11	EW	0.0124	0.0277	0.0311	0.0769	0.0923	0.1233
12	EW	0.0172	0.0385	0.0431	0.0576	0.0691	0.1122
13	EW	0.0033	0.0074	0.0083	0.0591	0.0709	0.0792



Maximum Gap Closure for 5 OBE's + 1 SSE (With Perimeter Racks)
Horizontal North-South Relative Displacements (in)

Table 3.5-135 Relative Disp. Due to North-South Translation

1st Rack	2nd Rack	1 OBE	5 OBE's	1.12 X 5 OBE's	1 SSE	1.2 X 1 SSE	Total Disp.
SW	1	0.0118	0.0359	0.0402	0.2010	0.2412	0.2814
1	2	0.0514	0.0127	0.0142	0.0966	0.1159	0.1301
2	NW	0.0396	0.0141	0.0158	0.2953	0.3544	0.3702
SW	3	0.0168	0.0177	0.0198	0.1514	0.1817	0.2015
3	4	0.0028	0.0273	0.0306	0.0982	0.1178	0.1484
4	NW	0.0141	0.0233	0.0261	0.1699	0.2039	0.2300
SW	5	0.0001	0.0534	0.0598	0.1907	0.2288	0.2886
5	6	0.0227	0.0248	0.0278	0.0799	0.0959	0.1237
6	NW	0.0226	0.0374	0.0419	0.1932	0.2318	0.2737
SW	7	0.0002	0.0484	0.0542	0.3354	0.4025	0.4567
7	8	0.0197	0.0343	0.0384	0.0716	0.0860	0.1244
8	9	0.0342	0.0937	0.1049	0.0994	0.1192	0.2242
9	10	0.0078	0.0020	0.0022	0.0536	0.0643	0.0665
10	NW	0.0069	0.2209	0.2474	0.1410	0.1692	0.4166
SW	11	0.0333	0.0746	0.0836	0.3205	0.3846	0.4682
11	12	0.0395	0.0282	0.0316	0.0429	0.0515	0.0831
12	13	0.0133	0.2370	0.2654	0.0969	0.1163	0.3817
13	NW	0.0070	0.2370	0.2654	0.1313	0.1576	0.4230

Table 3.5-136 Relative North-South Disp. Due to Rotation

1st Rack	2nd Rack	1 OBE	5 OBE's	1.12 X 5 OBE's	1 SSE	1.2 X 1 SSE	Total Disp.
SW	1	0.0056	0.0125	0.0140	0.0173	0.0208	0.0348
1	2	0.0147	0.0329	0.0368	0.0368	0.0442	0.0810
2	NW	0.0091	0.0203	0.0228	0.0195	0.0234	0.0462
SW	3	0.0022	0.0049	0.0055	0.0123	0.0148	0.0203
3	4	0.0025	0.0056	0.0063	0.0154	0.0185	0.0247
4	NW	0.0003	0.0007	0.0008	0.0031	0.0037	0.0045
SW	5	0.0013	0.0029	0.0033	0.0183	0.0220	0.0252
5	6	0.0022	0.0049	0.0055	0.0326	0.0391	0.0446
6	NW	0.0010	0.0022	0.0025	0.0143	0.0172	0.0197
SW	7	0.0011	0.0025	0.0028	0.0182	0.0218	0.0246
7	8	0.0029	0.0065	0.0073	0.0450	0.0540	0.0613
8	9	0.0233	0.0521	0.0584	0.0708	0.0850	0.1433
9	10	0.0239	0.0534	0.0599	0.0801	0.0961	0.1560
10	NW	0.0024	0.0054	0.0060	0.0361	0.0433	0.0493
SW	11	0.0177	0.0396	0.0443	0.1099	0.1319	0.1762
11	12	0.0521	0.1165	0.1305	0.2251	0.2701	0.4006
12	13	0.0391	0.0874	0.0979	0.1996	0.2395	0.3374
13	NW	0.0048	0.0107	0.0120	0.0844	0.1013	0.1133



Maximum Gap Closure for 5 OBE's + 1 SSE (With Perimeter Racks)

Table 3.5-137 Summary of East-West Relative Disp.
Summary of Total North-South Gap Closure (Translation and Rotation)

1st Rack	2nd Rack	Total Trans. Closure	Total Rot. Closure	Total Closure Between	Initial Gap Between Racks	Final Gap Between Racks	Gap Status
WW	1	0.2418	0.0552	0.2970	10.500	10.203	Open
WW	2	0.2426	0.0730	0.3156	9.750	9.434	Open
1	3	0.1035	0.0871	0.1906	1.750	1.559	Open
2	4	0.1308	0.0799	0.2107	1.250	1.039	Open
3	5	0.1017	0.0720	0.1736	0.750	0.576	Open
4	6	0.1004	0.0380	0.1384	0.630	0.492	Open
5	7	0.2512	0.0578	0.3090	0.550	0.241	Open
5	8	0.2750	0.0700	0.3449	0.550	0.205	Open
6	8	0.2632	0.0612	0.3243	0.550	0.226	Open
6	9	0.3123	0.0844	0.3968	3.380	2.983	Open
6	10	0.1860	0.0656	0.2516	3.380	3.128	Open
8	11	0.4349	0.1535	0.5884	0.790	0.202	Open
9	12	0.4190	0.1654	0.5844	0.790	0.206	Open
10	13	0.4560	0.1138	0.5698	0.790	0.220	Open
11	EW	0.3327	0.1233	0.4560	3.270	2.814	Open
12	EW	0.1890	0.1122	0.3012	3.270	2.969	Open
13	EW	0.5044	0.0792	0.5835	3.270	2.686	Open

Table 3.5-138 Summary of North-South Relative Disp.

1st Rack	2nd Rack	Total Trans. Closure	Total Rot. Closure	Total Closure Between	Initial Gap Between Racks	Final Gap Between Racks	Gap Status
SW	1	0.2814	0.0348	0.3162	5.250	4.934	Open
1	2	0.1301	0.0810	0.2111	0.500	0.289	Open
2	NW	0.3702	0.0462	0.4163	5.750	5.334	Open
SW	3	0.2015	0.0203	0.2218	6.000	5.778	Open
3	4	0.1484	0.0247	0.1732	0.750	0.577	Open
4	NW	0.2300	0.0045	0.2344	4.750	4.516	Open
SW	5	0.2886	0.0252	0.3139	7.500	7.186	Open
5	6	0.1237	0.0446	0.1683	0.750	0.582	Open
6	NW	0.2737	0.0197	0.2934	3.250	2.957	Open
SW	7	0.4567	0.0246	0.4813	7.050	6.569	Open
7	8	0.1244	0.0613	0.1856	0.790	0.604	Open
8	9	0.2242	0.1433	0.3675	0.790	0.422	Open
9	10	0.0665	0.1560	0.2225	0.790	0.568	Open
10	NW	0.4166	0.0493	0.4659	1.720	1.254	Open
SW	11	0.4682	0.1762	0.6444	87.740	87.096	Open
11	12	0.0831	0.4006	0.4837	0.790	0.306	Open
12	13	0.3817	0.3374	0.7192	0.790	0.071	Open
13	NW	0.4230	0.1133	0.5363	1.720	1.184	Open

3.5.3.1.15 Borated Stainless Steel Functionality

Borated stainless steel (BSS) is utilized in the ATEA spent fuel pool rack design as the neutron absorber. BSS is an excellent material for use in spent fuel pools and has been used in all of ATEA's racks. While it is an effective neutron poison, it also exhibits high corrosion resistance in the borated water environment of the spent fuel pool. It also exhibits good structural properties in strength and ductility. The ATEA-spent fuel rack designs utilize BSS as a neutron absorber only, and is functionally designed as a non-structural component. The BSS plates are designed to transmit only compressive loads within the structural framework of the racks. No tension or bending loads are transmitted given the inherent cell-to-cell gaps, the specific bearing load transmission features between the BSS and adjacent structural cells, the compliance of the interlocking features of the BSS plates, and the compliance of the non-fixity free-standing conditions of the BSS cell itself.

Interlocking fingers (straight mortises and tenons) machined along the edges of the BSS plates serve a dual purpose. Four individual BSS plates are assembled to form a square tube cell without the use of mechanical (i.e., screws or pins) or fusion (i.e., weld or adhesive) joining processes. The BSS cell slides inside the rack frame cell as an interlocked unit during fabrication. The interlocking fingers are designed such that sufficient clearances are provided to permit the joint to rotate and slip. The joint mitigates fuel assembly impact loading within the BSS cell while maintaining proper finger overlap and sufficient plate engagement. The design tolerances are such that a minimum engagement of one-half of a plate thickness is ensured. While the design provides compliance for internal loads, i.e., fuel assembly impact loads, the mortise and tenon joint maintains the square cell geometry when transmitting loads between the structural cells.

The transmission of lateral loads within the ATEA type 2A-B rack structural frame is achieved through a series of bearing retainer plates and corner tabs welded to the stainless steel cells. The retainer plates also serve to axially constrain the BSS cell within its designated rack cell. Lateral gaps between the BSS and stainless steel integral cell in addition to the non-fixity features of the BSS cell itself serve to mitigate bending loads in the BSS plates.

The transmission of lateral loads between the ATEA type 3A-E rack structural frame and the BSS cells is achieved through a series of stainless steel "bands" located at discrete axial locations along the length of the BSS cells. The band is assembled as two pieces fitting into mortice joints on the BSS plates and then welded to each other to form an integral band around the BSS cell. Given the freestanding boundary conditions of the BSS cell and lateral gaps between the bands and adjacent structural cells, rigid body motion is allowed with negligible bending moments produced in the BSS cell. Transmission of loads are entirely bearing in nature.

The BSS plates are sandwiched between the stainless steel structural cells for the ATEA type 4 racks with the transmission of loads being bearing in nature. Any moment loads due to type 1 rack impact would be in-plane and result in negligible stresses. Impact between the type 4 racks and the pool wall does not exist.

Results from the rack analyses show that subsequent rack frame loads and displacements are insufficient to load the BSS cell in bending or tension.

Dynamic loadings were generated by computer models for the various rack designs. These models included the BSS plates and the various rack component masses. G-force loadings were generated at locations where the bearing retainer plates axially constrain the BSS plates within the type 2 stainless steel rack cell and also at the rack base plate seating surface for the type 3 racks. The retainer plate welds and rack base plate are designed to carry the full vertical dynamic loadings from the BSS plates/cells to the stainless steel rack structure. Analyses contained in the Sections 3.5.3.1.2.5 and 3.5.3.1.12 demonstrate the integrity of the retainer plate weld tabs and baseplate respectively.

Lateral loads and subsequent moments and displacements were also generated for the rack cells. Resulting displacements were small and within the available design gaps. In addition, the BSS plates offer very little resistance due to its lack of restraint at the ends as the plates are only captured and not fixed (welded or pinned) to the rack structure. The in-plane bending (across the width of the plate) displacement due to its own mass is negligible, and bowing along the plate length is precluded by the interlocking fingers with adjacent plates.

Thermal Stresses in BSS

When a freshly discharged fuel assembly is stored in a Borated Stainless Steel (BSS) cell, the BSS plate temperature increases. The temperature distribution is isotropic in each section, so that the BSS cell expands in an isotropic way (without stresses).

The amount of expansion, calculated in a very conservative way (assuming a saturated boiling temperature, 238.9°F, in the BSS cell and only 120°F in the SS cell outside) can be evaluated as follows:

Lateral Expansion:

$$\begin{aligned} &= \alpha(\Delta T)L_1 & \text{Where} & \alpha = 8.872\text{E-}6 \text{ in/in/}^\circ\text{F at } 238.9^\circ\text{F} \\ &= (8.872\text{E-}6)(238.9-120)(8.4) & & L_1 = 8.4 \text{ in. (BSS width)} \\ &= 0.009 \text{ in.} < \text{Existing Gap} = 0.016 \text{ in.} \end{aligned}$$

Vertical Expansion:

$$\begin{aligned} &= \alpha(\Delta T)L_2 & \text{Where} & L_2 = 145.7 \text{ in. (BSS height)} \\ &= (8.872\text{E-}6)(238.9-120)(145.7) = 0.154 \text{ in.} < \text{Existing Gap} = 0.197 \text{ in.} \end{aligned}$$

Therefore, under no circumstances will the BSS be constrained by the surrounding SS cell. Further, an additional gap exists between the notches in the BSS plates due to laser cutting during the manufacturing process.

Therefore, the BSS plates will adequately function as the neutron attenuator and will provide a safe environment for storing spent fuel and fresh nuclear fuel assemblies.

3.5.3.1.16 U.S. Tool & Die Rack Structural Evaluation

Racks 1 through 6 are resident racks and will be kept in the new pool configuration. Those racks are referred as Racks 1 through 6. Those racks have been licensed in the Rochester Gas & Electric's Ginna spent fuel pool, NRC SER dated November 14, 1984, Amendment 65 to License No. DPR-18. Hereafter, this is referred as 1985 Licensing Basis.



1. The following information is being furnished to you for your information only. It is not to be used for any other purpose.

2. The following information is being furnished to you for your information only. It is not to be used for any other purpose.

The gaps in the new configuration are designed such that new ATEA racks do not impact U.S. Tool and Die racks under normal and all seismic conditions. However, due to hydrodynamic coupling, there will be some load transfer between resident and new racks. To establish these loads, the new seismic analysis includes all racks in the pool, in the whole pool model. The new seismic loads are generated for both resident and new racks.

Tables 3.5-139 and -140 provide summary of seismic loads on U.S. Tool and Die racks. The loads are summarized from new analysis and also from 1985 Licensing Basis. Review of these tables indicates that the new seismic loads on U.S. Tool and Die racks and rack support are lower than the original licensing basis. This is true for both OBE and SSE conditions. Therefore, the stresses in the U.S. Tool and Die racks will be lower than the 1985 Licensing Basis.

Table 3.5-139 Seismic Loads on Racks 1 through 6 - at the Base of Rack

	U.S. Tool & Die Analysis 1985 Licensing Basis			New Analysis Without Perimeter Racks Standard configuration			New Analysis With Perimeter Racks Extended Configuration		
	Fx lbs	Fy lbs	Fz lbs	Fx lbs	Fy lbs	Fz lbs	Fx lbs	Fy lbs	Fz lbs
Operating Basis Earthquake									
Standard Fuel	156,200	170,000	411,133	43,971	70,896	230,700	39,998	70,429	253,875
Consolidated Fuel	153,000	160,200	451,146				48,436	103,952	443,316
Mixed Fuel							28,896	47,966	254,084
Safe Shutdown Earthquake									
Standard Fuel	164,300	231,500	475,723	88,832	126,000	328,920	91,248	122,074	332,543
Consolidated Fuel	184,700	239,300	565,564	85,776	176,640	558,600	80,999	163,138	555,543
Mixed Fuel							69,395	110,225	552,970

Notes:

1. Reported results with perimeter racks are ratioed from analysis results to reflect maximum 138 fuel assemblies in Racks 1 through 6.
2. Maximum loads among Racks 1 through 6 are reported.
3. Empty spaces in the above table means, the results from other case envelopes this loading configuration.
4. The X direction is East, the Y direction is North and the Z direction is vertical.

Table 3.5-140 Seismic Support Pad Load on Racks 1 through 6 Load on Each Pad

	U.S. Tool & Die Analysis 1985 Licensing Basis		New Analysis Without Perimeter Racks Standard Configuration		New Analysis With perimeter racks Extended Configuration	
	Horizontal lbs	Vertical lbs	Horizontal lbs	Vertical lbs	Horizontal lbs	Vertical lbs
Operating Basis Earthquake						
Standard Fuel	115,432	205,567	24,584	122,976	22,818	114,145
Consolidated Fuel	110,762	225,573			23,873	169,285
Mixed Fuel					17,513	118,426
Safe Shutdown Earthquake						
Standard Fuel	141,939	237,862	87,636	193,440	78,324	172,761
Consolidated Fuel	151,144	282,782	103,596	250,680	76,601	246,162
Mixed Fuel					52,086	193,349

Notes:

1. Reported results with perimeter racks are ratioed from analysis results to reflect maximum 138 fuel assemblies in Racks 1 through 6.
2. Maximum loads among Racks 1 through 6 are reported.
3. Empty spaces in the above table means, the results from other case envelopes this loading configuration.

Summary

The loads and stresses in the U.S. Tool and Die racks are lower than the 1985 Licensing Basis. Therefore, the U.S. Tool and Die racks meets the structural acceptance criteria.

3.5.3.1.17 Spent Fuel Pool and Liner Structural Evaluation

This section demonstrates compliance of RG&E Ginna Unit 1 spent fuel pool and pool liner structural integrity with the requirements of NUREG-0800, Standard Review Plan 3.8.4, Appendix D requirements. The spent fuel pool evaluation is based on a conservative interpretation of the American Concrete Institute's Code Requirements for Nuclear Safety Related Concrete Structures ACI 349-85 (Reference 3.20). The pool liner evaluation is based on a conservative interpretation of the American Institute of Steel Construction's Building Code AISC-9th Edition (Reference 3.21).

The design of new high density storage racks is such that it preserves the original licensing basis (NRC SER dated November 14, 1984), here after referred to as the 1985 licensing basis, for the spent fuel pool liner and pool concrete. The new ATEA storage racks are free standing racks, and they are supported on the pool floor only. The gaps between the rack and the pool are designed such that the new racks do not impose any additional loadings on the pool wall. These conditions are verified throughout the analysis. The new racks are high density storage racks and they will store more fuel. The number of support legs are designed such that the new racks do not impose any higher loading to the pool liner or the pool concrete. This also verified during analysis. The support legs are positioned on the liner such that they are away from the liner weld seams.

The pool and the liner temperatures are kept the same as the original design basis. Therefore, there are no additional thermal loadings on the pool or the liner. The pool water level is kept the same as the original design basis. Therefore, there are no additional hydrostatic or hydrodynamic loads on the pool or the liner.

This design requires, only, verification of bearing loads on the liner and concrete.

Acceptance Criteria - Spent Fuel Pool Liner

The spent fuel pool liner is designed to AISC Code. The storage rack support pads are designed such that they do not rest on liner weld seam. The support pads primarily induce bearing loads on the liner.

- The redesign only changes floor bearing loads
- Bearing Allowable $0.9 F_y$ Per AISC
- Liner Fatigue Analysis per AISC, Appendix K

Acceptance Criteria - Spent Fuel Pool Concrete

The spent fuel pool concrete is designed per requirements ACI 349-85. The storage racks being free standing structure, primarily induces bearing load on concrete at support pad locations. The redesign only changes floor bearing loads.

Bearing Allowable $\phi (0.85 f_c)$ Per ACI 349, Section 10.15

- Demonstrate that there are no rack-to-wall impacts

Pool Liner Evaluation

The pool liner bearing stress analysis is performed in Section 3.5.3.1.9.1.2. Table 3.5-131 presents the results of the stress analysis. The results indicate that there is a large margin against AISC Code allowable. Section 3.5.3.1.11 presents the result of the pool liner fatigue analysis. The results indicate that the pool liner meets the fatigue requirements of the AISC Code, Ninth Edition, Section 5, Appendix K, and the liner has adequate fatigue life.

Therefore, the structural integrity of the liner is maintained.

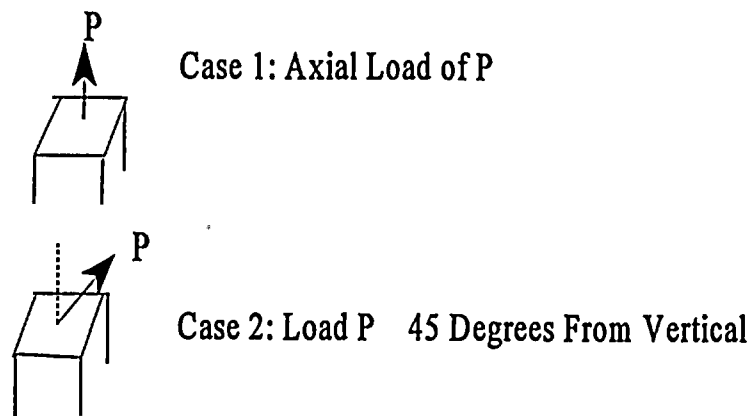
Spent Fuel Pool Structural Evaluation

This vertical reaction is transferred directly downward to the concrete through the liner plate. The maximum applied concrete bearing stresses for all load combinations is less than 3,570 psi. The maximum bearing stresses and the comparison of maximum bearing stresses to allowable are presented in Section 3.5.3.1.9.1.2, which indicates an adequate margin against the ACI 349-85 Code. Therefore, the structural integrity of the spent fuel pool is maintained.

3.5.3.1.18 Stuck Fuel Assembly - Uplift Force

This section demonstrates compliance of Rochester Gas & Electric's Ginna spent fuel storage racks with Standard Review Plan - NUREG-0800, Section 3.8.4, Appendix D, 'upward force on the racks caused by postulated stuck fuel assembly' requirements. The standard for the stuck fuel assembly condition stipulates that the spent fuel racks so designed and constructed such that, if maximum uplift force of the spent fuel crane is applied, the stresses in the rack should be within service Level B stress of ASME Section III, Subsection NF (Reference 3.19).

Two postulated events are considered, namely:



Acceptance Criteria:

The Standard Review Plan 3.8.4, Appendix D (Reference 3.4) provides the load combination to be considered and acceptable stress limits for this load combination. The load combination per SRP 3.8.4 is:

$$D + L + T_o + P_f$$

Where:

- D is dead weight load, these are negligible at the top of rack.
- L is live load, these are zero since there is no live load
- T_o is normal condition thermal load and is negligible at the top of tube
- P_f is upward force on the racks caused by postulated stuck fuel assembly.

The allowable stress limits are the Level B stress limits per ASME Section III, Subsection NF for Class 3 component supports (Reference 3.19). These limits per NF-3251 and Table NF-3552(b)-1 are:

Primary membrane stress	1.33 S
Primary membrane plus bending stress	1.995 S

The structural tubes are fabricated from ASTM A240 Type 304L material. The S value at 150° F from ASME Section III, Appendix I, Table I-7.2 is 15.7 ksi (Reference 3.19). Therefore, the allowable stress for this condition are:

Primary membrane stress	$1.33 \times 15.7 = 20.881 \text{ ksi}$
Primary membrane plus bending	$1.995 \times 15.7 = 31.322 \text{ ksi}$

Stuck Fuel Assembly - Uplift Analysis

There are two one-ton hoists on the fuel handling bridge. One extends on each side of the bridge (East and West). Only one hoist is used to remove a stuck fuel assembly.

Therefore, the total uplift force $P = 2,000 \text{ lbs}$

Fuel cell - Structural Tube Cross Section Properties:

	Type 2 and Type 4 Racks	Type 3 Racks
Tube outside dimension (2 x c)	8.2992 in	8.496 in
Tube inside dimension	8.1417 in	8.3386 in
Tube thickness - t	0.0787 in	0.0787 in
Tube cross section area - A	2.59 in ²	2.65 in ²
Tube moment of inertia - I	29.17 in ⁴	31.29 in ⁴

For a given load, the stresses in the Type 2 (and Type 4) rack tubes will be highest, due to lower cross section properties. The following analysis is performed for Type 2 Rack structural tubes, and the results will be applicable to Type 3 and type 4 racks also.

Case 1: Vertical Uplift Force

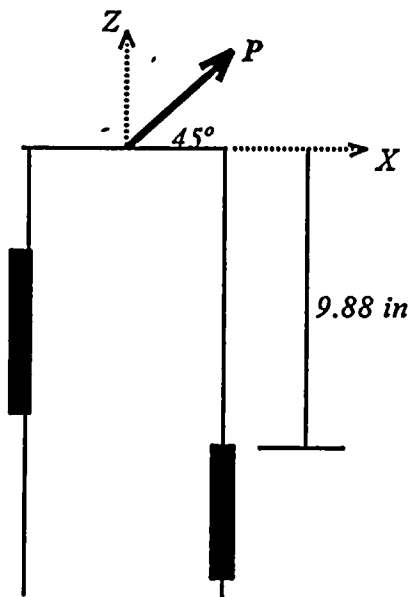
The vertical $P = 2,000 \text{ lb}$ force will produce axial stress in the tube.

$$\begin{aligned}
 \sigma_A &= \text{Load} / \text{Cross Section Area} \\
 &= P / A \\
 &= 2,000 / 2.59 \\
 &= 772 \text{ psi} < 20,881 \text{ psi (Primary membrane allowable 1.33S at 150° F)}
 \end{aligned}$$

$$\begin{aligned}
 \text{Design Factor} &= [(\text{Allowable} - \text{Actual}) / \text{Actual}] \times 100 \\
 &= [(20,881 - 772) / 772] \times 100 = 2,605\% \quad \therefore \text{Large margin}
 \end{aligned}$$



Case 2: Uplift Force 45 Degree From Vertical Axis



The $P = 2,000$ lb is applied 45 degrees from vertical.

$$F_x = 2,000 \times \cos 45^\circ = 1414.2 \text{ lb}$$

$$F_z = 2,000 \times \sin 45^\circ = 1414.2 \text{ lb}$$

For bending moment, conservative moment up to the second tab is used,

$$L = 9.88 \text{ inch}$$

$$\begin{aligned} \text{Bending moment } M &= F_x \cdot L \\ &= 1414.2 \times 9.88 \\ &= 13,972 \text{ in.lb} \end{aligned}$$

$$\sigma_{\text{bend}} = \frac{M c}{I} = \frac{13,972 \times \frac{8.2992}{2}}{29.17} = 1,988 \text{ psi}$$

$$\sigma_{\text{axial}} = \frac{F_z}{A} = \frac{1414.2}{2.59} = 546 \text{ psi}$$

$$\begin{aligned} \text{Membrane plus bending stress} &= 1,988 + 546 \\ &= 2,534 \text{ psi} < 31,322 \text{ psi, 1.995S for 304L at } 150^\circ \text{ F} \end{aligned}$$

$$\begin{aligned}\text{Design Factor} &= [(\text{Allowable} - \text{Actual}) / \text{Actual}] \times 100 \\ &= [(31,322 - 2,534) / 2,534] \times 100 = 1,136\% \therefore \text{Large margin}\end{aligned}$$

The weld stresses in the (BSS) upper retainers are calculated in Section 3.5.3.1.2. The stresses in all other hardware e.g., tabs, base plate, tube to base plate weld, support legs, etc., are much lower than the fuel tube stresses calculated here.

Conclusion:

Rochester Gas & Electric's Ginna Unit 1 high density spent fuel storage racks meets the Level B stress limits of ASME Section III, Subsection NF, Class 3 component support requirements for stuck fuel assembly - maximum uplift force. The design has minimum margin of safety of 11.4 against allowable stress.

3.5.3.1.19 Storage Rack Lifting Analysis

This section demonstrates compliance of existing Region 1 resident Wachter storage racks and new ATEA storage racks with NUREG-0612 (Reference 3.16), heavy load lifting requirements. The standard for NUREG-0612 heavy load lifting requirements stipulates that the structure to be lifted be designed and constructed such that it has a minimum specified safety factor to preclude drop of structure on any safety related system or equipments at nuclear power plants. Existing Region 1, three Wachter racks will be removed from the spent fuel pool and seven new ATEA racks will be placed in the spent fuel pool.

Four lifting points, at the bottom plate, are provided on each rack. The lifting points are diagonally across from each other. Each lifting beam-cable can be attached to diagonally opposite lifting point. This facilitates either redundant or non-redundant lifting. The single failure proof, 30-ton auxiliary building crane will be used to lift resident racks from the spent fuel pool and to lift new ATEA racks into the spent fuel pool.

Each rack weighs more than one fuel assembly plus the fuel handling tool. For this reason, the racks are classified as heavy load per NUREG-0612 criteria. Analysis is performed for each rack to ensure compliance with the lifting requirements of NUREG-0612. The lifting acceptance criteria is:



NUREG-0612 (Control of Heavy Loads at Nuclear Power Plants), Section 5.1.6 (Reference 3.16)

	Safety Factor	Design Criteria
Redundant Lift	5	Ultimate
Non-redundant Lift	10	Ultimate

The lifting stress analysis is performed for existing Region 1 Wachter storage racks and the new ATEA storage racks. The results are summarized in the following table:

	Materials of Construction	Dry Weight lb	Lifting Stress S psi	Material Tensile Strength Su at 150° F	Safety Factor Su / S
Wachter Racks (These racks will be removed from the pool)					
Type A3 Rack	304 SS	31,366	1,105	73,000	66
Type B Rack	304 SS	26,533	964	73,000	76
Type C Rack	304 SS	23,453	550	73,000	133
ATEA Racks (These racks will be installed in the pool)					
Type 2B Rack*	304L SS	19,341	4,780	68,100	14

* Stresses in Rack 2B envelopes all other new ATEA racks. Stresses are developed using very conservative point load application.

An adequate margin exists for lifting existing Region 1 Wachter storage racks and new ATEA storage racks for either redundant or non-redundant lifting.

3.5.3.2 Accident Conditions

Mechanical Accident Evaluation

This section demonstrates compliance with RG&E's Ginna spent fuel storage system with the Standard Review Plan - NUREG-0800, Appendix D, hypothetical accident condition requirements. The standards for hypothetical accident conditions stipulate that the spent fuel storage system be so designed and constructed such that, if it is subject to the specified accident conditions, spent fuel assemblies should remain in safe configuration. This means, a) the off-site radiation dose should be within regulatory limit; and b) the fuel should remain subcritical.

The major hypothetical accident conditions evaluated are:

- a) Fuel assembly drop during fuel handling in the spent fuel pool
- b) Spent fuel pool canal gate drop
- c) Spent fuel pool storage rack drop
- d) Tornado missile impact
- e) Spent fuel cask drop

Several of these hypothetical conditions are eliminated by administrative procedure and/or by the use of a single-failure proof lifting system. Assessment of other conditions was performed by structural analysis. Well proven classical methods were used in the performance of these analyses.

Detailed information supporting these analyses are presented here.

3.5.3.2.1 Methodology and Assumptions

The basis for these analyses is an equating of the kinetic energy of the falling missile at impact with the elastic and plastic strain energy; i.e., an energy balance.

The evaluation of the various accidents was based upon the conservative assumption that under stress from a uniform vertical load, the structural tubes will reach compressive yield using a reduced effective tube area. In order to judge the reasonableness of methodology, two results should be established; namely ductility factor and total deformation. The ductility factor is defined as the ratio of total strain to plastic strain. The total deformation is calculated directly from the energy balance. The elastic and plastic strains are based upon the deformations and the height of the target structure. The greater the height of the target structure, the lesser will be the plastic strain. The target structure is selected as that portion of the racks above the borated stainless steel. Therefore, the calculated plastic strains and hence ductility factors are very conservative.

For drops onto the top surface of the racks, the checkerboard pattern means that the number of structural tubes is about one half of the number of storage cells. As the dropped object impacts the top of the racks, the affected tubes yield. However, the effect does not remain localized and will spread to the surrounding tubes through the strong interconnection provided by the welded connecting tabs. The assumption of the spreading of load only to immediately adjacent tubes is very conservative. Sufficient interconnecting tabs are used to prevent general or local elastic buckling

of the tubes. This design provides for capacity to accommodate the various drop accidents. The extent of compressive yield was determined after completion of the various load drops. The stress values for buckling were determined and found to be sufficiently high.

The hydrodynamic effects have been neglected in the accident drop analyses to provide conservative results. In addition, no benefit is taken for deformation or energy absorption of the falling object.

3.5.3.2.2 Acceptance Criteria

The standards for the hypothetical accident conditions stipulate that the spent fuel storage system be designed and constructed such that, if it is subject to the specified accident conditions, spent fuel assemblies should remain in safe configuration. This means, a) the off-site radiation dose should be within regulatory limit; and b) the fuel should remain subcritical. This has been verified by confirming function capability of spent fuel storage racks and the spent fuel pool as follows:

Straight Deep Drop

The falling fuel assembly is stopped prior to impinging upon the fuel pool floor liner.

Straight Deep Drop Onto Support Leg

The load transmitted to the concrete will not result in crushing of concrete so as to prevent an uncontrollable leak in the pool.

Shallow Drops and Tornado Missile Impact

The acceptance criteria for top of rack impacts are that the required inelastic deformation must be less than 10% of the length of the deforming structural mechanism and that the ductility factor remains less than 20 (per Table 4-4 of Reference 3.32). The ductility factor of 20 as a limit has been accepted by NRC Staff in review of Bechtel Topical Report, BC-TOP-9A, Revision 2, September 1974. Significant distortion of the cells will be limited to the footprint of impact and the adjacent fuel cells.

3.5.3.2.3 Fuel Assembly Drop Analysis

For hypothetical fuel assembly drops, four cases were examined:

- a) Straight deep drop through cell.
- b) Same as above, except a support leg is present at the base of the cell.
- c) Shallow drop in which a dropped assembly strikes the top of a rack and falls flat on top of the rack.
- d) Shallow drop in which a dropped assembly strikes the top of a rack in a vertical position.

Unconsolidated, fuel assembly drops were evaluated for the conditions outlined above. The canister containing consolidated fuel (weighing 2,638 lb) is considered heavy load per NUREG-0612 criteria and will be transported within spent fuel pool using a special tool suspended from a single failure proof auxiliary building crane. In a safety evaluation report dated December 31, 1984 the NRC Staff reviewed and approved modifications to the auxiliary building crane in order to meet the crane single-failure criteria of NUREG-0612 and NUREG-0554. Therefore, handling of consolidated fuel will be performed in accordance with the guidelines of NUREG-0612 with regard to limiting the chance of unacceptable heavy load drop (reference "NRC Staff Safety Evaluation Supporting

Amendment 12 to Facility Operating License No. DPR-18, RG&E Ginna, Docket 50-244," dated December 16, 1988).

Design Parameters for Fuel Assembly Drop Analyses:

The requirements of the accident are that a fuel assembly, along with the handling tool, drops from an operating height.

Weights

	Weight in air Lbs	Weight in water Lbs
Fuel Assembly with control components	1450	1307
Fuel handling tool	<u>324</u>	<u>284</u>
Total	1774	1591

Maximum fuel assembly height above racks during fuel handling	12 inch
Height of the fuel assembly	160 inch

For deep drops, the drop height (160 + 12)	172 inch
For shallow drops, the drop height	12 inch

304L Stainless Steel material properties at 150° F (from ASME Section III, Appendix I)

Young's Modulus	$E = 27.9 \times 10^6 \text{ lb/in}^2$
Yield strength	$S_y = 23,150 \text{ psi or } 23.15 \text{ ksi}$
Ultimate Strength	$S_u = 68,100 \text{ psi or } 68.1 \text{ ksi}$

3.5.3.2.3.1 Fuel Assembly - Straight Deep Drop

For this hypothetical accident drop of the fuel assembly deep drop two cases were analyzed. The first is the drop through the cell and impacting on the bottom plate remote from any support legs. The second case is the deep drop inside through the fuel cell containing the support leg.

The following applies equally to Type 2, Type 3 and Type 4 racks for both of these drops.

Weight of fuel assembly + weight of handling tool = 1,591 lbs or 1.591 kips
Drop height 172 inch

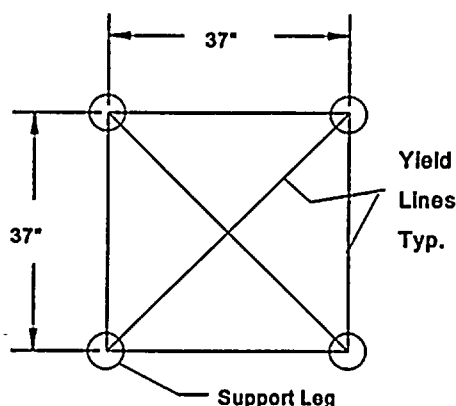
Bottom plate thickness 1.18 inch

3.5.3.2.3.1.1 Fuel Assembly Falls Through Cell to Base Plate

Impact Energy: $IE = W \times d$
 $IE = 1.591 \times 172 = 273.652 \text{ in-kips}$

Type 2 and Type 3 Racks

The drop in the middle between support legs will produce maximum deformation of the rack. In effect, a two-way slab develops. The approximate spacing of adjacent support legs is 4 x pitch of 9.2323 for type 3 racks (~ 37 inches). The Type 3 rack is limiting, because the maximum spacing between the support legs is in the Type 3 Rack. The results presented below will envelope Type 2 racks.



During 172 inch fuel assembly drop impact, the welds connecting the tube to the base plate will fail. The base plate will detach from the cells in a 37" x 37" region. The 37" x 37" plate will have support at the four legs and also will have a support from remaining plate. This means the edges will have fixed support. For conservatism, the energy absorbed in breaking welds is neglected. All kinetic energy is absorbed in forming plastic hinges of the 1.18 inch thick bottom plate. The plastic hinge lines are shown in above figure.

For fully plastic hinge of a plate $M_{pl} = (\sigma_y t^2) / 4$

$$M_{PL} = 8.059 \text{ in-kips/in}$$

where M_{PL} = Plastic Moment

$t = 1.18$ inches, thickness of the bottom plate

$\sigma_y = 23.15$ ksi at 150° F for 304L Stainless Steel

For a 37" x 37" two way flat plate.

$$P = 16 m_{PL} = 128.9 \text{ kips Fully Plastic Load}$$

External energy = Internal energy

$$W d = P \delta$$

$$\delta = 273.652 / 128.9 = 2.12 \text{ inch} < 13.7 \text{ inch} \therefore \text{O.K.}$$

Where 13.7 is the distance between the bottom plate and the pool liner. Therefore, the deformed plate will not impact the pool liner.

$$\delta = \frac{b}{2} \theta \text{ where } b = 37 \text{ inches}$$

$$\theta = 0.1146 \text{ radians}$$

$$\epsilon_{\text{bend}} = \frac{\Delta L}{L} = \left[\frac{(t / 2) \theta}{b / 4} \right]$$

$$\text{Bending Strain } \epsilon_{\text{bend}} = 0.007$$

where t = thickness of plate 1.18 inch

$L = b/4$ there will be four plastic moments in length b , $\therefore L = b/4$

$b = 37$ inch spacing between support legs

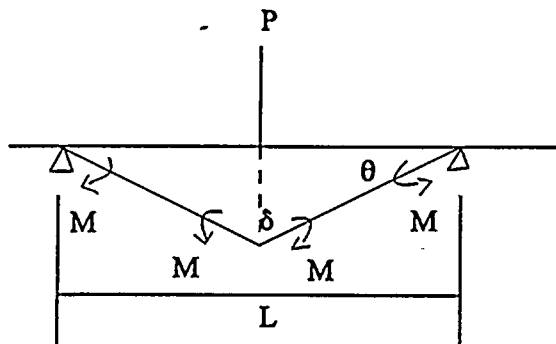
For 2.12 inch deformation of bottom plate, the falling object or the bottom plate will not impact the pool liner. ASTM Specification A 240-93a, Table 2 specifies a minimum elongation of 40% for Type 304L stainless steel material. The type 304L material is ductile and has adequate margin to accommodate 0.007 strain during fuel assembly drop. A major conservatism is to neglect the energy required to fail all the base welds in a 37" x 37" area of base plate.



and about the same number of people are now living in the same place as they were in 1950. The population of the world is now about 2.5 billion people, and it is expected that it will reach about 4 billion people by the year 2050. This is a very large increase in population, and it is a very rapid increase. It is a very rapid increase in population, and it is a very rapid increase in population.

Type 4 Racks

A drop in the middle between support legs will produce maximum deformation of the rack. The spacing of adjacent support legs is 5 x pitch of 8.43 for Type 4 racks ($L = 42.15$ inches).



During 172 inch fuel assembly drop impact, the welds connecting the tube to the base plate will fail. The base plate will detach from the cells. The 42.15" plate will have support at the two legs. This means the edges will have fixed support. For conservatism, the energy absorbed in breaking welds is neglected. All kinetic energy is absorbed in forming plastic hinges of the 1.18 inch thick bottom plate with 1.97 inch thick web. The base plate with 1.97 inch thick web forms a T cross section beam. The plastic hinge lines are shown in above figure.

For fully plastic hinge of the base plate (T Cross Section)

$M_{PL} = Z \sigma_y$ where Z is the plastic section of modulus.

$$Z = 34.15 \text{ in}^3$$

For fully plastic hinge of a plate $M_{PL} = 34.15 \sigma_y$

$$M_{PL} = Z \sigma_y = 790.5725 \text{ in-kips}$$

where $\sigma_y = 23.15 \text{ ksi}$ at 150° F for 304L Stainless Steel

For a simply supported beam:

$$\frac{P}{2} \delta = \Sigma M_{PL} \theta = 2 M_{PL} \theta$$

$$\delta = (L/2) \theta$$

$$P L = 8 M_{PL}$$

Loads required to form fully plastic hinge:

$$P = 150.05 \text{ Kips}$$

Equating Internal Strain Energy to the Kinetic Energy

External energy = Internal energy.

$$W d = P \delta$$

$$273.652 = 150.05 \delta$$

$$\delta = 273.652 / 150.05 = 1.82 \text{ inch} < 7.8 \text{ inch} \therefore \text{O.K.}$$

Where 7.8" is the distance between the bottom web and the pool liner. Therefore, the deformed beam will not impact the pool liner.

$$\delta = \frac{L}{2} \theta \text{ where } L = 42.15 \text{ inches}$$

$$\theta = \delta \frac{2}{b}$$

$$\theta = 0.0864 \text{ radians}$$

$$\epsilon_{bend} = \frac{\Delta L}{\text{Length}} = \left[\frac{c \theta}{L / 4} \right]$$

$$\text{Bending Strain } \epsilon_{bend} = 0.0342$$

where $c = 4.165"$ distance between neutral axis and outermost fibre

Length = $L/4$ since there will be four plastic moments in between supports, \therefore Length = $L/4$

$L = 42.15$ inch spacing between support legs

For 1.82 inch deformation of bottom plate, the falling object or the bottom plate will not impact the pool liner. ASTM Specification A 240-93a, Table 2 specifies a minimum elongation of 40% for Type 304L stainless steel material. The Type 304L material is ductile and has adequate margin to accommodate 0.0342 strain during fuel assembly drop. A major conservatism is to neglect the energy required to fail the base welds between fuel cell and bottom plate.



ALL INFORMATION CONTAINED HEREIN IS UNCLASSIFIED EXCEPT WHERE SHOWN OTHERWISE

3.5.3.2.3.1.2 Fuel Assembly Drops into Cell and Strikes Support Leg

For this hypothetical fuel assembly deep drop, the fuel assembly drops through the fuel cell onto the support leg.

The external energy at the point of contact: $W h = 1.591 \times 172 = 273.652$ in-kips

At this energy, the support leg female threads will shear first. The female threads are in 304L stainless steel tube, where as the male threads are in high strength ASTM-A564 Type 630 stainless steel. The tensile strength of 304L tube bar material is 68.1 ksi, whereas for the 630 precipitation hardened steel is 140 ksi. Therefore, the female threads will strip first.

<u>Hardware</u>	<u>Material</u>	<u>σ_u at 150° F</u>
Cylinder	304L SS	68.1 ksi
Threaded Rod	A564, Type 630	140
Neck down Portion	A564, Type 630	140
Support pad	F304L	63.25

Shear area of internal threads: (From Machinery's Handbook, 23rd Edition, page 1279)

$$A_n = 3.1416 \times n \times L_e \times D_{s_{min}} \left[\left(\frac{1}{2n} \right) + 0.57735 (D_{s_{min}} - E_{n_{max}}) \right]$$

where n = number of threads per inch, for M80x6 threads $n = 6$ mm or 4.23 threads/inch

L_e = length of thread engagement, 40 mm or 1.57 inch

$D_{s_{min}}$ = minimum major diameter of external threads, 79.32 mm or 3.123 inch

$E_{n_{max}}$ = maximum pitch diameter of internal thread, 76.478 mm or 3.011 inch

Substituting

$$A_n = 11.915 \text{ in}^2$$

Ultimate shear strength of the female threads:

$$P_u = (S_u/2) \times A_n = 405.7 \text{ kips}$$

where $S_u = 68.1$ ksi for 304L stainless steel at 150° F

After stripping the female threads, the rack bottom plate will provide support and also absorb the impact energy. For conservative evaluation, all remaining energy of the drop is used to calculate the impact load where the cylindrical portion of the female support leg impacts the bottom bearing pad and neglects the energy absorbed in the bottom plate.



Energy of the drop = $W h = 1.591 \times 172 = 273.652$ in-kips

Energy consumed in shearing threads = 95.747 in-kips

Remaining energy for impact to the bearing pad is = $273.652 - 95.747 = 177.905$ in-kips

This energy is converted to get initial velocity = $(1/2) m V^2$

Again only the weight of the fuel assembly (1.591 kips) is used to get maximum velocity after shearing threads.

$$177.905 = (1/2) (1.591/386.4) V^2$$

$$\therefore V^2 = 86,414 \text{ (in/sec)}^2$$

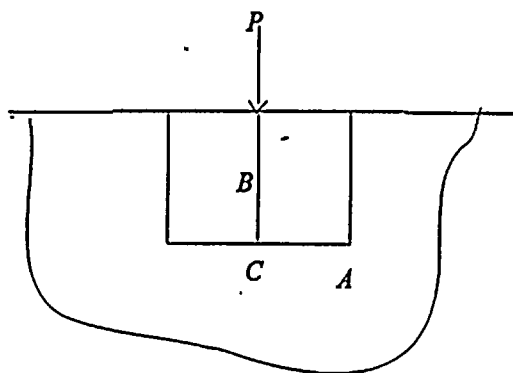
The support leg will travel 36 mm before it impacts the bearing pad. For conservative impact, the target is considered rigid and the velocity after impact is considered zero. The initial velocity of $V_o = \sqrt{86,414}$ in/sec and $V_f = 0.0$, $s = 36$ mm, and using constant deceleration:

$$a = -\frac{V_o^2}{2 s} = \frac{86414}{2 \times \frac{36}{25.4}} = -30,485 \text{ in/sec}^2 \text{ OR } -79 \text{ g's}$$

The impact load is = $W \times \text{deceleration}$
= 1.591×79
= 125.7 kips.

This impact load is lower than the load required to shear female threads (405.7 kips). For this case the inelastic strain energy is confined to the M80x6 threaded portion of the support leg. The maximum load imparted to the spent fuel pool floor is limited to ultimate strength of the threaded portion of the leg and is 405.7 kips.

Due to limited mechanism for inelastic energy absorption, the support leg female threads will fail. The load imparted to the floor will pass through the stainless steel liner. The stresses in the reinforced concrete floor are calculated using Boussinesq's solution (Reference 3.35), where P is equal to the maximum force transferred through the support legs to the floor. Using the Boussinesq solution, the maximum concrete compressive stress is at point C.



At point C

$r = 0$

$t = 0.25''$ pool liner thickness

$z = \text{bearing pad diameter} + 2t = 6.6929 + 2 \times 0.25 = 7.1929 \text{ in}$

$$\sigma_z = -P \left[\frac{3}{2\pi} \frac{z^3}{(r^2 + z^2)^{\frac{5}{2}}} \right] = -\frac{P}{A_{eq}}$$

$$A_{eq} = 108.36 \text{ in}^2$$

$$\begin{aligned} \text{Concrete Compressive Stress} &= P / A_{eq} \\ &= 3,744 \text{ psi} < 4,462.5 \text{ psi} \therefore \text{O.K.} \end{aligned}$$

where concrete allowable stress is 4,462.5 psi for accidental impact load for 3D confined concrete.

For normal condition, concrete allowable bearing stress = $\phi (0.85) f_c$
(per ACI 349-85, section 10.15)

For accident condition with impact load, allowable compressive stress = $\phi (0.85) f_c \times 2 \times \text{DIF}$

where: $\phi = 0.7$ per section 9.3 of ACI 349-85

$F_c = 3,000$ psi minimum strength 28 days cured concrete

$\text{DIF} = 1.25$ Dynamic impact factor for high strain rate per Table C-1 of ACI 349-85

$$\begin{aligned} \therefore \text{concrete allowable stress} &= 0.7 \times 0.85 \times 3,000 \times 2 \times 1.25 \\ &= 4,462.5 \text{ psi} \end{aligned}$$

In addition, the concrete Code ACI 349-85, Section 9.2.6 states that "when considering these concentrated loads, local section strengths and stresses may be exceeded provided there will be no loss of intended function of any safety related systems." Since 3 foot thick reinforced concrete spent fuel pool floor is supported on hard rock and is completely confined, the localized spalling of concrete will not jeopardize the safety function of the pool.

The indications are that, at distance below the support pad equal to the diameter of the support pad (6.6929"), the stresses are below allowable stresses. The concrete directly under the support pad is a local condition with three-dimensional confinement and, therefore, will not be damaged by the impact load.

3.5.3.2.3.2 Fuel Assembly - Shallow Drops

For this hypothetical accident drop of the fuel assembly, shallow drops, two cases were analyzed.

The acceptance criteria for top of rack impacts are that the required inelastic deformation must be less than 10% of the length of the deforming structural mechanism and that the ductility factor remains less than 20.

For drops onto the tops of the racks, the mathematical model consists of a vertical prismatic member with a height equal to the distance from the top of the rack to the top of the borated stainless steel. Because inelastic response is confined to this upper region, the values calculated for inelastic strain and ductility factors are conservative. If the entire rack were to be considered, the ductility factors would be reduced. The number of tubes considered in this model is the number of tubes directly impacted plus the number of tubes immediately adjacent. Due to the strong interconnection between tubes, this assumption is conservative. As the dropped object impacts the top of the racks, the affected tubes yield; however, the effect does not remain localized. It will spread to the surrounding tubes through the strong interconnection provided by the welded connecting tabs. The assumption of the spreading of load only to immediately adjacent tubes is conservative.

First buckling strength of the structural tube is calculated. From this it will be investigated whether the structural tube buckling occurs in elastic or plastic range.

Euler Buckling of Structural Tube Between Connection Tab Plates

ℓ = clear length between pitch of the tabs

I = cross section moment of inertia of the structural tube

A = cross section area of the structural tube

E = Young's Modulus of the tube material at 150°F

$$\sigma_{cr} = \frac{EI\pi^2}{Al^2}$$

Rack type	$l=\text{pitch}$ <u>in</u>	<u>A</u> <u>in²</u>	<u>I</u> <u>in⁴</u>	<u>E</u> <u>lb/in²</u>	<u>σ_{cr}</u> <u>ksi</u>
Type 2	49.29	2.59	29.17	27.9×10^6	1,277
Type 3	49.29	2.65	31.29	27.9×10^6	1,338
Type 4	48.23	2.59	29.17	27.9×10^6	1,333

Since σ_{cr} is well above the yield stress, the above results indicates that buckling will not occur in the elastic range.

3.5.3.2.3.2.1 Flat Impact on Top Interface of the Racks

For this hypothetical accident, the fuel assembly with handling tool is dropped from 12 inches above the rack, the fuel assembly impacts the top of the rack and falls flat on top of the rack.

For this case it is assumed that the fuel assembly is dropped vertically onto the top of the rack. After initially striking the top of the rack, the fuel assembly and handling gear rotates and falls flat on top of the racks. The total kinetic energy delivered to the top of the racks is little diminished due to the initial strike. This is due to the fact that the linear kinetic energy is converted to the rotational kinetic energy by means of a couple equal to the weight and inertial force of the fuel rod times the horizontal component of the distance between the center of gravity of the falling fuel assembly and the point of initial strike upon the top of the racks.

The kinetic energy at impact = $W \times d$

where: Weight of the fuel assembly and the tool is 1,591 lb.

The drop height for shallow drop is 12 inch + half height of fuel assembly
 $d = 12 + (160 / 2) = 92$ inch

Kinetic energy at impact = $W \times d = 1591 \times 92 = 146,372$ in-lb

Pitch of fuel cells:	Type 2 Rack	8.43 inch
	Type 3 Rack	9.23 inch
	Type 4 Rack	8.43 inch

For all the accident analyses presented in this section, the total number of tubes considered in the analysis is that contained within the footprint of the impacted area, plus the tubes that are immediately adjacent. The length of fuel assembly is 160 inch or approximately 18 pitch. For new racks, every other cell is a structural tube. Therefore, initially a minimum of 9 structural tubes will



be impacted. The other 9 adjacent structural tubes will also absorb impact energy. So effectively, 2 x 9 or 18 structural tubes will participate in absorbing impact energy. The top 10 inch portion, above the borated stainless steel portion of the tube, will absorb energy.

The Type 2 rack structural tubes have the minimum cross section area, and will have the largest deformation during fuel drop accident. The following calculations were performed for Type 2 racks. However, the results envelope all three type of racks.

A_{eff} - effective cross section area for 18 structural tubes.

$$A_{eff} = 2.59 \times 18 = 46.62 \text{ in}^2$$

The top 10 inches of the tube, above the borated stainless steel, will absorb all energy. Therefore, $h = 10 \text{ inch}$

$$\text{Elastic Strain Energy} = \frac{1}{2} \sigma_y^2 \frac{h_b}{E} A_{eff} = 4,478 \text{ in-lb}$$

The elastic strain energy absorbed is less than the total drop energy. Therefore, there will be some inelastic deformation.

Total drop energy = Elastic strain energy + Inelastic strain energy

$$146,372 = 4,478 + \text{Inelastic strain energy}$$

$$\therefore \text{Inelastic strain energy} = 146,372 - 4,478 = 141,894 \text{ in-lb}$$

$$\text{Inelastic Strain Energy} = \sigma_y h \epsilon_{in} A_{eff} = 141,894 \text{ in-lb}$$

$$\epsilon_{in} = 0.0131$$

$$\epsilon_{el} = \frac{\sigma_y}{E} = 0.00083$$

$$\delta = (\epsilon_{el} + \epsilon_{in})(10) = (0.00083 + 0.0131)(10) = 0.14 \text{ in}$$

$$\text{Ductility Factor} = \frac{\epsilon_{el} + \epsilon_{in}}{\epsilon_{el}} = \frac{0.00083 + .0131}{.00083} = 16.8$$

Ductility factor = 16.8 < 20 \therefore O.K.

3.5.3.2.3.2.2 End-On Impact

During an end-on impact hypothetical accident, the fuel assembly with handling tool is dropped from 12 inches above the rack, and the fuel assembly impacts the top of the rack vertically.

The drop energy $W \times d$ is $1591 \times 12 \approx 19,100$ in-lb

where $W = 1,591$ lb (weight of the fuel assembly and the tool)

The drop height is 12 inches.

For all the accident analyses presented in this section, the total number of tubes considered in the analysis is that contained within the footprint of the impacted area, plus the tubes that are immediately adjacent. Initial contact will engage two structural tubes. However, due to interconnection between the tubes, a total of 8 tubes will absorb impact energy.

The Type 2 rack structural tubes have the minimum cross section area, and will have the largest deformation during a fuel drop accident. The following calculations were performed for Type 2 racks. However, the results envelope all three type of racks.

A_{eff} - effective cross section area for 8 structural tubes.

$$A_{eff} = 2.59 \times 8 = 20.72 \text{ in}^2$$

The top 10 inches of the tube, above the borated stainless steel, will absorb all energy. Therefore, $h = 10$ inch

$$\text{Elastic Strain Energy} = \frac{1}{2} \sigma_y^2 \frac{h}{E} A_{eff} = 1,990 \text{ in-lb}$$

The elastic strain energy absorbed is less than the total drop energy. Therefore, there will be some inelastic deformation.

Total drop energy = Elastic strain energy + Inelastic strain energy

$$19,100 = 1,990 + \text{Inelastic strain energy}$$

$$\therefore \text{Inelastic strain energy} = 19,100 - 1,990 = 17,110 \text{ in-lb}$$

$$\text{Inelastic Strain Energy} = \sigma_y h \epsilon_{in} A_{eff} = 17,110 \text{ in-lb}$$

$$\epsilon_{in} = 0.00357$$

$$\epsilon_{el} = \frac{\sigma_y}{E} = 0.00083$$

$$\delta = (\epsilon_{el} + \epsilon_{in})(10) = (0.00083 + 0.00357)(10) = 0.044 \text{ in}$$

$$\text{Ductility Factor} = \frac{\epsilon_{el} + \epsilon_{in}}{\epsilon_{el}} = \frac{0.00083 + 0.00357}{0.00083} = 5.3$$

Ductility factor = $5.3 < 20$ \therefore O.K.



3.5.3.2.4 Tornado Missile Impact

A tornado missile impact on the storage racks was considered. Design values for tornado wind speed and missile characteristics are those established in NUREG-0800, Standard Review Plan 3.5.1.4 (revision 2, July 1981). The missile is characterized as a 1490 pound wood pole, 35 feet in length with a diameter of 13.5 inches. A tornado wind velocity of 132 mph (59 meter/per second) is considered per Ginna UFSAR, Section 3.5.2.1. The impact energy when the missile hits the storage racks is calculated in RG&E Letter to NRC dated January 18, 1984, Docket No 50-244 (Reference 3.39) and is summarized below:

Vertical kinetic energy at impact	79,000 ft-lb
Horizontal kinetic energy at impact	8,800 ft-lb

The vertical missile impact produces the largest deformation of the racks. The rack deformation due to horizontal missile impact will be lower than the vertical impact. Both of these impact are evaluated in the following section.

The acceptance criteria for top of rack impacts are that the required inelastic deformation must be less than 10% of the length of the deforming structural mechanism and that the ductility factor remains less than 20.

Vertical Missile Impact

The wooden pole diameter is 13.5 inches. The diagonal dimensions of structural tubes is 11.74 inches for Type 2 and Type 4 racks, and 12.02 inch for Type 3 Racks. Therefore, as a minimum two structural tubes will be impacted by a vertical impact.

For drops onto the tops of the racks, the mathematical model consists of a vertical prismatic member with a height equal to the full length of the fuel tube. The number of tubes considered in this model is the number of tubes directly impacted plus the number of tubes immediately adjacent. Due to the strong interconnection between tubes, this assumption is conservative. As the dropped object impacts the top of the racks, the affected tubes yield; however, the effect does not remain localized. It will spread to the surrounding tubes through the strong interconnection provided by the welded connecting tabs. The assumption of the spreading of load only to immediately adjacent tubes is very conservative.

The vertical impact energy is 79,000 ft-lb or 948,000 in-lb

Initial contact will engage two structural tubes. However, due to interconnection between the tubes, a total of 8 structural tubes will absorb impact energy.

The Type 2 rack structural tubes have the minimum cross section area, and will have largest deformation during a missile impact. The following calculations were performed for Type 2 racks. However, the results envelope all three types of racks.

A_{eff} - effective cross section area for 8 structural tubes.

$$A_{eff} = 2.59 \times 8 = 20.72 \text{ in}^2$$

The wooden pole will split on impact. Also the wood is a good energy absorber. However, the energy absorbed in the wooden pole is neglected as a conservatism. The impact will be of a long duration; for that reason, the entire length of the fuel tube (158.5 inch) will absorb the impact energy. Therefore, $h = 158.5$ inch

$$\text{Elastic Strain Energy} = \frac{1}{2} \sigma_y^2 \frac{h}{E} A_{eff} = 31,542 \text{ in-lb}$$

The elastic strain energy absorbed is less than the total kinetic energy. Therefore, there will be some inelastic deformation.

Total missile impact energy = Elastic strain energy + Inelastic strain energy

$$948,000 = 31,542 + \text{Inelastic strain energy}$$

$$\therefore \text{Inelastic strain energy} = 948,000 - 31,542 = 916,458 \text{ in-lb}$$

$$\text{Inelastic Strain Energy} = \sigma_y h \epsilon_{in} A_{eff} = 916,458 \text{ in-lb}$$

$$\epsilon_{in} = 0.0121$$

$$\epsilon_{el} = \frac{\sigma_y}{E} = 0.00083$$

$$\delta = (\epsilon_{el} + \epsilon_{in})(10) = (0.00083 + 0.0121)(158.5) = 2.05 \text{ in}$$

$$\text{Ductility Factor} = \frac{\epsilon_{el} + \epsilon_{in}}{\epsilon_{el}} = \frac{0.00083 + .0121}{.00083} = 15.6$$

Ductility factor = 15.6 < 20 \therefore O.K.

Horizontal Missile Impact

The horizontal kinetic energy of the missile impact is 8,800 ft-lb. This impact energy is much less than the vertical missile impact. In addition, due to the length of the pole being 35 feet, the large number of structural tubes will absorb the impact energy. For this reason, the rack deformation and ductility factor due to horizontal missile impact will be less than those of the vertical missile impact.



1. The first of the three main parts of the report is a description of the problem and the objectives of the study.

2. The second part of the report is a description of the methods used in the study.

3.5.3.2.5 Gate Drop

The gate separating the spent fuel storage pool from the cask loading pit is located on the east end of the spent fuel storage pool. The gate is approximately 28' long and 2' 6.5" wide. The gate weighs approximately 2100 pounds. The canal gate is considered a heavy load per NUREG-0612 criteria. The gate handling procedures will be changed such that it will be lifted within the spent fuel pool using a special tool suspended from a single-failure proof auxiliary building crane. In a safety evaluation report dated December 31, 1984, the NRC Staff reviewed and approved modifications to the auxiliary building crane in order to meet the crane single-failure criteria of NUREG-0612 and NUREG-0554. Therefore, handling of the canal gate will be performed in accordance with the guidelines of NUREG-0612 with regard to limiting the chance of unacceptable heavy load drop.

3.5.3.2.6 Rack Drops

The lifting analysis of the racks was performed to qualify the racks to lifting criteria of NUREG-0612. Section 3.5.3.1.19 provides results of the lifting analysis. The results indicate adequate margin against lifting by either a redundant or non-redundant lift system.

The installation procedures will preclude moving a rack over a previously installed rack. Racks will be lifted in the vicinity of the spent fuel pool using single-failure proof crane and lifting attachments. This will preclude rack drop analysis. However, the analysis is performed to verify structural strength of the design to withstand rack drops. If a rack drops to the floor, the maximum total force would be limited to the crush strength of the racks. The crush strength of racks is provided in this section.

During rack drops, most of the energy will be absorbed in the crushing of racks. Therefore, rack buckling and crush strength are calculated first..

Euler Buckling of Structural Tube Between Connection Tab Plates

$$\sigma_{cr} = \frac{E I \pi^2}{A \ell^2}$$

Earlier calculation for Euler's buckling of the structural tubes has shown that for all three type racks, the σ_{cr} is much more higher than the σ_y . Therefore, the tubes will not buckle as a beam in the elastic range.

Overall Rack Buckling

$$\sigma_{cr} = \frac{E I \pi^2}{A L_1^2}$$

Where L_1 = effective length for buckling, $2 \times$ height of racks = $2 \times 158.5 = 317$ inch
 A = cross section area of structural members in a rack
 I = cross section moment of inertia of rack structural members
 E = Young's Modulus = 27.9×10^6 lb/in² for 304L SS at 150°F
 (Note: Lowest of East-West or North-South properties are taken)

RACK Type	A in ²	I _{north-south} in ⁴	σ_{cr} ksi
2A	113.9	43,791	1,054
2B	129.5	64,009	1,354
3A	92.7	32,726	967
3B	82.1	25,998	868
3C	66.2	12,079	500
3D	66.2	12,079	500
3E	84.8	26,008	840
4	25.9	292	31

All of these σ_{cr} are higher than the σ_y ; therefore, racks will not buckle in beam mode in elastic range.

Local Plate Buckling

Crush strength of each rack is based upon the effective area, reduced for buckling times the compressive yield. This represents full mobilization of all the cells of the rack. The justification for this is based upon compressive yield of the cells without general elastic buckling.

Reference 3.37 - Blodgett pp. 2.12-4 through 9.

Type 2 and Type 4 Racks

$$\sigma_{CR} = \frac{\pi^2 K_c E}{12(1-\nu^2)} \left(\frac{t}{b} \right)^2 = \frac{\pi^2 (4)(27900)}{12(1-0.3^2)} \left(\frac{0.0787}{8.14} \right)^2 = 9.43 \text{ ksi}$$

where t = tube wall thickness = 0.0787 in

b = inside dimension of structural tube = 8.14 in

$K_c = 4$ (Reference 3.37, Blodgett)



Type 3 Racks

$$\sigma_{CR} = 8.982 \text{ ksi, using } t = 0.0787 \text{ in and } b = 8.34 \text{ in}$$

Crush Strength

- 1) Crush strength based upon effective crush area and yield strength of material.
- 2) Elastic buckling of individual tubes or the rack as a whole is precluded.

Using conservative assumptions:

$$\frac{A_{eff}}{A} = \frac{\frac{\sigma_y + \sigma_{cr}}{2}}{\sigma_y}$$

where A = total cross-sectional area of the structural tube

where σ_y = yield stress = 23.15 ksi for 304L stainless steel @ 150° F

A = total cross sectional area of the tubes.

A_{eff} = effective area of tubes, reduced to account for local buckling,

Note,

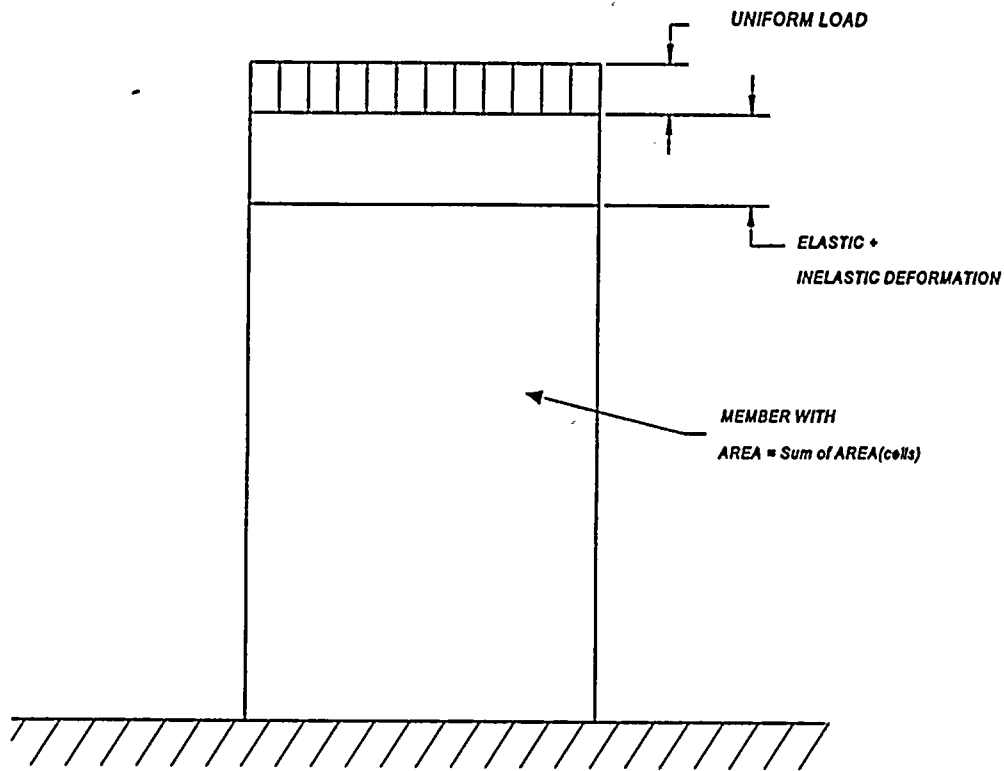
$$\text{Type 2 Racks} \quad \frac{A_{eff}}{A} = 0.704$$

$$\text{Type 3 Racks} \quad \frac{A_{eff}}{A} = 0.694$$

Methodology and Models

The mathematical model for developing the rack crush strength is that of uniform compressive yield under a uniform applied load at the top shown in the following sketch.

Crush Strength Model



Crush strength of each rack is based upon the effective area, reduced for buckling times the compressive yield. This represents full mobilization of all the cells of the rack. The justification for this is based upon compressive yield of the cells without general elastic buckling.

Tabulation of Results

Material $\sigma_y = 23,150$ psi @ 150°F

Rack No.	Cross Section Area A in ²	A_{eff} / A	Effective Crush Area A_{eff} in ²	Crush Force $A_{eff} \times \sigma_y$ kips	Number of Legs	Impact Load per Leg kips
2A	113.9	0.704	80.19	1856	12	155
2B	129.5	0.704	91.17	2111	16	132
3A	92.7	0.694	64.33	1489	12	124
3B	82.1	0.694	56.98	1319	11	120
3C	66.2	0.694	45.94	1064	8	133
3D	66.2	0.694	45.94	1064	8	133
3E	84.8	0.694	56.85	1362	12	114
4	25.9	0.704	18.23	422	2	211

The impact load on each leg due to rack drop is less than the leg load due to deep fuel assembly drop on leg (405.7 kips). Therefore, concrete stress due to rack drop are below allowable.

3.5.3.2.7 Cask Drop

The auxiliary building crane is used in moving the spent fuel shipping cask. The crane is electrically interlocked to prevent movement over the spent fuel storage racks. These interlocks may be defeated by keys, and when defeated, indicate the condition by rotating flashing yellow or red lights.

The auxiliary building crane meets the single-failure proof criteria of NUREG-0554 and NUREG-0612. The crane is rated 32.5 tons; however, the maximum critical load is 30 tons, which is characterized as a fully loaded spent fuel cask with a redundant yoke. No single-failure of any lifting component of the crane will result in the drop of any load up to 32.5 tons. The 30-ton hook is used for handling heavy loads such as a spent fuel cask. The crane is capable of stopping and holding the load under all conditions, including the safe shutdown earthquake UFSAR Section 9.1.4..1.

The NRC Staff, in its Safety Evaluation of November 14, 1984, has judged that the auxiliary building crane meets the intent of Guideline 7 of NUREG-0612, Section 5.1.1. The NRC Staff, therefore, does not postulate a cask drop or tip accident which could damage stored spent fuel (Section 2.5.1 of Reference 3.23).

3.5.3.2.8 Summary of Accident Drop Results

The straight deep drop cases require an exactitude (i.e., falls through cell with no contact) which has a very low probability of occurring. Nevertheless, the consequences of such an accident were examined and, while damage to the fuel rack bottom plate or support leg could be expected, no damage would occur to the spent fuel pool floor.



The shallow drop was examined and it was found that with ductility factor less than 20 and deformation less than one inch, the distortion of the cells would be confined to the portion of cells above the borated stainless steel, and hence, not affect the K factor used in the criticality analysis.

The conservatism used in the mechanical accident analyses for various drops indicate that, minor distortion of the rack is limited in the vicinity of the impact area. There is no gross deformation of the rack away from the impact area.

Individual hypothetical accident cases are summarized below.

Fuel Assembly - Straight Deep Drop

The kinetic energy of the falling fuel assembly is such that it can be expected that the bottom plate of the racks will be separated from the bottom of the cells due to failure of the welds (bottom plate to cell). The bottom plate would be supported by the support legs, located nominally at 37" on center for Type 2 and Type 3 racks. It is found that the bottom plate would yield and deform, deflecting about 2.12" with the fuel assembly impacting at the midpoint between support legs. For Type 4 racks, the bottom plate would yield and deform, deflecting about 1.82" with fuel assembly impacting, approximately, at the midpoint between support legs. Therefore, it is concluded that this would not result in any distress to the spent fuel pool floor.

Fuel Assembly - Straight Deep Drop onto Support Leg

For this case the inelastic strain energy is confined to the M80x6 threaded portion of the support leg. The maximum load imparted to the spent fuel pool floor is limited to ultimate strength of the threaded portion of the leg and is 405.7 kips.

Due to limited mechanism for inelastic energy absorption, the support leg female threads will fail. The load imparted to the floor will pass through the stainless steel liner. The stresses in the reinforced concrete floor are calculated using Boussinesq's solution (Reference 3.35). The indications are that, at distance below the support pad equal to the diameter of the support pad (6.6929"), the stresses are below allowable stresses. The concrete directly under the support pad is a local condition with three-dimensional confinement and, therefore, will not be damaged by the impact load. The maximum deformation of the bottom plate will be 1.42 inches (36 mm) after female threads are stripped.

Fuel Assembly - Shallow Drops

For this case it was assumed that the fuel assembly is dropped vertically onto the top of the rack. After initially striking the top of the rack, the fuel assembly and handling gear rotates and falls flat on top of the racks. The total kinetic energy delivered to the top of the racks is little diminished due to the initial strike. This is due to the fact that the linear kinetic energy is converted to the rotational kinetic energy by means of a couple equal to the weight and inertial force of the fuel rod times the horizontal component of the distance between the center of gravity of the falling fuel assembly and the point of initial strike upon the top of the racks. The results of the analysis indicate that distortion of cells will be limited to the portion of the cells above the top of the borated stainless steel. The ductility factor is less than 20 for both shallow drops and the maximum deformation of the top of the rack is 0.14 inches.

The results of the analysis indicate that distortion of the cells will be limited to the portion of the cells above the top of the borated stainless steel.

<u>Accident</u>	<u>Inelastic Strain (above BSS)</u>	<u>Ductility Factor</u>	<u>Total Deformation (inches)</u>
F.A., Shallow Drop, Flat Impact	0.0131	16.8	0.14
F.A., Shallow Drop, End-on Impact	0.00357	5.3	0.044

Tornado Missile Impact

Vertical and horizontal tornado missile impacts were considered. The wooden pole missile is dropped on top of the racks. Considering the impact energy and the footprint of the impact among vertical and horizontal impact, the vertical impact causes the highest deformation and highest ductility factor for the racks. The results indicate that the distortion of the cell will be limited to the footprint area and adjacent fuel cells. The deformation of the top of the impacted fuel cell will be 2.05 inches and ductility factor of structural tubes will be limited to 15.6.

Gate Drop, Rack Drop and Cask Drop

The consolidated fuel, pool canal gate, storage racks and the spent fuel shipping cask are considered heavy loads per NUREG-0612. There will be administrative control for movement of these hardware in the spent fuel pool area. Also they will be lifted using a single-failure proof crane and a single-failure proof lifting system. Handling of these hardware in the spent fuel pool area will be performed in accordance with the guidelines of NUREG-0612 with regard to limiting the chance of unacceptable heavy load drop. Reference 3.23, NRC Staff safety evaluation report provides exclusion of heavy load drops meeting these criteria.

3.5.3.2.9 Loss of Spent Fuel Pool Cooling

Differential Temperature Induced Loads - Abnormal Condition (T_a)

This thermal condition is produced when the pool water bulk temperature increases due to loss of artificial cooling. The pool liner temperature is kept the same as the normal operating temperature to generate conservative stresses in the rack. The most conservative analysis of the rack would then be to assume that the bottoms of the legs of the rack remain in their original positions and that the uniform temperature of the rack itself has reached to accident condition temperature. The maximum loading would thus be caused by the constraint at the bottoms of the legs and the uniform thermal growth in the rack.

Section 3.5.3.1.10 presents the analysis and results of the rack thermal analysis under abnormal condition (T_a). The results indicate adequate margin exists in the storage racks to accommodate differential temperature induced load due to loss of artificial cooling.

3.5.3.3 Tabulation of Results

Table 3.5-141 Results of Support Leg Stresses

Load Combinations	Maximum Stress (psi)	Allowable Stress (psi)	Design Factor (%)
<i>D + L (Level A)</i>			
Primary Membrane (Pm)	6,156	15,700	155.0
Primary Membrane+ Bending (Pm + Pb)	16,995	23,550	38.6
<i>D + L + E (Level B)</i>			
Primary Membrane (Pm)	6,156	20,880	239.2
Primary Membrane+ Bending (Pm + Pb)	16,995	31,322	84.3
Average Shear Stress	2,109	9,420	346.7
<i>D + L + E' (Level D)</i>			
Primary Membrane (Pm)	7,651	26,448	245.6
Primary Membrane+ Bending (Pm + Pb)	24,640	39,672	61.0
Average Shear Stress	3,306	28,123	750.7
Welds: <i>D + E (Level A)</i>	11,677	21,000	79.8
<i>D + E + Ta (Level B)</i>	11,733	27,930	138.0
<i>D + E' + Ta (Level D)</i>	18,302	29,400	60.6
Base Metal: <i>D + E (Level A)</i>	8,257	9,260	12.1
<i>D + E + Ta (Level B)</i>	8,297	11,725	41.3
<i>D + E' + Ta (Level D)</i>	12,942	28,123	117.3

Notes:

L - Live load is zero.

Design Factor (%) = $[(\text{Allowable} - \text{Actual}) / \text{Actual}] \times 100$

Table 3.5-142 Results of Concrete Stresses

Load Combinations	Maximum Stress (psi)	Allowable Stress (psi)	Design Factor (%)
<i>D</i>			
Maximum Slab Bearing	520	3,570	586.5
Boussinesq's Solution	779	3,570	358.2
<i>D + E</i>			
Maximum Slab Bearing	1,207	3,570	195.8
Boussinesq's Solution	1,811	3,570	97.1
<i>D + E'</i>			
Maximum Slab Bearing	1,501	3,570	137.8
Boussinesq's Solution	2,251	3,570	58.5

Notes:

Concrete's bearing allowable = $\phi (0.85)fc' = 0.70(0.85)3000 \text{ psi} * 2^1 = 3,570 \text{ psi}$

1. Since Area of concrete \gg area of pad = $\pi d^2/4 = 35.18 \text{ in}^2$, bearing allowable is increased by factor of 2 per Reference 3.5.2.2.2.1.
2. L- Live load is zero
3. T_a - Thermal load is zero for concrete.

Table 3.5-143 Results of Spent Fuel Pool Liner Stresses

Load Combinations	Maximum Stress (psi)	Allowable Stress (psi)	Design Factor (%)
<i>D + L + E</i>			
Liner Bearing Stress	1,207	23,400	1838.7
<i>D + L + E'</i>			
Liner Bearing Stress	1,501	23,400	1459.0

Table 3.5-144 Results of Tab Stresses

Load Combinations	Maximum Stress (psi)	Allowable Stress (psi)	Design Factor (%)
<i>D + L + E + To (Level A)</i>			
Primary Membrane (Pm)	660	15,700	Large
Primary Membrane + Bending (Pm + Pb)	5,759	23,550	Large
Range of Primary + Secondary	15,615	46,300	196
Average Primary Shear Stress	4,021	9,420	134
Weld Stress (Fillet Weld)			
Shear	6,308	21,000	232
Primary Membrane + Bending (Pm + Pb)	9,659	21,000	117
Range of Primary + Secondary	19,515	46,300	137
<i>D + L + E + Ta (Level B)</i>			
Primary Membrane (Pm)	660	20,881	Large
Primary Membrane + Bending (Pm + Pb)	5,759	31,322	Large
Range of Primary + Secondary	15,562	44,080	183
Average Primary Shear Stress	4,021	9,420	134
Weld Stress (Fillet Weld)			
Shear	6,308	27,930	343
Primary Membrane + Bending (Pm + Pb)	9,659	27,930	189
Range of Primary + Secondary	19,462	44,080	126

Load Combinations	Maximum Stress (psi)	Allowable Stress (psi)	Design Factor (%)
$D + L + E' + Ta$ (Level D)			
Primary Membrane (Pm)	1,162	26,448	Large
Primary Membrane + Bending (Pm + Pb)	10,148	39,672	291
Range of Primary + Secondary	19,951	44,080	120
Average Primary Shear Stress	7,768	28,123	262
Weld Stress (Fillet Weld)			
Shear	11,262	29,400	161
Primary Membrane + Bending (Pm + Pb)	16,916	29,400	74
Range of Primary + Secondary	26,719	44,080	65



Table 3.5-145 Results of Tube Stresses

Load Combinations	Maximum Stress (psi)	Allowable Stress (psi)	Design Factor (%)
<i>D + L + E + To (Level A)</i>			
Primary Membrane (Pm)	4,543	15,700	246
Primary Membrane + Bending (Pm+Pb)	4,872	23,550	383
Range of Primary + Secondary	14,728	46,300	214
Average Shear Stress	1,265	9,420	Large
<i>D + L + E + Ta (Level B)</i>			
Primary Membrane (Pm)	4,543	20,881	360
Primary Membrane + Bending (Pm + Pb)	4,872	31,322	542
Range of Primary + Secondary	14,675	44,080	200
Average Shear Stress	1,265	9,420	Large
<i>D + L + To + Pf (Level B)</i>			
Primary Membrane (Pm)	5,443	20,881	283
Primary Membrane + Bending (Pm + Pb)	7,205	31,322	334
Range of Primary + Secondary	17,008	44,080	159
<i>D + L + E' + Ta (Level D)</i>			
Primary Membrane (Pm)	6,979	26,448	279
Primary Membrane + Bending (Pm + Pb)	7,202	39,672	450
Range of Primary + Secondary	17,005	44,080	159
Average Shear Stress	1,265	9,420	Large



ALL INFORMATION CONTAINED HEREIN IS UNCLASSIFIED DATE 11-11-2001 BY 60322 UCBAW/SJS

Load Combinations		Maximum Stress (psi)	Allowable Stress (psi)	Design Factor (%)
Tube-to-Base Plate Fillet Weld				
$D + L + E + T_o$ (Level A)	Base Metal	11,957	46,300	287
	Weld	16,575	46,300	179
$D + L + E + T_a$ (Level B)	Base Metal	11,957	44,080	268
	Weld	16,575	44,080	166
$D + L + E' + T_a$ (Level D)	Base Metal	20,652	44,080	113
	Weld	29,969	44,080	47

Table 3.5-146 Results of Base Plate Stresses

Load Combinations	Maximum Stress (psi)	Allowable Stress (psi)	Design Factor (%)
$D + L + E + T_o$ (Level A)			
Primary Membrane (Pm)	767	15,700	Large
Primary Membrane + Bending (Pm + Pb)	4,286	23,550	Large
Range of Primary + Secondary Stress	10,227	46,300	353
$D + L + E + T_a$ (Level B)			
Primary Membrane (Pm)	767	20,881	Large
Primary Membrane + Bending (Pm + Pb)	4,286	31,322	Large
Range of Primary + Secondary Stress	5,842	44,080	Large
$D + L + E' + T_a$ (Level D)			
Primary Membrane (Pm)	767	26,448	Large
Primary Membrane + Bending (Pm + Pb)	4,286	39,672	Large
Range of Primary + Secondary Stress	5,842	44,080	Large

3.5.3.4 Discussion of Results and Significance

The analysis and design of the Ginna Spent Fuel Storage Racks provide assurances that the racks will perform the functions as required.

The assembly of structural tubes creates a sufficiently stiff and strong rack structure. The associated inter-rack connections and welding provide the necessary strength and stiffness to accommodate all of the rack loading conditions. In addition, a large number of support legs provide for a wide distribution of force and reactions and adequate structural margins.

The various loadings and resulting consequences were examined in detail by means of nonlinear dynamic analysis. One of the major loading effects is the impact of fuel assemblies against the cell walls. While the impact effect is of very short duration, it enhances the potential for sliding and tipping. Consequential impact effects were analyzed; namely the impact of support legs upon the spent fuel pool floor during tipping.

Given the evaluated seismic events, the changes in the final position of the racks are small as compared to the initial position prior to the seismic event. The effect of tipping is such that no net change of position results. The only changes in position result from sliding; however, the results of the 3D whole pool multi-rack analyses and the 3D single rack model studies indicate little net change in the gaps between racks. The maximum closure of gaps is such that no significant changes in the gaps result during any single seismic event. Furthermore, the combined gap closures resulting from a combination of 5 OBE's and 1 SSE show that there are no rack-to-rack or rack-to-wall impacts.

The conservatisms inherent in the criteria and methodology indicate that the racks have sufficiently large margins as shown by comparisons of calculated and allowable stresses.

Detailed results are found in sections 3.5.3.1 and 3.5.3.2, which provide the results of the normal condition and accident condition evaluations respectively. Section 3.5.3.3 provides a tabulation of all results.

3.5.3.5 Conclusion

It is shown that the spent fuel storage system structures at RG&E's R. E. Ginna Unit 1 are robust and that they provide safe storage of spent fuel under any of the normal, upset or hypothetical accident conditions. The design and supporting analyses of the high density free standing storage racks indicate that the spent fuel and the consolidated fuel canister can be stored safely in the new ATEA designed racks.

During the seismic events, impacts will occur on the racks due to the impacts of the fuel assemblies or canisters as well as the impacts of the rack legs on the floor during tipping. The analyses show during OBE or SSE seismic events, there are no rack-to-rack or rack-to-wall impacts.

The racks themselves are very rigid structures, capable of resisting large loads. The fact that the racks are free to slide has two significant effects; 1) the lateral forces are thereby limited, and 2) the sliding dissipates energy. The tipping of the racks is limited by the restoring moment due to the weight of the rack, the fuel, and the contained water. The hydrodynamic coupling is also a restorative force. The effect of the water coupling is also an energy dissipator. The hydrodynamic



pressures develop in order to force water from a closing gap. The vibratory nature of seismic events, while resulting in amplified loading, also results in rapid load reversals. The free standing characteristics of the racks and the hydrodynamic coupling are very effective in responding to the rapid load reversals.

Stresses in the new ATEA racks and in the existing U.S. Tool & Die racks, pool liner and spent fuel pool are below allowable. The deformations of this hardware are within allowable limits. Also, the results show the ruggedness of the spent fuel rack design.

The structural evaluation presented here shows that the RG&E's Ginna Unit 1 spent fuel storage system meets all applicable structural criteria to maintain a subcritical array for the spent fuel and keep radiation exposure within federal limits. The analysis of the spent fuel storage system demonstrates that the structure satisfies the requirements of Part 50 of Title 10 of the Code of Federal Regulations. Results of the analysis show the design satisfies the statutory requirements for licensing.

3.5.3.6 Anticipated Impact on Operations of R. E. Ginna Nuclear Plant

The racks are structurally designed to provide storage for spent fuel assemblies or consolidated fuel canisters without restriction. Both spent fuel or consolidated fuel canisters can be safely stored in any of the racks without restrictions.

The high density spent fuel storage racks are free standing; hence free to slide or tip without rack to rack impacts under seismic events. Both the old and new racks do not impact the walls of the spent fuel pool under any of the normal, abnormal and faulted conditions. These conditions include seismic OBE and SSE conditions. During seismic events, loads from the rack supports onto the spent fuel storage pool floor are within the allowable concrete bearing stresses. The liner itself will not be subject to any significant loads due to any sliding of the racks.

Under the hypothetical accident drop of a fuel assembly or tornado missile impact, minor distortion of the racks will occur. These rack distortions are limited to the foot print area of the impact and fuel cell in the vicinity of the impact area. There will be no gross distortions of the racks or any adverse effects upon the plant structures or equipment.

For the consolidated fuel canister, pool canal gate and spent fuel shipping cask, administrative procedures will require lifting this hardware using NUREG-0612, single failure proof crane and single failure proof lifting and rigging system. Also, during the removal of the old racks and during the installation of the new racks, that movement over the spent fuel pool shall be performed using single failure proof lift system.

In summary, the functioning of the racks under the specified loading, or events, will have no detrimental consequences to the spent fuel pool or plant operation.

3.6 REFERENCES

- 3.1 NUREG-0800, Standard Review Plan, Section 3.5.1.4, "Missile Generated by Natural Phenomena," U.S. Nuclear Regulatory Commission, Revision 2, July 1981.
- 3.2 NUREG-0800, Standard Review Plan, Section 3.7.1, "Seismic Design Parameters," U.S. Nuclear Regulatory Commission, Revision 2, August 1989.
- 3.3 NUREG-0800, Standard Review Plan, Section 3.7.3, "Seismic Subsystem Analysis," U.S. Nuclear Regulatory Commission, Revision 2, August 1989.
- 3.4 NUREG-0800, Standard Review Plan, Section 3.8.4, Appendix D, "Technical Position on Spent Fuel Pool Racks," Revision 1, July 1981.
- 3.5 NUREG-0800, Standard Review Plan, Section 3.8.5, "Foundations," U.S. Nuclear Regulatory Commission, Revision 1, July 1981.
- 3.6 NUREG-0800, Standard Review Plan, Section 9.1.2, "Spent Fuel Storage," U.S. Nuclear Regulatory Commission, Revision 3, July 1981.
- 3.7 OT Position, "Review and Acceptance of Spent Fuel Storage and Handling Applications," dated April 14, 1978 and the modifications to this document dated January 18, 1979, U.S. Nuclear Regulatory Commission.
- 3.8 U.S. NRC Regulatory Guide 1.13, "Spent Fuel Storage Facility Design Basis," Revision 1, December 1975
- 3.9 U.S. NRC Regulatory Guide 1.29, "Seismic Design Classification," Revision 3, September 1978
- 3.10 U.S. NRC Regulatory Guide 1.60, "Design Response Spectra for Seismic Design of Nuclear Power Plants," Revision 1, December 1973.
- 3.11 U.S. NRC Regulatory Guide 1.61, "Damping Values for Seismic Design of Nuclear Power Plants," Revision 0, October 1973.
- 3.12 U.S. NRC Regulatory Guide 1.92, "Combining Modal Responses and Spatial Components in Seismic Response Analysis," Revision 1, February 1976.
- 3.13 U.S. NRC Regulatory Guide 1.117, "Tornado Design Classification," Revision 1, April 1978.
- 3.14 U.S. NRC Regulatory Guide 1.124, "Service Limits and Loading Combinations for Class I Linear Type Components Supports," Revision 1, January 1978.
- 3.15 U.S. NRC Regulatory Guide 1.142, "Safety-Related Concrete Structures for Nuclear Power Plants," Revision 1, October 1981.

- 3.16 NUREG-0612, "Control of Heavy Loads at Nuclear Power Plant," U. S. NRC, July 1980.
- 3.17 NUREG-0554, "Single-Failure-Proof Cranes for Nuclear Power Plants," U. S. NRC, May 1979.
- 3.18 ANSI-57.2-1983, "Design Requirements for Light Water Reactor Spent Fuel Storage Facilities at Nuclear Power Plants."
- 3.19 American Society of Mechanical Engineers, Boiler and Pressure Vessel Code, Section III, 1989 Edition.
- 3.20 ACI 349-85, "Code Requirements for Nuclear Safety Related Concrete Structures," American Concrete Institute, 1985.
- 3.21 AISC-1989, "Manual of Steel Construction - Part 5, Specification and Codes," American Institute of Steel Construction, 9th Edition, 1989.
- 3.22 Updated Final Safety Analysis Report, "Rochester Gas & Electric, R. E. Ginna Nuclear Power Plant, Docket 50-244" Revision 13-1, July 1996.
- 3.23 NRC - Safety Evaluation by the Office of Nuclear Reactor Regulation Supporting Amendment 12 to Facility Operating License No. DPR-18, Rochester Gas & Electric Corp., R. E. Ginna Nuclear Power Plant, Docket No 50-244, dated December 16, 1985.
- 3.24 NRC Letter to RG&E - Mr. Kober dated November 14, 1984. Safety Evaluation Report to Amendment No. 65 "Increase of the Spent Fuel Storage Capacity," License No. DPR-18, Docket No. 50-244.
- 3.25 U.S. Tool & Die Inc., " Seismic Analysis Spent Fuel Storage Racks Modified to 100% Storage Density in Region 2," Report No. 8369-00-0013," Revision 1, March 1, 1984.
- 3.26 U.S. Tool & Die Inc., "Mechanical Analysis, Spent Fuel Storage Racks Modified to 100% Storage Capacity in Region 2," Report No. 8369-00-0014, Revision 2, September 1984.
- 3.27 "Nuclear Reactors and Earthquakes," TID-7024, US Atomic Energy Commission, August 1963.
- 3.28 Welding Research Council Bulletin Number 151, "Further Theoretical Treatment of Perforated Plates with Square Penetration Patterns," W. J. O'Donnell, June 1970.
- 3.29 DOE/RW-0184, Characteristic of Spent Fuel, High-Level Waste, and Other Radioactive Waste Which May Require Long Term Isolation," December 1987.
- 3.30 EPRI NP-6159, "An Assessment of Boraflex Performance in Spent-Nuclear-Fuel Storage Racks," Electric Power Research Institute, December 1988.

- 3.31 EPRI TR-100784, "Borated Stainless Steel Application in Spent Fuel Storage Racks," Electric Power Research Institute, June 1992.
- 3.32 Bechtel Topical Report "Design of Structures For Missile Impact," BC-TOP-9A, Revision 2, September 1974.
- 3.33 Marks Handbook, "Standard Handbook for Mechanical Engineers," Seventh Edition, McGraw Hill Book Company.
- 3.34 Oberg, E. Et al, "Machinery's Handbook," 23rd Edition, Industrial Press Inc., New York, 1990
- 3.35 Theory of Elasticity, 3rd Edition, Timoshenko and Goodier, McGraw-Hill, N.Y., 1970.
- 3.36 Mechanical Engineering Design, 5th Edition, Shigley and Mischke, McGraw-Hill, N.Y., 1989, pp. 735 and 751.
- 3.37 Design of Welded Structures, O.W. Blodgett, James F. Lincoln Arc Welding Foundation, Cleveland, OH, 1991.
- 3.38 Singh-1990, "Structural Evaluation of Onsite Spent Fuel Storage: Recent Developments," S. Singh, et. Al., Proceedings of the Third Symposium, Orlando, Florida, December 1990. North Carolina State University, Raleigh, NC 27695, pp V/4-1 through V/4-18.
- 3.39 Letter from John E. Maier, RG&E to Harold R. Denton, USNRC, "Application for Amendment to Operating License," Docket 50-244, January 18, 1984.
- 3.40 ANSYS, Engineering Analyses System User's Manual, Version 5.2, 1995.
- 3.41 SIMQKE - "A Program for Artificial Motion Generation," Department of Civil Engineering, Massachusetts Institute of Technology, November 1976.
- 3.42 Analysis and Design of Flight Vehicle Structures, E. F. Bruhn, Tri-State Offset Printing, 1965.
- 3.43 ASME Code Case N-510-1, "Borated Stainless Steel for Class CS Core Support Structures and Class 1 Component Supports, Section III, Division 1," December 12, 1994.

4.0 CRITICALITY EVALUATION

4.1 INTRODUCTION

Two regions comprise the spent fuel storage racks for the R.E. Ginna Nuclear Power Station. Region 1 maintains a maximum k_{eff} (K_{max}) ≤ 0.95 for fresh fuel with nominal enrichments up to 5.0 wt% ^{235}U . This is accomplished by a combination of absorber flux traps, a checkerboard of fresh and highly burned assemblies, and Integrated Fuel Burnable Absorber (IFBA) credit for fresh assemblies with nominal enrichments above 4.0 wt% ^{235}U . Region 2 maintains the 0.95 criticality criterion by using fixed absorber plates and burnup credit. This region accommodates nominal initial enrichments up to 5.0 wt% ^{235}U , with an associated minimum burnup of 47.25 GWd/mtU. Loading curves relating the required burnup to the initial enrichment of the spent fuel assemblies govern placement of spent fuel into either region.

The KENO V.a Monte Carlo program determines K_{max} for both Region 1 and 2 using storage rack models with unborated water at nominal pool temperatures. K_{max} includes the sum of the KENO V.a calculated k_{eff} , the KENO V.a bias, penalties related to fabrication tolerance uncertainties, and statistically combined uncertainties related to these parameters. This sum ensures that K_{max} will be less than or equal to 0.95 with a 95% probability at a 95% confidence level. Evaluations of the reactivity effects of abnormal and accident conditions ensure that these conditions also satisfy this criticality criterion under the double contingency principle.

The criticality safety analyses for the Ginna Unit 1 storage racks conform to applicable codes and standards ^{4.1-4.6}. The results of the analyses show that the combination of fixed absorbers and burnup credit inherent in the designs enables both the Region 1 and Region 2 racks to satisfy the criticality safety criterion, i.e., $K_{\text{max}} \leq 0.95$. A summary of the burnup requirements for loading fuel in either region is provided below. The limiting accident condition is a misplaced assembly in Region 2. The criticality criterion is satisfied for this, and any other abnormal event by a minimum soluble boron concentration in the storage pool coolant of 450 ppm during fuel movement.

4.1.1 Region 1 Normal Condition

A borated stainless steel rack, Type 3, comprises Region 1. This region accommodates fuel with initial enrichments up to 4.0 wt% ^{235}U (nominal) for either fresh fuel without IFBA or up to 5.0 wt% ^{235}U (nominal) with appropriate IFBA loadings. Fresh assemblies must be stored in a checkerboard arrangement so that fresh fuel is not directly adjacent to other fresh fuel. The positions adjacent to the fresh fuel, i.e., with flat surfaces facing each other, must be filled with fuel with a burnup appropriate to its initial enrichment, or left empty. The relationship between the burnup and initial enrichment is defined by a burnup versus enrichment, or loading, curve. There is a further physical restriction on fuel assembly loading in Region 1 in addition to the loading curve due to the rack design. As described in Section 1.3.1, lead-in funnels are provided for the cells that accept fresh fuel assemblies. The cells without a funnel may only contain spent fuel. Figure 4.1-1 illustrates the burnup versus initial enrichment loading curve for spent fuel in Region 1. Figure 4.1-3 illustrates allowable loading arrangements for fresh fuel assemblies and spent fuel assemblies with enrichments and burnups in areas A and B of Figure 4.1-1. The burnup requirements, including a 5% burnup 'measurement' uncertainty, are tabulated in Table 4.1-1. Table 4.1-3 lists the calculated k_{eff} values



from the KENO V.a calculation and K_{\max} which includes all biases and uncertainties for Region 1 for normal conditions. These results are based upon a fresh Westinghouse Optimized Fuel Assembly (OFA) stored adjacent to a Westinghouse Standard assembly. The Westinghouse OFA assembly is most reactive for fresh fuel while the Westinghouse Standard assembly is most reactive for burned fuel satisfying the loading curve for Region 1. Consolidated fuel canisters are also bounded by these assemblies and thus must conform to the same loading curve.

4.1.2 Region 2 Normal Condition

The tight pitch of the Region 2 cells requires burnup credit and fixed absorbers to satisfy the criticality criterion. Three rack cell configurations comprise Region 2 (see Figure 4.3-1). Type 1 cells are the Boraflex cells that form Region 2 for the existing license. Two racks of Type 2 cells, containing borated stainless steel (BSS) absorber plates, have been added to increase the capacity of Region 2. The capacity can be increased in the future by the addition of Type 4 racks on the north and south faces of the Type 1 rack configuration, (see Figure 4.3-1). This type also contains BSS absorber plates.

Figure 4.1-2 shows the burnup versus initial enrichment curves for Region 2, as well as the inventory of fuel as of 06/09/96 in the Ginna storage pool. Figure 4.1-4 illustrates allowable loading arrangements for assemblies with enrichments and burnups in areas A₁, A₂, B, and C of Figure 4.1-2. Table 4.1-2 lists the required burnup values. The central, solid curve is the base curve for storage in Region 2 for all type racks. It is based upon the requirements of the Boraflex rack, Type 1, with an assumed amount of Boraflex degradation/shrinkage. While no significant degradation has been shown, or anticipated, in the Ginna Boraflex racks, a significant margin has been included in this analysis to mitigate effects from possible degradation/shrinkage in the future. Figure 4.1-2 illustrates that the majority of the fuel currently stored in Region 2 falls above the curve. The dashed upper and lower curves prescribe a checker board pattern of loading burned fuel to accommodate those assemblies that fall below the base curve. Assemblies with burnups above the base curve, A1 and A2 may be placed directly adjacent to each other, i.e., flat surfaces facing each other. Assemblies below the curve in area B shall only be placed adjacent to assemblies from area A1, or a water hole. They shall not be directly adjacent to each other. Assemblies in area C shall be stored either adjacent to water holes or in Region 1. For a nominal 5.0 wt% ²³⁵U assembly, the base line requires a minimum burnup of 47.25 GWd/mtU. This includes a 5% uncertainty associated with the measurement of the assembly burnup.

Table 4.1-4 lists KENO V.a calculated reactivity values for Region 2 normal conditions. These results are for a Westinghouse 14x14 Standard fuel assembly design. This fuel type bounds the other assembly designs at Ginna with acceptable burnups for storage in Region 2. Consolidated containers are also bounded by this design and may be stored in Region 2 governed by the loading curve.

4.1.3 Abnormal Conditions

The analysis evaluates the abnormal and accident conditions listed below. These conditions are subject to the Double Contingency Principle^{4,6} which allows consideration of the soluble boron in the pool water. Allowance for soluble boron mitigates any reactivity increase and allows the storage rack to satisfy the criticality criterion.



THE UNIVERSITY OF CHICAGO PRESS, 5 EAST LEXINGTON AVENUE, NEW YORK, N. Y. 10017

Abnormal or accident conditions consider several dropped assembly scenarios, misloading an assembly, and seismically induced conditions. Dropped assembly accidents include an assembly dropped on top of the rack (T-bone or shallow drop), outside the rack (side drop), and through a rack cell (deep drop). The misloading accident, i.e., storage of a fuel assembly in violation of the administrative controls, is bounded by assuming the misloaded assembly is fresh with an enrichment of 4 wt% ^{235}U . The bounding accident for Regions 1 and 2 is a misloaded assembly in the Boraflex rack of Region 2. The Δk for this accident is about 0.05. Assuming a soluble boron concentration of 450 ppm in the pool water provides sufficient margin to mitigate any reactivity increases from this, or other, credible accidents.

ANSI/ANS-57.2^{4,1}, Section 6.4.2.1.3, lists the credible abnormal occurrences that must be considered for criticality safety analyses. Those listed above reflect the credible accident for the Ginna storage pool, i.e., shallow drop, deep drop, side drop, misloaded assembly, and horizontal movement of racks due to seismic events. The following occurrences specified in ANSI/ANS-57.2 were not considered:

1. Tipping of the storage rack was not analyzed because the Ginna storage rack fits tightly into the pool.
2. A stuck fuel assembly with a crane providing an uplifting force is construed to mean that the assembly hangs up due to contact between the assembly and the rack structural material. The structural analysis of this event indicates no damage to the racks (Section 3.5.3.1.18). Thus, there is no impact on criticality safety.
3. The only significant objects that could fall into or on the spent fuel rack other than a fuel assembly is the spent fuel handling bridge and the pool gate. The spent fuel handling bridge is restrained to Seismic Class I rails by Seismic Class I restraints to prevent it from jumping the tracks in the event of an earthquake. Seismic Class I anchors retain the winch mechanism on the fuel handling bridge floor. Redundancy is provided on the gate lifting mechanism to preclude a gate drop accident. Thus, there is no impact on criticality safety.
4. No rotating equipment is in the vicinity of the spent fuel pool. Thus, missiles generated by the failure of rotating machinery are not pertinent. Natural phenomena, i.e., a tornado missile, has been analyzed (Section 3.5.3.2.4). There is minimal damage to the top of the storage racks. However, fuel within the rack may be damaged. This damage may cause radiological releases and bowing in the fuel. However, the damage will not have a significant impact on the criticality safety of the storage racks.

4.2 ANALYTICAL METHODS

This section describes the methods used to ensure the criticality safety of the Ginna storage racks. The base analysis methodology employs the SCALE 4.2 code system^{4,7} with KENO V.a. CASMO-3^{4,8} supplements SCALE 4.2 for evaluation of tolerance effects and generation of spent fuel isotopics. These methods provide the basis for generating the burnup versus enrichment curves that govern loading of fuel into the storage racks. Integrated into the Region 2 curves is the consideration of Boraflex degradation in rack Type 1. A brief discussion of these items involved in generating the loading curve is provided in this section.

4.2.1 Criticality Analysis Methodology

The KENO V.a Monte Carlo program calculates the absolute reactivities for the various storage rack configurations. All analyses use the revised 44 group cross section set^{4,9}. This cross section set is processed by the CSAS routines of SCALE 4.2. This system of codes has been verified with extensive in-house benchmarks against critical configurations directly applicable to spent fuel storage pool storage analyses.

The benchmark cases have been chosen to demonstrate the applicability of the SCALE 4.2 system with the 44 group cross section library to spent fuel storage rack analyses. A series of 37 critical configurations closely modeling storage rack configurations have been analyzed. These experiments span a range of fuel enrichments, assembly/pin spacings, and materials interspersed between the fuel arrays applicable to the Boraflex and BSS racks evaluated in this analysis. Additionally, twelve mixed-oxide critical configurations have been examined to verify calculations for burnup credit, i.e., inclusion of plutonium effects. A description of the benchmark cases and a complete discussion of results is provided in Section 4.4.1.

The results from the benchmark calculations indicated no discernable trend relative to enrichment, pin pitch, fuel rod size, or fuel composition. However, they do suggest a trend of increasing bias as a function of the spacing between the edges of the fuel arrays. This is further influenced by the materials inserted into the space between the edges. The Region 1 racks have a spacing of about 3.7 cm (1.45") between the edges of fuel assemblies centered in the rack cells. The KENO V.a bias that corresponds to this spacing, including BSS and SS absorber plate effects, is $-0.0070 \pm 0.0009 \Delta k$. The edge-to-edge spacing between fuel assemblies in Region 2 is about 1.64 cm (0.646"). The KENO V.a bias associated with this spacing is $0.0056 \pm 0.0009 \Delta k$. As noted in Section 4.4.1, independent benchmark calculations presented in the International Handbook of Evaluated Criticality Safety Benchmark verify this trend for typical assembly edge-to-edge spacings for tight lattice storage racks.

4.2.2 Tolerance Evaluation/Burnup Isotopic Generation with CASMO-3

The analysis considers nominal dimensions for modeling both the storage racks and the fuel assemblies. To ensure a margin of safety, the reactivity effects caused by potential variations from the nominal and/or conditions assumed in the analysis must be factored into the analysis. The CASMO-3 program determines tolerance and moderator temperature effects, as well as, burnup isotopics. CASMO-3 is a multi group two-dimensional transport theory program developed for burnup calculations on Light Water Reactor (LWR) fuel assemblies or simple pin cells. The code handles a geometry consisting of cylindrical fuel rods of varying composition in an infinite square pitch array. This capability allows the evaluation of fuel assembly type differences, fuel assembly fabrication tolerances, e.g., enrichment, pellet diameters, etc., and rod consolidation effects. Typical fuel-storage-rack modeling capabilities allow evaluation of rack fabrication tolerances and moderator temperature effects in the storage pool. In addition to its use for sensitivity studies, CASMO-3 provides depletion data for burnup credit evaluations.

The application of burnup credit uses reactivity equivalence of fuel assemblies defined in an initial enrichment versus burnup curve. This allows a tighter pitch for storage of fuel assemblies without restrictive limits on enrichment. An alternative application of reactivity equivalencing is the determination of a curve relating initial enrichment versus the number of IFBA rods for an assembly. For the Ginna storage racks such a curve is defined for fuel with nominal initial enrichments above 4.0 wt%. Similar to the burnup versus enrichment curve, an assembly IFBA rod versus enrichment curve provides equivalency with an unrodded assembly. CASMO-3 is used to generate this curve for the optimal burnup point for IFBA assemblies to be stored in the Ginna storage racks.

4.2.3 Burnup Credit Methodology

Typically, a burnup credit analysis applies a uniform, average burnup distribution over the entire length of the assembly. However, a uniform distribution may underestimate the burnup at the center of the assembly while overestimating the burnup at the top and bottom. To adequately utilize burnup credit, an estimate of the reactivity effects of the axial burnup distribution relative to a uniform distribution must be determined and appropriately applied to the results. Alternatively, the explicit axial distribution can be modeled in the KENO V.a calculation to remove the need for application of an axial burnup penalty. This analysis uses the latter method and is based upon a best estimate of axial burnup shapes and fuel/moderator temperatures for the Ginna plant.

The Ginna spent fuel racks contains three primary types of 14x14 fuel assemblies: the Westinghouse Standard, the Exxon Standard, and the Westinghouse OFA assemblies. The latter generally have axial blankets (currently ranging from natural to about 2.6 wt% ^{235}U) and varying numbers of IFBA rods. The older, Standard assemblies contained neither axial blankets nor IFBA rods. Analytical axial burnup profiles were obtained from RGE for several OFA and Standard assemblies for various enrichment and burnup ranges. From these shapes, best estimates for the burnup profiles for burnup ranges from 10 to 20, 20 to 30, 30 to 40, and 40 to 50 GWd/mtU were chosen. The 23-node analytical profiles were reduced to seven axial zones: the burnup for the three upper and three lower zones are to top and bottom three nodal points while the central zone represents an average of the 17 central nodal points of the analytical profile. Such a seven zone model has been shown to be a reasonable approximation to more axial nodes^{4,10}. For each burnup range the seven zone distribution is normalized to 1 to enable generation of an axial shape for an average burnup by a simple multiplicative process.

CASMO-3 generates the isotopic concentrations for each segment of the axial profile. The segment concentrations are influenced by the axial fuel and moderator temperature distributions that effect the plutonium buildup occurring during depletion. A higher moderator temperature causes spectral "hardening" (a shift of the neutron energy spectrum to higher energy values) which increases conversion of ^{239}Pu from ^{238}U . Additionally, higher fuel temperatures cause Doppler broadening of the ^{238}U resonance structure, also increasing ^{239}Pu production. Typical core average axial moderator and fuel temperature profiles were obtained from RGE and used in the CASMO-3 depletions for the generation of isotopics for KENO V.a.

To reduce the amount of data transfer between CASMO-3 and KENO V.a, only selected actinide isotopes (^{235}U , ^{238}U , ^{236}U , ^{239}Pu , ^{240}Pu , ^{241}Pu), ^{16}O and equilibrium¹⁴⁹ Sm (xenon and iodine are eliminated in both rack models) at shutdown (no decay considered) are explicitly considered in the analysis. The other isotopes are represented by an equivalent ^{10}B concentration. CASMO-3 is used to determine the equivalency. Section 4.4.2 provides an additional description of the methodology and lists the isotopic concentrations for the base calculations.

The ability of CASMO-3 to predict isotopics has been illustrated by a comparison between CASMO-3 predicted and the measured isotopic values for the YANKEE ROWE Power Plant Cores I, II, and IV3.A^{4.11, 4.12}. The ratio of ^{238}U , ^{235}U , ^{236}U , ^{239}Pu , ^{240}Pu , ^{241}Pu , and ^{242}Pu to the initial ^{238}U concentration was compared for the measured and CASMO-3 predicted results. The CASMO-3 predictions were shown to be well within the statistical variations of the measured values. No observed bias is seen for any isotope except ^{242}Pu with CASMO-3 consistently under predicting the measured values by about 9%. Since ^{242}Pu is not an important contributor to k_{eff} , this effect is negligible for this analysis. Based on these results, it is concluded that the uncertainty of CASMO-3 predicted isotopics is bounded by the conservative methodology and the application of a 5.0% burnup uncertainty.

4.2.4 Boraflex Degradation/Shrinkage Methodology

Recent industry-wide blackness testing of Boraflex panels at other reactor storage sites has indicated shrinkage and gap formation in the Boraflex absorber sheets. Additional industry experience with the material has shown degradation, i.e., loss of the polymer material, in the sheets. The effects of both the degradation and the shrinkage of Boraflex in the Type 1 racks of Region 2 are evaluated and factored into the generation of the loading curves for Region 2.

The previous licensing report for Region 2 of the Ginna racks^{4.13} evaluated the effects of a 4% shrinkage and a 4" gap. This was considered a conservative assumption supported by generic studies for rack geometries^{4.14}. Recent blackness testing at other storage pools has indicated gaps ranging from 9" to 12" in length. Other loss of Boraflex into the spent fuel pool has also been postulated recently. The following assumptions and methodologies are used to evaluate the effects of both of these loss mechanisms on the reactivity of the storage racks:

1. Based upon the most recent indication of a 12" gap, an equivalent shrinkage, 8.3% based upon a 144" Boraflex plate, or gap is assumed. For the shrinkage evaluation, it is assumed that the shrinkage is uniform over the length and width of the plate. Thus an equal gap forms at the top and bottom, and at either side of the plate, i.e., 4.15% of the dimension at each edge. No density change is made to the remaining absorber material to reflect the shrinkage. KENO V.a evaluates the shrinkage reactivity effects.
2. The gap evaluation examined a single 12" gap over the length of the plate with an 8.3% shrinkage over the width. The model assumes that the location of the gap is randomly distributed on each plate of the cell. To provide a reasonable model, an array of 16 rack cells is modeled with each of the 32 absorber plates (2 plates per cell) randomly assigned a 12" gap. Appropriate boundary conditions provide an infinite array of this rack. The model assumes a 144" fuel zone with a 144" absorber plate. However, for additional conservatism, the gaps are limited to the central 132 inches of the cells to simulate the most reactive region when axial reflector fuel is used. Water replaces the absorber material in the gap with no

when axial reflector fuel is used. Water replaces the absorber material in the gap with no density modification of the remaining absorber material. The evaluation uses KENO V.a to assess gapping reactivity effects.

3. A detailed CASMO-3 model of the Boraflex rack evaluates the reactivity effects of the potential degradation of the absorber material. This degradation model reduces the thickness of the absorber material in the cell. The evaluation examines various degraded configurations to provide a bounding assessment of the effect. These configurations include replacement of the absorber with water, reduction of the density of the absorber material by the assumed boron loss, and a homogeneous mixture of degraded absorber and water in the absorber region. An evaluation of the required boron concentration in the pool water to compensate for varying amounts of degradation is also provided.

No significant degradation and/or shrinkage is anticipated in the Ginna racks. Indeed, fuel loading practices for Region 2 at Ginna ^{4,15} should reduce damage to the absorber material. However to address any potential absorber loss, the generation of the loading curve for Region 2 for Rack Type 1 includes allowances for Boraflex degradations. A sixteen cell infinite KENO V.a model with both a 12" gap, including 8.3% shrinkage on the width, and reduction of the absorber thickness by 50% provides the geometrical basis for the allowances. Thus, a conservative margin is provided to accommodate a combination of potential gapping and degradation beyond that currently experienced in the industry. This is well beyond that expected for the Ginna storage rack.

4.3 CRITICALITY ANALYSES

The spent fuel racks are divided into two administratively controlled regions (see Figure 4.3-1). Region 1 is designed to accommodate a full core off-load of assemblies. Thus, it must be able to store assemblies ranging from zero to very high burnups. This region comprises 5 modular racks of a borated stainless steel rack design designated as rack Type 3. Rack Type 3 combines a flux trap with a checkerboard pattern of fresh and burned fuel to insure criticality safety. Region 2 provides the bulk of the storage for burned fuel assemblies. It consists of three rack types: Type 1 is the Boraflex design currently licensed; Type 2 is a free standing, BSS absorber plate rack design; Type 4, also a BSS design, is a single row design that may be attached to the north and south faces of the Boraflex rack region for additional storage in the future. Section 1.3 provides a description of the new rack types to be placed in the Ginna storage pool. Figure 1.1-1 illustrates the general arrangement of rack types in the pool.

Section 4.3.1 describes the base input parameters for all the analyses. Section 4.3.2 describes the evaluation of the reactivity effects due to manufacturing tolerances for the rack and fuel assemblies, as well as uncertainties related to storage of fuel in the racks, i.e., fuel assembly type, fuel assembly position, boraflex degradation/shrinkage, and coolant temperature effect. Sections 4.3.3 and 4.3.4 discuss the analysis for normal conditions for Regions 1 and 2. This is followed by a discussion of the evaluation of the interface effects between rack types in Section 4.3.5. Section 4.3.6 describes the accident condition evaluation. The results of these analyses are discussed in Sections 4.3.7. Section 4.3.8 discusses storage of consolidated fuel containers in the storage racks. Finally, Section 4.3.9 relates the results of the analyses to the acceptance criteria for criticality safety.

4.3.1 Input Parameters

This section lists the input parameters used in the analysis of the storage racks. This includes fuel assembly dimensions, rack dimensions, and material specifications.

4.3.1.1 Fuel Assembly Description

Three basic fuel assemblies are stored in the Ginna spent fuel storage racks: Westinghouse Standard assemblies, Exxon Standard assemblies, and Westinghouse OFA assemblies. Table 4.3-1 shows the significant specifications and dimensions for these assemblies. No dimensions are provided for intermediate spacer grids and end fittings since these items are not modeled in the CASMO-3 or KENO V.a calculations. The criticality analysis uses the nominal dimensions of the fuel assembly components to determine k_{eff} . Tolerances are evaluated and included in the determination of K_{max} that is compared to the 0.95 criticality safety criterion.

In addition to an intact fuel assembly, the reactivity of consolidation containers containing fuel rods from up to two assemblies is evaluated. Table 4.3-2 provides information on the structure of the consolidated containers.

4.3.1.2 Spent Fuel Storage Rack Dimensions

A sketch of the Ginna storage rack is provided in Figure 4.3-1. This shows the arrangements of the various rack types to form Regions 1 and 2. Region 1 consists of five modules, or racks, of rack Type 3. Rack 3E contains five cells with the cell internal dimension enlarged to accommodate severely bowed or damaged fuel assemblies. Tables 4.3-3a and 4.3-3b provide the dimensions significant to the criticality analysis. As illustrated in Figure 4.3-1, Region 2 initially will be formed with rack Type 1, the existing Boraflex racks, and Type 2 racks 2A and 2B. Analysis is also provided for peripheral racks, Type 4, that may be added to the north and south faces of rack Type 1 (see Figure 4.3-1). Type 4 racks will be added if additional storage is required in the future. The significant dimensions for these rack types are provided in Tables 4.3-4 through 4.3-6. These tables form the bases for the analytical models described in a later section. Nominal values are used primarily in the evaluation of k_{eff} , and the effects of tolerances are included to determine K_{max} .

4.3.1.3 Material Specifications

Tables 4.3-7 and 4.3-8 provide the region material compositions and number densities used in the models. The first table lists the non-fuel materials. The second table provides the fuel number densities for the analyzed fresh fuel enrichments and the burnup isotopics for fuel with an initial enrichment of 5 wt% ^{235}U burned to 45 GWd/mtU, the upper point for the burnup versus enrichment curves. Section 4.4.2 contains the isotopic number densities for other initial enrichments and limiting burnups used in the analysis.

4.3.2 Tolerance/Uncertainty Evaluation

The fuel rack tolerance results are described in Section 4.3.2.1. Section 4.3.2.2 describes penalties associated with off-center fuel placement while an evaluation of the coolant temperature effect on rack reactivity is provided in Section 4.3.2.3. Tolerance penalties associated with the fuel assembly design, enrichment, and theoretical density are described in Section 4.3.2.4. Section 4.3.2.5 discusses



the reactivity differences among the three fuel assembly types. A summary of the tolerances, uncertainties, and biases applied to the KENO V.a results is provided in Section 4.3.2.6. Table 4.3-12 summarizes the tolerance, uncertainty, and bias values from this evaluation. Additionally, the KENO V.a bias, discussed in Section 4.4.1, is included in this table for completeness.

4.3.2.1 Fuel Rack Tolerance Analysis Methodology

The tolerance penalties associated with the different rack designs are obtained with the CASMO-3 computer code. Rack Types 2, 3, and, specifically, the cells for damaged fuel assemblies in rack 3E are evaluated using a model of 4 rack cells in CASMO-3. Periodic boundary conditions are used to provide an infinite rack model. These models closely approximate the rack configurations sketched in Figures 4.3-2 and 4.3-6. Such models are necessary to evaluate the alternating cell types in these. Rack Type 1 is modeled as an infinite array of Boraflex cells (Figure 4.3-5). The Type 4 rack evaluation diverges from that of the others. Since it is only one cell wide, it is modeled as infinite in one direction. Due to the large water gaps between the Type 4 racks, the pool wall, and the Type 1 racks (Figure 4.3-1), geometry limitations in CASMO-3 preclude either including the Type 1 racks or the pool wall in the model. However, since the primary contribution to the tolerance penalty, as observed for the other rack types, is the water gap between the Type 4 cells, modeling only the Type 4 rack is sufficient and provides a relatively small tolerance penalty. The bounding tolerances for each rack type are listed in Table 4.3-12. Note that the damaged cells of rack 3E (Figure 4.3-4) will not be distinguished from the other Type 3 cells since they are more limiting and only a limited number of Type 3E cells are placed along the outer edge rack 3E.

4.3.2.2 Off-Center Fuel Assembly Analysis

The off-center study evaluates the reactivity effects of fuel assembly movement within the rack cell by placing assemblies in a corner of the cell. This results in an uneven distribution of water between the outer edge of the assembly and the can and places assemblies closer together which may increase reactivity. Due to limitations in CASMO-3, the assemblies can only be arranged in groups of four (except for rack Type 4). Larger off-center groupings require the use of KENO V.a for evaluation. Based on previous calculations with KENO V.a and CASMO-3 the reactivity effect from off-center assembly spacing is not significant. This is illustrated in the listing the off-center penalty for each rack type in Table 4.3-12.

4.3.2.3 Storage Pool Coolant Temperature Effects

The rack analyses were performed for a nominal pool temperature of 68 °F (293 °K). An evaluation of the reactivity changes associated with temperature variations around this nominal value was performed with CASMO-3. The evaluation examined the temperature range from 50 to 212 °F to cover both credible 'cooldown' and 'heatup' events in the spent fuel pool. The reactivity increases from about 0.001 to 0.002 Δk as the temperature is lowered from 68 °F to 50 °F, depending upon rack type, see Table 4.3-12. For all rack types the reactivity decreases as the pool temperature is raised. For this evaluation, pool temperature decreases to about 50 °F are considered credible so a penalty is taken only for the Δk increase from 68 to 50 °F. Pool temperatures below 50 °F are not considered credible and represent an accident condition covered by the double contingency principle. For temperatures below 50 °F, the reactivity change is less than +0.0002 Δk for any rack type. Such small reactivity changes are easily covered by the effect of the 450 ppm minimum boron concentration in the pool water.

4.3.2.4 Fuel Assembly Mechanical Tolerances

This section addresses the reactivity effects due to manufacturing tolerances on the various dimensions of the 14x14 pin fuel assembly types. The major assembly types are the Exxon Standard, the Westinghouse Standard, and the Westinghouse OFA fuel assembly. The variables examined are dimensional changes of the fuel pellet diameter, the pellet cladding ID and OD, the guide tube and instrument tube ID and OD values, the fuel theoretical density, and the enrichment. These penalties are determined with the CASMO-3 code. Bounding penalties are obtained for assembly component parts by varying the component dimension over the allowable tolerance range. The statistically combined tolerance penalty for the fuel pellet, guide tube, instrument tube, and fuel cladding is reported for convenience for each assembly. The fuel pellet enrichment and theoretical density penalties reported separately to illustrate that the enrichments reported for the loading requirements are indeed nominal values. Table 4.3-9 provides a listing of the fuel assembly tolerance penalties. The Exxon assembly is seen to have the largest tolerance penalty for both manufacturing and enrichment variations while the Westinghouse OFA assembly shows the largest penalty related to the variation in theoretical density. A statistical combination of the individual results shows that the Exxon assembly penalty bounds the other assemblies. Thus, the penalty for this assembly is used in the determination of K_{\max} and incorporated into the summary Table 4.3-12.

4.3.2.5 Most Reactive Fuel Type

Three basic types of intact fuel plus twelve lead test assemblies are stored in the Ginna rack. In addition to the intact assemblies, there are several consolidated fuel containers currently in the rack. Thus, the evaluation of the reactivity of different fuel types logically is divided into two areas: intact fuel and consolidated fuel. The evaluation of these fuel types is discussed in this section.

4.3.2.5.1 Intact Fuel Assemblies

A CASMO-3 evaluation of the reactivity of each fuel assembly in a rack type configuration is performed for the two types of Westinghouse assemblies and the Exxon assembly. Table 4.3-10 lists the reactivity differences between the assemblies as a function of burnup for an infinite array of rack Type 1 cells. The Westinghouse OFA assembly is seen to be the most reactive for fresh fuel for normal reactor enrichments, while the Westinghouse Standard assembly is the most reactive for fuel with burnups above about 12 GWd/mtU. The Exxon assembly is bounded by the two Westinghouse assemblies. A separate study for low enrichments, i.e., about 1.95 wt%, showed the Westinghouse Standard assembly to be most reactive even when fresh (the enrichment is similar to that for burned assemblies). These results were factored into the final KENO V.a rack analyses to provide the most reactive conditions by appropriate use of the most reactive fuel in the models. Thus, no penalty is required to correct for fuel assembly type.

In addition to the three basic types of fuel assemblies, 12 Lead Test Assemblies are also stored in the spent fuel rack. They are two each of B&W and Exxon Standard assembly designs, four Exxon Annular Pellet designs, and four Westinghouse Standard mixed-oxide designs. CASMO-3 evaluations of these assemblies showed that their reactivities are bounded by that of the Westinghouse Standard assembly. Thus, they are subject to the same restrictions as the Westinghouse Standard assembly.



THE UNIVERSITY OF CHICAGO PRESS

4.3.2.5.2 Consolidated Fuel Containers

KENO V.a is used to evaluate the reactivity of the consolidation containers for both normal and abnormal conditions. For the normal condition, an evaluation is made of the intact containers in the storage racks. The evaluation examines fresh fuel enrichments of 1.6 and 2.22 wt% ^{235}U at storage pool temperatures, $\sim 68^\circ\text{F}$, for each major type fuel assembly. The container model includes only the outer walls of the container with dimensions bounded by Table 4.3-2. The reactivity worth of the inner plate is also assessed in the evaluation. The reactivity of the container is optimized with a series of cases varying both the number of pins and the pin pitch. The evaluation examines storage of only consolidation containers in a rack or a combination of intact fuel assemblies and containers. The accident case considers a loss of containment of the container that allows the fuel pins to spill into the storage pool. For convenience, a 19×19 array of pins (361) is examined (3 more than available in a full container). The pitch of the array is optimized to provide a bounding accident condition. In addition the effect of the minimum concentration of soluble boron in the pool water, 450 ppm, is determined. This evaluation, for both the normal and abnormal conditions, ensure that the storage of consolidation canisters satisfies the criticality safety criterion for both full and partially filled containers.

4.3.2.6 Summary of Biases, Penalties, and Uncertainties in Analysis

The calculated k_{eff} from KENO V.a results must be adjusted to account for methodology bias and, penalties and uncertainties associated with differences between the calculational model and variations in key parameters of the model. The methodology bias is discussed in Section 4.2.1. Manufacturing tolerance uncertainties and penalties are discussed in Section 4.3.2, as are other uncertainties associated with the choice of parameters factored into the models. These biases, penalties, and uncertainties are summarized in Table 4.3-12 for the four rack types. An additional uncertainty relative to the self shielding of ^{10}B in Boraflex^{4.13} is also included in the rack Type 1 summary. The last row lists the approximate adjustment factor to obtain K_{max} obtained from the additive and statistical combinations of these values. An estimate of the projected calculational uncertainty based upon one million neutron histories, 0.0007, is assumed to obtain this factor.

4.3.3 Region 1 Analysis

Region 1 (rack Type 3) stores spent and fresh fuel in a checkerboard pattern. All interior Region 1 cells are formed by four borated stainless steel sheets (see Section 1.3.1 for a detailed description). Each cell containing a spent assembly also contains a stainless steel casing which surrounds the borated stainless steel plates. Table 4.3-3a lists the dimensions of the rack cell that are explicitly modeled with KENO V.a. Based upon the evaluations for the most reactive assembly (Section 4.3.2.5), a Westinghouse OFA assembly represents the bounding fresh assembly while a Westinghouse Standard bounds the spent assemblies. A discussion of the geometrical model and the burnup credit methodology for Region 1 is provided in this section.

4.3.3.1 Region 1 Geometry Models

The base KENO V.a model represents an infinite rack array in the x-y plane. The axial dimension includes an active fuel length of 144" (365.76 cm) with a 12" (30.48 cm) top and bottom water reflector. The structure of the cells, four BSS rack cells (two with and two without the SS casings), are explicitly modeled in the x-y plane. Periodic boundary conditions on the outer faces of the four combined cell models generate an infinite x-y array of Region 1 cells. Figure 4.3-2 illustrates the base model with two fresh OFA assemblies and two spent Standard assemblies. The axial



THE UNIVERSITY OF CHICAGO PRESS

representation of the infinite model is shown in Figure 4.3-3. Note that this rack has lead-in funnels in the cells without SS casings to facilitate loading of off-loaded fuel. Fresh fuel must only be placed in these cells, not in those with SS casings (and without lead-in funnels) and are so modeled. Reversing the positions increases the reactivity of this region by about 0.2% Δk .

4.3.3.2 Burnup Credit

The application of burnup credit requires more calculations than the typical fresh fuel analysis. The reactivity effect of the following items must be evaluated and factored into the analysis:

- Operating history including fuel and moderator temperature,
- Axial burnup distributions as a function of burnup, and
- Measured burnup uncertainty.

These items contribute to the residual reactivity of the burned fuel, especially for the axial distribution. For a Region 2 type rack which contains burned fuel adjacent to burned fuel, consideration of the axial burnup distribution is necessary to adequately define the loading curve. However, for a checkerboard of fresh and burned fuel, the fresh fuel completely dominates the system's reactivity. Thus, consideration of a uniform average burnup shape for the checker boarded spent fuel is all that is required. This is illustrated in Section 4.4.2.

The following methodology describes the steps to calculate the burnup versus enrichment curve for Region 1. A CASMO-3 hot-full-power depletion with core average fuel and moderator temperatures is performed to determine the isotopic concentrations for the average burnup of an assembly. A second CASMO-3 calculation provides the base k_{inf} for a fuel assembly with all isotopes for rack temperature conditions (note that xenon and iodine are removed) at shutdown. A third CASMO-3 rack model calculates the k_{inf} with only the shutdown fuel pin concentrations of ^{16}O , ^{235}U , ^{238}U , ^{236}U , ^{239}Pu , ^{240}Pu , ^{241}Pu , and ^{149}Sm (xenon and iodine are eliminated in both models). A small amount of ^{10}B is added to the fuel pin until the k_{inf} from the second CASMO-3 calculation agrees with that of the first. In this manner, the added ^{10}B simulates the neutron absorption of the isotopes not present in the KENO V.a model. These concentrations are inserted in the KENO V.a model and k_{eff} calculated. If the k_{eff} is not satisfactory, the burnup is changed and the entire process repeated until a target K_{max} of about 0.94 is obtained. This is then repeated for additional enrichment values. The burnup/enrichment pairs provide the points to define a polynomial fit to the burnup versus enrichment curve of Figure 4.1-1 that generates the values in Table 4.1-1. Based upon the conservatism inherent in the model and the penalties applied, the proximity to the 0.95 criticality limit is justified.

4.3.4 Region 2 Analysis

Region 2 consists of rack Types 1, 2, and 4. Type 1 is the existing Boraflex rack which contain 840 cells in a 30 x 28 array. The Type 2 racks (see Figure 1.1-1) consist of two borated stainless steel (BSS) racks, rack 2A (8 x 11 array) and rack 2B (9 x 11 array). Type 4 racks consist of six individual racks of 10 cells each (Figure 1.3-13) and are attached to North and South faces of the Type 1 racks. An infinite model of each of the Types 1 and 2 racks provides the evaluation for these racks. The single row dimension, and positioning of the Type 4 rack preclude an individual analysis of this rack. The evaluation for this rack is combined into a model containing both rack Types 1 and 2.

4.3.4.1 Region 2 Geometry Models

Individual infinite (in x-y plane) rack models are used for rack Types 1 and 2. The evaluation of Type 4 requires consideration of interactions with Type 1 to adequately evaluate the reactivity of this rack type. Since a combination of rack types is required, a model is developed that examines all the Region 2 rack types together for the evaluation of Type 4. In all cases, the use of the Westinghouse Standard assembly provides bounding results for spent fuel in this region.

4.3.4.1.1 Rack Type 1 - Boraflex Rack

The Boraflex rack contains only a single cell configuration. A model of this cell was created and combined into a multi-cell array with periodic boundary conditions to create an infinite array in x-y extent (see Figure 4.3-5). The axial model is similar to that for Region 1, as illustrated in Figure 4.3-3. The nominal dimensions listed in Table 4.3-4 were used in the explicit model of this rack. As noted in Section 4.2.4 a significant amount of Boraflex degradation is included in the model. The model contains a 16x16 array of cells with Boraflex panels each containing a randomly distributed 12" axial gap, a 8% width shrinkage, and a 50% reduction in the plate thickness. A nominal rack model without degradation provides a measure of the reactivity change obtained from this degraded model.

4.3.4.1.2 Rack Type 2 - Borated Stainless Steel Rack

The BSS racks contain two cell types. One type is manufactured from 3 mm, borated stainless-steel plates (SS304 B7), and the other consists of a 2 mm, unborated stainless-steel can (SS304L). Figures 1.3-8 and 1.3-12 provide illustrative drawings for this rack type. The two basic cells are fabricated into a checkerboard pattern with a nominal 2.32 mm water gap located between cells in the x-y directions. The model of the 2x2 array of the two different cells uses a periodic boundary condition to create an infinite array in the x-y plane (see Figure 4.3-6).

4.3.4.1.3 Region 2 Combined Model for Rack Type 4 Evaluation

Rack Type 4 (Figure 1.3-13) is similar in design to rack Type 2. However, there are some notable differences. This type consists of only a single row of cells with a relatively large water gap between rack Type 4 and either rack Type 1 or the pool-wall (see Figure 1.1-1). The large water gaps allows the absorber cells to be fabricated with BSS plates only between adjacent Type 4 cells, i.e., in the east-west direction. Based on the single row configuration, this type can be adequately analyzed only in combination with the adjacent Type 1 rack. A combined model was developed for the interface effect evaluations (Section 4.3.5) for Types 1, 2 and 4, i.e., the south face of Type 1 (see Figure 4.3-7). It was used for the evaluation of this rack. The south face of Type 1 was chosen since this face does not contain Boraflex. This lack of Boraflex facing the Type 4 rack makes this more reactive than the north face. Inclusion of Type 2 allows a good assessment of the total reactivity of Region 2.

The base interface model is described in Section 4.3.5. Modifications to this model were made to implement the degraded Boraflex model into the Type 1 model. Thus, a bounding, geometrical model of Region 2 is contained in this evaluation.



4.3.4.2 Region 2 Loading Curve Generation

As mentioned above for Region 1, the application of burnup credit requires several basic calculational steps: 1) determine appropriate axial power shapes as a function of burnup, 2) determine axial intervals to be modeled, and generate burnup isotopics and cross sections for these burnup intervals, 3) integrate operating history data into the model directly or through appropriate penalties to be applied to the final results, and 4) iterate on burnup for a series of enrichments to develop an acceptable burnup versus enrichment curve for the storage rack design. For a rack containing completely burned fuel axial effects are significant and must be assessed. This section provides a brief description of the methodology for the burnup credit analysis. Details for these steps are provided in Section 4.4.2. This methodology for burnup credit is very similar to that accepted by the U.S. Nuclear Regulatory Commission^{4.10, 4.13, 4.16}.

4.3.4.2.1 Base Burnup vs Enrichment Curve Generation

Generation of the burnup versus enrichment curve includes consideration of axial burnup effects and fuel irradiation conditions. This information is used to obtain the isotopic concentrations of the burned fuel for the analysis. A brief description of this process is provided in this section.

Axial profiles are determined for selected average burnup values from three dimensional fuel cycle design data for the Ginna reactor. These profiles are then collapsed into the seven axial segments used in the KENO V.a model. The top and bottom three segments are exactly the same burnups, and spacings, of the 3D fuel cycle design calculations. The center burnup segment is adjusted to balance the average assembly burnup to the desired burnup value when weighted with the burnups at the ends of the assembly. Previous studies have shown that the seven axial zone model provides results equivalent to a 15 axial segment model^{4.10} which nearly duplicates the nodes in the fuel cycle design analysis.

A CASMO-3 hot-full-power depletion is performed to determine the isotopic concentrations in each axial segment at the appropriate burnup and fuel and moderator temperature. A second CASMO-3 calculation provides the base k_{inf} for a fuel assembly with all isotopes for the rack temperature condition at shutdown. A third CASMO-3 rack model calculates the k_{inf} with only the shutdown fuel pin concentrations of ^{16}O , ^{235}U , ^{238}U , ^{236}U , ^{239}Pu , ^{240}Pu , ^{241}Pu , and ^{149}Sm (xenon and iodine are eliminated in both rack CASMO-2 calculation). A small amount of ^{10}B is added to the fuel pin until the second CASMO-3 k_{inf} agrees with the first. In this manner, the added ^{10}B simulates the neutron absorption of the isotopes not present in the KENO V.a model. To generate the curve, an iteration process is used to determine the minimum burnup to give a target k_{eff} , about 0.94 for this case. If for the initial burnup, the KENO V.a is not satisfactory, the burnup is changed, and the entire process repeated for a given burnup profile. This method is repeated for several enrichments to obtain the burnup/enrichment pairs for the loading curve in Figure 4.1-2. A polynomial is fit to the burnup versus enrichment curve of Figure 4.1-2 to allow generation of the points in Table 4.1-2. Based upon the conservatism inherent in the model, the use of bounding axial profiles, and the penalties applied, the proximity to the 0.95 criticality limit is justified.

4.3.4.3 Generation of the Loading Curve for Abnormal Assemblies

Figure 4.1-2 defines the burnup versus enrichment requirements for the Region 2 storage racks. Fuel located above the base curve, areas A1 and A2, can be loaded anywhere in Region 2 next to fuel with burnups above the base line. Most of the burned fuel assemblies currently residing in the racks



(diamonds in Figure 4.1-2) fall in areas A1 or A2. To allow flexibility, and to preclude filling the Region 1 rack with lower burned assemblies, evaluations are made to determine the administrative controls to load fuel assemblies falling below the curve in Figure 4.1-2 . These evaluations examine two classes of fuel assemblies below the base curve: those with average burnup within a specified burnup range below the burnup versus enrichment curve limit, area B, and those with burnup below this range, area C.

The analysis develops secondary curves to allow storage of those assemblies with burnups (Figure 4.1-2) up to about 15% below the normal curve, defined as area B. Following the above procedure for the normal curve, an administrative loading scheme is developed that relies on the two secondary curves in Figure 4.1-2 (the upper and lower boundary lines). The intercept of the polynomial fit to the base curve is adjusted to fit a burnup point 10% below the base curve at 5.0 wt% ^{235}U nominal enrichment. This value is further reduced 5% to account for measured burnup uncertainty to give a total value of $(0.9)(0.95) = 0.855$ below the 5.0 wt% enrichment curve value. This curve has the same slope as the base curve. Based upon this lower curve, CASMO-3 rack calculations generate the upper boundary polynomial line. This is done with a rack model containing four cells that checker board the lower line fuel with estimated values on the upper line for 5.0 wt% ^{235}U fuel. The burnup for the upper line is adjusted until the k_{inf} of the model equals that for the base line. Once the burnup is defined, the intercept of the base line polynomial is adjusted to fit this point. Thus, the upper curve also has the same slope as the base curve. It is noted that for lower burnups, the burnups in area B may be significantly lower than 10% of the nominal curve. The above calculations define a checker-board loading scheme. Area B assemblies with burnups above the lower burnup boundary must be loaded directly adjacent (in a checker board pattern) to area A1 assemblies with burnups above the upper burnup boundary line. Another acceptable loading pattern for these fuel assemblies is alternating rows of A1 and B assemblies. If the B fuel is placed on the outside edge of a rack near the pool wall, A1 fuel must be placed directly adjacent to it in the rack. KENO V.a calculations at several enrichments verify the validity of the additional curves.

Fuel with burnups and enrichments below the lower boundary line, designated area C fuel, require an alternate loading scheme for storage in the Region 2 fuel racks. The limiting area C fuel assembly is fresh fuel at a nominal enrichment of 4.0 wt% ^{235}U . A KENO V.a calculation for this condition uses two 4.0 wt% ^{235}U fresh fuel assemblies diagonally opposite each other in a checker board pattern with two water locations (no assemblies). Thus, the use of water holes adjacent to fuel will satisfy the loading criteria for any enrichment/burnup combination. This arrangement may be used in place of storing fuel below the line in Region 1.

4.3.5 Interface Effects

The interaction between Regions 1 and 2, i.e., interface effects, is also examined, as well as that between the Boraflex racks and BSS racks in Region 2. Three areas of the racks in the pool were modeled to assess these effects. The areas of interest as shown in Figure 4.3-7 are:

1. Interfaces between (1) racks 3C and 2B and (2) racks 2B and 3E.
2. Interfaces between racks 1, 4F, and 3A.
3. Interfaces between racks 1, 4C, and 2A.



THE UNIVERSITY OF CHICAGO LIBRARY

1967

Figures 4.3-8, 4.3-9, and 4.3-10 show sketches of each model. The same KENO V.a geometry models were identical for the examination of the 2B/3C interface and the 2B/3E interface. The only difference was the position of a spike in the neutron starting distributions at the interface of interest. A similar start type application was applied to models 2 and 3 listed above for the other interfaces. In each model, sufficient concrete, 19.7" (50 cm), and water, 12" (30.48cm) is modeled to adequately represent reflective surfaces.

4.3.6 Accident Analysis

The accident analyses examine the following assembly drop conditions for each region: an assembly dropped horizontally on top of rack Types 2 and 3 and an assembly dropped vertically beside racks 2B and 3E. For both Regions 1 and 2, the effect of a misplaced assembly was also examined to ensure criticality safety. For a seismic event, the reduction in the rack Types 2 and 3 rack-to-rack separation distance was examined. These accidents are extremely improbable, and any associated reactivity increase can be mitigated by the soluble boron in the pool water. As part of this analysis, the reactivity effect of the soluble boron in the water was evaluated to determine the reactivity margins for the accident conditions.

The KENO V.a accident models are based on the infinite, or finite base models for both regions. Only modifications necessary to describe the accident condition are made to the base models. This allows assessment of the impact of the accident by examining the reactivity difference between the results from normal and accident models.

4.3.6.1 Region 1 Assembly Drop Analyses

Region 1 assembly drop analyses include the T-bone (shallow drop), side drop, and deep drop accidents. The following paragraphs describe the models for each accident.

The T-bone accident is a class of shallow-drop accidents in which the dropped assembly is assumed to lay horizontally atop the rack (see Figure 4.3-11). The dropped assembly is represented as a full assembly in both the x and y directions. Periodic boundary conditions on the right and bottom faces approximate a dropped assembly at the center of a 24 x 24 cell rack region. The rack deformation from the dropped assembly is negligible (Section 3.5.3.2.3.2.1). However, for conservatism, the model places the dropped assembly in direct contact with the top of the active fuel region of the assemblies in the rack, i.e., the upper nozzles are neglected. This provides a bounding accident scenario. For a reference case the same model is used with the dropped assembly replaced with water. The difference between the k_{eff} of the accident and the reference case provides the reactivity increase of the accident.

The T-bone model bounds the other shallow-drop accident, the vertical drop, in which the dropped assembly falls into a storage space and impacts upon the top of a stored assembly but remains vertically above the assembly. Since the upper and lower endfitting dimensions will maintain at least a 4" (10.16 cm) gap between the active fuel regions, the accident is less reactive than the modeled T-bone accident. Any reactivity effects from the minor bowing that may result in the stored assembly due to the impact will be negligible relative to the margin obtained from the soluble boron in the pool water.



ALL INFORMATION CONTAINED HEREIN IS UNCLASSIFIED DATE 08-14-2010 BY 60322 UCBAW

The Region 1 side-drop model required modification to the rack Type 3 finite model (Figure 4.3-4) in that the southwest corner cell of rack 3E was removed and replaced with a fresh assembly immediately next to racks 3E and 2B (see Figure 4.3-12). This configuration is not considered possible, but is used for conservatism. This is the only location that exists where an assembly can be vertically dropped and have fuel on two adjacent faces without an absorber material between the dropped assembly and those in the racks. Based upon this consideration it is also the most reactive configuration for a side drop accident. A second case with the dropped assembly replaced with water provides the base case for determination of the reactivity increase due to the accident.

The deep-drop accident considers a fuel assembly dropped into a rack cell (see Figure 4.3-13). The assembly is assumed to impact the bottom plate of the rack which is supported by pads on about 37" (94 cm) centers. It is assumed that an assembly drops at the center of a section and deforms the rack base plate to the maximum determined from the structural analyses, 2.12" (Section 3.5.3.2.3.1.1). Thus, the drop causes a concave depression in the plate, with assemblies positioned along the curved surface, Figure 4.3-13. Due to the complexity of explicitly modeling the accident condition, a bounding analysis is used. The analysis assumed all fuel assemblies in the rack were displaced 3.2" (8.13 cm) below the bottom of the rack. The Δk from a base model is determined as well as the minimum boron concentration pool water needed to reduce the system below the 0.95 limit. Note that due to the similarity in construction of rack Types 2, 3, and 4, the results from the Type 3 rack bounds those from Types 2 and 4.

The misplaced assembly accident assumes that during loading an assembly is placed in a location that violates the loading curve requirements. The accident model assumes that a fresh 4.0 wt% ^{235}U fuel assembly is placed into a spent rack location between four fresh assemblies (see Figure 4.3-14) in the Region 1 finite model. The model focuses the neutron starting distribution into the misplaced assembly to ensure that the assembly is adequately sampled. The result of this model is then compared with that of the normal condition, finite model to assess the Δk effect of the misplaced assembly.

4.3.6.2 Region 2 Assembly Drop Analyses

Four accidents were examined for the Region 2 racks: the T-bone on rack Type 2, side drop, misplaced assembly, and deep drop into a storage cell. The accident models assumed that the rack contained the highest allowable fresh fuel enrichment. The dropped assembly is assumed to be fresh 4.0 wt% ^{235}U fuel. The use of the maximum enrichment provides a bounding accident analysis with respect to fuel loadings.

The model for the Region 2 T-bone accident is similar to that for Region 1. For Region 2, rack Type 2 was used for the accident model since in a normal condition it is slightly more reactive than Type 1. Figure 4.3-11 provides a sketch of the model with the dropped assembly laying horizontally across the top of the rack. The Δk is determined from the results from cases with and without the dropped assembly.

The side-drop accident for Region 2 has already been considered in that used for Region 1. The dropped assembly is positioned adjacent to rack Type 3 of Region 1 and Type 2 of Region 2 (Figure 4.3-12). As noted in the discussion for the Region 1 accident, this is a bounding analysis and an individual assessment for the other rack types of Region 2 is unnecessary. If rack Type 4 is installed



1. The following information is being furnished to you for your information and use only. It is not to be distributed outside your organization.

2. This information is being furnished to you for your information and use only. It is not to be distributed outside your organization.

in the pool (Figure 4.3-1), there is insufficient space to place an assembly between the rack and the pool wall. However, prior to its installation, there is sufficient room for a dropped assembly to lodge between the wall and rack Type 1. This again is bounded by the analysis for the dropped assembly located in the corner of Types 2 and 3. The worst case for rack Type 1 is a drop on the south side of the array which does not contain Boraflex on the outer surface. This is equivalent to the assembly dropped adjacent to the Type 2 rack cell which also does not contain BSS. Thus, only a single layer of stainless steel separates the assemblies. The stainless steel in the Type 1 rack is about 0.01" (0.0254 cm) thicker than the Type 2. Due to the mild absorption of the stainless steel, this will reduce the effect of the drop in the Type 1 rack. In addition, based upon the results from the Type 2 and 3 side drop (Table 4.3-13), the effect is minimal and a low level of soluble boron reduces maintains k_{eff} within acceptable limits.

A misplaced assembly model was created for rack Types 1 and 2 similar to that for Region 1. In each model a 4.0 wt% ^{235}U fuel assembly is placed either into the Boraflex cell of rack Type 1 (see Figure 4.3-15), or into the stainless steel cell of rack Type 2. The misplaced assembly is placed in a location to provide a bounding reactivity increase. Both models focus the starting neutrons into the misplaced assembly. The Boraflex rack model includes Boraflex degradation and assumes that the misplaced assembly is placed in the most reactive checker board location of spent fuel assemblies. The model assumes an infinite array of 144 cells with a 4 wt% ^{235}U OFA assembly near the center of the array. The results of these models are then compared with those of the finite geometry models to assess the Δk effect of the misplaced assembly.

The deformation due to the deep drop accident for rack Types 2 and 4 is equivalent to that for rack Type 3 (Figure 4.3-13). Thus, they are covered by that analysis. Rack Type 1 has been fabricated differently from the Type 2, 3, and 4 racks. Rather than a single base plate across the bottom of each rack, individual plates are welded at the bottom of each cell to support the fuel assembly. Thus, under the hypothetical drop accident (Figure 4.3-16), it is assumed that the bottom welds break. This will allow a maximum of 14" (35.56 cm) of the assembly to be exposed below the rack. Due to the unique construction of each cell, there is no damage, or deformation, in surrounding cells. Two types of fuel assemblies can be considered for this accident. For a spent assembly that can be stored in the cell in which it is dropped, the post accident condition is equivalent to a partially inserted assembly during loading and results in no impact on criticality safety. Similarly for a fresh 4.0 wt% ^{235}U fuel assembly, this accident is bounded by the misplaced assembly accident. The portion of the dropped assembly in the cell is equivalent to a misplaced assembly and is bounded by that evaluation. The 14" (35.56 cm) displacement below the rack is equivalent the portion of an assembly that protrudes from the rack during insertion. This portion is essentially isolated from the assemblies in the rack and thus does not affect the reactivity of the rack. Thus, since this accident condition is bounded by the misplaced assembly accident; the minimum soluble boron concentration in the pool is sufficient to offset any reactivity increase.

4.3.6.3 Seismic Analysis

The structural analysis for the seismic accident indicates that there will be no impacts between adjacent racks or between the racks and the pool walls (Section 3.5.3.1.14). Thus, there is no mechanism for significant permanent rack deformations in either rack region. The analysis shows that during the worst seismic event, the gaps between the racks will always be greater than 0.071" (0.18 cm), see Table 3.5-137 and 3.5-138 column labeled 'Final Gap Between Racks'. This includes



both lateral movement and momentary swaying of the rack during the seismic event. Thus, there is no physical contact between adjacent racks. Based upon these results, an evaluation of the reactivity effect of rack movement was made for Regions 1 and 2 and for the interfaces between these regions. The specific models for the seismic events are discussed below.

4.3.6.3.1 Region 1 Seismic Analysis

The Region 1 based plates normally are spaced 0.79" (2.0 cm) apart (see Figure 3.5-36), approximately maintaining the rack cell pitch. For the seismic analysis, it is assumed that each rack Type 3 base plate touches that of the adjacent rack. The geometry model for the Region 1 seismic model is identical to Region 1 interface model sketched in Figure 4.3-7, except that the nominal water gaps between the base plates are reduced to zero width, i.e. the base plates are touching. The Δk effect of the Region 1 seismic event is determined from the difference between the nominal water gap model and the model without water gaps between the base plates.

4.3.6.3.2 Region 2 Seismic Analysis

As in Region 1, the seismic event may cause the free standing Region 2 racks to shift, one relative to the other, such that the base plates may touch each other. This accident has no effect on the current criticality analysis, since an infinite array of cells is considered without inter-rack spacings. Thus, the base model is identical to a seismic model. So even if the racks move directly adjacent to each other or if the cans sway and touch at the top without rack movement, the resulting geometry is no more limiting than the infinite lattice. This is verified further by the explicit interface models for Region 1 and 2 in the next section.

4.3.6.3.3 Interface Region Seismic Analysis

The seismic event is assumed to move all the racks so that their base plates are touching. This was modeled for the Type 1, 2, and 3 racks. For Type 4 a more severe result was modeled. This model assumed that the Type 4 racks were compressed until they touched the edges of the Type 1 racks. All these conditions are beyond the seismic conditions projected by the structural analyses in Section 3.5.3.1.14. At the interface between the two regions, the seismic event is assumed to reduce the spacing between Regions 1 and 2. The combined interface model is used with a reduced spacing between the regions of 0.004" (0.01 cm). Again, this bounds any actual calculated minimum gap of 0.071" (0.18 cm), which reduces the separation between cells from 1.57" (4.0 cm) to 0.85" (2.17 cm). The difference between the results of the seismic and the base interface models determine the Δk of the event. As with the interface models, the size of the racks requires an examination of selected portions of the racks (see Figure 4.3-7). The first evaluation examined the Type 2 and 3 movement. The evaluation seismic effects on the Type 1 racks, were divided into effects for Types 1, 2A, and 4C, i.e., the south face of the rack, and the north face, Types 1, 3A, and 4F. The south face is expected to show the highest increase in reactivity because of the lack of Boraflex on the south face of the Type 1 rack.

4.3.7 Summary of Results

This section lists the results from the various analyses for the Ginna storage racks. They show that the racks satisfy the 0.95 criticality safety criterion for both normal and abnormal conditions. The bases for this conclusion are provided in this section.

4.3.7.1 Analytical Results for Region 1

The results for the normal condition of Region 1 are listed in Table 4.1-3 which provides the calculated k_{eff} and the maximum k , K_{max} as a function of burnup and enrichment. Accident condition reactivities are summarized in Table 4.3-13. A brief discussion of these results is given in this section.

4.3.7.1.1 Normal Condition Results

Each model used in this analysis provides a calculated k_{eff} based upon nominal dimensions. Thus, the effects of variations around the nominal and biases must be combined with the calculated k_{eff} to determine maximum K-effective (K_{max}). Table 4.3-12 summarizes the Region 1 penalties, uncertainties, and biases that are used to obtain K_{max} . K_{max} is calculated for Region 1 as follows:

$$K_{\text{max}} = k_{\text{eff}} + \Delta k_{\text{bias}} + \Delta k_{\text{pen}} + \sqrt{(1.763 * \sigma_c)^2 + (1.763 * \sigma_{\text{bias}})^2 + (\sigma_{\text{tol}})^2}$$

where,

- k_{eff} is the calculated k from KENO V.a;
- Δk_{bias} is the KENO V.a methodology bias;
- Δk_{pen} is the sum of penalties for pool temperature and off-center placement;
- σ_c is the KENO V.a statistical uncertainty in k_{eff} ;
- σ_{bias} is the uncertainty in the KENO V.a methodology bias;
- σ_{tol} is the sum of tolerance uncertainties.

The Region 1 analyses considered fresh 4.0 wt% ^{235}U fuel checker boarded with spent fuel. The spent fuel burnup versus enrichment curve illustrated in Figure 4.1-1 specifies the minimum burnup versus enrichment for the loading spent fuel adjacent to fresh assemblies in this region. The target k_{eff} used to generate the curve was approximately 0.92 to provide a K_{max} of about 0.94. The KENO V.a results are shown in Table 4.1-3. These results are based upon 1,000,000 neutron histories (1000 batches of 1003 neutrons), as are all KENO V.a results. As seen, the highest K_{max} for any enrichment is 0.943 with a margin to the limit of 0.0081. This verifies that the Region 1 racks satisfy the criticality safety criterion for fresh fuel with a nominal enrichment less \leq 4.0 wt% ^{235}U .

The minimum burnup values listed in Table 4.1-3 are those that provide the desired k_{eff} from KENO V.a. However, the loading of assemblies in the rack is based upon 'measured' burnups from the plant computer. To account for the uncertainty in the measured burnup, the calculated burnups used in the loading curve are increased by 5%. The 5% value is based upon the flux map measurement uncertainty of the incore detectors^{4,17} and is similar to the uncertainty of other Westinghouse plants^{4,18,4,19}. Since burnup is the integrated power over time, the power uncertainty limits the maximum uncertainty in burnup to less than 4% for the integrated power and 5% for the local power. Thus, a 5% value has been conservatively selected for the uncertainty of the assembly average measured burnup.



4.3.7.1.2 Burnup Versus Enrichment Curve

A polynomial curve is generated to allow easy determination of the burnup limit at a given nominal enrichment based on the data points in Table 4.1-3. A multiple regression analysis is performed on the enrichment/burnup points, and a third order polynomial is determined. The resulting polynomial curve that differentiates Region A from Region B in Figure 4.1-1 is:

$$y = -53.570547 + 38.06359x - 7.81411x^2 + 0.692842x^3$$

where x is nominal enrichment in wt% ^{235}U and y is in terms of either MWd/kgU or GWd/mtU. Based upon this polynomial, the minimum burnup for fuel with a nominal enrichment of 4.0 wt% ^{235}U is 28 GWd/mtU. For the loading curve and Table 4.1-1, this value is multiplied by 1.05 to account for the burnup measurement uncertainty. Thus, for fuel with a nominal enrichment of 5.0 wt% ^{235}U fuel, a minimum burnup of 29.4 GWd/mtU is required for the spent fuel to be loaded in Region 1. Table 4.1-1 lists the acceptable burnups versus enrichments based upon the above polynomial fit to verified points at enrichments of 2.22, 3, 4, and 5 wt%.

4.3.7.1.3 IFBA Rod Requirements

The previous licensing analysis^{4,10} used the concept of reactivity equivalencing for storage of fuel assemblies with nominal enrichments greater than 4.0 wt% ^{235}U in the Region 1 racks. This concept, based upon the reactivity decrease associated with the addition of Integral Fuel Burnable Absorbers, is retained for fuel with nominal enrichments greater than 4.0 wt% ^{235}U . The IFBA analysis performed for the previous licensing report was not repeated in its entirety. However, CASMO-3 calculations were performed to verify that the IFBA requirements specified in that analysis remain valid for the BSS racks of Region 1. Similarly, the k_{∞} reference criticality reactivity point was verified as 1.458 for fresh fuel in Ginna core geometry with a nominal enrichment of 4.0 wt% ^{235}U . Thus, the results, and appropriate use of the results from the previous analysis remains applicable to storage of fuel assemblies with nominal enrichments greater than 4.0 wt% ^{235}U in the Region 1 racks. For completeness, the appropriate IFBA sections of the previous licensing document are listed in Section 4.4.3.

4.3.7.1.4 Accident Conditions

The results for the analysis of the assembly drop accidents, i.e., T-bone, misplaced assembly, side drop and deep drop, are discussed in this section. In addition, the results from the seismic event are provided for all rack types.

a) Assembly Drop Accidents - The Region 1 assembly drop analyses include the T-bone, side drop, deep drop (or drop through) accidents, and the misplaced assembly. Table 4.3-13 summarizes the results from these analyses. The T-bone accident has a minimal effect on reactivity, i.e., within the statistical uncertainty of the cases, even though it is a very conservative model. The misloading of a 4 wt% ^{235}U fresh assembly between four adjacent assemblies shows only a small reactivity increase, about 1% Δk . The deep drop accident with maximum expected deformation of the base plate shows essentially no change in reactivity. The dropping of an assembly in the cask lay down area (Figure 4.3-12), in the corner between racks 3E and 2B, shows the largest increase for a dropped assembly, about 4% Δk . Since application of the soluble boron credit is allowed by the double



W. B. G. & Co. 1000 Broadway, New York, N. Y.

W. B. G. & Co. 1000 Broadway, New York, N. Y.

W. B. G. & Co. 1000 Broadway, New York, N. Y.

W. B. G. & Co.
1000 Broadway
New York, N. Y.

contingency principle, 300 ppm boron was added to the water in the model. This reduced the reactivity about 2% Δk below the base case, or about 6% Δk below the accident value. Thus, a small concentration of boron in the pool water, <300 ppm, easily compensates for the reactivity from any of these accidents.

b) Seismic Conditions - As discussed in Section 4.3.6.3, the seismic event is assumed to have moved all the racks so that their base plates are touching. This was modeled for the Type 1, 2, and 3 racks. For Type 4 a more severe result was modeled. This model assumed that the Type 4 racks were compressed until they touched the edges of the Type 1 racks. All these conditions are beyond the post-event conditions projected by the structural analyses in Section 3.5.3.1.14. The results of the analyses are listed in Table 4.3-15.

The first evaluation examined the Type 2 and 3 movement. The accident results in about a 0.4% Δk increase in reactivity over the normal condition. Due to the number of Type 1 racks in Region 2, the evaluation of seismic effects on the Type 1 racks examined only portions of Region 1 (see Figure 4.3-7). The effect on Type 1, and racks 2A and 4C, i.e., the south face of the rack, and Type 1 and racks 3A and 4F, the north face, were considered individually. The south face, as expected, showed the highest increase, about 1% Δk . This was expected due to lack of Boraflex on the south face of the Type 1 rack. The north face showed an increase equivalent to that for Types 2 and 3 alone, about 0.4% Δk . Due to the small change in reactivity associated with this accident, the 300 ppm soluble boron required to cover the side-drop accident is more than sufficient to cover the seismic event effects.

4.3.7.2 Analytical Results for Region 2

The Region 2 analysis requires a more in-depth discussion since burnup credit is more extensively applied in Region 2. The results for the normal conditions are discussed in Section 4.3.7.2.1. Development of the burnup versus enrichment curve is addressed in Section 4.3.7.2.2. A discussion of the auxiliary curves that allow the loading of abnormal assemblies is provided in Section 4.3.7.2.3. Finally accident condition results are related in Section 4.3.7.2.4.

4.3.7.2.1 Analytical Results for Normal Conditions

Each model used in this analysis provides a calculated k_{eff} based upon nominal dimensions. Thus, adjustments are made to the calculated k_{eff} to obtain the maximum k_{eff} (K_{max}). Table 4.3-12 summarizes the Region 2 uncertainties, penalties, and biases and combines the individual values to provide the overall adjustment as a function of rack type. These values are then applied to the k_{eff} calculated by KENO V.a as follows:

$$K_{max} = k_{eff} + \Delta k_{bias} + \Delta k_{pen} + \sqrt{(1.763 * \sigma_c)^2 + (1.763 * \sigma_{bias})^2 + (\sigma_{tol})^2}$$



where,

- k_{eff} is the calculated k from KENO V.a;
- Δk_{bias} is the KENO V.a methodology bias;
- Δk_{pen} is the sum of penalties for pool temperature, ^{10}B self-shielding, and off-center placement;
- σ_c is the KENO V.a statistical uncertainty in k_{eff} ;
- σ_{bias} is the uncertainty in the KENO V.a methodology bias;
- σ_{tol} is the sum of tolerance uncertainties.

As discussed in Section 4.4.2.4, a significant amount of Boraflex degradation, i.e., both gapping and loss of thickness, are included in the base model for the Type 1 rack (providing a Δk margin of 0.048, see Section 4.4.2.4). To facilitate the management of the loading of the rack, a single loading curve for all three rack types is desired. Thus, the loading curve for Type 1 is bounding. This rack represents the base model that is used to generate the loading curve. Subsequently, the application of this curve to Types 2 and 4 will validate the conservatism of a single loading curve for all rack types in Region 2. The burnup versus enrichment curve for Region 2 is illustrated in Figure 4.1-2. It specifies the minimum burnup versus enrichment for loading spent fuel in this region. The target k_{eff} used to generate the curve was about 0.93 to provide a K_{max} of about 0.94. The results of the KENO V.a calculations are shown in Table 4.1-4 for all the rack types comprising Region 2. As seen, the highest K_{max} for any enrichment is 0.946 with a margin to the limit of 0.004. This verifies that the Region 2 racks satisfy the criticality safety criterion. Also recall that the values for the Type 4 rack result from a finite model that combines all three types in Region 1 and represents the more reactive south face. This combination shows that the infinite models used to generate the results for Types 2 and 3 provides an additional margin in the results over that from a more explicit finite model.

4.3.7.2.2 Base Burnup Versus Enrichment Curve

As with Region 1, a polynomial curve is generated for Region 2 to allow easy determination of the burnup limit at a given enrichment. For Region 2, the base curve fits the data points from the Type 1 results in Table 4.1-4. A multiple regression analysis is performed on the enrichment/burnup points, and a third order polynomial is determined. The resulting polynomial curve that differentiates regions A1 and A2 from regions B and C in Figure 4.1-2 is:

$$y = -27.058824 + 17.69608x - 0.41176x^2 - 0.04902x^3$$

where x is the nominal enrichment in wt% ^{235}U and y is in terms of either MwD/KgU or GWd/mtU. Based upon this polynomial, the minimum burnup for fuel with a nominal enrichment of 5.0 wt% ^{235}U is 45 GWd/mtU. For the loading curve or Table 4.1-2, this value is multiplied by 1.05 to account for the burnup measurement uncertainty. Thus, for fuel with a nominal enrichment of 5.0 wt% ^{235}U fuel, a minimum burnup of 47.25 GWd/mtU is required for the spent fuel to be loaded in Region 1. Table 4.1-2 lists the acceptable base minimum burnups versus nominal enrichments from the above polynomial fit to verified points at nominal enrichments of 1.6, 3, 4, and 5 wt%.

4.3.7.2.3 Loading Curve for Abnormally Burned Assemblies

Figure 4.1-2 shows the base line curve and all assemblies that are currently stored in the Ginna storage rack. As noted most assemblies have burnups above the loading curve, areas A1 and A2. However, some assemblies do not meet the minimum burnup requirements. This condition is the result of accommodating a significant amount of Boraflex degradation into the models. Without this degradation model, all assemblies would satisfy the curve for the Boraflex rack, as is noted in the current license. However, with the Boraflex degradation all assemblies do not meet the loading requirements. These assemblies can be loaded into Region 2 with more restrictive administrative controls. An auxiliary set of loading curves is obtained for assemblies $\leq 10\%$ below the base curve, defined by area B. These assemblies must be loaded in a checker board arrangement with fuel assemblies with burnups above the upper curve, in area A1. These curves are defined by the following polynomials:

$$y_l = -33.584697 + 17.69608x - 0.41176x^2 - 0.04902x^3$$

$$y_u = -19.565780 + 17.69608x - 0.41176x^2 - 0.04902x^3$$

where,

y_l is the equation of the lower line defining the lower limit of area B, and

y_u is the equation of the upper line defining the lower limit of area A1.

These lines are based upon the KENO V.a results for storage of fuel with a nominal enrichment of 5.0 wt% ^{235}U with burnups at 38.5 and 55.2 GWd/mtU in a checker board arrangement in rack Type 1. Table 4.1-4 lists the K_{max} for this point. This value was obtained by applying an axial correction factor to the case that was evaluated for a uniform axial shape, see Section 4.4.2. The polynomial fit was generated based upon the constants of the base curve with the intercept chosen to pass through the required 5 wt% ^{235}U upper and lower burnup points. Points at 3 and 4 wt% ^{235}U were evaluated to verify the conservatism of this curve. For the 3 and 4 wt% ^{235}U enrichments, upper/lower burnups of 18/25 and 29.1/40 GWd/mtU were assumed in the calculation, respectively. These burnups are within the upper and lower curves, i.e., requiring upper/lower burnups of 15.2/29.9 and 28.8/43.5 GWd/mtU for 3 and 4 wt%, respectively. The k_{eff} values for the chosen burnups were 0.92840 and 0.90950, respectively. Both values satisfy the criticality criterion with all factors included. Thus, even though the upper burnup is in area A2, the criticality criterion is met. This shows that there is conservatism built into the polynomial.

4.3.7.2.4 Results for Accident Conditions

The results for the accidents considered for Region 2 are listed in Table 4.3-14. These include the T-bone and misplaced assembly analysis for rack Type 2 and the misplaced assembly and deep drop accident for Type 1. The side-drop accident for all rack types is bounded by that listed in Table 4.3-13 for the drop into the corner of racks 2B and 3E (Figure 4.3-12). The deep drop accident for Types 2 and 4 are equivalent to that for Type 3 since the base plates are of similar construction and will experience the same damage for this accident. Due to the fabrication similarity between rack Types 2 and 4, the accident results for these two racks will be equivalent. Since the reactivity increases are minimal, an individual evaluation for Type 4 is not necessary.

A review of Table 4.3-14 shows that the reactivity changes for the Type 2 and Type 4 racks are less than 1% Δk for all the drop accidents. This small change is within the range of that for Type 1 and easily covered by 450 ppm soluble boron. The Type 1 rack misplaced assembly gives a reactivity increase larger to that of the side-drop accident. The misplaced fresh assembly, see Figure 4.3-15, is assumed to replace an A1 assembly arranged in a checker board pattern with assemblies from area B. This is the bounding misplaced accident condition for this region. A minimum soluble boron concentration of 450 ppm reduces the reactivity to about 2% Δk below the reactivity of the normal condition. Thus, a small amount of soluble boron adequately negates the reactivity increase from this or any other accident condition.

4.3.8 Fuel Rod Consolidation

The storage racks currently contain several consolidated fuel containers and are designed to accommodate additional fuel consolidation in the future. Figure 4.3-17 provides a sketch of the consolidation canister with dimensions based upon Table 4.3-2. The storage of these containers was evaluated with a series of KENO V.a calculations for both normal and abnormal conditions. The results of these calculations confirm the criticality safety of storage of consolidation containers in the storage racks.

The evaluation of the consolidation canisters was made with modifications of the basic KENO V.a rack models. The modifications involved replacing spent fuel assemblies in each of the rack regions with a model of the consolidation canister. The base canister model assumed only a square stainless steel can with an outer square dimension of 8.02" (20.371 cm) and a wall thickness of 0.089" (0.2261 cm). These dimensions include tolerance values, see Table 4.3-2, to provide the largest interior dimension for the container, 7.842" (19.919 cm). This dimension will provide the largest pitch for the fuel rods in the container and thus optimize the reactivity. The base canister model contained 144" (356.76 cm) fuel rods without axial blankets or integral absorbers. For Region 1, fresh 2.22 wt% ^{235}U rods were placed in the container, while for Region 2, 1.6 wt% ^{235}U rods were modeled. The optimum reactivity of the container in each type rack was then obtained with a series of KENO V.a cases by varying both the number and pitch of the rods in the container model. Table 4.3-11 lists the optimized results of this evaluation for Rack types 1, 2, and 3. The similarity between rack Types 2 and 4 obviated the need for an evaluation for the Type 4 rack.

The results listed in Table 4.3-11 for Rack Type 1 show that for 1.6 wt% ^{235}U rods the criticality criterion is satisfied for the optimized container with either 196 rods from a Westinghouse standard assembly or 225 rods from a Westinghouse OFA assembly. These results are based upon the rack model with boraflex degradation. These results differ from the previous analysis^{4,13} for this rack in two respects. First, they show that there are no restrictions on the number of rods that can be placed in the container. Second, the optimized array size is 196 for Standard and 225 for OFA rods in this analysis for 1.6 wt% ^{235}U rods, and was 169 for Standard rods at 1.85 wt% and 196 for OFA rods at 1.95 wt% in the previous analysis. The optimization of rods is dependent upon both the configuration in which the rods are placed and upon the enrichment of the rods. For Rack Type 1 the enrichment is the primary cause for the differences. This was verified by repeating the calculations with the conditions used in the previous analysis which showed agreement essentially within the statistical uncertainty of KENO V.a. An additional evaluation was made to assess the effect of the center plate in this rack. The center plate was added to the model between the center pins in the container (for the array with an odd number of pins, it was placed to one side of the center

of the container). No re-optimization was made for this configuration, however due to the thinness of the plate, it is judged it will not significantly effect the optimization parameters. The insertion of the center plate reduced K_{\max} by about 2.7% Δk for both the OFA and Standard assemblies. Thus, there is significant conservatism in the models.

The Rack Type 2 results in Table 4.3-11 are similar to those of Rack Type 1 relative to the optimum pitch. The lower K_{\max} values reflect the conservatism inherent in this rack. This conservatism is based upon burnup versus enrichment curves based upon a degraded Rack Type 1 model that is applied to Rack Type 2. The Rack Type 3 results in Table 4.3-11 illustrate the effect of the configuration in which the container is placed. The Rack Type 3 configuration causes the optimum number of OFA rods to peak at 196 rather than 225 rods. Both Rack Type 2 and 3 results show that the criticality criterion is satisfied without modeling the center plate. Additional margin exists due to the presence of the center plate.

These results indicate that for normal conditions, the criticality condition is satisfied for storage of consolidation containers in locations for intact spent assemblies. The analysis examined the maximum fresh fuel enrichment allowed by the burnup versus enrichment curve for each region. Based upon the reactivity equivalency of these curves, spent fuel rods with enrichment and burnup pairs in the acceptable areas of these curves can fill the containers and satisfy the criticality criterion.

The abnormal condition considers all the rods spilling from the consolidation container into the storage pool. To bound the accident condition, it is assumed that the rods form into an optimized square array in the storage pool. A 19x19 array of rods is modeled that provides a 361-rod array to bound the maximum number of rods that can be stored in the container, 358. The evaluation considers arrays of both 1.6 and 2.22 wt% ^{235}U rods. CASMO-3 calculations determined the optimum pitch for these enrichments at about 1.95 cm and 2.05 cm, respectively for the 1.6 and 2.22 wt% ^{235}U rods in a square array. This optimized array of 144" (365.76 cm) long fuel rods was modeled with KENO V.a with an infinite water reflector to determine the k_{eff} of the array for both enrichments. For the 1.6 wt% ^{235}U rods, KENO V.a obtained a $k_{\text{eff}} \pm 1\sigma$ of 0.87510 ± 0.00059 , well below the 0.95 limit. For 2.22 wt% ^{235}U rods, the $k_{\text{eff}} \pm 1\sigma$ was 0.97697 ± 0.00059 in unborated water and 0.80706 ± 0.00056 with a moderator boron concentration of 450 ppm. The minimal concentration of boron in the moderator significantly reduces the reactivity of this accident. Based upon these results, with the minimum boron concentration of 450 ppm, the safety criterion is satisfied for the fuel rods that satisfy the spent fuel burnup versus enrichment curves for either Region 1 or 2.

4.3.9 Acceptance Criteria for Criticality

This criticality analysis evaluates Westinghouse-OFA fresh fuel and Westinghouse Standard fuel in the Region 1 and 2 racks of the R.E.Ginna Nuclear Power Plant. A maximum nominal enrichment of 4.0 wt% ^{235}U fresh fuel is justified for Region 1. Fresh fuel enrichments above 4.0 wt% ^{235}U to a nominal 5.0 wt% ^{235}U are allowed with an appropriate number of IFBA rods loaded in the assemblies. This is accomplished by a checker board loading plan with spent fuel loaded according to the curve in Figure 4.1-1. For Region 2, initial enrichments up to a nominal 5.0 wt% ^{235}U may be loaded according to the loading curve illustrated in Figure 4.1-2. Both normal and accident conditions have been evaluated for these two regions. The accidents considered are:

1. A dropped assembly on top, beside, and into the racks.
2. Rack movements for Region 1, 2, and the interface between Regions 1 and 2.
3. A misplaced assembly for Regions 1 and 2.

The analysis further demonstrates that the criticality criterion is not affected by the interaction of Region 1 and 2 racks under normal conditions.

Burnup is used as a mechanism to control the reactivity of the Region 1 and Region 2 storage racks. For Region 1, a nominal enrichment of 5.0 wt% ^{235}U requires a minimum burnup of 29.4 GWd/mtU to be loaded in a checker board pattern with fresh fuel with reactivities less than or equal to that for nominal 4.0 wt% ^{235}U fuel with no IFBA rods. The Region 2 racks require a minimum burnup of 47.25 GWd/mtU for a nominal enrichment limit of 5.0 wt% ^{235}U . The values used to determine the minimum burnup as a function of initial enrichment account for the effect of manufacturing and fuel assembly tolerance effects on reactivity. In addition, the tabulated minimum burnups listed in Tables 4.1-1 and 4.1-2 include a burnup 'measurement' uncertainty of 5%.

The evaluation of consolidated fuel containers demonstrates that the containers may be stored anywhere in Regions 1 and 2 following the loading requirements of that of the most restrictive rod in the consolidated container. This applies to either completely filled, 358 rods, or partially filled containers.

4.4 SUPPLEMENTARY INFORMATION

This section provides additional discussions about the evaluation of the KENO V.a bias and the procedure followed to generate the burnup versus enrichment curves. Section 4.4.1 describes the comparison between KENO V.a and experimental results and the evaluation of trends in the comparison. A description of the facets involved with generating the loading curves including an illustration of the axial shape effect is provided in Section 4.4.2.

4.4.1 KENO V.a Bias

The KENO V.a bias is evaluated in this section. An examination of light water reactor critical experiments for low-enriched ^{235}U lattices indicates a trend in the bias related to the separation distance between assemblies. A total of fifty-seven critical light water moderated, low-enriched fuel configurations are evaluated with KENO V.a and the 44 group cross section library. A trend of increased bias with the separation distance between fuel arrays is noted (see Figure 4.4-1) such that the bias reaches a maximum Δk of -0.0087 ± 0.0026 (1.763σ uncertainty) with a 2.576" (6.543 cm) spacing between the fuel arrays (Table 4.4-1). Based upon this trend the biases for Region 1 and Region 2 as related to the separation distance of the edges of the assemblies in the racks are $-0.0070 \pm 0.0009\Delta k$ for Region 1 (1.46" or 3.7 cm separation) and $-0.0056 \pm 0.0009 \Delta k$ for Region 2 (0.65" or 1.64 cm separation), see Table 4.4-1. A brief description of the critical experiments, determination of the bias, and validation of the trend is provided in this section.

4.4.1.1 Critical Experiments

A total of fifty-seven critical experiments was evaluated with KENO V.a to determine the bias inherent in its methodology. All experiments were conducted to simulate low-enriched, light-water reactor fuel arrays in storage pool configurations. This includes both UO_2 and mixed oxide fuel compositions. The experiments contain uranium enrichments from about 2.3 to 5.7 and plutonium

enrichments from 2 to 6 wt%. Rack geometry is simulated with variations on fuel array spacings and with interspersed absorber materials between the arrays. Thus, all these experiments are directly applicable to rack analyses. The experiments have been divided into four sets. The first examines a set of twenty-one critical configurations^{4.20} performed specifically for rack simulation for a single fuel enrichment. The second is a series of sixteen additional UO_2 criticals^{4.21} covering a range of enrichments and conditions. The third is a set of twelve mixed oxide criticals^{4.22} that are included to support analysis of spent fuel. The last set comprises eight other UO_2 critical configurations that have been approved for an international data base^{4.23}. This last set includes results from the MCNP Monte Carlo code^{4.24} and KENO V.a with the 27 group cross section set. These other calculations provide an independent verification of the results and trends for the 44 group KENO V.a results.

The first set of benchmark cases are 21 experiments representing close proximity water storage of LWR fuel. The fuel enrichment for these experiments is 2.459 wt%. The configurations examined the effects of fuel array spacing, soluble boron in the moderator, and interspersed absorbers between fuel arrays. The absorbers included B_4C rods, stainless steel sheets, and borated aluminum sheets with four different boron concentrations. These experiments span the general range of applicability for storage rack calculations and thus form the base set for the bias determination. Table 4.4-1 lists the calculated and experimental k_{eff} values plus the bias for this series of experiments. For the group as a whole, the average bias is about -0.0056 with a standard deviation of about 0.0024. However, examination of the bias as a function of spacing indicates a trend in the data. Figure 4.4-2 provides a plot of the bias as a function of separation distance between fuel arrays. The data plotted includes both water gaps and cases with interspersed absorber materials, i.e., B_4C rods and stainless steel and borated aluminum sheets. The trend of increasing bias is apparent in all cases. The trend appears to indicate that the bias will continue to increase as the spacing increases. However, eventually the fuel arrays will be isolated from each other and the bias is expected to return to the zero spacing value. The International Handbook cases discussed later show this behavior for the water gap bias. The largest bias occurs for spacings between 6 and 7 centimeters and then returns to a value close to the bias at the zero spacing for a spacing of about 12 cm.

Data for interspersed absorbers is being reviewed and is not available at this time. However, examining the sparse data from these experiments, seems to indicate that the spacing for the largest bias is dependent upon the amount of absorber present. The higher the amount of absorber material, the smaller the spacing for the minimum in the bias. This is most easily seen by reviewing the B_4C rod cases which contain a large amount of absorber and comparing these with the various borated aluminum sheet cases. Note that the data for 0.4 wt% ^{235}U borated aluminum is suspect due to the large uncertainty in the boron content of the sheets. It also appears that the magnitude of the bias decreases as the absorber increases. The variation of the spacing for the bias minimum and bias magnitude with the absorber content seems reasonable, since these materials increase the isolation of fuel arrays and tend to reduce the spacing required for full isolation. These trends will be factored into the biases applied to the Ginna storage rack analyses.

The next two sets of benchmark comparisons were performed to widen the range of applicability of the calculations. The UO_2 critical experiments cover a wider range of enrichments and some additional absorber materials. The KENO V.a bias for these sets is listed in Table 4.4-2. Since there was little spacing variation in these cases, the average bias is -0.0023 ± 0.0025 , indicating essentially no bias. No trend is noted relative to enrichment in these cases. The mixed oxide criticals



ALL INFORMATION CONTAINED HEREIN IS UNCLASSIFIED DATE 08-14-2001 BY 60322 UCBAW

100-461614-100

100-461614-100

100-461614-100

comparisons, Table 4.4-3, provide a bias relative to plutonium in fuel rods that is applicable to burnup credit. The cases primarily varied the lattice pitch and the effect of boron in the moderator. No obvious trends are noted and the average bias of the set is -0.0023 ± 0.0033 . Thus, these cases extend the benchmarks to various enrichments and fuel mixtures without any indication of bias trends relative to these parameters.

The B&W critical data provides a good set for bench-marking methodologies for rack calculations. However, the data stops at a spacing with a large bias and does not illustrate the expected reduction in the bias as the spacing continues to increase. The data obtained from the International Handbook ^{4.23} supplies several spacing points beyond those from B&W for water between the fuel arrays. In addition, it provides comparisons of results from other analysis methodologies. This data enables verification of the expected trend for larger spacings. Additionally, it provides independent verification of the calculational techniques. Table 4.4-4 provides the results from the Handbook and those calculated with KENO V.a using the 44 group cross section set. The Handbook critical experiments have a critical k_{eff} of 0.9998. Results are provided from a) KENO V.a with the 27 groups SCALE set, and b) MCNP with the continuous energy cross section set. Figure 4.4-2 illustrates the trends in the data of Table 4.4-4. The figure shows substantial agreement for the trend with the edge-to-edge spacing among the different methods. However, the absolute biases differ. The MCNP results, with a continuous energy set, give the smallest bias, as would be expected from the cross section representation. The 44 group set gives intermediate results both for the Handbook benchmarks and for the B&W experiments. The 27 group set has the largest bias which illustrates the rationale for the migration to the 44 group set for criticality analyses. The figure shows a valley in the bias for spacings between six and eight centimeters. As expected the bias decreases as the spacing increases beyond this range and seems to be approaching the zero spacing bias. Figure 4.4-3 shows plots of the 44 group KENO V.a results and a least square fit of the data. The fit curve clearly indicates the trend of the data with a valley around eight centimeters and a return to the zero spacing bias as the spacing increases beyond the valley. This trend will be considered for the biases applied to the Region 1 and 2 storage racks.

The absorber material in both Region 1 and the replacement racks in Region 2 is borated stainless steel. The minimum boron content in the stainless steel is 1.7 wt%. The absorber material in the Type 1 rack is Boraflex with a boron content of about 34 wt% boron. The ^{10}B areal density of the BSS plates range from about 0.006 to 0.007 g/cm², the Boraflex sheet is about 0.02 g/cm², and that of the borated aluminum plates used in the experiment from about 0.0008 to 0.01 g/cm². Thus, the absorber content of the BSS and Boraflex is within, or near, the range of the experimental plates. In addition to the boron, the stainless steel in the BSS plates serves as a mild absorber. The bias associated with stainless steel plates was also evaluated with the experimental configurations. Rather than try to relate the bias to a specific absorber density, the average of the biases for the interspersed B-Al and SS sheets is obtained at each spacing interval and a least square fit generated to allow estimation of the biases for the Regions 1 and 2 spacings. A review of the data indicated that consideration of only the B-Al sheets provided the largest bias, for conservatism the averages used for the least squares fit only included these data. The fitting equation is:

$$y = -0.00348 - 0.00003s + 0.00027s^2 - 0.00152s^3$$

where,

y is the bias, and

s is the spacing in centimeters.

The edge-to-edge spacing between centered assemblies in Region 1 is about 1.46" (3.68 cm) and in Region 2 the spacing is about 0.65" (1.64 cm). Based on the above polynomial the bias for Region 1 is $-0.0070 \Delta k$ and for Region 2, $-0.0056 \Delta k$. The maximum standard deviation in the average value at the nearest experimental points to the actual spacings is taken as the uncertainty in the bias, 0.0009 in this case. These values will be used to include the uncertainty in the KENO V.a methodology into the criticality safety evaluation of the Ginna storage racks.

4.4.1.2 CASMO-3/KENO V.a Benchmarks

To provide assurance that CASMO-3 is consistent with KENO V.a, it is benchmarked against KENO V.a for selected critical configurations. CASMO-3 is a two-dimensional code that allows an explicit model of a fuel region in the x-y direction with the implicit reflective boundary conditions on the outer surfaces. Thus, CASMO-3 does not have the geometrical capability to adequately model the critical experiment directly. Thus, an indirect benchmark is necessary. This indirect benchmark is derived by modifying several critical configurations into a fuel region that can be modeled both by CASMO-3 and KENO V.a. These configurations provide the desired benchmark between KENO V.a and CASMO-3, and indirectly, with critical experiments. The comparisons between CASMO-3 and KENO V.a for Region 1 and 2 rack models also an independent verification of the KENO V.a absolute results.

Six critical arrangements⁴²⁰ are chosen for this comparison from the benchmark cases described in the previous section. Table 4.4-5 lists the configurations and significant information about the selected cases. Table 4.4-6 provides the results from CASMO-3 and KENO V.a. These results show that the bias between CASMO-3 and KENO V.a is generally similar to the KENO V.a bias obtained from the critical experiments. The CASMO-3/KENO V.a differences exhibit about the same trends as the KENO V.a bias. The last column in Table 4.4-6 lists the sum of K_{eff} , the bias, and the uncertainty to give K_{max} . As noted this value is generally slightly greater than the CASMO-3 value.

The comparisons between CASMO-3 and KENO V.a for Region 1 and 2 rack models also serve as a benchmark, as well as an independent verification of the KENO V.a absolute results. The comparison is shown in Table 4.4-7 and again shows excellent agreement between the two codes. Although the KENO V.a k_{eff} value slightly underestimates the CASMO-3 result, application of the KENO bias and uncertainties provides the maximum k_{eff} which exceeds the CASMO-3 result. Since all absolute values quoted for KENO V.a for the analysis have the bias applied, conservative results are obtained by use of KENO V.a rather than CASMO-3 values.

4.4.1.3 KENO V.a Infinite to Finite Model Comparison

The base analyses use models of the racks that are infinite in the x-y direction. Due to the size of the rack regions this is generally a good assumption with some conservatism. Table 4.4-8 which lists the Δk between the infinite and finite models for each rack. The result for rack Type 1 illustrates the



THE UNIVERSITY OF CHICAGO PRESS

slight conservatism in the model for a regular rack array. Rack Types 2 and 3 do not have BSS plates in the cells that face the pool walls and create a smaller storage region than Type 1. Thus, this comparison was performed to ensure that the infinite model is indeed conservative relative to an actual finite model. The results in Table 4.4-8 show that this is the case even with the BSS removed from the edges. This comparison shows about a 0.5% Δk conservatism in the models for the BSS racks.

4.4.2 Burnup Credit Methodology

Typically, a burnup credit analysis uses a uniform, average burnup distribution over the entire length of the assembly. This distribution underestimates the burnup at the center of the assembly and overestimates the burnup at the top and bottom. To adequately utilize burnup credit the axial effects must be understood. This requires that an estimate of the reactivity effects of the axial burnup distribution relative to a uniform distribution must be determined and appropriately applied to the results. Alternatively, the explicit axial distribution can be modeled in the KENO V.a calculation. This removes the need for application of an axial burnup penalty. This analysis uses the latter method which is described in this section. This includes a description of the assumptions used to generate both the axial burnup profile and the number densities for the axial segments. This methodology for burnup credit is very similar to that already accepted by the U.S. Nuclear Regulatory Commission^{4,10,4.13,4.16}.

4.4.2.1 Axial Profile Generation

The axial effects have been found to vary with the amount of burnup. Indeed in the range from about 10 to 20 GWd/mtU, the use of a uniform axial shape provides conservative results. Also, for storage of fresh fuel adjacent to burned fuel, the use of a uniform axial burnup shape is conservative. However, from about 20 to 50 GWd/mtU, the axial burnup shape has a significant effect. To provide an estimate of the effect typical axial burnup shapes were obtained from several irradiated assemblies of the Ginna Nuclear Power Plant, see Table 4.4-9. These covered both OFA and Standard assemblies with burnups ranging from 10 to about 48 GWd/mtU. The selected assemblies covered a range of enrichments, axial blanket enrichments, core positions, and different cycles. The bulk of the data represented Westinghouse OFA assemblies with axial blankets from later cycles since these are, and will be, the most numerous assemblies. However, data from an ANF assembly of Standard Westinghouse design was also examined. This assembly did not have axial blankets and the axial shapes from this assembly were chosen as representative, and bounding for axial blanketed fuel. Figures 4.4-4 through 4.4-7 show a comparison of the normalized shapes for the examined assemblies. The shapes were broken into 10 GWd/mtU ranges from 10 to 50 GWd/mtU. A review of the figures show the curves are very similar over each region. The OFA assemblies with natural uranium blankets show higher burnups in all nodes except the top and bottom two nodes which contain axial blankets. Assembly 'E60' contains a 2.6 wt% ²³⁵U blanket and shows lower burnup in the central region than the assemblies with blankets of natural enrichments. The non-blanket assembly 'Q16' also shows a lower central burnup especially in the important top and bottom three nodes. The axial shape from this assembly was chosen to provide the axial effects for this reason, i.e., the lower burnups in the lower and upper three nodes. Note that while the natural uranium blankets have lower burnups in the outer two nodes, these are blanket zones that are essentially dead relative to rack reactivity. Thus, they can be ignored. The 2.6 wt% ²³⁵U assembly does have slightly lower burnup in the bottom node in the 10 to 20 GWd/mtU range. However, in the next two lower nodes and the three top nodes it is less than the non-blanket assembly. This behavior is ignored for

two reasons: first, the top nodes provide the most reactivity due to irradiation temperature effects, and second, in this region the axial effects are minimal or nonexistent. Thus, the axial profile data from assembly 'Q16' was chosen as representative of the typical burnup profile for the Ginna core. Table 4.4-10 lists the relative axial profile obtained from typical fuel cycle analyses for this assembly as a function of end-of-cycle burnup. Figure 4.4-8 provides a plot of the absolute burnup as a function of height for each cycle of irradiation and Figure 4.4-9 shows the relative distribution.

A previous analysis showed that a seven-zone axial model was sufficient to represent the axial effects^{4,10}. This model explicitly represents the burnup in the top and bottom three nodes of the twenty-three analytical nodes. The central 17 nodes are averaged together to provide a single central zone. The central zone average value may be modified slightly to maintain the relative burnup equal to 1.0 if the sum of all seven zones does not equal 1.0. This maintains the desired average burnup associated with the shape. Figure 4.4-10 illustrates the seven node model for the 40/50 GWd/mtU burnup range. Note that the KENO V.a model assumes a 144" active fuel height while most of the past and current fuel had a height of about 141". To accommodate the added height, the extra length is added to the central portion of the curve, as noted by the gap at the center of the seven zone shape in Figure 4.4-10. Similar seven zone models are obtained for the other burnup ranges. Table 4.4-11 lists the relative axial shapes for each range in the seven zone model with the midpoint height of each node. For the analysis for Region 2, burnups of 21, 34, and 45 GWd/mtU were required for 3, 4 and 5 wt% ²³⁵U initial enrichments. The shapes for these burnups are just the product of the relative distribution times the average burnup. Table 4.4-12 lists the zone burnup values for the burnups examined in this analysis. These burnups are used to obtain the nuclide concentrations in each zone.

4.4.2.2 Axial Profile Isotopic Concentration Generation

CASMO-3 generates the isotopic concentrations for each segment of the axial profile. The axial fuel and moderator temperature distributions influence the plutonium buildup that occurs as a function of depletion. A higher moderator temperature causes spectral "hardening" (a shift of the neutron energy spectrum to higher energy values) which increases conversion of ²³⁸U to ²³⁹Pu. Additionally, higher fuel temperatures cause Doppler broadening of the ²³⁸U resonance structure, also increasing ²³⁹Pu production. To capture this effect, mid-cycle average axial moderator and fuel temperature profiles were obtained for the Ginna core. These data were used to approximate the average temperature data for the seven axial zones in the model. In addition, since the axial burnup profile represents a cumulative axial power distribution, the relative axial burnup values were used to obtain the average power in each zone. Due to the similarity in the profiles, the 40-50 GWd/mtU range burnup profile was used to obtain the power distribution that was used for all ranges. The temperature data and the power data are used by CASMO-3 to deplete the fuel to the desired burnup for each initial enrichment and each axial zone. Table 4.4-13 lists the seven zone data for 3.0 wt% ²³⁵U initial enrichment and an average burnup of 21 GWd/mtU. The first table lists the input data for the CASMO-3 calculations. The second set of tables provides the nuclide concentrations in for each zone in terms of atoms/barn-cm. This data was used directly in KENO V.a for the evaluation at this enrichment and burnup. Similar data for 4.0 wt%/ 34 GWd/mtU and 5.0 wt%/45 GWd/mtU is listed in Tables 4.4-14 and 4.4-15.

The isotopic concentration data was obtained by the following procedure. A CASMO-3 hot full power depletion is performed to determine the isotopics for each axial segment at the appropriate burnup, fuel and moderator temperature. These calculations are for Standard fuel assemblies without IFBA rods. A CASMO-3 calculation provides the base k_{inf} for a fuel assembly with the shutdown isotopes at rack conditions. A second CASMO-3 rack model calculates the k_{inf} with only the shutdown fuel pellet concentrations of ^{16}O , ^{235}U , ^{238}U , ^{236}U , ^{239}Pu , ^{240}Pu , ^{241}Pu , and ^{149}Sm (xenon and iodine are eliminated in both rack models). Previous analyses have shown that the use of shutdown isotopics without xenon essentially provides the maximum reactivity after irradiation. It provides conservative values when decay greater than about seven months is considered. A small amount of ^{10}B is added to the fuel pin until the second CASMO-3 model k_{inf} agrees with the first. Tables 4.4-13 through 4.4-15 list the concentrations with the ^{10}B equivalent. In this manner, the added ^{10}B simulates the neutron absorption of the deleted isotopes for the KENO V.a model.

A similar process is used to generate the isotopic concentrations for the cases that use a uniform assembly average burnup, e.g., for the Region 1 analysis. Tables 4.4-16 and 4.4-17 list data for assembly average burnups. Table 4.4-16 provides the concentrations for cases used to provide the auxiliary lines for the Region 2 curve at 5 wt%. These curves allow storage of 5 wt% ^{235}U initial enrichment assemblies with burnups of 38.5 and 52.2 GWd/mtU adjacent to each other. Note that for these curves a uniform distribution was used. However, it was corrected with the axial shape factor appropriate to the burnup range discussed in the next section. Table 4.4-17 provides the isotopic concentrations for the average burnups required for the Region 1 checker boarded burned fuel.

4.4.2.3 Axial Reactivity Effects

The axial burnup shapes are integrated into the models for Region 2 and thus the effects are explicitly considered in the results. However, it is instructive to evaluate the magnitude of the effect. In addition, this evaluation illustrates that the number of histories and distribution of the neutron start types are sufficient to 'see' the effect. Table 4.4-18 lists the results of the evaluation for each rack type. The axial burnup distribution used to determine the base line for the Region 2 loading curve is used for this evaluation. As noted from the table, all the Region 2 racks have about the same axial effect. Note that for the 3.0 wt% ^{235}U enrichment at 21 GWd/mtU burnup, the axial effect is almost nil, i.e., within statistical uncertainty. Thus, the values may be plus or minus. This effect varies with burnup and ranges from about 2% Δk for the 40-50 GWd/mtU range to about 0.0% Δk for about 21 GWd/mtU range. Reviewing the rack Type 1 results in Table 4.4-18, which shows both the degraded and the normal condition of the rack, the effect is relatively insensitive to the absorber material in the rack. Due to the magnitude of the differences, it is apparent that the statistics of the KENO V.a cases are recognizing the different axial zones and their importance. The Region 1, rack Type 3 results show a negative Δk of about 0.5%. This confirms the assertion that for a fresh/burned combination, a uniform axial distribution provides conservative results. However, as is apparent for Region 2 the effect is significant and must be factored into the final k_{eff} , either implicitly, as is done here, or by a larger margin to the 0.95 safety limit.



4.4.2.4 Boraflex Degradation Model Margin

The loading curves for rack Type 1 and Region 2 include margin for potential Boraflex degradation. Table 4.4-19 lists the results of an assessment of the margin in the Boraflex degradation model. The uniform axial shape cases from Table 4.4-18 for rack Type 1 with and without the degraded model are compared. The table shows that the degraded model provides a Δk margin of 0.048 over the normal condition model. Thus, there is approximately a 5% margin in the loading curves for Region 2 to accommodate potential Boraflex loss.

4.4.3 Westinghouse IFBA Documentation

The following discussion of the IFBA credit was obtained from the previous licensing submittal^{4,13}. The results have been verified with the CASMO-3 code and remain unchanged for the current analysis. This verification also included verification of the infinite multiplication factor equivalencing. The text that follows has been extracted without change from the previous licensing report. Table 7 and Figure 8 cited in the text are appended to the end of the text, as are references.

"4.2 IFBA Credit Reactivity Equivalencing

"Storage of fuel assemblies with nominal enrichments greater than 4.0 w/o U^{235} in the Region 1 spent fuel storage racks is achievable by means of the concept of reactivity equivalencing. The concept of reactivity equivalencing is predicated upon the reactivity decrease associated with the addition of Integral Fuel Burnable Absorbers (IFBA)⁽¹³⁾. IFBAs consist of neutron absorbing material applied as a thin ZrB_2 coating on the outside of the UO_2 fuel pellet. As a result, the neutron absorbing material is a non-removable or integral part of the fuel assembly once it is manufactured.

"Two analytical techniques are used to establish the criticality criteria for the storage of IFBA fuel in the fuel storage rack. The first method uses reactivity equivalencing to establish the poison material loading required to meet the criticality limits. The poison material considered in this analysis is a zirconium diboride (ZrB_2) coating manufactured by Westinghouse. The second method uses the fuel assembly infinite multiplication factor to establish a reference reactivity. The reference reactivity point is compared to the fuel assembly peak reactivity to determine its acceptability for storage in the fuel racks.

"4.2.1 IFBA Requirement Determination

"A series of reactivity calculations are performed to generate a set of IFBA rod number versus enrichment ordered pairs which all yield the equivalent K_{eff} when the fuel is stored in the Region 1 spent fuel racks. The following assumptions were used for the IFBA rod assemblies in the PHOENIX models:

- 1. The fuel assembly parameters relevant to the criticality analysis are based on the Westinghouse 14x14 OFA design (see Table 1 . . . for fuel parameters). [editor's note: Table 1 is fully reproduced in Table 4.3-1].*
- 2. The fuel assembly is modeled at its most reactive point in life.*



3. *The fuel pellets are modeled assuming nominal values for theoretical density and dishing fraction.*
4. *No credit is taken for any natural enrichment or reduced enrichment axial blankets.*
5. *No credit is taken for any U^{234} or U^{236} in the fuel.*
6. *No credit is taken for any spacer grids or spacer sleeves.*
7. *The IFBA absorber material is a zirconium diboride (ZrB_2) coating on the fuel pellet. Each IFBA rod has a nominal poison material loading of 1.67 milligrams B^{10} per inch, which is the minimum standard loading offered by Westinghouse for 14x14 OFA fuel assemblies.*
8. *The IFBA B^{10} loading is reduced by 5 percent to conservatively account for manufacturing tolerances and then by an additional 10% to conservatively model a minimum poison length of 92 inches.*
9. *The moderator is pure water (no boron) at a temperature of 68°F with a density of 1.0 gm/cm³.*
10. *The array is infinite in lateral (x and y) and axial (vertical) extent. This precludes any neutron leakage from the array.*

"Figure 8 [ed. note: Figure 8 is fully reproduced at the end of this text] . . . shows the constant K_{eff} contour generated for the Region 1 spent fuel racks. Note the endpoint at 0 IFBA rods where the nominal enrichment is 4.0 w/o and at 64(1X) IFBA rods where the nominal enrichment is 5.0 w/o. The interpretation of the endpoint data is as follows: the reactivity of the fuel rack array when filled with fuel assemblies enriched to a nominal 5.0 w/o U^{235} with each containing 64(1.0X) IFBA rods is equivalent to the reactivity of the rack when filled with fuel assemblies enriched to a nominal 4.0 w/o and containing no IFBAs. The data in Figure 8 . . . is also provided on Table 7 [ed. note: Table 7 is fully reproduced at the end of this text] . . . for the 1.0X, 1.5X and 2.0X IFBA rods.

"It is important to recognize that the curve in Figure 8 . . . is based on reactivity equivalence calculations for the specific enrichment and IFBA combinations in actual rack geometry (and not just on simple comparisons of individual fuel assembly infinite multiplication factors). In this way, the environment of the storage rack and its influence on assembly reactivity is implicitly considered.

"The IFBA requirements of Figure 8 . . . were developed based on the standard IFBA patterns used by Westinghouse. However, since the worth of individual IFBA rods can change depending on position within the assembly (due to local variations in thermal flux), studies were performed to evaluate this effect and a conservative reactivity margin was included in the development of the IFBA requirement to account for this effect. This assures that the IFBA requirement remains valid at intermediate enrichments where standard IFBA



1. The first part of the document is a list of names and addresses of the members of the committee.

2. The second part of the document is a list of names and addresses of the members of the committee.

patterns may not be available. In addition, to conservatively account for calculational uncertainties, the IFBA requirements of Figure 8 . . . also include a conservatism of approximately 10% on the total number of IFBA rods at the 5.0 w/o end (i.e., about 6 extra IFBA rods for a 5.0 w/o fuel assembly).

"Additional IFBA credit calculations were performed to examine the reactivity effects of higher IFBA linear B^{10} loadings (1.5X and 2.0X). These calculations confirm that assembly reactivity remains constant provided the net B^{10} material per assembly is preserved. Therefore, with higher IFBA B^{10} loadings, the required number of IFBA rods per assembly can be reduced by the ratio of the higher loading to the nominal 1.0X loading. For example, using 2.0X IFBA in 5.0 w/o fuel assemblies allows a reduction in the IFBA rod requirement from 64 IFBA rods per assembly to 32 IFBA rods per assembly (64 divided by the ratio 2.0X/1.0X).

"4.2.2 Infinite Multiplication Factor

"The infinite multiplication factor, K_{∞} , is used as a reference criticality reactivity point, and offers an alternative method for determining the acceptability of fuel assembly storage in the Region 1 spent fuel racks. The reference K_{∞} is determined for a nominal fresh 4.0 w/o fuel assembly.

"The fuel assembly K_{∞} calculations are performed using the Westinghouse licensed core design code PHOENIX-P⁽¹¹⁾. The following assumptions were used to develop the infinite multiplication factor model:

1. The Westinghouse 14x14 OFA fuel assembly was analyzed (see Table 1 [ed. note: Table 4.3-1]. . . . for parameters). The fuel assembly is modeled at its most reactive point in life and no credit is taken for any discrete burnable absorbers in the assembly.
2. All fuel rods contain uranium dioxide at a nominal enrichment of 4.0 w/o U^{235} over the entire length of each rod.
3. The fuel array model is based on a unit assembly configuration (infinite in the lateral and axial extent) in Ginna reactor geometry (no rack).
4. The moderator is pure water (no boron) at a temperature of 68 °F with a density of 1.0 gm/cm³.

"Calculation of the infinite multiplication factor for the Westinghouse 14x14 OFA fuel assembly in the Ginna core geometry resulted in a reference K_{∞} of 1.458. This includes a 1% ΔK reactivity bias to conservatively account for calculational uncertainties. This bias is consistent with the standard conservatism included in the Ginna core design refueling shutdown margin calculations.

"For IFBA credit, all 14x14 fuel assemblies placed in the Region 1 spent fuel racks must comply with the enrichment-IFBA requirements of Figure 8 . . . or have a reference K_{∞} less or equal to 1.458. By meeting either of these conditions, the maximum rack reactivity will then be less than 0.95, . . ."

"Bibliography

" ...

- 11. Nguyen, T.Q. et.al., "Qualification of the PHOENIX-P/ANC Nuclear Design System for Pressurized Water Reactor Cores," WCAP-11596-P-A, June 1988 (Westinghouse Proprietary).*

...

- 15. Davidson, S.L., et. al, "VANTAGE 5 Fuel Assembly Reference Core Report, Addendum 1," WCAP-10444-P-A, March 1986."*

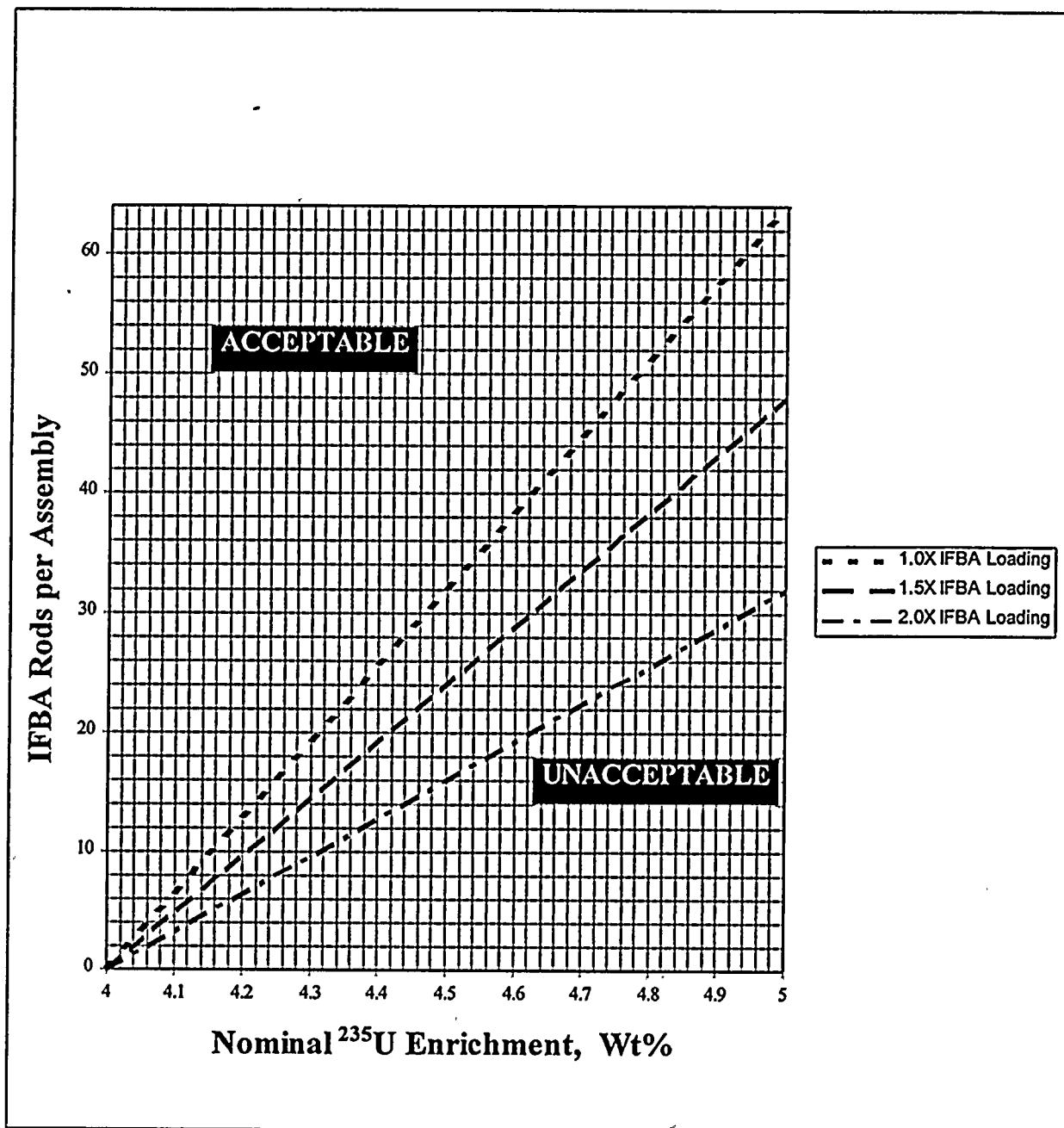
" ..."



Table 7 Ginna Region 1 Spent Fuel Rack IFBA Requirement

<i>Nominal Enrichment (w/o)</i>	<i>1.0X(1.67 mg./in) IFBA Rods in Assembly</i>	<i>1.5X(2.51 mg./in) IFBA Rods in Assembly</i>	<i>2.0X(3.34 mg./in) IFBA Rods in Assembly</i>
<i>4.0</i>	<i>0</i>	<i>0</i>	<i>0</i>
<i>4.5</i>	<i>32</i>	<i>24</i>	<i>16</i>
<i>5.0</i>	<i>64</i>	<i>48</i>	<i>32</i>

Figure 8 Ginna Region 1 Spent Fuel Rack IFBA Requirement



[ed. note: End of material from reference 4.13]



4.5 REFERENCES

- 4.1 ANSI/ANS 57.2 - 1983, "Design Requirements for Light Water Reactor Spent Fuel Storage Facilities at Nuclear Power Plants," approved October 1983.
- 4.2 American National Standard, "Validation of Calculational Methods for Nuclear Safety Criticality Safety," ANSI N16.9-1975.
- 4.3 NRC Standard Review Plan NUREG-0800, SRP 9.1.2, "Spent Fuel Storage," Rev. 3, July 1981.
- 4.4 USNRC Position Paper - "OT Position for Review and Handling Application," April 14, 1978, revised January 18, 1979.
- 4.5 USNRC Reg. Guide 1.13, "Spent Fuel Storage Facilities Design Basis," Proposed Rev.2, published Dec. 1981.(Provides supplementary information relative to ANS 57.2)
- 4.6 ANSI N16.1-1975, "American National Standard for Nuclear Criticality Safety in Operations with Fissionable Materials Outside Reactors."
- 4.7 'SCALE 4.2, Modular Code System for Performing Standardized Computer Analyses for Licensing Evaluation," NUREG/CR-0200, Revision 4, November 1993, Oak Ridge National Laboratory.
- 4.8 "CASMO-3, A Fuel Assembly Burnup Program," STUDSVIK/NFA-89/3, November 1989, Studsvik of America Inc.
- 4.9 'SCALE 4.3, Modular Code System for Performing Standardized Computer Analyses for Licensing Evaluation for Workstations and Personal Computers," Volume 3, Section M4, NUREG/CR-0200, Revision 5, September 1995, Oak Ridge National Laboratory. (Note the revised library released in May 1996 was used for the analysis).
- 4.10 Docket 50-302, Florida Power Corporation, Letter from P.M. Beard, FPC, "Updates Shooley Evaluation and Replaces Attachment 3 with a Nonproprietary Version of Report BAW-2209, Rev 1. 'Crystal River Unit 3 Spent Fuel Storage Pool B Criticality Analysis,' per discussions with NRC re FPC 950126 Application," March 9, 1995. Note: BAW-2209, R01(95/02/28) is contained in Doc. 83104, pp 091-171.
- 4.11 R.J. Nodvik, "Evaluation of Mass Spectrometric and Radiochemical Analysis of Yankee Core 1 Spent Fuel," WCAP-6068, March 1966, Westinghouse Electric Corporation, Pittsburgh, PA 15230.
- 4.12 R.J Nodvik, et al, "Supplementary Report on Evaluation of Mass Spectrometric and Radiochemical Analysis of Yankee Core 1 Spent Fuel, Including Isotopes of Elements Thorium Through Curium," WCAP-6086, August 1969, Westinghouse Electric Corporation, Pittsburgh, PA 15230.



1. The first part of the document is a list of names and addresses of the members of the committee.

2. The second part of the document is a list of names and addresses of the members of the committee.

- 4.13 "Criticality Analysis of The R.E. Ginna Nuclear Power Plant Fresh and Spent Fuel Racks, and Consolidated Rod Storage Canisters," dated June 1994, Attachment A of Letter R.C. Mecredy, RGE, to A.R. Johnson, NRC, Subject: "Technical Specification Improvement Program," Rochester Gas & Electric, Docket No. 50-244, May 5, 1995.
- 4.14 "An Assessment of Boraflex Performance in Spent-Nuclear-Fuel Storage Racks," K. Linquest and D.E. Kline, NP-6159, Electric Power Research Institute, December 1988.
- 4.15 Letter R.C. Mecredy, RGE, to G. Vissing, US. NRC, "Response to NRC Generic Letter 96-04, dated June 26, 1996; Subject: Boraflex Degradation in Spent Fuel Pool Storage Racks," R.E. Ginna Nuclear Power Plant, October 24, 1996.
- 4.16 "Amendment No. 181 To Facility Operation License No. NPF-3 (TAC No. M86933)," Docket No. 50-346, Letter US Nuclear Regulatory Commission to Toledo Edison Co., November 19, 1993. (Approval of an enrichment increase for the Davis Besse Nuclear Power Station, Unit 1 spent fuel storage pool).
- 4.17 Ginna Technical Specifications, Section SR 3.2.1.1, Page B.3.2-6, Amendment 65.
- 4.18 "Sequoyah Nuclear Plant (SQN) - Request for License Amendment to Technical Specifications (TS) - Spent-Fuel Pool Storage Capacity Increase," Docket Numbers 50-327 and 50-328, 4/27/92.
- 4.19 "North Anna Power Station, Unit No. 1, Technical Specifications," Docket No. 50-338, Amendment No. 178, 3/94.
- 4.20 BAW-1484-7, "Critical Experiments Supporting Close Proximity Water Storage of Power Reactor Fuel," N. M. Baldwin, et al., July 1979.
- 4.21 The UO_2 Criticals Data were obtained from the following:
- 4.21a. S.R. Bierman, et al., "Critical Separation Between Subcritical Clusters of 2.35 wt% ^{235}U Enriched UO_2 Rods in Water with Fixed Neutron Poisons," PNL-2438, Battelle Pacific Northwest Laboratories, October 1977.
- 4.21b. S.R. Bierman, et al., "Critical Separation Between Subcritical Clusters of 4.31 wt% ^{235}U Enriched UO_2 Rods in Water with Fixed Neutron Poisons," NUREG/CR-0073 (PNL-2615), Battelle Pacific Northwest Laboratories, March 1978.
- 4.21c. S.R. Bierman et al., "Criticality Experiments with Subcritical Clusters of 2.35 wt% and 4.31 wt% ^{235}U Enriched UO_2 Rods in Water with Uranium or Lead Reflecting Walls," NUREG/CR-0796 (PNL-2827), Pacific Northwest Laboratory, April 1979.
- 4.21d. R.I. Smith and G.J. Konzek, "Clean Critical Experiment Benchmarks for Plutonium Recycle in LWRs," EPRI NP-196, Vols I and II, Electric Power Research Institute, April 1976 and September 1978.



- 4.21e. E.G. Taylor et al., "Saxton Plutonium Program Critical Experiments for the Saxton Partial Plutonium Core," WCAP-3385-54, Westinghouse Electric Corp., Atomic Power Division, December 1965.
- 4.22 The Mixed Oxide Criticals Data were obtained from the following:
- 4.22a. R.I. Smith and G.J. Konzek, "Clean Critical Experiment Benchmarks for Plutonium Recycle in LWRs," EPRI NP-196, Vols I and II, Electric Power Research Institute, April 1976 and September 1978.
- 4.22b. E.G. Taylor et al., "Saxton Plutonium Program Critical Experiments for the Saxton Partial Plutonium Core," WCAP-3385-54, Westinghouse Electric Corp., Atomic Power Division, December 1965.
- 4.22c. S.R. Bierman, et al., "Criticality Experiments with Low Enriched UO_2 Fuel Rods in Water Containing Dissolved Gadolinium, PNL-4976, Battelle Pacific Northwest Laboratory, February 1984.
- 4.23 "International Handbook of Evaluated Criticality Safety Benchmark Experiments," Volume IV, LEU-COMP-THERM-002, "Low Enriched Uranium Systems, Water-Moderated $\text{U}(4.31)\text{O}_2$ Fuel Rods In 2.54-Cm Square-Pitched Arrays," NEA/NSC/DOC(95)03/IV, Nuclear Energy Agency, Paris.
- 4.24 "MCNP4, Monte Carlo N-Particle Transport Code System," using Continuous Energy ENDF/B-V cross sections.

**Table 4.1-1 Polynomial Generated for Spent Fuel Burnup vs Enrichment Requirements
for the Region 1 Racks**

Initial Wt% ²³⁵ U (Nominal)	Minimum Burnup, GWd/mtU	Initial Wt% ²³⁵ U (Nominal)	Minimum Burnup, GWd/mtU
2.22	0.00	3.6	15.24
2.3	1.12	3.7	16.15
2.4	2.47	3.8	17.07
2.5	3.75	3.9	17.98
2.6	4.99	4.0	18.90
2.7	6.17	4.1	19.83
2.8	7.30	4.2	20.78
2.9	8.39	4.3	21.74
3.0	9.45	4.4	22.73
3.1	10.47	4.5	23.75
3.2	11.47	4.6	24.79
3.3	12.43	4.7	25.88
3.4	13.38	4.8	27.01
3.5	14.32	4.9	28.18
3.6	15.24	5.0	29.40



**Table 4.1-2 Polynomial Generated Burnup vs Enrichment Requirements for the Region 2
Racks**

Initial Wt% ²³⁵ U (Nominal)	Minimum Burnup, GWd/mtU			Initial Wt% ²³⁵ U (Nominal)	Minimum Burnup, GWd/mtU		
	Base	Upper	Lower		Base	Upper	Lower
1.14		0.00		3.0	22.05	29.92	15.20
1.2		1.04		3.1	23.50	31.37	16.65
1.3		2.77		3.2	24.93	32.80	18.08
1.4		4.48		3.3	26.35	34.21	19.49
1.5		6.18		3.4	27.74	35.61	20.89
1.6	0.00	7.87		3.5	29.12	36.99	22.27
1.7	1.67	9.54		3.6	30.47	38.34	23.62
1.8	3.33	11.20		3.7	31.81	39.68	24.96
1.9	4.98	12.85		3.8	33.13	41.00	26.28
2.0	6.61	14.48		3.9	34.42	42.29	27.57
2.015	6.85	14.72	0.00	4.0	35.70	43.57	28.85
2.1	8.22	16.09	1.37	4.1	36.95	44.82	30.10
2.2	9.83	17.69	2.97	4.2	38.19	46.06	31.34
2.3	11.41	19.28	4.56	4.3	39.40	47.27	32.55
2.4	12.98	20.85	6.13	4.4	40.59	48.46	33.74
2.5	14.53	22.40	7.68	4.5	41.76	49.62	34.90
2.6	16.07	23.94	9.22	4.6	42.90	50.77	36.05
2.7	17.59	25.46	10.74	4.7	44.02	51.89	37.17
2.8	19.10	26.96	12.24	4.8	45.12	52.99	38.27
2.9	20.58	28.45	13.73	4.9	46.20	54.07	39.35
3.0	22.05	29.92	15.20	5.0	47.25	55.12	40.40

Table 4.1-3 KENO V.a Region 1 (Rack Type 3) Results of Burnup vs Enrichment Calculations

Description	Calculated		K_{max}^a	Margin To 0.95, Δk
	k_{eff}	$1\sigma_c$		
4 wt% fresh/ 2.22 wt% at 0 GWd/mtU	0.91977	0.00072	0.94159	0.00841
4 wt% fresh / 3 wt% at 9 GWd/mtU	0.91877	0.00069	0.94058	0.00942
4 wt% fresh/ 4 wt % at 18 GWd/mtU	0.92144	0.00070	0.94326	0.00674
4 wt% fresh/ 5 wt% at 28 GWd/mtU	0.91990	0.00068	0.94171	0.00829

a) K_{max} is calculated with the formula listed in Section 4.3.7.1.1, i.e.,

$$K_{max} = k_{eff} + \Delta k_{bias} + \Delta k_{pen} + \sqrt{(1.763 * \sigma_c)^2 + (1.763 * \sigma_{bias})^2 + (\sigma_{tol})^2}$$

where the values for Δk_{bias} , Δk_{pen} , σ_{bias} , and σ_{tol} are obtained from Table 4.3-12. For example, the K_{max} for the 2.22 wt% assembly in rack Type 3 is

$$\begin{aligned} K_{max} &= 0.91977 + 0.00701 + 0.00133 \\ &\quad + \sqrt{(1.763 * 0.00072)^2 + (1.763 * 0.0009)^2 + (0.01332)^2} \\ &= 0.94159 \end{aligned}$$



Table 4.1-4 KENO V.a Region 2 (Rack Types 1, 2, & 4) Results of Burnup vs Enrichment Calculations

Description	Calculated		K_{max}^a	Margin To 0.95, Δk
	k_{eff}	$1\sigma_c$		
Rack Type 1 Standard Assys				
5 wt% at 45 GWd/mtU,axial model, degraded rack model	0.93091	0.00059	0.94817	0.00183
4 wt% at 34 GWd/mtU, axial model, degraded rack model	0.92806	0.00061	0.94532	0.00468
3 wt% at 21 GWd/mtU, axial model, degraded rack model	0.92099	0.00058	0.93824	0.01176
5 wt% at 38.8 checkerboarded with 5 wt% at 55.2 GWd/mtU, degraded rack model, corrected to axial model			0.94375	0.00625
1.6 wt% fresh fuel, degraded rack model	0.92898	0.00056	0.94623	0.00377
4.0 wt% fresh fuel checker boarded with waterholes	0.92311	0.00078	0.94042	0.00958
Rack Type 2 Standard Assys				
5 wt% at 45 GWd/mtU axial model	0.91951	0.00058	0.93500	0.01500
4 wt% at 34 GWd/mtU axial model	0.91629	0.00057	0.93178	0.01822
3 wt% at 21 GWd/mtU axial model	0.90914	0.00057	0.92463	0.02537
1.6 wt% fresh fuel	0.91265	0.00054	0.92813	0.02187
Rack Type 4 Standard Assys				
5 wt% at 45 GWd/mtU axial model, degraded Type 1 rack model	0.91718	0.00060	0.93190	0.01810
4 wt% at 34 GWd/mtU axial model, degraded Type 1 rack model	0.91511	0.00060	0.92983	0.02017
3 wt% at 21 GWd/mtU axial model, degraded Type 1 rack model	0.90751	0.00057	0.92778	0.02222
fresh 1.6 wt% fuel, degraded Type 1 rack model	0.91077	0.00059	0.92548	0.02452

a) K_{max} is calculated with the formula listed in Section 4.3.7.2.1, i.e.,

$$K_{max} = k_{eff} + \Delta k_{bias} + \Delta k_{pen} + \sqrt{(1.763 * \sigma_c)^2 + (1.763 * \sigma_{bias})^2 + (\sigma_{tol})^2}$$

where the values for Δk_{bias} , Δk_{pen} , σ_{bias} , and σ_{tol} are obtained from Table 4.3-12. For example, the K_{max} for rack Type 1 at 5 wt% at 45 Gwd/mtU is

$$\begin{aligned} K_{max} &= 0.93091 + 0.00561 + 0.00358 \\ &\quad + \sqrt{(1.763 * 0.00059)^2 + (1.763 * 0.0009)^2 + (0.00784)^2} \\ &= 0.94817 \end{aligned}$$

Table 4.3-1 Fuel Assembly Parameters

Description	Exxon	W Std	W OFA
Rods/Assy	179	179	179
Guide Tubes/Assy	16	16	16
Instrument Tubes/Assy	1	1	1
IHM Wt, Kg/assy	370-374.5	383-398	349-356.5
Rod Pitch, in	0.556	0.556	0.556
Pellet OD, in	0.3565±0.0008	0.3669±0.0008	0.3444±0.0008
Pellet Density, %TD	95±2.0	95±2.0	95±2.0
Max Enrichment, wt% no IFBAs with IFBAs	4.0±0.05 -	4.0±0.05 -	4.0±0.05 5.0±0.05
Pellet Dish Factor, %	1.187±2.0	1.187±2.0	1.1926±2.0
Active Fuel Lgth, in	141-144	141-144	141-144
Clad OD, in	0.424±0.0025	0.422±0.0025	0.400±0.0025
Clad Thickness, in	0.030±0.0025	0.0243±0.0025	0.0243±0.0025
Clad Material	Zirc-4	Zirc-4	Zirc-4
Guide Tube OD, in	0.524±0.005	0.539±0.005	0.528±0.005
GT Thickness, in	0.015±0.0055	0.017±0.0055	0.019±0.0055
GT Material	Zirc-4	SS ^a	Zirc-4
Inst. Tube OD, in	0.424±0.005	0.422±0.005	0.399±0.005
IT Thickness, in	0.039±0.004	0.0240±0.004	0.0235±0.004
IT Material	Zirc-4	SS	Zirc-4
IFBA Number/Assy Boron Loading, mg/in	-	-	0 - 64 1.67 - 3.34

a) Modeled conservatively as Zirc-4



Table 4.3-2 Consolidation Canister Specifications

Description	Values
Outer square dimension, in	8.00±0.02
Wall thickness, in	0.093±0.004
Height, in Including Lids at top/bottom Without Lids at top/bottom Canister lid height, in - top/bottom	168±0.06 156 1/4±0.06 5 7/8
Material of construction Body Lids Divider Plate	SS304 SS304 SS304
Divider Plate Thickness, in Centered Within, in Length, in	0.093±0.004 1/32 153 5/16±0.06
Max rods/container	2x179



CONFIDENTIAL - SECURITY INFORMATION

CONFIDENTIAL - SECURITY INFORMATION

Table 4.3-3a Region 1, Rack Type 3 Cell Dimensions

Description	Design Dimensions	Model Dimensions
Cell Pitch, cm(in)	23.45±0.2(9.2323)	23.45
Cell ID, cm(in)	20.68 +0.2/-0.1 (8.1418)	20.68
Wall Thickness, cm(in) SS304L BSS	0.20±0.018(0.0787) 0.25 +0.05/-0.0(0.0984)	0.20 0.25
Nominal gap, cm(in)/min	2.07(0.815)/1.95 min*	2.07
Peripheral row BSS support Belt plate width, cm(in) SS thickness, cm(in)	0.8(0.3228) 0.20 ±0.018(0.0787)	0.8 0.20
BSS Parameters BSS density, g/cc Boron content, wt% ¹⁰ B wt% in natural boron Plate length, in	7.73 -7.78 1.7 min 18.14 145.7	7.73 1.7 18.14 144.0

- a) A minimum tolerance of 1.85 cm is assumed for the analysis to provide additional margin for the Type 3 rack.

Table 4.3-3b Region 1, Rack Type 3 Damaged Fuel Cell Dimensions

Description	Design Dimensions
Cell Pitch, cm(in)	23.45±0.2(9.2323)
Cell ID, cm(in)	22.1 +0.2/-0.1(8.701)
Wall Thickness, cm(in) SS304L BSS	0.2±0.018(0.0787) 0.30 +0.05/-0.0(0.1181)
Nominal Gap, cm(in)/minimum Between damaged cells Between damaged/normal cells	0.55(0.2165)/ 0.43 min 1.36(0.5354)/1.13 min
BSS Parameters BSS density, g/cc Boron content, wt% ¹⁰ B wt% in natural boron Plate length, in	7.73 -7.78 1.7 min 18.14 145.7

Table 4.3-4 Region 2, Rack Type 1 Cell Dimensions

Description	Design Dimensions	Model Dimensions
Cell Pitch, in	8.43 +0.06/-0.0	8.43
Cell ID (without poisons), in	8.25 +0.06/-0.0, square	8.25
Wall Thickness, in	0.09 ± 0.004	0.09
Wall Material	SS-304	SS-304
SS Poison support sheet thickness, in	0.062 ± 0.003	0.062
Cell ID with poison, in	8.113	8.113
Boraflex Poison, length, in width, in thickness, in ¹⁰ B Self Shielding Bias Min ¹⁰ B content, g/cm ²	144 ± 1/16 7.625 ± 0.0625 0.075 ± 0.007 +0.0014 0.020	144 ^a 6.33 ^a 0.038 ^a - 0.020

- a) Boraflex shrinkage/degradation model includes a 12" gap in length randomly positioned, within the central 132" of the plate, a 8% width shrinkage, and a 50% loss in thickness.

Table 4.3-5 Region 2, Rack Type 2 Cell Dimensions

Description	Design Dimensions	Model Dimensions
Cell Pitch, cm(in)	21.412±0.2(8.43)	21.412
Cell ID, cm(in)	20.68 +0.2/-0.1(8.1418)	20.68
Wall Thickness, cm(in) SS304L BSS	0.2 ± 0.018(0.0787) 0.3 +0.05/-0.0(0.1181)	0.2 0.3
Nominal Gap, cm(in)/minimum	0.232(0.0913)/0.15 min	0.232
BSS Parameters BSS density, g/cc Boron content, wt% ¹⁰ B Wt% in natural boron Plate length, in	7.73 -7.78 1.7 min 18.14 145.7	7.73 1.7 18.14 144.0

Table 4.3-6 Region 2, Rack Type 4 Cell Dimensions

Description	Design Dimensions	Model Dimensions
Cell Pitch, cm(in)	21.412±0.2(8.43)	21.412
Cell ID, cm(in)	20.68 +0.2/-0.1 (8.1418)	20.68
Wall Thickness, cm(in) SS304L BSS	0.2 ± 0.018(0.08) 0.25 +0.05/-0.0(0.10)	0.2 0.25
Nominal gap thickness, cm(in) between Type 4 cells (nominal/min) between Type 4 and rack Type 1 between Type 4 and pool wall	0.082(0.03228)/0.03 min 3.0(1.18) min 13.334(5.25) min	0.082 3.0 13.334
BSS Parameters BSS density, g/cc Boron content, wt% ¹⁰ B Wt% in natural boron Plate length, in	7.73 -7.78 1.7 min 18.14 145.7	7.73 1.7 18.14 144.0

Table 4.3-7 Material Compositions for Non-Fuel Regions

Material Compositions for Stainless Steel SS304L
($\rho = 8.0 \text{ g/cc}$)

<u>Element</u>	<u>Weight Fraction</u>	<u>Atom/b-cm</u>
Cr	0.180	1.66779E-2
Mn	0.020	1.75387E-3
Fe	0.720	6.21117E-2
Ni	0.080	6.56661E-3

Material Compositions for Borated Stainless SS304 B6
($\rho = 7.73 \text{ g/cc}$)

<u>Element</u>	<u>Weight Fraction</u>	<u>Atom/b-cm</u>
Cr	0.180	1.61151E-2
Mn	0.020	1.69468E-3
Fe	0.663	5526419E-2
Ni	0.120	9.51448E-3
B	0.017	7.31794E-3

Material Compositions for Zircaloy-4
($\rho = 6.56 \text{ g/cc}$)

<u>Element</u>	<u>Weight Fraction</u>	<u>Atom/b-cm</u>
Zr	0.9829	4.25652E-2
Sn	0.0140	4.65903E-4
Fe	0.0021	1.48550E-4
Cr	0.0010	7.59770E-5

Material Compositions for Boraflex
($\rho = 1.7 \text{ g/cc}$)

<u>Element</u>	<u>Weight Fraction</u>	<u>Atom/b-cm</u>
H	0.030	3.04701E-2
¹⁰ B	0.0618	6.31428E-3
¹¹ B	0.2751	2.55761E-2
C	0.190	1.61945E-2
O	0.220	1.40812E-2
Si	0.2232	8.13601E-3

Material Compositions for Water and Concrete

KENO V.a Standard Compositions @ T= 293°K
Density of Water = 1.0 g/cc



Table 4.3-8 Fuel Material Number Densities

KENO V.a Fresh Fuel Standard Composition Parameters

Wt% ²³⁵ U	Fractional TD	Temp, °K	Wt% ²³⁸ U
1.6	0.95	293	98.4
2.22	0.95	293	97.78
4.0	0.95	293	96.0

**Axial Burnup Region Number Densities for 5.0 Wt% Initial Enrichment Fuel
At 45 GWd/mtU Average Burnup, Atom/b-cm**

Level	Burnup	²³⁵ U	¹⁶ O	²³⁶ U	²³⁸ U	¹⁴⁹ Sm
1	21.97	6.5805E-04	4.6040E-02	9.1978E-05	2.1400E-02	1.1504E-07
2	36.60	4.2226E-04	4.6040E-02	1.2979E-04	2.1136E-02	1.1678E-07
3	45.11	3.1547E-04	4.6040E-02	1.4412E-04	2.0952E-02	1.1550E-07
4	49.15	2.7799E-04	4.6040E-02	1.4937E-04	2.0864E-02	1.2008E-07
5	42.12	3.6395E-04	4.6040E-02	1.3988E-04	2.1002E-02	1.3026E-07
6	33.55	4.6717E-04	4.6040E-02	1.2524E-04	2.1176E-02	1.2931E-07
7	20.11	6.9888E-04	4.6040E-02	8.6650E-05	2.1431E-02	1.2438E-07
Average	45	3.2281E-04	4.6040E-02	1.4409E-04	2.0958E-02	1.2364E-07

Level	Burnup	²³⁹ Pu	²⁴⁰ Pu	²⁴¹ Pu	¹⁰ B
1	21.97	1.1721E-04	2.5577E-05	1.3166E-05	1.4923E-05
2	36.60	1.3755E-04	4.5800E-05	2.7853E-05	2.3099E-05
3	45.11	1.4105E-04	5.5424E-05	3.4953E-05	2.6417E-05
4	49.15	1.4550E-04	6.0421E-05	3.8844E-05	2.8880E-05
5	42.12	1.4988E-04	5.4273E-05	3.4922E-05	2.6902E-05
6	33.55	1.4418E-04	4.4430E-05	2.7446E-05	2.2480E-05
7	20.11	1.1854E-04	2.3898E-05	1.2260E-05	1.4145E-05
Average	45	1.4492E-04	5.6043E-05	3.6072E-05	3.2281E-04



Table 4.3-9 Assembly Tolerance Penalties (Δk)

Assembly Type	Manufacturing	Theoretical Density	Enrichment, 0.05 wt% ΔE	Statistical Combination
Westinghouse OFA	0.00266	0.00293	0.00419	0.00576
Westinghouse Standard	0.00303	0.00266	0.00408	0.00574
Exxon Standard	0.00303	0.00279	0.00413	0.00583

Table 4.3-10 Reactivity Uncertainty Associated With Fuel Assembly Type

Burnup, GWd/mtU	CASMO-3 k-infinity for a 4 Wt% Assembly in Rack Type 1		
	Westinghouse Standard	Exxon Standard	Westinghouse OFA
0	1.13164	1.12100	1.13448
10	1.04405	1.03429	1.04584
20	0.96854	0.95816	0.96385
30	0.89811	0.88629	0.88318

Table 4.3-11 Consolidation Container Results

Wt% ²³⁵ U	No. Rods	Fuel Assy Type	KENO V.a Results		
			k _{eff}	1σ	K _{Max}
Rack Type 1					
1.6	196	Standard	0.92765	0.00058	0.94490
1.6	225	OFA	0.92534	0.00054	0.94259
Rack Type 2					
1.6	196	Standard	0.91538	0.00058	0.93087
1.6	225	OFA	0.91196	0.00057	0.92745
Rack Type 3					
2.22	196	Standard	0.92307	0.00074	0.94489
2.22	196	OFA	0.92169	0.00072	0.94351



.....

..

Table 4.3-12 Summary of Rack Type Uncertainties, Penalties, And Credits

Description	Region 1	Region 2		
	Type 3	Type 1	Type 2	Type 4
Methodology Bias & Calculational Penalties				
Δk_{bias} - KENO.V.a Bias (44 Group)	0.00701	0.00561	0.00561	0.00561
Penalties:				
Pool Temperature Penalty (50 to 212°F),	0.00133	0.00218	0.00207	0.00207
Boraflex B10 Self Shielding Penalty	0.00000	0.00140	0.00000	0.00000
Assy Off-Center Placement Penalty	<u>0.00000</u>	<u>0.00000</u>	<u>0.00000</u>	<u>0.00083</u>
Δk_{pen} - sum of penalties	0.00133	0.00358	0.00207	0.00290
Total = $\Delta k_{bia} + \Delta k_{pen}$	0.00834	0.00919	0.00768	0.00851
Tolerance Uncertainties and Statistical Uncertainties				
Tolerance Uncertainties:				
Fuel Assy Manufacturing Tolerance	0.00583	0.00583	0.00583	0.00583
Rack Fabrication Tolerance	<u>0.01198</u>	<u>0.00524</u>	<u>0.00484</u>	<u>0.00092</u>
σ_{tol} - sum of tolerance uncertainties	0.01332	0.00784	0.00758	0.00590
σ_c - Calculational Uncertainty ^a	0.00070	0.00070	0.00070	0.00070
σ_{bias} - Methodology Bias Uncertainty	0.00090	0.00090	0.00090	0.00090
Total (Statistically Combined)	0.01348	0.00809	0.00784	0.00624
Total adjustment to k_{eff}	0.02182	0.01728	0.01552	0.01475

a) Based upon a typical sigma of 0.0007 for 1,000,000 neutron histories for KENO V.a cases.



Table 4.3-13 Region 1, Rack Type 3, Dropped Assembly Accident Results

Model	$\Delta k \pm 1.763\sigma$
Rack Type 3 T-bone	0.0017 ± 0.0018
Rack Type 3 Misplaced assembly	0.0114 ± 0.0015
Rack Type 3 Deep Drop Accident	0.0008 ± 0.0018
Rack Type 2/3 Side Drop	0.0393 ± 0.0016
Side Drop with 300 ppm Boron	-0.0222 ± 0.0017

Table 4.3-14 Region 2, Rack Types 1, 2, & 4, Dropped Assembly Accident Results

Model	$\Delta k \pm 1.763\sigma$
Rack Type 2 T-bone	0.0079 ± 0.0015
Rack Type 2 Misplaced Assembly	0.0097 ± 0.0015
Racks Type 2 & 4 Deep Drop Accident ^a	0.0008 ± 0.0018
Rack Type 1 Misplaced Assembly - Lower Curve	0.0469 ± 0.0013
Rack Type 1 Misplaced Assy , 450 ppm Boron, Base	-0.0196 ± 0.0014
Rack Type 1 Deep Drop Accident ^b	0.0469 ± 0.0013

a) Same as deep drop for rack Type 3 since base plate construction is similar.

b) Bounded by the Rack Type 1 misplaced assembly accident.

Table 4.3-15 Seismic Event Accident Results

Model	$\Delta k \pm 1.763\sigma$
Rack Types 2 and 3	0.0043 ± 0.0026
Rack Types 1, 2A, & 4C	0.0085 ± 0.0026
Rack Types 1, 3A, & 4F	0.0045 ± 0.0026



Table 4.4-1 KENO V.a BIAS vs Separation Distance

Case	Core	Spacing cm	B4C Pins	Boron ppm	Plates	Calculated		Experimental		Bias Δk_{eff}
						k_{eff}	1σ	k_{eff}	1σ	
1	i	--	--	0	--	0.9965	0.0010	1.0002	0.0005	-0.0037
2	ii	0.00	0	1037	--	0.9982	0.0006	1.0001	0.0005	-0.0019
3	iii	1.64	0	764	--	0.9996	0.0006	1.0000	0.0006	-0.0004
4	iv	1.64	84	0	--	0.9952	0.0010	0.9999	0.0006	-0.0047
5	v	3.27	64	0	--	0.9959	0.0010	1.0000	0.0007	-0.0041
6	vi	3.27	64	0	--	1.0066	0.0010	1.0097	0.0012	-0.0031
7	vii	4.91	34	0	--	0.9946	0.0009	0.9998	0.0009	-0.0052
8	viii	4.91	34	0	--	1.0015	0.0010	1.0083	0.0012	-0.0068
9	ix	6.54	0	0	--	0.9943	0.0007	1.0030	0.0009	-0.0087
10	x	4.91	--	143	None	0.9950	0.0006	1.0001	0.0009	-0.0051
11	xi	1.64	--	514	SS	0.9956	0.0006	1.0000	0.0006	-0.0044
12	xii	3.27	--	217	SS	0.9937	0.0006	1.0000	0.0007	-0.0063
13	xiii	1.64	--	15	1.614%B/AL	0.9949	0.0010	1.0000	0.0010	-0.0051
14	xiv	1.64	--	92	1.257%B/AL	0.9942	0.0010	1.0001	0.0010	-0.0059
15	xv	1.64	--	395	0.401%B/AL	0.9906	0.0009	0.9998	0.0016	-0.0092
16	xvi	3.27	--	121	0.401%B/AL	0.9892	0.0009	1.0001	0.0019	-0.0109
17	xvii	1.64	--	487	0.242%B/AL	0.9932	0.0004	1.0000	0.0010	-0.0068
18	xviii	3.27	--	197	0.242%B/AL	0.9929	0.0004	1.0002	0.0011	-0.0073
19	xix	1.64	--	634	0.100%B/AL	0.9955	0.0004	1.0002	0.0010	-0.0047
20	xx	3.27	--	320	0.100%B/AL	0.9942	0.0005	1.0003	0.0011	-0.0061
21	xxi	4.91	--	72	0.100%B/AL	0.9918	0.0005	0.9997	0.0015	-0.0079
Average =						0.9954		1.0010		-0.0056
Standard Deviation =						0.0038		0.0027		0.0024

Table 4.4-2 Additional UO₂ Critical Experiment Comparisons

Case	Case ID	Case Description	Wt% ²³⁵ U	Boron ppm	Calculated		Bias
					k _{eff}	1 σ	Δk _{eff}
1	p2438x05	No Absorber Plates	2.35	0	0.9968	0.0009	-0.0032
2	p2438x17	Boral Absorber Plates	2.35	0	0.9961	0.0009	-0.0039
3	p2438x28	Stainless Steel Absorber Plates	2.35	0	0.9958	0.0010	-0.0042
4	p2615x14	Stainless Steel Absorber Plates	4.31	0	0.9979	0.0011	-0.0021
5	p2615x23	Cadmium Absorber Plates	4.31	0	0.9995	0.0011	-0.0005
6	p2615x31	Boral Absorber Plates	4.31	0	0.9987	0.0011	-0.0013
7	p3314a	0.226 cm Boraflex Absorber Plates	4.31	0	1.0027	0.0011	0.0027
8	p3314b	0.452 cm Boraflex Absorber Plates	4.31	0	1.0016	0.0011	0.0016
9	e196u6n	0.615" Pitch	2.35	0	0.9951	0.0010	-0.0049
10	epru615b	0.615" Pitch	2.35	464	0.9947	0.0010	-0.0053
11	epru75	0.750" Pitch	2.35	0	0.9943	0.0010	-0.0057
12	epru75b	0.750" Pitch	2.35	568	0.9986	0.0008	-0.0014
13	e196u87c	0.870" Pitch	2.35	0	0.9976	0.0009	-0.0024
14	epru87b	0.870" Pitch	2.35	286	0.9999	0.0008	-0.0001
15	saxu56	2 Lattice Pitches, SS Clad, 0.56" Pitch	5.74	0	0.9950	0.0011	-0.0050
16	saxu792	2 Lattice Pitches, SS Clad, 0.792" Pitch	5.74	0	0.9988	0.0011	-0.0012
Average =					.9977		-0.0023
Standard Deviation =					0.0025		0.0025

Table 4.4-3 Mixed Oxide Critical Experiment Comparisons

Case	Case ID	Case Description	Wt% Pu	Boron ppm	Calculated		Bias	
					k_{eff}	1σ	Δk_{eff}	1σ
1	epri70un	UO2/PuO2 Square Lattice, 0.700" Pitch	2	0	0.9969	0.0011	-0.0031	0.0011
2	epri70b	UO2/PuO2 Square Lattice, 0.700" Pitch	2	681	1.0008	0.0010	0.0008	0.0010
3	epri87un	UO2/PuO2 Square Lattice, 0.870" Pitch	2	0	1.0018	0.0011	0.0018	0.0011
4	epri87b	UO2/PuO2 Square Lattice, 0.870" Pitch	2	1090	1.0083	0.0009	0.0083	0.0009
5	epri99un	UO2/PuO2 Square Lattice, 0.990" Pitch	2	0	1.0051	0.0009	0.0051	0.0009
6	epri99b	UO2/PuO2 Square Lattice, 0.990" Pitch	2	767	1.0072	0.0009	0.0072	0.0009
7	saxton52	UO2/PuO2 Square Lattice, 0.52" Pitch	6.6	0	1.0001	0.0011	0.0001	0.0011
8	saxton56	UO2/PuO2 Square Lattice, 0.56" Pitch	6.6	0	0.9993	0.0011	-0.0007	0.0011
9	saxtn56b	UO2/PuO2 Square Lattice, 0.56" Pitch	6.6	337	1.0006	0.0000	0.0006	0.0000
10	saxtn792	UO2/PuO2 Square Lattice, 0.792" Pitch	6.6	0	1.0031	0.0011	0.0031	0.0011
11	saxtn735	UO2/PuO2 Square Lattice, 0.735" Pitch	6.6	0	1.0010	0.0012	0.0010	0.0012
12	saxtn104	UO2/PuO2 Square Lattice, 1.04" Pitch	6.6	0	1.0036	0.0011	0.0036	0.0011
Average =					1.0023		0.0023	
Standard Deviation =					0.0033		0.0033	

Table 4.4-4 International Handbook Critical Experiments

Spacing Between Fuel Arrays, cm	Δk KENO V.a 27 Group Cross Sections	Δk MCNP, Continuous Energy Cross Sections	KENO V.a, 44 Group Cross Sections	
			Handbook Criticals	B&W Criticals
0	-0.0084	-0.0011	-0.0039	--
4.46	-0.0079	-0.0030	-0.0048	--
6.39	-0.0108	-0.0028	-0.0072	--
7.57	-0.0092	-0.0077	-0.0068	--
8.01	-0.0067	-0.0043	-0.0040	--
8.41	-0.0110	-0.0042	-0.0060	--
10.05	-0.0036	-0.0006	-0.0042	--
11.92	-0.0094	-0.0021	-0.0042	--
0	--	--	--	-0.0019
1.636	--	--	--	-0.0004
4.907	--	--	--	-0.0051
6.54	--	--	--	-0.0087

Table 4.4-5 CASMO-3/KENO V.a Benchmark Configurations

Core	Fuel Region Separation, cm	Isolation Plate	Mod Temp, °C	PPM Boron
III	1.636	-	18.0	764
IX	6.54	-	17.5	0
XIII	1.636	Al, 1.614 wt%B	20.0	15
XVI	3.272	Al, 0.401 wt%B	17.5	121
XXI	4.907	Al, 0.100 wt%B	16.5	72
XII	3.272	SS	26.0	217

Table 4.4-6 CASMO-3/KENO V.a Infinite Array Benchmark Comparison

Core	CASMO-3 k_{inf}	KENO V.a $k_{inf} \pm 1\sigma$	Δk KENO V.a - CASMO-3	KENO V.a Bias	KENO V.a K_{max}^a
III	1.12299	1.11758 ± 0.00048	-0.00541	-0.00045	1.120236
IX	1.07976	1.07214 ± 0.00059	-0.00762	-0.00874	1.096324
XIII	1.10406	1.09490 ± 0.00063	-0.00926	-0.00509	1.103581
XVI	1.09909	1.09040 ± 0.00061	-0.00869	-0.01086	1.104940
XXI	1.09151	1.08473 ± 0.00060	-0.00678	-0.00787	1.095787
XII	1.10643	1.09701 ± 0.00058	-0.00942	-0.00608	1.105645

a) K_{max} is the sum of k_{inf} , the bias, and 1.763 times the sum of the squares of the uncertainties associated with the bias and k_{inf} .

Table 4.4-7 CASMO-3/KENO V.a Infinite Array Benchmark Comparison

Rack Type	CASMO-3 k_{inf}	KENO V.a $k_{inf} \pm 1\sigma$	Δk KENO V.a - CASMO-3	KENO V.a Bias	KENO V.a K_{max}^a
Type 1	0.86548	0.86614 ± 0.00054	0.00066	-0.0056	0.87359
Type 2	0.90356	0.89964 ± 0.00053	-0.00392	-0.0056	0.90708
Type 3	0.91894	0.91060 ± 0.00073	-0.00834	-0.0079	0.92054

a) K_{max} is the sum of k_{inf} , the bias, and 1.763 times the sum of the squares of the uncertainties associated with the bias and k_{inf} .

Table 4.4-8 KENO V.a Infinite to Finite Model Comparison

Rack Type	Δk (infinite - finite)	1σ
Rack Type 1	0.0032	0.0008
Rack Type 2		
BSS on Edge of Finite Model	0.00439	0.0008
No BSS on Edge of Finite Model	0.00645	0.0008
Rack Type 3		
BSS on Edge of Finite Model	0.00661	0.0010
No BSS on Edge of Finite Model	0.00975	0.0010



Table 4.4-9 Ginna Fuel Assemblies Used for Axial Shape Evaluation

Fuel Assembly ID	Assy Type	Cycle	Burnup, GWd/mtU
A62	OFA, Blanket	21	15.19
A62	OFA, Blanket	22	27.21
A62	OFA, Blanket	23	33.97
A62	OFA, Blanket	26	48.48
D77	OFA, Blanket	24	12.96
D77	OFA, Blanket	25	27.87
D77	OFA, Blanket	26	44.11
C63	OFA, Blanket	23	12.88
C63	OFA, Blanket	24	27.08
C63	OFA, Blanket	25	39.67
C63	OFA, Blanket	26	45.03
C56	OFA, Blanket	23	14.22
C56	OFA, Blanket	24	27.62
C56	OFA, Blanket	25	32.30
C56	OFA, Blanket	26	37.51
E60	OFA, Blanket	25	15.65
E60	OFA, Blanket	26	34.42
Q16	ANF Std, No Blkt	14	10.72
Q16	ANF Std, No Blkt	15	23.01
Q16	ANF Std, No Blkt	16	33.53
Q16	ANF Std, No Blkt	17	44.84



1. The first part of the document is a list of names and addresses. The names are listed in the first column, and the addresses are listed in the second column. The names are: John Doe, Jane Doe, and Bob Doe. The addresses are: 123 Main St, 456 Main St, and 789 Main St.

Table 4.4-10 Relative Axial Shapes for Typical Non-Axial Blanket Standard Fuel Assemblies

Assy Burnup, GWd/mtU =			10.715	23.011	33.526	44.844
Assy ID & Cycle of Irradiation =			Q16 Cy 14	Q16 Cy 15	Q16 Cy 16	Q16 Cy 17
Node	Height, in	Midpt, in	Relative Burnup			
1	6.15	3.075	0.490901	0.485724	0.472708	0.488181
2	12.30	9.225	0.806533	0.813611	0.806777	0.813375
3	18.45	15.375	0.987681	1.000956	0.997793	1.00252
4	24.60	21.525	1.074382	1.084308	1.082622	1.081126
5	30.75	27.675	1.112366	1.117726	1.116626	1.106949
6	36.90	33.825	1.127018	1.128938	1.12808	1.113705
7	43.05	39.975	1.130751	1.130677	1.129869	1.113839
8	49.20	46.125	1.130098	1.128373	1.127602	1.111498
9	55.35	52.275	1.127298	1.12468	1.124023	1.108554
10	61.50	58.425	1.123472	1.120377	1.119967	1.105544
11	67.65	64.575	1.119832	1.116031	1.11591	1.102667
12	73.80	70.725	1.115912	1.111642	1.111853	1.099835
13	79.95	76.875	1.112086	1.107383	1.108036	1.097293
14	86.10	83.025	1.107699	1.102864	1.104098	1.094773
15	92.25	89.175	1.10294	1.09817	1.099922	1.092164
16	98.40	95.325	1.097154	1.092564	1.095031	1.089399
17	104.55	101.475	1.088661	1.084612	1.087872	1.08514
18	110.70	107.625	1.074382	1.071879	1.07606	1.077848
19	116.85	113.775	1.04797	1.04776	1.052914	1.062015
20	123.00	119.925	0.997107	1.000217	1.006144	1.025176
21	129.15	126.075	0.898553	0.903872	0.909622	0.936067
22	135.30	132.225	0.713299	0.714658	0.717413	0.745652
23	141.45	138.375	0.415119	0.41315	0.409473	0.446793



Table 4.4-11 Relative Axial Shapes for the Seven Zone Axial Model

Assy Burnup, GWd/mtU =			10.715	23.011	33.526	44.844
Assy ID & Cycle of Irradiation =			Q16 Cy 14	Q16 Cy 15	Q6 Cy 16	Q16 Cy 17
Node	Height, in	Height, cm	Relative Burnup			
1	6.15	15.621	0.491	0.486	0.473	0.488
2	12.30	31.242	0.807	0.814	0.807	0.813
3	18.45	46.863	0.988	1.001	0.998	1.003
4	125.55	318.897	1.099	1.098	1.099	1.092
5	131.70	334.518	0.899	0.904	0.910	0.936
6	137.85	350.139	0.713	0.715	0.717	0.746
7	144.00	365.760	0.415	0.413	0.409	0.447

Table 4.4-12 Axial Burnup Shapes for the Region 2 Loading Curve

Assy Initial Enrichment, Wt% =			3	4	5
Assy Burnup, GWd/mtU =			21.00	34.00	45.00
Node	Height in	Height, cm	Node Burnup, GWd/mtU		
1	6.15	15.621	10.20	16.07	21.97
2	12.3	31.242	17.09	27.43	36.60
3	18.45	46.863	21.02	33.92	45.11
4	125.55	318.897	23.06	37.37	49.15
5	131.7	334.518	18.98	30.93	42.12
6	137.85	350.139	15.01	24.39	33.55
7	144	365.76	8.68	13.92	20.11

Table 4.4-13 Irradiation Input Data and Isotopic Concentrations for 3 Wt% Initial Enrichment Fuel at 21 GWd/mtU Burnup In Region 2

Zone	Uppper Boundary, cm	Zone Burnup, GWd/mtU	Fuel Temperature, °K	Moderator Temperature, °K	CASMO-3 Zone Power, W/gU
1	15.621	10.20	805.94	557.70	15.52416
2	31.242	17.09	867.05	558.16	25.86533
3	46.863	21.02	928.16	558.35	31.88013
4	318.897	23.06	932.57	574.28	34.73219
5	334.518	18.98	887.60	590.85	29.76694
6	350.139	15.01	829.27	591.59	23.71172
7	365.760	8.68	770.94	592.07	14.20803

Axial Burnup Region Number Densities, Atom/b-cm

Level	Burnup, GWd/mtU	²³⁵ U	¹⁶ O	²³⁶ U	²³⁸ U	¹⁴⁹ Sm
1	10.20	4.6345E-04	4.6040E-02	4.0905E-05	2.1987E-02	7.0831E-08
2	17.09	3.4726E-04	4.6040E-02	6.0203E-05	2.1827E-02	7.8726E-08
3	21.02	2.9213E-04	4.6040E-02	6.8757E-05	2.1713E-02	8.1832E-08
4	23.06	2.6977E-04	4.6040E-02	7.2601E-05	2.1666E-02	8.6537E-08
5	18.98	3.2605E-04	4.6040E-02	6.4526E-05	2.1765E-02	8.8019E-08
6	15.01	3.8452E-04	4.6040E-02	5.5108E-05	2.1878E-02	8.3143E-08
7	8.68	4.9549E-04	4.6040E-02	3.6081E-05	2.2025E-02	7.3739E-08
Average	21	2.9541E-04	4.6040E-02	6.8760E-05	2.1725E-02	8.4910E-08

Level	Burnup, GWd/mtU	²³⁹ Pu	²⁴⁰ Pu	²⁴¹ Pu	¹⁰ B
1	10.20	7.9185E-05	1.3750E-05	5.1063E-06	6.4851E-06
2	17.09	1.0171E-04	2.6739E-05	1.3023E-05	1.0251E-05
3	21.02	1.0928E-04	3.3917E-05	1.7595E-05	1.2369E-05
4	23.06	1.1414E-04	3.7909E-05	2.0480E-05	1.3609E-05
5	18.98	1.1053E-04	3.1282E-05	1.6341E-05	1.1580E-05
6	15.01	1.0065E-04	2.3841E-05	1.1271E-05	9.3555E-06
7	8.68	7.4853E-05	1.1527E-05	4.0172E-06	5.7635E-06
Average	21	1.1108E-04	3.4359E-05	1.8077E-05	1.2496E-05



* 2004年，中国GDP为15.98万亿元，比上年增长9.7%，其中第一产业增加值1.67万亿元，增长4.3%；第二产业增加值6.43万亿元，增长12.1%；第三产业增加值7.88万亿元，增长9.5%。

14 14

Table 4.4-14 Irradiation Input Data and Isotopic Concentrations for 4 Wt% Initial Enrichment Fuel at 34 GWd/mtU Burnup in Region 2

Zone	Uppper Boundary, cm	Zone Burnup, GWd/mtU	Fuel Temperature, °K	Moderator Temperature, °K	CASMO-3 Zone Power, W/gU
1	15.621	16.07	805.94	557.70	15.52416
2	31.242	27.43	867.05	558.16	25.86533
3	46.863	33.92	928.16	558.35	31.88013
4	318.897	37.37	932.57	574.28	34.73219
5	334.518	30.93	887.60	590.85	29.76694
6	350.139	24.39	829.27	591.59	23.71172
7	365.760	13.92	770.94	592.07	14.20803

Axial Burnup Region Number Densities, Atom/b-cm

Level	Burnup, GWd/mtU	²³⁵ U	¹⁶ O	²³⁶ U	²³⁸ U	¹⁴⁹ Sm
1	16.07	5.6255E-04	4.6040E-02	6.5780E-05	2.1690E-02	9.3550E-08
2	27.43	3.7849E-04	4.6040E-02	9.5834E-05	2.1467E-02	9.9113E-08
3	33.92	2.9530E-04	4.6040E-02	1.0780E-04	2.1312E-02	1.0033E-07
4	37.37	2.6207E-04	4.6040E-02	1.1286E-04	2.1237E-02	1.0513E-07
5	30.93	3.4179E-04	4.6040E-02	1.0278E-04	2.1371E-02	1.1147E-07
6	24.39	4.3079E-04	4.6040E-02	8.9221E-05	2.1526E-02	1.0842E-07
7	13.92	6.0756E-04	4.6040E-02	5.9153E-05	2.1732E-02	9.9625E-08
Average	34	2.9901E-04	4.6040E-02	1.0802E-04	2.1319E-02	1.0478E-07

Level	Burnup, GWd/mtU	²³⁹ Pu	²⁴⁰ Pu	²⁴¹ Pu	¹⁰ B
1	16.07	1.0013E-04	2.0203E-05	9.2139E-06	1.0533E-05
2	27.43	1.2273E-04	3.8390E-05	2.1475E-05	1.6809E-05
3	33.92	1.2814E-04	4.7397E-05	2.7845E-05	2.0217E-05
4	37.37	1.3283E-04	5.2374E-05	3.1720E-05	2.2295E-05
5	30.93	1.3354E-04	4.4857E-05	2.6875E-05	1.9272E-05
6	24.39	1.2503E-04	3.4904E-05	1.9731E-05	1.5624E-05
7	13.92	9.7316E-05	1.7494E-05	7.6889E-06	9.5098E-06
Average	34	1.3104E-04	4.8234E-05	2.8681E-05	2.0526E-05

Table 4.4-15 Irradiation Input Data and Isotopic Concentrations for 5 Wt% Initial Enrichment Fuel at 45 GWd/mtU Burnup in Region 2

Zone	Upper Boundary, cm	Zone Burnup, GWd/mtU	Fuel Temperature, °K	Moderator Temperature, °K	CASMO-3 Zone Power, W/gU
1	15.621	21.97	805.94	557.70	15.52416
2	31.242	36.60	867.05	558.16	25.86533
3	46.863	45.11	928.16	558.35	31.88013
4	318.897	49.15	932.57	574.28	34.73219
5	334.518	42.12	887.60	590.85	29.76694
6	350.139	33.55	829.27	591.59	23.71172
7	365.760	20.11	770.94	592.07	14.20803

Axial Burnup Region Number Densities, Atom/b-cm

Level	Burnup, GWd/mtU	²³⁵ U	¹⁶ O	²³⁶ U	²³⁸ U	¹⁴⁹ Sm
1	21.97	6.5805E-04	4.6040E-02	9.1978E-05	2.1400E-02	1.1504E-07
2	36.60	4.2226E-04	4.6040E-02	1.2979E-04	2.1136E-02	1.1678E-07
3	45.11	3.1547E-04	4.6040E-02	1.4412E-04	2.0952E-02	1.1550E-07
4	49.15	2.7799E-04	4.6040E-02	1.4937E-04	2.0864E-02	1.2008E-07
5	42.12	3.6395E-04	4.6040E-02	1.3988E-04	2.1002E-02	1.3026E-07
6	33.55	4.6717E-04	4.6040E-02	1.2524E-04	2.1176E-02	1.2931E-07
7	20.11	6.9888E-04	4.6040E-02	8.6650E-05	2.1431E-02	1.2438E-07
Average	45	3.2281E-04	4.6040E-02	1.4409E-04	2.0958E-02	1.2364E-07

Level	Burnup, GWd/mtU	²³⁹ Pu	²⁴⁰ Pu	²⁴¹ Pu	¹⁰ B
1	21.97	1.1721E-04	2.5577E-05	1.3166E-05	1.4923E-05
2	36.60	1.3755E-04	4.5800E-05	2.7853E-05	2.3099E-05
3	45.11	1.4105E-04	5.5424E-05	3.4953E-05	2.6417E-05
4	49.15	1.4550E-04	6.0421E-05	3.8844E-05	2.8880E-05
5	42.12	1.4988E-04	5.4273E-05	3.4922E-05	2.6902E-05
6	33.55	1.4418E-04	4.4430E-05	2.7446E-05	2.2480E-05
7	20.11	1.1854E-04	2.3898E-05	1.2260E-05	1.4145E-05
Average	45	1.4492E-04	5.6043E-05	3.6072E-05	3.2281E-04



Table 4.4-16 Isotopic Concentrations for Fuel for Region 2 Auxiliary Curves, Atom/b-cm

Enrichment, Wt %	Burnup, GWd/mtU	²³⁵ U	¹⁶ O	²³⁶ U	²³⁸ U	¹⁴⁹ Sm
5.0	52.2	2.4763E-04	4.6040E-02	1.5282E-04	2.0832E-02	1.1451E-07
5.0	38.8	4.0229E-04	4.6040E-02	1.3335E-04	2.1066E-02	1.2873E-07
4.0	40.0	2.3482E-04	4.6040E-02	1.1638E-04	2.1211E-02	1.0064E-07
4.0	29.1	3.5997E-04	4.6040E-02	9.9148E-05	2.1403E-02	1.0839E-07
3.0	25.0	2.4699E-04	4.6040E-02	7.6063E-05	2.1651E-02	8.4683E-08
3.0	18.0	3.3627E-04	4.6040E-02	6.2279E-05	2.1778E-02	8.4126E-08

Enrichment, Wt %	Burnup, GWd/mtU	²³⁹ Pu	²⁴⁰ Pu	²⁴¹ Pu	¹⁰ B
5.0	52.2	6.3354E-05	4.0144E-05	1.4439E-04	3.1155E-05
5.0	38.8	4.8842E-05	3.0860E-05	1.4294E-04	2.4623E-05
4.0	40.0	1.3277E-04	5.5454E-05	3.3446E-05	2.3452E-05
4.0	29.1	1.2770E-04	4.1271E-05	2.4286E-05	1.8037E-05
3.0	25.0	1.1583E-04	4.1120E-05	2.2419E-05	1.2589E-05
3.0	18.0	1.0576E-04	2.8949E-05	1.4549E-05	9.8012E-06

Table 4.4-17 Average Isotopic Concentrations for Region 1 Loading Curve, Atom/b-cm

Enrichment, Wt %	Burnup, GWd/mtU	²³⁵ U	¹⁶ O	²³⁶ U	²³⁸ U	¹⁴⁹ Sm
3.0	9	4.8608E-04	4.6040E-02	3.6932E-05	2.1930E-02	7.5148E-05
4.0	18	5.2911E-04	4.6040E-02	7.1679E-05	2.1582E-02	1.0825E-07
5.0	28	5.5621E-04	4.6040E-02	1.0952E-04	2.1231E-02	1.3556E-07

Enrichment, Wt %	Burnup, GWd/mtU	²³⁹ Pu	²⁴⁰ Pu	²⁴¹ Pu	¹⁰ B
3.0	9	1.1790E-05	4.1949E-06	7.6900E-08	6.0879E-06
4.0	18	2.3888E-05	1.1999E-05	1.0873E-04	1.2043E-05
5.0	28	3.4759E-05	2.0835E-05	1.3291E-04	1.8966E-05



Table 4.4-18 Evaluation of Axial Shape Effects for All Rack Types

Description	Calculated		Δk_{axial}
	k_{eff}	1σ	
Rack Type 1 Standard Assys			
5 wt% at 45 GWd/mtU degraded	0.91080	0.00051	
5 wt% at 45 GWd/mtU degraded axial	0.93091	0.00059	0.02011
5 wt% at 45 GWd/mtU	0.86258	0.00053	
5 wt% at 45 GWd/mtU axial	0.88589	0.00059	0.02331
4 wt% at 34 GWd/mtU degraded	0.91188	0.00051	
4 wt% at 34 GWd/mtU degraded axial	0.92806	0.00061	0.01618
4 wt% at 34 GWd/mtU	0.86432	0.00056	
4 wt% at 34 GWd/mtU axial	0.88177	0.00059	0.01745
3 wt% at 21 GWd/mtU degraded	0.92397	0.00052	
3 wt% at 21 GWd/mtU degraded axial	0.92099	0.00058	-0.00298
3 wt% at 21 GWd/mtU	0.87495	0.00055	
3 wt% at 21 GWd/mtU axial	0.87403	0.00058	-0.00092
Rack Type 2 Standard Assys			
5 wt% at 45 GWd/mtU	0.89584	0.0005	
5 wt% at 45 GWd/mtU axial	0.91951	0.00058	0.02367
4 wt% at 34 GWd/mtU	0.89781	0.00052	
4 wt% at 34 GWd/mtU axial	0.91629	0.00057	0.01848
3 wt% at 21 GWd/mtU	0.90852	0.00055	
3 wt% at 21 GWd/mtU axial	0.90914	0.00057	0.00062
Rack Type 3 Standard Assys			
5 wt% at 45 GWd/mtU	0.88676	0.00071	
5 wt% at 45 GWd/mtU axial	0.88102	0.00069	-0.00574
4 wt% at 34 GWd/mtU	0.88692	0.00068	
4 wt% at 34 GWd/mtU axial	0.88052	0.0007	-0.0064
3 wt% at 21 GWd/mtU	0.88937	0.00070	
3 wt% at 21 GWd/mtU axial	0.88628	0.00070	-0.0031
Rack Type 4 Standard Assys			
5 wt% at 45 GWd/mtU	0.88400	0.00055	
5 wt% at 45 GWd/mtU axial	0.90496	0.00061	0.02096
4 wt% at 34 GWd/mtU	0.88472	0.00056	
4 wt% at 34 GWd/mtU axial	0.90379	0.00061	0.01907
3 wt% at 21 GWd/mtU	0.89626	0.00057	
3 wt% at 21 GWd/mtU axial	0.89432	0.00058	-0.00194

Table 4.4-19 Evaluation of Margin Provided by the Boraflex Degradation Model for Rack Type 1

Description	Calculated		$\Delta k_{\text{degraded}} \pm 1\sigma$
	k_{eff}	1σ	
5 wt% at 45 GWd/mtU degraded rack model	0.91080	0.00051	0.0482 ± 0.0007
5 wt% at 45 GWd/mtU nominal rack model	0.86258	0.00053	-
4 wt% at 34 GWd/mtU degraded rack model	0.91188	0.00051	0.0476 ± 0.0008
4 wt% at 34 GWd/mtU nominal rack model	0.86432	0.00056	-
3 wt% at 21 GWd/mtU degraded rack model	0.92397	0.00052	0.0490 ± 0.0008
3 wt% at 21 GWd/mtU nominal rack model	0.87495	0.00055	-

Figure 4.1-1 Region 1 Spent Fuel Burnup vs Enrichment Curve

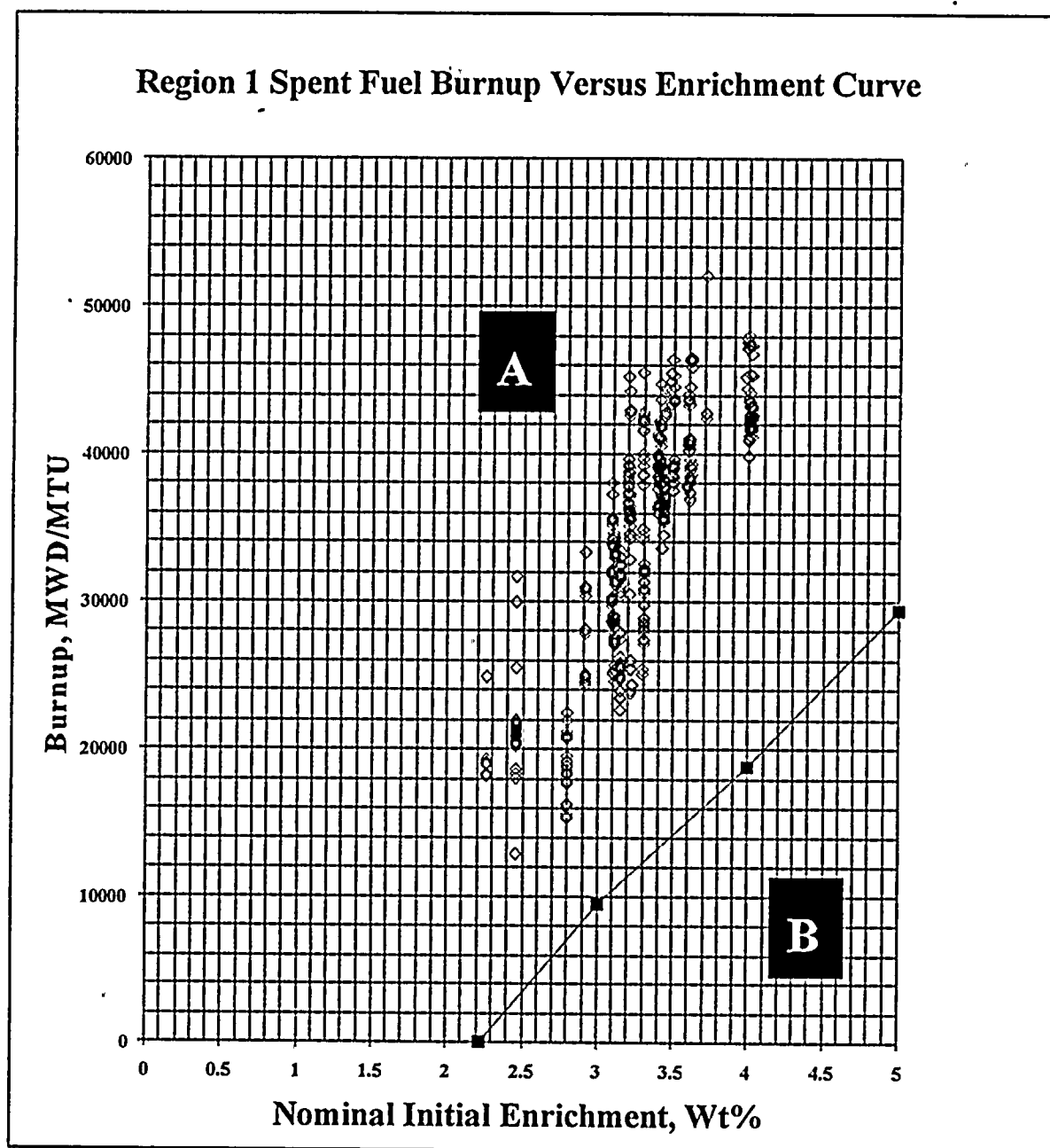


Figure 4.1-2 Region 2 Burnup vs Enrichment Curve

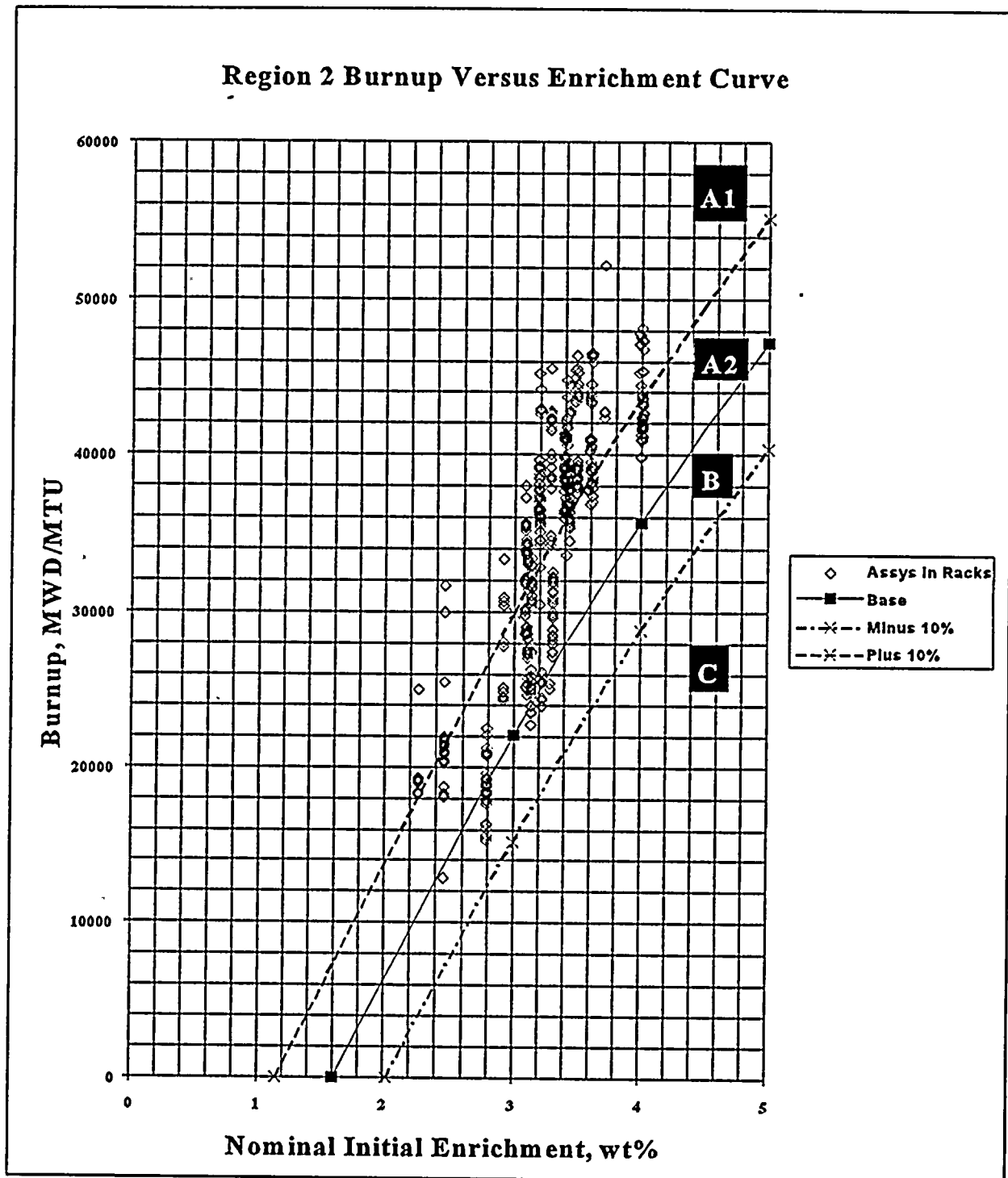
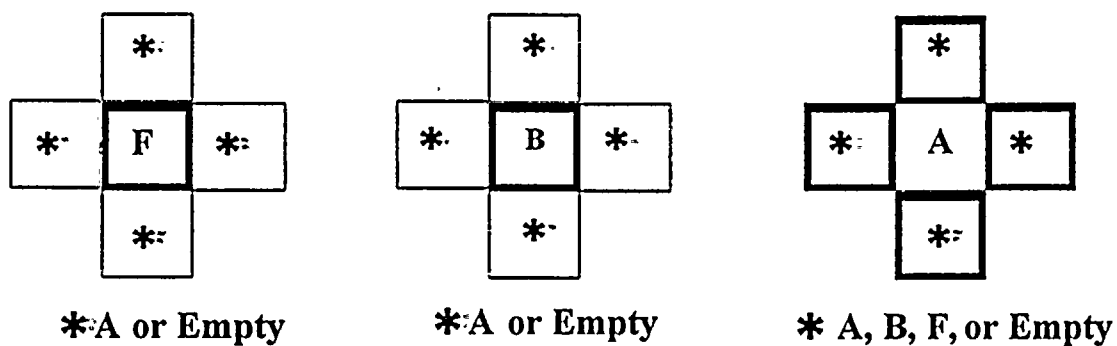


Figure 4.1-3 Sketch of Allowable Loading Configurations for Region 1



Cell With Integral
Lead-in Funnel



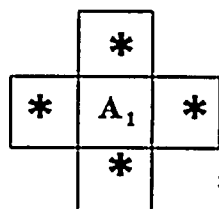
Cell Without Integral
Lead-in Funnel

F = Fresh Fuel Assembly.

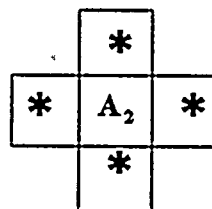
A = Fuel Assembly with Burnup and Enrichment in Area A of Figure 4.1-1.

B = Fuel Assembly with Burnup and Enrichment in Area B of Figure 4.1-1.

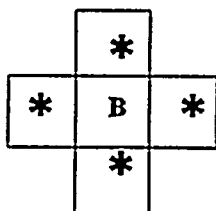
Figure 4.1-4 Sketch of Allowable Loading Configurations for Region 2



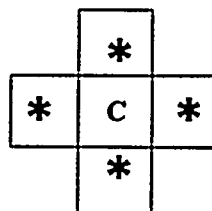
*** A₁, A₂, B,
or Empty**



*** A₁, A₂, or Empty**



*** A₁ or Empty**



*** Empty**

A₁ = Fuel Assembly with Burnup and Enrichment in Area A₁ of Figure 4.1-2.

A₂ = Fuel Assembly with Burnup and Enrichment in Area A₂ of Figure 4.1-2.

B = Fuel Assembly with Burnup and Enrichment in Area B of Figure 4.1-2.

C = Fuel Assembly with Burnup and Enrichment in Area C of Figure 4.1-2.



THE UNIVERSITY OF CHICAGO LIBRARY

1964

Figure 4.3-1 Ginna Spent Fuel Pool Configuration

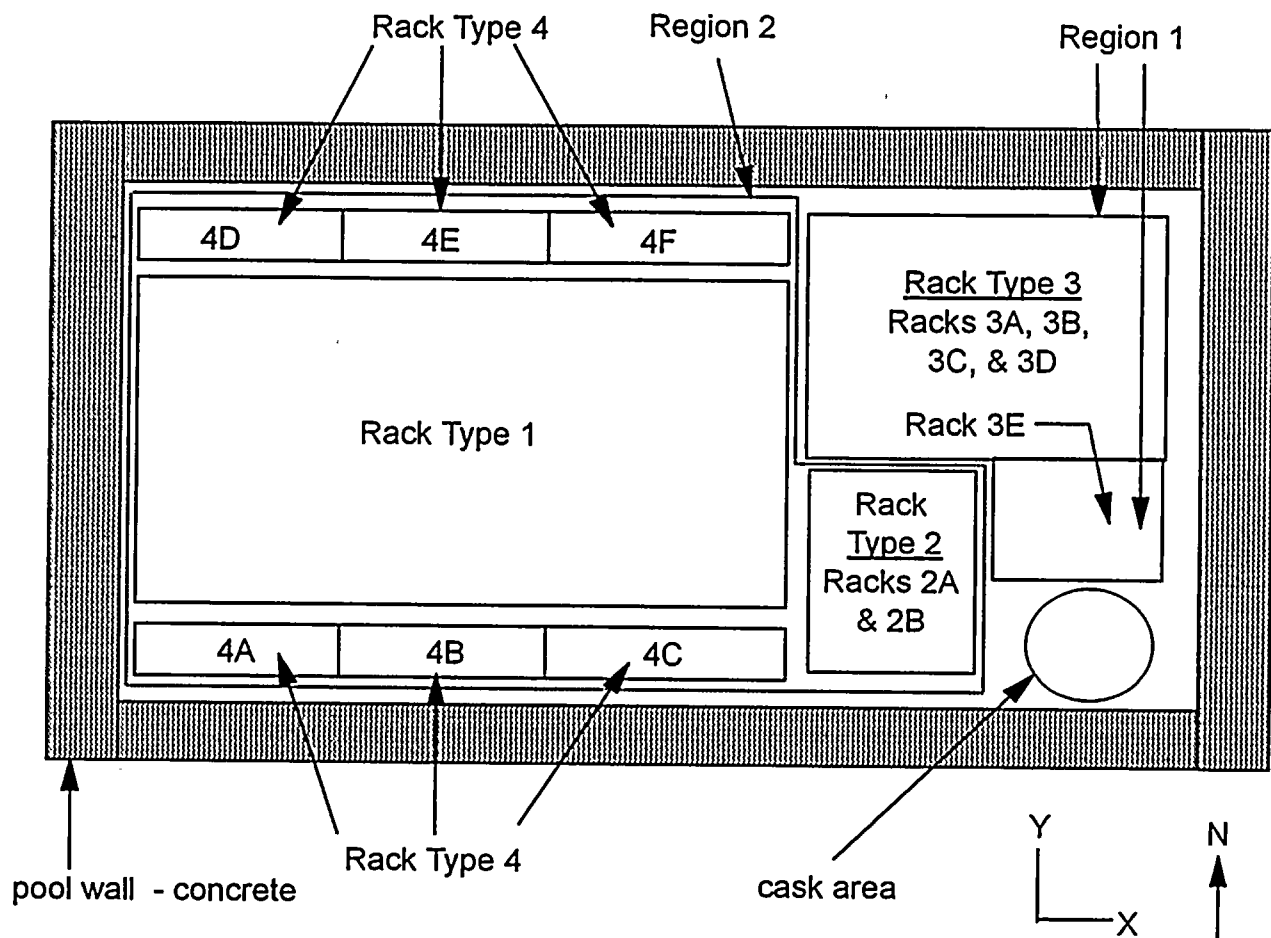
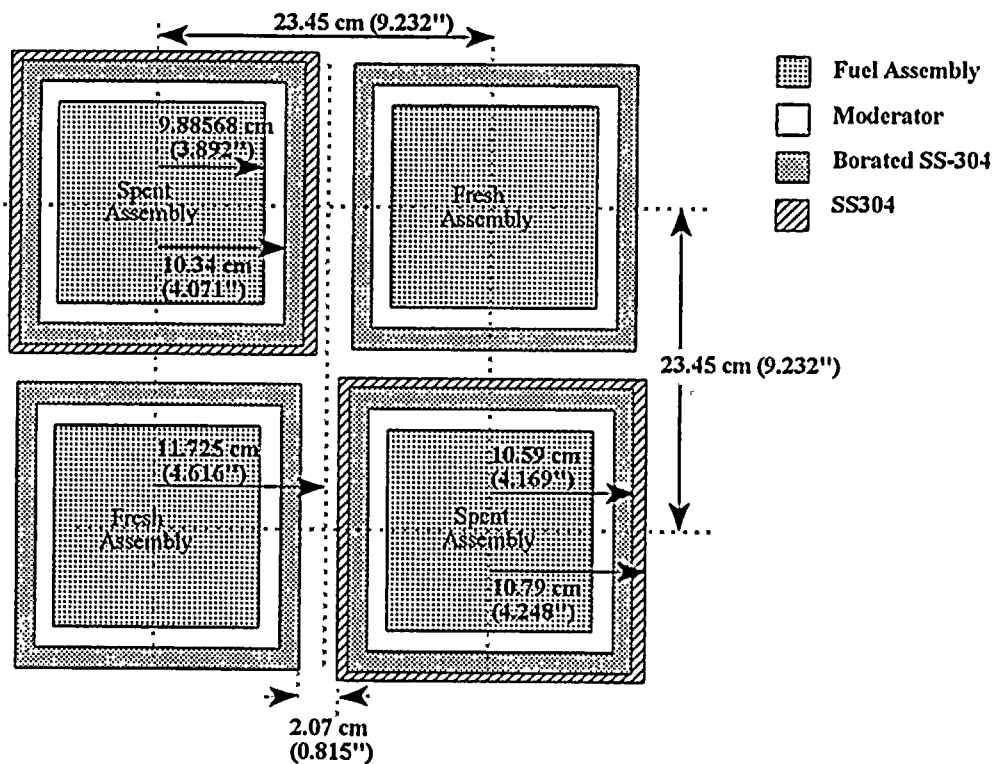


Figure 4.3-2 Region 1 Type 3 Base Cell Structure for Infinite Model





THE UNIVERSITY OF CHICAGO PRESS

Figure 4.3-3 Axial Profile of Finite And Infinite Base Models

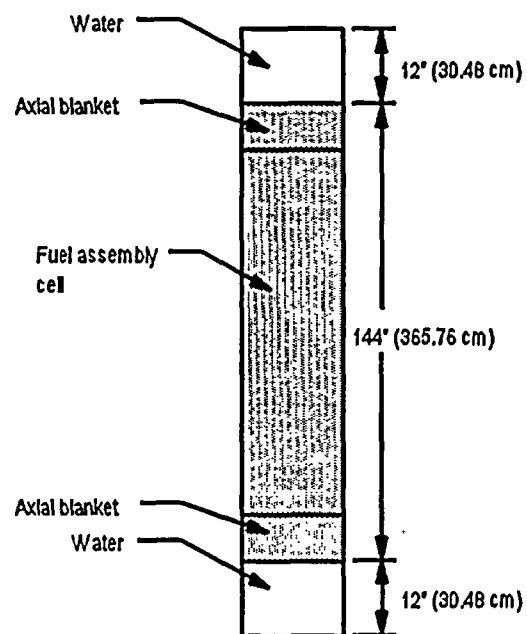
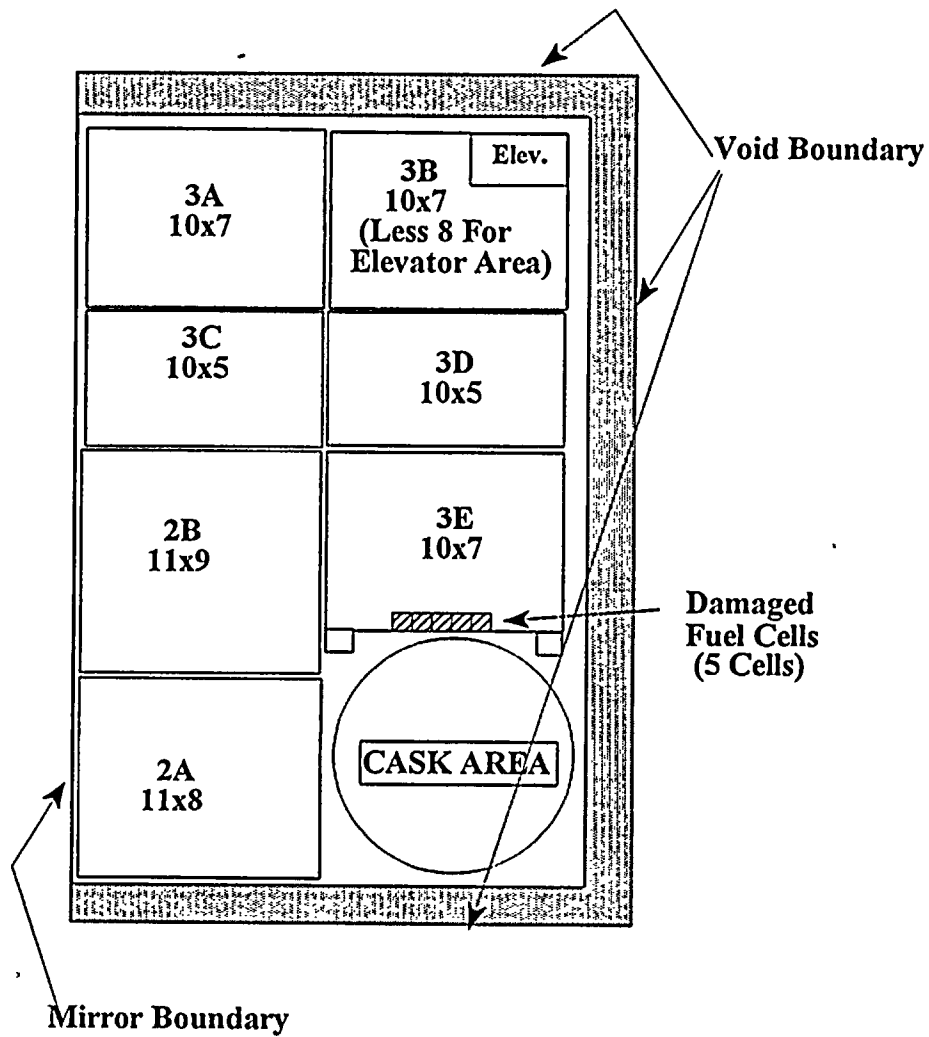


Figure 4.3-4 Region 1 - Rack Type 3 Finite Model





1. The first part of the document is a list of names and addresses of the members of the committee.

2. The second part of the document is a list of names and addresses of the members of the committee.

Figure 4.3-5 Region 2 Boraflex Rack (Type 1) - KENO V.a Model

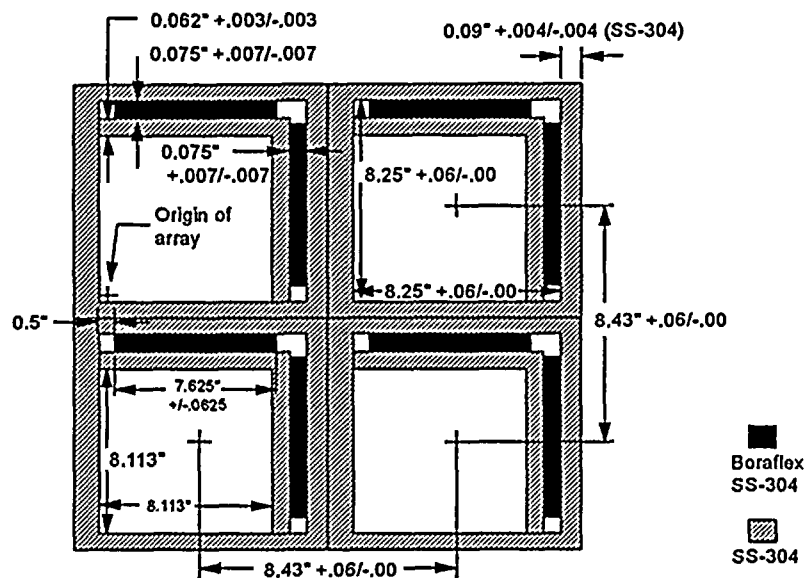
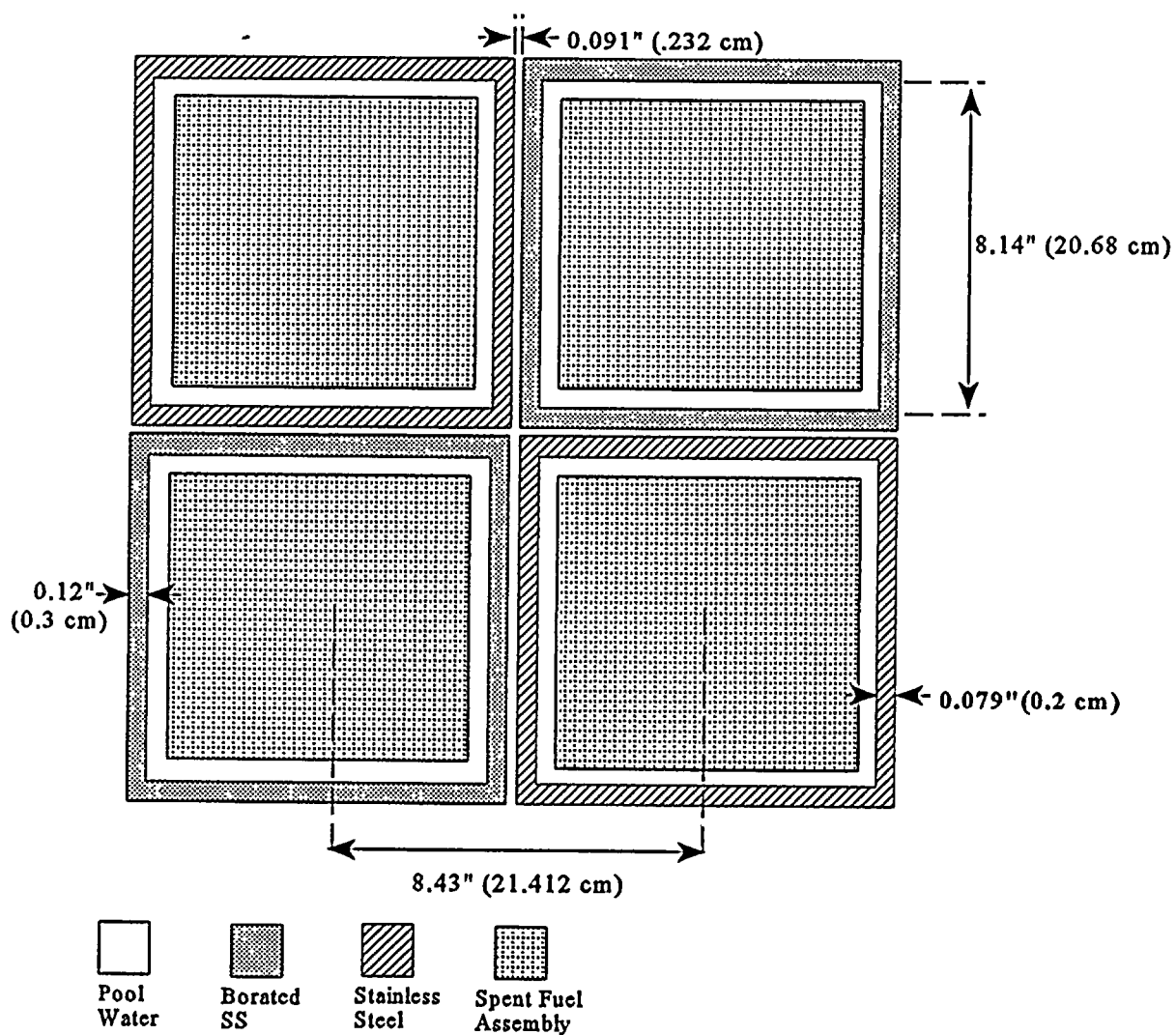


Figure 4.3-6 Region 2 Borated Stainless Steel (Type 2) Racks - KENO V.a Model





1. The first part of the document is a list of names and addresses of the members of the committee.

2. The second part of the document is a list of names and addresses of the members of the committee.

3. The third part of the document is a list of names and addresses of the members of the committee.

Figure 4.3-7 Areas Modeled to Examine Interface Effects between Rack Types and Regions

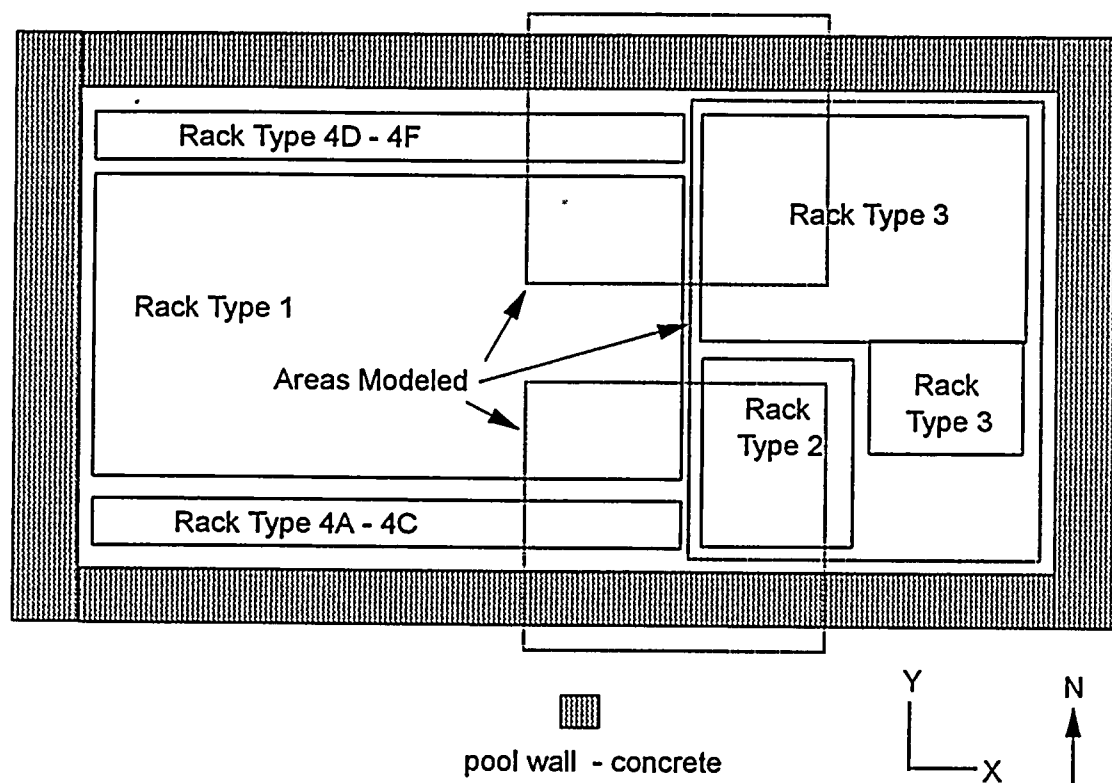


Figure 4.3-8 KENO V.a Model Used to Examine Interface Effects between (1) Rack Types 3C & 2B, and (2) Rack Types 2B & 3E

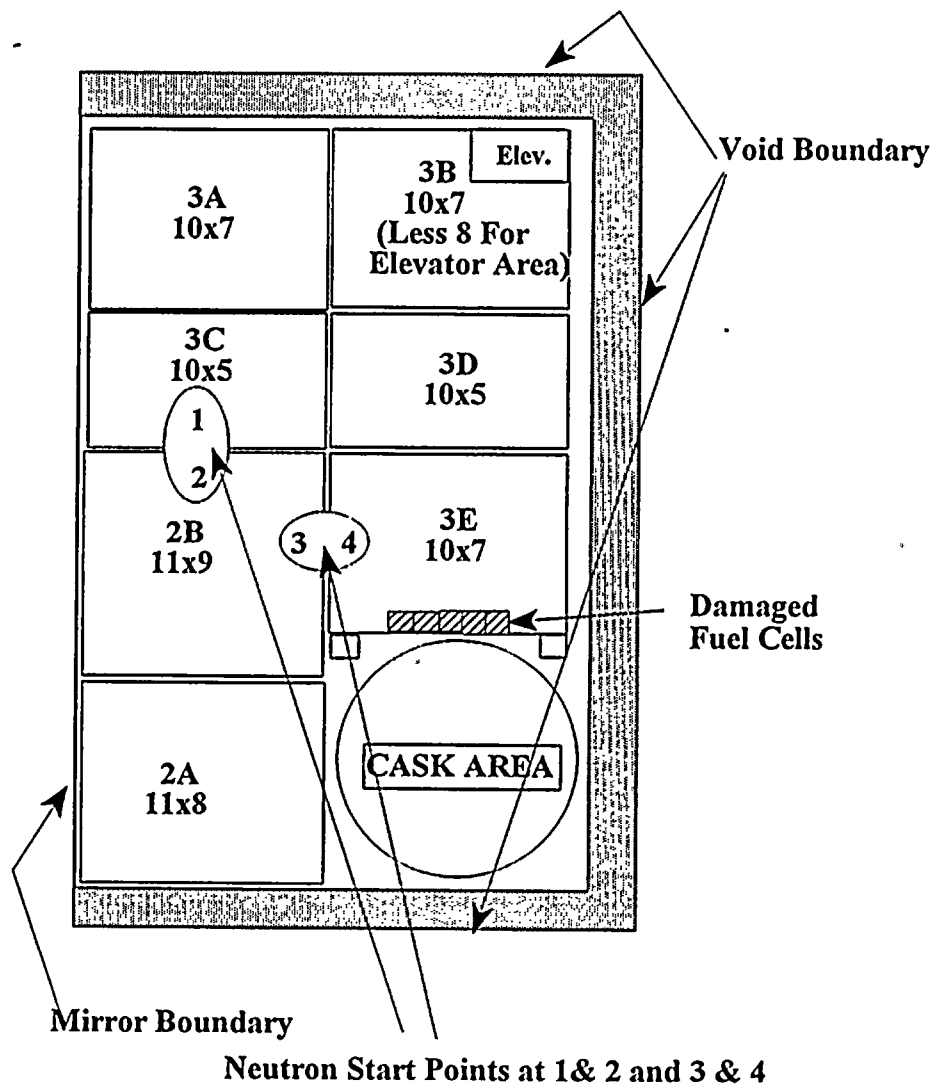




Figure 4.3-9 KENO V.a Model Used to Examine Interface Effects between Rack Types 1, 4F, and 3A

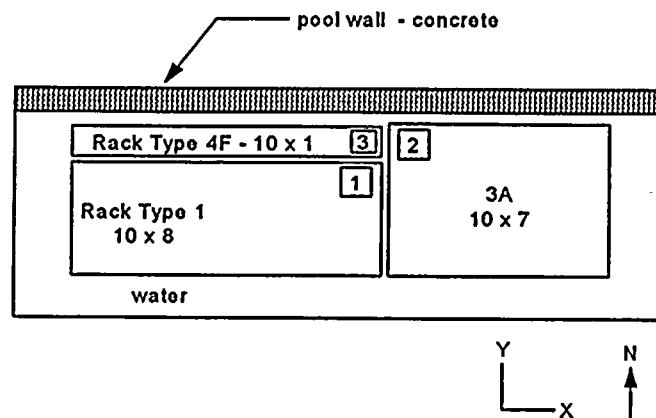
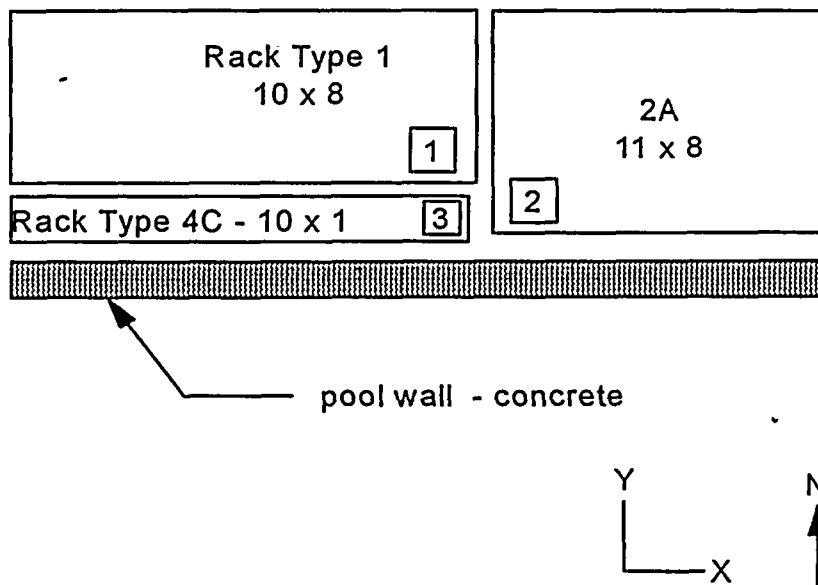


Figure 4.3-10 KENO V.a Model Used to Examine Interface Effects between Rack Types 1, 4C, and 2A





THE UNIVERSITY OF CHICAGO PRESS

Figure 4.3-11 KENO V.a Shallow Drop Accident Models

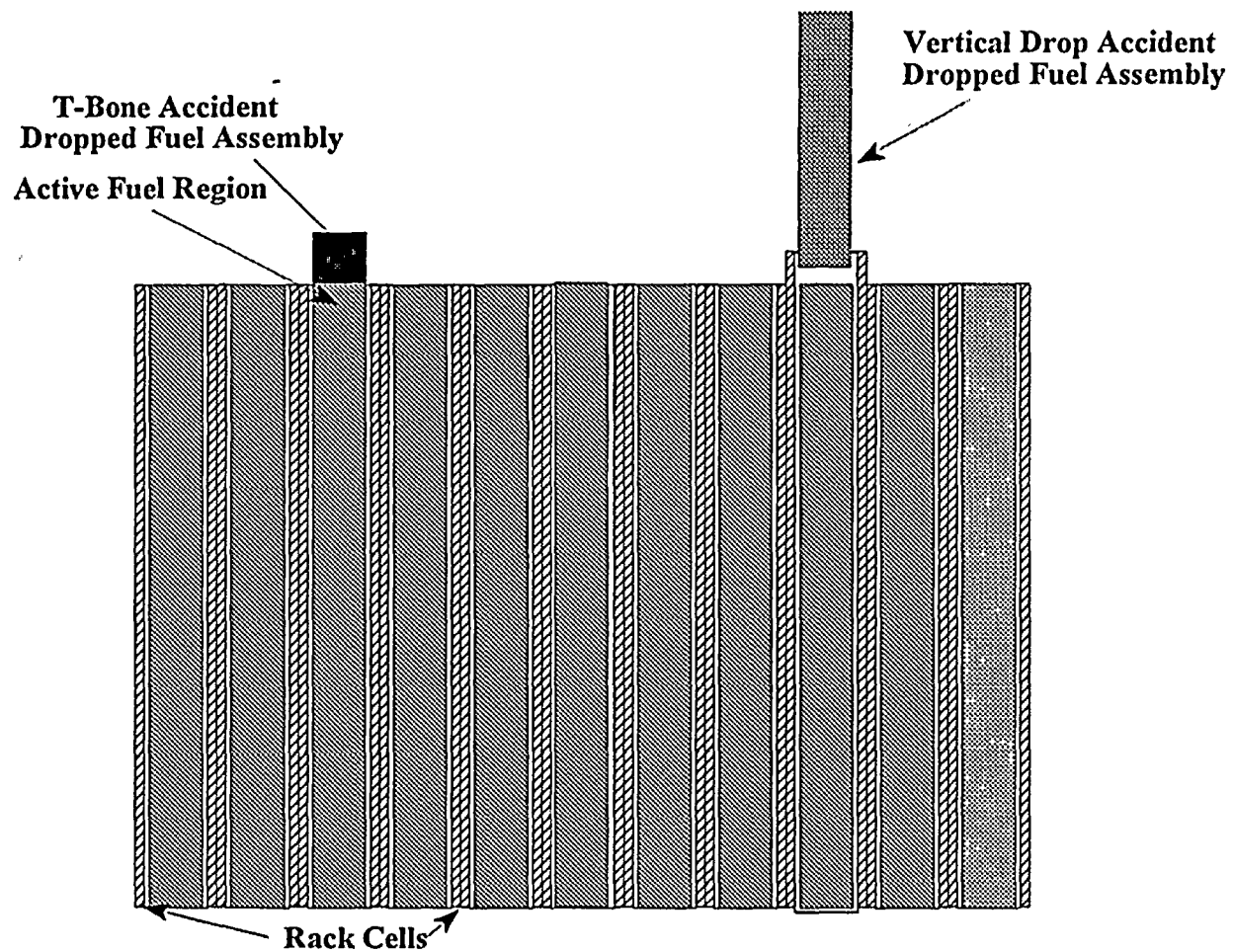
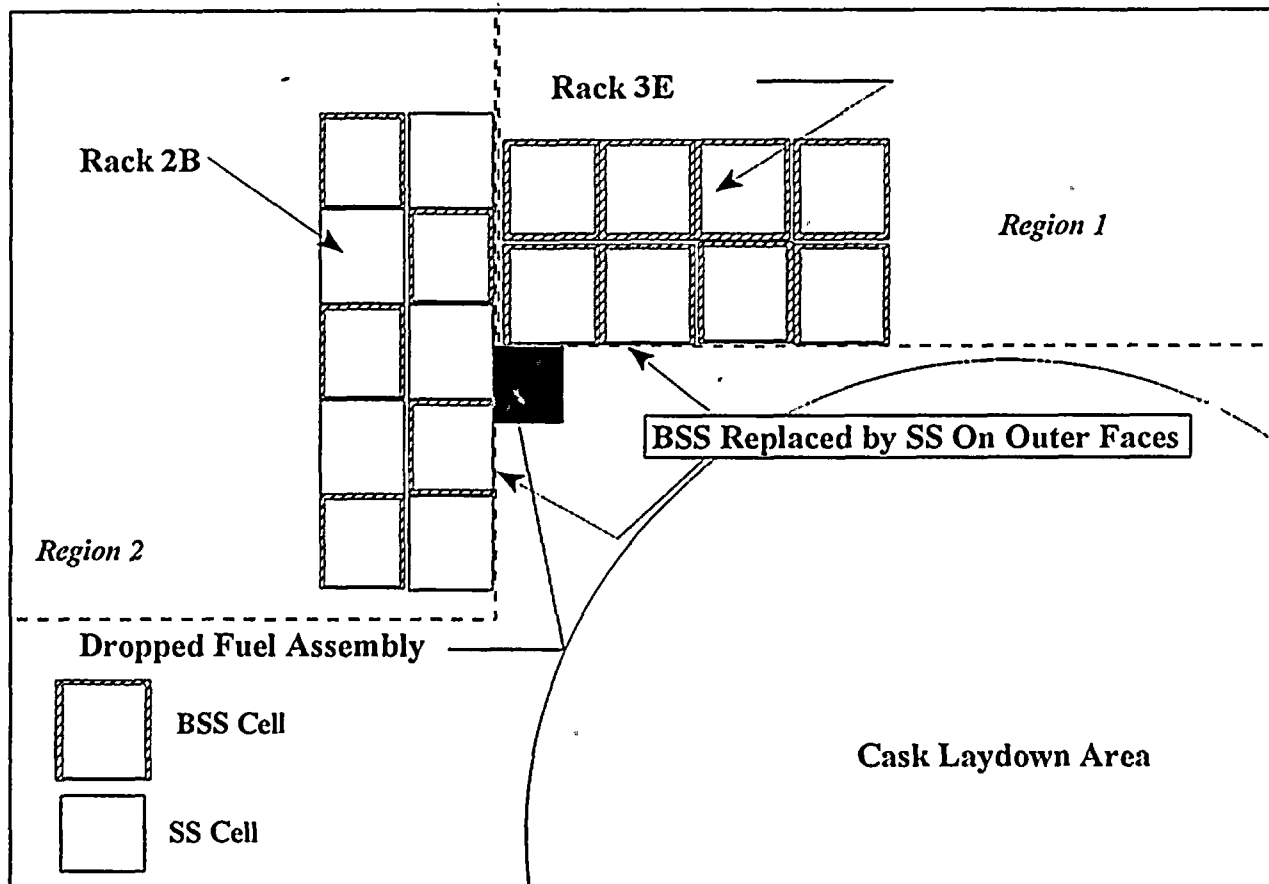


Figure 4.3-12 KENO V.a Side Drop Accident Model

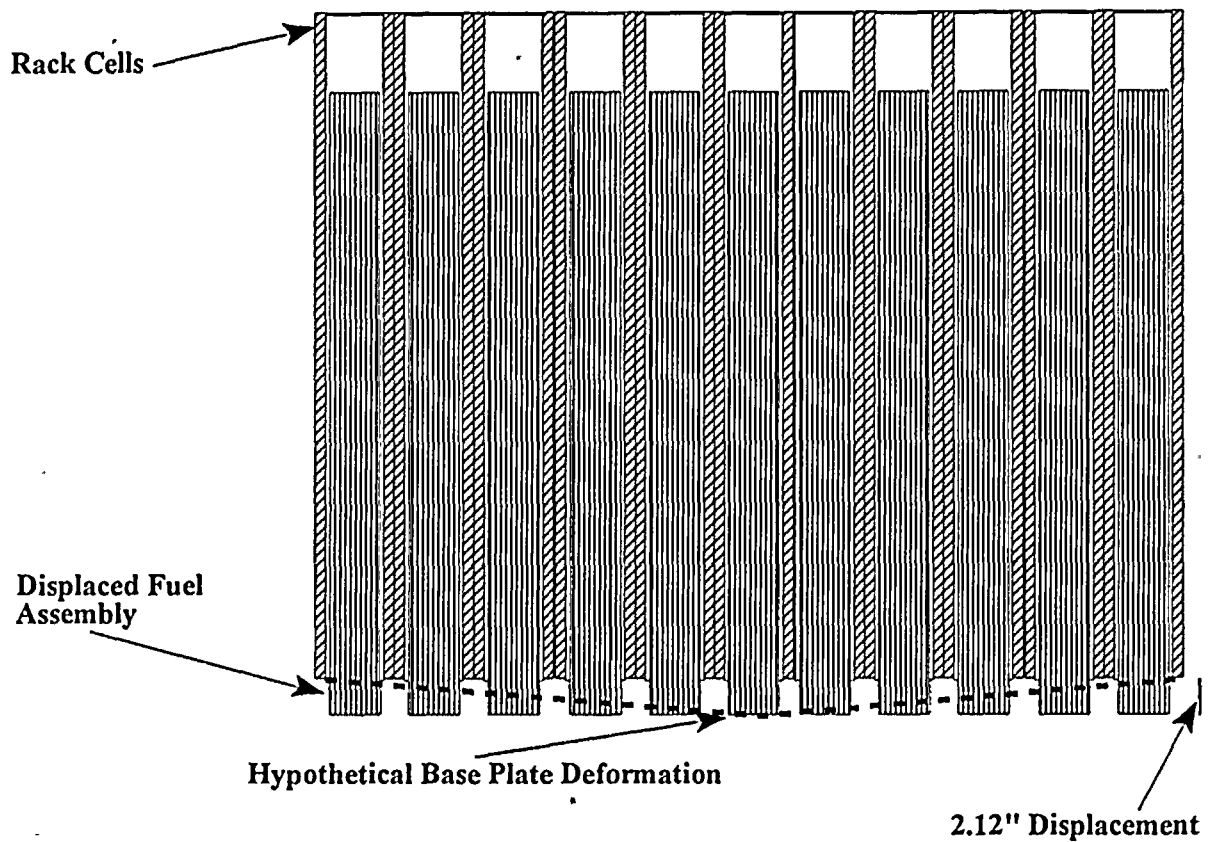




RECEIVED

1964

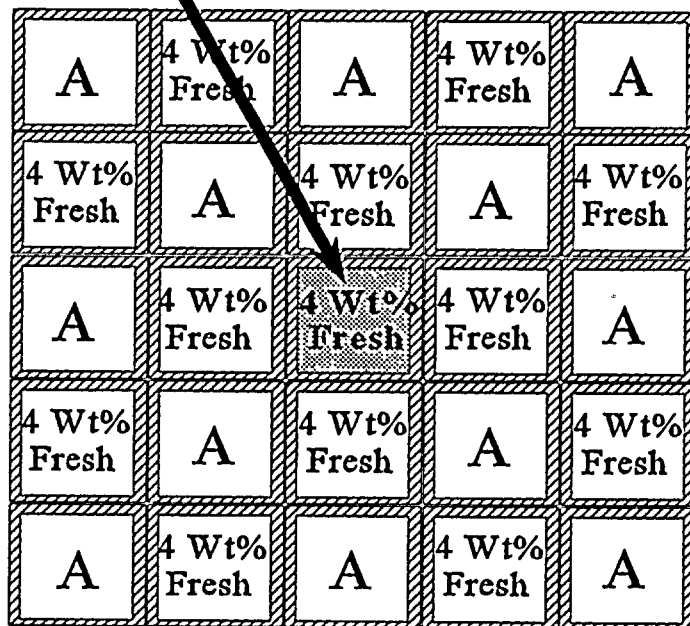
**Figure 4.3-13 KENO V.a Deep Drop Accident Model
for Rack Types 2, 3, and 4**



Rack Types 2, 3, & 4 Deep Drop Deformed Model

Figure 4.3-14 KENO V.a Region 1 Misplaced Assembly Model

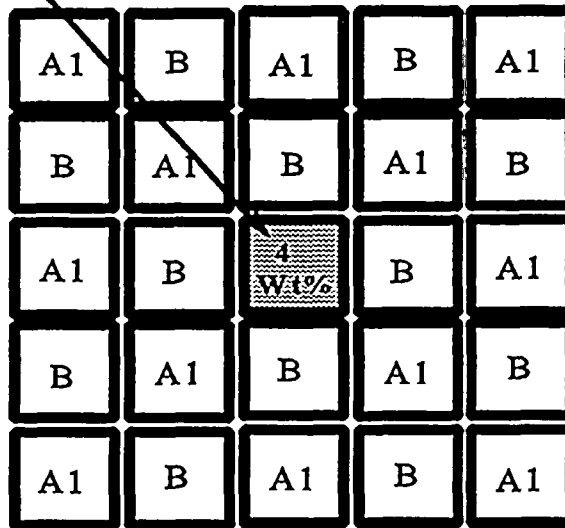
Misplaced Assembly



Region 1
Rack Type 3

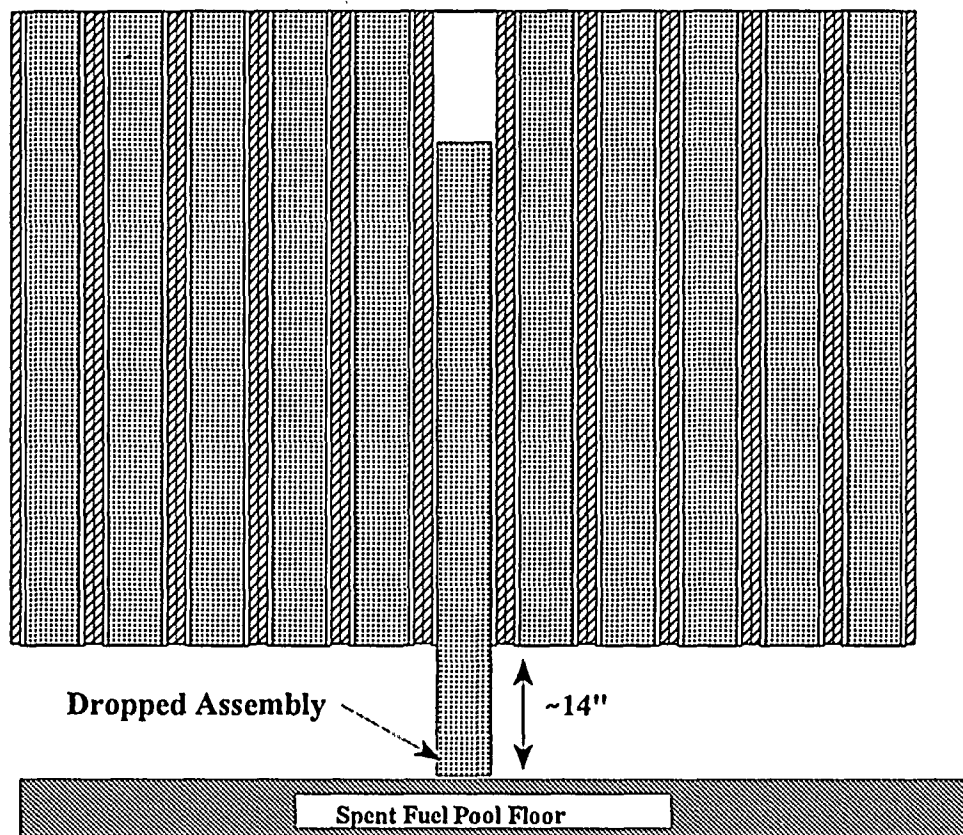
Figure 4.3-15 KENO V.a Region 2 Misplaced Assembly Model

Misplaced Assembly



**Region 2
Rack Type 1**

Figure 4.3-16 KENO V.a Rack Type 1 Deep Drop Accident Model



Deep Drop Deformation For Rack Type 1

Figure 4.3-17 Sketch of Consolidation Canister

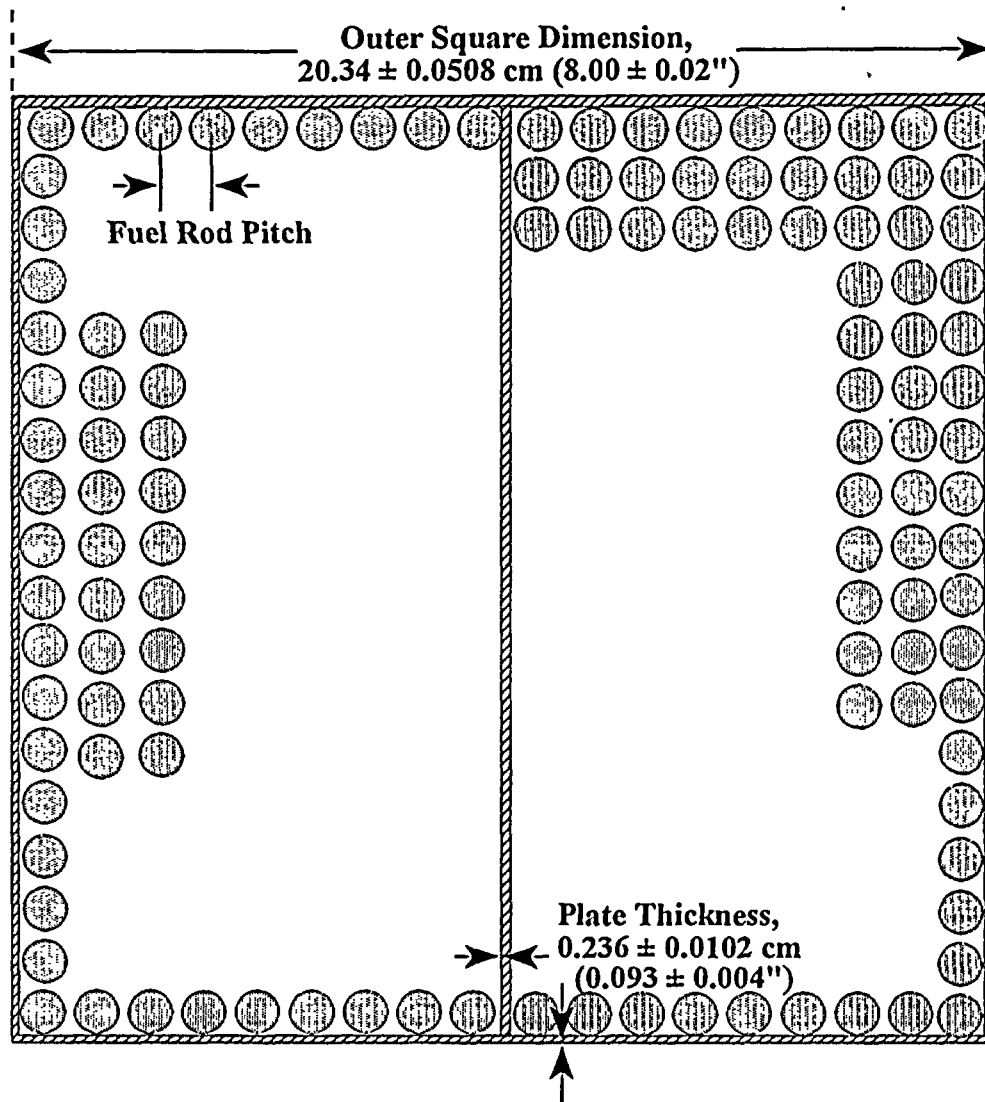




Figure 4.4-1 KENO V.a Results for B&W Criticals for Spacing Variations

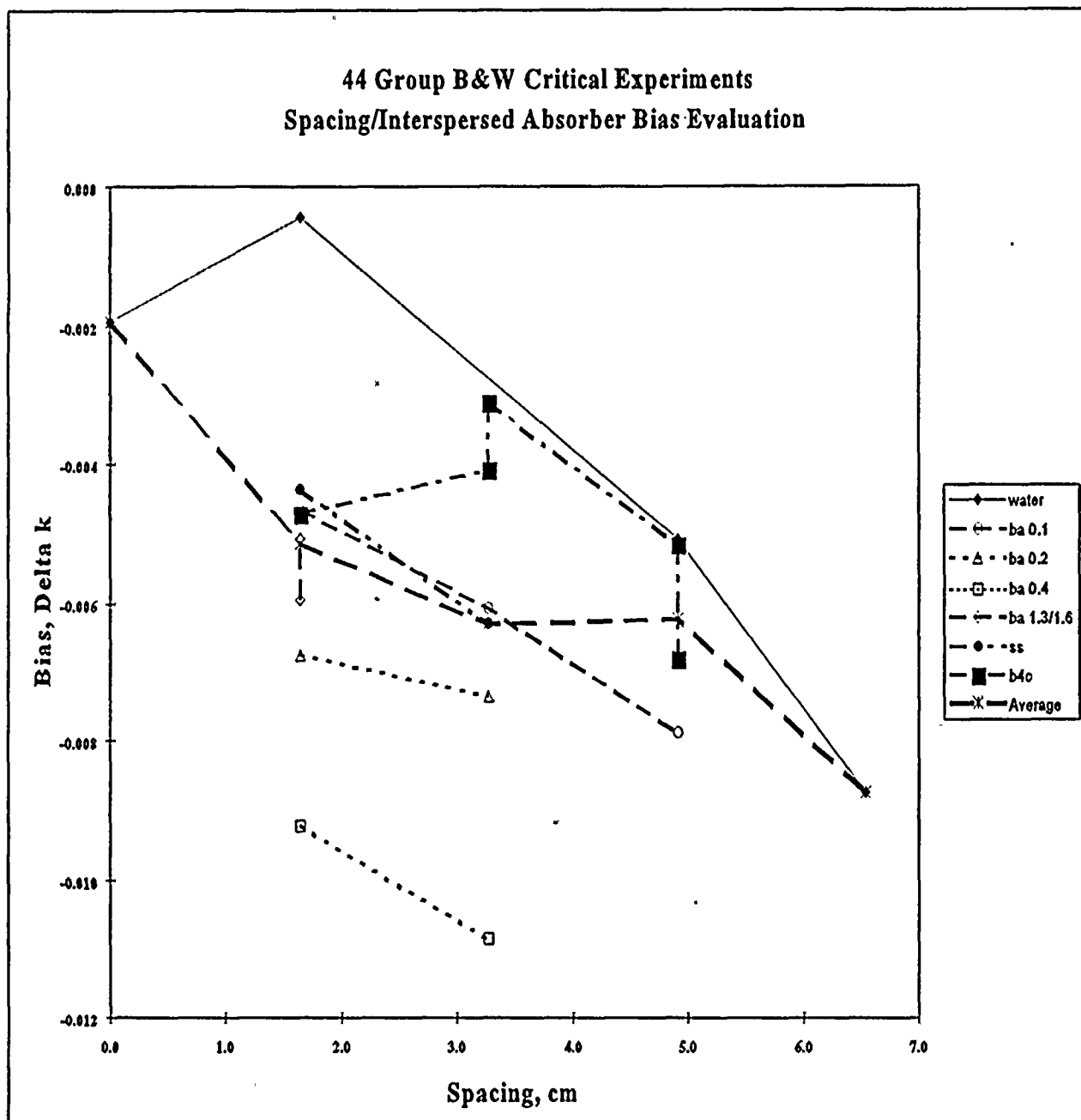


Figure 4.4-2 Results for Water Spacing Experiments from KENO V.a 27 and 44 Group and MCNP Continuous Group Cross Sections

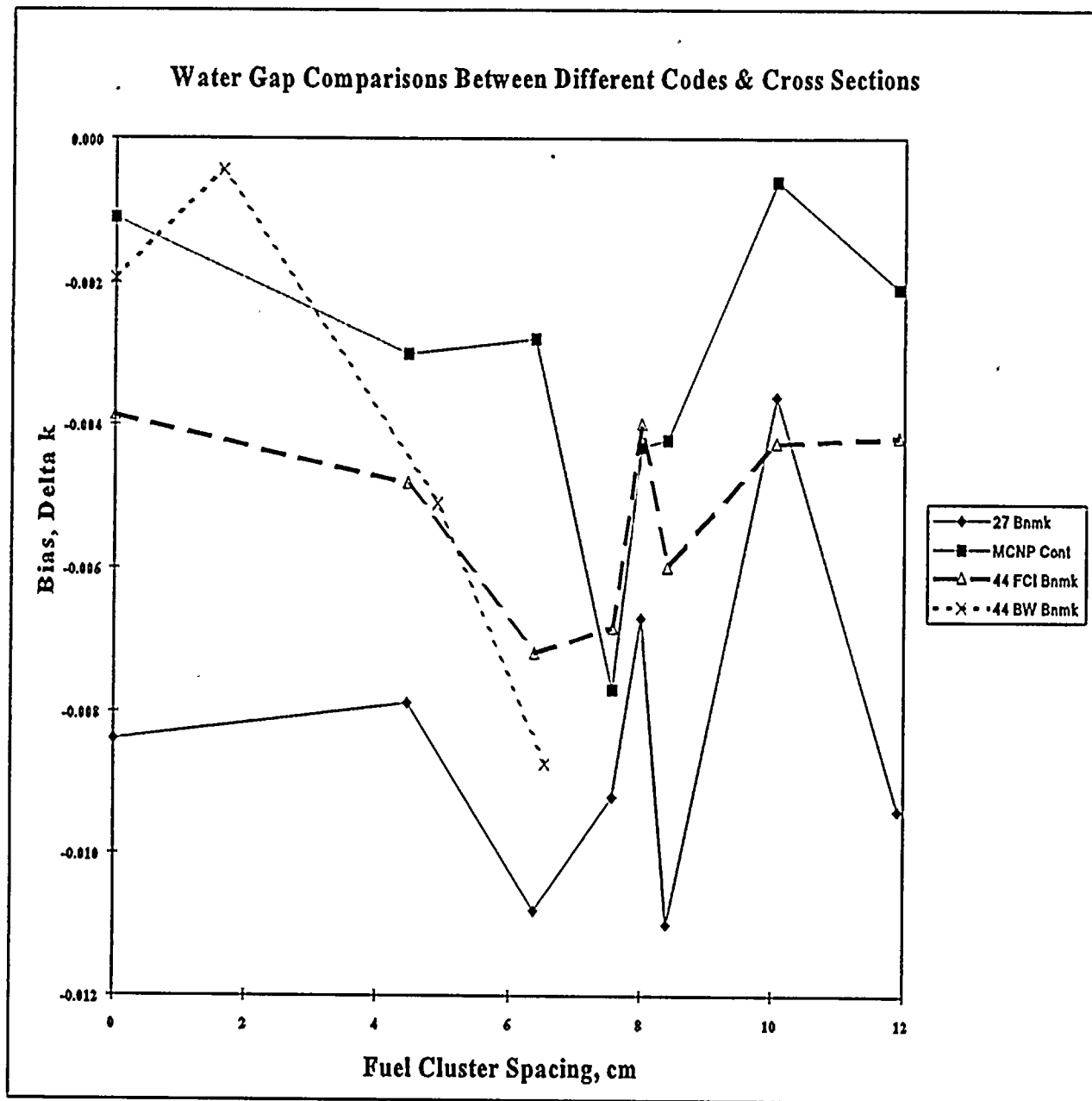




Figure 4.4-3 Least Squares Fit Through Results B&W Interspersed Absorber Experiments

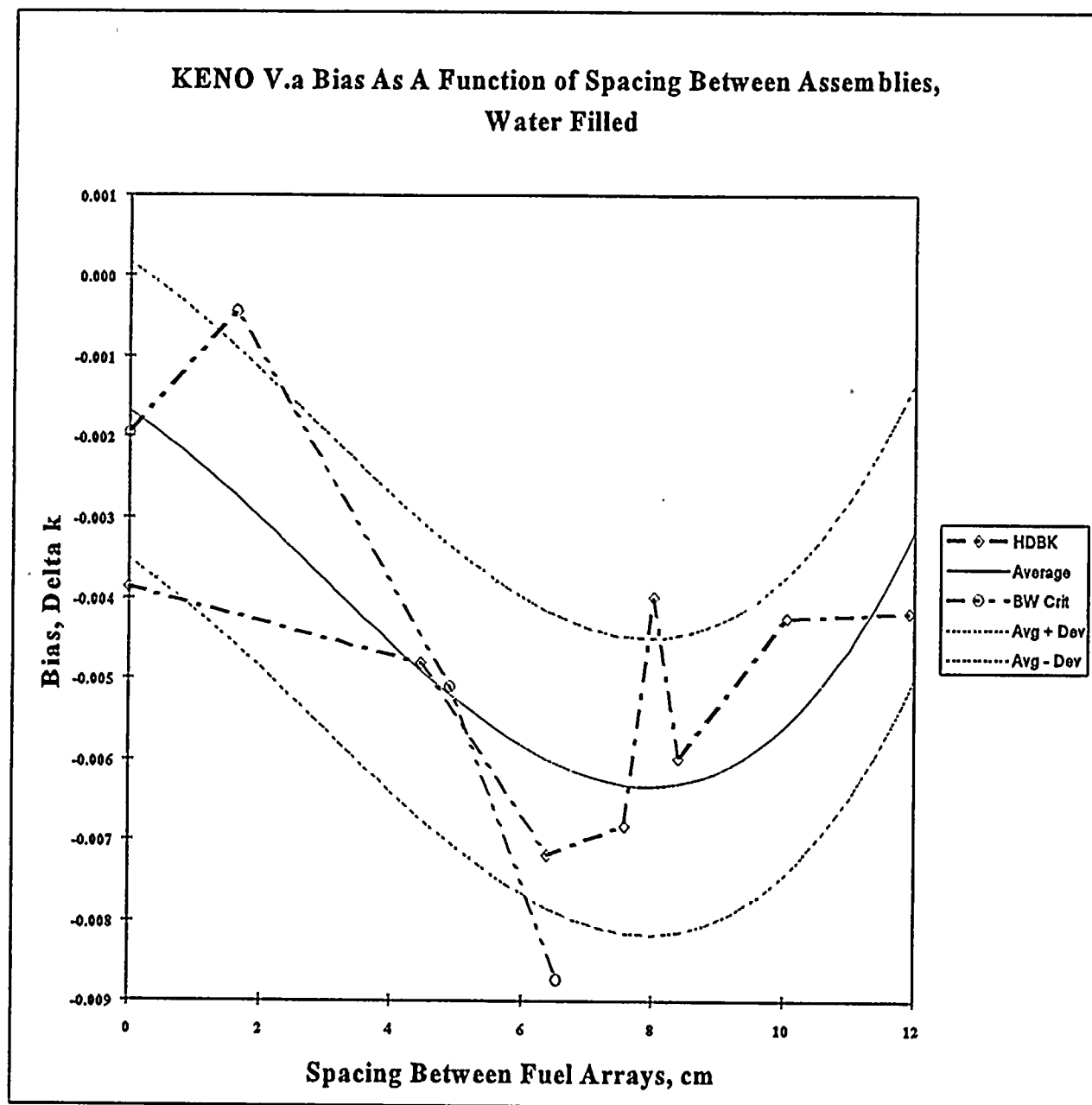


Figure 4.4-4 Typical Ginna Axial Burnup Shapes for Burnups between 10 and 20 GWd/mtU

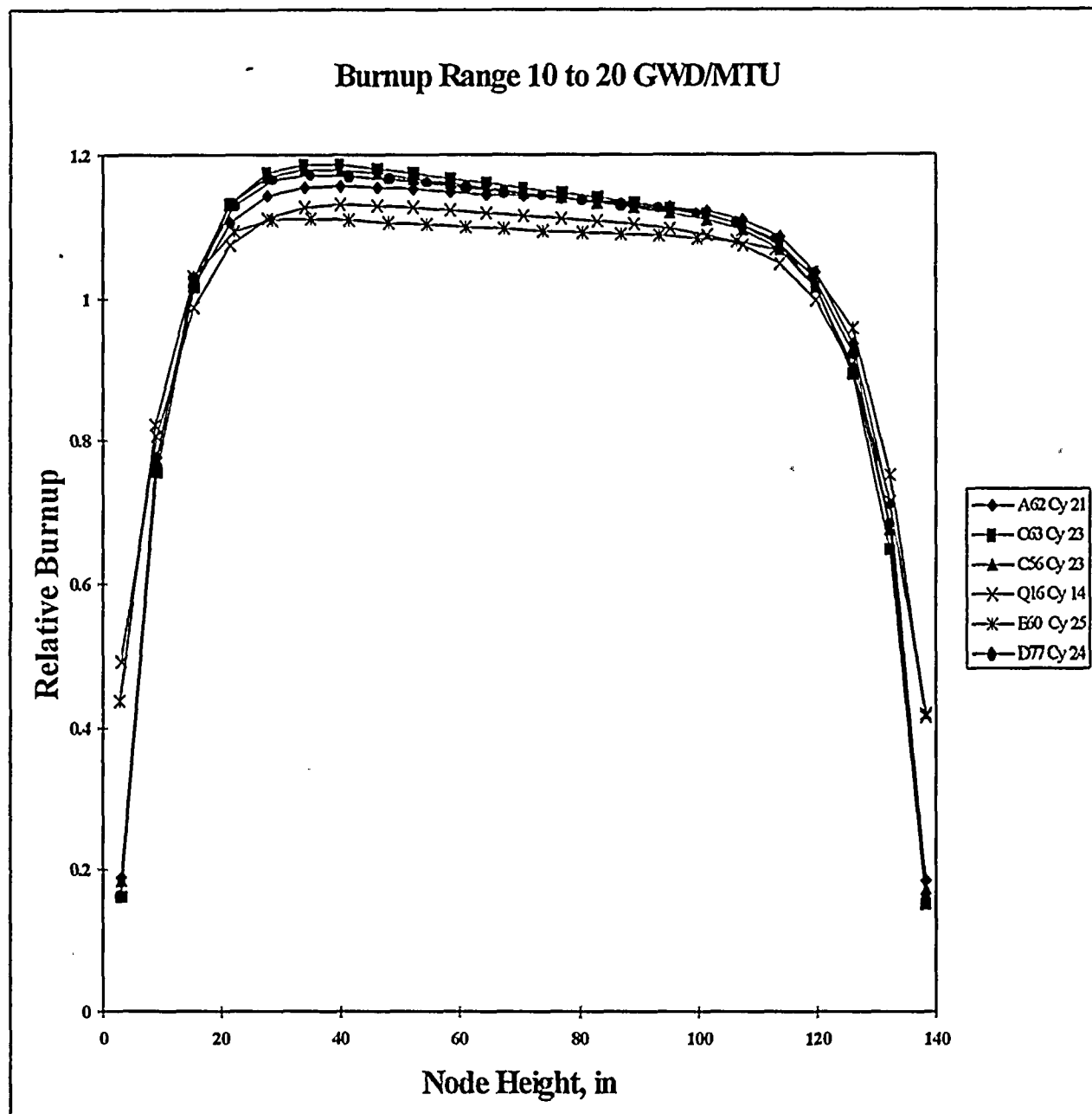




Figure 4.4-5 Typical Ginna Axial Burnup Shapes for Burnups between 20 and 30 GWd/mtU

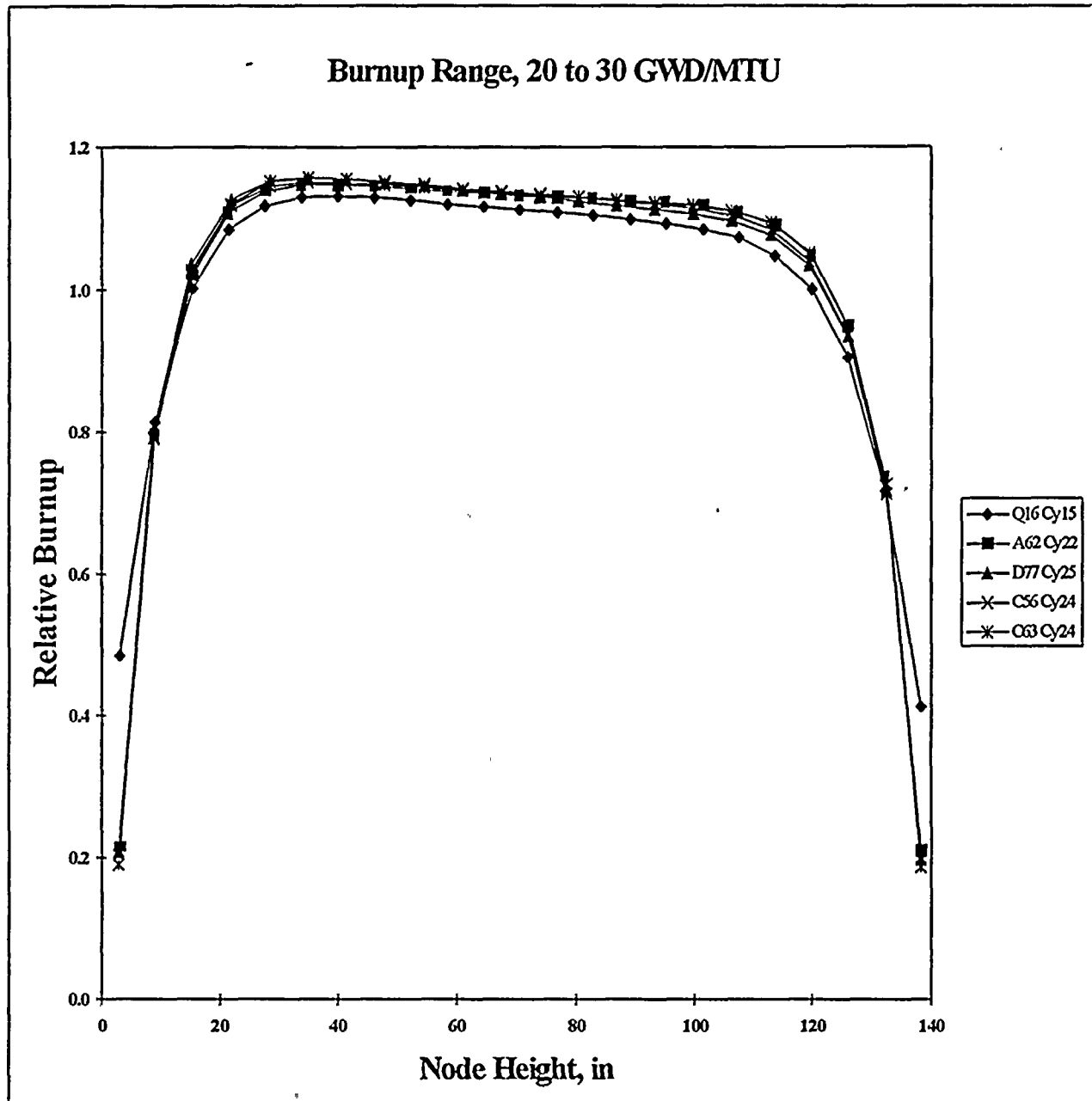


Figure 4.4-6 Typical Ginna Axial Burnup Shapes for Burnups between 30 and 40 GWd/mtU

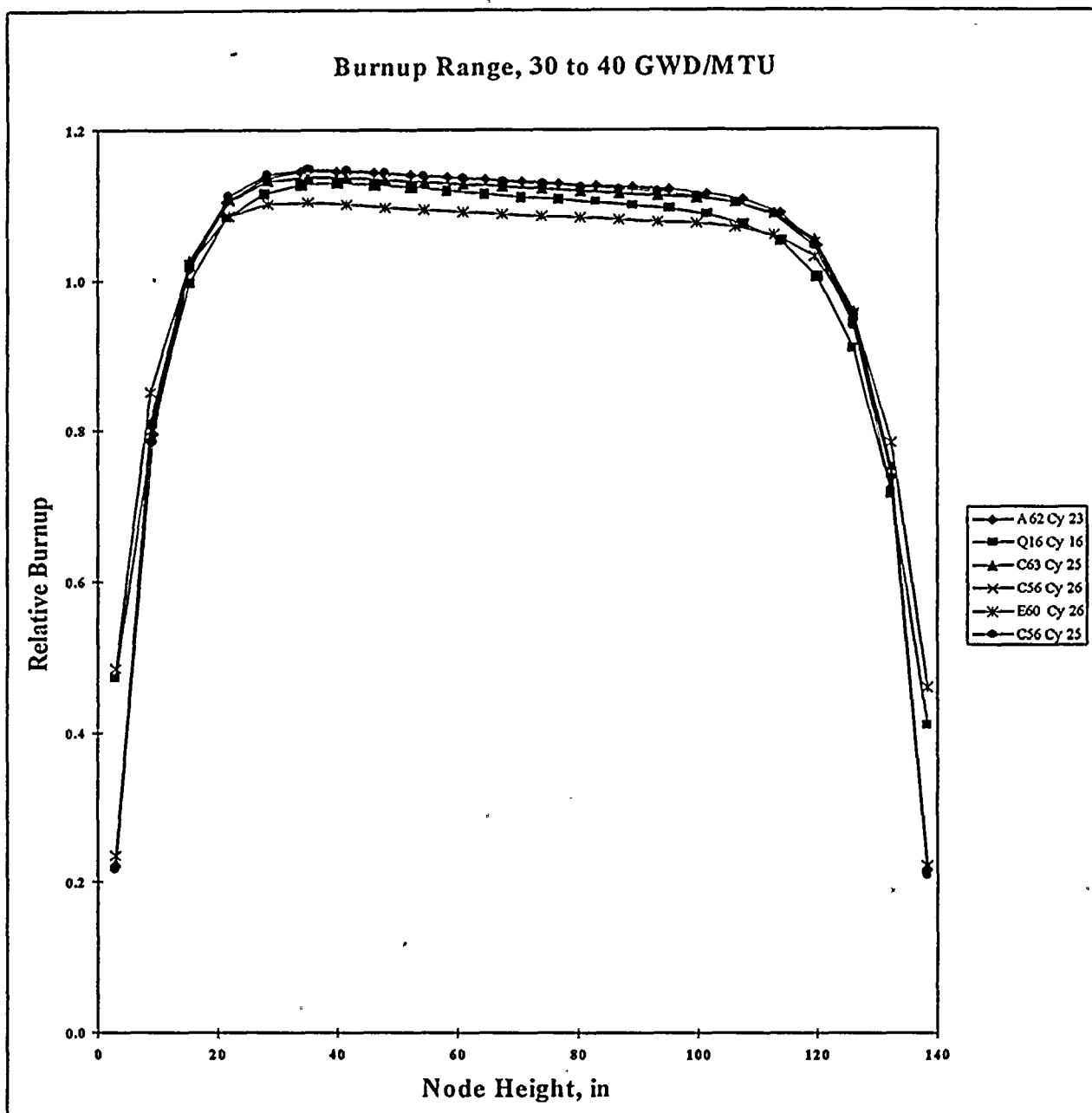




Figure 4.4-7 Typical Ginna Axial Burnup Shapes for Burnups between 40 and 50 GWd/mtU

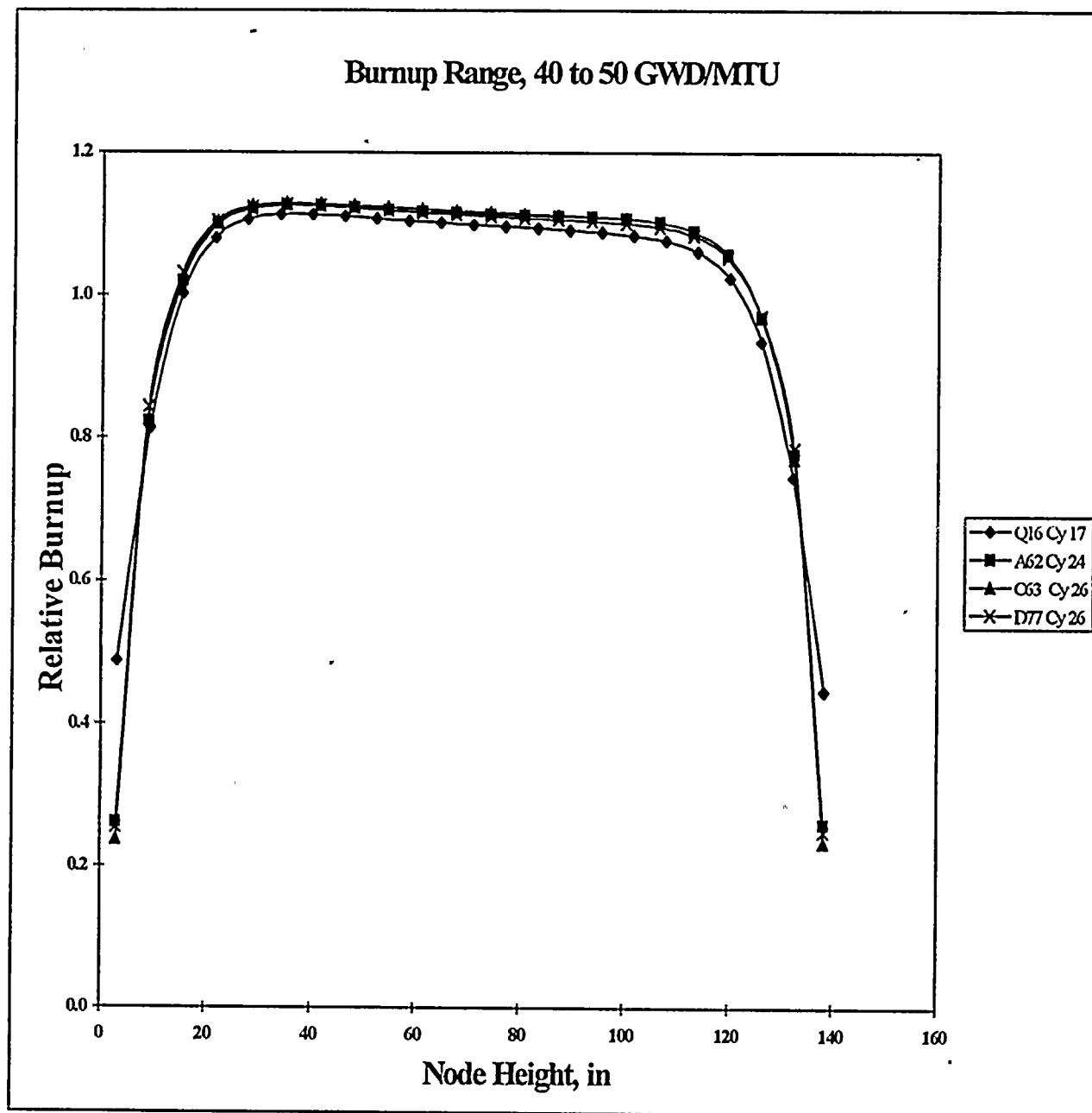


Figure 4.4-8 Non-Axial Blanket Shapes Used for Analysis

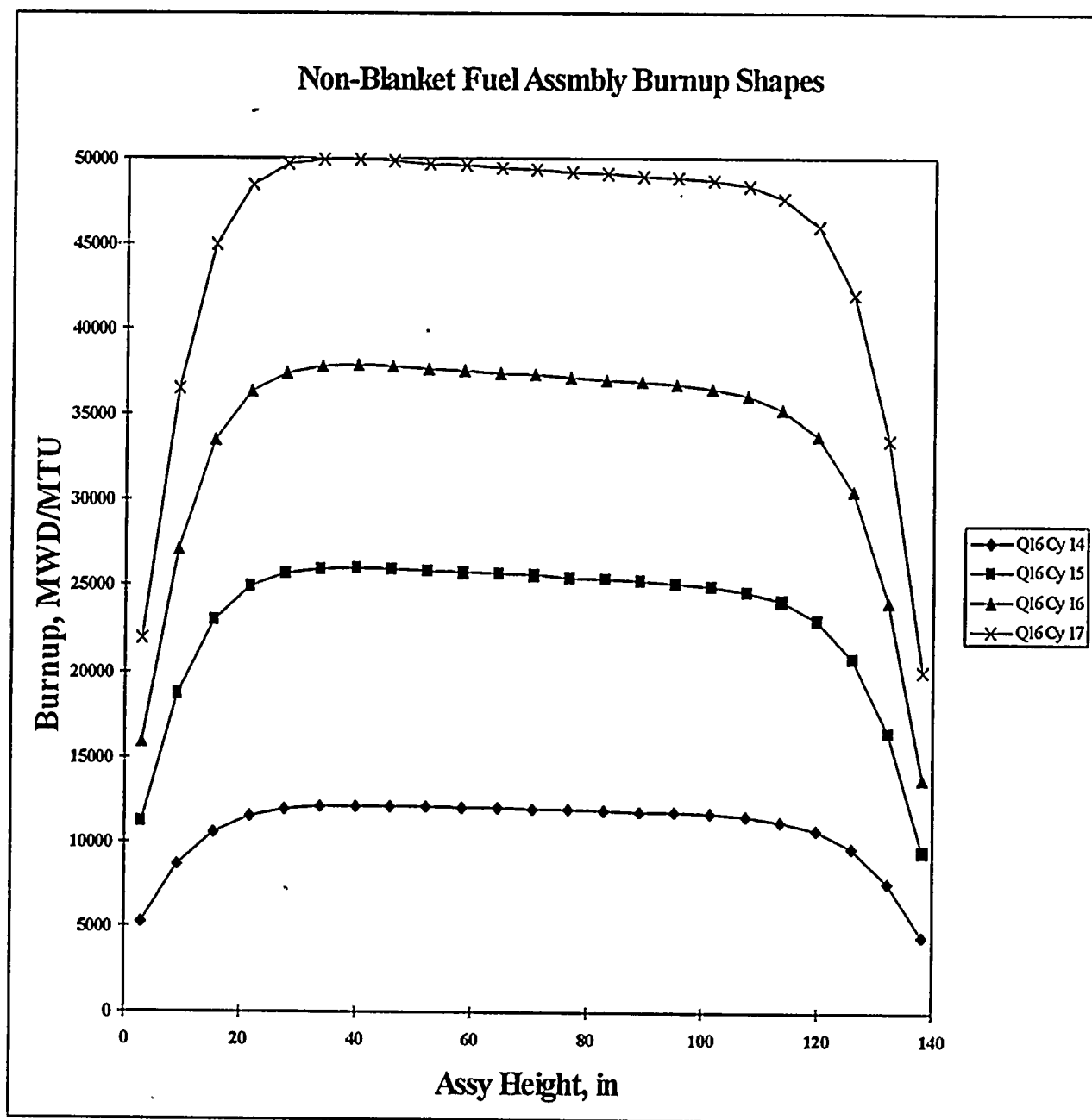


Figure 4.4-9 Relative Non-Blanket Axial Shapes Used in Analysis

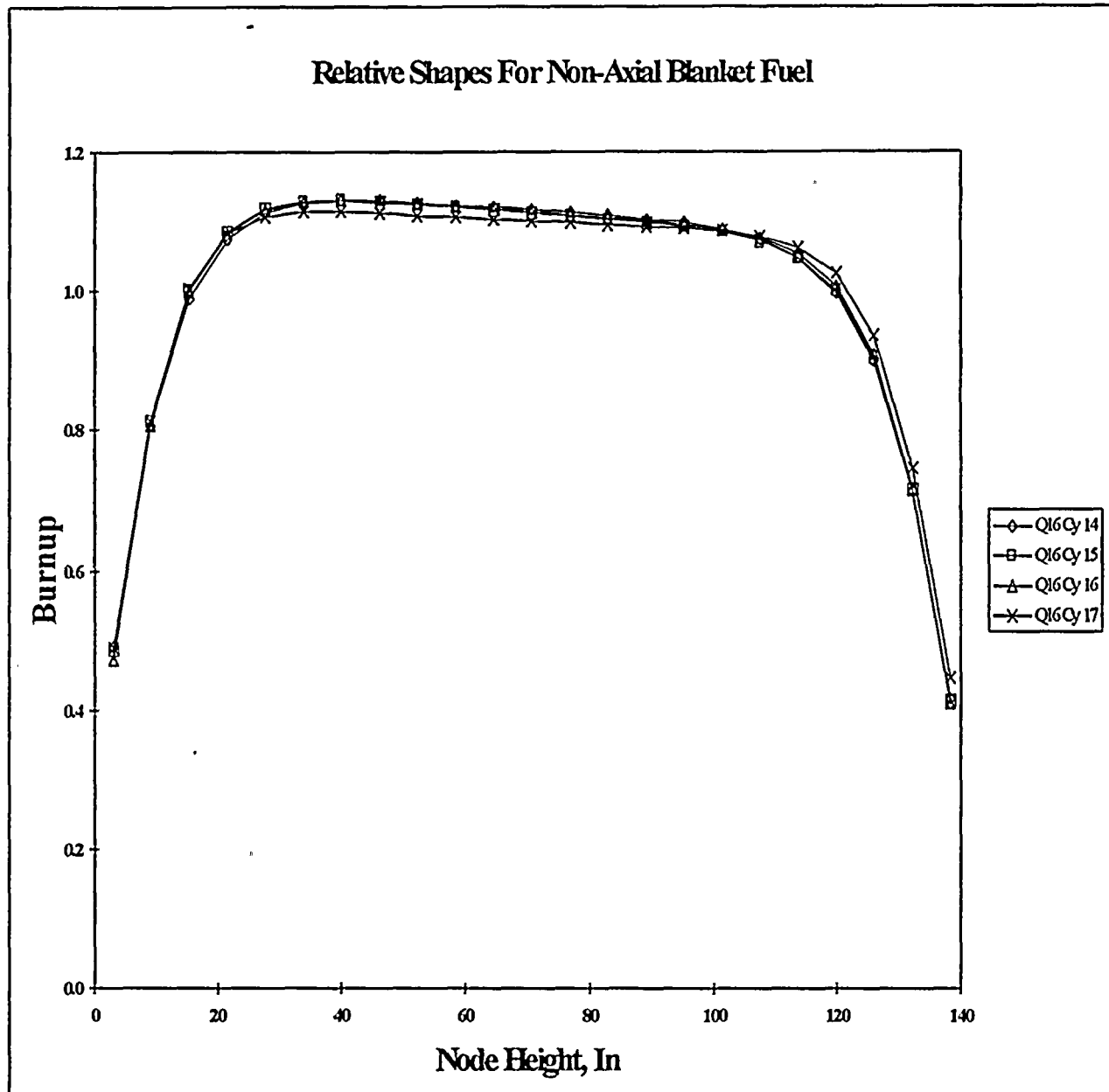
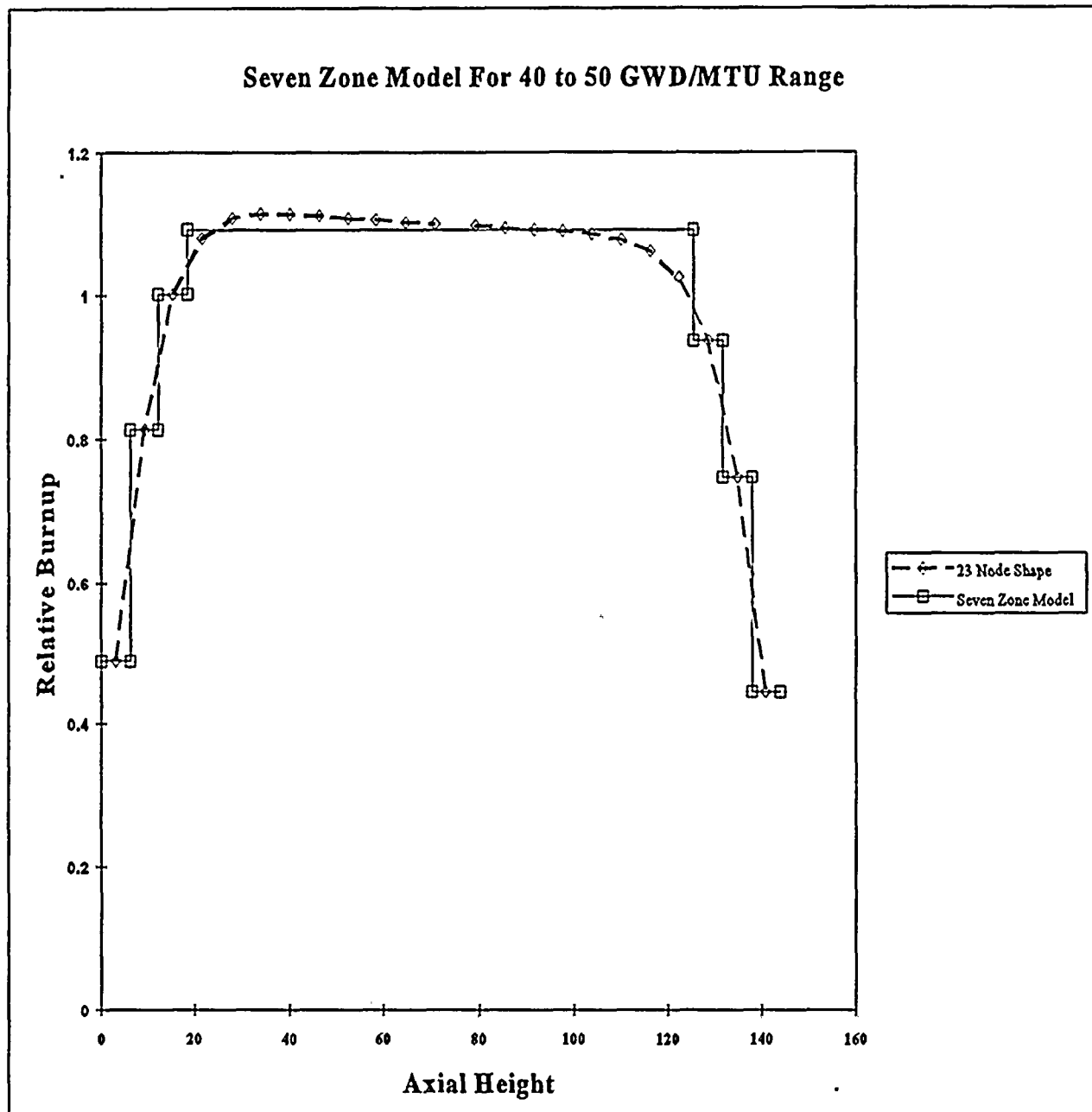


Figure 4.4-10 Illustration of Seven Zone Representation



5.0 THERMAL-HYDRAULIC EVALUATION

5.1 INTRODUCTION

Rochester Gas & Electric Co. is expanding the spent fuel storage capacity at its Ginna plant through installation of high density storage racks in the spent fuel storage pool. The pool capacity will be increased in two phases. The initial phase will increase the pool storage capacity by 305 locations with the installation of ATEA Type 2 and 3 racks. The second phase, if implemented by RG&E, will increase the capacity by an additional 48 storage locations with the installation of ATEA Type 4 racks. As discussed in Section 1.1, the pool total storage capacity of the spent fuel pool will be increased from its present capacity of 1016 to a total of 1369 locations with the implementation of both phases 1 and 2.

The increased storage capacity of the spent fuel pool will result in increased decay heat loads. The effect of the increased decay heat on the thermal performance of the spent fuel pool was determined for the final spent fuel pool configuration (both phase 1 and 2) at the maximum capacity. The required reactor hold-time based on conservative assumptions for the full core discharge schedule was determined using the existing heat removal capability of the spent fuel heat exchangers. Pool heatup rates at the maximum pool capacity were calculated accounting for the displaced water volume. Local fluid conditions and maximum clad temperature at the most limiting location in the pool were verified as acceptable.

RG&E may elect to utilize fuel consolidation as a future means of increasing the spent fuel pool storage capacity over the present design. Local fluid conditions for the limiting location in the spent fuel storage pool, conservatively determined for normal storage, were demonstrated as bounding compared to those for consolidated fuel canisters positioned throughout the spent fuel pool.

The following analyses for the thermal-hydraulic qualification of the spent fuel storage pool were performed for the ATEA Type 2, 3 and 4 racks:

- Calculation of Spent Fuel Decay Heat Loads
- Bulk Pool Heat Up Rate (upon loss of pool cooling)
- Local Pool Thermal Evaluations
 - Calculation of local fluid and fuel clad temperatures
 - Assessment of flow blockage on local fluid conditions
 - Assessment of gamma heating on the fluid conditions in the inter-canister gaps
- Impact of Pool Re-racking on Fuel Consolidation Limits

The results of these evaluations demonstrating the acceptable thermal-hydraulic performance of the Ginna spent fuel pool with increased storage capacity follow.

5.2 CRITERIA

The thermal-hydraulic analyses were performed in accordance with the requirements and guidelines set forth in the following:

- OT Position for Review and Acceptance of Spent Fuel Storage and Handling Applications, Dated April 14, 1978 and revised January 18, 1979, (Ref. 5.2.1),
- NUREG-0800 Standard Review Plan 9.1.3, Revision 1 (July 1981) and Standard Review Plan 9.2.5, Revision 2 (July 1981), (Ref. 5.2.2),
- A.G. Croff, ORIGEN2-A Revised and Updated Version of the Oak Ridge Isotope Generation and Depletion Code, ORNL-5621, (Ref. 5.2.3).

The thermal-hydraulic criteria include the following:

- Bulk pool does not exceed 150 °F under any SFP loading criteria
- Local boiling does not occur in the hot assembly except for the condition of a complete inlet flow blockage
- Maximum clad temperature remains below saturation for all non-flow blockage cases
- Adequate cooling for consolidated fuel canisters is provided with the increased pool storage capacity

5.3 ASSUMPTIONS

The maximum bulk fluid and clad temperatures for the Ginna spent fuel storage pool were calculated with the following conservative assumptions:

- Maximized decay heat load as a result of bounding fuel enrichment, bounding burn-up and bounding number of assemblies discharged to the SFP,
- Instantaneous discharge of the fuel to the spent fuel pool after a minimum reactor shutdown time of 100 hours
- Local hot channel peaking factor, $F_{\Delta H}^N = 1.75$, used for peaking for the hot fuel assembly
- Minimum water volume accounting for full pool storage capacity used for the calculation of the bulk pool heat-up rate

5.4 DISCUSSION OF SPENT FUEL COOLING

The existing spent fuel cooling system at the Ginna plant consists of three cooling loops. The primary loop (loop 2) is made up of spent fuel pump B, spent fuel pool heat exchanger B and piping. The backup loops include installed loop 1 with spent fuel pool pump A, spent fuel pool heat exchanger A and piping, and skid-mounted loop 3 with skid-mounted spent fuel pool pump, spent fuel pool standby heat exchanger, piping and hoses.

Loop 2 is designed to maintain the spent fuel pool water below 150 °F with a design basis heat load of 16×10^6 Btu/hr associated with a service water temperature of 80 °F. Loop 1 and loop 3 are each designed to remove 7.93×10^6 Btu/hr with a pool temperature of 150 °F and service water at 80 °F. Operated in parallel, they are capable of removing the design basis heat load. The source of service water for the SFP heat exchangers is Lake Ontario. No modifications to the existing SFP cooling system are planned as a result of the installation of the ATEA racks.

The availability of three pumps, three heat exchangers and associated parallel flow paths in the Ginna SFP System provides adequate protection against any postulated single failures. Therefore, redundancy exists in the Ginna spent fuel pool cooling system to ensure that full heat removal capability is available for the design basis heat load.

Service water to the spent fuel pool cooling system is provided by lake water supplied by Lake Ontario. Since the lake water temperature varies from winter to summer, the potential heat removal capability of the SFP cooling system also varies. With cooler lake water temperature, the heat removal capability of the SFP cooling system increases. Therefore, the necessary core shutdown required to ensure that the SFP temperature does not exceed its 150 °F limit is a function of lake water temperature. The required core shutdown times to prevent the SFP from exceeding the 150 °F limit were analyzed for lake water temperatures of 40 °F and 60 °F as well as for the design lake water temperature of 80 °F.

5.5 SPENT FUEL POOL CAPACITY AND DISCHARGE SCENARIOS

The following sections summarize the spent fuel pool capacity used as a calculational base and the discharge scenarios for the normal and full core offload.

5.5.1 Spent Fuel Pool Capacity

The discharge schedule is shown in Table 5.5-1. Beginning in 1997, a bounding 44 assembly batch discharge schedule based on an 18 month fuel cycle was assumed through the end of plant life.

The discharge schedule listed in Table 5.5-1 results in a total spent pool inventory of 1879 in the year 2029. This postulated loading scheme is conservative for determining the maximum Ginna spent fuel pool heat load since the present Ginna operating license expires in the year 2009. Additionally, the 1879 fuel assemblies assumed to be loaded exceeds the 1369 fuel assembly storage locations available in the pool after installation of the ATEA Types 2, 3 and 4 racks. These extra fuel assemblies could be accommodated by performing fuel consolidation. Presently, the Ginna fuel pool includes 11 fuel assemblies that have been consolidated and are stored in 8 fuel assembly locations. Additionally, 2 fuel assembly locations are presently being used to store non-fuel related hardware.

5.5.2 Core Offload Scenarios

Two core offload scenarios based on the core discharge schedule in Table 5.5-1 were used in the evaluation of the spent fuel pool.

5.5.2.1 Normal Discharge Scenario

The normal fuel storage scenario assumes that one reload batch is sequentially discharged from the core until space remains for one core offload. The newly discharged batch is assumed to have a decay time of 100 hours and the previously discharged batch has a decay time of 18 months consistent with Table 5.5-1.

5.5.2.2 Full Core Discharge Scenario

For a full core offload, one reload batch at a time is discharged from the reactor until vacant locations remain in the spent fuel storage pool for one batch plus one full core of fuel.

Both beginning of cycle (BOC) and end of cycle (EOC) scenarios were investigated for the full core offload. For the BOC scenario, the plant is assumed to operate for 30 days prior to shutdown. The decay heat for the previously discharged batch is assumed to be the decay time for the 30 day operation plus the decay time for the full core prior to discharge to the SFP. No credit is taken for the decay time associated with the refueling outage duration for the previously discharged batch. For the EOC scenario, the decay heat for the previously discharged 44 fuel assembly batch is based on an 18 month irradiation time.

For the discharged fuel assemblies, shown in Table 5.5-1, no additional decay time due outage duration was conservatively assumed to maximize the decay heat.

Table 5.5-1 Ginna Spent Fuel Pool Inventory (Actual & Projected)

Discharge Date	Average Burnup (MWD/MTU)	Number of Assemblies	Days of Decay to 9/18/2029
10/1/72	19572	70	20806
1/1/74	25135	12	20349
3/11/75	24054	24	19915
1/29/76	25048	37	19591
4/15/77	28831	41	19149
3/25/78	28579	41	18805
2/9/79	29429	40	18484
3/29/80	30721	36	18070
4/18/81	31258	15	17685
1/26/82	32281	19	17402
3/27/83	35200	21	16977
3/3/84	36714	28	16635
3/2/85	37342	29	16271
2/7/86	39119	31	15929
2/6/87	39421	32	15565
2/10/88	40281	33	15196
3/17/89	38118	36	14795
3/23/90	36995	37	14424
3/22/91	39473	29	14060
3/27/92	40057	37	13689
3/12/93	44705	37	13339
3/4/94	42397	27	12982
3/26/95	41518	37	12595
4/1/96	40674	41	12223
10/20/97	Proj:55000	44	11656
3/7/99	Proj:55000	44	11153
9/15/00	Proj:55000	44	10595
3/17/02	Proj:55000	44	10047
9/16/03	Proj:55000	44	9499
3/15/05	Proj:55000	44	8953
9/21/06	Proj:55000	44	8398
3/19/08	Proj:55000	44	7853
9/18/09	Proj:55000	44	7305
3/15/11	Proj:55000	44	6762
9/15/12	Proj:55000	44	6212

Table 5.5-1 Ginna Spent Fuel Pool Inventory (Actual and Projected) Continued

Discharge Date	Average Burnup (MWD/MTU)	Number of Assemblies	Days of Decay to 9/18/2029
3/15/14	Proj:55000	44	5666
9/15/15	Proj:55000	44	5117
3/15/17	Proj:55000	44	4570
9/15/18	Proj:55000	44	4021
3/15/20	Proj:55000	44	3474
9/15/21	Proj:55000	44	2925
3/15/23	Proj:55000	44	2379
9/15/24	Proj:55000	44	1829
3/15/26	Proj:55000	44	1283
9/15/27	Proj:55000	44	734
3/15/29	Proj:55000	44	187
9/18/29	-----	-----	-----
TBD		121	
Total		1879	

Note: Number of assemblies discharged through April 1996 are actual assemblies discharged to the SFP.

5.6 DECAY HEAT LOAD

The decay heat loads were determined with the ORIGEN2 computer code (Ref. 5.2.3). ORIGEN2 has been submitted previously for a similar application (Ref. 5.6.1). The code explicitly solves the coupled isotopic production and decay equations, properly accounts for the heat produced by all activation products and more than 100 actinide isotopes, and rigorously accounts for neutron absorption in the fission products. Whereas activation products produce a small fraction of the decay heat power, their contribution is included in this analysis for conservatism. A comparison between ORIGEN2 and ASB 9.2 methodology is included in Section 5.11.

5.6.1 Full Core Decay Heat Load

For this evaluation, the core was assumed to operate at 102% of the rated 1520 MWt core power for 18 month cycles. A conservative flat full power history was used for the entire cycle length. Consequently, the reactor was assumed to operate at 102% power for the entire cycle length with no reductions in power which normally occur during a typical cycle. No credit was taken for nuclide decay (and corresponding reduction in decay heat) during outage periods and during fuel transfer (i.e., the assembly, batch, or core offload was assumed to occur instantaneously). The maximum heat load resulting from a core offload was calculated at 100 hours after reactor shutdown.

To ensure that conservative decay heats were obtained, the decay heat for burnups of 15, 17.5, and 20 GWD/MTU were calculated. The 20 GWD/MTU burnup bounds the cycle length associated with an 18 month fuel cycle. In addition, a short irradiation period of 30 days, which corresponds to a cycle burnup of 1.1 GWD/MTU, was performed to investigate pool heat loads for a BOC core offload scenario. The resulting decay heat loads after 100 hours of decay were examined and the maximum value, which occurred after a burnup of 20 GWD/MTU, was used in this analysis.

5.6.2 Single Fuel Assembly Decay Heat Load

The heat load for a single fuel assembly was also computed. Both average and peak assembly heat loads are required for analysis. The heat load was based on an eighteen month cycle length and 44 fuel assembly batch size was assumed for each reload outage.

The power history of an individual fuel assembly has a significant effect on the decay heat prediction. Typically, fresh and once-burned fuel will operate above the average assembly power. This evaluation incorporated an assembly peaking of 1.35 for fresh fuel, 1.20 for once-burned and 1.00 for twice burned fuel. Calculations utilizing the decay heat load for an average fuel assembly were based on a 'peak' average fuel assembly operating at an assembly relative power of 1.35. This corresponds to a fresh fuel assembly in the reactor. The decay heat load for this 'peak' assembly after a shutdown time of 100 hours is greater than that for an assembly operating at the true core average power, i.e., having a 1.00 peaking factor.

The hot, or design, fuel assembly decay heat load was obtained by conservatively applying the design enthalpy rise factor for the Ginna core, $F_{\Delta H}^N = 1.75$, to the average assembly decay heat load.

5.7 REQUIRED CORE DECAY TIMES

The technical specification temperature limit for the Ginna spent fuel storage pool is 150°F. This temperature limit is achieved with the heat removal capability of the present SFP heat exchangers. The SFP heat load must not exceed the heat removal capability of the existing SFP heat exchangers at a 150°F pool temperature. In order to maintain the SFP bulk temperature below the technical specification limit, the fuel must be held in the core for a minimum shutdown time to ensure that the total SFP heat load is less than the heat removal capability of the existing Ginna SFP cooling system. Fuel may not be offloaded from the core, in any event, prior to a minimum shutdown time of 100 hours that is assumed for the radiological consequence analysis.

The required shutdown time to maintain the bulk pool temperature less than the 150°F technical specification limit was determined for lake temperatures of 80°F, 60°F and 40°F.

5.7.1 Single Batch Offload

The decay heat load for a 44 fuel assembly batch was determined for batch average burnups of 15, 30, 45 and 60 GWD/MTU. The maximum spent fuel pool decay heat load, after a 100 hour shutdown time, is 11.22×10^6 Btu/hr. This heat load includes the contribution due to all previously discharged batches, and occurred for the 15 GWD/MTU case. The contribution due to all previous discharged batches is 3.56×10^6 Btu/hr. Note that, in general, the long term decay heat load typically increases with increasing burnup. However, the 44 assembly batch modeled here utilized conservative peaking factors of 1.35 for a burnup of 0 to 20 GWD/MTU, 1.2 for a burnup of 20 to 36 GWD/MTU, and 1.0 for a burnup of 36 to 60 GWD/MTU. This modeling of a batch yielded a slightly higher decay heat load with 100 hours of decay after the 15 GWD/MTU burnup than did subsequent burnups with their reduced peaking factors. Thus, a conservative decay heat load was generated for the 44 assembly batch.

The single batch core offload can be performed after the required 100 hour shutdown time associated with the radiological requirement. The total spent fuel pool decay heat load at 100 hours is well within the 16×10^6 Btu/hr heat removal capability of the SFP heat exchangers at the 80°F maximum lake water temperature. Consequently, a normal 1/3 core offload after 100 hours decay will never result in the SFP approaching its design temperature limit of 150°F.

5.7.2 Full Core Offload

A full core offload scenario with a full inventory of spent fuel assemblies (1879 fuel assemblies assuming some consolidated rod canisters) results in the highest predicted decay heat loads. A comparison of decay heat loads for the full core offload at 30 days of operation and for core average burnups of 15, 17.5 and 20 GWD/MTU showed a conservative value was calculated for the 30 day core operation. This is because the once and twice burned fuel assemblies were not decayed for any cycle outage time before the full core offload outage.

For the 30 day core operation, the total decay heat load on the SFP after 100 hours is 21.7 MBtu/hr. Since this decay heat load exceeds the 16 MBtu/hr design limit heat removal capacity for 80°F lake water temperature, additional shutdown is required before initiating the full core offload at the design lake temperature scenario. The required delay time prior to completing the full core offload is obtained from a comparison of decay heat load against the SFP heat exchanger heat removal capability for the various lake water temperatures to ensure that the 150 °F SFP limit is not exceeded.

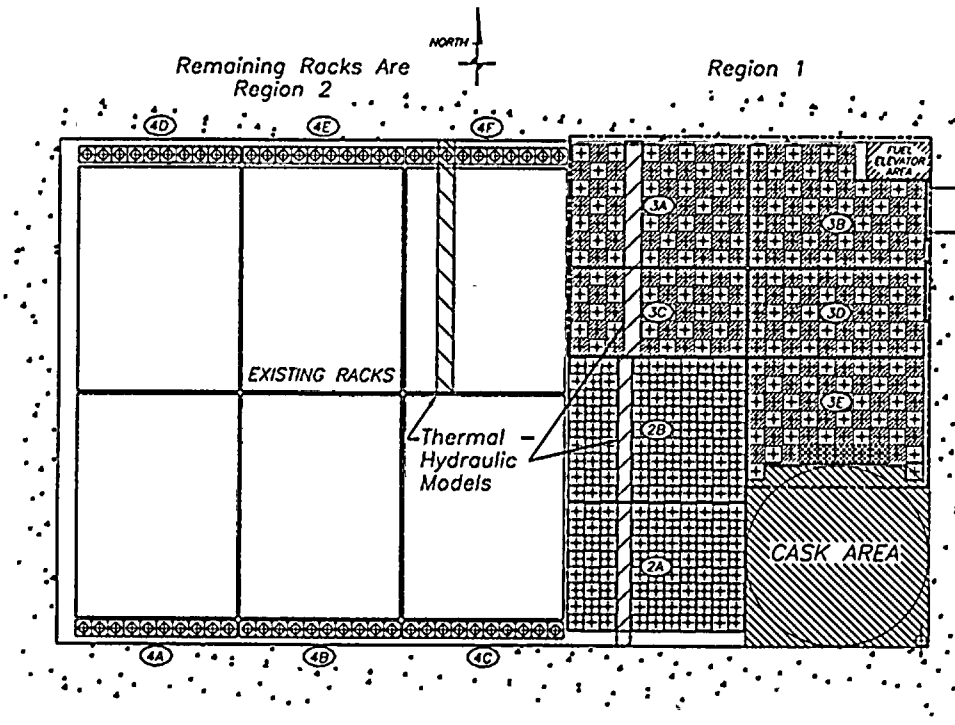
The required core delay times ensuring that the SFP design limit temperature of 150 °F is not exceeded for the full core offload scenario with a full inventory of spent fuel assemblies is summarized below for lake temperatures of 40 °F, 60 °F and 80 °F:

Lake Water Temperature °F	SFP Heat Exch. Capacity Mbtu/hr	Decay Heat Load Mbtu/hr	Delay Time Required for the 150 °F Tech. Spec. Limit Temp.
40	24.6	21.7	100 hours
60	20.4	20.4	132 hours
80	16.0	16.0	280 hours

5.8 LOCAL FUEL BUNDLE THERMAL-HYDRAULICS

The spent fuel pool at RG&E's Ginna plant, shown in Figure 5.8-1, is divided into two regions. Region I consists of flux type racks and Region II consists of high-density type racks. Two different rack designs are contained in Region II. Part of Region II contains ATEA Type 2 borated stainless steel racks; the remaining racks in Region II are the existing boraflex design (not removed as part of the pool re-rack). The existing high-density boraflex racks have ATEA Type 4 borated stainless steel side racks located between them and the pool wall in the gap. The ATEA side racks are located on the North and South walls of the SFP.

Figure 5.8-1 Spent Fuel Pool



The following table identifies the rack designs found in the Ginna SFP.

Region	Rack Type	Design
I	3A,B,C,D,E	ATEA BSS Flux Trap
II	2A,B	ATEA BSS High Density
II	Boraflex	Existing High Density
II	4A through 4F (Type 4 are side racks)	ATEA BSS High Density

BSS - Borated Stainless Steel
 3A, etc. - Letter denotes a particular array of canisters on a specific rack type.

5.8.1 Natural Circulation in the Spent Fuel Pool Storage Canisters

When fuel assemblies offloaded from the core are placed in the spent fuel pool into the canisters, cooling occurs by natural circulation. The density difference between the hot fuel assemblies and the cooler bulk pool fluid result in a thermal head. Pressure drop due to frictional losses in the downcomer, resistances due to rack leveling feet, inlet to the fuel canisters, bundle skin friction, fuel assembly (upper and lower) nozzles and grids and other losses in the flow path balance this buoyancy force.

The natural circulation cooling is analyzed to demonstrate that adequate cooling occurs in the hottest fuel assembly in the absence of inlet and outlet flow blockages preventing local boiling and maintaining the peak clad temperature below saturation. The hydraulic model consists of a row of fuel assemblies extending from the downcomer wall to the center of the pool. The pool water is assumed to flow downward between the periphery of the wall adjacent to the rack modules, then laterally in the region between the rack module bases and the pool floor, then upward through the fuel assemblies (Figure 5.8-2). A conservative pool-rack gap geometry is used to model the downcomer. This is conservative because flow is assumed to communicate with the canisters from the downcomer only which is modelled as a flow path only one row wide. In reality, flow reaches the canisters from other downcomer regions besides the downcomer segment modelled.

For the limiting Region I location, the assembly power is for a peak average assembly having a peaking factor of 1.35 (fresh fuel) and is from the most recently discharged batch having 100 hours of decay for the radiological requirement. The fuel assembly axial variation of power was modelled with a 1.55 chopped cosine shape; the results agreed very closely with those obtained using a uniform power shape.

The single row of fuel assemblies are modelled initially to establish the pressure drop boundary condition which is then imposed on the hot fuel assembly. All canisters in the row are conservatively assumed to contain a fuel assembly with the minimum decay time. A rack leveling foot is conservatively placed below each of the fuel assemblies as an added resistance to flow. In reality, a representative row selected for evaluation consists of approximately 12 or more fuel assemblies and has at most 4 or 5 support feet.

Once the pressure drop across the row of average fuel assemblies is calculated, the calculation is repeated. The pressure drop boundary condition obtained from the row of average fuel assemblies is imposed on the hottest fuel assembly for the region being analyzed. The hottest fuel assembly has a peaking factor of $F_{\Delta H}^N = 1.75$. A rack leveling foot is placed under the highest powered assembly. The placement of the rack leveling foot under the hot assembly increases the pressure drop across the assembly and minimizes the flow to the hottest assembly.

The inlet temperature of the water entering the downcomer and flowing in the region between the rack base and pool floor is assumed to be at the maximum pool bulk temperature of 150°F. Minimum rack-to-wall dimensions in the downcomer were modelled in order to maximize downcomer resistance thereby minimizing fuel assembly flow.

The fuel clad temperature for the hottest fuel assembly was calculated with a heat transfer coefficient for free convection. An additional resistance of 0.001 ft²-hr-°F/Btu was used for potential fouling on the fuel rods.

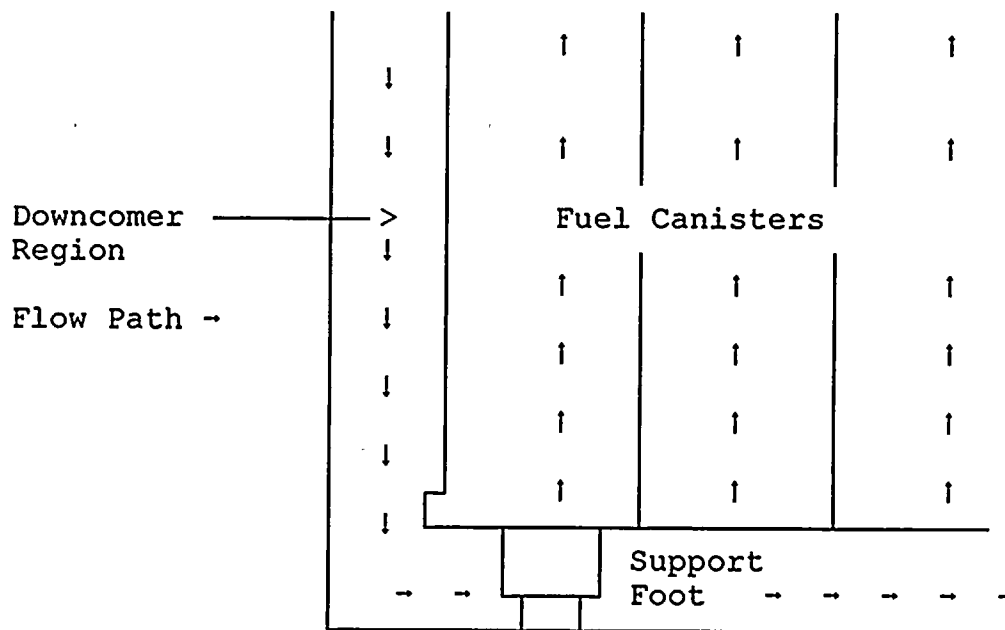
Due to the various canister designs present in the Ginna spent fuel pool, a single canister-type model was not used. The final pool configuration, upon completion of Phase II, required the application of three separate models to analyze the following geometries:

- Region I type 3 racks,
- Region II type 2 racks, and
- Region II with the existing boraflex and adjacent type 4 side racks.



Each of the models followed the general approach described above. The calculations were performed with Framatome Cogema Fuel's FSPLIT code (Ref. 5.7.1). FSPLIT is a PC based code which can be used for pressure drop/flow solutions for networks with water, heavy water, incompressible fluids, or gasses. The networks can be closed loop or simulated open loop. Forced flow and natural circulation problems can be analyzed with FSPLIT. The FSPLIT code has been previously used supporting licensing submittals.

Figure 5.8-2 Natural Circulation Flow Path



5.8.2 Effects of Gamma Heating in the Flux Trap Regions and Inter-Canister Gaps

The natural circulation in the flux trap regions (type 3 racks) and intercell gaps (type 2 racks) is driven by the pressure drop across the major flow path. Water enters the bottom of the canisters and flows upwards in two parallel paths. The major flow path is through the fuel assemblies and a secondary path is in the gaps between canister types where it is heated by the gamma heat produced in the stainless steel. This analysis verifies the absence of localized boiling in these secondary paths.

5.8.2.1 Region I Type 3 Flux Traps

Water enters the Region I flux traps through a rectangular opening at the top of the base plate. It flows upwards in the region between the canisters and exits at the level of the top of the canisters as shown in Figure 5.8-3. The top of every other type 3 canister has a lead in edge which forms a funnel that facilitates the insertion of offloaded fuel and which effectively blocks a significant part of the exit flow area along the canister width. This configuration is shown in Figure 1.3-4. Flow exits the flux trap region at the corner intersections of four canisters which are not obstructed by the funnel feature and rejoins the main flow.



Figure 5.8-3 Flux Trap Region

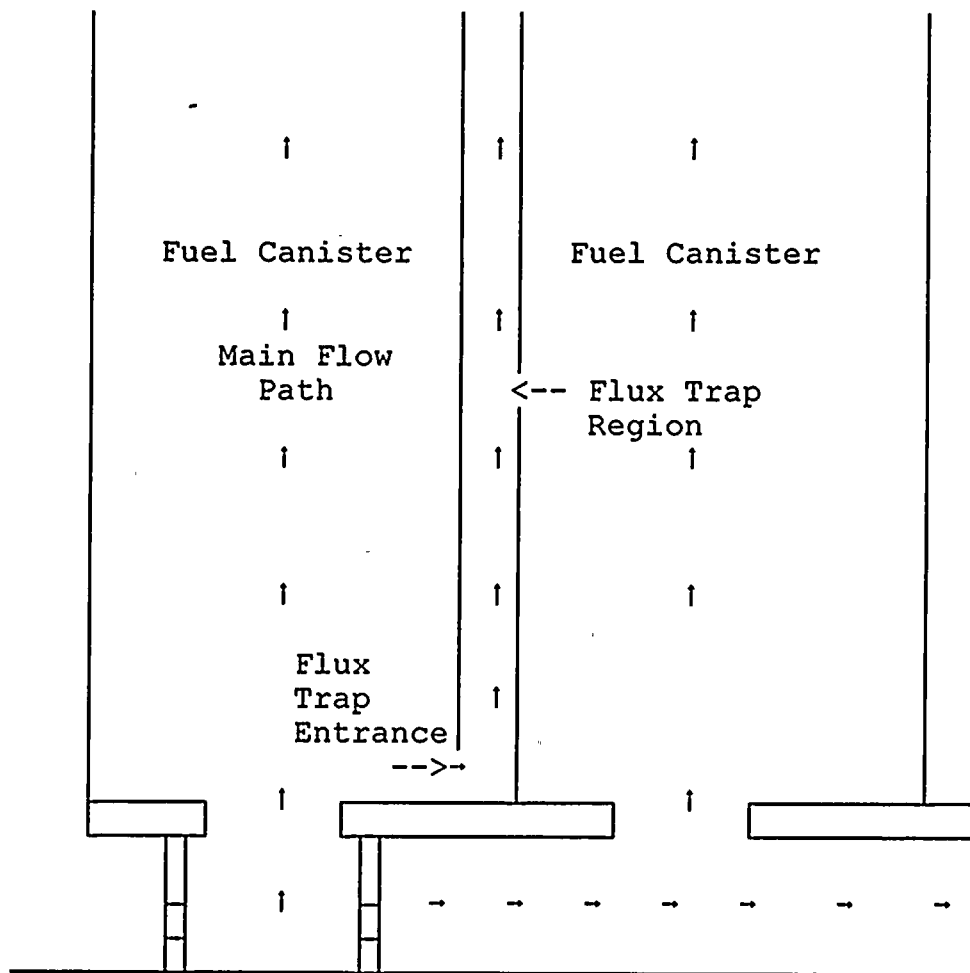


Diagram showing the flow path in the Type 3 Rack Flux Trap Region.

5.8.2.2 Region II Type 2 Inter-Canister Gaps

For the type 2 canister inter-canister gap, water enters an opening between the borated stainless steel plate and the canister wall above the base plate and flows upward approximately 12 feet and re-enters the main flow stream through a similar gap at the top (Figure 5.8-4). The boundary conditions for the flow in the inter-canister gap are the pressures where the flow enters the gap above the base plate and at the top where the flow exits the gap and re-enters the main flow stream.

For both gap configurations, all of the gamma heat production is deposited in the gap. The total wall thickness, including the borated stainless steel, is used to calculate the heat production.

Figure 5.8-4 Region II Type 2 Inter-Canister Gap

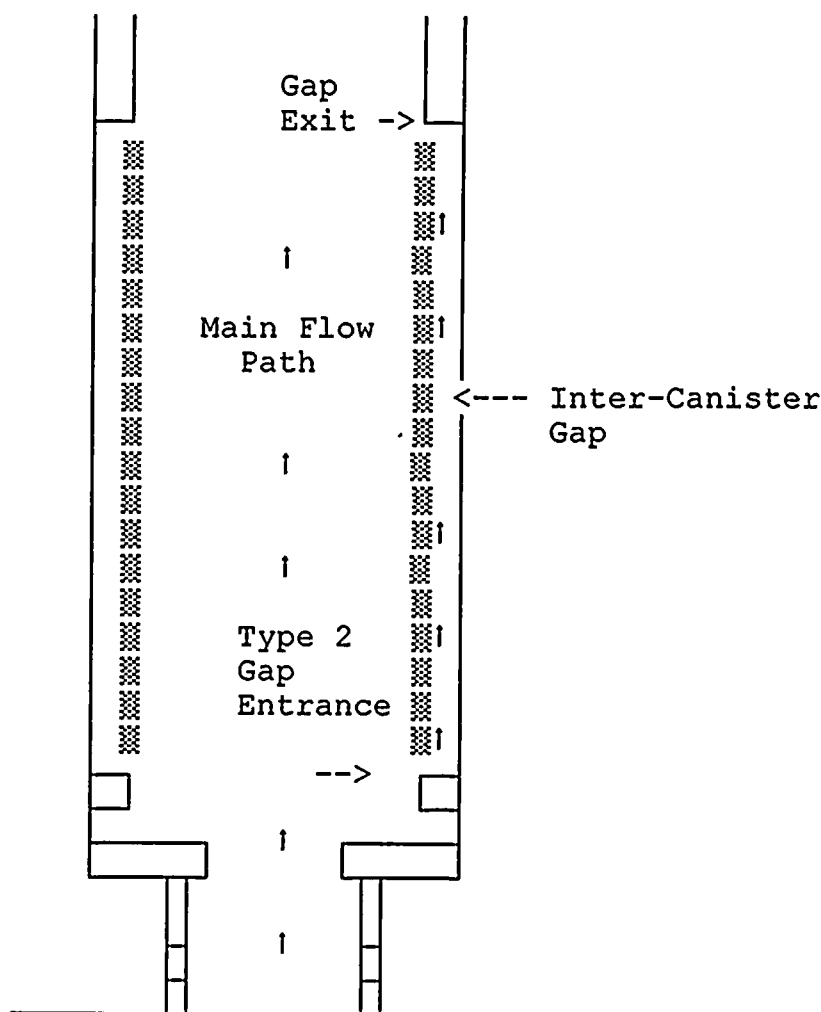


Diagram showing flow path in Rack Type 2 Inter-Canister Gap.

5.8.3 Flow Blockages

A partial flow blockage at the cell outlet was postulated with a fuel assembly lying on top of the rack. This configuration was modelled as a blockage of approximately 85% of the exit flow area of the hottest assembly located over a rack leveling foot to demonstrate that boiling would not occur.

A complete inlet blockage of the hottest assembly was also postulated. Using a counterflow flooding correlation, it was demonstrated that water would replace the exiting flow which was assumed to be steam.

5.8.4 Natural Circulation in the Consolidated Fuel Canisters

The natural circulation in the consolidated fuel canisters is calculated in a manner similar to that for the fuel cells. The boundary condition for the flow through the consolidated canisters is obtained from the natural circulation of the average fuel assemblies. Flow resistances are based on fuel rods in a close packed

triangular lattice at a consolidation rate of 2:1. This assumes that the fuel rods associated with two fuel assemblies are stored in one consolidated canister. The flow loss through the consolidated canister is primarily due to laminar friction losses along the rods which was determined to be approximately 50 times greater than canister inlet and exit flow losses.

RG&E may, at a future date, increase the storage capacity of the spent fuel pool through fuel consolidation. An evaluation was performed to ascertain the affects of additional fuel consolidation activities on the thermal-hydraulic results for the hottest fuel assembly. The analysis, in principal, is the same as that used for the fuel assemblies. Comparing to the Region I results, which were thermally limiting for the spent fuel pool, consolidated fuel canisters were placed in the fuel assembly row previously modelled to establish the pressure drop boundary condition for the hottest fuel assembly. An acceptable application of consolidated fuel canisters is possible provided the calculated pressure drop boundary condition from the row of fuel assemblies used for the hottest fuel assembly remains limiting.

Various configurations of consolidated fuel canisters were investigated:

- Full row of consolidated canisters in Region I,
- Single consolidated canister in a row of fuel assemblies,
- Full consolidation (2:1) and partial consolidation (1:1).

5.9 SPENT FUEL POOL THERMAL-HYDRAULICS ANALYSIS RESULTS

The results of the spent fuel thermal-hydraulic analyses performed are discussed in this section. The general methodology used is discussed in Section 5.8. Certain features of the analysis method are repeated and expanded in the discussions of the various analyses for clarity.

5.9.1 Region I with Type 3 ATEA Racks

The ATEA type 3 rack, flux trap design, is located in Region I of the Ginna spent fuel pool (Figure 5.8-1). This rack type was conservatively modelled as a single row of 12 canisters extending from the North wall southward to the middle of the spent fuel pool (Figure 5.8-1). The thermal-hydraulic model includes racks 3A and 3C; the single row (type 3 canisters) ends at the inter-rack gap between the type 3 and ATEA type 2 rack.

The minimum downcomer gap dimension, rack-to-pool wall, is 1.80 inches. Figure 5.9-1 shows the flow path. A single canister width is used for the width of the downcomer channel. Frictional flow losses in the downcomer were based on turbulent flow. Turn losses, contraction/expansion losses at the rack base to wall and through the support feet and base plate were based on well known expressions found in reference 5.8.1. The fuel assembly grid and nozzle pressure drop losses were based on the behavior of an orifice in the laminar flow regime. Frictional loss due to the fuel rod and canister skin friction was calculated assuming laminar flow through the canister. The total pressure drop loss of the fuel assembly was obtained by combining the grid and nozzle losses with the friction loss.

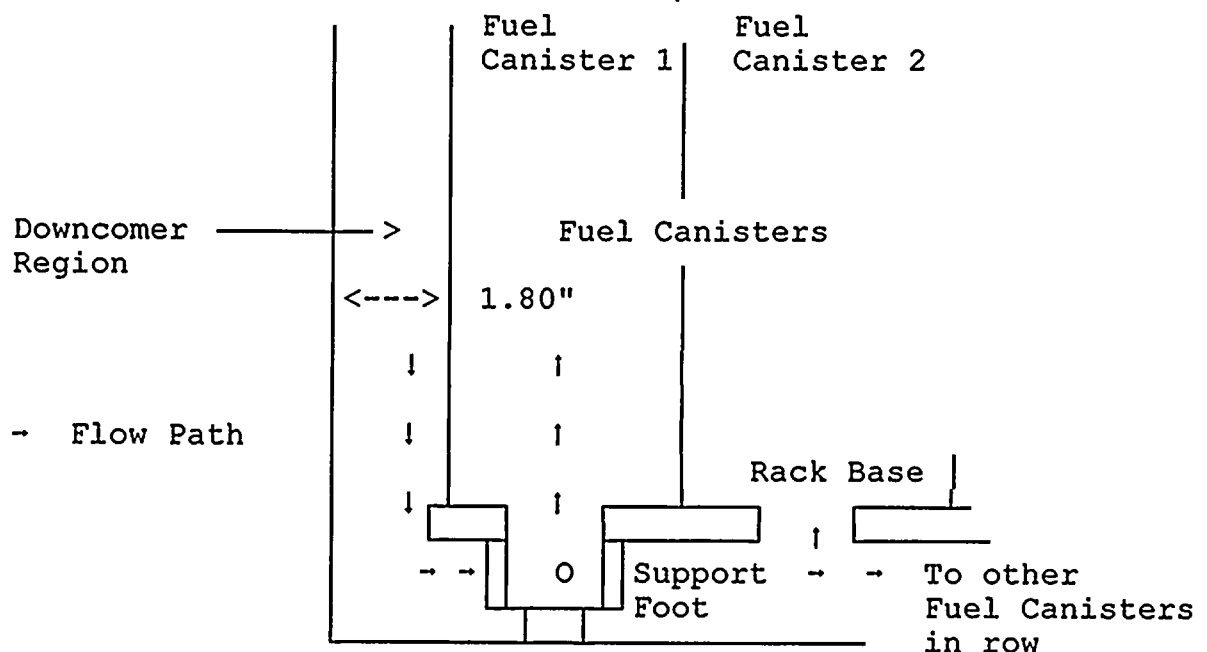
The results for the hottest assembly in a Region I type 3 rack are summarized in the following table.

Table 5.9-1 Region I Type 3 Rack Local Pool Cooling Results

	Assembly Peak	Assembly Flow (lbm/hr)	Temperature (°F)		
			Inlet	Outlet Fluid	Peak Clad
Region I Type 3	1.75	4260	150	222	232

Saturation temperature at the top of the rack is 238.9°F based on a minimum SFP water height of 23 feet above the top of the racks.

Figure 5.9-1 Natural Circulation Flow Path - Type 3 Rack



(Resistance Due to Support Foot Placed Under all Canisters in Model)

5.9.2 Region II with Type 2 ATEA Racks

The ATEA type 2 rack, high density design, is located in Region II of the Ginna spent fuel pool (Figure 5.8-1). This rack type was conservatively modelled as a single row of 17 canisters extending from the South wall northward to the middle of the spent fuel pool (Figure 5.8-1). The thermal-hydraulic model includes racks 2A and 2B; the single row (type 2 canisters) ends at the inter-rack gap between the type 2 and ATEA type 3 rack.

The row of fuel assemblies was modelled in a similar manner as discussed in Section 5.8.1. The minimum downcomer gap dimension, rack-to-pool wall, is 7.30 inches. A single canister width is used for the width of the downcomer channel.



The Ginna UFSAR states that prior to moving fuel from Region I to Region II, a cooling period of 60 days must have elapsed. The decay heat load for a 60 day decay time was used for the thermal-hydraulic model.

The results for the hottest assembly in a Region II Type 2 racks are summarized in the following table. The peak clad temperature calculated in Section 5.9.1 for the type 3 rack in Region I bounds the results for a Type 2 rack. This is primarily due to the significantly lower decay heat resulting from the minimum 60 day decay time required for assemblies located in Region II.

Table 5.9-2 Region II Type 2 Rack Local Pool Cooling Results

	Assembly Peak	Assembly Flow (lbm/hr)	Temperature (°F)	
			Inlet	Outlet Fluid
Region II Type 2	1.75	3180	150	181

Saturation temperature at the top of the rack is 238.9°F based on a minimum SFP water height of 23 feet above the top of the racks.

The results reported in Section 5.8.1 for the Region I, type 3 rack are bounding.

5.9.3 Region II with Type 4 ATEA Side Racks

The ATEA type 4 side racks are located along the North and South walls of the Ginna spent fuel storage pool in the pool-to-rack gap for the existing boraflex racks (Figure 5.8-1). The large existing gap along these walls, ranging from approximately 14 to 17 inches, permitted the additional storage using the type 4 racks. The actual placement of the racks into the pool occurs upon completion of Phase II.

The thermal-hydraulic model consisted of a single row of 15 canisters extending from the North wall southward to the middle of the spent fuel pool (Figure 5.8-1). The thermal-hydraulic model includes a single canister in rack 4-4F and a row of 14 canisters in one of the existing boraflex racks.

The row of fuel assemblies was modelled in a similar manner as discussed in Section 5.8.1. This model differs slightly due to the differences between the existing rack design and the ATEA Type 4 rack design. The existing boraflex racks have an I-beam around their perimeter supporting the main structure which resembles a rectangular honeycomb. Square flow holes are located in the I-beam permitting flow to transverse from the downcomer to central regions of the pool. The canister entrance flow hole in the base plate of the canisters is virtually identical for both designs (3.37 in. for the ATEA type 4 and 3.25 in. minimum for the existing boraflex canister).

The pressure loss through the I-beam was modelled as a restriction for flow to the boraflex racks. The loss coefficient for flow through the I-beam is similar in magnitude to that for flow through an ATEA support foot. The minimum downcomer gap dimension, rack-to-pool wall, is 3.59 inches for this analysis. A single canister width is used for the width of the downcomer channel.

Because of differences in inlet regions of the rack designs, the boraflex type was analyzed initially with the minimum rack-to-wall gap dimension to obtain the pressure drop boundary condition. The minimum downcomer rack-to-wall gap dimension of 3.59 inches was based on the presence of a type 4 canister. The canister pressure drop obtained for the boraflex type canister was then used as a boundary condition that existed across the ATEA Type 4 rack. The fuel assembly flow rate and temperature rise for the ATEA Type 4 rack was calculated based upon the assumed pressure drop boundary condition. -

The Ginna UFSAR states that prior to moving fuel from Region I to Region II, a cooling period of 60 days must have elapsed. The decay heat load for a 60 day decay time was used for the thermal-hydraulic model.

Since the ATEA type 4 and boraflex rack designs both have essentially equal flow areas (the boraflex is slightly larger than type 4), the results obtained for the ATEA Type 4 rack are equally applicable to both rack types. The ATEA Type 4 rack results are summarized in the following table.

Table 5.9-3 Region II Type 4 & Boraflex Rack Local Pool Cooling Results

	Assembly Peak	Assembly Flow (lbm/hr)	Temperature (°F)	
			Inlet	Outlet Fluid
Region II Type 4 & Boraflex	1.75	3600	150	177

Saturation temperature at the top of the rack is 238.9°F based on a minimum SFP water height of 23 feet above the top of the racks.

As with the ATEA Type 2 racks, the results reported in Section 5.8.1 for the Region I, type 3 rack are bounding due to the longer decay time associated with the fuel assemblies stored in Region II of the Ginna spent fuel pool.

5.9.4 Natural Circulation in the Region I Flux Trap Region

The pressures obtained from the Region I type 3 average fuel assemblies were applied as the boundary condition to obtain the flow in the Region I flux traps. The circulation in the flux trap regions is driven by the pressure differences in the fuel cells because the flow in these major paths is much higher. The gamma heating occurs in the stainless steel and water and is deposited directly into the flux trap region. For the analysis configuration described in Section 5.8.2, the following results were obtained for the Region I flux traps. The reported flow is contained in one gap between two adjacent canisters in Region I.

Flow (per gap): 38 lbm/hr
 Outlet Temperature: 221°F

5.9.5 Natural Circulation in the Region II Inter-Canister Gaps

The pressures obtained from the Region II type 2 average fuel assemblies were applied as the boundary condition to obtain the flow in the Region II flux traps. Pressures were selected at the height of the inlet to the inter-canister gap above the base plate and approximately 12 feet downstream where the flow from the gaps re-enters the main stream inside the canister. As with the Region I flux traps, the circulation in the inter-canister gaps is driven by the pressure differences in the fuel cells because the flow in these major flow paths is much higher. The gamma heating occurring in the stainless steel and water is deposited directly into the inter-canister gap region. For the analysis configuration described in Section 5.8.2, the following results were obtained for the Region II inter-canister gaps. The reported flow is contained in one gap between two adjacent canisters in Region II.

Flow (per gap): 12 lbm/hr
Outlet Temperature: 184°F

5.9.6 The Effect of Flow Blockage

The partial blockage of a canister outlet was analyzed assuming a dropped fuel assembly was laying on top of the rack. Utilizing the conservative assumption that the end fitting of the dropped fuel assembly obstructed the exit flow from the hottest assembly in Region I, the exit flow area was reduced by approximately 85%. The resulting bulk fluid temperature was determined to be 233 °F which is below saturation (238.9°F). The peak clad temperature for the outlet blockage is 244 °F. The peak clad temperature is slightly above the saturation temperature. Using a nucleation criterion from Lahey (Ref. 5.9.6), it was shown that bubbles may be present on the cladding surface but that local conditions would not support bubble growth. The heat flux necessary for active nucleation is approximately seven times greater than the hot fuel assembly heat flux. Consequently, adequate cooling of the canister is still maintained.

The second scenario that was investigated was the complete blockage of the fuel canister inlet. The complete blockage of a canister inlet prevents natural circulation flow from removing the decay heat. In the event of such a blockage, evaporative cooling removes the decay heat from the canister. Assuming steam flow exists in the hottest fuel assembly canister ($F_{\Delta H}^N = 1.75$), a counterflow flooding correlation of Wallis demonstrated that the liquid water entering the canister was sufficient to replenish the boil-off and prevent dry-out. As long as the required mass flux of liquid (needed to match the steam rate) is less than the flooding limit, adequate cooling of the assembly is assured even if the canister inlet is completely obstructed.

The counter-current flooding calculation was performed for minimum flow areas of one-half (0.139 ft²) and one-fourth (0.070 ft²) of the minimum fuel assembly tube region flow area. The minimum tube region flow area is 0.279 ft². It was conservatively assumed that the fluid pressure at the fuel assembly exit was atmospheric and no credit was taken for subcooling of the liquid entering the top of the assembly.

The results indicated that a safety margin of over 40 exists at the one-half area reduction and over 7 for the one-fourth area reduction. The clad temperature was calculated to be approximately 10 °F above the water saturation temperature.



1 2 3 4 5 6 7 8 9 10 11 12 13 14 15 16 17 18 19 20 21 22 23 24 25 26 27 28 29 30 31 32 33 34 35 36 37 38 39 40 41 42 43 44 45 46 47 48 49 50 51 52 53 54 55 56 57 58 59 60 61 62 63 64 65 66 67 68 69 70 71 72 73 74 75 76 77 78 79 80 81 82 83 84 85 86 87 88 89 90 91 92 93 94 95 96 97 98 99 100

1 2 3 4 5 6 7 8 9 10 11 12 13 14 15 16 17 18 19 20 21 22 23 24 25 26 27 28 29 30 31 32 33 34 35 36 37 38 39 40 41 42 43 44 45 46 47 48 49 50 51 52 53 54 55 56 57 58 59 60 61 62 63 64 65 66 67 68 69 70 71 72 73 74 75 76 77 78 79 80 81 82 83 84 85 86 87 88 89 90 91 92 93 94 95 96 97 98 99 100

5.9.7 Natural Circulation in the Consolidated Fuel Canister

The evaluation of cooling the consolidated fuel canister is identical in principle to the fuel assembly analysis. The decay heat load is much lower, based on a 5 year decay time. The local pressures from the Region I average fuel assembly analysis were applied as boundary conditions with a rack leveling foot placed below the consolidated fuel canister. The consolidated fuel canister contained two fuel assemblies worth of rods.

Decay heat for this analysis was selected by comparing the decay heat of peak average fuel assemblies after a 5 year decay having burnups of 15, 30, 45 and 60 GWd/mtU. The decay heat for a fuel assembly having 60 GWd/mtU was found to be bounding and was used for this evaluation.

The result for the consolidated fuel canister follows:

Flow:	120 lbm/hr
Outlet Temperature:	222°F
Peak Clad Temperature:	231°F

RG&E may, at a future date, increase the capacity of the Ginna spent fuel storage pool through consolidation. This evaluation assessed the impact of consolidated fuel canisters on the local pressure results from the Region I analysis.

Using the Region I thermal-hydraulic model, an analysis was performed to obtain the pressure drop boundary condition as was done for the row of average fuel assemblies. Consolidated fuel canisters having consolidation rates of 2:1 and 1:1 were modelled.

The results indicated that both configurations of consolidated fuel canisters would result in higher local pressure drops than were determined for the row of fuel assemblies. Applying these local pressures across the hottest fuel assembly as a pressure drop boundary condition would result in increased flow to the hottest assembly compared to the design results obtained with the fuel assemblies.

These evaluations indicate the thermal-hydraulic conditions determined with fuel assemblies in the fuel canisters in both Regions I and II remain bounding with increasing numbers of consolidated fuel canisters. With increasing numbers of consolidated fuel canisters, additional flow would be diverted to the hottest fuel assembly resulting in reduced bulk fluid and clad temperatures for the hottest assembly.

5.10 LOSS OF THE SPENT FUEL COOLING SYSTEM

The spent fuel pool temperature heat-up rate has been determined for a complete loss of the spent fuel heat removal system. No credit is taken for heat loss through the pool walls, evaporative cooling from the pool surface or convective cooling to the ambient air. The thermal inertia of the pool was determined by summing the contributions of the racks, fuel assemblies, the net pool water volume, and the SFP liner.

The heat-up rates are calculated for the time it takes the pool to heat from the 150°F technical specification limit temperature to the design limit for the SFP, 180°F. Values are reported for both the pool configuration with fuel assemblies and for complete consolidation. Complete consolidation places two fuel assemblies in a consolidated fuel canister placed in every location of the spent fuel pool. The table summarizes the heat-up rates for varying heat loads as a function of the lake water temperature.

Backup heat removal systems consisting of the original SFPCS and the portable skid mounted unit are available in the event of a failure of the primary SFPCS. The use of these backup systems provide heat up times to reach the 180°F structural integrity limit temperature greater than those listed in Table 5.10-1. The original SFPCS can be made operational in 45 minutes which is considerably less than the minimum time of 3.4 hours listed in Table 5.10-1 for full consolidation with an 80°F lake water temperature. After 45 minutes of heatup, the pool temperature would be 156.5°F for a heat up rate of 8.71° F/hr for full consolidation. The increase in water temperature would then drop to 4.4°F/hr after 45 minutes. An additional 5.3 hours would be available for repair or to place the skid mounted unit into operation before the pool water temperature reaches 180°F. The additional time of 5.3 hours is greater than the 3 hours required to bring the skid mounted system into operation. Similar results are obtained for lake water temperatures below 80°F. Thus, adequate time and cooling capacity are available to prevent the SFP water temperature from reaching 180°F.

Table 5.10-1 Loss of Pool Cooling and Heat-Up Time

Pool Configuration	Lake Water (°F)	Heat Load MBtu/hr	Heat-Up Time (Hours) 150°F → 180°F
Unconsolidated	40	21.7	2.8
Unconsolidated	60	20.4	3.0
Unconsolidated	80	16.0	3.8
Consolidated	40	21.7	2.5
Consolidated	60	20.4	2.7
Consolidated	80	16.0	3.4

The heat-up rate for a lake water temperature of 40°F is based on the decay heat after a 100 hour decay time based on the radiological requirement. The consolidated pool configuration is for full pool consolidation, i.e., two spent fuel assemblies are conservatively placed in a consolidated fuel canister in all locations.



5.11 COMPARISON BETWEEN ORIGEN2 RESULTS AND ASB 9-2 METHODOLOGY

ORIGEN2 does not use empirical-based methods to calculate decay heat but tracks the buildup and decay of the individual fission products within the reactor core during operation and shutdown. ORIGEN2 also includes the effect of element transmutation from neutron capture, both in fissile isotopes and fission products. Because ORIGEN2 performs a rigorous calculation of decay heat, it was used in the calculations for decay heat in this analysis. To provide additional information, a comparison of the full core decay heat power resulting from ORIGEN2 and that resulting from the Branch Technical Position ASB 9-2 for a core operating time of 15 GWD/MTU is shown below for several times after shutdown.

Table 5.11-1 Comparison between ORIGEN2 and ASB 9-2 Results for a full core offload (121 Fuel Assemblies, no pool inventory) with 15 GWD/MTU burnup

Decay Time (hours)	ORIGEN2 Results (kW)	ASB 9-2 Results	ASB 9-2/ORIGEN2
24	8041	9104	1.132
100	5050	5537	1.096
600	2351	2544	1.082
2400	1094	1101	1.006

This comparison shows that for the time of interest in this analysis, 100 hours, that the ASB 9-2 method predicts the decay heat for a full core to be within 10% of ORIGEN2.

5.12 REFERENCES

- 5.2.1 OT Position for Review and Acceptance of Spent Fuel Storage and Handling Applications, Dated April 14, 1978, and revised January 18, 1979.
- 5.2.2 NUREG-0800 Standard Review Plan 9.1.3, Revision 1 (July 1981), and Standard Review Plan 9.2.5 Revision 2 (July 1981), (Ref. 5.2).
- 5.2.3 A.G. Croff, ORIGEN2-A Revised and Updated Version of the Oak Ridge Isotope Generation and Depletion Code, ORNL-5621, (Ref. 5.3).
- 5.6.1 P.L. Holman, et. al., Kewaunee New and Spent Fuel Storage Rack Criticality Analysis, BAW-2095, November 1989. (FCF internal document).
- 5.7.1 FTI Document 32-1203121-01, "FSPLIT Certification Analysis," September 1991. (Code Verification)



- 5.8.1 Handbook of Hydraulic Resistance, 2nd Edition, I.E. Idelchik, Hemisphere Publishing Corp., 1986.
- 5.9.6 The Thermal-Hydraulics of a Boiling Water Nuclear Reactor, 2nd Printing, R.T. Lahey, Jr., and F.J. Moody, ANS/AEC Monograph Series on Nuclear Science and Technology Published by the ANS.

6.0 RADIOLOGICAL EVALUATION

The radiological safety analysis^[6.1,6.2] was performed in accordance with General Design Criteria 61 of 10 CFR Part 50 Appendix A^[6.3] to evaluate hypothetical accidents involving fuel damage to Regions 1 and 2 and dose rates due to the increased capacity. The analysis addressed:

- (1) offsite dose consequences at the site boundary (EAB) and at the low population zone boundary (LPZ) from these limiting hypothetical accidents:
 - (a) rack drop accident
 - (b) cask drop or tip accident
 - (c) gate drop accident
 - (d) consolidated canister drop accident
 - (e) fuel handling accident
 - (f) tornado missile accident
- (2) dose rates at the surface of the spent fuel pool and through the pool's concrete walls for the purposes of occupational exposure.

The analysis also addresses solid radwaste and gaseous releases.

From the standpoint of offsite doses, the important aspect of the proposed re-racking is that the pool will continue to be divided into two regions, Region 1 which requires fuel to have decayed a minimum time of 100 hours, and (2) Region 2 which requires fuel to have decayed for a minimum time of 60 days. These two regions are illustrated in Figure 6-1. Due to the two separate decay times, accidents occurring in either area can have varying radiological consequences.

6.1 ACCEPTANCE CRITERIA

6.1.1 Offsite Dose Exposure

Reference offsite dose values for evaluating hypothetical accidents involving fission product releases are specified in 10 CFR Part 100^[6.4] and are 25 rem to the whole body and 300 rem to the thyroid from iodine exposure. Both values are applicable to the exclusion area boundary (EAB) and the low population zone boundary (LPZ). Section 15.7.4. of the Standard Review Plan^[6.5] (SRP) specifies acceptance criteria of 25% of 10 CFR Part 100 guidelines¹ for postulated fuel handling accidents. However, the Ginna Station was designed and built prior to the SRP and is not required to meet the SRP limits. A previous fuel handling accident analysis showed an offsite dose of 96 rem thyroid^[6.6(c)] which has been previously accepted by the NRC as being "well within" 10 CFR Part 100 limits.

¹ Section 15.7.4.IV states that a plant's facilities are acceptable if reasonable assurance is provided that the calculated offsite radiological consequences of a postulated fuel handling accident are well within the 10 CFR Part 100 exposure guidelines.

6.1.2 Occupational Dose Exposure

Occupational exposure dose limits are specified in 10 CFR Part 20^[6.7] and are further controlled by plant procedures. The recommended dose rate that shall not be exceeded in accessible spaces adjacent the spent fuel pool is given in ANSI/ANS 57.2^[6.8] and is 2.5 mrem/hr to any persons occupying those spaces. The rate is specified for when the pool is at its design fuel inventory and at the minimum design water depth.

6.2 OFFSITE DOSE CONSEQUENCES

The following six hypothetical accidents potentially resulting in releases of fission products were evaluated:

- a) rack drop accident
- b) cask drop or tip accident
- c) gate drop accident
- d) consolidated canister drop accident
- e) fuel handling accident
- f) tornado missile accident

6.2.1 Rack Drop Accident

Installation and removal of the racks (heavy loads) will require use of the auxiliary building's 30 ton crane hook, which meets the single failure proof requirements of NUREG-0612^[6.9] for carrying heavy loads (see UFSAR Ch. 9.1.4.3.1)^[6.10]. In addition, during the re-racking, installation and removal procedures will prevent transport of racks over spent fuel. Thus, an accident involving the release of fission products from a rack drop accident is not plausible, and the offsite radiological dose consequences need not be determined for this accident.

6.2.2 Cask Drop/Tip Accident

Insertion and removal of a spent fuel cask will be conducted using the auxiliary building's 30 ton crane hook, which meets the single failure proof requirements of NUREG-0612 for carrying heavy loads (see UFSAR Ch. 9.1.4.3.1). In addition, during the removal and insertion of the cask, plant procedures and crane interlocks will prevent transport of the cask over spent fuel. Thus, an accident involving the release of fission products from a cask drop or tip accident is not plausible, and the offsite radiological dose consequences need not be determined for this accident.

6.2.3 Gate Drop Accident

The existing lifting mechanism for the spent fuel pool gate (to transfer canal) is not single failure proof. However, RG&E will modify the lifting mechanism to make it single failure proof in accordance with NUREG-0612 to prevent accidental dropping of the gate, which is considered a heavy load. This action will prevent potential fuel damage and the subsequent release of fission products. Thus, the offsite radiological dose consequences need not be determined for this accident.

6.2.4 Consolidated Canister Drop Accident

A consolidated canister can contain all of the fuel rods from two assemblies and is considered a heavy load per NUREG-0612 criteria. There will be administrative control for movement of the canisters in the spent fuel pool. The canisters will be lifted using a single-failure proof crane and a

single-failure proof lifting system and will be handled in accordance with the guidelines on NUREG-0612 with regard to limiting the chance of an unacceptable heavy load drop. This action will prevent potential fuel damage and the subsequent release of fission products. Thus, the offsite radiological dose consequences need not be determined for this accident.

6.2.5 Fuel Handling Accident

The dose models and methodology for calculating the thyroid and whole-body doses at the EAB and LPZ due to a fuel handling accident inside the auxiliary building are described in Section 15.7.3.2 of the UFSAR. The proposed re-racking of the Ginna SFP has not affected any assumptions or inputs (including source terms) used in the fuel handling accident as described in the UFSAR. The height of the Region 1 racks will remain the same as those currently installed, and it has been shown (UFSAR 15.7.3.1.4) that if a dropped fuel assembly impacts a stored assembly, the fuel rod cladding of the impacted assembly would not fail. Therefore, the current analysis for this accident as documented in the UFSAR remains valid and applicable.

The offsite dose consequences for a fuel handling accident occurring in the spent fuel pool are:

Dose	Dose (rem) at EAB	Dose (rem) at LPZ
0-2 hour thyroid	14	0.88
0-2 hour whole body	0.31	0.02

6.2.6 Tornado Missile Accident

Since Region 1 racks are to be replaced with ATEA-designed racks, the radiological dose consequences of the tornado missile accident in Region 1 must be re-evaluated. The dose models used to calculate the offsite thyroid and whole body doses are identical to the models used in the fuel handling accident analysis inside the auxiliary building (see section 15.7.3.2 of the UFSAR).

The thyroid dose was calculated using the following equation:

$$Dose(rem) = \sum_i A_i \frac{X}{Q} B DCF_i$$

where

- A_i = iodine activity(Ci) released from auxiliary building for isotope I
- X/Q = the 0-2 hour atmospheric dispersion factor at the site boundary and the 0-8 hour atmospheric dispersion factor at the low population boundary
- B = breathing rate ($3.47 \times 10^{-4} \text{ m}^3/\text{sec}$)
- DCF_i = adult thyroid inhalation dose conversion factor (rem/Ci) for iodine isotope I

The external whole body gamma radiation dose was calculated using the following semi-infinite cloud equation:

$$Dose(rem) = 0.25 \sum_i \overline{E}_{\gamma_i} A_i \frac{X}{Q}$$

where

0.25 = units conversion factor [(rad-m³-disintegration)/(Ci-MeV-sec)] to convert [(Ci-sec-MeV)/m³] to rads (or rems since quality factor is 1.0)

\bar{E}_{γ_i} = average gamma ray energy (MeV/disintegration) for isotope I

A_i = noble gas activity (Ci) released from the auxiliary building

X/Q = the 0-2 hour atmospheric dispersion factor at the site boundary and the 0-8 hour atmospheric dispersion factor at the low population boundary

Note that $0.25 \times \bar{E}_{\gamma_i}$ is the whole body dose conversion factor.

Since the pool is divided into two regions, it is possible that the hypothetical tornado missile, which is considered to be a 1,490 lb wooden pole, 35 ft in length and 13.5 inches in diameter (see UFSAR 9.1.2.7), could impact and damage the fuel in either region. The ATEA racks are being designed to replace the existing Region 1 racks and will have the same height as the current Region 1 racks. It has been determined in a separate analysis (see Section 3 of this report) that the resulting damage from the stated tornado missile to the ATEA-designed racks would be the assembly of direct impact and immediately adjacent assemblies for a total of nine damaged assemblies.

Since Region 1 is to contain freshly off-loaded fuel with a minimum of 100 hours of decay whereas Region 2's minimum decay time is 60 days, Region 1 damage will provide limiting dose consequences. Freshly off-loaded fuel is to be stored in a checkerboard pattern. To ensure that freshly off-loaded fuel is not stored in adjacent rack cells, the Region 1 racks will be loaded in a checkerboard pattern with fuel from Region 2 before off-loading fresh fuel.

Upon impact from the hypothetical tornado missile, the maximum damage to the Region 1 ATEA racks will be nine cells or nine assemblies. The worst case configuration would be five freshly off-loaded assemblies and four Region 2 assemblies. It was conservatively assumed that all assemblies had a peaking factor of 1.2. Additional assumptions and inputs are shown in Table 6A-1 in Appendix 6A. The resulting offsite dose consequences are shown below in Table 6.4-1. For comparison, the dose consequences resulting from the tornado missile accident occurring in Region 2 and damaging nine fuel assemblies (see UFSAR 9.1.2.7) were also calculated and are shown in Table 6.2-1.

Table 6.2-1 Offsite Radiological Consequences of a Hypothetical Tornado Missile Accident

Accident / Dose	Dose (rem) at EAB	Dose (rem) at LPZ
Tornado missile accident in Region 1 (100 hrs decay)		
0-2 hour thyroid	40	20
0-2 hour whole body	0.19	0.093
Tornado missile accident in Region 2 (60 days decay)		
0-2 hour thyroid	0.51	0.25
0-2 hour whole body	8.1E-4	4.0E-4

6.3 OCCUPATIONAL EXPOSURE

The Ginna Station Radiation Protection Staff and Procedures are currently adequate for supporting this major operation. The areas of potential concerns are documented in procedures. These include but are limited to: the risk of significant airborne activity, the protection of the divers and the workers from inadvertent and unplanned exposures, and the documentation of the dose from this campaign.

Work will be controlled by the Ginna Station RWP, and tracked using the automated electronic dosimetry program. This allows a very rapid update of the worker's doses as well as the total person-rem associated with the rerack.

Personnel traffic and equipment movement will be monitored and controlled to minimize contamination and radioactive waste generation, and to ensure that the work is in keeping with the ALARA dose minimization philosophy.

Divers will have multiple electronic and TLD dosimetry to ensure that correct monitoring of the doses is achieved. To support this, area radiation monitors will be installed into the spent fuel pool to anticipate any radiological changes.

Gaseous releases will be monitored at the pool by a Continuous Air Monitor which will be Noble Gas and Iodine capable. The plant effluent radiation monitoring system will also be available to monitor these conditions.

Ginna Station performed a rerack in 1984-1985 and the lessons learned were reviewed and will be applied to the upcoming project. As a result, we expect this to reduce the total exposure associated with the rerack from 14 Person-Rem in 1984-1985 to a range of 8 to 12 Person-Rem in 1998.

While offsite dose consequences are calculated for accident scenarios, there should be no significant releases to the atmosphere or receiving waters as a result of the rerack. Any releases which do occur should be well within the regulatory limits.

All of the Radiation Protection Professional Staff are Board Certified by the American Board of Health Physics (Parts 1 and 2). As a result, they have a high degree of training and experience to deal with developing situations.

Due to the proposed increase in spent fuel capacity, the dose rates at the outer surface of each concrete wall of the spent fuel pool and the dose rate at the pool surface were calculated. The spent fuel pool wall thicknesses are shown in Figure 6.2. The dose rates were calculated using the discrete ordinates transport codes, ANISN^[6.11], and DORT^[6.12]. ANISN is essentially a one-dimensional version of the two-dimensional DORT code and generally yields slightly more conservative results than the DORT code. The DORT code was used to verify the ANISN results. The macroscopic material cross sections were generated using the BUGLE-93^[6.13] microscopic cross section library.

The source terms for both codes were generated based upon:

- pool at full capacity
- fuel with a burnup of 60 GWD/MTU
- fuel with 100 hours of decay.

The resulting dose rates at locations of interest are shown in Table 6.3-1. All dose rates at the outer surfaces are small with the exception of the south wall, which has a dose rate of 101 rem/hr. This dose rate is not a concern, however, since the south wall faces the ground at elevations spanning the heights of the fuel assemblies. At elevations above the fuel, the concrete is nearly six feet thick and at this outer surface it becomes the north wall of the decontamination pit.

During normal operations, personnel working in the fuel storage area are exposed to radiation from the spent fuel pool. Operating experience has shown that the area radiation dose rates, which originate primarily from radionuclides in the pool water, are generally 1.0 to 2.0 mrem/hr. Radionuclide concentrations typical of those found in pool water are shown in Table 6.3-2. During fuel reload operations, the concentrations might be expected to increase due to crud deposits spalling from spent fuel assemblies and to activities carried into the pool from the primary system. However, experience to date has not indicated a major increase as a consequence of refueling.

Operating experience has also shown that there have been negligible concentrations of airborne radioactivity and no increases are expected as a result of the expanded storage capacity. A continuous air for airborne activities is available in the immediate vicinity of the spent fuel pool.

No increase in radiation exposure to operating personnel is expected; thus, neither the current health physics program nor the area monitoring system needs to be modified.

Table 6.3-1 Dose Rates at Locations of Interest Around Spent Fuel Pool from Fuel Assemblies (doses do not include contribution from radionuclides in the pool water)

Location	Dose Rate (Rem/hr)
Outer face of north wall (6' thick)	0.014
Outer face of west wall (6' thick)	0.014
Inner face of outer east wall (3.5' of concrete plus 3' of water through transfer canal)	0.22
Outer face of outer east wall (3.5' of concrete plus 3' of water through transfer canal plus 6' of concrete)	2.1×10^{-8}
At pool surface (through 26' of water)	8.0×10^{-10}

Table 6.3-2 Gamma Isotopic Analysis of Spent Fuel Pool Water for 1996

Radionuclide	Activity ($\mu\text{Ci/ml}$)
Co-58	5.15×10^{-5}
Co-60	5.84×10^{-5}
Cs-134	9.66×10^{-6}
Cs-137	7.55×10^{-5}
H-3	1.80×10^{-1}
Te-123m	5.81×10^{-6}
Sb-125	1.47×10^{-4}

6.4 SOLID RADWASTE

Spent resins are generated by the spent fuel pool purification system. The frequency for changing the resins is between two to three years. The floor of the spent fuel pool will be cleaned before any work and after each of the old Region 1 racks is removed. Appropriate work practices and the cleaning of the spent fuel pool floor will reduce the generation of spent resins by the purification system. It is not possible to separate out the activity of the spent fuel pool resin from the resin in the spent resin tank. Recent resin activity is shown in Table 6.4-1. Operating experience after the 1985 modification indicates that the increased storage capacity will not result in a significant change in generation of solid radwaste (disposal of the existing Region 1 racks immediately after the installation is discussed separately in Section 6.6).

There is no expected additional man-rem burden from the solid radwaste generated due to the increased capacity of the spent fuel pool.

Table 6.4-1 Radionuclide Analysis Report - Resin Activity, from the Spent Resin Tanks

RADIONUCLIDE	ACTIVITY
NON-TRANSURANIC	$\mu\text{Ci/gm}$
Co-58	4.63
Cs-137	15.04
Cs-134	1.29
Co-60	13.83
Mn-54	1.01
C-14	1.27
Tc-99	< LLD
I-129	< LLD
H-3	1.28
Sr-90	0.13
Ni-63	27.70
Fe-55	24.90
Sb-125	6.69

**Table 6.4-1 Radionuclide Analysis Report - Resin Activity, from the Spent Resin Tanks
Continued**

RADIONUCLIDE	ACTIVITY
TRANSURANIC	$\mu\text{Ci/gm}$
Po-238	0.014
Pu-239, 240	0.008
Pu-241	0.70
Cm-242	0.019
Cm-245/244	0.020

Resin Volume = 14ft³ or 0.4 m³
LLD = lowest level of detection

6.5 GASEOUS RELEASES

Table 6.5-1 summarizes the auxiliary building gaseous releases in 1994 and 1995. No significant increases are expected as a result of the reracking. There is no way to separate out the SFP contribution from the total exhausted from the auxiliary building.

Table 6.5-1 Gaseous Releases from the Auxiliary Building

1994	
Radionuclide	Curies
Xe-133	2.21×10^1
Xe-135	7.63
I-131	1.30×10^{-4}
Kr-85m	-----
Kr-87	-----
Kr-88	-----
I-133	1.62×10^{-4}
H-3	3.73×10^1
Cs-137	6.46×10^{-6}
1995	
Radionuclide	Curies
Xe-133	1.86×10^1
Xe-135	7.03
I-131	7.18×10^{-5}
Kr-85m	-----
Kr-87	-----
Kr-88	-----
I-133	1.22×10^{-4}
H-3	4.94×10^1
Cs-137	4.27×10^{-6}

Note: It is not possible to segregate the atmospheric releases from the spent fuel pool from the remainder of the auxiliary building.

6.6 RACK DISPOSAL

During the modification, three Wachter racks will be removed from the spent fuel pool: Type A3 (31,366 lbs), Type B (26,533 lbs), and Type C (23,453 lbs). The old Region 1 racks will be decontaminated, packaged, and shipped by truck to a facility licensed for the processing of low-level radioactive waste.

Shipment of the spent fuel pool racks to the processing facility will meet all the requirements set forth by applicable Departments of Transportation (Federal and State) and the American Association of State Highway and Transportation Officials.

6.7 CONCLUSIONS

Of the six limiting hypothetical accidents evaluated only two, the fuel handling and tornado missile accidents, result in the release of fission products to the environment. The offsite thyroid and whole body doses calculated for the exclusion area boundary and low population zone boundary are less than the acceptance criteria. Therefore, it can be concluded that in the event of these accidents, the proposed re-racking of the Ginna spent fuel pool does not adversely affect the health and safety of the public.

The increase in storage capacity does not adversely affect the dose rates at the pool surface or at other locations of interest nor will it adversely affect solid radwaste production and gaseous releases from the auxiliary building.

6.8 REFERENCES

- 6.1 32-1258146-00, Ginna Re-rack Radiological Safety Analysis, M.A. Rutherford.
- 6.2 32-1257240-00, GINNA Rerack Gamma Heating/Dose Analysis, T.L. Lotz.
- 6.3 Title 10, Chapter 1, Code of Federal Regulations, Part 50 Appendix A, General Design Criteria for Nuclear Power Plants, 4/30/93.
- 6.4 Title 10, Chapter 1, Code of Federal Regulations, Part 100, Reactor Site Criteria, 4/30/92.
- 6.5 NUREG-0800, Standard Review Plan for the Review of Safety Analysis Reports for Nuclear Power Plants, LWR Ed., USNRC, Current thru October 1990.
- 6.6 38-1247195-00, RG&E Radiological Safety Analysis Transmittals Received by FTI, M.A. Rutherford.

Referenced transmittals are:

(A) Letter from J.P. Ortiz (RG&E) to G.T. Fairburn (FTI), FR-96-013, dated July 19, 1996. SUBJECT: INPUT DATA FOR THE RADIOLOGICAL SAFETY ANALYSIS /DRAFT AIS NO. 51-1257365-00.

(B) This reference intentionally omitted.

References Continued

- (C) Letter from J.P. Ortiz (RG&E) to G.T. Fairburn (FTI), FR-96-022, dated August 19, 1996. SUBJECT: ACTION ITEM MM-07/10/96-8.2/INPUT TO THE MOST RECENT CONTROL ROOM DOSE ANALYSIS.
- 6.7 Title 10, Chapter 1, Code of Federal Regulations, Part 20, Standards for Protection Against Radiation, 3/31/95.
- 6.8 ANSI/ANS 57.2-1983, Design Requirements for Light Water Reactor Spent Fuel Storage Facilities at Nuclear Power Plants, American Nuclear Society, 10/7/83.
- 6.9 NUREG-0612, Control of Heavy Loads at Nuclear Power Plants, U.S. NRC, July 1980.
- 6.10 Updated Final Safety Analysis Report for R.E. Ginna Unit 1, Docket No. 50-244, current thru Rev.13-1, controlled copy #1243, 7/96.
- 6.11 ANISNBW - A One-Dimensional Discrete Ordinates Transport Code, B&W Version of ANISN-W User's Manual, NPGD-TM-491, Rev.8, Filepoint 2A4, FTI Lynchburg, VA, July 1993.
- 6.12 BWNT-TM-107, ORIG, DORT - Two dimensional Discrete Ordinates Transport (BWNT Version of RSIC/ORNL Code DORT), VA, Filepoint 2A4, FTI, Lynchburg, May 1995.
- 6.13 BUGLE-93 Production and Testing of the VITAMIN-B6 Fine Group and the BUGLE-93 Broad Group Neutron/Photon Cross-Section Libraries Derived from the ENDF/B-VI Nuclear Data, DLC-175, Oak Ridge National Laboratory, Oak Ridge, April 1994.
- 6.14 USAEC Reg. Guide 1.25, Assumptions Used for Evaluating the Potential Radiological Consequences of a Fuel Handling Accident in the Fuel Handling and Storage Facility for Boiling and Pressurized Water Reactors, 3/23/72.
- 6.15 NUREG/CR-5009, Assessment of the Use of Extended Burnup Fuel in Light Water Power Reactors. Baker, D.A.; Bailey, W.J.; Beyer, C.E.; et al. Battelle Memorial Institute, Pacific Northwest Laboratory, February 1988.
- 6.16 International Commission on Radiological Protection Publication 30 Supplement to Part 1, Limits for Intakes of Radionuclides by Workers, 1980.

Figure 6-1 Overview of Proposed Re-racking of the Ginna Spent Fuel Pool

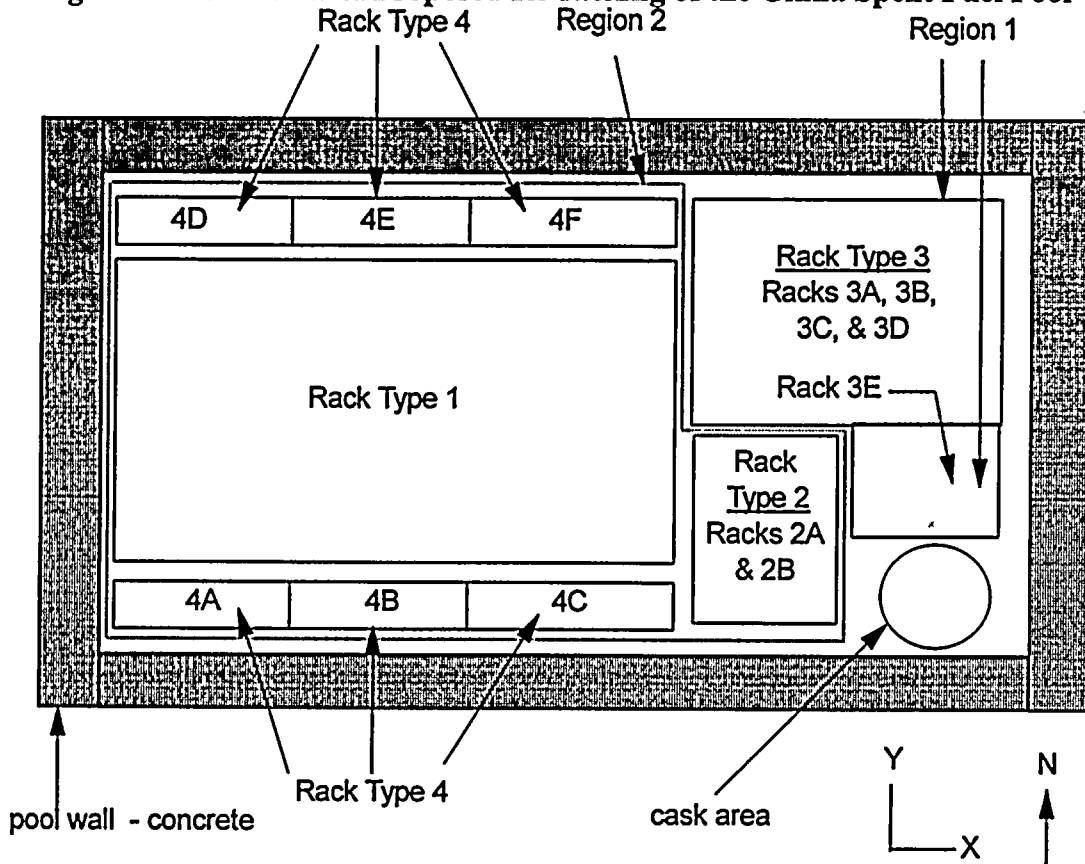
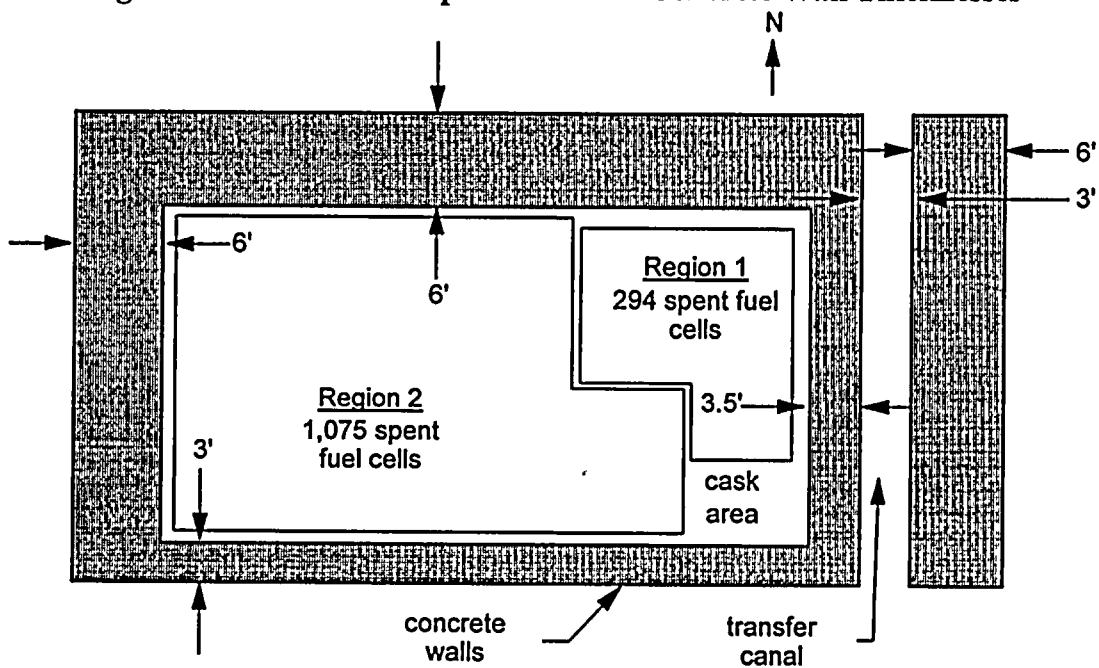


Figure 6-2 Overview of Spent Fuel Pool Concrete Wall Thicknesses





Appendix 6A Assumptions and Input

Key assumptions and input are presented in this appendix for the calculation of radiological dose consequences for the tornado missile accident.

Table 6A-1 Assumptions and Inputs Used in Determining Offsite Doses Due to Tornado Missile Accident Inside Auxiliary Building

Assumption or Input	Value	Basis for Value
Core power, MW _{th}	1551	1520 plus 2% uncertainty
Radial peaking factor	1.2	Conservative average value for damaged assemblies
Total # of rods in assembly	179	Consistent with current FH analysis
# of damaged assemblies	9	See section 3
Core source terms	----	Iodine and noble gas activity determined with ORIGEN2
Gap activity, %	I & NG, 10 Kr-85, 30 I-131, 12	Reg. guide 1.25; extended burnup factor applied to I-131 per NUREG-5009 ^(6.15)
Minimum water depth above damaged fuel assembly, ft	23	Reg. guide 1.25
Pool scrubbing factor elemental organic NG	133 1 1	Reg. guide 1.25 - overall effective decontamination factor is 100.
Iodine chemical species, % elemental organic	99.75 0.25	Iodine released from fuel to pool water, Reg. Guide 1.25.
Filtration	None assumed	
Site boundary atmospheric dispersion factor, sec/m ³	6.0 E-5	
Low population zone boundary atmospheric dispersion factor, sec/m ³	3.0 E-5	Table 15.7-1 of UFSAR
Iodine dose conversion factors (DCFs), rem/ci I-131 I-132 I-133 I-134 I-135	 1.07 E6 6.29 E3 1.81 E5 1.07 E3 3.14 E4	ICRP 30 ^(6.16)

Assumption or Input	Value	Basis for Value
Breathing rate, m ³ /sec	3.47 E-4	Reg. guide 1.25.
Fuel exposure for impacted spent fuel assembly, MWD/MTU	60,000	Reference 6.6(A)
Design missile	1490 lb wooden pole, 35 feet in length and 13.5" in diameter with a vertical velocity of 70 ft/sec.	UFSAR Ch. 9.1.2.7
Cooldown time for impacted spent fuel assemblies: Region 1 (Rack Type 3) Region 2 (Rack Types 2, 3, & 4)	100 hrs 60 days	UFSAR Ch. 15.7.3.2 & Ch. 9.1.2

Table 6A-2 Tornado Missile Accident Source Terms for Region 1 (100 Hours of Decay)

Nuclide	Activity(Ci) Released to Aux.Bldg
I-131	1.78E+03
I-132	1.24E+03
I-133	1.54E+02
I-134	Negligible
I-135	1.11E-01
Kr-83m	Negligible
Kr-85m	1.07E-02
Kr-85	1.28E+04
Kr-87	Negligible
Kr-88	Negligible
Xe-131m	2.31E+03
Xe-133m	5.31E+03
Xe-133	2.86E+05
Xe-135m	1.77E+00
Xe-135	5.35E+02
Xe-138	Negligible

Table 6A-3 Tornado Missile Accident Source Terms for Region 2 (60 Days of Decay)

Nuclide	Activity(Ci) Released to Aux.Bldg
I-131	2.28E+01
I-132	1.61E-02
I-133	Negligible
I-134	Negligible
I-135	Negligible
Kr-83m	Negligible
Kr-85m	Negligible
Kr-85	1.55E+04
Kr-87	Negligible
Kr-88	Negligible
Xe-131m	3.01E+02
Xe-133m	1.84E-02
Xe-133	2.81E+02
Xe-135m	Negligible
Xe-135	Negligible
Xe-138	Negligible

Table 6A-4 Dose Conversion Factors

Nuclide	Thyroid DCF Rem/Ci	Whole Body DCF Rem-m ³ /Ci-sec	Eave
I-131	1.07E+06	9.70E-02	0.39
I-132	6.29E+03	5.59E-01	2.24
I-133	1.81E+05	1.50E-01	0.60
I-134	1.07E+03	6.48E-01	2.59
I-135	3.14E+04	3.64E-01	1.46
Kr-83m	n/a	1.10E-02	0.044
Kr-85m	n/a	4.00E-02	0.16
Kr-85	n/a	5.75E-04	0.0023
Kr-87	n/a	1.98E-01	0.79
Kr-88	n/a	5.50E-01	2.2
Xe-131m	n/a	7.25E-04	0.0029
Xe-133m	n/a	5.00E-03	0.02
Xe-133	n/a	7.50E-03	0.03
Xe-135m	n/a	1.08E-01	0.43
Xe-135	n/a	6.25E-02	0.25
Xe-138	n/a	2.80E-01	1.12

Note that the whole body DCFs are calculated by multiplying the average energy of the emitted photons by 0.25 (see Section 6.2.6).

7.0 QUALITY ASSURANCE

7.1 DESCRIPTION OF SUPPLIER'S QUALITY ASSURANCE PROGRAM

FTI has a Quality Assurance Program for products and services designated as 'Safety-Related' and as 'Non-Safety Related'. This program is intended to comply with the requirements of 10 CFR 50, Appendix B (Quality Assurance Criteria for Nuclear Power Plants and Fuel Processing Plants) and the applicable requirements of the ASME Boiler & Pressure Vessel Code, Section III, Division I. The Quality Assurance Program is in compliance with ANSI N45.2 and its applicable daughter documents, and any applicable requirements in ANSI/ASME, NQA-1 which are not covered in the ANSI N45.2 Series.

The program also establishes methods to meet the quality requirements that are imposed by contracts with the customer or that, in the absence of such provisions, are imposed by the Product Line Manager. This program also provides for the implementation of the customer-specific procedures when required by the contract.

The scope of this program covers activities beginning with the authorization to proceed under customer contract and extending through the delivery of the final product. At the option of the Product Line Manager, it may also be applied to activities performed prior to the initiation of the contract.

This program has been reviewed and approved by RG&E and has been utilized in performing work in the past. A controlled copy of the FTI Quality Assurance Manual (Doc. No. 56-1201212) is maintained at RG&E by G. R. Amsden, Quality Assurance.

7.2 DESCRIPTION OF QUALITY ASSURANCE PLAN AND IMPLEMENTATION

FTI is the Prime Contractor for design, licensing analysis, fabrication, and installation of spent nuclear fuel storage racks. FTI is teamed with ATEA for design and fabrication, and FCF for the licensing analysis. Peyla Construction Management (PCM) will be responsible for the removal and disposal of the old racks and will install the new racks. ATEA is a subcontractor of FTI, and FCF and PCM are subcontractors to ATEA.

FTI is responsible for the overall project coordination and integration of the resources and the team. All work performed on the project, whether technical or administrative, will be performed in accordance with FTI's Quality Assurance Program (Doc. No. 56-1201212). Also, in accordance with the Project Management Plan (Doc. No. 56-1257505) project-specific tasks performed by FCF will utilize the FCF Quality Assurance Program (Doc. No. 56-1177617); project-specific tasks for ATEA will utilize the ATEA Quality Assurance Program (Rev. 0, dated April 18, 1995, as audited and approved by FTI; and project-specific tasks performed at Ginna by PCM will be performed in accordance with the FTI Quality Assurance Program (Doc. No. 56-1201212). Technical documents from RG&E and other organizations will be retained in the FTI Records Center and will be maintained in accordance with the contract requirements.

The ATEA storage racks are categorized as 'Safety-Related' products and as such are required to meet or comply with the requirements of 10 CFR 50, Appendix B.

7.2.1 Organization

Authority and an organization have been established under this project and are contained in the Project Management Manual noted in the above paragraphs. FTI retains the responsibility for the overall program effectiveness including work that is delegated to suppliers.

7.2.2 Quality Assurance

A Quality Assurance Program has been established that applies to all activities, products and services performed, procured and rendered on this project. FTI retains the overall responsibility for establishing and maintaining the project's Quality Assurance. The FTI Quality Assurance Program shall be performed in accordance with FTI document number 56-1201212.

7.2.3 Design Control

A design control program has been established for the project to provide a process to control design documents. These data affect the safety-related products and include for example, but are not limited to, design drawings, input for stress analysis, thermal hydraulics, seismic, physics, radiation, computer programs, materials, specifications, and system descriptions. Specifics of the design control processes are described in the FTI or subcontractors' Quality Assurance Program Manuals.

7.2.4 Procurement Document Control

Procurement of safety-related products and services are specified in procurement documents. Products and services are provided by approved suppliers.

7.2.5 Instructions, Procedures, and Drawings

Activities affecting quality of safety-related products and services are performed in accordance with documented instructions, procedures or drawings, which include appropriate quantitative and qualitative means of verifying quality. Required actions and responsibilities for preparation, review, approval and control of these documents are established in procedures and instructions.

7.2.6 Document Control

Measures for the review, approval and issuance of documents covering safety-related products and services and their associated changes are established internally to assure technical adequacy and the inclusion of quality control requirements prior to implementation. These measures include responsibilities for required independent reviews by qualified individuals including quality personnel for review and concurrence with respect to Quality Assurance-related aspects of documents to assure acceptability. Document control is applied to design, procurement and manufacturing documents including as-built documents and documents relating to computer codes, as well as instructions and procedures.

7.2.7 Control of Purchased Material, Equipment, and Services

When specified in the procurement document, FTI provides for Quality Assurance surveillance of suppliers during fabrication, inspection, testing and the release of safety-related products and services.

For commercial 'off-the-shelf' items, which are to be used as safety-related products and services, but where a specific Quality Assurance control appropriate for nuclear applications cannot be imposed in a practical manner, a receiving inspection and/or tests are performed and shall meet the acceptance criteria. These instructions are subject to the document control provisions.

Prior to placing an order with a new supplier, an evaluation is conducted by Quality Assurance personnel and appropriate engineering and/or procurement personnel. Such an evaluation may include an audit and is conducted in accordance with applicable FTI and/or their subcontractor's Quality Assurance Program.

7.2.8 Identification and Control of Materials, Parts, and Components

Identification requirements are established in Quality Assurance programs and are specified as necessary in the procurement documents for safety-related products and services. Identification and control procedures assure that identification is maintained on the item or on records that are traceable to the item to preclude use of incorrect or defective items. Identification of items can be traced to appropriate documentation such as design documents, procurement documents and/or inspection records. Identification of items is verified and documented prior to release of the item for further use.

7.2.9 Control of Special Processes

Established procedures are maintained to provide appropriate control over special processes for safety-related products and services. The processes that are controlled as special processes are the following: the process where direct inspection is impossible or disadvantageous; and processes where the results are highly dependent on the control of the process or the skill of the operator, or both. Examples of these processes are welding, casting, and explosive forming.

The special process procedures and certification of qualified personnel are maintained under document control. Special processes are performed by qualified personnel and accomplished under prescribed procedural controls. Recorded evidence of verification is maintained.

7.2.10 Inspection

Procedures are established that control manufacturing activities of safety-related products and services. These procedures provide control for the selection and identification of required inspection in a quality plan identifying the inspections to be performed, their location in the manufacturing process and the mandatory 'Hold Points' required by various organizations (i.e., Quality Assurance, the customer). This document is either prepared and/or approved by the Quality Assurance organization having the responsibility for the item to be inspected.

7.2.11 Test Control

Measures are established to control the testing of safety-related products and services. These measures include identification of required testing, development of procedures, a means of assessing the adequacy of tested items, and designation of responsibility for performing the various phases of the testing activities. Tests required during manufacturing are identified in the Quality Plan of the item. The measures established for the control of special processes include a provision for identifying the necessary qualification tests.

The test results are documented, evaluated, and their acceptability determined by a qualified, responsible individual or group. Modifications, repairs and replacements are tested in accordance with the original test or appropriate alternatives.

Test program requirements are incorporated as appropriated in purchase orders and will be reflected in the Quality Plan. Supplier testing activities are subject to auditing and monitoring for compliance during the surveillance activities.

7.2.12 Control of Measuring and Test Equipment

FTI maintains the means of controlling measuring and test equipment used on safety-related products and services. Programs were developed for considering such attributes as inherent stability, purpose of use, desired accuracy, and the degree of usage.

Measuring and test equipment are identified and traceable to the calibration test data and for other required documentation. The complete status of all items under the calibration system including personal acceptance gages, is recorded, maintained and controlled.

7.2.13 Handling, Storage, and Shipping

Procedures are established to control cleaning, packaging, shipping, storage and handling of safety-related products and services. Where required, these activities are accomplished by appropriately trained personnel.

The procedures include the control of cleaning, handling, storage, packaging, shipping and preservation on materials, components, and systems in accordance with design specification requirements to preclude unacceptable damage, loss, or deterioration by environmental conditions. The identification controls include considerations for identification of inspection, use, personnel training and qualification, auditing, non-conformance, and other appropriate requirements. These procedures may be in various forms, such as manufacturing procedures, shipping instructions, drawings, manufacturing routing sheets, cleaning specifications, and procedural training booklets.

7.2.14 Inspections, Tests, and Operating Status

Procedures are established to indicate the inspection, test and operating status of safety-related products and services during fabrication, installation and testing. These procedures control the application and removal of status indicators through the use of inspection control cards, shop travelers, or other documents. These procedures also control sequence changes and the identification of non-conforming items. The procedures document the sequence of required tests, inspections, and other safety-related operations.

7.2.15 Non-Conforming Materials, Parts, or Components

Procedures are established to control the identification, documentation, segregation, review and disposition of non-conforming safety-related products and services. They include notification of affected organizations if disposition is other than scrap. These procedures identify individuals or groups who are authorized to dispose of and approve non-conformance and describe the segregation and/or control of non-conforming items to prevent inadvertent use.

Documentation identifies the non-conforming items, describes the non-conformance, the disposition of the non-conformance, including reinspection requirements, and includes documented approval of the disposition. When non-conforming items are repaired or otherwise made suitable for their designed use, they are inspected and tested in accordance with the original inspection and test requirements or acceptable alternatives. The Quality Assurance Department is responsible for the review and approval of decisions proposed by Engineering.

7.2.16 Corrective Action

Procedures are established that provide corrective actions for safety-related products and services. These procedures include the initiation and documentation of corrective actions to preclude recurrence of significant conditions adverse to quality. Implementation of corrective action is verified by responsible individuals or organizations and is documented to close out the corrective action. Corrective action processing involves participation of Quality Assurance. These decisions are documented.

For significant conditions adverse to quality, the cause and corrective actions taken are documented and reported to management for review. Non-conformance reports are generated. These non-conformance reports are reviewed to determine the need for corrective action and are analyzed for trends. The results of these trend analyses are provided to management.

7.2.17 Audits

Procedures are established that provide a comprehensive system of Quality Assurance Program audits of activities affecting the quality of safety-related products and services. Audits are performed by qualified audit personnel using written procedures or checklists designed to provide an objective evaluation of the Quality Assurance Program and its effective implementation. Audits are planned and conducted by the quality organization responsible for its Quality Assurance Manual. Activities of the quality organization itself are audited by qualified auditors assigned by the General Management, having no direct responsibilities in the area to be audited. A written report that documents the audit results and corrective action is prepared by the team leader and distributed to the management of the organization being audited. The corrective actions to be proposed by the organization responsible for the finding are reviewed by the quality organization or by the team leader (when the quality organization was the audited area). Verification of corrective action (including re-audit of deficient areas, where appropriate) is performed and documented.

Provisions made for preparation, performance, reporting, and closing out of suppliers' audits are similar and meet the same requirements. Audit schedules are implemented in accordance with the Quality Assurance Manual. These audits ensure that procedures and activities comply with the overall Quality Assurance Program and provide a comprehensive independent verification and evaluation of quality-related procedures and activities.

8.0 ENVIRONMENTAL COST/BENEFIT ASSESSMENT

8.1 NEED FOR INCREASED STORAGE CAPACITY

The U.S. Department of Energy (DOE) has statutory and contractual obligations to accept Ginna spent fuel beginning in 1998. RG&E, in considering its capacity needs, assessed that the DOE would not be ready to accept spent fuel in 1998. This assessment has been confirmed by recent letter from DOE dated December 17, 1996, in which the DOE notified RG&E that it will not start acceptance of Ginna spent fuel in 1998.

Early in January 1997, the DOE released a draft proposal outlining a three-phase process for private firms to accept and transport waste from civilian reactors. According to the proposal, there would be two phases prior to operation of a Federal repository. The estimated duration of the phases is several years beyond 1998, subject to the DOE meeting the schedule for award of the contracts and Congress designating a Federal storage site. The DOE proposal, and its associated uncertainties, further confirms RG&E's need for increased storage capacity beyond 1998 to accommodate the Ginna spent fuel prior to operation of the Federal repository.

Table 5.5-1 shows the schedule of refueling outages to the end of license in September 2009. Additional discharges were conservatively incorporated beyond September 2009 for the purpose of determining a bounding decay heat load. The bounding decay heat load is based on an inventory of fuel rods in the spent fuel pool not to exceed the number of rods contained in 1,879 intact fuel assemblies (179 fuel rods/assembly x 1,879 assemblies=336,341 fuel rods).

The current spent fuel pool inventory is as follows: (a) 782 spent fuel assemblies (intact), (b) 8 consolidated rod canisters and 2 consolidated hardware canisters (from 11 intact fuel assemblies), (c) 1 fuel rod storage basket, (d) 5 storage locations with non-fuel components, and (e) 1 storage location not available for storage, for a total of 799 storage locations being occupied. The current licensed capacity is 1,016 fuel assemblies. Projected spent fuel discharges are conservatively estimated at 44 spent fuel assemblies during each of the projected refueling outages. Based on the current inventory and projected spent fuel discharges, Ginna loses the capability to discharge a full-core into the spent fuel pool in September 2000.

8.2 ESTIMATED CONSTRUCTION COSTS

The construction cost for the proposed reracking, including engineering, escalation, and allowance for funds used during construction is estimated at \$6 million.

8.3 ALTERNATIVES TO INCREASED STORAGE CAPACITY

Fuel Assembly Consolidation

Fuel assembly consolidation involves separation of the fuel rods from the fuel assembly hardware (grids, guide tubes, and nozzles). The nuclear industry, including RG&E, has conducted several programs over several years to demonstrate that rods can be consolidated with up to a ratio of 2 to 1 (rods from two fuel assemblies are stored in one canister). Rod consolidation to that ratio has been demonstrated to be achievable.

Utilities have also undertaken programs to consolidate assembly hardware. The programs have not achieved the desired consolidation rate of 10:1 (hardware from ten fuel assemblies are stored in one canister). Vendors have developed advanced consolidation machines to address lessons learned from the programs. These machines have not been demonstrated yet. At present, there is a degree of uncertainty with respect to the consolidation rate of hardware.

The economics of consolidation is highly dependent on the consolidation rates for fuel rods and hardware. With additional demonstration programs, fuel consolidation has the potential to be a strong alternative to building an Independent Storage Facility (ISFSI). RG&E has prepared this Licensing Report to allow future storage of consolidated spent fuel as an alternative to an ISFSI.

At present, increasing the capacity of the spent fuel pool by reracking is a better alternative (lower cost, lower uncertainty).

Independent Spent Fuel Storage Facility (ISFSI)

Constructing an ISFSI to increase capacity is not cost-effective compared with increasing capacity by reracking the spent fuel pool. There is a large fixed cost for constructing the facility and procuring the ancillary equipment for storing a limited number of storage casks. Because of this fixed cost, the cost of the ISFSI for the equivalent number of storage locations is more than 3 times the cost per location of reracking the spent fuel pool.

Shipment to another Reactor Site

Shipment of spent fuel to other non-RG&E reactor sites would require an increase in the storage capacity at those sites to accommodate Ginna spent fuel assemblies. Additional capacity at non-RG&E sites would have to be designed to store Ginna 14x14 spent fuel assemblies. In addition, utilities at those sites may charge storage fees separate from the cost of the increased capacity. The proposed reracking is the most cost-effective of all storage alternatives to increase capacity at the Ginna site. By modifying the spent fuel pool at Ginna, there are no additional costs associated with transportation to another site, modifications to accommodate 14x14 assemblies, and potential storage fees.

Other Alternatives

Permanent shutdown of Ginna because of lack of storage capacity for spent fuel was not a viable alternative. The costs of a permanent shutdown are significantly higher than the cost of reracking the spent fuel pool.

8.4 COMMITMENT OF MATERIAL RESOURCES

The material resources utilized in the spent fuel reracking are described in Section 1.0. These include primarily austenitic stainless steel as a structural material and borated stainless steel as a neutron absorber. The requirement for austenitic stainless steel for the reracking is a negligible amount of world production. The production of borated stainless steel can be accommodated by manufacturers in the U.S., Austria, Germany, and the Czech Republic. Levels of production of borated stainless steel can be adjusted to meet significantly higher demands.

The additional capacity in the spent fuel pool does not result in a permanent commitment of water, land, or air resources. The increased capacity will utilize the existing area of the spent fuel pool.

The proposed additional storage capacity in the spent fuel pool will not significantly foreclose the alternatives available with respect to any other licensing actions designed to ameliorate a possible shortage of spent fuel storage capacity.

8.5 HEAT RELEASED TO THE ENVIRONMENT

The heat removal capability of the spent fuel pool cooling system will remain unchanged as discussed in Section 5.4. After a shutdown, the full core will decay in the reactor vessel prior to movement to the spent fuel pool. The total heat load from the spent fuel assemblies, including a full core discharge, will remain within the limits of the existing spent fuel pool cooling system (Section 5.4). The heat released to the environment from this modification is bounded by existing heat loads from normal operation.